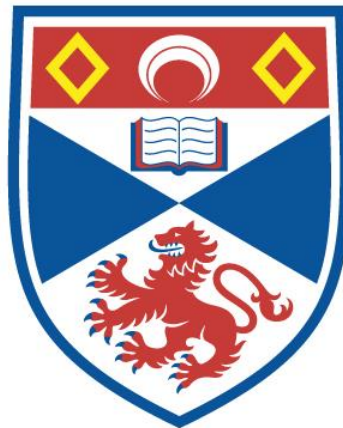


STELLAR PULSATION AND THE RV TAURI PHENOMENON

JOHN KINGSLEY WORRELL

A Thesis Submitted for the Degree of PhD
at the
University of St Andrews



1985

Full metadata for this item is available in
Research@StAndrews:FullText
at:

<http://research-repository.st-andrews.ac.uk/>

Please use this identifier to cite or link to this item:

<http://hdl.handle.net/10023/6509>

This item is protected by original copyright

This item is licensed under a
Creative Commons Licence

STELLAR PULSATION
AND THE
RV TAURI PHENOMENON

BY
JOHN K. WORRELL

A thesis submitted to the University of St. Andrews
in application for the degree of Doctor of Philosophy

St. Andrews

March 1985



BEST COPY

AVAILABLE

Text cut off in
original thesis

PAGE NUMBERS ARE
CLOSE TO THE
EDGE OF THE PAGE.

SOME NUMBERS HAVE
BEEN CUT OFF

SOME PAGES ARE SKEWED
FROM TIGHT BINDING
OF ORIGINAL THESIS

I John Kingsley Worrell hereby certify that this thesis which is approximately 65,000 words in length has been written by me, that it is the record of work carried out by me, and that it has not been submitted in any previous application for a higher degree.

March 1985


J.K. Worrell

I hereby certify that the candidate has fulfilled the conditions of the Resolution and Regulations appropriate to the degree of Ph.D. of the University of St. Andrews and that he is qualified to submit this thesis in application for that degree.

March 1985


T.R. Carson

I was admitted as a research student under Ordinance No. 12 on 1st October 1980 and as a candidate for the degree of Ph.D. on 1st October 1981; the higher study for which this is a record was carried out in the University of St. Andrews between 1980 and 1984.

March 1985


J.K. Worrell

In submitting this thesis to the University of St. Andrews I understand that I am giving permission for it to be made available for use in accordance with the regulations of the University Library for the time being in force, subject to any copyright vested in this work not being affected thereby. I also understand that the title and abstract will be published, and that a copy of the work may be made and supplied to any bona fide library or research worker.

ABSTRACT

On the basis of observational data it is argued that RV Tauri variables, and probably yellow semiregular (SRd) variables, are closely related in every way to type II cepheid stars. Assuming that a single mass ($\sim 0.6 M_{\odot}$) is applicable to all three classes of star linear, nonadiabatic pulsation models are calculated. Using these models, the observed effective temperatures, and periods for these stars new luminosities are calculated and compared with the observed luminosities. This comparison appears to confirm the relationships between the three classes implied by the observations for the globular cluster stars.

It is shown that an interaction of two or more pulsation modes could be responsible for the characteristic light curves of the RV and SRd stars but it is argued that this is unlikely.

One RV star and a high luminosity F star both exhibit pulsations with two periods. The periods together with the observed effective temperatures and linear pulsation calculations yield masses and luminosities for the two stars. On the basis of the linear pulsation calculations the peculiar characteristics of the pulsations are explained.

A sequence of nonlinear pulsation models based on the "standard" physics is presented. The light curves for some of these models show features characteristic of the RV stars. Strange behaviour found in the luminosity at the surface of some models is shown to be a product of an inadequate boundary condition. An alternative is suggested which cures the problem. Nonlinear models calculated with the new boundary condition eject matter, form very extended atmospheres, exhibit semiregular RV - like light curves with a (possibly) cyclic variation of the phase of light minima, and show long term variations of mean effective temperature. Strong shock waves exhibiting properties like those found in RV stars are found. It is suggested that the equilibrium diffusion approximation is inappropriate for these models and the consequences of its use discussed.

ACKNOWLEDGEMENTS

I would like to thank Dr T.R. Carson for suggesting the subject of this thesis, for the use of his opacity tables and nonlinear code, and for his encouragement and advice whilst this work was in progress.

I would also like to thank Prof. D.W.N. Stibbs for the use of facilities at the University Observatory and for his encouragement. Dr P.W. Hill and the staff of the University Computing Laboratory have greatly eased some of the computer related problems encountered and so I would also like to thank them. I would also like to thank Morag Driscoll for typing some of the earlier chapters in this volume and for her encouragement at that time.

Everybody at the Observatory has helped out in some way over the years but I should in particular like to thank Alan Bridger, Simon Jeffery, Alan MacFadzean, and Ian Skillen. To the research students and postdocs in general go my thanks for their own peculiar brand of encouragement.

Last of all, but definitely not least, I would like to thank my family and friends for their very substantial support over the years during which this work was pummelled into shape.

CHAPTER 1	INTRODUCTION	
CHAPTER 2	METHODS FOR LINEAR NONADIABATIC PULSATION.	
2.1	INTRODUCTION	5
2.2	THE EQUILIBRIUM MODEL	9
2.3	THE LINEAR NON-ADIABATIC PULSATION CALCULATION . .	17
2.3.1	The Work Integral For Linear Pulsation	27
2.4	THE EDDINGTON APPROXIMATION FOR RADIATIVE TRANSPORT	31
2.5	THE MOMENTUM EQUATION AT THE SURFACE	35
CHAPTER 3	CONVECTION AND PULSATION	
3.1	MODELS FOR THE INTERACTION OF CONVECTION AND PULSATION	43
3.2	THE MODEL OF CONVECTION ADOPTED	54
3.3	THE STATIC MODEL	57
3.4	THE LINEAR PULSATION MODEL	62
3.5	THE WORK INTEGRAL WITH VISCOSITY	67
CHAPTER 4	THE EQUATION OF STATE AND OPACITY	
4.1	THE EQUATION OF STATE.	69
4.1.1	The Basic Equations	69
4.1.2	The Partition Functions	73
4.1.3	Derivatives Of The Electron Number Density . . .	76
4.1.4	The Effect Of The Varying Partition Functions .	77
4.1.5	A Note On The Implementation Of The Equation Of State	79
4.2	THE TREATMENT OF STELLAR OPACITY	79
4.2.1	Use Of The Opacity Data	82
CHAPTER 5	SENSITIVITY OF THE CALCULATIONS TO ERRORS AND TO VARYING PHYSICS	
5.1	NUMERICAL ERRORS	88
5.2	PHYSICAL PERTURBATIONS	99
CHAPTER 6	THE PRESENT STATUS OF THE RV TAURI STARS	
6.1	OBSERVATIONS OF RV TAURI STARS AND THEIR RELATIONS.	106
6.2	PULSATION MODELS OF RV TAU STARS	131

6.3	THE EVOLUTIONARY STATUS OF THE RV TAU AND RELATED STARS	138
CHAPTER 7 LINEAR PULSATION RESULTS		
7.1	THE EFFECT OF VARIATIONS OF THE INPUT PHYSICS UPON PULSATION MODELS	142
7.1.1	Convection And The Carson Opacities	147
7.1.2	Sensitivity Of The Fundamental Blue Edges To Variations Of The Physics	150
7.1.2.1	Different Implementations Of The Carson Opacities	151
7.1.2.2	A Comparison Of Different Opacities	153
7.1.2.3	Blue Edges For Different Metallicities	156
7.1.2.4	The Effect Of The Eddington Approximation	159
7.1.2.5	The Running Wave Boundary Condition	161
7.1.2.6	The Effect Of Convection On The Blue Edges	163
7.2	RED EDGES FOR THE $M = 0.6 M_{\odot}$ INSTABILITY STRIP	164
7.3	NONADIABATIC EFFECTS	166
7.3.1	The Effects Of Extreme Nonadiabaticity	170
7.4	A SURVEY OF THE LUMINOSITY-TEMPERATURE PLANE FOR $M = 0.6 M_{\odot}$	174
CHAPTER 8 APPLICATIONS OF THE LINEAR PULSATION RESULTS: THE RV TAURI STARS		
8.1	THE RV AND SRD STARS	183
8.1.1	Resonances	202
8.2	A DETERMINATION OF THE MASS AND LUMINOSITY OF UU HER	212
8.3	A DETERMINATION OF THE MASS AND LUMINOSITY FOR THE HIGH LUMINOSITY F STAR HD161796	218
CHAPTER 9 NONLINEAR MODELS		
9.1	THE NONLINEAR PROGRAMME	225
9.2	MODELS WITH "STANDARD" PHYSICS	229
9.2.1	The Sequence For $\text{Log}(L/L_{\odot}) = 3.2$	230
9.2.1.1	$\text{Log}(T_{\text{eff}}) = 3.76$	231
9.2.1.2	$\text{Log}(T_{\text{eff}}) = 3.74$	232
9.2.1.3	$\text{Log}(T_{\text{eff}}) = 3.72$	235
9.2.1.4	$\text{Log}(T_{\text{eff}}) = 3.70$	236
9.2.1.5	$\text{Log}(T_{\text{eff}}) = 3.65$	237
9.2.2	The Sequence For $\text{Log}(L/L_{\odot}) = 3.5$	238
9.2.2.1	$\text{Log}(T_{\text{eff}}) = 3.72$	238
9.2.2.2	$\text{Log}(T_{\text{eff}}) = 3.70$	240
9.2.3	Driving Of The Pulsations	241

9.3	SPHERICAL GEOMETRY IN THE ATMOSPHERE	243
9.4	THE LUMINOSITY AT THE OUTER BOUNDARY	245
9.5	MODELS CONSTRUCTED USING RADIATION DILUTION . . .	249
9.5.1	Features Common To All Of The Models	250
9.5.2	The Model For $\text{Log}(L/L_{\odot}) = 3.2$	251
9.5.3	The Model For $\text{Log}(L/L_{\odot}) = 3.4$	255
9.5.4	The Deep Minimum For The $\text{Log}(L/L_{\odot}) = 3.2$ Model .	257
9.5.5	Damping Through Running Waves	259
9.5.6	Omission Of Molecules From The Equation Of State	259
9.5.7	Omission Of All Molecular Effects	260
9.5.8	The Effects Of Varying The Artificial Viscosity	261
9.5.9	The Luminosity Spikes	262
9.5.10	The Validity Of The Equilibrium Diffusion	
	Approximation	263
9.5.11	Shock Waves	265

CHAPTER 10 CONCLUSION

APPENDIX A REFERENCES

CHAPTER 1

INTRODUCTION

There are many stars which exhibit intrinsic variability and of these the stars undergoing radial pulsations are probably the most important. The regular, "clockwork", pulsations of the classical cepheids and RR Lyrae stars together with the slightly less regular type II cepheids provide a source of data through their periods which cannot be degraded by the presence of matter lying between them and the observer. The shape of the light curves, and where available the velocity curves, for the pulsating stars forms a further only slightly less robust piece of information. The classic application of these properties is the use of the empirical period - magnitude relation of the classical cepheid stars to determine the distances of galaxies. In a similar way RR Lyrae stars can be used to gauge the distances of globular clusters and type II cepheids are becoming useful as a means of probing the older components of the Galaxy. Although the radial pulsators make up between only one in a million and one in a hundred thousand they have an importance which outweighs their relative

paucity.

In conjunction with detailed models of pulsating stars information regarding the structure of the stars themselves can be derived. When more than one period is observed in a star then the information that can be derived is correspondingly increased. In the case of the nonradial pulsators, e.g. ZZ Ceti stars and the Sun, a great many periods are observed, and for the Sun very detailed information on the internal structure can be derived by fitting models to the observations.

However not all radial pulsators show regular pulsations. In particular the RV Tauri stars and some globular cluster stars classified as W Vir stars show varying degrees of irregularity with a strong tendency for alternate light minima to be of different depths. The apparently continuous progression from regular W Vir to semi-regular RV Tauri behaviour in the globular clusters suggests a close connection between these two classes of stars and prompts the question; "Why does irregularity set in?". The period - magnitude relation for the RV Tauri stars has a positive slope, for both field and cluster stars. This appears to violate the period - mean density relation for pulsating stars and so this too requires an explanation. The answering of these and many more questions regarding the RV Tauri stars is the primary concern of this thesis.

A secondary aim of this work is the investigation of the effects of differing approximations of the physics incorporated into theoretical models of stellar pulsation. Of these the most important source of uncertainty is probably the opacity and so a comparison of the properties of the pulsation models constructed using the "standard" Los Alamos opacities and with the Carson (1976) opacities is included. (N.B. a recent revision by Carson et al. 1984 of the latter opacities removes the most substantial differences.)

Chapter 2 describes the linear pulsation problem and the ancillary approximations and assumptions necessary together with the methods needed to construct the static stellar models and to solve the linear pulsation equations. The various theories of convection in pulsating stars are reviewed and the modifications necessary to include such a theory in the static and linear pulsation models are described in chapter 3. A description of the equation of state and the opacities together with the methods for using the opacity tables form chapter 4. In chapter 5 an attempt to quantify the propagation of errors through the calculations is given together with a description of a method for studying the effects of variations of the opacity upon the models. Chapter 6 is a review of the RV Tauri stars with the SRd stars and type II cepheids. Particular attention is paid to intercomparisons of the properties of the members of the three classes. In chapter 7 the results of the linear pulsation calculations made with the differing physical approximations are

described followed by a description of a survey of the HR diagram around the expected locations of the RV Tauri stars. The application of these results to the RV Tauri stars and type II cepheids is described in chapter 8. Analyses of the RV Tauri star UU Her and a peculiar F star, HD161796, in the light of the linear pulsation results follows. Chapter 9 is a description of nonlinear pulsation models constructed for the region of the HR diagram where RV Tauri stars are thought to be found. The final chapter concludes the study and in time honoured fashion suggests further lines of research.

CHAPTER 2
METHODS FOR LINEAR NONADIABATIC PULSATION.

2.1 INTRODUCTION

In this work we assume, without exception, that the stars are spherically symmetric non-relativistic and are in local thermodynamic equilibrium. We further assume that the pressure is isotropic and that the local equations for energy transfer are valid. The equations for time dependent stellar structure are most appropriately written in a Lagrangian formulation. The equations are;

the continuity equation,

$$\frac{\partial r}{\partial m} = \frac{1}{4\pi r^2 \rho} \quad [1]$$

the momentum conservation equation,

$$\frac{d^2 r}{dt^2} = -4\pi r^2 \frac{dp}{dm} - \frac{Gm}{r^2} \quad [2]$$

the first law of thermodynamics,

$$T \frac{dS}{dt} = \epsilon - \frac{\partial L}{\partial m} \quad [3]$$

and an appropriate equation for energy transport. Here r , m , p , T , L , ρ , S and ϵ represent the radial coordinate, the mass contained within a sphere of radius r , the total pressure, temperature, luminosity, density, specific entropy and the energy generation rate. Since it is well known, e.g. Rosseland (1949), that for stars of moderate to high central condensation the pulsation amplitude decreases very rapidly towards the centre of the star, we need only consider the stellar envelope external to the region of energy generation and so can dispose of ϵ .

In the bulk of this work the radiative diffusion approximation is used to represent the energy transport but some results are also obtained using an Eddington Approximation to radiative transport, Unno and Spiegel (1966), and a simple mixing length theory of convection. The set of equations is completed by the addition of the equation of state, that is, $p = p(\rho, T)$. We also need to know the stellar radiative opacity, κ , which enters into the equation for radiative energy transport.

With the omission of the energy generating regions, the luminosity, L , of a star in equilibrium becomes a constant and so we are left with three differential equations to solve. The problem is further simplified because for a star in equilibrium the problem now becomes an initial value problem rather than a boundary condition problem. A stellar envelope can be specified by a stellar mass, luminosity, effective temperature and a chemical composition which is assumed to be constant throughout.

There is no shortage of methods for solving the complete problem, i.e. for the construction of an equilibrium model of a stellar envelope and for solving the equations for the linear pulsation modes of this model. A simple method for constructing a stellar model is to state a set of conditions for the surface and to integrate down towards the centre of the star. This method has been used widely, e.g. Schwarzschild (1958) etc., and might be said to be the classical technique. An alternative method is to write the equations as a set of difference equations, e.g. Henyey et. al. (1964), which can then be solved by iteration. The same choice faces us in solving the linear pulsation equations. If we linearise the time dependent equations for stellar structure and assume a time dependence for the perturbations, $\sim e^{i\omega t}$, then we have an eigenvalue problem in ω . This can be solved by selecting boundary conditions at the envelope surface and base and then for a trial value of ω using a shooting method for integration, iterating on ω until the two integrations meet. The

combination of an integrated stellar model and shooting method for the linear pulsation problem has been used widely, e.g. Baker and Kippenhahn (1962,1965). Iben (1971) has used the difference equation method for the pulsation problem together with an integrated envelope model. This involves calculating a number of mean values of physical variables at points between the grid points for the difference equations and so a consistent method in which the differential equations for time dependent stellar structure are recast as difference equations and then the linearisation procedure carried out on these is probably to be preferred. Castor (1971) and Keeley (1977) have both used this type of method. In Castor's method the problem becomes that of solving a rational function for the eigenvalue, ω , and thence for the eigenvectors. This is accomplished by an iteration on ω for which we must provide a trial value. Keeley uses the inverse iteration method for which a trial value of the relevant eigenfunction must also be provided. I have adopted Castor's method.

In the following sections the construction of a stellar envelope, the formulation and solution of the pulsation equations, and the physical approximations and numerical methods necessary are presented.

2.2 THE EQUILIBRIUM MODEL

In this section the energy is assumed to be transported solely by radiation, and for this the diffusion approximation is adopted. The equations to be solved are;

$$\frac{dp}{dm} = - \frac{Gm}{4\pi r^4} \quad [5]$$

$$\frac{dr}{dm} = \frac{1}{4\pi r^2 \rho} \quad [6]$$

and $\frac{dt}{dm} = 0 \quad [7]$

$$\frac{dT}{dm} = - \frac{3}{4\sigma} \frac{Kl}{(4\pi r^2)^2 T^3} \quad [8]$$

Following Castor (1971) we adopt the following difference equations:

$$p_{I-1} - p_I = \frac{Gm_I}{4\pi r_I^4} \Delta m_{2I} \quad [9]$$

$$r_I^3 - r_{I-1}^3 = \frac{3}{4\pi} \frac{\Delta m_{I-1}}{\rho_{I-1}} \quad [10]$$

and
$$L = \frac{4\sigma}{3} (4\pi r_I^2)^2 \frac{T_{I-1}^4 - T_I^4}{\frac{1}{2}(K_{I-1}\Delta m_{I-1} + K_I\Delta m_I)} \quad [11]$$

$$= \text{constant}$$

The quantities m , r , and L are defined at zone interfaces and p , ρ , T , and K for the zones themselves. The surface of the star is at $I=N$ and the base of the envelope at $I=1$. We have defined, $\Delta m_{I-1} = (m_{I-1} - m_I)$ and $\Delta m_I = (m_I - m_{I+1})/2$. The $N - 1$ zones and N interfaces are laid out in the following way.



The form of the mean opacity has been chosen, as in Castor's work, for ease of handling since we can use a fine enough zone width to render the precise form unimportant. More care must be taken in the case of the more coarsely zoned nonlinear pulsation models.

The structure of the envelope will be specified by the mass, M , luminosity, L , effective temperature, T_{eff} , and the chemical composition. We must find the values of p , r , T , and ρ at the point where $m = M$. However since this would imply that the density and so the opacity are zero, we must choose a point a little way into the star. This point is specified by its optical depth, τ_0 , which is chosen to satisfy

$$\tau_0 \ll 1.$$

An alternative approach is to set the boundary at $\tau = 2/3$ using the Eddington approximation to give the conditions above this point. However whilst this is simple for the static model it is very difficult to treat this boundary correctly in the pulsation calculation, (e.g. Unno 1965).

If we now consider the radius, r , and mass at this optical depth to be effectively constant and taking the value of the temperature, T , from the exact grey relation for $\tau=0$, i.e.

$$T_0^4 = \frac{\sqrt{3}}{4} T_{eff}^4$$

we obtain,

$$p_0 = p_{r_0} + \frac{GM}{R^2} \frac{\tau_0}{\kappa(\rho_0, T_0)} \quad [12]$$

where,

$$p_{r_0} = \frac{1}{3} \alpha T_0^4$$

since the gas pressure $p_g = 0$ at the surface. ρ_0 , is, as yet, unknown. Two different methods have been used in this work for calculating the value of p_{N-1} . The first and simplest is to assume that all the star's mass lies within the outermost interface, i.e., $m_N = M$. In this case the difference equation for pressure gives,

$$p_{N-1} = \frac{1}{3} \alpha T_0^4 + \frac{GM_N}{r_N^2} \frac{Dm_{N-1}}{2} \frac{1}{4\pi r_N^2} \quad [13]$$

where,

$$\frac{Dm_{N-1}}{2} = \frac{4\pi r_N^2}{K_{N-1}} \chi_0$$

and,

$$K_{N-1} = K(\rho_{N-1}, T_{N-1}).$$

with $T_{N-1} = T_0$, ρ_{N-1} , and K_{N-1} are obtained by an iterative solution of these equations together with the equation of state. The alternative method is to assume that a small portion of the star's mass lies outside the outer interface, so,

$$m_{ext} = 4\pi r_N^2 \frac{\chi_0}{K_0}$$

and,

$$p_{N-1} = \frac{\alpha}{3} T_0^4 + \frac{GM_N}{r_N^2} \frac{Dm_{N-1}}{2} \frac{1}{4\pi r_N^2} \quad [14]$$

where,

$$Dm_{N-1} = m_{ext} + \frac{Dm_{N-1}}{2}.$$

This method seems to be favoured by Castor and by Stellingwerf (1974), whilst the former is used by Fox and Wood (1982). The quantities $Dm1_{N-1}$ and m_{ext} can be related by assuming an infinite sequence of zones of masses decreasing by a constant factor, α , outwards, i.e.,

$$\frac{Dm1_{I-1}}{Dm1_I} = \alpha > 1.$$

So,

$$m_{ext} = Dm1_{N-1} / (\alpha - 1)$$

and,

$$Dm2_N = \frac{1}{2} \left(\frac{\alpha + 1}{\alpha - 1} \right) Dm1_{N-1}. \quad [15]$$

It is not clear which of these two approaches should be preferred, especially in the case of an extended atmosphere. The first method would seem to give too sharp a boundary, whereas, although the latter method gives a smooth diminishing of the density, this part of the star is ignored in the pulsation calculations. The former method is the one chosen for most of the calculations in this work since it is far simpler to apply.

Assuming a value for the radius at the outermost interface, $r_N = R$, we now have all the variables defined for the outer interface and zone. The calculation from the $(I-1)^{th}$ interface and zone quantities from the I^{th} zone and interface quantities is easily carried out. First we find p_{I-1} , for some chosen zone mass $Dm1_{I-1}$, so,

$$p_{I-1} = p_I + \frac{G M_I}{r_I^2} \frac{Dm2_I}{4\pi r_I^2}. \quad [16]$$

The radiation equation is now solved iteratively together with the equation of state to give T_{I-1} and ρ_{I-1} . The equation is assumed to be solved correctly if,

$$\left| 1 + \frac{4\sigma}{3} \frac{(4\pi R_I^2)^2}{L} \frac{T_I^4 - T_{I-1}^4}{\frac{1}{2}(K_{I-1} \Delta m_{I-1} + K_I \Delta m_I)} \right| < \epsilon_R \quad [17]$$

and if the n^{th} iterate for the temperature, $T_{I-1}^{(n)}$ satisfies ;

$$\left| \frac{T_{I-1}^{(n)} - T_{I-1}^{(n-1)}}{T_{I-1}^{(n-1)}} \right| + \left| \frac{\rho_{I-1}^{(n)} - \rho_{I-1}^{(n-1)}}{\rho_{I-1}^{(n-1)}} \right| < \delta \quad [18]$$

I find that a reasonable choice for the tolerances is: $\epsilon_R, \delta = 1.10^{-5}$.

It can easily be seen that the first condition is very much more restrictive than the second in regions where,

$$\frac{T_I - T_{I-1}}{T_I} \ll 1.$$

In this situation the first condition can be allowed to fail in one or two zones although we find that a value of $5 \cdot 10^{-4}$ for ϵ_R will always give convergence.

The particular method used for the iteration is not very important. For the radiative models a Newton-Raphson method generally gives convergence in 3 - 4 steps. In order to guarantee convergence from the trial values we restrict the corrections. If,

$$\Delta T_{I-1}^{(n)} \equiv T_{I-1}^{(n)} - T_{I-1}^{(n-1)}$$

is the correction given by the Newton-Raphson method we apply a correction $\Delta T_{I-1}^{(n)'}$ calculated so that,

$$\Delta T_{I-1}^{(n)'} = \Delta T_{I-1}^{(n)} \cdot \min \left(1, \frac{0.2}{|\Delta T_{I-1}^{(n)} / T_{I-1}^{(n-1)}|} \frac{0.5}{|\rho_{I-1}^{(n-1)}|} \right),$$

where,

$$f_{I-1}^{(n-1)} = 1 + \frac{40}{3} \frac{(4\pi r_I^2)^2}{L} \frac{T_I^4 - T_{I-1}^4}{\frac{1}{2}(K_{I-1} Dm_{I-1} + K_I Dm_I)},$$

Once the values of T_{I-1} and ρ_{I-1} have been determined then we calculate r_{I-1} using,

$$r_{I-1}^3 = r_I^3 - \frac{3}{4\pi} \frac{Dm_{I-1}}{\rho_{I-1}} \quad [19]$$

and, of course, $m_{I-1} = m_I - Dm_{I-1}$. The other auxiliary quantities may then be calculated.

Trial values for starting the iteration for a zone and also the value of the zone mass are determined by using Euler's method to integrate the differential equations forward from I to I-1. The variables used for this are the logarithms of m, r, p, T, and ρ and the independent variable is $\log(p)$. The quantity Dm_{I-1}/m_I can become very small and so when this happens Dm_{I-1} is calculated using a Taylor series for $\exp(\log(m_{I-1}/m_I))$ so

$$\frac{Dm_{I-1}}{m_I} = - \sum_{j=1}^n \frac{(\log(m_{I-1}/m_I))^j}{j!}$$

where $n=3$ suffices for $\log(m_{I-1}/m_I) \lesssim 10^{-4}$. The zoning for this integration is determined using the restrictions;

$$\left| \frac{\delta m}{m} \right|, \left| \frac{\delta T}{T} \right|, \frac{5}{2} \left| \frac{\delta p}{p} \right|, \left| \frac{\delta r}{r} \right|, \frac{1}{3} \left| \frac{\delta K}{K} \right| < 2. \omega^{-2}$$

and,

$$\left| \frac{\delta T}{T} \right| > 3. \omega^{-3}$$

where δx denotes the increment or decrement in any variable. The

integration and relaxation of the envelope is stopped when one of the following conditions is satisfied;

$$\frac{M_I}{M} < 0.9$$

or $\frac{\Gamma_I}{R_{ph}} < 0.02$ and $\frac{M_I}{M} < 0.95$
 or $P_I > 10^{14}$

and

$$T_i > 2 \cdot 10^6 \text{ K.}$$

For a giant star these conditions will give a model of about 300 zones.

It is found that although the independent variable for the integration is $\log(p)$, the restrictions on T and on ρ dominate towards the surface of the star and particularly in the ionisation zone. The lower limit on ΔT is only significant in the very outermost zones where $\tau < 0.1$. Bednarek (1975) found that the pulsation eigenvalues diverge if the atmosphere zoning becomes too tight. Since this was probably caused by cancellation in the calculation of $T_r - T_{r-1}$, the lower limit on ΔT should avoid this problem. Certainly no such effect was found in these calculations.

If we wish to reduce the number of zones in the difference representation of the envelope then we simply integrate forwards for a number of steps so increasing the zone mass.

In order to complete the set of initial values we must find some way of specifying the outer radius of the star, r_N . This is done using an iterative process. We know the photospheric radius R_{ph} defined such that,

$$L = 4\pi R_{ph}^2 \sigma T_{eff}^4 \quad [20]$$

Taking an estimated value of r_N we calculate the stellar structure zone by zone until we find $T_{\gamma} > T_{eff}$. The photospheric radius is then interpolated and the value for r_N is corrected if,

$$\left| \frac{R_{ph}^{(n)} - R_{ph}^{(n-1)}}{R_{ph}^{(n-1)}} \right| > \epsilon_{ph}$$

where $\epsilon_{ph} = 10^{-5}$ and $R_{ph}^{(n)}$ is the n^{th} iterated approximation to R_{ph} . For the first correction to r_N we use,

$$r_N^{(2)} = r_N^{(1)} + \alpha (R_{ph}^{(1)} - R_{ph}^{(2)})$$

where $\alpha = 2$ is reasonable. Thereafter we use,

$$r_N^{(n+1)} = \frac{r_N^{(n)}(R_{ph}^{(n-1)} - R_{ph}^{(n)}) - r_N^{(n-1)}(R_{ph}^{(n)} - R_{ph}^{(n-1)})}{R_{ph}^{(n)} - R_{ph}^{(n-1)}}$$

The initial estimate for r_N is not particularly important and, $r_N = R_{ph}$, gives quite rapid convergence. Some improvement can be gained by using a simple model of the atmosphere. Assuming the atmosphere to be isothermal, that $(r_N - R_{ph})/R_{ph}$ is sufficiently small that g is constant, and that we can approximate the opacity by a power law,

$$K = K_0 (\rho / \rho_0)^\beta$$

where $\beta \approx 1$, we find,

$$r_N = R_{ph} + \frac{1}{\beta+1} \frac{\rho_0}{\rho_0 g_0} \log \left(1 + \frac{2}{3} \frac{\beta+1}{\rho_0} \frac{g_0}{K_0} \right) \quad [21]$$

Using ρ_0, g_0, K_0 , as calculated at the surface and $\beta = (\partial \log K / \partial \log \rho)_T$ gives a reasonable estimate of $r_N - R_{ph}$, which is always a little smaller than that given by the iteration.

2.3 THE LINEAR NON-ADIABATIC PULSATION CALCULATION

As stated in the introduction to this chapter the method adopted for the linear non-adiabatic pulsation calculation is that evolved by Castor (1971). This method is also reported in Cox (1980). In all that follows little deviation from the path adopted by Castor will occur.

Recall the equations for time dependent stellar structure,

$$\begin{aligned} \frac{d^2 r_I}{dt^2} &= - \frac{GM_I}{r_I^2} - 4\pi r_I^2 \frac{\rho_I - \rho_{I-1}}{\Delta m_{2I}}, \\ T_I \frac{ds_I}{dt} &= \frac{L_I - L_{I-1}}{\Delta m_{1I}}, \\ \frac{1}{\rho_I} &= \frac{4\pi}{3} \frac{r_{I+1}^3 - r_I^3}{\Delta m_{1I}}, \end{aligned}$$

and,

$$L_I = 2 \cdot \frac{4\sigma}{3} (4\pi r_I^2)^2 \frac{T_{I-1}^4 - T_I^4}{(K_{I-1} \Delta m_{1I-1} + K_I \Delta m_{1I})}.$$

We now perturb these equations keeping only terms linear in the perturbations, and assume that the time dependence for all perturbed quantities is $e^{i\omega t}$ where ω is complex. This gives us,

$$-\omega^2 \delta r_I = 4 \frac{G M_I}{r_I^3} \delta r_I - \frac{4\pi r_I^2}{Dm I} (\delta p_I - \delta p_{I-1}) \quad [22]$$

$$i\omega T_I \delta S_I = \frac{\delta L_I - \delta L_{I-1}}{Dm I} \quad [23]$$

$$\frac{\delta p_I}{\rho_I} = -4\pi \frac{r_{I+1}^2 \delta r_{I+1} - r_I^2 \delta r_I}{Dm I} \quad [24]$$

and,
$$\frac{\delta L_I}{L_I} = 4 \frac{\delta r_I}{r_I} + \left(4 \frac{T_{I-1}^4}{T_{I-1}^4 - T_I^4} - \frac{\kappa_{I-1} Dm_{I-1} \kappa_{I-1}}{\kappa_{I-1} Dm_{I-1} + \kappa_I Dm_I} \right) \frac{\delta T_{I-1}}{T_{I-1}} \quad [25]$$

$$+ \left(4 \frac{T_I^4}{T_I^4 - T_{I-1}^4} - \frac{\kappa_I Dm_I \kappa_I}{\kappa_I Dm_I + \kappa_{I-1} Dm_{I-1}} \right) \frac{\delta T_I}{T_I} - \frac{\kappa_I Dm_I \kappa_{I-1}}{\kappa_I Dm_I + \kappa_{I-1} Dm_{I-1}} \frac{\delta p_{I-1}}{\rho_{I-1}} - \frac{\kappa_I Dm_I \kappa_I}{\kappa_I Dm_I + \kappa_{I-1} Dm_{I-1}} \frac{\delta p_I}{\rho_I}.$$

The equations are completed with a linearised equation of state,

$$\frac{\delta Q_I}{Q_I} = \left[\left(\frac{\partial \log Q}{\partial \log T} \right)_{\rho_I} \right] \frac{\delta S_I}{C_{vI}} + \left[\left(\frac{\partial \log Q}{\partial \log \rho} \right)_S \right] \frac{\delta p_I}{\rho_I} \quad [26]$$

where Q is either p or T. The perturbations, $(\delta p/\rho)_I$, $(\delta T/T)_I$, $(\delta p/\rho)_I$, and $(\delta L/L)$ are now eliminated in equations [22,23] using equations [24,25,26]. This leaves us with one equation for each interface and one for each zone which we write in terms of,

$$X_I = \sqrt{Dm I} \delta r_I$$

and,

$$Y_I = T_I \delta S_I.$$

These variables are chosen so that in the adiabatic limit, i.e. $Y_I \rightarrow 0$ for $I = 1, N-1$, we have,

$$\sum_{I=1}^N (X_j)_I^* (X_k)_I = \delta_{jk} \sqrt{\sum_{I=1}^N |X_j|^2} \sqrt{\sum_{I=1}^N |X_k|^2}, \quad [27]$$

since we know that,

$$\int \left(\frac{\delta r}{r} \right)_j^* \left(\frac{\delta r}{r} \right)_k r^2 dm = \delta_{jk} \sqrt{\int \left(\frac{\delta r}{r} \right)_j^2 r^2 dm} \sqrt{\int \left(\frac{\delta r}{r} \right)_k^2 r^2 dm},$$

where the indices label the eigenmodes. The variable Y_I is chosen rather than, for example, $(\delta T/T)_I$ since this avoids the possibility of loss of significance in forming the left hand side of equation [23] in the deep, approximately adiabatic parts of the envelope.

Following Castor we write,

$$\left(\frac{\delta L}{L}\right)_I = BL_{11I} X_{I-1} + BL_{21I} Y_{I-1} + BL_{12I} X_I + BL_{22I} Y_I + BL_{13I} X_{I+1} \quad [28]$$

and also,

$$\left(\frac{\delta \rho}{\rho}\right)_I = DR_{1I} X_I + DR_{2I} X_{I+1}$$

defining the quantities DR_1 , DR_2 , and BL_{11} etc.. The equations for linear, non-adiabatic pulsation can now be written as,

$$\omega^2 X_I = G_{11I} X_{I-1} + G_{12I} X_I + G_{13I} X_{I+1} + G_{21I} Y_{I-1} + G_{22I} Y_I \quad [29]$$

and,

$$i\omega Y_I = k_{11I} X_{I-1} + k_{12I} X_I + k_{13I} X_{I+1} + k_{14I} X_{I+2} + k_{21I} Y_{I-1} + k_{22I} Y_I + k_{23I} Y_{I+1} \quad [30]$$

where,

$$k_{11I} = + \frac{L}{\Omega_{mlI}} BL_{11I}$$

$$k_{12I} = \frac{L}{\Omega_{mlI}} (BL_{12I} - BL_{11I+1}) \text{ etc.}$$

defining the symbols G_{11} etc. and K_{11} etc.. At the surface and the base of the envelope these equations are replaced with the relevant

boundary conditions which are,

$$X_1 = 0$$

[31]

and,

$$\delta L_1 = 0$$

for the envelope base, together with,

$$\left(\frac{\delta L}{L}\right)_N = 2 \left(\frac{\delta r}{r}\right)_N + \left(\frac{\delta J}{J}\right)_N \quad [32]$$

and some expression relating $(\delta p/p)_N$ and X_N at the surface. Here J is the average radiation intensity and equation [32] simply expresses the assumption that no radiation passes into the star from outside. In the diffusion approximation,

$$J = \frac{\sigma}{\pi} T^4.$$

For the last equation Castor (1971) uses,

$$\left(\frac{\delta p}{p}\right)_N = - \left(\frac{\omega^2 r_N^3}{G M_N} + 4 \right) \left(\frac{\delta r}{r}\right)_N, \quad [33]$$

that is, the condition for the perfect reflection of momentum at the star's surface. This is not a particularly good expression to use when either radiation pressure is important or when an extended atmosphere is present in which case momentum can escape through the surface carried by running waves. The momentum boundary condition will be considered in a later section.

We can write the two pulsation equations in a very convenient form by dropping X_1 from our list of variables and forming two vectors \underline{X} and \underline{Y} , each of $N-1$ elements. (From here on a symbol with a single underline will denote a vector, a symbol with a double underline a matrix and a $+$ represents the Hermitian transpose operation.) This gives us,

$$\omega^2 \underline{X} = \underline{G_1} \underline{X} + \underline{G_2} \underline{Y} \quad [34]$$

and,

$$i\omega \underline{Y} = \underline{K_1} \underline{X} + \underline{K_2} \underline{Y} \quad [35]$$

where the definition of the $(N-1) \times (N-1)$ square matrices $\underline{G_1}$ etc. is obvious. It is easy to show that,

$$G_{I+1} = G_I B_{I-1}$$

and so we see that the tridiagonal matrix $\underline{G_1}$ is symmetric. In the adiabatic approximation, where $\underline{Y} = 0$, we have,

$$\omega_{ad}^2 \underline{X}_{ad} = \underline{G_1} \underline{X}_{ad} \quad [36]$$

and so ω_{ad} is real. Since we expect that for most stars nonadiabatic effects will be small then ω_{ad} and \underline{X}_{ad} should be good approximations to the nonadiabatic eigenfrequency and vector for each particular eigenmode. The adiabatic problem is easily solved as we can call on Sturm's Theorem to locate the zeroes of the characteristic polynomial. A sequence of $m+1$ polynomials $\{f_k(x)\}$ is a Sturm sequence on the interval $[a,b]$ if;

i. $f_m(x)$ does not vanish on $[a,b]$,

ii. no two consecutive polynomials are zero,

and, iii. whenever $f_k(x) = 0$ then, $f_{k-1}(x) \cdot f_{k+1}(x) < 0$.

Sturm's theorem states that for a given value of x if we count the number of changes of sign as k varies from 0 to m then this is equal to the number of zeroes on the interval $[a,x)$. This allows us to count the number of zeroes on any interval and thus estimate the location of a root of the equations. In particular the presence of any sign changes in $\{f_k(0)\}$ would indicate dynamical instability. Using this to give a good enough estimate for the eigenfrequency we can then use the Newton-Raphson formula, or any other convenient iteration method to determine the exact value. Fortunately a subroutine using this algorithm for determining eigenvalues of real Hermitian matrices, and subsequently the corresponding eigenvectors, is available in the NAG library and this saved a good deal of tedious programming.

Given the adiabatic eigenfrequency ω_{ad} and the eigenvector \underline{X}_{ad} for a mode we can improve our estimate of the period, $P = 2\pi/\text{Re}(\omega)$ and estimate the growth rate, using the quasi-adiabatic approximation. Cox (1980) states that,

$$\left| \frac{(G_2 Y)_I}{(G_1 X)_I} \right| \sim \left| \frac{(k_2 Y)_I}{(k_1 X)_I} \right| \sim \left| \frac{(TSS)/(C_v T)}{\delta \rho / \rho} \right|.$$

Throughout most of the star this quantity is very small and so we can write,

$$i\omega_{ad} \underline{Y}_{q.a.} = \underline{K1} \underline{X}_{ad} \quad [37]$$

where $\underline{Y}_{q.a.}$ is the quasi-adiabatic approximation to \underline{Y} . This gives,

$$\omega_{q.a.}^2 \underline{X}_{ad} = \underline{G11} \underline{X}_{ad} + \frac{1}{i\omega_{ad}} \underline{G2} \underline{K1} \underline{X}_{ad}$$

i.e.,

$$\omega_{q.a.}^2 = \omega_{ad}^2 + \frac{\underline{X}_{ad}^+ \underline{G2} \underline{K1} \underline{X}_{ad}}{\underline{X}_{ad}^+ \underline{X}_{ad}} \quad [38]$$

However in the outer layers of the star the terms in \underline{Y} are of the same order of magnitude as those in \underline{X} and so a better approximation is gained using,

$$(i\omega_{ad} - \underline{K2}) \underline{Y}' = \underline{K1} \underline{X}_{ad}$$

to give,

$$\omega'^2 = \omega_{ad}^2 + \frac{\underline{X}_{ad}^+ \underline{G2} (i\omega_{ad} - \underline{K2})^{-1} \underline{K1} \underline{X}_{ad}}{\underline{X}_{ad}^+ \underline{X}_{ad}} \quad [39]$$

This is the approximation used by Castor (1971) as a starting value for an iteration to find ω . For stars where the nonadiabaticity is small, i.e. $\text{Im}(\omega)/\text{Re}(\omega) \ll 1$, this is a very good approximation indeed and even for stars where this condition is not satisfied it generally gives the correct sign for $\text{Im}(\omega)$. The weakness in using this formula to calculate the initial estimate for ω is that we must invert the matrix $(i\omega - \underline{K2})$. Whilst we can do this using no more than $22 \times (N-1)$ elements of storage it is still a very slow procedure taking many times as long as the iteration for the accurate solution of the

eigenproblem. Unfortunately there exists to my knowledge no better method for obtaining this starting value.

In order to solve the full nonadiabatic eigenproblem we rewrite the matrix equations [34,35] as a single equation defining the vector \underline{Z} of $2N - 3$ elements such that,

$$Z_{2I-1} = Y_I \quad \text{for } I=1, N-1$$

and,

$$Z_{2I-2} = X_I \quad \text{for } I=2, N-1.$$

In a similar manner the elements of $(\underline{G}_1 - \underline{I})$, \underline{G}_2 , \underline{K}_1 and $(\underline{K}_2 - i\omega)$, with the exception of the surface momentum equation, are interleaved to form the square matrix \underline{A} and we define another vector \underline{R} so that we can write

$$\underline{A} \underline{Z} = \underline{R} . \quad [40]$$

Here,

$$R_J = 0 \quad \text{for } J=1, 2N-6,$$

$$R_{2N-5} = -K_1 X_N ,$$

$$R_{2N-4} = -G_1 X_N ,$$

and

$$R_{2N-3} = -K_1 X_N .$$

Since the system of equations is homogeneous we are allowed to specify

X_N . This is chosen so that, $\left(\frac{S^r}{r}\right)_N = 1 ,$

fixing the normalisation of the eigenvectors. Given an estimate of ω the system is now solved using a simple generalised Gaussian elimination and back substitution algorithm to give \underline{Z} . Simple numerical experiments show that this solution is accurate to about 11 figures and since this is very close to the precision of the computer used nothing more sophisticated has been tried. This solution for \underline{Z} is now inserted into the equation for the momentum boundary condition,

$$G_{11N} X_{N-1} + G_{21N} Y_{N-1} + G_{13N} X_N = 0.$$

However since ω is only an estimate the right hand side will not be zero but a function of ω , i.e., $F(\omega)$. Our task is to solve for,

$$F(\omega) = 0.$$

This is performed by using the secant method to generate the next corrected estimate for ω . In practice it is a good idea to solve for,

$$\frac{F(\omega)}{X_2} = 0.$$

since this function contains fewer poles than does $F(\omega)$. In particular a whole set of poles lying close to each of the eigenfrequencies is removed. The reason for this is that both are rational functions of ω containing many poles at the same points on the complex plane and we effectively cancel out these poles in forming $F(\omega)/X_2$. The arguments behind this are given in Ralston (1965) but are not relevant to this discussion. The removal of the poles greatly improves convergence.

Since for a great many of the stars studied here the adiabatic eigenfrequency was a poor estimate of $\text{Re}(\omega)$ it was necessary to limit each correction to ω in order to prevent convergence to the wrong solution. This was done by finding the smallest interval between the first few adiabatic frequencies and choosing 1/5 of this value as the upper limit on each correction to $\text{Re}(\omega)$. Occasionally the initial estimate for ω is too close to the eigenfrequency for a previously calculated mode and so the solution converges to this rather than the required solution. This can be almost entirely negated by dividing the discriminant F by a factor $(\omega'_I - \omega_J)$ where ω'_I is the estimate to ω_I . In practise since we know that when ω_J is a pulsation eigenvalue $-\omega_J^*$ is also a pulsation eigenvalue we divide through by

$$(1 - \omega'_I/\omega_I)(1 + \omega'_I/\omega_J^*)$$

for the iteration for the I^{th} eigenvalue. If this fails then the value of the real part of the estimated ω'_I is increased slightly above its original value and the iteration restarted. The equations are considered to be solved when

$$\left| \frac{\omega^{(n)}}{\omega^{(n-1)}} - 1 \right| < 10^{-10}$$

which since the order of the method is ≈ 1.7 gives a fractional error 10^{-17} on ω .

Some experiments were made to try to develop an alternative method for performing this iteration. This involves modifying the pulsation equations so that they read,

$$\omega^2 X = G_1 X + G_2 Y$$

$$i\omega Y = \gamma (K_1 X + K_2 Y).$$

Clearly $\gamma = 1$ corresponds to the full nonadiabatic problem and $\gamma = 0$ to the adiabatic approximation. The method tried was to set $\gamma \ll 1$ and iterate until $|\omega^{(n)}/\omega^{(n-1)} - 1|$ was small and then to repeat this using $\gamma^{(n+1)} = \sqrt{\gamma^{(n)}}$ until $\gamma^{(n)} = 1$, whereupon we have the nonadiabatic solution. Unfortunately the transition from the adiabatic to the non-adiabatic solution turns out to be discontinuous for many of the stars of interest for which the nonadiabaticity is large. Occasionally the possibility arises that a mode might have been missed in the series of solutions. This can be checked by plotting the eigenfunctions and counting the nodes or, better, the number of times the phase of the eigenfunction flips through π^c .

2.3.1 The Work Integral For Linear Pulsation

The stability coefficient for the pulsation, η , defined as the logarithm of the factor by which the pulsation energy increases in a period, must now be calculated. In one period the pulsation energy increases by a factor of,

$$\left| e^{i\omega P} \right|^2 = \left| e^{-\text{Im}(\omega)P} \right|^2$$

so,

$$\begin{aligned} \eta &= -2 \operatorname{Im}(\omega) P \\ &= -4\pi \operatorname{Im}(\omega) / \operatorname{Re}(\omega). \end{aligned} \quad [41]$$

We can also find the rate of increase of the pulsation energy directly from the equations of motion. Rather than use the equations in the radial approximation it is more instructive to use the general Euler equation for fluid motion,

$$\frac{d\underline{v}}{dt} = -\frac{1}{\rho} \underline{\nabla} p - \underline{\nabla} \bar{\Phi}_g, \quad [42]$$

where we have ignored the viscous terms, and where $\bar{\Phi}_g$ is the gravitational potential. By performing a scalar multiplication of this equation by \underline{v} we obtain an equation for the conservation of mechanical energy,

$$\frac{d(\frac{1}{2}v^2)}{dt} = -\frac{1}{\rho} \underline{v} \cdot \underline{\nabla} p - \underline{v} \cdot \underline{\nabla} \bar{\Phi}_g, \quad [43]$$

as given by Ledoux and Walraven (1958). Integration over mass gives us the mechanical energy conservation for the whole star,

$$\frac{d}{dt} \int \frac{1}{2} v^2 dm = - \int \underline{v} \cdot \underline{\nabla} p dV - \int \underline{v} \cdot \underline{\nabla} \bar{\Phi}_g dm, \quad [44]$$

where the volume element $dV = dm/\rho$. Now it can be shown, e.g. Unno et al. (1979), that,

$$\int \underline{v} \cdot \underline{\nabla} \bar{\Phi}_g dm = \frac{1}{2} \int \frac{d\bar{\Phi}_g}{dt} dm. \quad [45]$$

Also,

$$\underline{\nabla} \cdot (\underline{v} p) = \underline{v} \cdot \underline{\nabla} p + p \underline{\nabla} \cdot \underline{v}$$

and the continuity equation can be written as,

$$\frac{d(\underline{v} p)}{dt} = \frac{1}{\rho} \underline{\nabla} \cdot \underline{v}$$

so,

$$\frac{d}{dt} \int \frac{1}{2} v^2 dm = \int \nabla \cdot (v p) dV + \int p \frac{d(\rho/\rho_0)}{dt} dm \quad [46]$$

$$+ \frac{1}{2} \frac{d}{dt} \int \frac{1}{2} \Phi_G dm.$$

Applying the divergence theorem we obtain the equation for the rate of change of mechanical energy,

$$\frac{d}{dt} \int \left(\frac{1}{2} v^2 + \frac{1}{2} \Phi_G \right) dm = \int p \frac{d(\rho/\rho_0)}{dt} dm - \int p v \cdot d\underline{S}. \quad [47]$$

The first term on the right is simply the work done on each mass element by the pressure forces. The surface integral represents the work done by the stellar envelope on the stars core and on the matter outside the star. We define the pulsation energy $E = \frac{1}{2} (v^2 + \Phi_G)$.

The equation [47] must be integrated over a period to give the change in the pulsation energy over a period. First, though, we return to the restricted case of radial pulsation, for which,

$$v \cdot d\underline{S} = \left(\frac{dr}{dt} \right)_R 4\pi R^2 \quad [48]$$

where R is the radius at the stars surface. The velocity at the envelope base is assumed to be zero. In the linear approximation,

$$p = p_0 \left(1 + \left| \frac{\delta p}{p} \right| \cos(\omega_R t + \phi_p) + O\left(\left(\frac{\delta p}{p}\right)^2\right) \right)$$

$$\frac{d(\rho/\rho_0)}{dt} = \frac{1}{\rho} \left(\left| \frac{\delta \rho}{\rho} \right| \omega_R \sin(\omega_R t + \phi_\rho) - O\left(\left(\frac{\delta \rho}{\rho}\right)^2\right) \right)$$

and,

$$v = -\omega_R |\delta v| \sin(\omega_R t + \phi_r)$$

where,

$$\omega_R \equiv \text{Re}(\omega).$$

The only terms which will survive the integration over time are the crossterms, e.g.,

$$\int \cos(\omega r t + \phi_p) \cdot \sin(\omega r t + \phi_r) dt = \frac{1}{2} P \sin(\phi_r - \phi_p).$$

So, the change in pulsation energy over a period,

$$\begin{aligned} \Delta E_p &= \pi \int \frac{P}{\rho} \operatorname{Im} \left(\left(\frac{\delta P}{\rho} \right)^* \left(\frac{\delta \rho}{\rho} \right) \right) dm \\ &\quad + 4\pi^2 p R R^3 \operatorname{Im} \left(\left(\frac{\delta P}{\rho} \right)_R^* \left(\frac{\delta R}{R} \right) \right) \end{aligned} \quad [49]$$

where the subscript, R, indicates a value at the stars surface. It is easy to show that the total pulsation energy, E_p , is given by,

$$E_p = \frac{1}{2} \omega R^2 \int_0^M \left| \frac{\delta r}{r} \right|^2 r^2 dm. \quad [50]$$

Observing that,

$$\eta = \left\langle \frac{d \log E_p}{dt} \right\rangle p = \frac{\Delta E_p}{E_p},$$

where $\langle \dots \rangle$ indicates averaging over a period, we now have an alternative expression for η which can be used to determine the contribution of each zone, or mass element, to driving the pulsation.

The method used above to obtain the work integrals may be applied directly to the discrete linear pulsation equations [29] and [30] as follows. For the velocities at each point we have the vector $i\omega \underline{X}$, and so by premultiplying the momentum equation by $i\omega \underline{X}^\dagger$ we get,

$$i\omega^3 |\underline{X}|^2 = i\omega \underline{X}^\dagger \underline{G}_1 \underline{X} + \underline{X}^\dagger \underline{G}_2 (i\omega \underline{X}) \quad [51]$$

This can be written as,

$$i\omega (\omega^2 \underline{J} - \underline{\Sigma}^2 \underline{J}) = \underline{C},$$

where,

$$\underline{J} \equiv \int |\delta r|^2 dm$$

the oscillatory moment of inertia, and,

$$\Sigma^2 J \equiv \int \left(4 \left| \frac{\delta r}{r} \right|^2 \frac{G \mu r}{r} - \Gamma_3 \left| \frac{\delta \rho}{\rho} \right|^2 \right) d\mu,$$

and,

$$C \equiv \int (\Gamma_3 - 1) \left(\frac{\delta \rho}{\rho} \right)_{\text{space}}^* (i\omega T \delta S)_{\text{space}} d\mu,$$

as in, for example, Cox (1980). It is clear that $|X|^2 = \int |\delta r|^2 d\mu$ and some simple, though boring, manipulations show that, for example,

$$\left(X^+ G_2 \right)_{\text{I}}^+ = (\Gamma_3 - 1)_{\text{I}} \text{Dm} 2_{\text{I}} \left(\frac{\delta \rho}{\rho} \right)_{\text{I space}},$$

and so, finally, the required identities are obtained. This last form of the mechanical energy integral can be used to test the consistency of the solutions and the real part of C gives the work integral.

2.4 THE EDDINGTON APPROXIMATION FOR RADIATIVE TRANSPORT

For the diffusion approximation for radiative transport to hold the assumption that the gas is optically thick must be true. This is clearly untrue in the stellar atmosphere and so we consider an alternative treatment, the Eddington Approximation given by Unno and Spiegel (1966).

The radiation equation may be written

$$\underline{\mu} \cdot \nabla I = -(\kappa + \sigma) \rho I + \kappa \rho B + \sigma \rho J \quad [5.2]$$

where $\underline{\mu}$, I, B, J, σ represent the direction cosine vector, the specific intensity and the scattering coefficient respectively.

Eddington's method consists of taking moments of this equation and solving the resulting set of equations under the assumption,

$$I(\alpha, \theta, \phi; t) = \sum_{i=0}^n \sum_{j=i}^i I_i^j(\alpha, t) S_i^j(\theta, \phi),$$

where $S_i^j(\theta, \phi)$ are spherical harmonics. We choose $n = 0$. The first two moment equations are,

$$\nabla \cdot \underline{E} = -4\pi \kappa \rho (J - B)$$

with

$$\underline{E} \equiv \int \mu I d\Omega,$$

the integral being over all angles, and,

$$\nabla \cdot \underline{K} = -(\kappa + \sigma) \rho \underline{E}$$

where

$$\underline{K} = \frac{1}{4\pi} \int \mu \mu I d\Omega.$$

It is simple to show that under the approximation adopted,

$$\underline{K} = \frac{1}{3} J \underline{I} \quad (\underline{I} \equiv \text{identity tensor})$$

and also

$$\underline{E} = -\frac{4\pi}{3(\kappa + \sigma)\rho} \nabla J.$$

We will drop σ in the following. For radiative equilibrium we have $\nabla \cdot \underline{E} = 0$ and so $J = B$. In other words,

$$\underline{E} = -\frac{4\pi}{3\kappa\rho} \nabla B,$$

which is just the diffusion approximation. In the general case we can

write,

$$J = B - \frac{1}{4\pi\kappa\rho} \nabla \cdot E,$$

so

$$E = -\frac{4\pi}{3} \frac{1}{\rho} \nabla \left(B - \frac{1}{4\pi\kappa\rho} \nabla \cdot E \right).$$

Now when radiation is the only transport mechanism,

$$\rho T \frac{dS}{dt} = -\nabla \cdot E$$

and so,

$$E = -\frac{4\pi}{3} \frac{1}{\kappa\rho} \nabla \left(B + \frac{T}{4\pi\kappa} \frac{dS}{dt} \right).$$

If we reduce this to the purely radial case and use $L = 4\pi r^2 F$ we get,

$$L = -\frac{4\pi}{3} \frac{(4\pi r^2)^2}{\kappa} \frac{\partial}{\partial m} \left(B + \frac{T}{4\pi\kappa} \frac{dS}{dt} \right). \quad [53]$$

Unno and Spiegel have shown how this treatment gives the correct behaviour in both the optically thick and thin limits. When radiative equilibrium holds then the new terms only affect the pulsating model, but when convective transport is taken into account $\nabla \cdot E_{\text{rad}} \neq 0$ and so the static envelope could well be affected. This last point is invariably omitted from practical calculations of stellar envelopes. This new equation for L can easily be implemented by adding a new term $(\delta L/L)'_I$ to $(\delta L/L)_I$, i.e.

$$\left(\frac{\delta L}{L} \right)'_I = -\frac{i\omega}{\alpha c} \frac{Y_{I-1}/K_{I-1} - Y_I/K_I}{T_{I-1}^4 - T_I^4}.$$

The relevant equation at the surface is obtained, as before, using the assumption that no radiation enters the star from outside, so,

$$(\delta L/L)_N = 2(\delta v/v)_N + (\delta J/J)_N$$

$$\begin{aligned} \text{with} \quad \delta J_N &= \delta B_N + \left(\frac{T}{4\pi\kappa} i\omega \delta S \right)_N \\ \text{so} \quad \left(\frac{\delta L}{L} \right)_N &= 2 \left(\frac{\delta v}{v} \right)_N + \left(\frac{\delta B}{B} \right)_N + i\omega \frac{Y_N}{4\pi B_N \kappa_N} \end{aligned}$$

Here we must approximate, again evaluating the final term at $N-1$.

Whether or not the new term will affect the calculations depends upon the ratio of the radiative relaxation time, τ_R , and the pulsation period since this determines the ratio of the two terms on the right hand side of [53]. Using the second T.d.S equation of thermodynamics gives this ratio as

$$\frac{\tau_R}{P} = \frac{C_p T}{8\sigma T^3 \kappa} \cdot \frac{1}{P}.$$

When τ_R is small compared with the period then we can expect little difference. The most usual cause for this term to become important is a large value of $1/P$ as in the case of nonradial oscillations of high order. However for some of the more luminous stars with extended atmospheres it could well be possible that κ could become small enough that the same effect is achieved for a relatively long period. This turned out to be the case for some of the stars in this study. Another case which seems now to be more important is the occurrence of shock waves in nonlinear models.

The effect of the new term in the radiation equation is to introduce a phase lag between the temperature and luminosity perturbations which should tend to increase the amplitude of the temperature perturbation and provide a further ^{so} _^urce of damping. The

larger temperature perturbations should also increase the energy of the outer layers making mass loss through pulsation more likely. A very strong shock wave is associated with a rapid change in the temperature and in models computed using the diffusion approximation this energy is radiated away almost immediately. The introduction of a delay in this radiation would retain more energy in the atmosphere possibly leading to an enhanced driving of mass loss.

2.5 THE MOMENTUM EQUATION AT THE SURFACE

The difference equation for momentum conservation from which X is calculated requires knowledge of the pressure perturbation for a zone outside the star and which is thus undetermined. Christy (196) got around this problem in his nonlinear work by setting $p_N = -p_{N-1}$ giving a pressure at the surface $p_S = (p_N + p_{N+1}) = 0$. This is inelegant and is of dubious validity for, at least, stars in which radiation pressure might be important.

A simple boundary condition for the linear model may be obtained by assuming that the gas pressure, p_g , vanishes at the surface so $p = p_r$. This is the approach taken by Fox and Wood (1982). We have equation [13] for the static model and

$$\delta p_{N-1} - \delta p_{rS} = - \frac{W_{N-1}}{2} \frac{1}{4\pi r_N} \left(4 \frac{G M_N}{v_N^3} + W^2 \right) \left(\frac{\delta r}{r} \right)_N \quad [54]$$

for the linear pulsations. If the radiation pressure at the surface, p_{rS} , is zero then

$$\left(\frac{\delta p}{p} \right)_{N-1} = - \left(4 + \frac{W^2 v_N^3}{G M_N} \right) \left(\frac{\delta r}{r} \right)_N \quad [55]$$

which is the boundary condition adopted by Castor (1971).

For the Castor boundary condition the momentum is reflected perfectly at the surface with no energy being lost to the exterior. When radiation pressure is included then some work is done, presumably on the radiation field. However since the expression for the radiation pressure is not strictly, if at all, valid in the optically thin regions because it assumes radiation and matter to be in equilibrium this should be regarded with scepticism. Moreover it is not necessarily true that $p_g = p_{r_g}$ is a good assumption, particularly for stars with extended atmospheres. When the pressure gradient is small and the pressure scale height of the order of the wavelength of the pulsational perturbations then the "surface" of the star is not well defined and energy can escape in the form of sound waves.

Linearising the momentum equation with the assumption that $g = Gm./r^2$ is roughly constant, along with the other static variables, over the range of radius in question gives,

$$\frac{\partial(\delta p/p)}{\partial x} = \frac{R}{H} \left(\left(\frac{\omega^2 r}{g} + 4 \right) \frac{\delta r}{r} + \frac{\delta p}{p} \right) \quad [56]$$

where $x = r/R$, and $H = g\rho/p$ is the pressure scale height. Clearly when $H/R \rightarrow 0$ we retrieve Castor's boundary condition. The condition for standing waves, that the perturbations should be evanescent outside the surface, can now be obtained as in Baker and Kippenhahn (1965), by assuming,

$$\frac{\delta p}{p} = \alpha \frac{\delta \rho}{\rho} ,$$

with $\alpha \approx 1$, ignoring the temperature perturbation which should be small.

Since,

$$\frac{\delta p}{\rho} = -3 \frac{\delta r}{r} - \frac{\partial}{\partial \log r} \left(\frac{\delta r}{r} \right),$$

we get, assuming $x \approx 1$,

$$\alpha \frac{\partial^2 z}{\partial x^2} + \left(4\alpha - \frac{R}{H} \right) \frac{\partial z}{\partial x} + \frac{R}{H} \left(\frac{\omega^2 R}{g} + 4 - 3\alpha \right) z = 0,$$

where $z = \delta r / r$. This gives a solution of the form $z \propto e^{kx}$ with,

$$k_{\pm} = \frac{R/\alpha H - 4 \pm \sqrt{(R/\alpha H - 4)^2 - 4R/\alpha H (\omega^2 R/g + 4 - 3\alpha)}}{2}.$$

When R/H is large,

$$\left(\frac{\alpha H}{R} \right) k_{\pm} = 1 - 2 \frac{\alpha H}{R} \left(\frac{\omega^2 R}{g} + 4 - 3\alpha \right), + 2 \frac{\alpha H}{R} \left(\frac{\omega^2 R}{g} + 4 - 3\alpha \right) \quad [57]$$

The first solution gives a kinetic energy per unit volume which becomes infinite but the second gives a bounded total kinetic energy.

Substituting $\partial/\partial x = k_-$ into equation [56] gives,

$$\frac{\delta p}{\rho} = - \frac{(\omega^2 R/g + 4) \delta r}{(1 - (H/R)k_-) r} \quad [58]$$

and for $H/R \rightarrow 0$ we again recover the Castor equation.

Consider now the case where H/R is sufficiently large for the term under the square root to be negative. This implies that there will be waves running out of the stars surface and so carrying away energy. The phase shift between $\delta p/\rho$ and $\delta r/r$ now means that the surface term in the work integral ceases to be negligible and so will tend to damp the pulsations. This surface contribution becomes,

$$-4 \pi^2 \rho R^3 \text{Im} \left(\frac{\omega^2 R/g + 4}{1 - (H/R)k_-} \right) \left| \frac{\delta r}{r} \right|^2.$$

This boundary condition assumes the existence of matter outside the surface of the star and so the static model for which it is applicable should be constructed with the boundary conditions given by equations [14,15]. We define p_s , the surface pressure as,

$$p_s = p_{r_0} + \frac{GM_N}{r_N^2} \frac{M_{ext}}{4\pi r_N^2},$$

and for the linear perturbation we have,

$$\delta p_s = \delta p_{r_0} - \frac{M_{ext}}{4\pi r_N^2} \left(4 \frac{GM_N}{r_N^3} + \omega^2 \right) \left(\frac{\delta r}{r} \right)_N,$$

so δp_{N-1} and δp_s are related by,

$$\delta p_{N-1} - \delta p_s = - \frac{Dm_{N-1} - M_{ext}}{4\pi r_N^2} \left(4 \frac{GM_N}{r_N^3} + \omega^2 \right) \left(\frac{\delta r}{r} \right)_N. \quad [59]$$

For δp_s we use equation [58] and so we have an equation for δp_{N-1} in terms of $\delta r_N / r_N$, where $r_N = R$.

Although this boundary condition should give a better representation of the physics at the surface its use is still largely crippled by the lack of a simple model for the static structure of the outer atmosphere. For example since $H \sim T$ for a near perfect gas the presence of a hot corona would lead to an increase of the lowest pulsation period at which running waves set in. Also for cooler stars with extended atmospheres created by pulsation raising the energy of the outer layers of the star we should expect a large value of H and so the existence of running waves. How this is related to, or interacts with, pulsation driven mass loss I do not know and in any case it can only be studied as a nonlinear problem.

All of this assumes that the thermal and radiative time scales, τ_w and τ_r , are short compared with the dynamical time scale, τ_{dyn} . If this is not true then the temperature perturbation, $t \equiv \delta T/T$, should be included, that is

$$\frac{\delta p}{p} = \chi_T t + \chi_\rho \frac{\delta \rho}{\rho}.$$

The same analysis as before gives

$$\chi_T(1 - CK)t + (\chi_\rho CK^2 + \chi_\rho(3C-1)K + S - 3\chi_\rho)z = 0.$$

where the variables $C = H/R$, and $S = 4 + \omega^2 R/g$ have been introduced.

A further equation is required to relate t and z . We have,

$$i\omega T \delta S = -L \frac{\partial L}{\partial m} \equiv -\frac{L}{4\pi R^3 \rho} \frac{\partial L}{\partial x}$$

where $l = \delta L/L$. Also

$$l = 2z + 4t + \frac{i\omega}{4\pi\sigma T^4 K} T \delta S$$

from section 2.4. The second T.dS equation is

$$T \delta S = C_v T (t - (\Gamma_3 - 1) \delta \rho / \rho)$$

or

$$-\frac{L}{4\pi R^3 \rho} \frac{\partial L}{\partial x} = i\omega C_v T (t - (\Gamma_3 - 1)(3 + K)z).$$

if the exponential x-dependence is assumed as before. So

$$i\omega \frac{4\pi R^3 \rho C_v T}{L} (t + (\Gamma_3 - 1)(3 + K)z) = -KL$$

and

$$(1 + \frac{C_v T}{4\pi\sigma T^4 K} \frac{L}{4\pi R^3 \rho C_v T} K) l = 2z + 4t.$$

We observe,

$$\tau_w \equiv 4\pi R^3 \rho C_v T / L$$

and

$$\chi_{rad} \equiv \frac{C_V T}{4\pi\sigma T^4 R}$$

For simplicity I define, $D = \omega\tau_{th}$ and $E = \omega\tau_{rad}$. Eliminating l gives

$$(4k + i(\omega + Ek))\epsilon = -(2k + i(\omega + Ek)(\Gamma_3 - 1)(3 + k))\zeta.$$

Combining this equation with the momentum equation and then ^{disregarding} the trivial, $\zeta = 0$, solution gives _^

$$aX^3 + bX^2 + cX + d = 0,$$

where $X \equiv CK$ and

$$a \equiv 4\chi_\rho + i\gamma\chi_\rho E$$

$$b \equiv -\alpha - C[2\chi_T + 12\chi_\rho + i(2\chi_\rho(S + \gamma)E - \gamma\chi_\rho D)]$$

$$c \equiv C[-2\chi_T + 4(S - 3\chi_\rho) + i((S - 3\gamma\chi_\rho)E - \gamma\chi_\rho D)] \\ + C^2[i3\gamma\chi_\rho D]$$

$$d \equiv C^2[i(S + 3\gamma\chi_\rho)D],$$

(N.B. $\gamma = C_p/C_V = (\Gamma_3 - 1)\chi_T/\chi_\rho + 1$). This is very like the equation published recently by Saio, Wheeler and Cox (1984), and in fact it was the appearance of the relation in their paper which prompted me to include my own calculation in this section. If $D \rightarrow 0$ then this reverts to a quadratic equation for X and a trivial $X = 0$ solution. The new terms in E and D enter only in the already small terms, $O(C)$, as phase shifts. D is always very small near the surface of a star and so the quadratic solutions, X , are always a good approximation.

Since C.E is also small this too can probably be neglected in most cases. One point of interest is that there is always an imaginary value of K,

$$k_0 \approx iCD(S + 3\gamma\chi_\rho),$$

and so a wave solution. However the energy carried should always be very small.

CHAPTER 3
CONVECTION AND PULSATION

Some consideration must now be given to the role of convection in pulsating stars. Since the pulsations in giant stars are driven by the interaction of radiation with the stellar material we should expect that the appearance of another transport mechanism should be important. Further, turbulent convection involves motions with length scales small enough that viscous forces can become important and so a new source of dissipation is introduced which naively we should expect to damp the pulsations. Whilst convection is generally thought to carry little of the energy flow near the blue edge of the "Great Sequence" it is known to be a very important transport mechanism nearer to the red-edge and it is thought to be the means whereby the stars beyond the red-edge remain stable against pulsation.

3.1 MODELS FOR THE INTERACTION OF CONVECTION AND PULSATION

A great deal of work has been done over the past twenty years with the aim of producing a theory for the interaction of convection and pulsation.

The pioneering work of Baker and Kippenhahn (1965) on linear pulsation included convection calculated using the standard mixing length formalism of Bohm-Vitense (1958) in the static models. For the pulsation models they assumed $\delta L_c = 0$ implying that the time scale for convection is very much greater than that for the pulsations. They found that for Cepheid models this produced a phase lag between the luminosity and velocity perturbations of about 180° which is greatly at variance with the observed value of $\sim 90^\circ$. Little convective damping was to be found.

Iben (1971) uses the same approximate model of convection although he also experiments with methods for limiting the convective flux by considering the maximum amount of ionisation energy a fluid blob can transfer. He again finds the overly large phase lags.

In order to remove the arbitrary assumption regarding the way in which the convection adjusts itself to following the pulsations Unno (1967) developed a simple time dependent mixing length model of convection. Unno assumes, as in all mixing length theories, that;

i. the mixing length is much smaller than the characteristic scale length of pulsation perturbations.

ii. the convective velocities are subsonic, (Boussinesq's Approximation),

iii. the turbulent viscosity and thermal conductivity due to the smaller eddies are as given by Bohm-Vitense's theory.

Under assumption i. Unno uses a horizontal averaging procedure to separate the convective perturbations from the pulsational variations. In this way he obtains differential equations for the convective velocity, u , and temperature, θ , perturbations as follows,

$$\frac{d\underline{u}'}{dt} + (\underline{u}' \cdot \nabla) \underline{u}' - \langle (\underline{u}' \cdot \nabla) \underline{u}' \rangle = -\frac{1}{\langle \rho \rangle} \nabla p' + \frac{\rho'}{\langle \rho \rangle} \nabla \langle p \rangle - (\underline{u}' \cdot \nabla) \underline{u}, \quad [60]$$

and

$$C_p \langle \rho \rangle \left\{ \frac{d\theta}{dt} + (\underline{u}' \cdot \nabla) \theta - \langle (\underline{u}' \cdot \nabla) \theta \rangle + \underline{u}' \cdot \nabla \theta \left(1 - \frac{\langle \nabla_{ad} \rangle}{\langle \nabla \rangle} \right) \right\} = -\nabla \cdot E_r'. \quad [61]$$

Here all primed quantities represent convective perturbations, $\langle \dots \rangle$

represents the horizontal averaging, and $\nabla \equiv \frac{d \log T}{d \log p}$, "ad" \Rightarrow adiabatic

The crucial step comes in finding approximate expressions for

$$\nabla \cdot E'_r$$

and

$$(\underline{u}' \cdot \nabla) x - \langle (\underline{u}' \cdot \nabla) x \rangle \equiv \mathcal{L}(x)$$

where x represents Θ or any component of \underline{u}' . In the mixing length theories the space derivatives are approximated using

$$\left| \frac{\partial}{\partial x_i} \right| \rightarrow \frac{1}{(l/2)}$$

Employing the Eddington Approximation, since $\partial L_r / \partial m \neq 0$, Unno finds

$$\nabla \cdot E'_r \approx \frac{4ac \langle \kappa \rangle \langle \rho \rangle \langle T^3 \rangle}{\eta} \Theta$$

where

$$\eta \equiv 1 + \frac{3}{4} (\langle \kappa \rangle \langle \rho \rangle l)^2$$

In the optically thick limit this becomes,

$$\nabla \cdot E'_r \approx \frac{4ac}{3} \frac{\langle T^3 \rangle}{\langle \kappa \rangle \langle \rho \rangle} \frac{1}{(l/2)} \Theta$$

Unno uses approximation ii. for the $\mathcal{L}(x)$ terms, giving,

$$\mathcal{L}(x) = \frac{|u'|}{l/2} x$$

So Unno's simple theory gives,

$$\left(\frac{d}{dt} + \frac{u}{l/2} \right) u = - \frac{Q \Theta}{2 \langle \rho \rangle \langle T \rangle} \frac{\partial \langle \rho \rangle}{\partial r} \quad [62]$$

$$\left(\frac{d}{dt} + \frac{u}{l/2} \right) \Theta + \frac{4ac \langle \kappa \rangle \langle T^3 \rangle}{c_p \eta} \Theta = \frac{u}{l/2} \frac{1}{H} \langle T \rangle (\langle \nabla \rangle - \langle \nabla_{ad} \rangle) \quad [63]$$

where $U = |u'|$, $H \equiv |\partial r / \partial \log(p)|$. These equations are interpreted by Unno so that in the static case (no pulsation) the time derivatives are dropped and this gives the static structure of the star when used with the definition,

$$F_c = \langle \rho \rangle \langle C_p \rangle U \theta.$$

However this is not the only interpretation. Gough (1977) derives essentially the same equations as [62,63] using a more sophisticated model and interprets the equations as equations of motion for blobs of fluid with velocity U and a temperature differing from the ambient temperature by θ . He drops the $\mathcal{L}(x)$ terms and notes that for the static case the approximation,

$$\left| \frac{d}{dt} \right| = \frac{U}{l/2}$$

yields equations which have the same basic form as those of Bohm-Vitense. However Gough's main line of reasoning is that the nonlinear effects should be represented by the mixing length annihilation hypothesis which gives the probability of a fluid blob created at time t_0 surviving until the present time t (Spiegel (1963)). This is written as,

$$\Pi(x, t; t_0) = \exp\left(\int_{t_0}^t U(x'; t'; t_0) / l(x'; t') dt'\right)$$

where $x(t)$ is the radial Lagrangian coordinate for the fluid blob. Solving the equations of motion for the fluid blob using the initial

conditions,

$$u(t_0) = 0$$

$$\theta(t_0) = \Delta T$$

he obtains expressions for u and θ . By postulating a constant production of fluid blobs such that the mass of blobs produced per second is

$$\frac{A}{r} g \text{ sec}^{-1}$$

he is able to calculate the convective flux and turbulent pressure. This theory is completed by the assumption of a quadratic function for the distribution of ΔT , the initial temperature perturbation, and then the calculation of the averaged flux and turbulent pressure.

Application of the Unno and Gough theories by Gonczi and Osaki (1980), and by Baker and Gough (1979) respectively show that when the turbulent stresses are ignored in the pulsation calculation then no appreciable stabilisation due to convection is found. The reintroductionⁱ of the turbulent pressure into the Gough model does, however, give a red edge as does the introduction of turbulent viscosity by Gonczi (1981, 1982) into the Unno theory. However, both theories exhibit a disturbing feature. When $\langle \nabla \rangle \rightarrow \langle \nabla_{ad} \rangle$, it is found

that the pulsation perturbations of the convection variables exhibit wild spatial oscillations which occur on a length scale shorter than the mixing length. This phenomenon is explained by both Baker and Gough, and Gonczi and Osaki, and appears to be inconsistent with the intuitive interpretation of the convective mixing length hypothesis. These authors have shown that it is the phase-lag between the convective perturbations and the pulsation dynamics which is responsible for this effect. Keeley (1977) has gone further and has removed these oscillations by introducing an empirical diffusion term into his equation for the convective flux perturbation. That is,

$$\frac{d\delta F}{dt} = -\frac{\delta F - \delta F_0}{\tau_c}$$

becomes,

$$\frac{d\delta F}{dt} = -\frac{\delta F - \delta F_0}{\tau_c} + l'^2 \frac{d^2 \delta F}{dr^2}$$

where δF_0 is the "instantaneous" flux perturbation, $\tau_c = u/(1/2)$ the convective time scale and l' is an arbitrary length chosen so that $l' \gg \lambda$. This modification successfully eliminates spatial variations on a length scale less than l' . An alternative device for removing these oscillations has been used by Saio (1980). He introduces the ad hoc hypothesis that the effect of the unresolved small scale convective eddies is to introduce dissipation of the convective perturbations on a time scale $1/\text{Re}(\omega)$. That is, the turbulent stress terms, for example, usually represented as,

$$\delta(\underline{u}' \cdot \nabla \underline{u}') - \langle \underline{u}' \cdot \nabla \underline{u}' \rangle = \frac{1}{\tau_c} \delta \underline{u}' - \frac{\delta \tau_c}{\tau_c^2} \underline{u}'$$

become,

$$\approx \left(\frac{1}{\tau_c} + \text{Re}(\omega) \right) \delta u' - \frac{\delta \tau_c}{\tau_c^2} u'.$$

Saio shows, as do Gough and Baker, and Gonczi and Osaki, that the scale length, ζ , for the spatial oscillations in the unmodified theory is,

$$\frac{\zeta}{l} \sim \frac{1}{2} \frac{1}{\text{Re}(\omega) \tau_c}.$$

In the modified model we have,

$$\frac{\zeta}{l} \sim \frac{1}{2} \left(\frac{1}{\text{Re}(\omega) \tau_c} + 1 \right)$$

and so the high frequency oscillations are removed. This device has been used in some of the calculations of this study.

Both these ad hoc devices will remove the offending oscillations but it would be preferable to have some such feature implicit in the theory. Ulrich (1976) has derived a simple nonlocal mixing length theory of convection for static envelopes. His expression for the nonlocal flux, F_{NL} , is,

$$l^2 \frac{dF_{NL}}{dz^2} = F_{NL} - \alpha F_L$$

where α determines the strength of the nonlocal effects and it can be expected that $0.9 < \alpha < 1$, $l \approx 1$, and F_L is the usual mixing length theory convective flux. This suggests that there is some justification for the introduction of a diffusion term into the equations.

Baker and Gough (1979) show that the turbulent pressure is of crucial importance to understanding the interaction of convection and pulsation. However they were unable to include the turbulent pressure correctly in their static models. Stellingwerf (1976) has shown that any attempt to solve the stellar structure equations including turbulent pressure correctly as an initial value problem is bound to meet with an insurmountable numerical instability at the outer edge of the convective zone. The cause of this can be traced back to the replacement of the spatial derivatives of the convective perturbations with local algebraic expressions whilst attempting to keep the derivatives of the convective velocity in the equations for the mean variables. So again the inadequacies of the local theory and the need for a nonlocal theory of convection become abundantly clear.

A fresh attempt to supply the required nonlocal theory is to be found in the work of Stellingwerf (1982a,b,1983a,b). He derives equations of motion for the convective perturbations and mean properties of a radially pulsating stellar envelope, and casts these as an equation for the conservation of energy which includes all the contributions of convection. At this point he discards the equation of motion for the convective eddies and introduces a transport equation for the convective elements in its place. The acceleration of the elements is provided by a buoyancy term proportional to the temperature perturbation and a source term is supplied which creates elements with a small initial velocity and then destroys them after

they have travelled a mean free path, l'' . The system must be completed by a further expression relating the convective velocity and temperature perturbations and for this Stellingwerf resorts to the standard mixing length theory, having shown that, $l'' = \frac{1}{4}l$. So in this formulation the nonlocal behaviour enters solely through a partial differential equation for the convective velocity or, more precisely, the convective kinetic energy, $\omega = u'^2$,

$$\frac{d\omega}{dt} = \frac{1}{r^2} \frac{\partial}{\partial r} \left(r^2 l'' \omega^{1/2} \frac{\partial \omega}{\partial r} \right) + \frac{\omega^{1/2}}{l''} (\omega_0 - \omega) - 2 \frac{\omega}{r^2} \frac{\partial}{\partial r} (r^2 \langle u \rangle)$$

where ω_0 is the buoyancy term driving the turbulence. Stellingwerf remarks that the sign of his diffusion term is the reverse of that which would be found by simply retaining the spatial derivatives in the mixing length theory. This is because no averaging of the properties of convective eddies with different histories has been performed in the simple mixing length theory. He goes on to show that his equation gives a sensible representation of convective overshooting in contrast to the counter intuitive behaviour to be expected from the naive mixing length theory.

Another nonlocal, time dependent mixing length theory of convection has recently been proposed by Eggleton (1983). In this work the author emphasises the need for a prescription for the convective perturbations which treats all the variables in a consistent manner. The theory proposed treats all aspects of

convection, including mixing, as one system and shows up connections between, for example, nuclear energy generation and convection not present in any other competing theory. His equation for the convective velocities is very like that of Stellingwerf, that is,

$$\frac{du'}{dt} + u' \frac{\partial u'}{\partial z} + \frac{u'^2}{L} = \frac{T \nabla_{ad}}{h} s' + \left(u' \left(\frac{\partial^2}{\partial z^2} - \frac{1}{L^2} \right) u' \right)$$

where h is the specific enthalpy, s' is the specific entropy perturbation, and z is a vertical coordinate (plane geometry). This should give the same overshooting behaviour as Stellingwerf's treatment. In this model, though, the nonlocal terms are present in the equations for all the variables and so should probably be preferred.

An entirely different approach to the problem of convection in a pulsating star has been taken by Deupree (1977a,b,c,d). In this work an attempt is made to model the convective flows numerically using a two-dimensional Euler-Lagrange difference scheme. His equations take the form of an energy conservation equation including all the convective energy terms, which is very like Stellingwerf's energy equation, together with simple equations for the large scale convective flows. The process of entrainment through which the kinetic energy of convection is degraded to thermal energy is simulated using an eddy viscosity. Whilst this two-dimensional model can be criticised for its restrictive geometry which imposes a

symmetry upon the motions which is not necessarily realistic, and for the unavoidable coarseness of the finite difference grid, the results do show reasonable agreement with observed properties. In particular a tolerable red edge to the RR Lyrae instability strip is found and also the phase lag problem is to a large extent alleviated.

Both of these features are also present in the more recent work of Stellingwerf described earlier and, more importantly, the structure of the stellar models and the mechanisms operating to produce stability appear to be very similar. Finding this sort of agreement between two very different models of convection seems to imply that a reasonable representation is almost within sight.

Whilst some sort of nonlocal theory of convection should be employed if it is hoped to make accurate calculations, this class of theory is very much more difficult to put into practice than a local theory. This difficulty arises from the introduction of the new second order derivative which requires the specification of a further pair of boundary conditions. The stellar envelope model can now no longer be treated as an initial value problem but must be solved as a boundary condition problem. For this reason a simple local theory of convection has been used in some of the work in this study. The local theory used is, at its most complex, the Unno theory but after experiments in which the response time of the convection was either made zero or infinite the latter model was selected for much of the

work.

3.2 THE MODEL OF CONVECTION ADOPTED

The equations adopted for the treatment of convection are taken from Unno (1967), Goczzi and Osaki (1980), and Goczzi (1981,1982). For the convective velocity, U , and temperature perturbations, Θ , we have, for $\nabla - \nabla_{\text{ad}} > 0$,

$$\frac{dU}{dt} + \frac{U^2}{L/2} = -\frac{Q}{2\rho T} \frac{\partial p}{\partial r} \quad [65]$$

and

$$\frac{d\Theta}{dt} + \frac{U\Theta}{L/2} + \frac{4\alpha cKT^3}{C_p \gamma} \Theta = \frac{U}{L/2} \frac{L/2}{H} T (\nabla - \nabla_{\text{ad}}) \quad [66]$$

where all the variables other than U and Θ are averaged over lengths greater than the mixing length. If $\nabla - \nabla_{\text{ad}} < 0$ then the U , Θ , and F_c are all zero and the energy transport is purely radiative. For the static model we determine l in the "traditional" manner using, $l = \alpha H$, where $\alpha \approx 1$ is a constant. However the behaviour of l for the pulsating star is not well established. A simple and reasonably plausible model is given in Unno (1976). Assuming that a convective element is born at a time t' with a mixing length, or size, proportional to the instantaneous pressure scale height, evolves according to the law $\rho l^3 = \text{constant}$ throughout its lifetime, then taking the time dependence for all pulsational perturbations to be $e^{i\omega t}$ he obtains, for a single element,

$$\left(\frac{\delta l}{l}\right)_{\text{single}} = \frac{\delta M}{H} e^{i\omega(t'-t)} - \frac{1}{3} \frac{\delta \rho}{\rho} (1 - e^{i\omega(t'-t)})$$

By assuming a constant birth rate and lifetime for the elements and a simple decay law, i.e. $\propto \exp((t'-t)/\tau_c)$, an average value is obtained,

$$\frac{\delta L}{L} = \frac{1}{1+i\omega\tau_c} \left(\frac{\delta H}{H} - \frac{i\omega}{3} \frac{\delta \rho}{\rho} \right). \quad [67]$$

The equations for energy transfer are completed by the definition of the convective flux,

$$F_c = \rho C_p u \theta$$

and a definition of η ,

$$\eta = 1 + \frac{3}{4} (\rho K L)^2.$$

The equation for the conservation of the mean momentum is modified to include viscosity using the equations given by Gonczi (1982). We have

$$\frac{\partial(\rho u)}{\partial t} + \nabla \cdot (\rho u u) + \nabla \cdot \underline{\underline{B}} = -\nabla P - \rho \nabla \Phi_g$$

where Φ_g is the gravitational potential, u is the velocity vector for the mean motion and $\underline{\underline{B}}$ is the viscous stress. This latter term can be written as,

$$\underline{\underline{B}}_{ij}(\underline{u}', \underline{u}) = 2\rho\nu(\underline{u}') \left[e_{ij} - \frac{1}{3} \delta_{ij} \nabla \cdot \underline{u} \right]$$

which for radial pulsations gives,

$$\left[\nabla \cdot \underline{\underline{B}} \right]_r = \frac{4}{3} \frac{1}{r^3} \frac{\partial}{\partial r} \left(\rho r^4 \nu \frac{\partial}{\partial r} \left(\frac{\dot{r}}{r} \right) \right).$$

The momentum equation now becomes,

$$\frac{d^2 r}{dt^2} + \frac{4}{3} (4\pi)^2 \frac{1}{r} \frac{\partial}{\partial m} \left(\rho r^4 \nu \frac{\partial}{\partial m} \left(\frac{1}{r} \frac{dr}{dt} \right) \right) = -\frac{Gm}{r^2} - 4\pi r^2 \frac{\partial p}{\partial m}. \quad [68]$$

In general the energy equation should also contain a viscosity term representing the appearance of the kinetic energy being converted to thermal energy. However it can be shown, e.g. Ledoux and Walraven (1958), that this term takes the form,

$$\nabla \cdot (\underline{u} \cdot \underline{\beta})$$

or for radial motions,

$$\frac{4}{3} r^2 \frac{\nu}{\rho} \left(\frac{\partial(v/r)}{\partial r} \right)^2$$

In the linear pulsation model this term disappears along with all the other nonlinear effects. The turbulent viscosity, ν , is assumed to take the same form as a molecular viscosity, i.e.,

$$\nu \propto u l'$$

where u is the characteristic velocity and l' the characteristic length of the small scale motions. The characteristic length for convection is the mixing length, l . However, in cases where the pulsation timescale, $1/\text{Re}(\omega)$, is shorter than the time taken for a convective eddy to travel its full distance before dissolution the length scale for the viscosity will be shorter. A reasonable expression for the turbulent viscosity is thus,

$$\nu = u^2 \tau_c \min(1, \tau_c \text{Re}(\omega)).$$

This is the expression favoured by Gonczi (1981).

This together with the equations for the total energy flux, an equation for the radiative energy flux, the continuity equation, the equation of state, and the opacity comprises the stellar model.

3.3 THE STATIC MODEL

We need to be able to calculate the temperature gradient, ∇ , given the luminosity and other mean physical variables at a given point. When $\nabla - \nabla_{\text{rad}} < 0$, then clearly the equation for radiative energy transport is all that is required. For the case where this is not true then we remove the time derivative terms from equations [65,66] and replace $\partial p / \partial r$ with $-Gm/r^2$. In choosing the finite difference scheme to represent these equations we observe that U , Θ , and F_z are "naturally" associated with zone interfaces. A number of zone variables have to be calculated at interfaces, and vice versa. The criterion employed to select the particular form of these averaged quantities is simplicity and plausibility. Since the width of the zones in a linear pulsation model is likely to be small it is unlikely that the precise form will be of much importance. Using $\langle x \rangle$ to represent the arithmetic mean of two interface quantities in a zone or two zone quantities at an interface, we choose the following equations,

$$L_{zI} = 4\pi r_I^2 \langle C_P \rho \rangle_I U_I \Theta_I \quad [69]$$

$$\frac{2U_I^2}{\Delta M_I} = \frac{1}{2} G_I \left\langle \frac{Q}{T} \right\rangle_I \Theta_I \quad [70]$$

$$2 \frac{U_I \Theta_I}{\Delta M_I} + \frac{4\alpha c}{\eta_I} \left\langle \frac{KT^3}{C_P} \right\rangle \Theta_I = \frac{U_I}{M_I} \langle T \rangle_I (\nabla - \langle \nabla_{\text{rad}} \rangle) \quad [71]$$

with,

$$M_I \equiv \frac{1}{G_I} \frac{\langle \rho \rangle_I}{\langle \rho \rangle_I}$$

$$C_{T_I} \equiv \frac{C_{T_I}}{V_I^2}$$

We also have,

$$L_{R_I} = - \frac{4\pi c}{3} \frac{(4\pi r_I^2)^2}{\langle \kappa_I \rho_I \rangle} \langle T_I^2 \rangle \langle T_I \rangle (T_I - T_{I-1}) \quad [72]$$

and so we define,
$$\nabla_I \equiv \frac{T_I - T_{I-1}}{\rho_I - \rho_{I-1}} \frac{\langle \rho \rangle_I}{\langle T \rangle_I}, \quad [74]$$

and of course,
$$L_I = L_{R_I} + L_{C_I}. \quad [73]$$

We use,

$$\eta_I = 1 + \frac{3}{4} \kappa^2 M_I^2 \rho_I \kappa_I \rho_{I-1} \kappa_{I-1} \quad [75]$$

since this gives more meaningful values of $\langle \kappa T^3 / C_p \rangle_I / M_I$ in both the optically thick and optically thin limits. This is similar to a scheme used by Keeley (1977).

The equations can be solved in two different ways. If it is assumed that the temperature gradient, ∇ , is known then the elimination of U and θ in equation [69] using [70] and [71] gives a quadratic equation for L_c . The luminosity calculated using this ∇_I and T etc will not, in general, be correct and so T_I , and so ∇_I , must be corrected and the process repeated until agreement is achieved. The alternative is to take the known value of L_I and to eliminate U and θ from the convective flux equation and then to substitute this into the equation for the total flux to give what is in effect a cubic equation in ∇_I . Both of these methods are covered in Cox and Giuli (1968). For this study the latter method is adopted.

We substitute equation [70] in equation [71] to give, if we ignore the trivial $\Theta_I = 0$ solution, a quadratic equation for $\Theta_I^{1/2}$. The physically meaningful solution of this equation is then used to eliminate U_I and Θ_I from equation [69], using [74], to give when substituted in [73],

$$\beta_I - (\nabla_{R_I} - \langle \nabla_{ad} \rangle_I) + A_I (\sqrt{\beta_I + B_I^2} - B_I)^3 = 0 \quad [76]$$

where,

$$\beta_I \equiv \nabla_I - \langle \nabla_{ad} \rangle_I$$

$$\nabla_{N_I} \equiv \frac{L_{R_I}}{4\pi r_I^2} \left(\frac{4ac G_I \langle T^2 \rangle_I \langle T \rangle_I^2 Dm_{2I}}{3 \langle k Dm_1 \rangle_I \langle \rho \rangle_I} \right)^{-1} \quad [77]$$

$$A_I \equiv \left(\frac{4ac \langle T^2 \rangle_I \langle T \rangle_I Dm_{2I}}{3 \langle k Dm_1 \rangle_I \langle \rho \rangle_I} \right)^{-1} \frac{\alpha \sqrt{2}}{8} \langle \rho C_p \rangle_I \left(\frac{M_I \langle Q \rangle_I}{G_I \langle T \rangle_I} \langle T \rangle_I \right) \quad [78]$$

$$B_I \equiv \frac{1}{\sqrt{2}} \left(\frac{G_I \langle Q \rangle_I}{M_I \langle T \rangle_I} \langle T \rangle_I \right)^{1/2} \left(\frac{4ac \langle k T^3 \rangle_I}{4_I \langle C_p \rangle_I} \right) \quad [79]$$

This is most conveniently solved by dividing equation [76] by $(\nabla - \langle \nabla_{ad} \rangle_I)$ and so introducing the variable z_I where,

$$z_I \equiv - \frac{\beta_I - \nabla_{R_I} - \langle \nabla_{ad} \rangle_I}{\nabla_{R_I} - \langle \nabla_{ad} \rangle_I}$$

$$\equiv \frac{\nabla_{R_I} - \nabla_I}{\nabla_{N_I} - \langle \nabla_{ad} \rangle_I} \quad [80]$$

Clearly when $\nabla_I = \nabla_{R_I}$, for the radiative case, we have $z_I = 0$, and when $\nabla_I \rightarrow \langle \nabla_{ad} \rangle_I$ giving the fully convective case we have $z_I \rightarrow 1$. This is, then, a convenient parameter for measuring the effectiveness of convection. We now rearrange equation [76] in order to solve for z_I ,

and find,

$$z_I^{4/3} + \left(\frac{\nabla n_I - \langle \nabla n \rangle_I}{A_I} \right)^{1/3} \frac{1}{2B_I} z_I^{2/3} + \frac{(A_I (\nabla n_I - \langle \nabla n \rangle_I))^{1/3}}{2B_I} (z_I - 1) = 0. \quad [81]$$

If we represent the coefficient of $z_I^{2/3}$ by $\alpha\beta$ and that of $(z_I - 1)$ by α then on comparing this equation with equation 14.82 in Cox and Giuli we see that,

$$B_{\text{Cox-Giuli}} \equiv \alpha\beta$$

and,

$$a_{\text{Cox-Giuli}} \equiv \frac{1}{\alpha\beta^2} \equiv 2A_I B_I.$$

This last quantity is dimensionless and in the theory described by Cox and Giuli is a constant determined by the eddy geometry. However here, since we have included terms to improve upon the treatment of optically thin convection and since a finite difference approximation has been used this is not the case. For instance we have the ratio of differently weighted mean opacities,

$$\dots \left\langle \frac{kT^3}{c_p} \right\rangle \cdot \frac{Wm z_I}{\langle k/m \rangle_I} \dots$$

Examining the behaviour of $2A_I B_I$ in the optically thick regions then gives us some idea of how the various averagings of the zones affect the model. We find that this quantity is generally within 2 or 3% of its expected "perfect zoning" value.

The algorithm for the iteration to find T_I is essentially the same as that used for the radiative model. A zone mass is selected and this gives the pressure in the new zone, and the other variables are estimated by an integration from the last zone to this. The temperature gradient is calculated using the equation appropriate to the current value of $(\nabla_{R_I} - \langle \nabla_{ad} \rangle_I)$, and the function,

$$f^{(n)} \equiv \nabla_I^{(n)} - \frac{T_{I-1}^{(n)} - T_I}{T_{I-1}^{(n)} + T_I} \cdot \frac{\rho_{I-1}^{(n)} + \rho_I}{\rho_{I-1}^{(n)} - \rho_I} \quad [82]$$

is calculated. If,

$$|f^{(n)}| > \epsilon_c$$

then T_I is corrected. The correction to T_I is calculated using the secant method which is simply a Newton-Raphson method in which the derivative is approximated as,

$$f'(T) = \frac{f^{(n)} - f^{(n-1)}}{T^{(n)} - T^{(n-1)}}$$

so,

$$T^{(n+1)} = T^{(n)} - f^{(n)} \cdot \frac{T^{(n)} - T^{(n-1)}}{f^{(n)} - f^{(n-1)}} \quad [83]$$

The use of this formula obviates the need for second derivatives of the thermodynamic variables which would require either complicated though feasible additions to the equation of state, or the time consuming calculation of numerical derivatives. It is found that, on average, this method requires only one iteration more than the Newton formula in the radiative model. However the first step of the iteration must be made using some alternative formula and for this we

use,
$$T_{I-1}^{(2)} = T_{I-1}^{(1)} \left(1 + \frac{1}{2} \left[\left(\frac{1 + C_I}{1 - C_I} \right) \frac{T_I}{T_{I-1}} - 1 \right] \right) \quad [84]$$

where,

$$C_T \equiv \nabla_T \frac{P_{T-1} - P_T}{P_{T-1} + P_T}.$$

The zoning is determined in the same way as for the radiative models with the exception that a further condition is introduced to ensure that L_c/L does not change too rapidly from zone to zone. If h is the increment in pressure chosen as before then we choose the new h' according to,

$$h' = \min(h, h_c)$$

with,

$$h_c \equiv 0.02 \left| \frac{\Delta p}{p} \frac{L_c}{\Delta L_c} \right|$$

and where ΔL_c and Δp are the changes in L_c and p across the previous zone. This has been found to give a reasonable resolution for L_c/L .

3.4 THE LINEAR PULSATION MODEL

The equations for pulsation with convection in the linear approximation are obtained using the same procedure as for their radiative counterparts. That is the explicitly time dependent terms are reintroduced and the equations perturbed. On subtracting the static structure equations and keeping only first order terms we obtain the required equations.

The momentum equation must be modified to include the viscosity terms as given by equations [68]. We require,

$$\frac{1}{r} \frac{\partial}{\partial m} (\rho^2 r^6 \nu \frac{\partial}{\partial m} (\frac{1}{r} \frac{d\delta r}{dt}))$$

at the I^{th} zone interface, and so [...] in zones I and I-1,

$$\frac{1}{r_I} \frac{1}{\partial m 2_I} \left\{ [\dots]_I - [\dots]_{I-1} \right\}.$$

So,

$$[\dots] = \rho_I^2 \langle r^6 \nu \rangle \frac{i\omega}{\partial m 2_I} \left(\frac{X_{I+1}}{r_{I+1} \sqrt{\partial m 2_{I+1}}} - \frac{X_I}{r_I \sqrt{\partial m 2_I}} \right),$$

since $r_I = X_I (\partial m 2_I)^{1/2}$. The only uncertainty is in the form for the zone value of $r^6 \nu$ since both r and ν are interface quantities. So we have,

$$\begin{aligned} \omega^2 X_I &= \frac{i\omega}{r_I \sqrt{\partial m 2_I}} \left[\frac{\rho_I^2 \langle r^6 \nu \rangle}{\partial m 2_I} \left(\frac{X_{I+1}}{r_{I+1} \sqrt{\partial m 2_{I+1}}} - \frac{X_I}{r_I \sqrt{\partial m 2_I}} \right) \right. \\ &\quad \left. - \frac{\rho_{I-1}^2 \langle r^6 \nu \rangle}{\partial m 2_{I-1}} \left(\frac{X_I}{r_I \sqrt{\partial m 2_I}} - \frac{X_{I-1}}{r_{I-1} \sqrt{\partial m 2_{I-1}}} \right) \right] \quad [86] \\ &= G_{11I} X_{I-1} + G_{21I} X_{I-1} + G_{12I} X_I + G_{22I} X_I + G_{13I} X_{I+1}. \end{aligned}$$

It is clear that the dependence of this equation upon ω is no longer simple and the Sturm sequence method which assumes $\omega^2 \in \mathbb{R}$, is no longer applicable to finding the adiabatic solution. However experience shows that the change in $\text{Re}(\omega)$ due to the introduction of the viscous terms is small. This means that a reasonable estimate of ω for starting the iterative solution of the full nonadiabatic equations can be obtained simply by dropping the viscous terms.

The energy transport equation requires the quantity $\delta L/L$. From the expression for the total luminosity we get,

$$\frac{\delta L}{L} = \frac{L_R}{L} \left(\frac{\delta L}{L} \right)_R + \frac{L_C}{L} \left(\frac{\delta L}{L} \right)_C. \quad [87]$$

The equation for $\delta L_R/L_R$ is exactly the same as for the radiative model. From the equation [69] for L_C we have,

$$\left(\frac{\delta L}{L} \right)_{L_C} = 2 \frac{\delta v_I}{v_I} + \frac{\delta \langle \rho c_p \rangle_I}{\langle \rho c_p \rangle_I} + \frac{\delta u_I}{u_I} + \frac{\delta \theta_I}{\theta_I}. \quad [88]$$

Replacing the time derivative terms in equations [65] and [66], replacing $-Gm/r^2$ with a difference equation for $\partial p/\partial r$ and using χ rather than αH the pulsational perturbations $\delta U/U$ and $\delta \theta/\theta$ can be obtained in the usual way. The equations can be written as,

$$a_I(\omega) \left(\frac{\delta u}{u} \right)_I = b_I(\omega) \left(\frac{\delta \theta}{\theta} \right)_I + c_I(\omega) \chi + d_I(\omega) \psi \quad [89]$$

and,

$$e_I(\omega) \left(\frac{\delta \theta}{\theta} \right)_I = f_I(\omega) \left(\frac{\delta u}{u} \right)_I + g_I(\omega) \chi + h_I(\omega) \psi \quad [90]$$

for each zone, where each coefficient is a rational function of ω . These equations are solved and then the resulting expressions for $\delta U/U$ and $\delta \theta/\theta$ substituted into equation [88] to give,

$$\left(\frac{\delta L}{L} \right)_C = CL11_I \chi_{I-1} + CL21_I \psi_{I-1} + CL12_I \chi_I + CL22_I \psi_I + CL13_I \chi_{I+1} \quad [91]$$

where again all the coefficients are rational functions of ω .

It can be seen that the coefficients of the χ and ψ vectors in the convective pulsation problem have a very much more complicated ω dependence than their counterparts in the radiative problem. Whilst

it is still possible to use the same methods to solve the eigenvalue problem, it should be expected that many more solutions are present and, perhaps, new modes of pulsation, or whatever, exist. However the enumeration of the pulsation modes of the nonadiabatic equations has yet to be achieved for the radiative model let alone the convective model. A very rudimentary view of this problem can be attained by eliminating the spatial derivatives from the pulsation equations, with the exception of the luminosity gradient for which a simple linear approximation is used. This procedure gives the one-zone model as described by, for example, Baker (1966) for the radiative model, and by Unno (1967) with convection included. The form of the resulting characteristic equation for the radiative model is, as is well known, a cubic equation in $i\omega$. The solutions of this equation are a complex conjugate pair $i\omega_{1,2}$ corresponding to pulsation and a much smaller real root $i\omega_3$ which corresponds to secular variations on a thermodynamic time scale. For the convective system two new $i\omega_{4,r}$ terms are introduced, one from each of the equations relating $\delta U/U$ and $\xi\theta/\theta$. There are thus five roots to be found. Unno derives approximate solutions for the complex conjugate pair and shows that their value is little changed by the introduction of convection. However he goes no further than this.

Rather than attempt an approximate analysis of the system which would involve much complicated algebra I have resorted to a numerical method in order to obtain, to a high accuracy, the roots of this system for selected values of the input parameters. The results show;

i. a complex conjugate pair $i\omega_{1,2}$ with $|\text{Re}(\omega_{1,2})| \sim 1/\tau_d$, τ_d being the dynamical time scale,

ii. a single real root $i\omega_3$ with $i\omega_3 \sim 1/\tau_{th}$ where τ_{th} is the thermodynamical time scale,

iii. a single real root $i\omega_4$ for which $i\omega_4 \sim 1/\tau_r$ and τ_r is the radiative time scale as given in section 2.4,

iv. a single real root $i\omega_5$ with $i\omega_5 \sim 1/\tau_c$.

So the $\omega_{1,2}$ are two new modes, one of which represents the decay of perturbations in the radiation field and the other which represents the growth of convective perturbations. The first, radiative, mode arises from the perturbations due to the convective motion and so we should expect that the phenomena are, as with the convective mode, of a localised nature and not global effects such as pulsation. However this cannot completely remove the possibility that when the spatial derivatives are reintroduced into the equations new families of global modes will be found. The problem of formally enumerating the families of the modes in stellar models is something which has sadly been neglected but which, as is evident from such work as Cox et.

al. (1980), of great importance.

3.5 THE WORK INTEGRAL WITH VISCOSITY

Although the expression for the work integral given in section 2.3.1 is valid when convection is included, the inclusion of viscous dissipation requires the introduction of a further term. When the viscous stress is included in the Euler equation we have,

$$\frac{d\underline{v}}{dt} + \frac{1}{\rho} \nabla \cdot \underline{\underline{\mathcal{B}}} = -\frac{1}{\rho} \nabla p - \nabla \Phi_G$$

where $\underline{\underline{\mathcal{B}}}$ is the viscous stress tensor. Proceeding as before we obtain the work integral. That is, for the viscous term we have,

$$\frac{dW_{vis}}{dt} = \int \underline{v} \cdot (\nabla \cdot \underline{\underline{\mathcal{B}}}) dV$$

which for radial pulsation becomes,

$$\frac{dW_{vis}}{dt} = \int \dot{r} \frac{4}{3} \frac{1}{r^3} \frac{\partial}{\partial r} \left(\rho r^4 \frac{\partial}{\partial r} \left(\frac{\dot{r}}{r} \right) \right) dV \quad [93]$$

Since $\dot{r} = \text{Re}(i\omega) |r| e^{i(\omega t + \theta)}$ we obtain,

$$\Delta W_{vis} \equiv \oint \frac{dW_{vis}}{dt} dt = \frac{(4\pi)^2}{3} \int_0^R \text{Im} \left(\left[i\omega \frac{\partial}{\partial r} \left(\rho r^4 v \frac{\partial (sr/r)}{\partial r} \right) \right]^* \frac{sr}{r} \right) dr \quad [94]$$

which is equivalent to Gonczi's (1981) expression. An integration by parts observing that v vanishes at both boundaries of the envelope gives,

$$\Delta W_{vis} = -\frac{4\pi}{3} \int \text{Re}(\omega) v r^2 \left| \frac{\partial (sr/r)}{\partial r} \right|^2 dm. \quad [95]$$

This is calculated in the finite difference scheme as,

$$\Delta W_{vis} = -\frac{(4\pi)^2}{3} \text{Re}(\omega) \sum_I \rho_I^2 \langle r^4 v \rangle \left| \frac{X_{I+1}}{r_{I+1} \sqrt{M_I} Z_{I+1}} - \frac{X_I}{r_I \sqrt{M_I} Z_I} \right| \quad [96]$$

where $\langle \dots \rangle$ is the same average as used previously for the viscosity term.

CHAPTER 4

THE EQUATION OF STATE AND OPACITY

4.1 THE EQUATION OF STATE.

4.1.1 The Basic Equations

In order to complete the set of equations for stellar structure it is necessary to have an equation expressing the relation between p , ρ , T ; the equation of state.

If the formation of molecules is ignored we can write,

$$p = p_{\text{ions}} + p_e + p_r$$

The radiation pressure, $p_r = (1/3)aT^4$, where a is the radiation pressure constant. The pressure due to atoms and ions,

$$p_{\text{ions}} = \frac{\rho}{m_H \mu_{\text{ions}}} kT$$

where m_H is the mass of a hydrogen atom, μ_{ions} is the mean molecular mass due to atoms and ions only and k is the Boltzmann constant. If the chemical abundances are specified by mass as X_i (i denoting the atomic species) with $\sum_i X_i = 1$ then,

$$\frac{1}{\mu_{\text{ions}}} = \sum_i X_i / A_i$$

where A_i is the atomic weight of an atom of the species i . The electron pressure, $p_e = n_e kT$, where n_e is the electron number density. The degree of ionisation of each ionic species is determined by means of the Saha Equation. In the case of negligible degeneracy and in the nonrelativistic regime this can be written,

$$\frac{n_{ij+1}}{n_{ij}} n_e = \alpha_{ij+1}$$

n_{ij} is the number density of the atomic species i , j times ionised and

$$\alpha_{ij+1} = 2 \frac{B_{ij+1}}{B_{ij}} \left(\frac{m_{ij+1}}{m_{ij}} \frac{m_e kT}{h^2} \right)^{3/2} e^{-\chi_{ij+1}/kT} \quad [97]$$

In this, B_{ij} is the partition function for the ionic species (ij) , m_{ij} is the corresponding mass, χ_{ij} is the energy required to remove an electron from that ion, m_e is the electron mass and h a form of Planck's Constant. The partition functions are a complicated function of the ionisation equilibrium and will be treated in some detail in a later section. We can safely assume,

$$\frac{m_{ij+1}}{m_{ij}} = 1.$$

Only the first negative ion will be considered for each ionic species and it is simplest to include this separately in the summation.

The total number, n_i , of ions in a given volume of the atomic species i is a constant and gives us an expression,

$$n_i = \left(\sum_{j=0}^{z_i} n_{ij} \right) + n_{i-1} \quad [98]$$

and also

$$n_i = \frac{\rho}{M_H} \frac{X_i}{A_i} \quad [99]$$

It is clear from [97] that

$$u_{ij} = u_{i0} \prod_{k=1}^j \left(\frac{\alpha_{ik}}{u_e} \right) \quad [100]$$

$$u_{i-1} = u_{i0} \frac{u_e}{\alpha_{i-1}}$$

Writing

$$\beta_{ij} = \prod_{k=1}^j \left(\frac{\alpha_{ik}}{u_e} \right),$$

$$\beta_{i-1} = \frac{u_e}{\alpha_{i-1}},$$

we can substitute [100] into [98] to get,

$$u_i = u_{i0} \left(\sum_{j=1}^{z_i} \beta_{ij} + 1 + \beta_{i-1} \right),$$

and so [97] gives,

$$u_{i0} = \frac{\rho}{u_H} \frac{X_i}{A_i} \left(\sum_{j=1}^{z_i} \beta_{ij} + 1 + \beta_{i-1} \right)^{-1}. \quad [101]$$

A j times ionised atom will have contributed j electrons to the gas and so we have,

$$u_e = \sum_{i=1}^N \left(\sum_{j=1}^{z_i} j u_{ij} - u_{i-1} \right) \quad [102]$$

which with [99], [100] and [101] becomes

$$u_e = \frac{\rho}{u_H} \sum_{i=1}^N \frac{X_i}{A_i} \left(\frac{\sum_{j=1}^{z_i} j \beta_{ij} - \beta_{i-1}}{1 + \sum_{j=1}^{z_i} \beta_{ij} + \beta_{i-1}} \right) \quad [103]$$

This is our basic equation for the ionisation equilibrium. Given an auxiliary equation for B_{ij} and a pair of values from the set p, T, ρ we can solve for n_e and for the third quantity from that set.

In order to perform the pulsation calculations it is necessary to calculate the specific heat capacity, C_v , and at least two of Γ_1 , $(\Gamma_2 - 1)/\Gamma_2$, $(\Gamma_3 - 1)$. These quantities are defined as;

$$C_v \equiv (\partial E / \partial T)_\rho; \quad \Gamma_1 \equiv \left(\frac{\partial \log P}{\partial \log \rho} \right)_{ad}$$

and

$$(\Gamma_2 - 1) / \Gamma_2 = (\partial \log P / \partial \log T)_{ad}$$

$$(\Gamma_3 - 1) = (\partial \log T / \partial \log \rho)_{ad}$$

where E is the specific internal energy. We also calculate the auxiliary functions,

$$\chi_T \equiv \left(\frac{\partial \log \rho}{\partial \log T} \right)_P$$

and

$$\chi_\rho \equiv \left(\frac{\partial \log P}{\partial \log \rho} \right)_T$$

Here

$$E = \frac{3}{2} \frac{kT}{\mu_H \mu_{ion}} + \frac{3}{2} \frac{n_e kT}{\rho} + \frac{aT^4}{\rho} + E_{ion},$$

where the contributions are due to the heavy ions, the electrons, radiation, and the ionisation energy per unit mass. This final term is given by,

$$E_{ion} = \sum_{i=1}^N \frac{X_i}{A_i} \frac{\sum_{j=1}^{Z_i} \left(\sum_{k=1}^{Z_i} \chi_{ik} \right) \beta_{ij} - \chi_{i-1} \beta_{i-1}}{1 + \sum_{j=1}^{Z_i} \beta_{ij} + \beta_{i-1}} \cdot [104]$$

In this treatment we have ignored the excitation energy.

It is evident from an inspection of these equations that we will require the quantities,

$$\eta_T \equiv \left(\frac{\partial \log n_e}{\partial \log T} \right)_P,$$

$$\eta_\rho \equiv \left(\frac{\partial \log n_e}{\partial \log \rho} \right)_T,$$

and

$$E_{ion T} \equiv \left(\frac{\partial E_{ion}}{\partial \log T} \right)_P.$$

However we first consider the partition functions.

4.1.2 The Partition Functions

The partition functions are given by,

$$B_{ij} = \sum_{k=1}^{\infty} g_{ijk} W_{ijk} e^{-E_{ijk}/kT} \quad [105]$$

Where g_{ijk} is the statistical weight, W_{ijk} the probability of population and E_{ijk} the excitation energy of the k^{th} excited state of the j times ionised i^{th} element. In this calculation we follow Fischel and Sparks (1971), with a few simplifications. The Bohr model is used to calculate g_{ijk} and E_{ijk} , ie,

$$g_{ijk} = m_{ij} n_k^2$$

and

$$E_{ijk} = \chi_{ij} - \frac{\chi_{ij}}{n_k^2} \quad [106]$$

where m_{ij} is the ground state partition function, and n_k the principle quantum number for the k^{th} state.

The populations of states with higher values of k are reduced by the effects of perturbations due to neighbouring particles. It is assumed by Fischel and Sparks that the linear Stark effect represents this adequately and that all the free electrons act as quasistatic perturbers, Griem (1967). This gives a simple expression for W_{ijk} ,

$$W_{ijk} = \min \left(1, \frac{6.14 \cdot 10^5}{2.61 n_e^{2/3}} \left(\frac{Z_{ijk}^*}{n_k} \right)^4 \right),$$

here n_q is the total number of quasistatic charged perturbbers given by

$$n_q = \sum_{i=1}^N \left(\sum_{j=1}^{Z_i} j^{3/2} n_{ij} \right) + n_e. \quad [107]$$

In this simple treatment we approximate the screened nuclear charge, Z_{ijk}^* as,

$$Z_{ijk}^* = \chi_{ij} / R h c$$

R being the Rydberg constant and c the velocity of light. The intention is to form a power series in $(1/n_k)$. We define, $p_{ij} = n_k$ such that $\log(W_{ijk}) = 0$,

$$4 \log p_{ij} = 14.69 - \frac{2}{3} \log n_q + 4 \log Z_{ijk}^* \quad [108]$$

so for $n_k < p_{ij}$,

$$W_{ijk} = 1$$

otherwise

$$W_{ijk} = \left(\frac{p_{ij}}{n_k} \right)^4. \quad [109]$$

Dropping the ij subscripts and taking $n_k = k = n$ we can write, for

$$p > 1, \quad B = m + \sum_{n=2}^p m n^2 e^{-\chi/kT} \cdot e^{(\chi/kT)/n^2} + \sum_{n=p+1}^{\infty} m n^2 \frac{p^4}{n^4} e^{-\chi/kT} \cdot e^{(\chi/kT)/n^2}.$$

Defining $D = \chi/kT$ we expand the second exponential as,

$$e^{D/n^2} = 1 + D/n^2 + D^2/2n^4.$$

As is well known the error is $D^2/6n^6$ which since $D < 1$ should be sufficiently accurate for most values of n . This gives

$$B = m + m e^{-D} \sum_{n=2}^P (n^2 + D + \frac{D^2}{2n^2}) + m e^{-D} p^4 \sum_{n=p+1}^{\infty} (\frac{1}{n^2} + \frac{D}{n^4} + \frac{D^2}{2n^6}).$$

We define the generalised ξ -function

$$\xi(i, p) = \sum_{k=0}^{\infty} \frac{1}{(k+p)^i},$$

and so

$$B = m + m e^{-D} \left\{ \frac{1}{6} p(p+1)(2p+1) - 5 + D(p-2) + \frac{1}{2} D^2 (\xi(2, 3) - \xi(2, p+1)) \right\} \quad [110] \\ + m e^{-D} p^4 \left\{ \xi(2, p+1) + D \xi(4, p+1) + \frac{1}{2} D^2 \xi(6, p+1) \right\}.$$

The calculation of the approximate partition function has now been reduced to an evaluation of the ξ -functions.

A number of algorithms for determining the ξ -functions have been examined. The simplest method seems to be to use

$$\xi(i, p) \approx \frac{1}{2} \int_p^{\infty} \left(\frac{1}{x^i} + \frac{1}{(x-1)^i} \right) dx$$

for large j since the fractional error is $\sim (1/j)^3$. An alternative might be to use an Euler Maclaurin Formula but this is really no better. For $j > 4i$ we use the integral expression alone, for $j > 2i$ we use

$$\xi(i, p) = \sum_{k=0}^{4i} \frac{1}{(k+p)^i} + \frac{1}{2} \int_{4i+1}^{\infty} \left(\frac{1}{x^i} + \frac{1}{(x-1)^i} \right) dx$$

and for $j > 2i$ we use

$$\xi(i, p) = \xi(i, 1) - \sum_{k=1}^{p-1} \frac{1}{k^i}$$

The technique gives partition functions which are in good agreement with those quoted by Fischel and Sparks (1971).

4.1.3 Derivatives Of The Electron Number Density

We can calculate n_T and n_ρ , also E_T , analytically. Comparison of [102] and [107] will show that the functions n_e and n_q are very similar. Take partial derivatives of each we obtain

$$n_{ex} = A n_{qx} + B$$

$$n_{qx} = C n_{ex} + D$$

where x is either T or ρ , and A, \dots are functions of n_e, n_q and T .

We can now solve for n_{ex} and n_{qx} . Clearly we require the derivatives of α_{ij} for all i and j . If,

$$y_x \equiv \left(\frac{\partial \log y}{\partial \log x} \right)$$

where x is either T or ρ , then,

$$\alpha_{ij+1,x} = B_{ij+1,x} - B_{ij,x} + (3/2 + \chi_{ij+1}/kT) T_x$$

and so we must find the derivatives of the partition functions,

$$\left(\frac{\partial B_{ij}}{\partial \log x} \right) = \sum_{k=1}^{\infty} g_{ijk} \left(\frac{\partial \log W_{ijk}}{\partial \log x} + \frac{E_{ijk}}{kT} T_x \right) W_{ijk}$$

Since $\log(W_{ijk}) = \min(0, C_{ijk} - 2/3 \log(n))$,

$$\begin{aligned} \frac{\partial \log W_{ijk}}{\partial \log x} &= -\frac{2}{3} n_{qx} \quad , \text{ if } W_{ijk} < 1 \\ &= 0 \quad \text{otherwise.} \end{aligned}$$

So

$$\begin{aligned} \frac{\partial B_{ij}}{\partial \log x} &= T_x \sum_{k=1}^{\infty} g_{ijk} W_{ijk} e^{-E_{ijk}/kT} \frac{E_{ijk}}{kT} \\ &\quad - \frac{2}{3} n_{qx} \sum_{k=1}^{\infty} g_{ijk} W_{ijk} e^{-E_{ijk}/kT} (1 - W_{ijk}), \end{aligned}$$

where $\theta(x)$ is the step function,

$$\begin{aligned}\theta(x) &= 1, & x > 0 \\ &= 0, & x < 0.\end{aligned}$$

Using the same approximations and definitions as for B_{ij} we obtain,

$$\begin{aligned}\frac{\partial B_{ij}}{\partial \log x} &= T x u v e^{-u} \left\{ (p-1 + D(\xi(2,2) - \xi(2,p)) \right. \\ &\quad \left. + \frac{1}{2} D(\xi(4,2) - \xi(4,p)) + p^4 (\xi(4,p+1) \right. \\ &\quad \left. + D(\xi(6,p+1) + \frac{D}{2} \xi(8,p+1))) \right\} \\ &\quad - \frac{2}{3} u q x u v e^{-u} p^4 \left\{ \xi(2,p+1) + D(\xi(4,p+1) + \frac{D}{2} \xi(6,p+1)) \right\}.\end{aligned}$$

If we integrate this term numerically then we find satisfactory agreement with the analytic expression for B and so we adopt this set of approximations.

All the required thermodynamic quantities can now be easily calculated.

4.1.4 The Effect Of The Varying Partition Functions

On comparing the equation of state calculated using the varying partition functions with that computed using constant values I find that the differences are very small indeed. The function probably of most relevance is $(\Gamma_3 - 1)$ since this has a direct influence upon the work integral, that is

$$C = \int (\Gamma_3 - 1) \left(\frac{\delta P}{P} \right)^{\frac{1}{2}} i \omega T \delta S d m.$$

In all cases the depth of the wells in $(\Gamma_3 - 1)$ due to ionisation of the various elements is increased. For a Type II Cepheid this increase peaks at around 0.3% at the minimum of the well. In the case of a main sequence star this rises to about 1% in both the H I/He I and the He II ionisation zones. This increase in the effect is to be expected because of the very much greater density of this type of star. From the general trend of the effect it should be expected that the use of varying partition functions would lead to a marginal increase in driving through the Γ -mechanism. However the actual results show an increase in stability by 18%, 35%, and 5% for the fundamental mode through to the second overtone mode in solar models. Iben (1971) has also included partition functions in pulsation calculations but using a cruder model of the summation cut-off. He reports similar negative results for giant pulsators..

The most obvious effect of the inclusion of varying partition functions is to slow the programme down to a crawling pace and so apart from a hand full of exploratory calculations they have been abandoned in favour of the constant partition functions set equal to the ground state values.

4.1.5 A Note On The Implementation Of The Equation Of State

Some care must be taken in performing these calculations since the ratio of the numbers of ionic species can be very large and very small. For this reason we handle n_e and α_{ij} etc. as logarithms and so, for instance, [100] becomes,

$$\log n_{ij} = \log n_{i0} + \sum_{k=1}^j (\log \alpha_{ik} - \log n_{ke})$$

and [98] becomes

$$\log \alpha_{ij} = K + \log \beta_{ij+1} - \log \beta_{ij} + \frac{3}{2} \log T - \frac{\chi_{ij+1}}{kT}.$$

We now define, $\gamma_i = \max_j (\log(\beta_{ij}), \log(\beta_{i-1}))$ and redefine $\log(\beta_{ij})$ to be $\log(\beta_{ij}) - \log(\gamma_i)$ for all j . In this way we avoid all overflows and can easily control the number of underflows by ignoring all those terms that would be too small, i.e. $< 10^{-12}$, to contribute to the summations $\sum_j (\beta_{ij} + 1 + \beta_{i-1})$ and $\sum_j (j\beta_{ij} - \beta_{i-1})$. This is now written

$$\sum (\beta_{ij} + \gamma_i + \beta_{i-1}) \text{ etc.}$$

4.2 THE TREATMENT OF STELLAR OPACITY

In order to determine the temperature gradient throughout the star we need to know the opacity of the material. The methods used in these calculations have been reviewed by Carson (1976). In common with almost all treatments of stellar pulsation we ignore the

frequency dependency of the opacity and use an averaged value. The most appropriate form for this is the Rosseland Mean Opacity,

$$\frac{1}{K_r(\rho, T)} = \frac{\int_0^\infty \frac{1}{K(\rho, T; \nu)} \frac{dB}{dT} d\nu}{\int_0^\infty \frac{dB}{dT} d\nu}$$

where ν is the radiation frequency and B is the integrated Planck intensity. The effects of conduction are usually combined with the Rosseland opacity for radiation to give a combined opacity. The calculation of the thermal conductivity is summarised in Carson (1971).

The calculation of the radiative opacity is a formidable task involving the use of some model of the atoms accurate enough to give reasonable values of occupation numbers, oscillator strengths and energies for the electron states whilst being simple enough to make the calculations practicable. There is still disagreement over the form of the atomic model to be adopted with Cox (e.g. Cox (1965), Cox et al. (1965)) and his colleagues at Los Alamos favouring a hydrogenic model and Carson (e.g. Carson et al. (1968)) advocating a hot Thomas Fermi atomic model for the "metals". In the Carson calculations H and He are treated using the best available theoretical and experimental data for cross-sections and energy levels, with the hydrogenic approximation used for the highly excited levels of He. The data for the heavier elements are calculated using the "hot" Thomas-Fermi model together with experimental ionisation energies. An

iteration on the electron degeneracy parameters common to all atoms is performed, until charge neutrality is achieved. Experimental electron affinities are used to calculate the contribution of negative ions to the ionization equilibrium at low temperatures as is the formation of a number of molecules. The negative ions also contribute to the absorption. Allowance is made for the Rayleigh scattering by all neutral atoms, molecules and by He. Finally the electron scattering is determined from the Klein-Nishina formula and the conductive opacity calculated using a method of Hubbard and Lampe (1968). The Carson opacities are similar to the Cox opacities in general appearance but a number of important differences are present in that;

- i. the opacity for $\log(T) < 4.2$ is smaller by up to factor of 2,
 - ii. at $\log(T) \approx 4.7$ a HeII ionisation feature in the form of a small hump appears,
 - iii. for $\log(T) > 4.7$ the opacities are generally larger,
- and,
- iv. when $5.4 < \log(T) < 6.4$ a significant hump caused by the final ionisation stages of C and O (with a small contribution from N) is apparent at lower densities.

The question of which of the two methods gives the most realistic results is difficult to address and remains unanswered. Carson (1976) has stated his belief that this can only be decided by the comparison of stellar structure, evolution, and pulsation calculations made using

the respective sets of opacity data with the observed properties of the stars.

4.2.1 Use Of The Opacity Data

The opacity data exists in the form of a table. For the Carson opacities the data points are spaced equally at intervals at $\Delta \log(\rho) = 1$ and with $\Delta \log(T) = 0.1$ for $\log(T) < 5.0$ and $\Delta \log(T) = 0.2$ for $\log(T) > 5.0$. The boundaries of the table are at $\log(T) = 3.2$ and 9.0 , and such that, $-11 < \log(\rho) - 2.(\log(T)-4) \leq -2$. This range of values in $\log(T)$ is ample but it is sometimes the case for very extended envelopes that points are required for densities lower than are found on the table. Since the data points for $\log(T) < 3.9$ are unreliable through some failure of the calculations, these points are replaced with points calculated using Christy's (1966) analytic approximation to the Cox-Stewart opacities. This procedure has also been followed by Carson et al. (1981), Jeffery (1982) and Bridger (1983). They find that this procedure does not introduce any unreasonable behaviour at the matching point. There are two alternative methods for using a table such as this, the simplest being some sort of interpolation and the other is to fit a function to the data.

Almost all the calculations so far made with the Carson opacities have used linear interpolation for this purpose, e.g. Carson et al. (1981), Carson and Stothers (1976). As an alternative these authors have experimented with quadratic interpolation reporting small shifts in the blue-edge of the instability strip for $M/M_{\odot} = 0.6$ stars, and have also used linear interpolation in a table with double the usual density of points. The shift, $\delta \log(T_{\text{eff}})$ from the usual results are given here.

$\log(L/L_{\odot})$	Quadratic	1/2 spacing
2.0	-0.004	0
2.5	+0.001	-0.003

This seems reasonable when the density of the points is considered. However any simple interpolation algorithm such as these suffers from a severe deficiency in that the resulting function is not differentiable. The effect of this upon the pulsation work function, is shown, together with the opacity throughout the star, in figs. 4.1-4. The various spikes in the work function occurring in the region of radiative dissipation are clearly spurious, as is much of the detail on the opacity plots. I can see little advantage in the quadratic interpolation and indeed it might even be worse than the linear algorithm.

A very much more suitable method is interpolation using cubic spline functions, (see e.g. Conte and de Boor (1972)). Basically a spline interpolant is a piece wise polynomial interpolant defined so that at all places it has two continuous derivatives. Some additional assumptions must be made to define the derivatives at the edges of the table interpolated. The spline interpolant is generally stored as a table containing the knots, (points through which the interpolant must pass) and the coefficients of a set of basis functions, from which it is easy to calculate the desired function. The particular representation chosen for some of the calculations which appear in this work was the B-spline, e.g. Cox (1972) or deBoor (1972). Fortunately an efficient two dimensional B-spline fitting routine is available, along with many others, in the NAG library. Unfortunately the computer used for these calculations, a VAX 11/780, is endowed with too small an exponent range to permit the full use of this routine.

The method used for the spline interpolation involved a preliminary interpolation using cubic splines and, in places, an extrapolation in $\log(\rho)$ for each value of $\log(T)$ of the opacity table onto a new coordinate system in terms of $\log(T)$, and $u = \log(\rho) + 12 + 2.(\log(T) - \log(T_0))$ (here $\log(T_0) = 3.5$) from which the B-spline interpolant is then calculated. Unfortunately it is not possible to use all of the table to form the interpolant since too large a table brings about a cascade of simultaneous underflows and

overflows. This seems to be unavoidable for the machine available. The limits on the table are reduced to;

$$3.3 < \log T < 7.0$$

$$\text{and } 1 < u < 6$$

For $u < 1$ we use linear extrapolation. Unfortunately this is a fairly common occurrence although it is limited to a few zones in the density inversion region of the more luminous $\log(L/L_{\odot}) > 2.5$ and $M/M_{\odot} < 1.2$, stars. More serious is the fact that a great many models reach $u = 6$ before the envelope is sufficiently deep that the lower pulsation boundary condition is properly satisfied, i.e. $X \approx 10^{-3}$ or even 10^{-2} . The best method for extending the range in density beyond $u = 6$ seems to be to return to a linear interpolation in the original data. Since this occurs when the opacity is fairly smooth the spurious effects are largely absent.

Another way of using the opacity data is to derive some sort of fit to the data. This can be an analytic fit as used by Christy (1966) or by Stellingwerf (1974), or a numerical fit such as a spline-surface. In an attempt to find a smooth differentiable function to represent the Carson opacities a number of least squares spline fits were calculated. The results are not particularly inspiring since only for the zero metal opacities can reasonable residuals be obtained for a reasonable number of knot points. Even this fit shows a great many points at which the difference between the

tabulated and fitted opacity is 20% or more. This is unacceptable since it washes out most of the important details as can be seen from fig. 4.4. In order to try and rectify this situation fits to κ/P_e and to κ/n_e were attempted. These too proved to be impracticable. It appears that there is just too much detail in the opacities for a numerical fit to be possible indeed it seems that the table itself barely manages to resolve all the structure. The features do not conform to the rectangular coordinates of the table implying that a fit based on these coordinates is unlikely to be successful and so an analytic fit is much to be preferred. This should be attempted at some time in the future.

From the various figures given it can be seen that linear, and quadratic, interpolation give a reasonable representation of the opacity whilst a spline fit does not. The hybrid spline and linear interpolation seems to give by far the best results. However in most of the more luminous models computed in the present work nature conspires to place a very significant part of the envelope on the low density edge of the opacity tables available. The spline method is necessarily unreliable at the edge of the table because of the assumptions necessary to define the splines at the boundary. This makes the errors on the results derived using the splined tables poorly known and so for this reason (and also because of the late completion of the splining programmes) most of the results in this study have been derived using linear interpolation. The other methods

are used only to get an idea of the errors associated with the interpolation methods.

Figures 4.1 - 4.4

$$M/M_{\odot} = 0.8$$

$$\log(L/L_{\odot}) = 1.25$$

$$\log(T_{\text{eff}}) = 3.88$$

$$X = 0.75, Y = 0.25$$

a) $\log(\mathcal{K})$ with $\log(M - M_r)$

b) work function with $\log(M - M_r)$

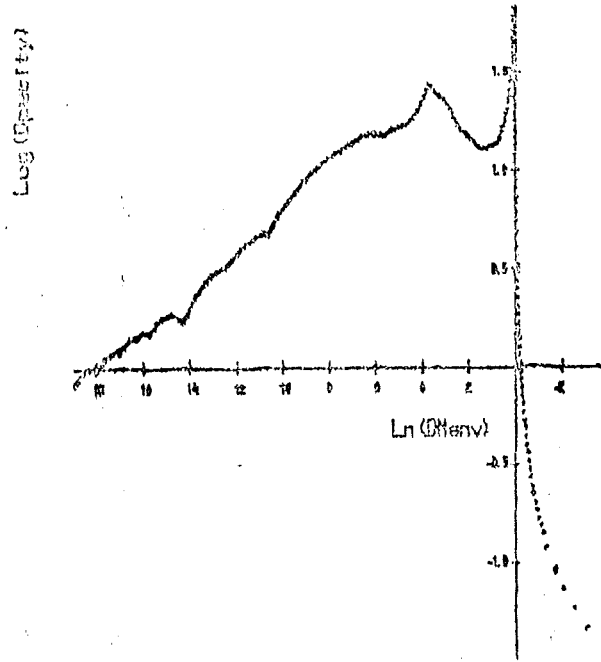
c) work integral with $\log(M - M_r)$

Mass 0.800 M_{\odot}

Luminosity 17.0 L_{\odot}

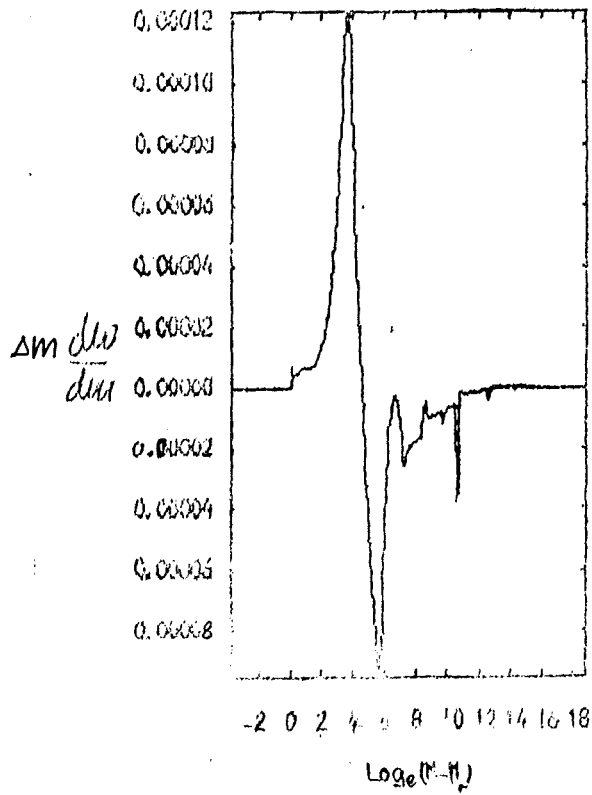
T_{eff} 7525 B K.

a)



b)

08001238



c)

08001238

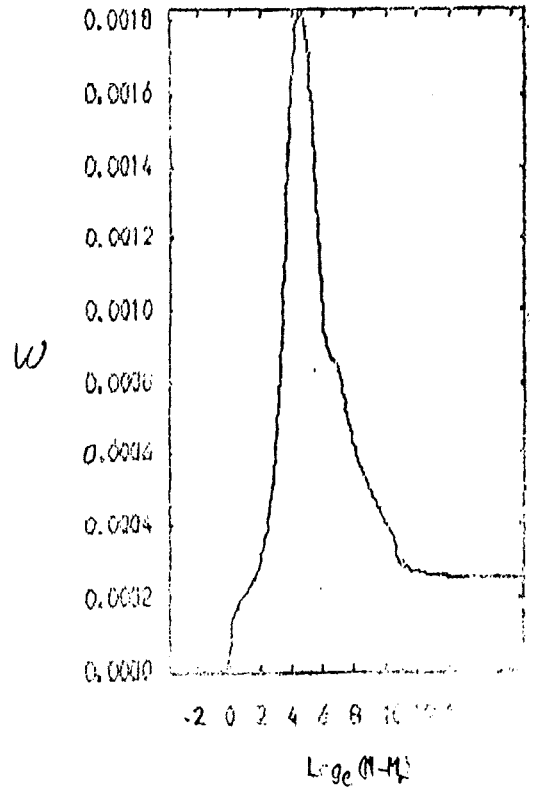
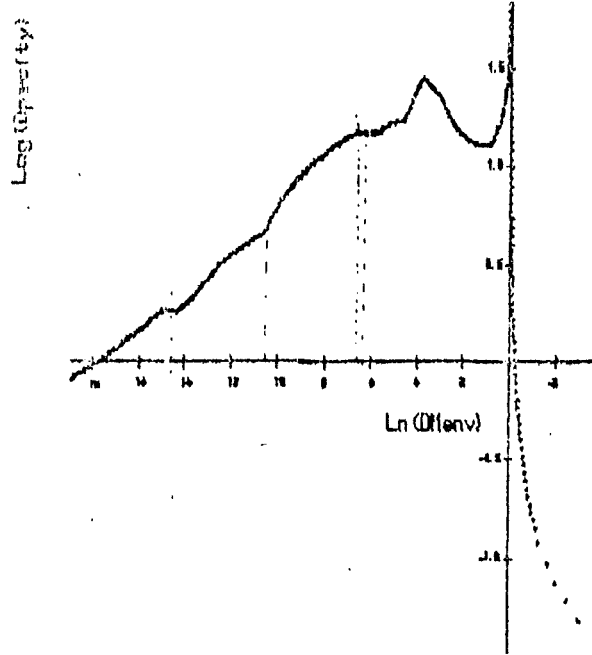


Fig. 4.1 Linear interpolation.

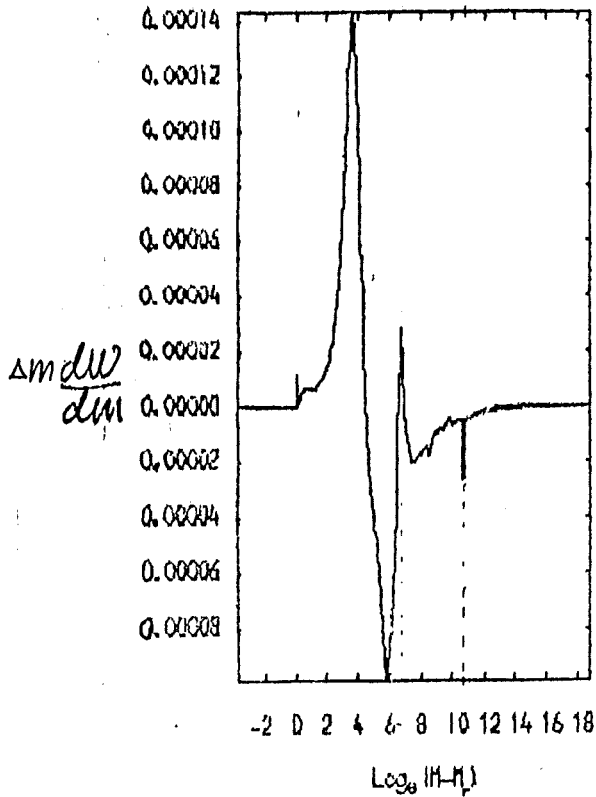
Mass $0.830 M_{\odot}$
 Luminosity $17.8 L_{\odot}$
 $T_{\text{eff}} 7535.6 \text{ K}$

a)



b)

QUOTST11



c)

QUOTST11

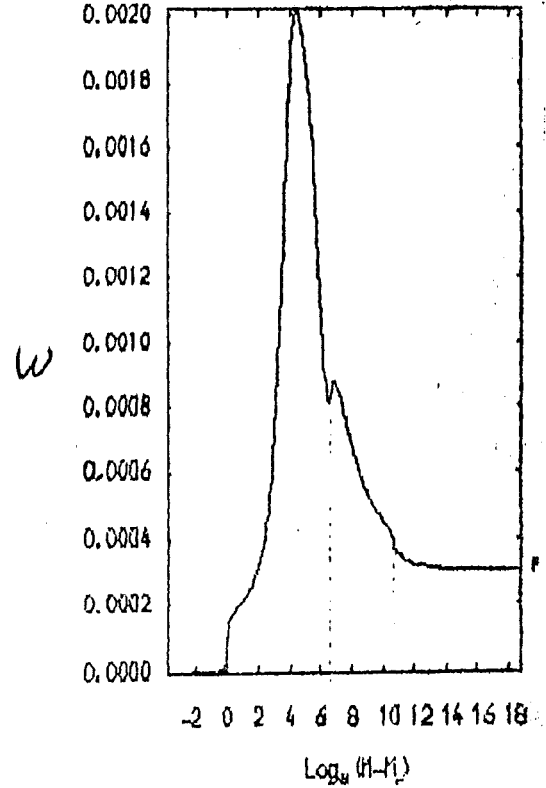


Fig. 4.2 Quadratic interpolation.

Mass 0.800 M_{\odot}
 Luminosity 17.8 L_{\odot}
 T_{eff} 7565.8 K.

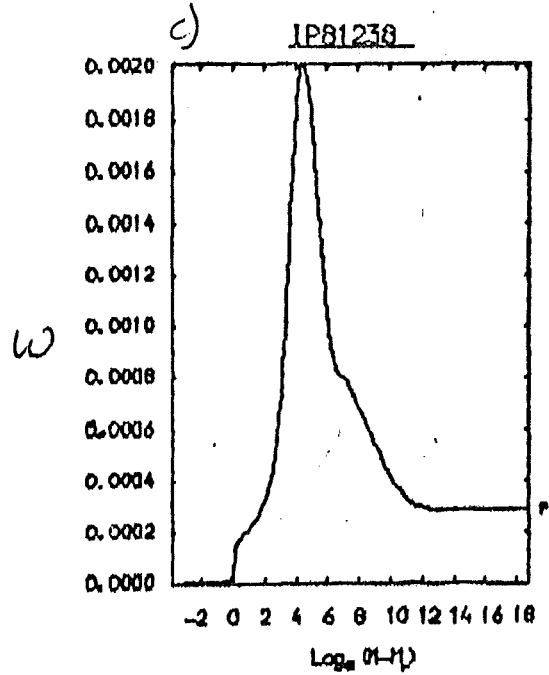
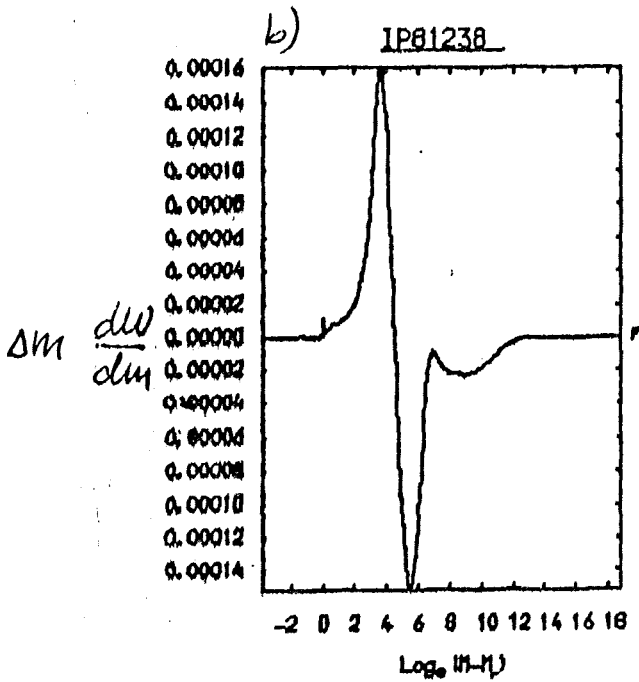
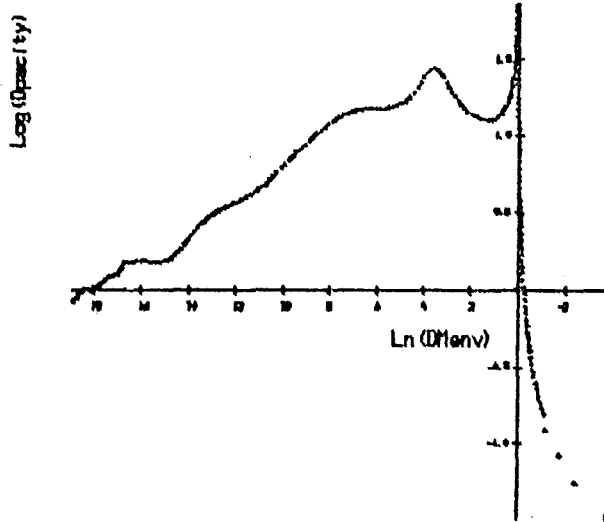


Fig. 4.3 Cubic spline interpolation

Mass $0.87 M_{\odot}$

Luminosity $17.8 L_{\odot}$

$T_{\text{eff}} 7505 \text{ K}$

a)

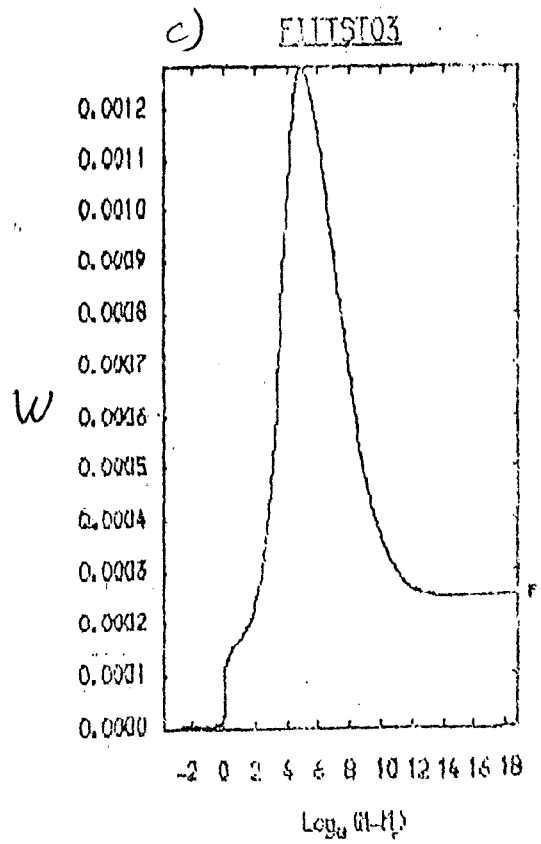
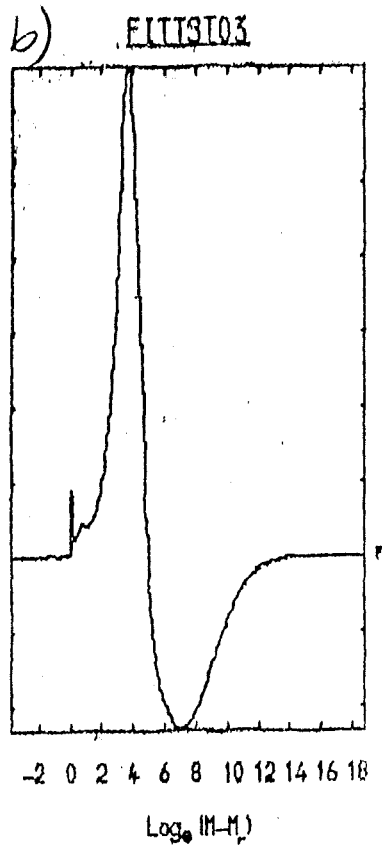
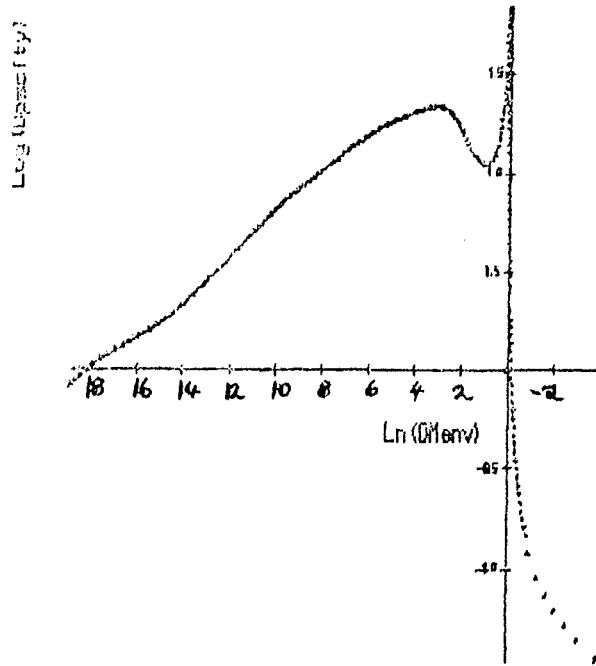


Fig. 4.4 Cubic spline least squares fit.

CHAPTER 5

SENSITIVITY OF THE CALCULATIONS TO ERRORS AND TO VARYING PHYSICS

5.1 NUMERICAL ERRORS

All of the variables which comprise the stellar model will be to some degree uncertain. This arises, if we ignore such effects as roundoff, from the fact that we cannot solve the radiation equation and the equation of state exactly. Normally the uncertainties generated in this way can be made very small and so disregarded. However the computer available to me, a VAX 11/780, has a short word length which gives only six or seven significant figures in single precision or sixteen in double precision. Because of the way in which the St. Andrews system is set up it is imperative, for reasons of speed, that single precision be used in the equation of state calculations even though the luxury of double precision can be permitted in most other parts of the programme. For this reason it seemed sensible to look at the way in which the errors propagate through the calculations.

We will consider a simple equation analogous to the radiation equation. We calculate x_{n+1} from x_n using,

$$|f(x_{n+1}, x_n)| < \epsilon' \quad [111]$$

where ϵ' specifies the accuracy to which this calculation is performed. We can calculate an upper limit to the error on x_{n+1} , ie

$$\delta x_{n+1}, \quad |\delta x_{n+1}| < \left(\epsilon' + \left| \frac{\partial f}{\partial x_n} \right| |\delta x_n| \right) / \left| \frac{\partial f}{\partial x_{n+1}} \right| \quad [112]$$

Clearly if $\epsilon' = 0$,

$$|\delta x_{n+1}| \leq \left| \frac{\partial f}{\partial x_0} \right| |\delta x_0| / \left| \frac{\partial f}{\partial x_{n+1}} \right|$$

and so if the initial value of x , x_0 , is known δx_{n+1} remains zero.

Equation [112] can be rewritten as,

$$\left| \frac{\partial f}{\partial \log x_{n+1}} \right| \left| \frac{\delta x_{n+1}}{x_{n+1}} \right| < \left(\epsilon' + \left| \frac{\partial f}{\partial \log x_n} \right| \left| \frac{\delta x_n}{x_n} \right| \right)$$

and so it can be seen that

$$\left| \frac{\delta x_n}{x_n} \right| < \left(n \epsilon' / \left| \frac{\partial f}{\partial \log x_n} \right| + \left| \frac{\delta x_0}{x_0} \right| \left| \frac{\partial f}{\partial \log x_0} \right| / \left| \frac{\partial f}{\partial \log x_n} \right| \right) \quad [113]$$

This implies that $\left| \frac{\partial f}{\partial \log x_n} \right| \left| \frac{\delta x_n}{x_n} \right|$ will grow linearly, assuming $\left| \frac{\partial f}{\partial \log x_n} \right|$ does not fall too rapidly.

In the stellar envelope the error is introduced through the radiation equation solved such that,

$$\left| 1 + \frac{40}{3} \frac{(4\pi r^2)^2}{L} \frac{T_{i-1}^4 - T_i^4}{\frac{1}{2}(k_{e,i-1} + k_{e,i})} \right| < \epsilon_R \quad [114]$$

A further source of uncertainty is introduced by the equation of state which is solved iteratively so that

$$\left| \frac{\delta k_{e,i}}{k_{e,i}} \right| < \epsilon_{eos} \quad [115]$$

The continuity equation and the momentum equation are themselves error free and only accumulate the errors given by [114] and [115]. Equation [115] accumulates an error from the pressure and introduces a new error whenever it is used. We can linearise [114],

$$\alpha_T \left| \frac{\delta T_{I+1}}{T_{I+1}} \right| + \alpha_p \left| \frac{\delta p_{I+1}}{\rho_{I+1}} \right| < \epsilon_R + \Delta(r_I, \rho_I, T_I)$$

Where Δ contains the error carried over from the last zone.

Linearising the equation of state gives us,

$$\left| \frac{\delta p}{p} \right|_I + \left(\frac{p_e}{p} \right)_I \left| \frac{\delta n_e}{n_e} \right|_I > \left| (1 + 3(p_r/p)_I) \left(\frac{\delta T}{T} \right)_I + \left(\frac{p_g - p_e}{p} \right)_I \left(\frac{\delta p}{\rho} \right)_I \right| \quad [116]$$

Here $|\delta p/p|_I$ introduces errors accumulated from previous zone calculations. These equations can be rearranged to give upper limits upon $|\delta T/T|$ and $|\delta p/p|$. The error determination is completed by

introducing the linearised continuity and momentum equations, giving,

$$\left| \frac{\delta r}{r} \right|_{I+1} \leq \left(\frac{r_I}{r_{I+1}} \right)^3 \left| \frac{\delta r}{r} \right|_I + (1 - r_I/r_{I+1}) \frac{(1 + r_I/r_{I+1} + (r_I/r_{I+1})^2)}{3} \left| \frac{\delta p}{\rho} \right|_I \quad [117]$$

and

$$\left| \frac{\delta p}{p} \right|_{I+1} \leq \frac{p_I}{p_{I+1}} \left| \frac{\delta p}{p} \right|_I + 4(1 - p_I/p_{I+1}) \left| \frac{\delta r}{r} \right|_I \quad [118]$$

The expressions used are;

$$\Delta_I = 4 \left| \frac{\delta r}{r} \right|_{I+1} + \left| \frac{K_{pI+1}}{1 + K_I/K_{I+1} (Q_{mI}/Q_{mI+1})} \right| \left| \frac{\delta p}{\rho} \right|_{I+1} + \left| \frac{K_{TI+1}}{1 + K_I/K_{I+1} (Q_{mI}/Q_{mI+1})} - \frac{4}{1 - T_I^4/T_{I+1}^4} \right| \left| \frac{\delta T}{T} \right|_{I+1} \quad [119]$$

$$\left| \frac{\delta p}{p} \right|_I = \frac{p_{I+1}}{p_I} \left| \frac{\delta p}{p} \right|_{I+1} + 4(1 - p_{I+1}/p_I) \left| \frac{\delta r}{r} \right|_{I+1} \quad [120]$$

$$\left| \frac{\delta T}{T} \right|_I = \left(\frac{p_e}{p} \right)_I \epsilon_{eos} + \frac{|\alpha_{pI}| |\delta p_I/p_I|}{(1 + 3(p_r/p)_I) |\alpha_{TI}|} + \frac{|\delta r_I| + |\Delta_I|}{|\alpha_{TI}|} \quad [121]$$

$$\left| \frac{\delta p}{\rho} \right|_I = \left(\frac{p_e}{p} \right)_I \epsilon_{eos} + \frac{(1 + 3(p_r/p)_I) |\delta T/T|_I + |\delta p/p|_I}{(1 - (p_r/p)_I)} \quad [122]$$

$$\left| \frac{\delta r}{r} \right|_I = \left(\frac{r_{I+1}}{r_I} \right)^3 \left| \frac{\delta r}{r} \right|_{I+1} + (1 - r_{I+1}/r_I) \frac{(1 + r_{I+1}/r_I + (r_{I+1}/r_I)^2)}{3} \left| \frac{\delta p}{\rho} \right|_{I+1} \quad [123]$$

$$\alpha_{TI} \equiv \frac{4}{1 - (T_{I+1}/T_I)^4} - \frac{K_{TI}}{1 + K_{I+1}/K_I (Q_{mI+1}/Q_{mI})} \quad \alpha_{pI} \equiv - \frac{K_{pI}}{1 + K_{I+1}/K_I (Q_{mI+1}/Q_{mI})}$$

N.B. δ_R^* is not the value from which the next correction to T_r is calculated but an extrapolated value given by $\delta_{R_r}^* = \delta_{R_r}^{(n)} \cdot (\delta_{R_r}^{(n-1)} / \delta_{R_r}^{(n-2)})^\gamma$, where γ is the order of the iterative method. For the Newton-/raphson method $\gamma = 2$. Since $(r_r / r_{r-1}) > 1$ equation [122] could be a dangerous source of errors.

These equations give upper limits to the errors and not the probable error. We can expect that the probable error will, if the errors are randomly distributed, be considerably smaller. If this is the case then we should combine them according to,

$$\left| \frac{\delta z}{z} \right|' = \sqrt{\left| \frac{\delta x}{x} \right|^2 + \left| \frac{\delta y}{y} \right|^2}$$

rather than,

$$\left| \frac{\delta z}{z} \right|' = \left| \frac{\delta x}{x} \right| + \left| \frac{\delta y}{y} \right|.$$

Clearly

$$\left| \frac{\delta z}{z} \right|' < \left| \frac{\delta z}{z} \right|.$$

This simple model for the accumulation of errors has been programmed. The data is presented in tables 5.1 + 2 and figs.5.1 - 6. It can be seen that;

- i. the errors increase as a power of the pressure p in the interior of the star.

ii. the upper bound error grows very much more rapidly than does the "statistical" error,

iii. the upper bound error is approximately proportional to the number of zones in the model, whilst the "statistical" error varies very nearly inversely with the number of zones. (see table 5.1 and figure 5.2),

iv. the errors decrease when the equation of state error, ϵ_{eos} , is decreased with ϵ_{eos} dictating the lower limit of the overall error just below the ionization zone from which the errors subsequently grow. (see table 5.2 and figure 5.3)

Whilst it is not clear whether or not an increase in the number of zones would improve the errors it is clear that a reduction in the upper limit on the equation of state errors would. Unfortunately the error on the equation of state cannot be improved without resorting to the widespread use of double precision variables, a measure which would more than double the required computing time. Whilst for the 5G RR Lyrae model the probable error is always reasonable it seems to become distressingly large at the base of an envelope constructed for $\log(L/L_{\odot}) = 3.5$ and $\log(T_{eff}) = 3.75$, and the upper limit error is ludicrously large. However it should be pointed out that the integration for an envelope would not be carried beyond $\log(p) = 14$ for a pulsation calculation.

Table 5.1

Variation of the Errors at the Envelope Base with the Number of Mass Zones

No. of zones(N)	$ \delta T/T $	$ \delta T/T $
60	0.381	$3.55 \cdot 10^{-4}$
136	1.166	$1.43 \cdot 10^{-4}$
259	1.852	$7.24 \cdot 10^{-5}$

$$N \cdot |\delta T/T|_{\text{stat}} \approx 2 \cdot 10^{-2}$$

$$(1/N) \cdot |\delta T/T|_{\text{nb}} \approx 7 \cdot 10^{-3}$$

Table 5.2

Variation of the Errors at the Envelope Base with the Equation of State Error for a 5G Model

ϵ_{eos}	$ \delta T/T $
$2 \cdot 10^{-6}$	$1.93 \cdot 10^{-4}$
$2 \cdot 10^{-7}$	$1.93 \cdot 10^{-5}$
$2 \cdot 10^{-10}$	$4.36 \cdot 10^{-7}$

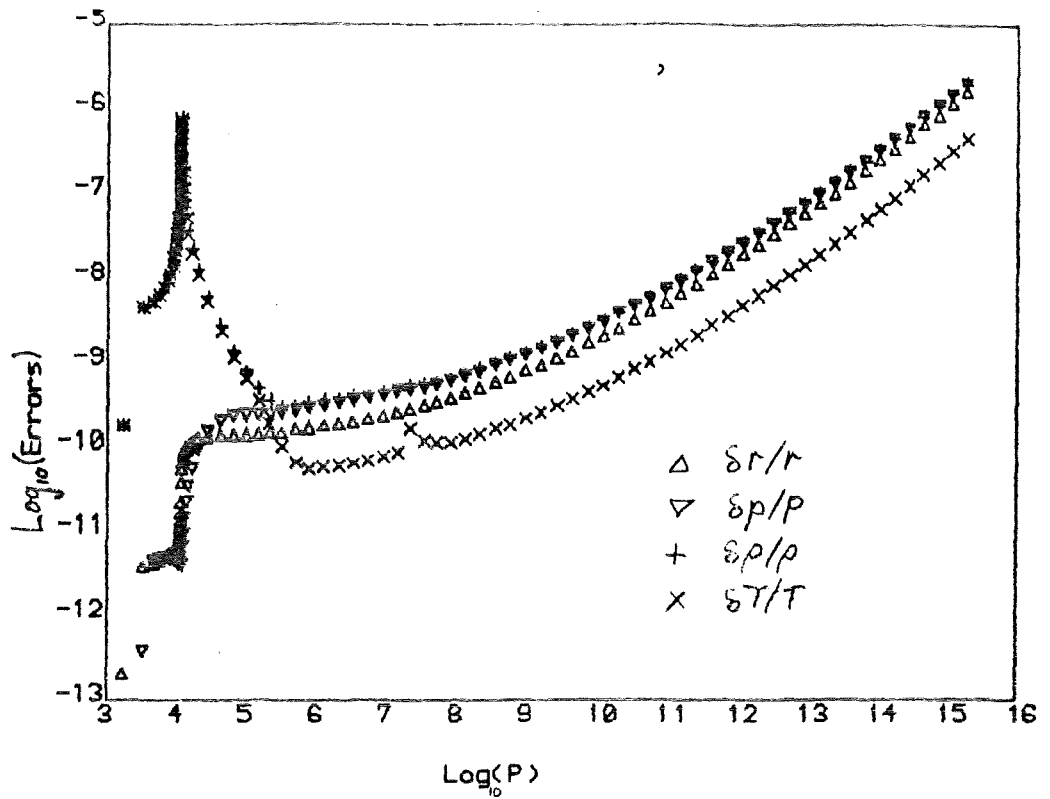


Fig. 5.1 "Statistical" errors for a 5G ($Z = 0$) model, with $\xi_{eos} = 2 \cdot 10^{-10}$ (i.e. $M/M_{\odot} = 0.58$, $T_{eff} = 6500K.$, $L/L_{\odot} = 38.5$, $X = 0.7$, $Y = 0.3$)

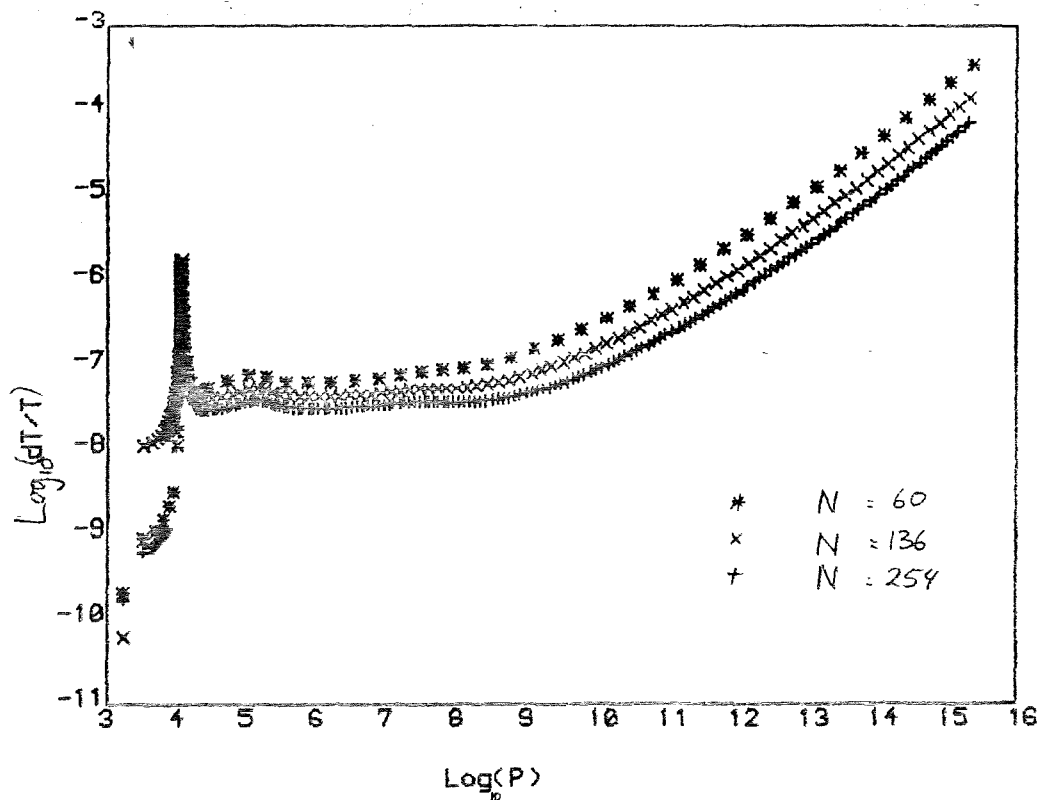


Fig. 5.2 The effects of changing the number of zones upon the "statistical" errors for the 5G model with $\xi_{eos} = 2 \cdot 10^{-6}$.

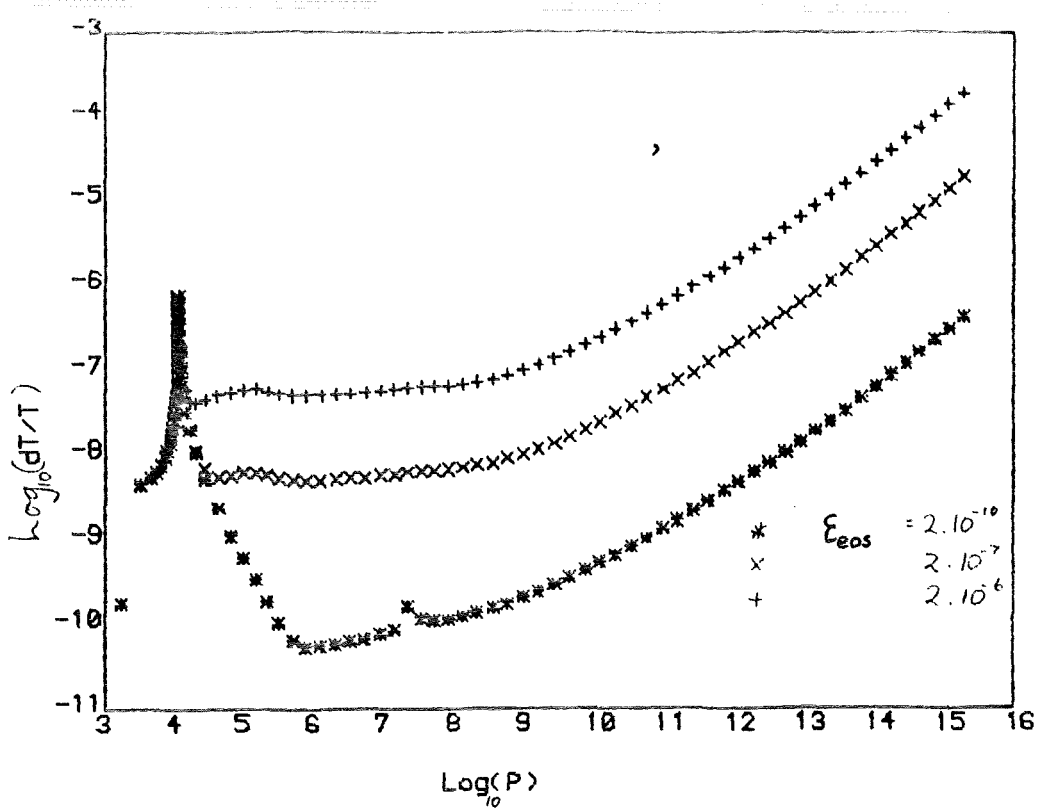


Fig. 5.3 The effects of changing ϵ_{eos} upon the "statistical" error for the temperature.

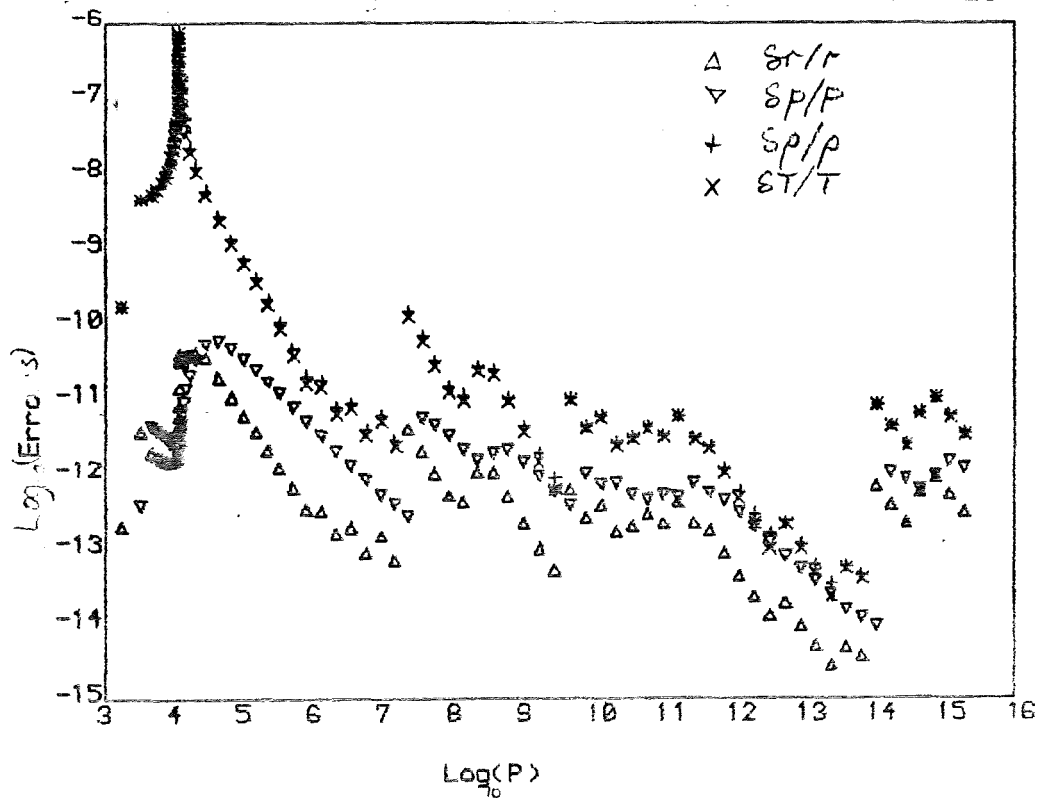


Fig. 5.4 "Statistical" errors for the 5G model when the $(r_{\text{ext}}/r_{\text{int}})^3$ term has been removed from the equation for the density errors.

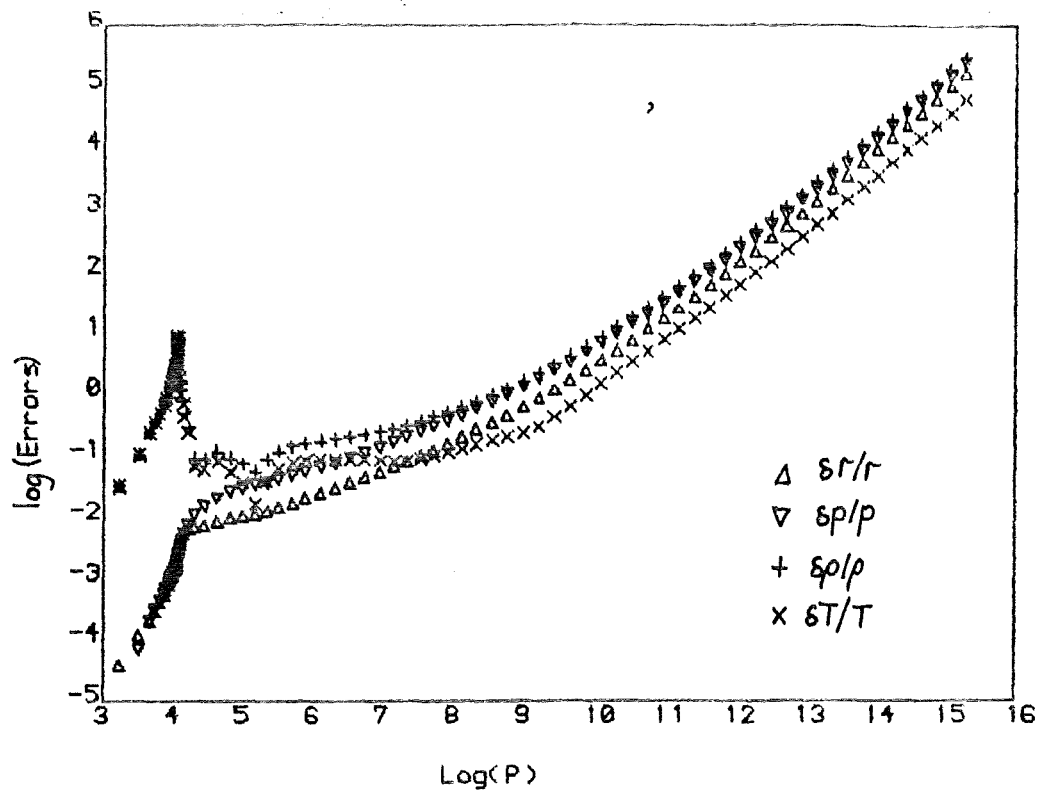


Fig. 5.5 Upper limit errors for the 5G model with the extrapolation of the local errors suppressed, $\epsilon_{eos} = 2 \cdot 10^{-6}$.

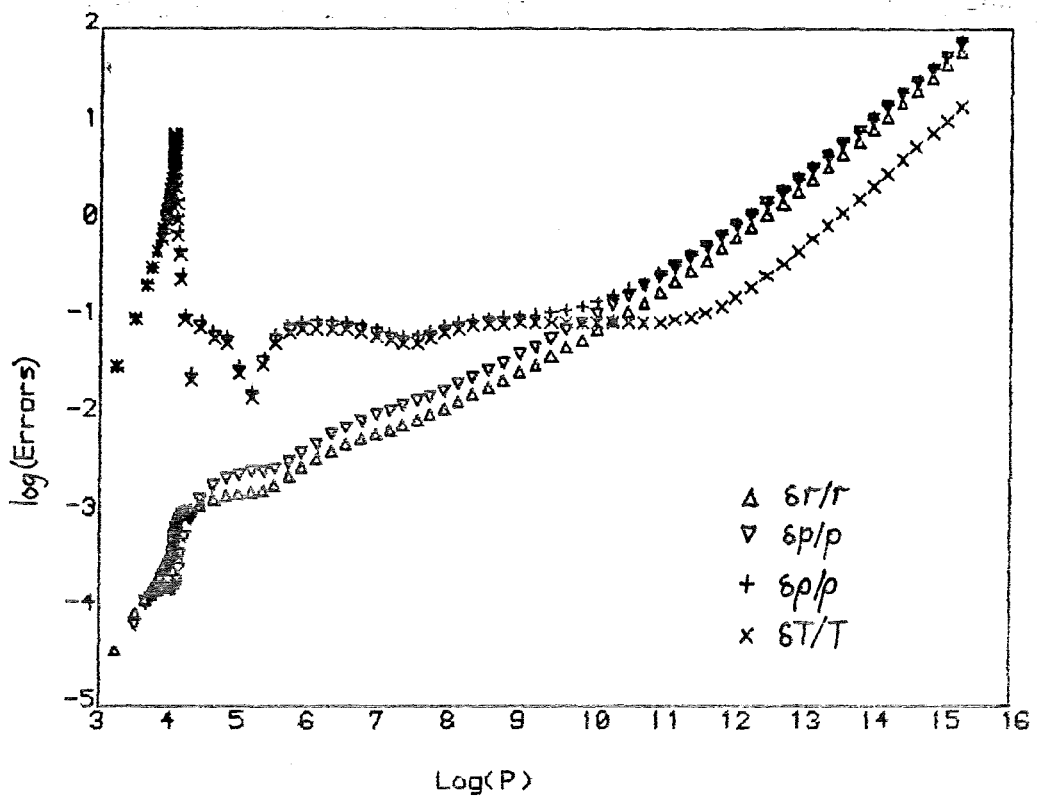


Fig. 5.6 "Statistical" errors for the 5G model with the extrapolation of the local errors suppressed, $\epsilon_{eos} = 2 \cdot 10^{-6}$.

This rapid growth of the error is brought about by the $(r_i/r_{i-1})^3$ term in equation [122]. We can rearrange this to give us

$$\left| \frac{\delta r}{r} \right|_{i-1} \leq \left(\frac{r_N}{r_{i-1}} \right)^3 \left| \frac{\delta r}{r} \right|_N + \sum_{j=i}^N (r_j/r_{j-1}) \frac{(1+r_j/r_{j-1} + (r_j/r_{j-1})^2)}{3} \left| \frac{\delta \rho}{\rho} \right|_j$$

Since (r_N/r_{i-1}) can be as large as 100 (even larger for some very luminous stars) it is not difficult to see how such a large increase in error can arise. Recomputing the errors with this and other terms removed in turn confirms this, as can be seen from a comparison of figs. 5.1 and 5.4.

The difference between the "statistical" and upper-bound errors can be seen by comparing figs. 5.5 and 5.6. Since the data for these figures is computed using the last applied correction rather than the next expected correction the reduction of the errors by the final step of the iteration can be seen by comparing figs. 5.1 and 5.6. If this simple error calculation can be trusted then it would seem to lay rather stringent limits on the depth of a stellar envelope. Unfortunately it has proved necessary to set the lower boundary rather deeper than this limit in order that the approximation $X = 0$ be satisfied. However since the pulsation amplitude is very small in this part of a star it is to be hoped that the errors incurred will be negligible. However I suspect that even for the probable error calculation I am overestimating the error.

The logical and desirable step now would be to calculate the effect these errors have upon the pulsation eigenvalues, and eigenvectors. This turns out to be an insurmountable task. If we consider the adiabatic problem,

$$\omega^2 \underline{X} = \underline{G} \underline{X},$$

then using the orthogonality of the eigen-vectors it can be shown, e.g. Wilkinson (1956), that,

$$\delta(\omega_j^2) = \frac{\underline{X}_j^+ \delta \underline{G} \underline{X}_j}{\underline{X}_j^+ \underline{X}_j}.$$

Here $\delta \underline{G}$ is the perturbation on \underline{G} . The derivation of this formula hinges upon our ability to write $\delta \underline{X}_j = \sum_{j \neq k} \epsilon_{jk} \underline{X}_k$ and then use the orthogonality property to eliminate the ϵ_{jk} s. If we calculate $\delta \underline{G}$ using our values for the errors obtained above then we find that,

$$\frac{\delta(\omega_j^2)}{\omega_j^2} \ll \omega^{-5}$$

for most cases and never greater than $5 \cdot 10^{-5}$. This is reassuring.

However, consider now the nonadiabatic case in which ω becomes complex. $\text{Im}(\omega)/\text{Re}(\omega)$ is typically rather small. We calculate ω as a root of a polynomial (or to be more exact a rational function) and so it is perhaps instructive to look at the following simple analogy. Consider

$$\omega^2 + b\omega + c = 0$$

where

$$b^2 - 4c < 0 \text{ and } |1 - 4c/b^2| \ll 1.$$

So $\text{Im}(\omega)/\text{Re}(\omega) \ll 1$. Now look at the effect of a small change on b or c ,

$$\frac{\partial \omega_{\pm}}{\partial b} = \frac{1}{2} \left(-1 \mp \frac{ib}{\sqrt{|b^2 - 4c|}} \right).$$

So

$$\delta \omega_{\pm} = \frac{1}{2} \left(-1 \mp \frac{ib}{\sqrt{|b^2 - 4c|}} \right) \delta b$$

and

$$\left| \frac{\text{Im}(\delta \omega_{\pm})}{\text{Re}(\delta \omega_{\pm})} \right| = \frac{b}{\sqrt{|b^2 - 4c|}} \gg 1.$$

In fact

$$\frac{|\text{Im}(\delta \omega_{\pm})/\text{Im}(\omega_{\pm})|}{|\text{Re}(\delta \omega_{\pm})/\text{Re}(\omega_{\pm})|} = \left(\frac{b}{\sqrt{|b^2 - 4c|}} \right)^2$$

and so it might be dangerous to assume that the error on the adiabatic period represents the error on the nonadiabatic complex frequency.

We look now at the matrix form of the linear pulsation equations i.e. equations [29,30]. If the difference equations are not satisfied exactly we will have,

$$\begin{aligned} \omega'^2 \underline{X}' &= \underline{G1}' \underline{X}' + \underline{G2}' \underline{Y}' \\ i\omega' \underline{Y}' &= \underline{K1}' \underline{X}' + \underline{K2}' \underline{Y}' \end{aligned} \quad [124]$$

The ' indicates that these quantities are all perturbed from the true values.

Now the problem to be solved revolves around the errors on the matrices $\underline{G1}$, $\underline{G2}$, $\underline{K1}$, $\underline{K2}$. We write $\underline{G1}'$ etc. in terms of a perturbation $\underline{\delta G1}$ and the "perfect" value $\underline{G1}$ which gives us expressions for the perturbations $\underline{\delta W/W}$, $\underline{\delta X}$ and $\underline{\delta Y}$,

$$(\omega_k^2 - \underline{G1})\underline{\delta X}_k - \underline{G2}\underline{\delta Y}_k = -2\omega_k^2 X_k \left(\frac{\underline{\delta W}}{W}\right)_k + \underline{\delta G1}X_k + \underline{\delta G2}Y_k \quad [125]$$

$$(i\omega_k - \underline{K2})\underline{\delta X}_k - \underline{K1}\underline{\delta Y}_k = -i\omega_k Y_k \left(\frac{\underline{\delta W}}{W}\right)_k + \underline{\delta G1}X_k + \underline{\delta K2}Y_k. \quad [126]$$

In principle, given the eigenvalue and eigenvectors together with $\underline{\delta G1}$ etc. we can set an element of $\underline{\delta X}$ to take the value zero and then solve for the rest of the perturbations. However we do not know $\underline{\delta G1}$ etc. but only upper bounds on each element. This means that the best we can do is to find an upper bound on $|\underline{\delta W/W}|$.

Eliminating $\underline{\delta Y}_k$ in [126], we get,

$$\begin{aligned} (\omega_k^2 - \underline{G1})\underline{\delta X}_k - \underline{G2}(i\omega_k - \underline{K2})^{-1}\underline{K1}\underline{\delta X}_k - \\ + \left(\frac{\underline{\delta W}}{W}\right)_k (2\omega_k^2 X_k + i\omega_k \underline{G2}(i\omega_k - \underline{K2})^{-1}Y_k) \\ = \underline{\delta G1}X_k + \underline{\delta G2}Y_k + \underline{G2}(i\omega_k - \underline{K2})^{-1}\underline{\delta K1}X_k \\ + \underline{G2}(i\omega_k - \underline{K2})^{-1}\underline{\delta K2}Y_k. \end{aligned} \quad [127]$$

In the adiabatic problem it is now possible, where the perturbations are small, to expand $\underline{\delta X}_k$ in terms of the eigen-vectors, since they form a complete set, that is,

$$\underline{\delta X}_k = \sum_{j \neq k} \epsilon_{kj} X_j$$

Since the adiabatic eigen-vectors are orthogonal the x -terms can be eliminated. For the nonadiabatic problem the eigenvectors are not

orthogonal and it is not known whether or not they comprise a complete set so little is gained by using them as the basis for an expansion of $\underline{\delta X}_k$.

However if the nonadiabaticity is small then we can write,

$$\underline{X}_k = \underline{X}_{ak} + \sum_{j \neq k} (\mathcal{U}_{jk} \underline{X}_{aj} + i \mathcal{V}_{jk} \underline{X}_{aj})$$

where \underline{X}_{aj} are adiabatic eigenvectors and $|\mathcal{U}_{jk}|, |\mathcal{V}_{jk}| \ll 1$, and,

$$\underline{\delta X}_k = \sum_{j \neq k} (\underline{\epsilon}_{jk} \underline{X}_{aj} + i \mathcal{M}_{jk} \underline{X}_{aj})$$

Premultiplying [127] by $\underline{X}_k^\dagger = \underline{X}_{ak}^\dagger + \sum_{j \neq k} (\mathcal{M}_{jk} \underline{X}_{aj}^\dagger - i \mathcal{V}_{jk} \underline{X}_{aj}^\dagger)$ it can be seen that all the $\underline{\delta X}_k$ terms are of the same order as $(|\mathcal{U}_{jk}| + |\mathcal{V}_{jk}|) \cdot (|\underline{\epsilon}_{jk}| + |\mathcal{M}_{jk}|)$ and so should be small with the exception of the terms in $\underline{X}_{ak}^\dagger$, i.e.,

$$\underline{X}_{ak}^\dagger (\omega_k^2 - \omega_{aj}^2) \underline{X}_{aj} = (\omega_k^2 - \omega_{aj}^2) \underline{\epsilon}_{jk} |\underline{X}_{ak}|^2$$

The only nonzero term is $(\omega_k^2 - \omega_{ak}^2) |\underline{X}_{ak}|^2$ which is also small. The second term is more of a problem, i.e.,

$$\underline{X}_{ak}^\dagger \underline{G}_2 (i\omega_k - \underline{k}_2)^{-1} \underline{k}_1 \underline{X}_{aj}$$

Now,

$$(\omega_k^2 - \omega_{ak}^2) |\underline{X}_{ak}|^2 \approx \underline{X}_{ak}^\dagger \underline{G}_2 (i\omega_{ak} - \underline{k}_2)^{-1} \underline{k}_1 \underline{X}_{ak},$$

so it seems likely that this term is also of the same magnitude as the nonadiabatic terms. So I think it reasonable to estimate an upper bound for $|\delta\omega/\omega|$ using,

$$\begin{aligned} & \left| \frac{\delta\omega}{\omega} \right|_k \left[2\omega_k^2 |\underline{X}_k|^2 + i\omega_k \underline{X}_{ak}^\dagger \underline{G}_2 (i\omega_k - \underline{k}_2)^{-1} \underline{Y}_k \right] \\ & \approx \left| \underline{X}_k \underline{\epsilon G}_1 \underline{X}_k + \underline{X}_k^\dagger \underline{\epsilon G}_2 \underline{Y}_k + \underline{X}_k^\dagger \underline{G}_2 (i\omega_k - \underline{k}_2)^{-1} (\underline{\epsilon k}_1 \underline{X}_k + \underline{\epsilon k}_2 \underline{Y}_k) \right|. \end{aligned} \quad [130]$$

However since we can expect $|\delta\omega|$ to be dominated by $\text{Re}(\delta\omega)$ it is unlikely that any information regarding the reliability of $\text{Im}(\delta\omega)$ can be obtained in this way, although it seems likely that the total error should still be of the order of that on the adiabatic period.

It is possible to gain some idea of the error by directly applying numerical perturbations. The method chosen was to generate numbers, δ , randomly distributed over the range $(-\xi, \xi]$ and adding them to either the relevant physical variables according to $x = x(1 + \delta)$ before the matrices \underline{G}_1 etc. were calculated, or directly to the matrices themselves. $\xi = 10^{-3}$ was chosen for a set of calculations. Case 1 refers to the former option and Case 2 to the latter. A further possibility, Case 3, involves choosing ξ to be the error given by the equations [119-123]. The results are given in tables 5.3 - 4. The results seem to confirm quantitatively the conclusions drawn from the naive treatment of the errors given earlier. That is, perturbations of the physical variables in the static model seem to produce a small and manageable perturbation in the eigenvalues. The large difference between the perturbations for Cases 1+2 seems to imply that the matrix elements themselves are insensitive to perturbations of the physical variables. Whilst it is conceivable that the matrix elements are constructed from combinations of the physical variable which can be calculated exactly or with only a local error (that is, no accumulation from preceding zone calculations) I cannot prove this, and indeed it seems a little unlikely. However

Table 5.3

$M/M_{\odot} = 0.58, T_{\text{eff}} = 6500, L/L_{\odot} = 38.5, X = 0.7, Z = 0.0, \text{Christy Opacity}$

	P_0	η_0	$ \delta P/P $	$ \delta \eta/\eta $
Reference	0.5367	0.1636	-	-
Case 1	0.5368 +0.0004	0.01637 +0.0001	$8 \cdot 10^{-4}$	$7 \cdot 10^{-3}$
Case 2	0.5274 +0.004	0.011 +0.04	$8 \cdot 10^{-3}$	~ 1
Case 3	0.5367	0.01636	$7 \cdot 10^{-8}$	$6 \cdot 10^{-5}$

Table 5.4

$M/M_{\odot} = 0.6, T_{\text{eff}} = 10^{3.75}, L/L_{\odot} = 10^{3.5}, X = 0.745, Z = 0.25, \text{Carson Opacity}$

	P_0	η_0	$ \delta P/P $	$ \delta \eta/\eta $
Reference	37.1597	1.244	-	-
Case 1	37.1428	1.249	$5 \cdot 10^{-4}$	$4 \cdot 10^{-3}$
Case 2	23.3552	1.157	$5 \cdot 10^{-1}$	$8 \cdot 10^{-2}$
Case 3	37.1560	1.247	$8 \cdot 10^{-6}$	$2 \cdot 10^{-3}$

For cases 1+2, $\xi = 10^{-3}$

since this treatment of the errors seems unlikely to produce any solid results it seems pointless to spend any further time on it.

5.2 PHYSICAL PERTURBATIONS

A problem related to the calculation of errors is that of calculating the effect a perturbation of some input function has upon the structure of the star and then on the pulsation characteristics. Since the physics that is needed to calculate the structure of stars is still fairly uncertain this could be of importance. In particular, for nondegenerate stellar envelopes, the opacity is still not known to a tolerance better than 10%. The most usual method used to study the effects of different opacity calculations is simply to compute models using each possible set of data. This is clumsy and can only give a small part of the information which should be present and which could point the way to those parts of the (ρ, T) plane for which improvements in the opacity calculations are most urgent. Whilst it is possible to study simplified equations in order to determine just what effect some change in the opacity at a particular point has upon the pulsation it is not possible to see how changes distributed throughout the envelopes accumulate to produce an effect. What is needed is some sort of derivative of the relevant physical variables with respect to the function in question, (here the opacity). This has been attempted for the stellar structure problem by Refsdal and Stabell (1972) using a fairly crude numerical perturbation method in order to discover the

effects of uncertainties in the opacity upon Horizontal Branch models. A very much more sophisticated, general method has been developed by Epstein et. al. (1983) involving the calculation of functional derivatives of the various physical variables. They apply this theory to a study of opacity uncertainties in neutron star models.

Consider now the effect of a small perturbation $\Delta K(\rho, T)$ upon the opacity $K(\rho, T)$ at a given point,

$$\tilde{K}(\tilde{\rho}, \tilde{T}) \equiv K(\rho, T) + \Delta K(\rho, T)$$

since the physical variables will also be perturbed. If these perturbations are also small,

$$\tilde{K}(\tilde{\rho}, \tilde{T}) = K(\rho, T) \left(1 + K_{\rho} \frac{\delta \rho}{\rho} + K_T \frac{\delta T}{T} \right) + \Delta K(\rho, T)$$

if $\delta K(\rho, T) \equiv \tilde{K}(\tilde{\rho}, \tilde{T}) - K(\rho, T),$

$$\frac{\delta K}{K} = K_{\rho} \frac{\delta \rho}{\rho} + K_T \frac{\delta T}{T} + \frac{\Delta K}{K},$$

where

$$K_{\rho} \equiv \left(\frac{\partial \log K}{\partial \log \rho} \right)_T, \quad K_T \equiv \left(\frac{\partial \log K}{\partial \log T} \right)_{\rho}$$

We now perturb the difference equations for stellar structure,

$$\rho_I \left(\frac{\delta \rho}{\rho} \right)_I - \rho_{I-1} \left(\frac{\delta \rho}{\rho} \right)_{I-1} = 4(\rho_I - \rho_{I-1}) \left(\frac{\delta r}{r} \right)_I \quad [131]$$

$$r_{I-1}^3 \left(\frac{\delta r}{r} \right)_{I-1} - r_I^3 \left(\frac{\delta r}{r} \right)_I = \frac{1}{3} (r_I^2 + r_I r_{I-1} + r_{I-1}^2) (r_I - r_{I-1}) \left(\frac{\delta \rho}{\rho} \right)_{I-1} \quad [132]$$

$$\begin{aligned} & 4 \left(\frac{\delta r}{r} \right)_I + \left(\frac{4 T_I^4}{T_{I-1}^4 - T_I^4} - \frac{K_{I-1} \kappa_{mlI} K_{I-1}}{K_I \kappa_{mlI-1} + K_I \kappa_{mlI}} \right) \left(\frac{\delta T}{T} \right)_{I-1} - \frac{K_{I-1} \kappa_{mlI-1} K_{I-1}}{K_I \kappa_{mlI-1} + K_I \kappa_{mlI}} \left(\frac{\delta \rho}{\rho} \right)_{I-1} \\ & + \left(\frac{4 T_I^4}{T_I^4 - T_{I-1}^4} - \frac{K_I \kappa_{mlI} K_{I-1}}{K_I \kappa_{mlI-1} + K_I \kappa_{mlI}} \right) \left(\frac{\delta T}{T} \right)_I - \frac{K_I \kappa_{mlI} K_{I-1}}{K_I \kappa_{mlI-1} + K_I \kappa_{mlI}} \left(\frac{\delta \rho}{\rho} \right)_I \quad [133] \\ & = \frac{K_{I-1} \kappa_{mlI-1}}{K_I \kappa_{mlI-1} + K_I \kappa_{mlI}} \left(\frac{\Delta K}{K} \right)_{I-1} - \frac{K_I \kappa_{mlI}}{K_I \kappa_{mlI-1} + K_I \kappa_{mlI}} \left(\frac{\Delta K}{K} \right)_I \end{aligned}$$

and,

$$\left(\frac{\delta p}{\rho}\right)_I = \chi_{\rho I} \left(\frac{\delta p}{\rho}\right)_I + \chi_{T I} \left(\frac{\delta T}{T}\right)_I \quad [134]$$

r_N is a boundary condition and so $(\delta r/r)_N = 0$. Thus we have to find $(\delta r/r)_I$, $(\delta p/p)_I$, $(\delta T/T)_I$, and $(\delta \rho/\rho)_I$ for $I = 1, N-1$. We can write these equations in a convenient matrix form,

$$\left(\frac{\delta r}{r}\right) = \underline{A} \left(\frac{\delta p}{\rho}\right) \quad [135]$$

$$\left(\frac{\delta p}{\rho}\right) = \underline{B} \left(\frac{\delta r}{r}\right) \quad [136]$$

$$4 \left(\frac{\delta r}{r}\right) + \underline{C} \left(\frac{\delta T}{T}\right) + \underline{D} \left(\frac{\delta p}{\rho}\right) = \underline{E} \left(\frac{\Delta \kappa}{\kappa}\right) \quad [137]$$

and

$$\left(\frac{\delta p}{\rho}\right) = \underline{\chi}_{\rho} \left(\frac{\delta p}{\rho}\right) + \underline{\chi}_{T} \left(\frac{\delta T}{T}\right). \quad [138]$$

Solving for $(\delta T/T)$ we find,

$$\left((4\underline{I} + \underline{D}\underline{B})\underline{A}(\underline{I} - \underline{\chi}_{\rho}\underline{B}\underline{A})^{-1}\underline{\chi}_{T} + \underline{C} \right) \left(\frac{\delta T}{T}\right) = \underline{E} \left(\frac{\Delta \kappa}{\kappa}\right) \quad [139]$$

The sensitivity of (T) , and of course all the other variables, is contained in the matrix, ^{to variations in κ}

$$\left((4\underline{I} + \underline{D}\underline{B})\underline{A}(\underline{I} - \underline{\chi}_{\rho}\underline{B}\underline{A})^{-1}\underline{\chi}_{T} + \underline{C} \right)^{-1} \underline{E}.$$

As is expected this is an upper triangular matrix, and this is characteristic of an initial value problem. This matrix is analogous to the functions calculated by Epstein et al. and the form of the matrix is essentially the same as that of the step functions found in that work. This matrix approach can be generalized to the full general boundary value problem, however that will not be attempted

here.

The matrix can most easily be calculated for each zone of the stellar model in the following manner. Define:

$$\begin{aligned} t_I &\equiv (\delta T/T)_{N-I+1} \\ d_I &\equiv (\delta \rho/\rho)_{N-I+1} \\ \pi_I &\equiv (\delta P/P)_{N-I+1} \\ \kappa_I &\equiv (\delta v/v)_{N-I+1} \\ h_I &\equiv (\Delta K/K)_{N-I+1} . \end{aligned}$$

Equations [135-138] can now be written for the I^k zone,

$$\pi_I = MP_I \pi_{I-1} + MR_I \kappa_{I-1} \quad [142]$$

$$\kappa_I = CR_I \kappa_{I-1} + CW_I d_I \quad [143]$$

$$\begin{aligned} 4\kappa_{I-1} + RT1_I t_{I-1} + RT2_I t_I + RW1_I d_{I-1} + RW2_I d_I \\ = RK1_I h_{I-1} + RK2_I h_I \end{aligned} \quad [144]$$

and

$$\pi_I = ET_I t_I + EW_I d_I . \quad [145]$$

Where all the quantities for zone $I-1$ are known. Substituting for

[145] in [128] and solving for t_I and d_I we get, e.g.

$$\begin{aligned} t_I = [EW_I (-4\kappa_{I-1} - RT1_I t_{I-1} - RW1_I d_{I-1} + RK1_I h_{I-1} + RK2_I h_I) \\ - RT2_I (MP_I \pi_{I-1} + MR_I \kappa_{I-1})] / [RT2_I EW_I - RW2_I ET_I] \end{aligned} \quad [146]$$

Now we define the vectors carrying the functional derivatives for each zone,

$$\begin{aligned} \zeta_I &\equiv (\underline{KT}_I^T) \underline{k}, \\ \alpha_I &\equiv (\underline{KD}_I^T) \underline{k}, \\ \chi_I &\equiv (\underline{KR}_I^T) \underline{k}, \end{aligned} \quad [147]$$

and,
$$\pi_I \equiv (\underline{KP}_I^T) \underline{k}.$$

The vectors for the I^{th} zone contain I nonzero elements and N-I-1 zeros. The elements are easily calculated, e.g. for J = 1, I-2

$$\begin{aligned} [\underline{KT}_I^T]_J &= (-E D_I R T_{I-1} [\underline{KT}_{I-1}^T] - E T_I R D_{I-1} [\underline{KD}_{I-1}^T] - R D_{I-2} M P_I [\underline{KP}_{I-1}^T])_J \\ &\quad - (4 E D_I + R D_{I-2} M R_I) [\underline{KR}_{I-1}^T]_J / (R T_{I-2} E D_I - R D_{I-2} E T_I), \end{aligned} \quad [48a]$$

$$\begin{aligned} [\underline{KT}_I^T]_{I-1} &= (-E D_I R T_{I-1} [\underline{KT}_{I-1}^T]_{I-1} - E T_I R D_{I-1} [\underline{KD}_{I-1}^T]_{I-1} - R D_{I-2} M R_I [\underline{KP}_{I-1}^T]_{I-1} \\ &\quad - (4 E D_I + R D_{I-2} M R_I) [\underline{KR}_{I-1}^T]_{I-1} + E D_I R K_{I-1}) \\ &\quad / (R T_{I-2} E D_I - R D_{I-2} E T_I), \end{aligned} \quad [48b]$$

and

$$[\underline{KT}_I^T]_I = E D_I R K_{I-1} / (R T_{I-2} E D_I - R D_{I-2} E T_I). \quad [48c]$$

The vectors for the density derivative are calculated in an identical way and from this the radius vectors are easily obtained using [143], for J = 1, I,

$$[\underline{KR}_I^T]_J = C R_I [\underline{KR}_{I-1}^T]_J + C D_I [\underline{KD}_I^T]_J. \quad [49]$$

We can complete the calculation by using [145] to find \underline{KP}_I . For

$J = 1, I,$

$$[kP^T]_J = ET_I[kT^T]_J + EW_J[kD^T]_J. \quad [150]$$

This is all straightforward and not at all difficult: the problem lies in the amount of storage and the time that this requires since both are proportional to $N.(N-1)/2$.

We must now look at the perturbed pulsation equations,

$$2\omega^2 X \left(\frac{\delta\omega}{\omega} \right) + (\omega^2 - G_1) \delta X - G_2 \delta Y = \delta G_1 X + \delta G_2 Y \quad [151]$$

and

$$i\omega Y \left(\frac{\delta\omega}{\omega} \right) + (i\omega - K_2) \delta Y - K_1 \delta X = \delta K_1 X + \delta K_2 Y. \quad [152]$$

Again δX_N and $\delta X_1 = 0$, and so we have $2.(N-1)$ equations for the $N-2$ unknown δX_I s, $N-1$ unknown δY_I s and $\delta\omega/\omega$. This system is easily solved by a method similar to that used for the pulsation problem itself. That is, we define Z such that,

$$Z_{2I-1} \equiv Y_I$$

$$Z_{2I} \equiv X_{I+1}$$

for $I = 1, N-1$, and likewise δZ except that,

$$\delta Z_{2N-2} \equiv X_N \frac{\delta\omega}{\omega}.$$

Defining matrices \underline{H} , to contain the coefficients of $\underline{\delta Z}$, and $\underline{\Delta}$ containing the right hand side of [151,152] we have,

$$\underline{H} \underline{\delta Z} = \underline{\Delta}.$$

\underline{H} has diagonals and a single full column \underline{H}' consisting of,

$$H'_{2I-1} = i\omega Y_I / X_N \quad \text{and} \quad H'_{2I} = 2\omega^2 X_I / X_N, \quad \text{for } I = 1, N-1.$$

If we expand $\underline{\Delta}$ as,

$$\underline{\Delta} = \underline{K} \underline{k} + \underline{K}_\tau \underline{k}_\tau + \underline{K}_\rho \underline{k}_\rho$$

where \underline{K} is a matrix of $N-1$ columns and $2N-1$ rows, then it is clear that all we need do is to calculate \underline{H}^{-1} in order to find the dependence of the pulsation upon changes to the opacity (or for that matter any other input function). In particular if, as seems likely, we require only $\delta\omega/\omega$ then we need only calculate the $2.(N-1)^{th}$ row of $(\underline{H})^{-1}$ or, better, the $2.(N-1)^{th}$ column of $(\underline{H}^T)^{-1}$. This is easily done using a very slightly modified Gaussian elimination algorithm, yielding a vector containing the required information for $\delta\omega/\omega$. Calculating these vectors for a number of modes permits the examination of not only the dependence of pulsation periods and growth rates but also of the resonance locations etc.

These calculations have not yet been performed but it is intended that they will be done when time permits.

CHAPTER 6
THE PRESENT STATUS OF THE RV TAURI STARS

6.1 OBSERVATIONS OF RV TAURI STARS AND THEIR RELATIONS.

The most obvious ⁿad critical property of a RV Tauri variable is a light curve which shows minima of alternating depth. For some stars, e.g. AC Her, this alternation and the depths of the minima is very regular whilst for others the minima interchange more or less frequently so that for some extreme cases, e.g. DF Cyg, the alternation is little more than statistical. As well as the alternation the depths of the minima can also be highly variable and very deep minima can sometimes occur as for example for R Sct in 1983 (Howell et al. 1983). Formal periods for the RV Tau (or RV class) stars defined as the time elapsed between successive deep minima lie between about 30 and 100 days. However there is strong evidence suggesting that the time interval between two consecutive minima regardless of the depth is the more physically significant period. This shorter period, taken to be one half the formal period, will be used from here on.

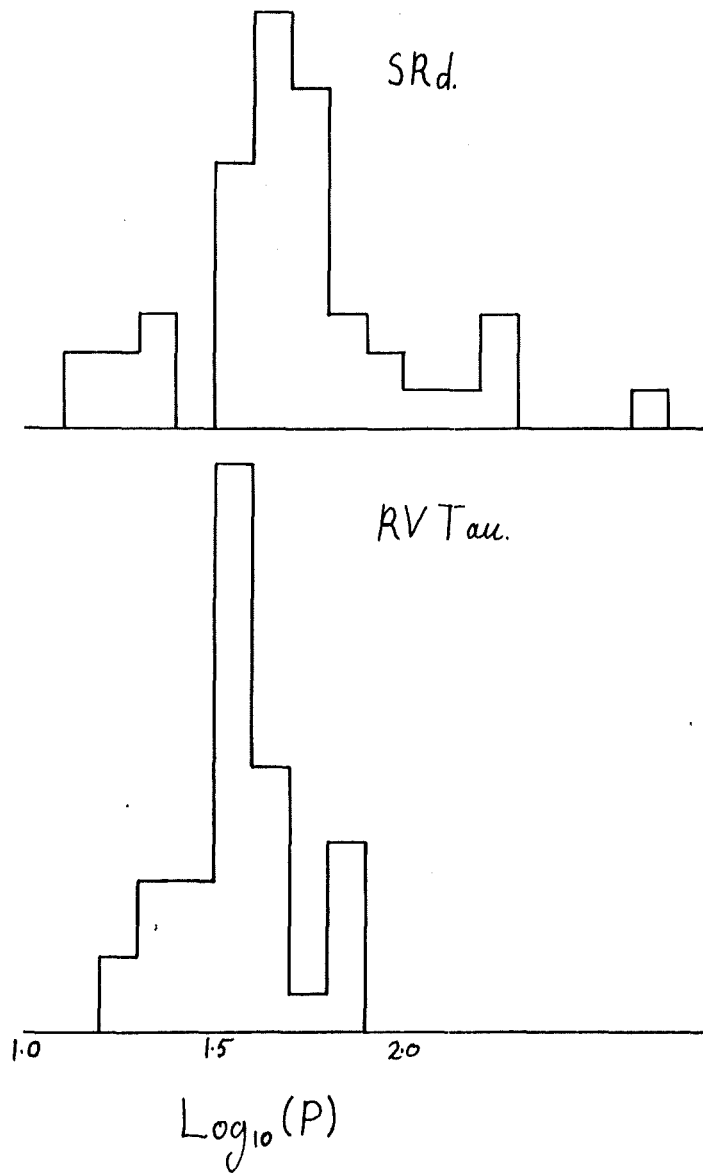


Fig. 6.1. Period - frequency histograms for field RV and SRd stars with spectra taken from Kukarkin (1969a - 1976).

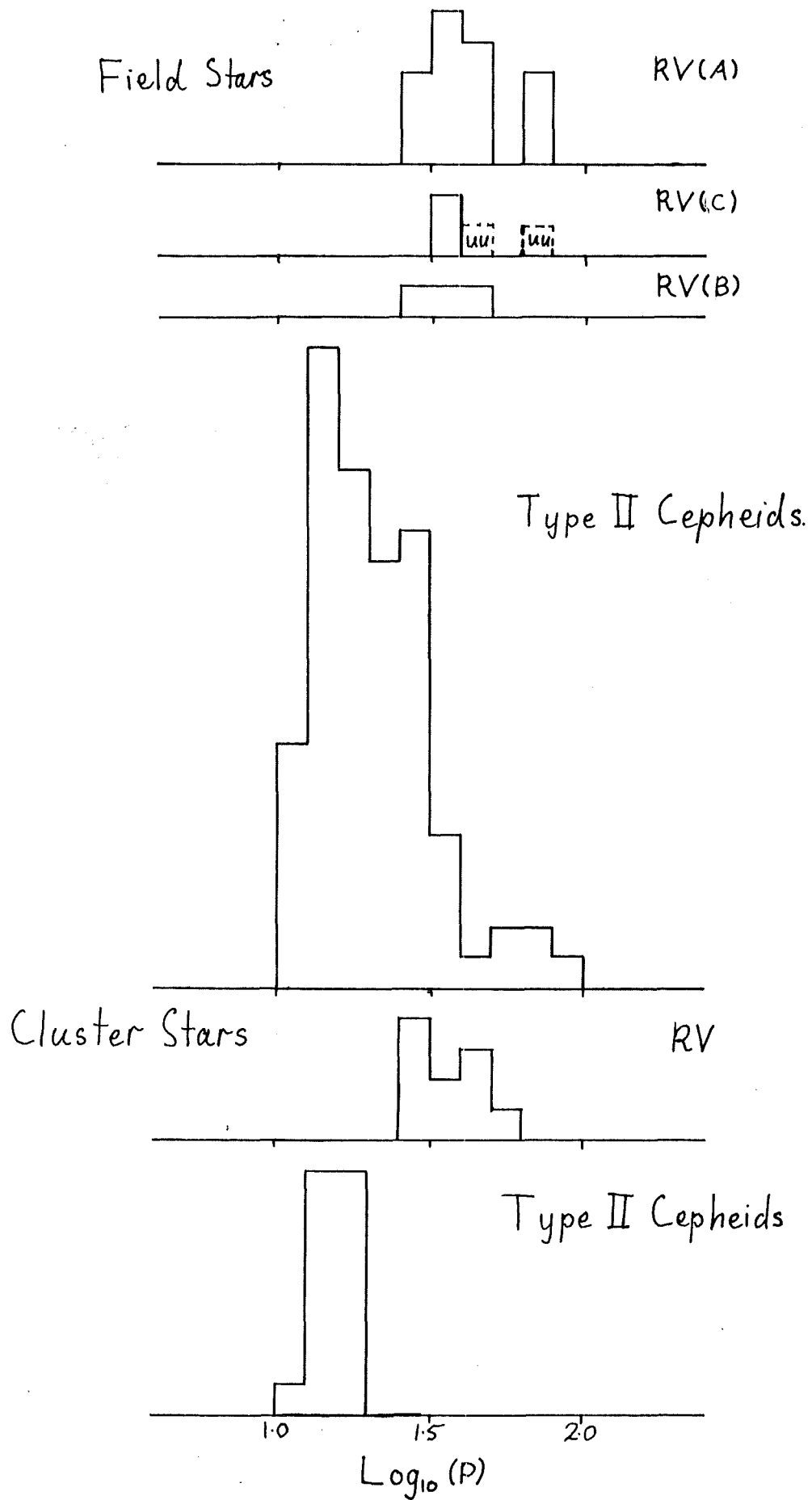


Fig. 6.2 Period - frequency histograms for Dawson's (1979) field RV samples and Harris's (1984) type II cepheids.

Table 6.1

CW, RV and SRd stars in the G.C.V.S.

	Vol. 1+2	Supp. 1	Supp. 2	Supp. 3	Total
CW +CW?	96	7	3	1	107
CW	80	4	1	1	86
RV + RV?	104	1	3	1	108
RV	77	1	0	0	78
RV (F-K)	35	0	3	0	38
SRd + SRd?	47	0	3	3	53
SRd	45	0	2	0	47
SRd (F-K)	40	0	1	0	41

One piece of evidence supporting the shorter period is the tendency of certain longer period W Vir (or CW) stars to exhibit minima of alternating depth (Erleksova 1970) of which the best example is SZ Mon for which this behaviour had been found by Stobie (1970) and Lloyd-Evans (1970). Also what velocity curves there are for RV stars suggest a variation on the shorter rather than the formal period. The first piece of evidence suggests a connection between these two classes of stars and when other properties are taken into consideration it seems that the RV stars form an extension of the CW stars to longer periods. This sequence is further extended by the inclusion of the yellow semi-regular variables or SRd stars, again with the shorter period. This latter group shares the RV Tauri phenomenon even though the shallower minimum is usually little more than a still-stand at rising light or, frequently, absent. Periods for the SRd stars tend to be more unstable than for the RV stars but the amplitudes are more stable.

There is one RV star, UU Her, which according to Payne - Gaposhkin, Brenton and Gaposhkin (1943) exhibits two modes of pulsation. They identify a 91 day RV - like mode and a 70 day Cepheid - like mode which appear alternately. However there are at least three portions of the light curve (JD 21360 - 21550, JD 25700 - 25900, and JD 29650 - 29900) to which I would prefer to assign a period of about 45 days. This seems to imply that the RV behaviour here is associated with an overtone pulsation (presumably

the first overtone) and also reinforces the argument that the correct period to associate with the formal RV period is twice that of a pulsation mode. The evidence for the RV/W Vir stars in the globular clusters implies that in the majority of cases the fundamental mode gives rise to the RV pulsations. Since UU Her is the only RV star to show a clear double mode behaviour (it is possible that SU Gem might be the only other such star) it seems reasonable to assume for the moment that the fundamental mode is the correct one to use in association with the RV stars. In the figures which follow UU Her is shown with both periods.

It seems, then, that these three classes of stars could be closely related and so a comparison of their properties should be important.

In a review of the RV stars Stothers (1963) shows that their periods are not evenly distributed over the range. This can be seen clearly from figs. 6.1 + 6.2. (UU Her, denoted "UU", is shown with both the possible periods.) The first figure shows the period distribution for all those RV and SRd stars found in the General Catalogue of Variable Stars (G.C.V.S.) (Kukarkin et al. (1969a, 1969b, 1971, 1974, 1976)) with spectra in the range F-K. This range of spectra encompasses all the well observed stars in these classes and is used as a criterion for removing stars which have superficially similar light curves, e.g. SRa,b,c stars, but which are different in

other respects. This greatly reduces the number of RV stars but has little effect upon the samples of SRd and CW stars. (Table 6.1 contains the relevant data.) Even then it is not at all certain that all the stars are correctly classified since, most importantly, the distinction between the RV and SRd stars is not clear. The period-frequency distributions for all three classes of star show strong main peaks. Secondary peaks for the RV and CW stars also seem to be real. Taking smaller but more certain samples of RV and SRd stars from Dawson's (1979) photometric study gives part of fig. 6.2. Similar data for the few known RV and SRd stars found in globular clusters selected from Stothers (1963), Rosino (1978) and Harris (1984) are given along with the data for CW stars (Harris 1984). Both samples of field RV stars show very similar distributions suggesting that the smaller sample is representative but the same does not hold for the SRd sample. The cluster RV stars seem to show a double peaked distribution but bearing the last observation in mind this should be treated with caution. There does not seem to be any striking difference between the field and cluster period distributions for any of the classes considered.

There is a convincing peak in the distribution of CW stars at $\log(P) = 1.15$ and the hint of a second peak at $\log(P) = 1.45$. If it were possible to combine the three classes of stars then this second peak in the CW distribution would appear as the lower period wing of a large peak centred about $\log(P) = 1.5 - 1.7$. However the absence of a

reliable knowledge of the numbers in each class renders this very uncertain.

A number of RV stars show very long period variations in their mean luminosities for which the periods are ~ 1000 days or between 13 and 25 times the formal periods. These are referred to as the RVb stars as opposed to the RVa stars which are known not to exhibit this phenomenon. This cyclic variation may also be accompanied by a variation of amplitude, as for RV Tau itself, or by a variation in period (DF Cyg). CU Del shows spontaneous changes of phase and BT Lac shows a secular decrease of period at the rate of 4.10^{-4} days/cycle. Mantegazza (1978) has carried out a Fourier analysis of the light curve of the RVa star EP Lyr and finds a very long period ~ 7000 days along with the possibility of an overtone oscillation in near resonance. It might be, then, that the long period variations exist in more RV stars than those for which it has been detected if not all.

After the characteristic light curves the most distinctive feature of the RV and SRd stars are the spectra. From a comprehensive survey of these spectra Preston et al. (1962) were able to define three reasonably homogeneous groups of RV star and distinguish them from the SRd stars. These groups are distinguished as follows:

Group A (RV(A))

All spectral features indicate an M.K. type G or K. TiO bands may appear at light minima along with weak Balmer emission at rising light. This is by far the largest of the groups. Dawson (1979) subdivides the group into A₁ with TiO and A₂ without. With only two exceptions, TT Oph and TX Oph which show only emission, none of the members of A₂ show emission.

Group B (RV(B))

This group contains stars for which the spectra are markedly peculiar at all phases. The hydrogen line types are F5 - G0 but CaII lines correspond to an earlier type. Hydrogen emission is moderately strong for all members of this class. It is the resultant

weakening of the hydrogen lines which leads to the discrepancy in the spectral types. The most striking feature of the spectra in this group is the occurrence of strong CN and CH features varying with phase. This led Rosino (1951) to classify AC Her as Rp. The carbon features can be very strong at light minima but absent at other phases. Preston et al. (1962) state that it is impossible to confuse these stars with the members of group A.

Group C (RV(C))

The stars of this group resemble those in group B in all respects with the exception that the CN and CH features so prominent in that group are absent here. Unfortunately since the carbon features of the group B stars are so dependent on the phase, good phase coverage is

required to distinguish the members of groups B and C.

The spectra of the SRd stars are also peculiar, showing a very smooth continuum from which CN and most metallic blends are absent indicating a spectral type earlier than G2. However the absence of H-absorption and the structure of the G-band imply a later type. The most distinctive feature of SRd spectra is the strong Balmer emission present as late as light maximum. Preston et al. (1962) find hydrogen emission lines here for only two of the RV stars in their sample and even these are much weaker than the corresponding lines for an SRd star. They conclude that this is the most useful spectroscopic criterion for distinguishing between the two classes of star.

Some doubt exists as to the homogeneity of group B. All of the stars in this group appear to possess their own peculiarities. AC Her shows many signs of being a peculiar carbon star and indeed has been shown by Baird (1981) to be metal poor but carbon rich. Since the molecular bands are very strong in comparison with the the atomic lines for the same elements Baird suggests that the existence of a substantial circumstellar cloud is implied. AR Pup, possibly a member of group B, has spectra similar to those of AC Her. UY CMa lies in the "forbidden" region of the period-frequency distribution ($\log(P) = 1.735$) and EP Lyr has been accused of binarity (Wenzel 1961)

although this seems to be largely unfounded.

Estimates for the physical parameters of a number of RV and SRd stars have been found by Dawson (1979) using D.D.O. photometry. This information has been supplemented with data drawn from the reviews on globular cluster variables by Rosino (1978) and Stothers (1963). The former is favoured in all cases. Temperatures are derived from (B-V) for the former and estimated from mean spectral types for the latter using Bohm-Vitenses' (1973) calibrations for metal poor stars in both cases. Bolometric corrections are extracted from the same source where required. The data for M5 V42 and V84 are taken from Demers and Harris (1974). These data are presented in Table 6.2. Gehrz (1971) has detected large infrared excesses from RV stars and so it is possible that temperatures and bolometric corrections derived from photometry are misleading. The infrared excesses strongly suggest the presence of circumstellar matter. However the spectra of the RV stars are peculiar and so unless the temperatures can be derived from a detailed analysis of individual lines this source of information should also be regarded with suspicion. Temperatures have been derived from high resolution spectra for two RV stars by Baird (1981) for AC Her for which he finds $T_{eff} = 7000$ K, and by Luck (1981) for R Sct near secondary light minimum giving $T_{eff} = 4400$ K. Dawson's (1979) photometric values are $T_{eff} = 4950$ K and 4720 K respectively. The limited agreement in the case of R Sct is adequate for our purposes but the discrepancy for AC Her is a little disturbing. However Dawson

Table 6.2.1 Galactic type II cepheids from Demers and Harris (1974)

	P(days)	log(P)	$\langle M_v \rangle$	$\langle B-V \rangle$	T_{eff} K	log(T_{eff})	B.C.	$\langle M_{bol} \rangle$	log(L/L $_{\odot}$)
RU Cam	22.182	1.346	-2.220	1.080	4414.891	3.645	-0.540	-2.760	3.004
RS Peg	19.907	1.299	-2.140	0.980	4650.721	3.668	-0.368	-2.508	2.903
k Pav	9.057	0.957	-1.600	0.670	5464.874	3.738	-0.059	-1.659	2.564
AU Peg	2.399	0.380	-0.680	0.600	5667.610	3.753	-0.057	-0.737	2.195
ST Pup	19.099	1.281	-2.210	0.560	5786.823	3.762	-0.061	-2.271	2.808
SW Tau	1.581	0.199	-0.400	0.330	6522.589	3.814	0.008	-0.392	2.057
XX Vir	1.349	0.130	-0.280	0.290	6659.779	3.823	0.044	-0.236	1.994
AL Vir	10.280	1.012	-1.700	0.560	5786.823	3.762	-0.061	-1.761	2.604
TX Del	6.166	0.790	-1.330	0.730	5296.878	3.724	-0.078	-1.408	2.463
UY Eri	2.218	0.346	-0.630	0.470	6064.290	3.783	-0.063	-0.693	2.177
W Vir	17.219	1.236	-2.040	0.730	5296.878	3.724	-0.078	-2.118	2.747

Table 6.2.2 Galactic RV(A) stars from Dawson (1979)

	P(days)	log(P)	$\langle M_v \rangle$	$\langle B-V \rangle$	T_{eff} K	log(T_{eff})	B.C.	$\langle M_{bol} \rangle$	log(L/L $_{\odot}$)
RV Tau	39.349	1.595	-4.600	0.000	4620.000	3.665	-0.580	-5.180	3.972
U Mon	46.130	1.664	-2.800	0.000	5430.000	3.735	-0.260	-3.060	3.124
R Sct	72.000	1.857	-3.500	0.000	4720.000	3.674	-0.540	-4.040	3.516
V Vul	37.860	1.578	-3.600	0.000	5440.000	3.736	-0.250	-3.850	3.440
UZ Oph	43.720	1.641	-4.800	0.000	4880.000	3.688	-0.470	-5.270	4.008
DY Aql	65.710	1.818	-0.900	0.000	3680.000	3.566	-1.270	-2.170	2.768
564 Oph	35.300	1.548	-4.700	0.000	4000.000	3.602	-0.980	-5.680	4.172
TT Oph	30.540	1.485	-1.800	0.000	4910.000	3.691	-0.450	-2.250	2.800
TX Oph	67.665	1.830	-5.600	0.000	5300.000	3.724	-0.310	-5.910	4.264
SS Gem	44.655	1.650	-0.900	0.000	5300.000	3.724	-0.300	-1.200	2.380
R Sge	35.297	1.548	-1.600	0.000	4960.000	3.695	-0.480	-2.080	2.732
TW Cam	43.700	1.640	-4.600	0.000	4710.000	3.673	-0.580	-5.180	3.972
DF Cyg	24.904	1.396	-3.200	0.000	5090.000	3.707	-0.400	-3.600	3.340
SU Gem	25.060	1.399	-2.800	0.000	4810.000	3.682	-0.480	-3.280	3.212
RX Cap	33.975	1.531	2.900	0.000	4990.000	3.698	-0.400	2.500	0.900

Table 6.2.3 Galactic RV(B) stars from Dawson (1979)

	P(days)	log(P)	$\langle M_v \rangle$	$\langle B-V \rangle$	T_{eff} K	log(T_{eff})	B.C.	$\langle M_{bol} \rangle$	log(L/L $_{\odot}$)
AC Her	37.731	1.577	0.100	0.000	4950.000	3.695	-0.440	-0.340	2.036
EQ Cas	29.185	1.465	1.300	0.000	5290.000	3.723	-0.305	0.995	1.502
EP Lyr	41.715	1.620	4.500	0.000	5960.000	3.775	-0.100	4.400	0.140

Table 6.2.4 Galactic RV(C) stars from Dawson (1979)

	P(days)	log(P)	$\langle M_v \rangle$	$\langle B-V \rangle$	T_{eff} K	log(T_{eff})	B.C.	$\langle M_{bol} \rangle$	log(L/L $_{\odot}$)
UU Her	45.000	1.653	-3.300	0.000	5687.000	3.755	-0.170	-3.470	3.288
453 Oph	35.224	1.547	-3.700	0.000	5570.000	3.746	-0.183	-3.883	3.453
360 Cyg	33.543	1.526	-5.400	0.000	5520.000	3.742	-0.244	-5.644	4.158

Table 6.2.5 Galactic SRd stars from Dawson (1979)

	P(days)	log(P)	$\langle M_V \rangle$	$\langle B-V \rangle$	T_{eff} K	log(T_{eff})	B.C.	$\langle M_{bol} \rangle$	log(L/L $_{\odot}$)
SX Her	53.445	1.728	-4.800	0.000	3975.000	3.599	-1.112	-5.912	4.265
TX Per	38.825	1.589	-4.250	0.000	3870.000	3.588	-1.445	-5.695	4.178
WY And	54.500	1.736	-3.400	0.000	3640.000	3.561	-3.050	-6.450	4.480
RU Cep	54.500	1.736	-5.500	0.000	3620.000	3.559	-3.284	-8.784	5.414
Z Aur	55.500	1.744	-5.500	0.000	4020.000	3.604	-1.010	-6.510	4.504
TW Aql	48.000	1.681	-4.800	0.000	4950.000	3.695	-0.191	-4.991	3.897
SV UMa	38.000	1.580	-4.750	0.000	4610.000	3.664	-0.396	-5.146	3.958
AB Leo	65.100	1.814	-6.080	0.000	4130.000	3.616	-0.825	-6.905	4.662

Table 6.2.6

Globular cluster type II cepheids
from Demers and Harris (1979)

	P(days)	log(P)	$\langle M_V \rangle$	$\langle B-V \rangle$	T_{eff} K	log(T_{eff})	B.C.	$\langle M_{bol} \rangle$	log(L/L _o)
W Cen 29	14.723	1.168	-2.180	0.850	4976.223	3.697	-0.179	-2.359	2.844
43	1.156	0.063	-0.540	0.360	6421.552	3.808	-0.016	-0.556	2.122
48	4.477	0.651	-1.210	0.530	5877.868	3.769	-0.064	-1.274	2.410
60	1.349	0.130	-0.450	0.290	6659.779	3.823	0.044	-0.406	2.062
61	2.275	0.357	-0.500	0.530	5877.868	3.769	-0.064	-0.564	2.126
92	1.346	0.129	0.030	0.430	6191.846	3.792	-0.054	-0.024	1.910
M3 154	15.276	1.184	-2.710	0.510	5939.367	3.774	-0.065	-2.775	3.010
M80 1	15.631	1.194	-1.580	0.590	5697.182	3.756	-0.058	-1.638	2.555
M13 1	1.459	0.164	-0.420	0.190	7015.524	3.846	0.095	-0.325	2.030
2	5.117	0.709	-1.440	0.300	6625.217	3.821	0.035	-1.405	2.462
6	2.113	0.325	-0.410	0.410	6256.624	3.796	-0.046	-0.456	2.082
M10 2	18.750	1.273	-2.290	0.650	5522.046	3.742	-0.057	-2.347	2.839
3	7.870	0.896	-1.370	0.640	5550.859	3.744	-0.056	-1.426	2.471
M14 1	18.707	1.272	-2.270	0.750	5242.038	3.720	-0.089	-2.359	2.843
2	2.786	0.445	-0.680	0.200	6979.109	3.844	0.097	-0.583	2.133
7	13.614	1.134	-1.530	0.690	5408.288	3.733	-0.063	-1.593	2.537
17	12.078	1.082	-1.520	0.650	5522.046	3.742	-0.057	-1.577	2.531

Table 6.2.6 (continued)

	P(days)	log(P)	$\langle M_V \rangle$	$\langle B-V \rangle$	T_{eff} K	log(T_{eff})	B.C.	$\langle M_{bol} \rangle$	log(L/L $_{\odot}$)
M14 76	1.888	0.276	-1.490	0.230	6871.000	3.837	0.089	-1.401	2.460
M15 1	1.439	0.158	-0.010	0.270	6729.458	3.828	0.061	0.051	1.879
M2 1	15.560	1.192	-1.990	0.480	6032.817	3.781	-0.064	-2.054	2.722
5	17.539	1.244	-2.110	0.470	6064.290	3.783	-0.063	-2.173	2.769
6	19.231	1.284	-2.270	0.490	6001.503	3.778	-0.065	-2.335	2.834

Table 6.2.7 Globular cluster RV stars from Demers and Harris (1974), Rosino (1978), and Stothers (1963)

	P(days)	log(P)	$\langle M_V \rangle$	$\langle B-V \rangle$	T_{eff} K	log(T_{eff})	B.C.	$\langle M_{bol} \rangle$	log(L/L $_{\odot}$)
M5 42	25.704	1.410	-3.200	0.530	5877.868	3.769	-0.064	-3.264	3.206
84	26.485	1.423	-3.120	0.550	5817.011	3.765	-0.062	-3.182	3.173
ω Cen 1	29.512	1.470	-2.910	0.770	5187.759	3.715	-0.102	-3.012	3.105
M2 11	33.884	1.530	-3.280	0.500	5970.357	3.776	-0.065	-3.345	3.238
M56 6	44.668	1.650	-2.190	0.610	5638.191	3.751	-0.057	-2.247	2.799
M22 8	33.500	1.525	-1.900	0.000	5284.218	3.723	-0.080	-1.980	2.692
9	43.855	1.642	-1.300	0.000	5284.218	3.723	-0.080	-1.380	2.452

Table 6.2.8 Globular cluster SRd stars from Rosino (1978)

	P(days)	log(P)	$\langle M_V \rangle$	$\langle B-V \rangle$	T_{eff} K	log(T_{eff})	B.C.	$\langle M_{bol} \rangle$	log(L/L $_{\odot}$)
M3 138	39.811	1.600	-1.420	0.900	4848.420	3.686	-0.244	-1.664	2.566
225	44.668	1.650	-1.590	0.900	4848.420	3.686	-0.244	-1.834	2.634
M13 11	46.238	1.665	-1.930	1.000	4602.565	3.663	-0.401	-2.331	2.832
M22 5	46.345	1.666	-1.660	0.850	4976.223	3.697	-0.179	-1.839	2.636
M56 3	50.816	1.706	-1.450	0.700	5380.220	3.731	-0.066	-1.516	2.506
M3 95	51.642	1.713	-1.770	1.100	4369.181	3.640	-0.577	-2.347	2.839

Table 6.2.9 Galactic type II cepheids from Kwee (1968)

	P(days)	log(P)	$\langle M_V \rangle$	$\langle B-V \rangle$	T_{eff} K	log(T_{eff})	B.C.	$\langle M_{bol} \rangle$	log(L/L $_{\odot}$)
527 Sgr	1.259	0.100	-0.560	0.320	6556.623	3.817	0.017	-0.543	2.117
2 Aql	1.671	0.223	-0.560	0.420	6224.147	3.794	-0.050	-0.610	2.144
839 Sgr	1.841	0.265	-0.560	0.460	6095.932	3.785	-0.061	-0.621	2.149
UY Eri	2.208	0.344	0.000	0.410	6256.624	3.796	-0.046	-0.046	1.918
AU Peg	2.399	0.380	0.000	0.650	5522.046	3.742	-0.057	-0.057	1.923
465 Oph	2.838	0.453	-0.560	0.620	5608.931	3.749	-0.056	-0.616	2.147
AP Her	10.399	1.017	-2.000	0.550	5817.011	3.765	-0.062	-2.062	2.725
1072 Sgr	13.397	1.127	-2.570	0.500	5970.357	3.776	-0.065	-2.635	2.954
802 Sgr	13.490	1.130	-2.130	0.560	5786.823	3.762	-0.061	-2.191	2.776
410 Sgr	13.804	1.140	-2.610	0.500	5970.357	3.776	-0.065	-2.675	2.970
CS Cas	14.689	1.167	-2.670	0.500	5970.357	3.776	-0.065	-2.735	2.994

Table 6.2.9 (continued)

	P(days)	log(P)	$\langle M_V \rangle$	$\langle B-V \rangle$	T_{eff} K	log(T_{eff})	B.C.	$\langle M_{\text{bol}} \rangle$	log(L/L $_{\odot}$)
FI Sct	14.894	1.173	-2.690	0.500	5970.357	3.776	-0.065	-2.755	3.002
1187 Sgr	15.101	1.179	-2.250	0.560	5786.823	3.762	-0.061	-2.311	2.824
741 Sgr	15.205	1.182	-2.260	0.560	5786.823	3.762	-0.061	-2.321	2.828
CZ Sct	15.417	1.188	-2.280	0.560	5786.823	3.762	-0.061	-2.341	2.836
AL Sct	15.596	1.193	-2.290	0.560	5786.823	3.762	-0.061	-2.351	2.840
377 Sgr	16.218	1.210	-2.330	0.560	5786.823	3.762	-0.061	-2.391	2.856
481 Oph	16.406	1.215	-2.350	0.560	5786.823	3.762	-0.061	-2.411	2.864
CO Sct	17.100	1.233	-2.840	0.500	5970.357	3.776	-0.065	-2.905	3.062
W Vir	17.298	1.238	-2.400	0.560	5786.823	3.762	-0.061	-2.461	2.884
1303 Sgr	18.493	1.267	-2.930	0.500	5970.357	3.776	-0.065	-2.995	3.098
CC Lyr	23.988	1.380	-3.220	0.520	5908.537	3.771	-0.064	-3.284	3.214

Table 6.2.10 Globular cluster type II cepheids
from Kwee (1968)

		P(days)	log(P)	$\langle M_V \rangle$	$\langle B-V \rangle$	T_{eff} K	log(T_{eff})	B.C.	$\langle M_{bol} \rangle$	log(L/L $_{\odot}$)
M2	1	15.560	1.192	-2.240	0.530	5877.868	3.769	-0.064	-2.304	2.822
	5	17.539	1.244	-2.390	0.550	5817.011	3.765	-0.062	-2.452	2.881
	6	19.320	1.286	-2.570	0.570	5756.785	3.760	-0.060	-2.630	2.952
M3	154	15.276	1.184	-2.880	0.510	5939.367	3.774	-0.065	-2.945	3.078
M5	42	25.704	1.410	-3.280	0.540	5847.363	3.767	-0.063	-3.343	3.237
	84	26.485	1.423	-3.200	0.560	5786.823	3.762	-0.061	-3.261	3.204
M10	2	18.750	1.273	-2.470	0.580	5726.909	3.758	-0.059	-2.529	2.912
	3	7.870	0.896	-1.550	0.590	5697.182	3.756	-0.058	-1.608	2.543
M13	1	1.459	0.164	-0.460	0.450	6127.733	3.787	-0.059	-0.519	2.108
	2	5.105	0.708	-1.370	0.510	5939.367	3.774	-0.065	-1.435	2.474
	6	2.113	0.325	-0.300	0.550	5817.011	3.765	-0.062	-0.362	2.045

Table 6.2.10 (continued)

		P(days)	log(P)	$\langle M_v \rangle$	$\langle B-V \rangle$	T_{eff} K	log(T_{eff})	B.C.	$\langle M_{bol} \rangle$	log(L/L $_{\odot}$)
M15	1	1.439	0.158	-0.480	0.240	6835.341	3.835	0.084	-0.396	2.058
M80	1	15.631	1.194	-1.760	0.540	5847.363	3.767	-0.063	-1.823	2.629
ω Cen	29	14.723	1.168	-2.280	0.840	5002.188	3.699	-0.167	-2.447	2.879
	43	1.156	0.063	-0.740	0.350	6455.058	3.810	-0.008	-0.748	2.199
	48	4.477	0.651	-1.410	0.520	5908.537	3.771	-0.064	-1.474	2.490
	60	1.349	0.130	-0.650	0.280	6694.528	3.826	0.053	-0.597	2.139
	61	2.275	0.357	-0.700	0.520	5908.537	3.771	-0.064	-0.764	2.206
	92	1.346	0.129	-0.180	0.460	6095.932	3.785	-0.061	-0.241	1.997

himself states that the strong carbon bands of the group B stars make their temperatures very uncertain and it seems reasonable to suppose that this disagreement between the two methods is confined to this one group.

The temperatures along with comparable data for a selection of Type II cepheids derived from $(B-V)_c$ values taken from Demers and Harris (1974) are plotted against period in figs. 6.3 + 6.4. Two points are clear from this. The first is that the points for the RV stars and the Type II cepheids appear to belong to a single distribution for both field and cluster stars. Although there is a rather greater spread in temperature for the RV stars this can be seen as a continuous increase in the spread with increasing period for all the stars. It could be that the greater spread is just a reflection of the greater difficulty of measuring RV temperatures due to the presence of the gas shell. However since the same trend is probably present in the CW stars from which circumstellar matter appears to be absent (Gehrz and Hackwell 1974) the more positive view would seem to be in order.

The luminosities of the RV and SRd stars present something of a problem. Consider the data for the globular cluster RV Tauri stars presented in Table 6.2 and as fig. 6.5 + 6.7. The values for $\langle M_V \rangle$ are derived from the $\langle m_{pg} \rangle$ values given in Stothers (1963) using a conversion formula found in Allen (1973) (A.Q.) and the $(m-M)_{pg}$ values

Symbols for Figs. 6.3 - 6.10

- △ Type II Cepheids (field + cluster)
- ▽ RV(A) stars (field)
- + RV(B) stars (field)
- × RV(C) stars (field + cluster)
- SRd stars (field + cluster)

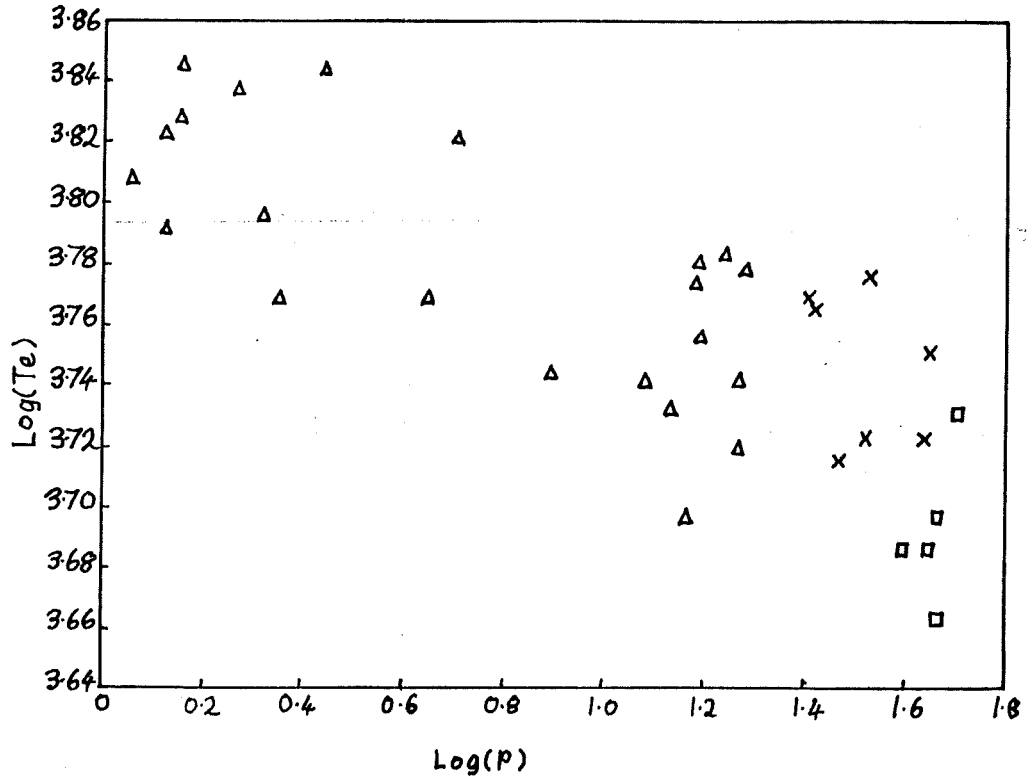


Fig. 6.3 Log(P) - Log(T_{eff}) for cluster type II cepheids, RV, and SRd stars taken from Demers and Harris (1974), Stothers (1963), and Rosino (1978).

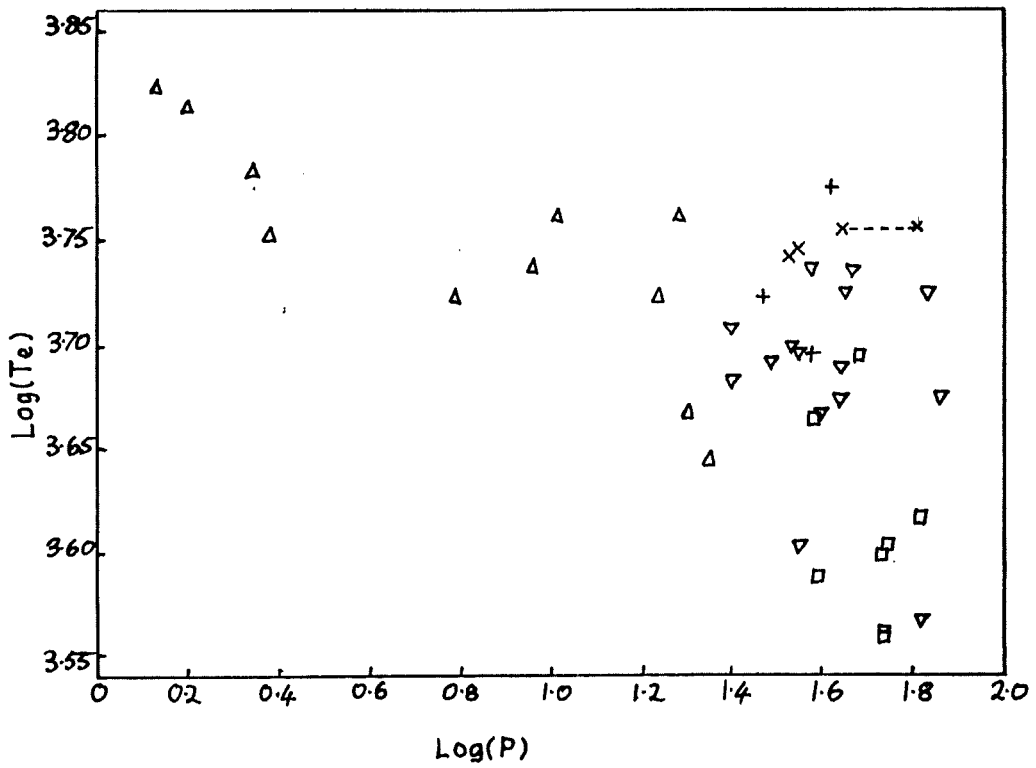


Fig. 6.4 Log(P) - Log(T_{eff}) field type II cepheids, RV, and SRd stars taken from Demers and Harris (1974), and Dawson (1979).

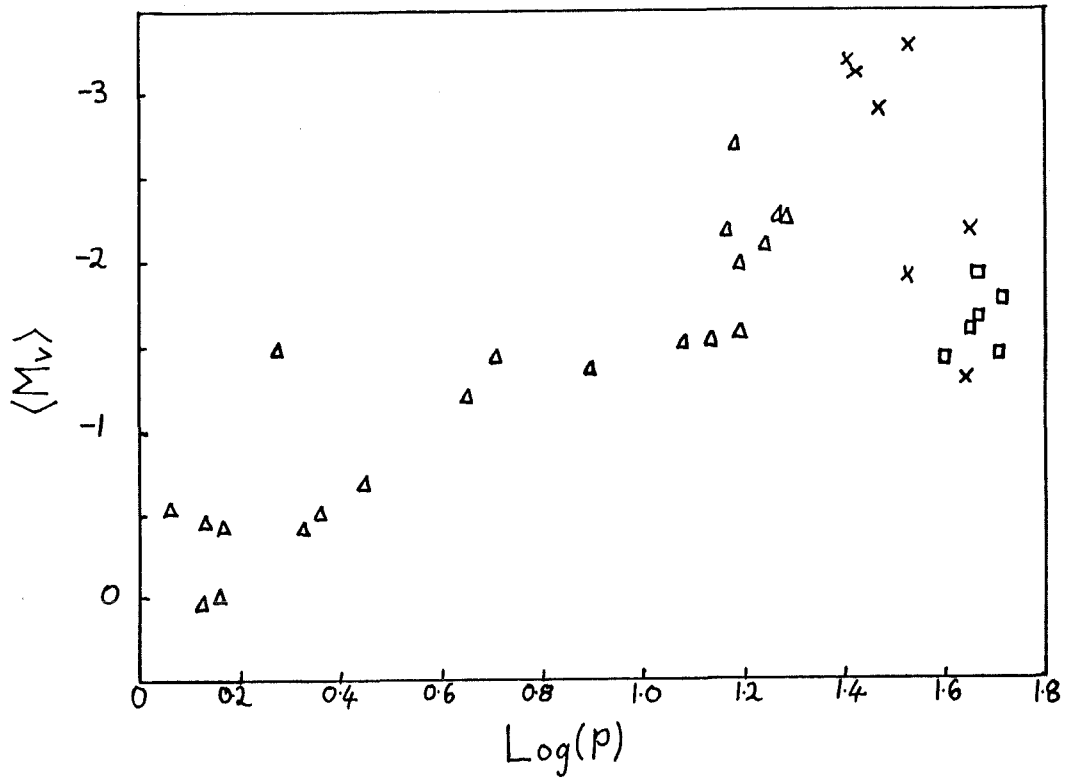


Fig. 6.5 $\text{Log}(P) - \langle M_V \rangle$ for cluster type II cepheids, RV, and SRd stars.

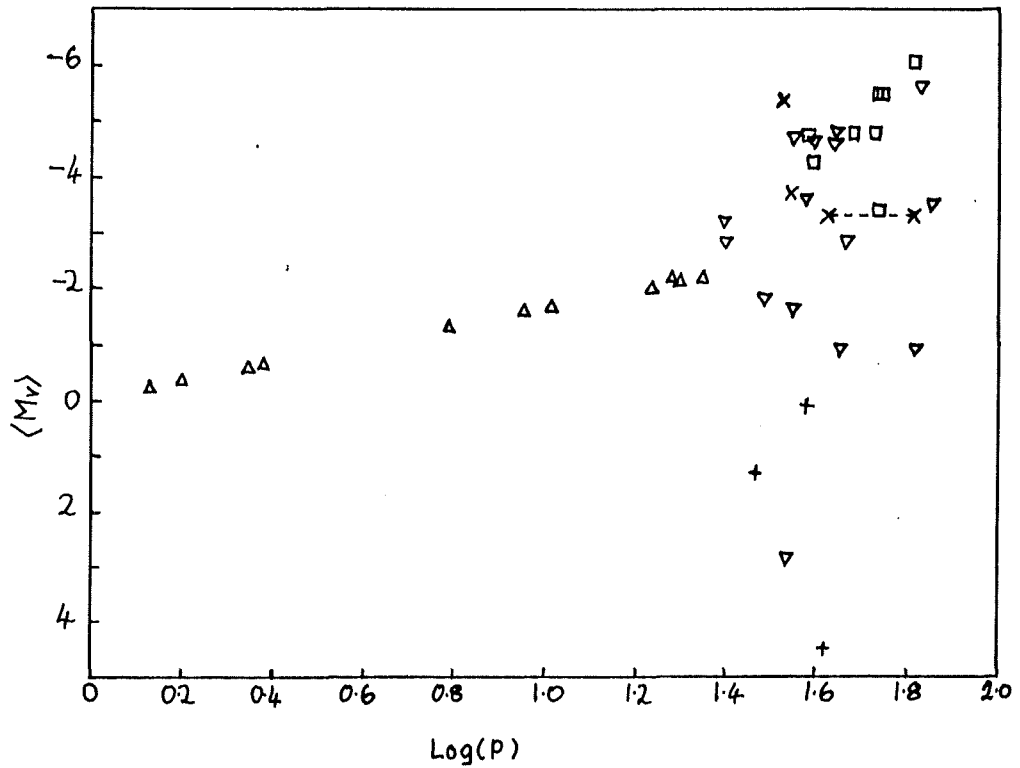


Fig. 6.6 $\text{Log}(P) - \langle M_V \rangle$ for field type II cepheids, RV, and SRd stars.

are taken from Lang (1974) with the horizontal branch adjusted to match that adopted by Demers and Harris (1974). Data for the cluster Type II cepheids from the latter paper are also plotted in this figure. Again the tables of Bohm-Vitense (1973) furnish $(B-V)_0$ to T_{eff} conversions and the bolometric corrections. It is clear that although the short period end of the RV sample coincides with the CW stars, the long period stars do not show the same trend at all. In fact there appears to be a decrease of luminosity with increasing period for which

$$\langle M_v \rangle = 0.076P - 5.15$$

or

$$\langle M_v \rangle = 6.1 \log P - 11.8.$$

In his study of RV luminosities Du Puy (1973) discards stars whose membership of the class he suspects, retaining ω Cen V1, M56 V6, and M2 V11 and introduces AP Sct (NGC 6712 V2). If the former stars are considered we find

$$\langle M_v \rangle = 0.014P - 3.5$$

or

$$\langle M_v \rangle = 1.2 \log P - 4.8$$

which, although the slope is smaller than for the full sample, still opposes that of the CW stars. This difference cannot be accounted for by the bolometric corrections as seems to be suggested by Rosino

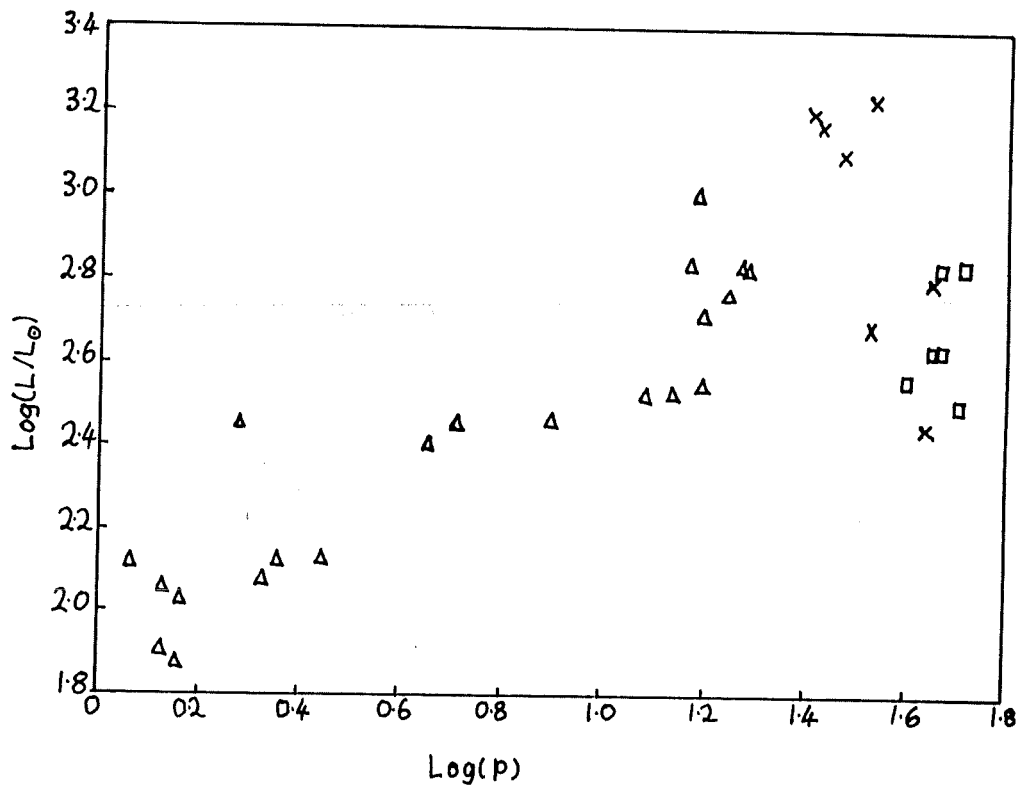


Fig. 6.7 $\text{Log}(P) - \text{Log}(L/L_{\odot})$ for cluster type II cepheids, RV, and SRd stars.

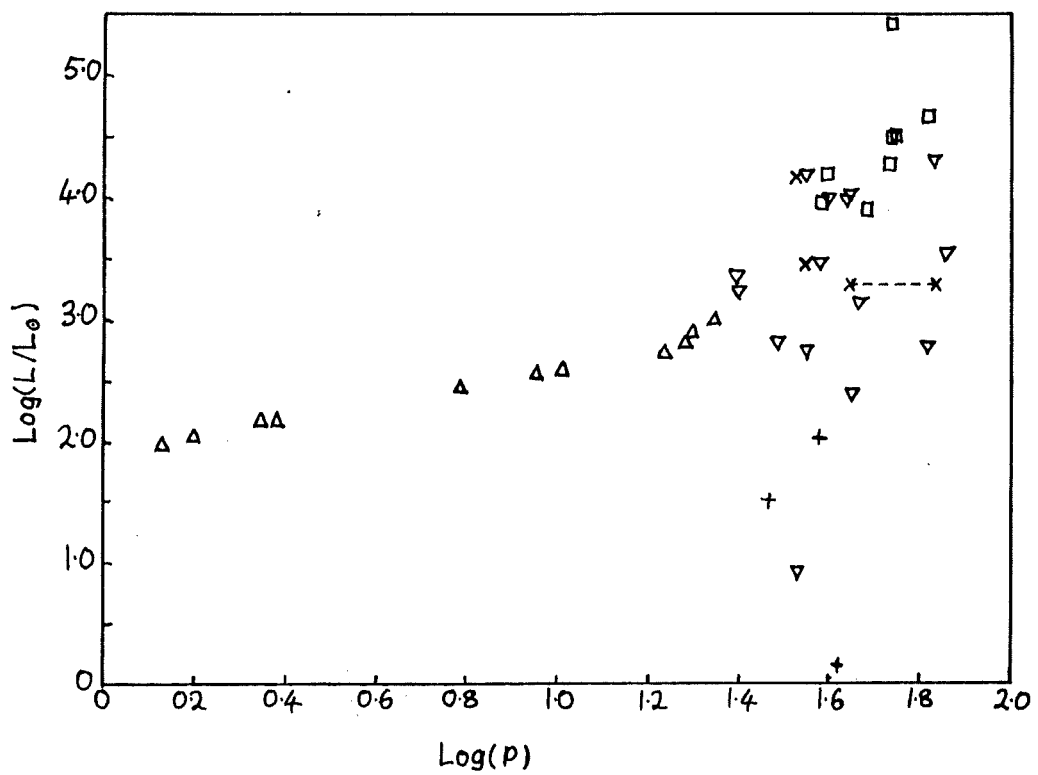


Fig. 6.8 $\text{Log}(P) - \text{Log}(L/L_{\odot})$ for field type II cepheids, RV, and SRd stars.

(1978). However this may well not be the correct interpretation since the RV and SRd stars appear to split into two well separated groups. One of these groups forms an extension of the CW stars and the other, in which all the SRd stars are found, lies well below them. It is not easy to decide whether the stars in the first group are true full-blooded RV Tauri stars since the alternation of minima is not particularly strong which leads to both M5 V42 and V84 being classified as either RV or CW.

Du Puy (1973) uses a number of different methods to estimate the absolute magnitudes of the field RVs. From statistical and secular parallaxes he finds that for samples selected by period $-3.7 < \langle M_V \rangle < -3.0$ with an increase in $\langle M_V \rangle$, the sample mean, with period, i.e.

$$\langle M_V \rangle = 0.010.P - 3.5$$

or

$$\langle M_V \rangle = 0.9 \log P - 4.6$$

From spectral classification he originally derived

$$-7 < \langle M_V \rangle < -4$$

but this assumes unrealistically high masses and the amended magnitudes given in Barnes and Du Puy (1975) are in agreement with the values derived from parallaxes.

Dawson (1979) has used his observations in the D.D.O. photometric system to estimate the absolute magnitudes of the RV and SRd stars in his sample of a limited selection of phases. These are included in table 6.2. A plot of $\langle M_v \rangle$ with period for the CW and RV stars in the galactic field, fig. 6.6, shows an effect similar to that found for the globular cluster stars. A plot of luminosity with period, fig. 6.8, shows a similar pattern. The scatter is very much greater than for the cluster magnitudes but a slight diminishing of $\langle M_v \rangle$ with increasing period can be detected with a slope similar to that of the smaller sample of cluster stars. Dawson shows that there is a considerable uncertainty for his magnitude estimates and so a large part of the scatter could derive from this. However if the shallower slope given by the three "reliable" cluster stars is the correct one to use then the scatter for the cluster stars is not much less than for the field stars. Either way the evidence suggests that a great many RV stars have magnitudes considerably lower than would be expected if they were simply a continuation of the CW class. However a glance at the data for the SRd stars shows a very different picture. These stars do appear to form a continuation of the period luminosity law even though the slope is rather steeper,

$$\langle M_v \rangle = -0.045P - 2.6$$

or

$$\langle M_v \rangle = -4.8 \log P - 3.3$$

as opposed to

$$\langle M_v \rangle = -0.089P - 0.48$$

or

$$\langle M_v \rangle = -1.6 \log P - 0.07.$$

The $P-\langle M_v \rangle$ relation for the field SRd stars contrasts sharply with that of the field RV Tauri stars and with the cluster SRd stars. The latter difference could derive from the use of photographic magnitudes to give one set of SRd luminosities and photometric indicators to give the other. Photometric indicators could be rendered inaccurate by the spectral peculiarities of the SRd stars and the photographic magnitudes, a blue band observation, might be an unreliable source of luminosities for the relatively cool SRd stars. On the other hand the low luminosity group in the globular cluster data also contains a number of RV stars for which the temperatures are much the same as their brighter brethren. It might be that the lower luminosities of the SRd/RV group are the result of a potent source of circumstellar absorption which for some unknown reason is absent from the field SRd stars. This latter explanation is probably more likely to be the explanation for the lower luminosities of the field RV stars.

The decrease of luminosity with increasing period becomes perplexing when one considers the fact that there are long period RV Tauri stars with periods 50 or so times greater than those of BL Her stars which have very similar luminosities and for which T_{eff}^4 is no more than a factor of 2 or 3 larger. This implies a mass for the RV star of about $10^{-1} M_{\odot}$, in the more extreme cases, which is very much smaller than the $M \approx 0.6 M_{\odot}$ estimated for the Type II cepheids. To add to the mystery, stars with very long periods showing the characteristics of CW stars have been observed in M31 by Baade and Swope (1963). These stars have very large absolute magnitudes suggesting a turnup in the period-luminosity law (van den Bergh 1974).

Observations of the RV, SRd and CW stars in the infrared have been made by Gehrz (1972), and by Gehrz and Hackwell (1974). From an inspection of the flux distributions it is immediately clear that the RV and SRd stars show considerable infrared excesses. The flux curves can be either smooth or show strong features. In a preliminary report Gehrz and Woolf (1970) conclude that the "RV stars comprise a unique infrared class".

The members of group A₁ generally have well developed silicate features whilst the RV(A₂) stars display smooth flux curves. The infrared flux for the classic group B star AC Her is very large and shows features at longer wavelengths

which are not found in any of the other stars. AC Her is known to be carbon rich Baird (1981) and Dawson (1979) has shown that the infrared excesses correlate with metallicities for group A stars. This implies that the differences in the infrared features can be ascribed to differing chemical compositions. R Sct is strange in that it has only a very small infrared excess. A very small infrared excess proves to be characteristic of the SRd stars with one exception, TX Per, which shows a typically RV-like excess. Since R Sct also has a relatively long period for an RV star, 144 days, and since that for TX Per is relatively short Gehrz (1972) suggests that these stars be reclassified on this basis. However R Sct shows a typical RV light curve and so I choose not to follow this suggestion.

The results of an infrared survey of ten CW stars covering the entire period range up to 22 days tell a very different story. The conclusion formed by Gehrz and Hackwell (1974) is that the CW stars radiate as almost perfect blackbodies. Not a trace of an infrared excess is found.

The conclusion, then, is that the RV stars are surrounded by extended dust and gas shells which are absent from the CW stars. This is strengthened by the identification of strong optical circumstellar lines in RV spectra and their complete absence from CW stars (Gehrz and Hackwell 1974). The relative strength of the molecular bands and atomic lines in AC Her (Baird 1981) adds further weight to the

arguments for circumstellar gas. The implication is that mass loss has taken place, or is taking place, in the RV Tauri stars and perhaps in the SRd stars but not to any appreciable extent in the CW stars. This would appear to be a fundamental physical distinction between the CW stars on the one hand and the RV/SRd stars on the other.

Is it possible that flux redistribution by the circumstellar shells is responsible for the anomalously low luminosities of some of the stars? In order to test this, flux distributions were constructed by taking V and T_{eff} from Dawsons' data and using this to define a Planck function which was extended into the infrared regions by taking the infrared fluxes from Gehrz (1972) and by postulating a free-free emission "tail" fitted to the longest wavelength data point. By comparing this with the blackbody flux alone, corrections to the bolometric magnitudes were generated. These corrections are given in table 6.3. Only one of the corrections, that for RV Tau itself, is large enough to make any significant difference to the luminosities for these stars. The implication is that obscuration by circumstellar material will not explain the low luminosities of many RV Tauri stars. This is in broad agreement with Barnes and Du Puy (1975) although my luminosity corrections are larger than theirs. The temperature and luminosity data has been combined to construct H-R diagrams, figs. 6.9 + 6.10, for completeness.

Table 6.3

Corrections to RV luminosities from infrared photometry

	$\text{Log}(L/L_{\odot})$	$\Delta \text{Log}(L/L_{\odot})$	$\text{Log}(L'/L_{\odot})$
AC Her (B)	2.036	0.143	2.179
U Mon (A_1)	3.124	0.121	3.245
RV Tau (A_1)	3.972	0.579	4.551
R Sct (A_1)	3.516	0.016	3.532
TW Cam (A_2)	3.972	0.334	4.316
DF Cyg (A_2)	3.340	0.239	3.579
SU Gem (A_2)	3.212	0.391	3.603
R Sge (A_2)	2.732	0.198	2.930
V Vul (A_1)	3.440	0.137	3.577

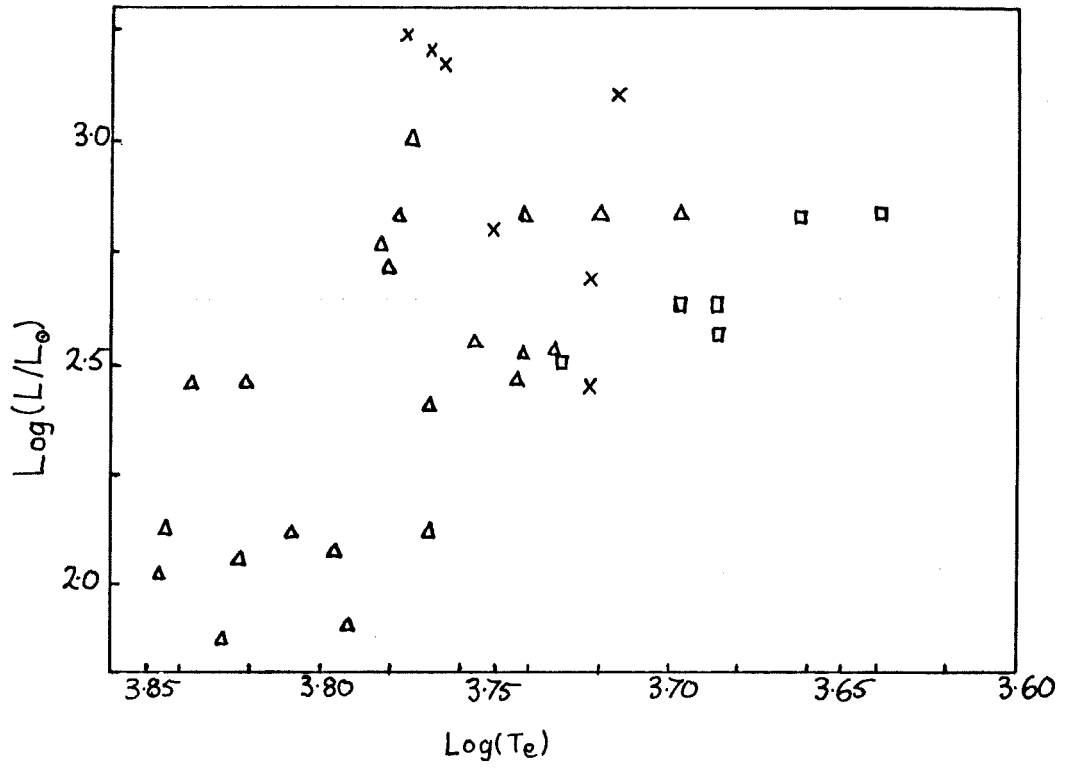


Fig. 6.9 H-R diagram for cluster type II cepheids, RV, and SRd stars.

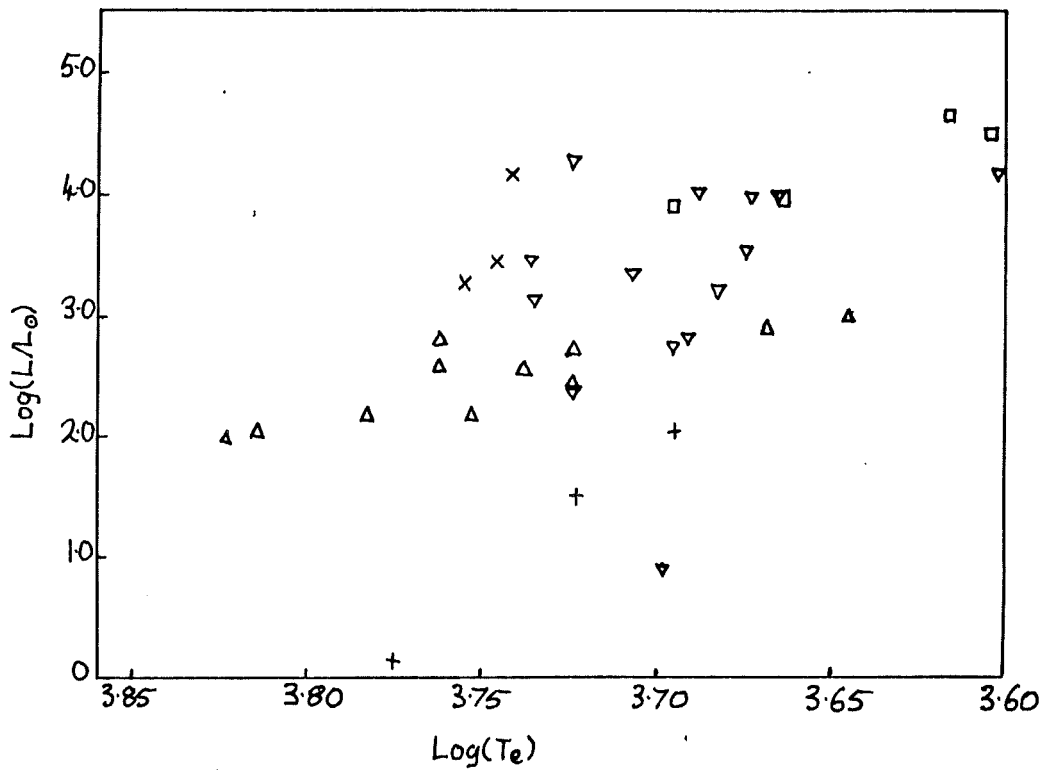


Fig. 6.10 H-R diagram for field type II cepheids, RV, and SRd stars.

Abundance estimates for samples of RV and SRd stars in the galactic field have been determined by Dawson (1979) using D.D.O. photometry. For the group A stars the abundance can be determined well from a CN strength indicator. The abundances derived for the group C stars are more uncertain since the D.D.O. system is not designed to handle the low metallicities found for them. In the case of the B stars neither of the two indicators in the system, a UV excess and the CN strength, are reliable because of the Balmer emission and anomalous bands, and so the abundances, which are determined from the UV excess, cannot be regarded as reliable. For this latter group the abundances derived depend strongly upon whether or not a peculiar mixture of elements is assumed and upon the assumed luminosity class. If EP Lyr is assumed to be peculiar then $[Fe/H] = -0.75$ otherwise it is -1.9 which seems unreasonable. Baird (1981) has made a study of AC Her using high dispersion spectra and finds $[Fe/H] = -1.2$ but finds $[C/H] = -0.7$ indicating a substantial carbon enrichment. Since the UV excess measures the abundance of the Fe peak elements (Kraft 1979) Dawsons estimate, $[Fe/H] = -0.6$, does not give particularly good agreement. However Bairds abundances do show that the group B stars are chemically peculiar with a mixture of elements similar to that found in the carbon stars.

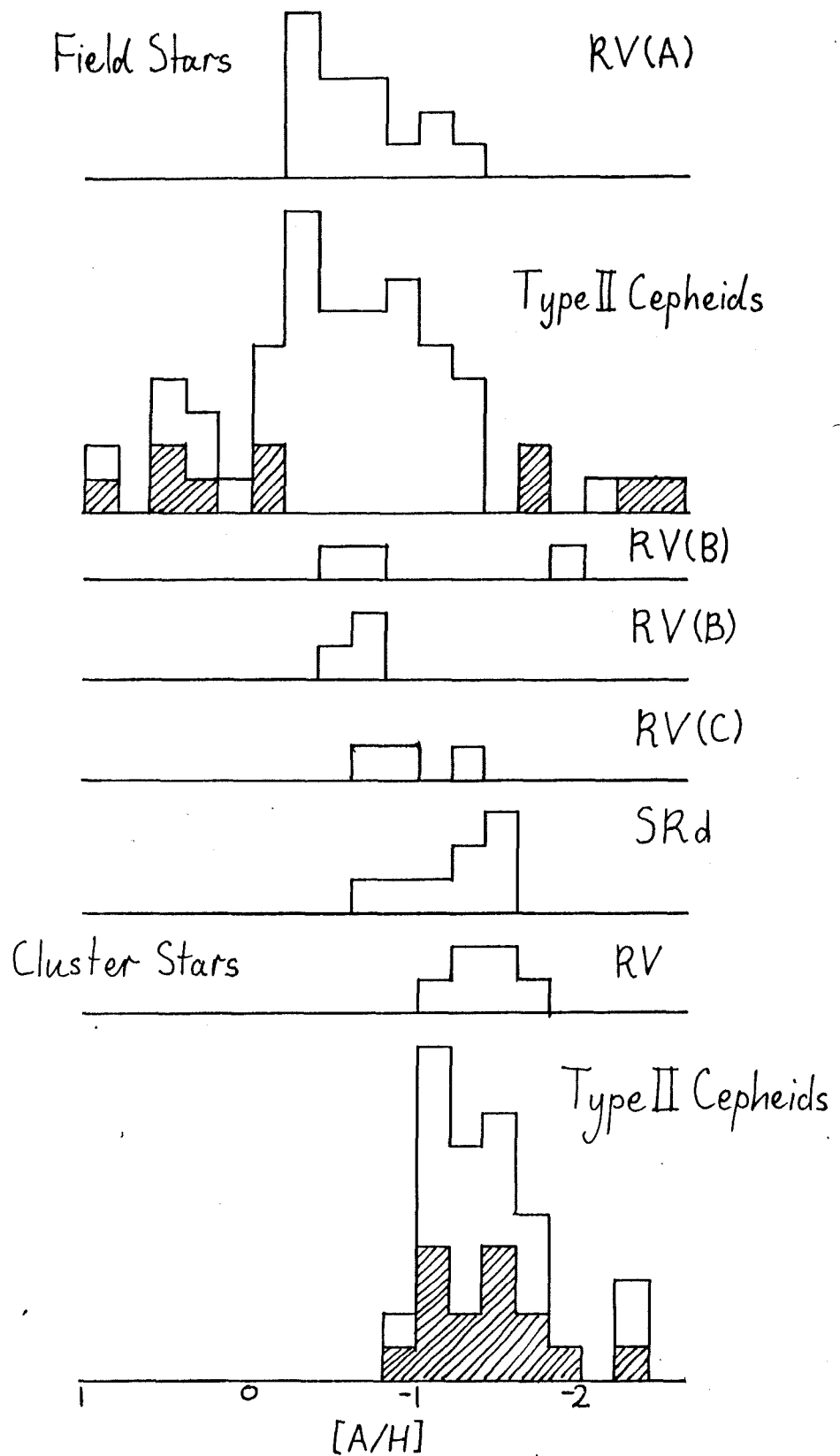


Fig. 6.11 Metallicity - frequency histograms for field RV, and SRd stars (Dawson (1979)), field type II cepheids (Harris (1981)), cluster RV stars and type II cepheids (Harris (1984)). The cross-hatching indicates the BL stars ($P < 8$ days).

The SRd stars turn out to be very metal poor. There are two exceptions; CE Vir which appears to be either a metal rich subgiant or a carbon star, and UW Lib which shows the characteristics of a G0-3 dwarf. Both are consequently discarded. Preston and Wallerstein (1963) have studied SX Her in detail finding $[Fe/H] = -1.8 \pm 0.7$ which is in reasonable agreement with Dawson's $[Fe/H] = -1.4$. A single cluster variable, M2 V11, is included in Dawson's sample of RV stars and for this he finds $[Fe/H] = -1.3$.

Harris (1981) has used Washington photometry to obtain abundances for 63 field Type II cepheids which he shows form a transition population between the disk and halo. In a later paper (Harris 1984) he gives abundances of the clusters containing six RV stars and forty-one type II cepheids taken from Pilachowski (1984). M2 V11 is included in this sample and the abundance of the cluster is close to that derived for the star by Dawson. Comparing the abundance-frequency diagrams given in fig. 6.11 shows that the RV stars and the Type II cepheids have the transitional abundance distribution. The group C stars show a distribution lying midway between that of the globular cluster and transitional population. For the SRd stars the peak stands squarely in the halo population but there is a tail running back to the transitional population. It is interesting that the double mode RV star UU Her has a metallicity considerably lower than those of the other RV(C) stars. In this respect and because of its long (70 day) period it is similar to the

SRd stars. It is, however, very much hotter. If EP Lyr is assumed to have a carbon star composition (second histogram) the group B stars fall into the transitional population, otherwise there is a wide dispersion in abundance (first histogram). For the clusters the RV and CW stars again show very similar distribution.

It would seem, then, that the RV and the majority of CW stars belong to the same metallicity populations whether they are found in the field or in globular clusters. The SRd stars seem not to belong to this population although they could well be true members of Population II, their shorter period relations being the group C RV Tauri variables. The abundances of Baird (1981), and less conclusively of Dawson (1979), indicate considerable metal deficiencies in the RV(B) stars which would seem to fit in with current theories of the formation of R stars. This would set the group B stars in amongst the metal poor grouping.

The kinematics of the RV and SRd stars in the field have been studied by Joy (1952). He finds that there is a clear division of his stars into a low velocity group (group 1) with time averaged velocities less than 70 km/s and a high velocity group (group 2). The group mean velocities are 28 km/s and 154 km/s respectively. When the distribution of the stars in the galaxy is considered then the low velocity stars are found to lie reasonably close to the galactic equator ($\langle b \rangle \approx 13^\circ$) whilst the rest lie scattered from the equator

($\approx 28^\circ$). The relation of the radial velocities with galactic longitude shows the high velocity stars lying around the locus predicted for a halo population. The SRd stars belong to population II according to their kinematics and space distribution, a conclusion which is strongly reinforced by their metal paucity. On the other hand similar considerations indicate that the RV(A) stars belong to an intermediate, old disk population. The status of the RV(C), and of course the RV(B), stars is uncertain but would tend to suggest that they lie somewhere in between these two main groupings.

A more recent study of the kinematics and space distributions of the type II cepheids by Harris (1981), and Harris and Wallerstein (1984) shows that these too split into two major components, that is, a high velocity, dispersed and metal poor group and a larger, old disk grouping. There are also metal rich stars with a high velocity dispersion to be found in the galactic bulge.

When the type II cepheids, RV, and SRd stars are considered as a whole there are two separate populations which, presumably, have evolved from different mixtures of elements. There is a metal poor halo population containing type II cepheids and SRd stars, and perhaps also RV(C) and RV(B) stars, and a relatively metal-rich old disk population containing another group of type II cepheids and the RV(A) stars.

It is just possible that the mean velocities of the RVb stars might illuminate the unexplained origin of the long period light variations. The RVb star U Mon has a variation in mean velocity on a period of 2320 days which is equal to the period for the mean light variations (Joy 1952). If it is assumed that both these variations are due to binarity then we find

$$R \geq 920 R_{\odot}$$

$$\text{and } M \geq 0.61 M_{\odot},$$

if the orbit is assumed to be circular and the orbital plane to lie nearly on the line of sight. There would seem to be too many RVb stars ($\sim 10-25\%$) for the conditions imposed on the orientation of the orbit to hold. One explanation for the light variations which can very probably be ruled out for many stars is a variation of the energy generation. A particularly good example is BT Lac which shows a light variation of 1.4^m over a period of 654 days. Since

$$\log(P) \approx 0.75 \log(L/L_{\odot}) \approx 0.3 M_{bol}$$

we have $\Delta \log(P) \approx 0.4$. This cannot have passed unnoticed.

As was mentioned earlier the spectra of RV Tau stars display a plethora of peculiarities. A number of these are shared by either the W Vir stars or the SRd stars, or both, but a few seem to be restricted to the RV stars. The work on RV spectra is confined to AC Her (Sanford (1955), Baird (1981) and Yoshioka 1979), R Sct (Preston 1962) and U Mon (Preston 1964).

When the radial velocities derived from the major absorption lines are corrected for long term variations the velocity curve for U Mon is found to be highly repetitive with a period equal to the short period for the light variations. As the velocity approaches the maximum infall velocity a new blue shifted component appears and doubled lines exist for a while. This phenomenon, which is also observed in CW stars, is explained by the existence of a phase shift across the atmosphere so that the outer atmosphere is still collapsing as the next shock emerges into the atmosphere to drive the renewed expansion. The regularity and periodicity of the velocity curve is, as was noted earlier, strong evidence for the significance of the shorter period as the pulsation period.

Preston (1964) also finds metallic emission during rising light with velocities between those of the doubled absorption components along with HeI emission and the ubiquitous H α emission. The HeI emission implies the presence of a strong shock. He finds that the velocities are greater for more highly ionised lines indicating a velocity gradient in the atmosphere. Further, he finds two sharp sets of H + K CaII lines with velocities of -45 and -83 km/s respectively which he demonstrates are not of interstellar origin. His explanation for this last observation is the existence of expanding circumstellar gas shells.

For R Sct Preston (1962) finds weak metallic emission at secondary light maximum with velocities between those of the components of doubled absorption lines as for U Mon. The doubling persists through the subsequent decline in light. He finds TiO absorption at the following deep minimum. From a curve of growth analysis Preston (1962) finds that the blue component of the doubled lines is formed in hotter material than its companion. As well as this he finds evidence for veiling of the blue component, that is a source of continuous emission overlying its place of origin. The Balmer emission appears to take place in this layer below the source of the red absorption component and is undisplaced relative to the metallic emission system. In addition he finds abnormally strong low ionisation level lines which suggest the presence of circumstellar material. He suggests that this circumstellar material is also the source of the TiO bands.

Baird (1984) finds that the metallic line emission and the absorption doubling are also present in AC Her. However in this case the splitting is much greater, with a highly red shifted line system moving at +60 km/s in comparison with the +30 km/s of the main velocity curve. This is present at the rise to both light maxima and since it also appears in the spectra of Sanford (1955) would seem to be a regular occurrence. In his search for an explanation of this phenomenon Baird (1984) examines the suggestion by Karp (1975) that such line splitting might be produced by a temperature inversion in

the atmosphere due to the passage of a shock. This mechanism predicts that the relative strength of the two components is indicative of the direction of the motion of the atmosphere, and that the separation of the components should increase with line strength. Baird (1984) demonstrates that this latter prediction is not fulfilled but on the contrary the reverse is true. Further, he suggests that this implies the existence of two separate lines with overlapping wings. There is also evidence for veiling of the blue component as was found by Preston (1962) for R Sct suggesting that, again, the blue component is produced deeper in the atmosphere. Baird estimates that the material producing the red component falls through $\sim 56 R_{\odot}$ during the 15 days the line is present. To explain these two layers falling with very different velocities he proposes a model in which the more rapidly falling layer lies deepest with the emission being produced in a layer sandwiched in between. However, as he himself realises, this predicts that the red component and not the blue component should be more heavily veiled contrary to the observations.

The important point, though, is that the observations imply that matter is regularly driven out to great distances from the stars surface before some, at least, falls back. This would suggest that the circumstellar matter could be the product of continuing pulsation driven mass loss.

Recently, on 29 September 1982, R Sct underwent a very pronounced light minimum, 3^m below mean light, for which a spectrum was obtained by Howell et al. (1983). The spectrum is very peculiar showing virtually none of the usual absorption features but in their place a mass of emission lines. It might almost be that the spectrum has simply been inverted. The only absorption features present are very strong TiO bands. Howell et al. (1983) suggest that the emission is simply a normal chromospheric emission revealed by the disappearance of the photospheric illumination. On the basis of the line velocities they deduce that it is produced close to the stellar surface. However the emission vanishes completely as soon as the luminosity begins to grow and this is a phenomenon which would seem not to fit the chromospheric emission hypothesis. On the basis of their observations the authors suggest that the RV Tau stars are very similar to the RCB stars, a resemblance which they say extends to many other properties. They also speculate that the RV stars might evolve into RCB stars with, perhaps, sufficient mass loss to bare the helium rich layers. Further, they raise the possibility that RV stars might share the RCB property of hydrogen deficiency.

6.2 PULSATION MODELS OF RV TAU STARS

No attempt has been made to calculate nonlinear pulsation models of RV stars or, indeed, SRd stars. There is a single example of an analysis based upon linear pulsation models by Takeuti and Petersen

(1983). However over the past twenty years a number of workers in the field have stumbled across nonlinear models showing characteristics reminiscent of the RV stars.

The first of these serendipitous models is one constructed by Christy (1966) in an attempt to model W Vir. The relevant parameters are;

$$M = 0.88 M_{\odot}$$

$$L = 1.8 \cdot 10^3 L_{\odot} \quad (M_{bol} = -3^m.4)$$

$$T_{off} = 5500 \text{ K}$$

$$Y = 0.45$$

$$Z = 0.002$$

$$P = 18.5 \text{ days}$$

He finds very rapid growth of the pulsation driven predominantly by the H/HeI ionisation zone ($\Delta W_{H/HeI} \propto \lambda \Delta W_{HeII}$). In an attempt to find a simple explanation for the period alternation he calculates P_1/P_0 finding $P_1/P_0 \approx 2/3$ and suggests that an alternately constructive and destructive interference of these two modes is responsible for the effect. However he also observes that the outer zones oscillate with a period double that of the main pulsation and that the outer zone itself escapes from the model altogether. He estimates that this mass loss occurs at a rate of $5.6 \cdot 10^{-6} M_{\odot}/\text{yr}$ - a not insubstantial figure. The outer zone appears to be driven out by a series of very strong shocks which Christy (1966) suggests cool radiatively more rapidly than they should through the deficiencies of the diffusion

approximation. There is one major difference between the light curve of Christy's model and the observed light curves and that is that in the model the alternation occurs in the light maximum as opposed to the light minimum as observed.

In his comprehensive theoretical study of classical cepheids Stobie (1969) finds another example of RV-like behaviour for the following model parameters;

$$M = 9 M_{\odot}$$

$$L = 10^4 L_{\odot} \quad (M_{bol} = -5^m.23)$$

$$T_{eff} = 4700 \text{ K}$$

$$Y = 0.15$$

$$Z = 0.04$$

$$P = 28.7/33.1 \text{ days}$$

$$P_{\text{annual}} = 62.8 \text{ days}$$

He finds a maximum light amplitude of $\delta M_{bol} = 2^m.25$ with successive maxima/minima differing by $0^m.25/0^m.75$. The behaviour of the outer atmosphere is similar to that in Christy's (1966) model although in this case mass is not lost. The light curve is like that of some of the more restrained RV stars and the period, although short, is not too short to be that of one of the shorter period RV stars. On the other hand the temperature is low and the observations of Dawson (1979) indicate masses no greater than $3 M_{\odot}$. However the model does suggest that RV Tau behaviour can be found in a wide variety of models. The important factor seems to be the value of L/M which is

2.10^3 in Christy's (1966) model and 10^3 in Stobie's (1969) model.

Alternation has been produced in a very different way in some of the models calculated by Deupree and Hodson (1976) using Deupree's (e.g. 1975, 1977a) 2-dimensional convection/pulsation programme. The mechanism behind the behaviour is rooted in the convective motions which are found to be damped out in alternate cycles. Since it is the action of the opacity bottling up the radiation which modulates the light output, the periods for which convection is active show greater luminosities. My objection to this model is that all of the light curves I have seen produced using this particular model of convection show significant variations from period to period. Indeed the model quoted by Deupree and Hodson (1976) as their example is the "standard" 5g model for an RR Lyrae pulsator which certainly should not alternate in the manner found.

The most promising nonlinear models in the literature seem to be those in the recent work of Bridger (1983) on the W Vir stars. He finds that amongst a set of twenty-five models distributed over the instability strip, four of the more luminous models ($L/M = 1.3$ and $2.0 \cdot 10^3$) show some evidence of alternation. These models have the following parameters;

Model	Log(L/L _⊙)	Log(T _{eff})	P(days)	δM _{bol}
14	2.9	3.74	16.0	1 ^m .4
15	2.9	3.73	17.4	1 ^m .6
22	3.1	3.77	17.1	1 ^m .05
24	3.1	3.75	20.6	1 ^m .6

where the mass is in all cases 0.6 M_⊙. The most interesting of these is model 14. This model exhibits two modes of pulsation; a cepheid-like mode with the 16 day period, and an RV-like mode which has a formal period of 32 days with "semi-periods" of 19 and 13 days. Every 8 - 10 periods the pulsation switches mode taking 3 - 4 periods to accomplish this feat. As in the Christy (1966) model the outermost zones oscillate with a doubled period although for these models mass was not lost. For another model (20) Bridger (1983) reports that the initial pulsation was very erratic because of the rather wild behaviour of the outer zone. However, after a while this outer zone took off with a velocity greater than the escape velocity and from then on the pulsation was stable. The RV-like portion of the light-curve for model 14 looks in many ways very like those of the tamer RV stars found, in particular, in the globular clusters (Erleksova 1970). Mode switching has been observed to occur in at least one and probably two field RVs. UU Her definitely exhibits two pulsation modes, again, one cepheid-like with a 70 day period and the other RV-like with a formal period of 91 days giving a period ratio of ≈ 0.7 if the short period is assumed for the RV mode. The strange

thing about this is that it would seem to be the overtone mode which is producing the alternation whereas various authors in the past (e.g. Wood 1974) have found that mass loss and irregularities are more likely to occur in the fundamental mode. This is a little disturbing. It is also possible that SU Gem shows more than one mode.

The important results of these models is that in all cases the formal period is twice the pulsation period and that there is no qualitative difference between the basic physics of the cepheid and RV models.

Takeuti and Petersen (1983) have attempted to explain the RV light curves in terms of resonances. At these longer periods and to obtain a simple alternation it is expected that the relevant resonance condition is $P_1/P_0 = 0.5$. In this model the formal period of the pulsation would be equal to the fundamental period with the second maximum being a "super-bump" in the same way as the $P_2/P_0 = 0.5$ resonance gives rise to the bumps in the BL Her stars (e.g. Carson and Stothers 1982). One immediate but tentative criticism which can be raised is that the phase of the bump in the BL Her stars is a highly critical function of the period ratio but even though the RV light curves can be highly erratic the times of both minima are always very nearly equally spaced. Another criticism, which is certainly valid, is that at the high L/M values which characterise these stars, adiabatic linear pulsation models, as used in the study by Takeuti and

Petersen (1983), do not give a good representation of the pulsation. In fact the behaviour is not even the same in quality as for the full non-adiabatic theory; let alone in quantity. For this reason the resonance hypothesis has been reexamined. However, on the basis of their adiabatic models Takeuti and Petersen (1983) conclude that the resonance condition cannot be satisfied for the observed periods, luminosities, and temperatures. Further, they find that even when the resonance condition is discarded it is still not possible to construct models satisfying the observations of the higher period RV stars for reasonable masses. Their estimates of the masses required are, like Du Puys' (1971), ludicrously small ($\sim 10^{-2} M_{\odot}$). Takeuti and Petersen (1983) appeal to nonlinear effects to save the day but whilst these do generally raise the period it is hardly likely that they can change it by the order of magnitude required. As a rough guide Ledoux and Walraven (1958) give

$$P_{nl}/P_l = (w^2/(2w-1))^{3/2}$$

where P_{nl} and P_l are the nonlinear and linear periods respectively, and w is the maximum value of the ratio of the stars radius to its equilibrium value. For the nonlinear period to be much larger than the linear period a very large amplitude is required.

6.3 THE EVOLUTIONARY STATUS OF THE RV TAU AND RELATED STARS

Gingold (1974) has followed the evolution of a $0.6 M_{\odot}$ star in detail from the horizontal branch (HB), through the helium shell burning phase, and on to the final contraction following the extinction of the energy source leading to the white dwarf stage. The star makes a number of passes across the pulsation instability strip. Horizontal branch stars lying within the instability strip are identified with RR Lyrae stars. Later, after a preliminary bluewards excursion, the star moves to the red crossing the instability strip fairly rapidly before turning to climb the H.R. diagram travelling parallel to the strip. The luminosity continues to grow through the exhaustion of core helium and then through the helium shell burning phase during which the energy output of the hydrogen shell source rises above that of the helium shell. The star is now thermally unstable and a low amplitude thermal oscillation sets in. Soon the instability switches from the oscillatory mode to a monotonically growing mode which marks the onset of the first helium shell flash. Nonlinear effects modify the monotonic perturbation to a series of relaxation oscillations, fourteen in this case, each of which produces a considerable transitory change in luminosity ($\log(L/L_{\odot}) = 3.2-3.8$). For all but the last cycle, which occurs when the envelope mass is very small, $0.005 M_{\odot}$, the corresponding temperature perturbation is small taking the star over the range $\log(T_{\text{eff}}) \simeq 3.59-3.62$. However, during the last cycle the star executes a long loop to the blue

reaching $\log(T_{eff}) \simeq 4.49$ before swinging back towards the instability strip. Following this dramatic phase the evolution turns back bluewards and the star evolves with an approximately constant luminosity ($\log(L/L_{\odot}) \simeq 3.6$) to reach $\log(T_{eff}) \simeq 5.5$ from whence it drops down the H.R. diagram to its final stage as a white-dwarf.

According to Gingold (1974) the portion of the evolutionary track of relevance to the RV and SRd stars is probably the helium shell flashing phase. Here the luminosities and temperatures should be comparable with those of the observed stars. In a histogram (fig.5 from Gingold 1974) he shows that the star spends about the same length of time at all points of the range $\log(L/L_{\odot}) \simeq 3.05-3.70$, with about twice as long close to $\log(L/L_{\odot}) \simeq 3.0$, representing about $1/6^{th}$ of its post-HB lifetime. Gingold (1974) has compared the ratio of the lifetimes for AGB stars and HB stars with the ratio of the numbers of RV and RR Lyr stars in ω Cen and finds that there are about a factor of ten fewer RV stars observed than are predicted. Since post-HB models with lower masses have much lower maximum luminosities ($0.51 M_{\odot}$ models do not even reach the red-giant stage) a spread in initial masses could explain the difference. However there are differences between theory and observation which are more difficult to explain.

In a later paper Gingold (1976) presents an analysis of the type II cepheids based upon a comprehensive set of evolutionary tracks. He examines three sequences of which two consist of models

with varying total mass but constant core mass for $Y = 0.3$ and 0.2 respectively, and a third in which the total mass is held constant whilst the core mass is varied. For a range of masses the stars make two slow passes across the instability strip with $\log(L/L_{\odot}) \approx 3.0-3.3$ in addition to the single rapid transit made by the $0.6 M_{\odot}$ model. These results are displayed in the form of a histogram giving his prediction of the number of stars to be found in a given luminosity range on the instability strip. The transits mentioned above form a high, narrow peak in the distribution at $\log(L/L_{\odot}) \approx 2.25$ for the $Y = 0.3$ constant core mass sequence, and $\log(L/L_{\odot}) \approx 2.05$ for the $Y = 0.2$ sequence. This peak can be identified with the BL Her stars and for the $Y = 0.2$ models fits very well with the observed distribution. There is a small peak in the constant core mass distributions at $\log(L/L_{\odot}) \approx 2.55-2.7$ and above that the distribution is flat extending to $\log(L/L_{\odot}) \approx 3.7$. This high luminosity tail is produced by the sensitivity of the flash luminosities to the mass. Although there is a secondary peak in the observed distribution at $\log(L/L_{\odot}) \approx 2.5$ the W Vir stars form a broad peak centred on $\log(L/L_{\odot}) \approx 2.75$ which falls off steadily up to $\log(L/L_{\odot}) \approx 3.3$. As a means of correcting this Gingold (1976) suggests that mass loss occurs during the high luminosity phases of the later evolution. The sequence of constant core mass models already shows that the luminosity of the flash driven crossing falls with mass. If the mass loss increases with luminosity, or better, if there is a low

luminosity cutoff, then this would clearly tend to pull the stars down to form a more concentrated distribution at a lower luminosity.

Gingold (1974) has already identified the RV stars with the stars undergoing helium shell flashes. The observations of Gehrz (1972) show that these stars have experienced, or are experiencing, considerable mass loss. So if the identification of the RV stars with the luminous He-shell flashing stars is correct the mass loss hypothesis of Gingold (1976) gains credence. However, infrared observations of the type II cepheids themselves (Gehrz and Hackwell 1974) show no evidence at all for circumstellar material. This implies that unless there is some way for the circumstellar matter to cease to be visible in the infrared, the type II cepheids cannot be those same stars which have lost mass.

CHAPTER 7
LINEAR PULSATION RESULTS

7.1 THE EFFECT OF VARIATIONS OF THE INPUT PHYSICS UPON PULSATION
MODELS

As stated in the introduction one of the aims of this dissertation is to examine the effects of variations in the assumed physics upon the results of linear pulsation theory. The two greatest sources of uncertainty are in the opacity and in the treatment of convection.

Recently Simon (1982) has made a plea for more work to^{be} done on heavy element opacities. This plea owes its existence largely to the greater success of pulsation models constructed using the Carson opacities when compared with those employing the Los Alamos opacities (e.g. Cox and Stewart 1965). When the source of the differences is sought the evidence points to the opacity due to the metals. Standard Los Alamos models all predict period ratios for the double mode type I cepheids (P_1/P_0) and for the bump cepheids (P_2/P_0) far greater than

those observed for the masses predicted by evolution calculations. On the other hand the period ratios predicted for the RR Lyrae stars are in accordance with the observations. Assuming the source of the discrepancy to lie in the opacity this suggests the problem is rooted in the metals opacity. In a seminal paper Fricke, Stobie and Strittmatter (1971) attacked the problem by computing pulsation models using artificially modified opacities. They find that multiplying the opacity in the regions well below the HeII ionisation zone by a factor greater than one alleviates the discrepancy somewhat. Continuing along the same tack Simon (1981) finds that increasing the opacity by a factor of around 2 for the temperatures greater than 10^5 K removes the discrepancy altogether. He elaborates on this theme (Simon 1982) by modifying the Stellingwerf opacity formula so that the metallic contribution is multiplied by a factor slightly larger than 2. This removes the period ratio discrepancy in the population I variables without introducing problems into the population II calculations.

Until recently the Carson opacities showed a bump in the region around $\log(T) \approx 5.4$ which was produced by the elements carbon, nitrogen, and oxygen. Whilst the methods of Carson et al. (1968) have been criticised (e.g. Cloutman 1973) the opacities computed using those methods do show the features required to reconcile pulsation theory with the observations. However Carson has now reexamined the problem (Carson et al. 1984) and finds that when the calculation is improved the bump disappears leaving an opacity which

is very like the Los Alamos opacity. If the intention is to look at the effects of an opacity with a bump then the Carson opacity has this bump and should be no less valid than the opacities produced by the ad hoc modifications described above. In fact when most of the calculations were performed there was little reason to regard the Carson opacities as anything other than another valid, alternative approximation to the real opacity.

However the opacity is by no means the only source of uncertainty. It is conceivable that some other improvement or variation of the input physics could give rise to a similar effect. The prime candidate is convection. In this respect it is unfortunate that convection is so very poorly understood in relation to pulsations. However an optimistic outlook has been adopted and sequences of models incorporating convection in one form or another have been constructed. The effect of differing models of the convection/pulsation coupling is examined in a later section.

Although the opacity and convection are the physical areas most likely to yield significant uncertainties there are other areas which should be scrutinised. The treatment of radiative transport in the atmospheres of pulsating stars is far from perfect (e.g. Castor 1971). It is usually assumed that the radiative relaxation time is short compared with the pulsation period. For short periods or in the case of very rarefied atmospheres this is not always true. An

alternative to the diffusion approximation, which embodies this assumption, is the Eddington approximation of Unno and Spiegel (1966) outlined in section 2.4. The effects of this alternative have been examined in a number of models. Another flaw in the radiation treatment is the assumption of plane parallel geometry in the atmosphere. This is plainly not true for a great many of the more luminous models. However the absence of any convincing tractable treatment of sphericity makes this unavoidable. In an attempt to improve upon the usual treatment Fadeev and Tutukov (1981) use a radiation dilution coefficient in their boundary condition for the radiation equation, but have not carried the modification through into the differential equations. Fox and Wood (1982) have adopted an ad hoc treatment of sphericity which involves a locally defined optical depth which unfortunately is not guaranteed to be monotonic with geometric depth.

Another source of uncertainty lies in the boundary condition adopted for the momentum equation. Quite apart from the problem of deciding where the stellar surface lies, there is the possibility that pulsational energy can propagate through the surface in the form of running waves. This can occur if, for a given period, the temperature is high enough or if the gravitational force is sufficiently low. The latter could well be important for models of type II cepheids or, more likely, RV Tauri stars.

There are three ways in which these uncertainties manifest themselves in linear pulsation models. The growth rate of oscillations is likely to be the property most sensitive to variations since all of the uncertainties considered affect energy transport, that is the retention of pulsation energy by the star. In particular all introduce new sources of dissipation. Convection can also introduce a new driving term through the effects of turbulent pressure, which is omitted from my models, and also, less realistically, through the turbulent viscosity term. The Carson opacity tends to be "bumpier" than the Los Alamos counterpart and so can be expected to contribute both driving and dissipation.

The second property to be affected is the pulsation period. In this case the effects can be expected to be very much smaller unless the nonadiabaticity, the degree of coupling of the dynamics with the energy transport, is very pronounced. Finally it is quite likely that the phase-lag between the velocity perturbation and luminosity will be affected. Since this is a property of the energy transport mechanism it should be sensitive to variations. However since the observed stars of interest have highly nonsinusoidal light curves this property is suitable only for the crudest comparison with the observations.

7.1.1 Convection And The Carson Opacities

Stellar models constructed using the Carson opacities which include metals possess a convection zone coinciding with the CNO bump which models using the Los Alamos opacities lack. (N.B. All the models described from here on were constructed using a mixing length, l , given by $l/H_p = 1$.) At high luminosities, $\log(L/L_\odot) \geq 3.25$, the difference is striking. This convection zone is always inefficient with $(L_c/L)_{\text{CNO}_{\text{MAX}}} = 0.58$ for $\log(L/L_\odot) = 4.0$. Table 7.1 shows the results for a selection of models. The strength of the convection zone shows no variation with effective temperature. When the luminosity rises from $\log(L/L_\odot) = 3.25$ to 4.0 the peak fraction of luminosity carried by convection rises steadily

A similar but stronger convection zone driven by the CNO bump is described by Stothers (1976) in a study of massive, luminous main sequence stars.

This convection zone forces the temperature gradient down and so prevents the radiation pressure from rising to the levels found in some of the more luminous radiative models. The Eddington luminosity is clearly exceeded locally and so the possibility of dynamical instability must be born in mind. As a matter of course a search is made for dynamically unstable modes in the adiabatic approximation. Stability in the adiabatic limit should ensure stability when nonadiabatic effects are reintroduced (for example Fox and Wood

Table 7.1 $(L_e/L)_{\text{CNOmax}}$ for various models using the Carson opacity for $Z = 0.005$ with $M = 0.6 M_\odot$

$\text{Log}(L/L_\odot) \setminus \text{log}(T_{\text{eff}})$	3.58	3.67	3.76
4.00	0.58	0.57	0.57
3.75	0.34		0.34
3.50	0.20		0.19
3.25	0.07		0.07

1982). So far none of the models have displayed dynamical instability.

A number of models for the interaction of pulsation and convection have been programmed. The choice of the model can be made from; the Unno theory, instantaneous relaxation of convection to follow the pulsation, or a zero convective flux perturbation. In addition turbulent viscosity may be included and Saio's modification of the small scale turbulence is available. The choice of the model does not make a radical difference to the behaviour of the lower luminosity stars, for example for RR Lyrae or classical cepheid models as has been reported by Baker and Gough (1979), and Gonczi and Osaki (1981). However for some of the stars in this work the choice becomes critical and, I think, shows up short comings in the theory.

The ratio of the convective time scale and the pulsation period is the critical quantity. As an example consider a star with $M = 0.6 M_{\odot}$, $\log(L/L_{\odot}) = 3.5$, $\log(T_{\text{eff}}) = 3.76$, $1/H_p = 1$. In the H/HeI ionisation zone $\tau_{\text{conv}}/\tau_{\text{dyn}} = 7.4 \times 10^{-2}$, whilst at the centre of the HeII ionisation zone $\tau_{\text{conv}}/\tau_{\text{dyn}} = 33$. The mass of the H/HeI ionisation zone is very small and much less than that of the HeII ionisation zone which would make it unlikely that it should have much effect upon the dynamics of the model. This would imply that it is safe to use the simple $\delta L_c/L = 0$ model. A comparison of the pulsation properties of this model shows startling differences.

	P_{oad}	P_o	P_i
$\delta L_c/L = 0$	47.6	31.25	16.65
Unno	"	52.57	13.78
Unno + Saio	"	52.53	13.77
Instantaneous	"	52.59	13.81

Evidently it is the H/HeI ionisation zone that dominates the behaviour. An examination of the eigenvectors confirms this. Figs. 7.1+7.2 show the eigen vectors for the first and second models. There is a very considerable difference in the effect of the H/HeI ionisation zone at $\log(p) = 2.9$ upon $\zeta r/r$. The effect of the HeII zone at $\log(p) = 4.0$ is rather smaller. I find it difficult to believe that the H/HeI ionisation zone could influence the dynamics to this extent. It seems to me that the effect is massively overestimated probably because of the omission of nonlocal effects and the turbulent pressure in the calculations. Consequently the safest approach is to drop the convective terms from the pulsation equations. This has been done in the remainder of the calculations in this dissertation. One advantage of this is that a direct comparison can be made with other work, for example Saio, Wheeler and Cox (1984).

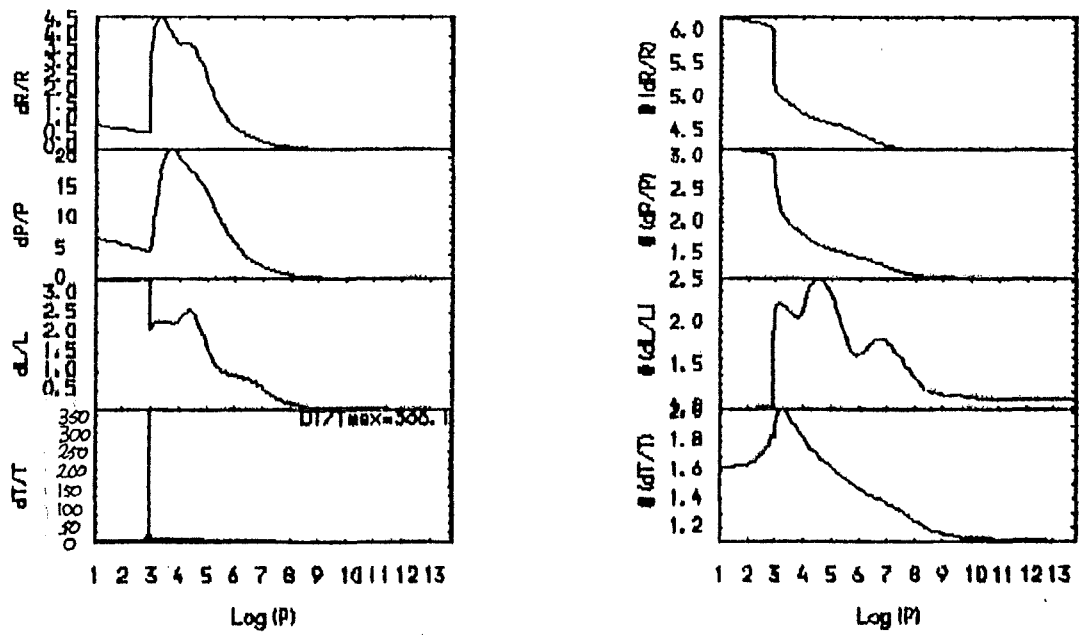


Fig. 7.1 Eigenfunctions for the fundamental mode using the approximation $\delta L_e / L_e = 0$ (see text)

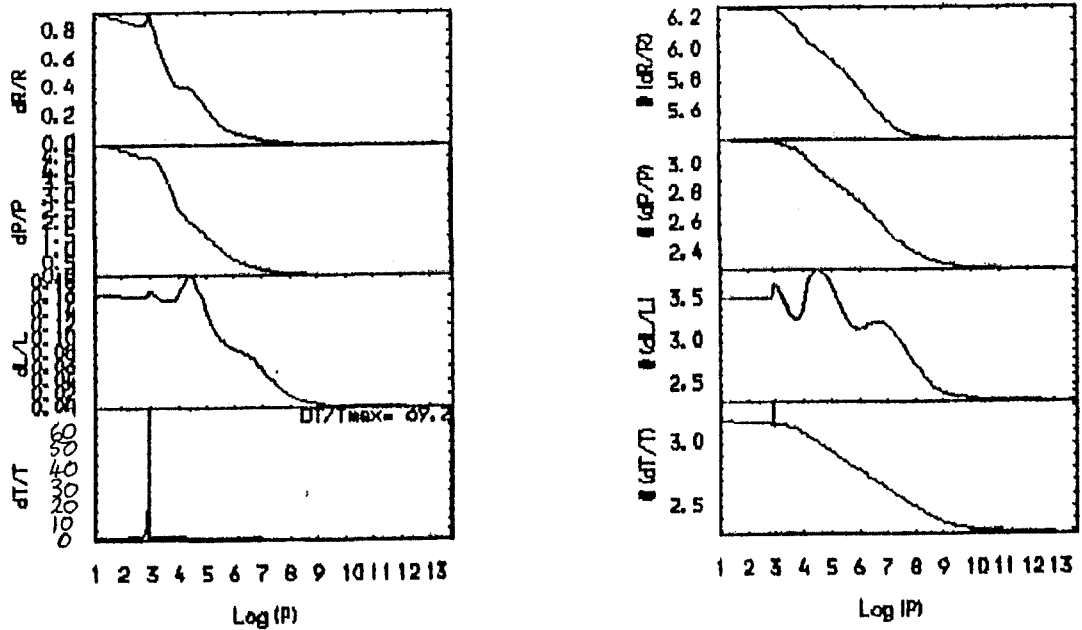


Fig. 7.2 Eigenfunctions for the fundamental mode using the Unno model for $\delta L_e / L_e$ (see text)

7.1.2 Sensitivity Of The Fundamental Blue Edges To Variations Of The Physics

Apart from the lower luminosities (RR Lyrae stars) the overtone blue edges lie redwards of the fundamental blue edge and so the bluewards limit for all the radial modes of pulsation is the fundamental blue edge. The overtone blue edges are also far more sensitive to the outer boundary condition, since the peak of the oscillatory moment of inertia moves towards the surface as the mode order increases, and also to the zoning because the local wave number increases with mode order. A further problem is that the outer node of the 2nd overtone eigenfunction moves out towards the surface to around zone N-2. This means that the eigenfunction is poorly resolved. This effect has previously been observed by Fox and Wood (1982).

At very high luminosities problems start to creep in. As L/M rises the path of the stellar model across the Carson opacity table moves towards the low density boundary and eventually substantial regions have to be calculated using extrapolated opacities. This can become a rather hair raising occupation when the CNO bump is prominent. The result of this is that the highest luminosity to which a model sequence is taken is often dictated by the limitations of the opacity tables. When convection is included in the models this effect is mellowed and models with $L/M \sim 2.10^6$ have been constructed. At the

very highest luminosities the nonadiabaticity becomes very important and the organisation and behaviour of the pulsation modes becomes exceedingly complicated. This has already been documented for high luminosity helium stars by Wood (1976), Saio and Wheeler (1983), and more comprehensively by Saio, Wheeler and Cox (1984). The high luminosity behaviour includes the appearance of new modes. The behaviour of the blue edges also becomes qualitatively different.

The method used to locate the blue edges when the modes are all well behaved, that is for $L/M \leq 2.10^3$, is an iteration on $\log(T_{eff})$ solving for $\eta = 0$. A bisection algorithm is employed. The iteration is halted when either,

$$|(\log(T_{eff}))^{(n)} - (\log(T_{eff}))^{(n-1)}| < 10^{-2}$$

or

$$|\eta / \eta_{max}| < 10^{-2}$$

where η_{max} is the greatest value of the magnitude of the growth rate found so far for that iteration.

7.1.2.1 Different Implementations Of The Carson Opacities -

Blue edges have been computed for $M = 0.6 M_{\odot}$, $Z = 0.00$ and 0.02 using linear interpolation, bicubic spline interpolation, and a spline surface fitted to the Carson tables. There is not any radical difference in approach between the linear and quadratic interpolation and so the latter is omitted. As can be seen from fig. 7.3 all three methods give concordant results for the metal free table. So far as

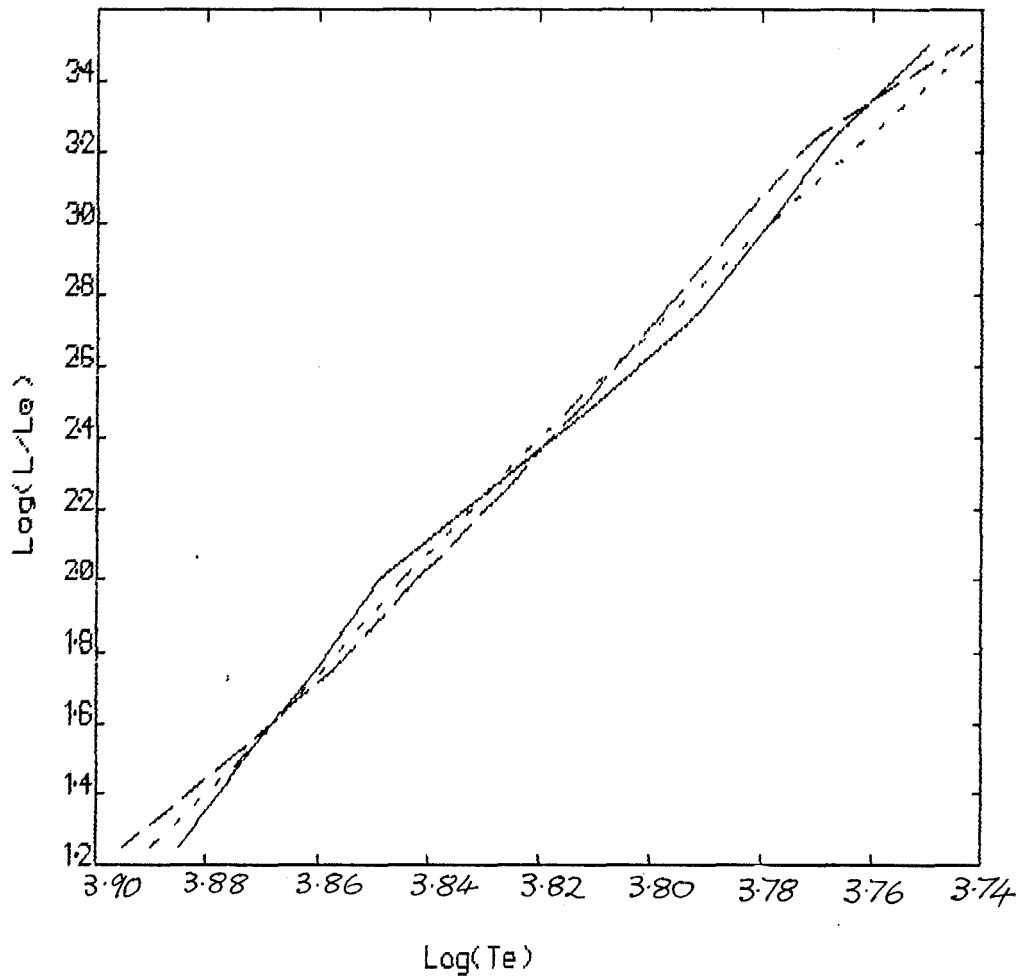


Fig. 7.3

Blue edges using different opacity implementations for $Z = 0.000$

- = linear interpolation
- - - = cubic spline interpolation
- · - = fitted spline surface

the interpolation method is concerned we can adopt an uncertainty of $\delta \log_{10}(T_{eff}) = 0.006$ or $\delta T_{eff}/T_{eff} = 0.015$ for any given luminosity. This is encouraging. Fig. 7.4 shows the corresponding data for $Z = 0.02$. It is not encouraging. The behaviour of results from the fitted opacity surface is not at all like that of the interpolated opacities. As was mentioned in section 4.2 (on the opacity implementation) it is virtually impossible to resolve the metallic opacity data with fewer points than are present in the table. The fitted surface must therefore be counted as a failure.

Comparison of the linear and spline interpolation results for this metallicity does not give particularly inspiring results either. The uncertainties are estimated to be $\delta \log_{10}(T_{eff}) = 0.01$ or $\delta T_{eff}/T_{eff} = 0.023$ at the lowest luminosity rising to twice this value at $\log_{10}(L/L_{\odot}) = 3.0$. It is not clear which method should be adopted. Plainly in an ideal world the cubic spline technique should be favoured since it provides the best differentiability and "smoothness" properties (e.g. Aalberg et al. 1967). However the preliminary interpolation onto a new rectangular grid introduces a new source of uncertainty. Worse, the splines are poorly defined at the edges of the table. Since the models tend towards the low density edge of the table this greatly reduces my faith in the veracity of the results obtained with the spline method. The more luminous a star is then the more strongly it will be affected by this source of error and so the increase of the uncertainty with luminosity comes as no surprise. For

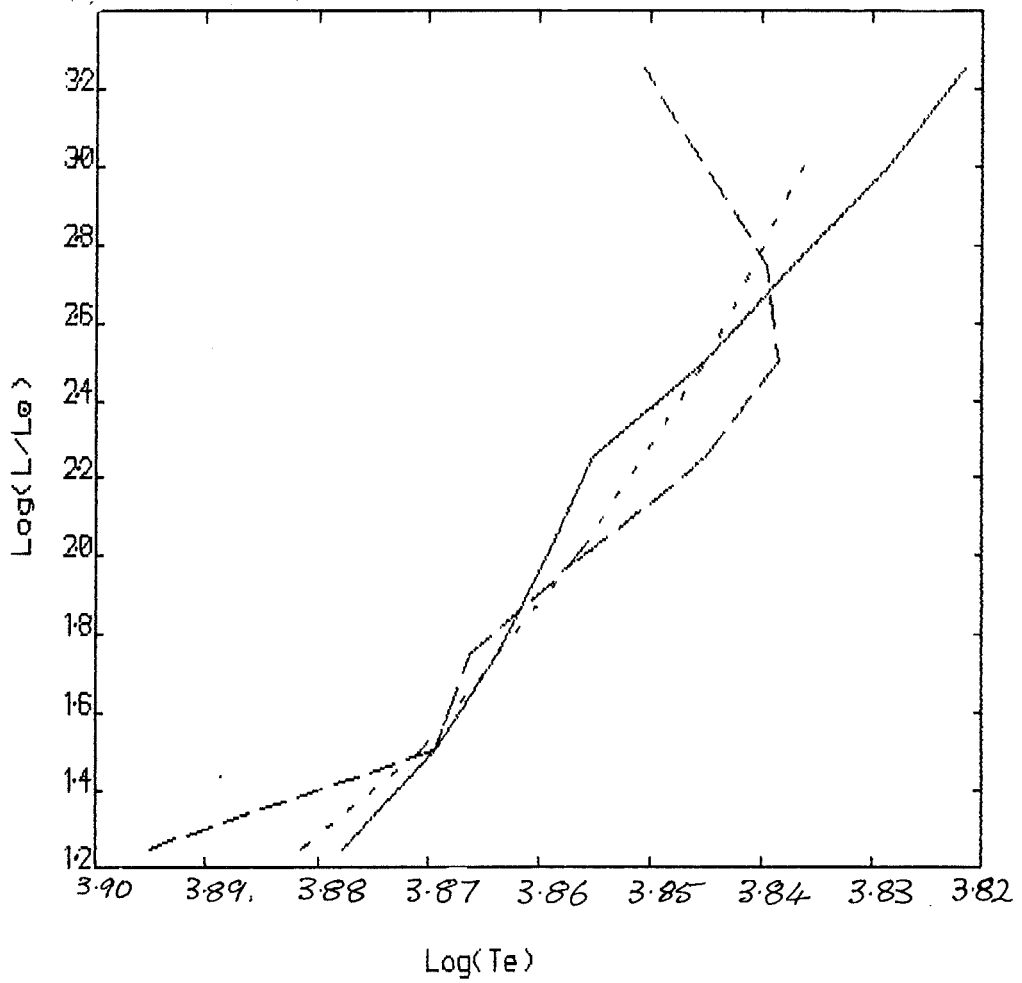


Fig. 7.4

Blue edges using different opacity implementations for $Z = 0.020$

- = linear interpolation
- = cubic spline interpolation
- · - · = fitted spline surface

this reason the linear interpolation method, for all its faults, is retained for the bulk of the results obtained in the following chapters.

7.1.2.2 A Comparison Of Different Opacities -

Carson, Stothers and Vemury (1981) made calculations of fundamental blue edges using the Carson opacity tables for $M = 0.6 M_{\odot}$, $\log(L/L_{\odot}) = 2.0, 2.5, 3.0$ for $Z = 0.000, 0.005, 0.010, 0.020$. However these calculations were made using the Baker-Kippenhahn momentum boundary condition applied at $\tau = 2/3$. Models computed using this boundary condition are not comparable with nonlinear models and it is in any case difficult to make a good approximation to the radiative transport when $\tau \ll 1$ does not hold. I adopt the Castor-Iben boundary condition as given in section 2.5 which is applied at $\tau \approx 0$. The effect of the differing boundary conditions upon the blue edges is seen in fig. 7.5 for $Z = 0.005$.

Blue edges for $Z = 0.000$ computed using linear interpolation in the Carson tables and the Stellingwerf opacity fit (as the best available representation of the Los Alamos opacities) are displayed in fig. 7.6. The additional blue edge is interpolated from King, Cox and Hodson (1981) with $Z = 0.001$, a difference which should be negligible considering the very small effect of metallicity variations when the Los Alamos opacities are used. Comparison of the King and Carson blue

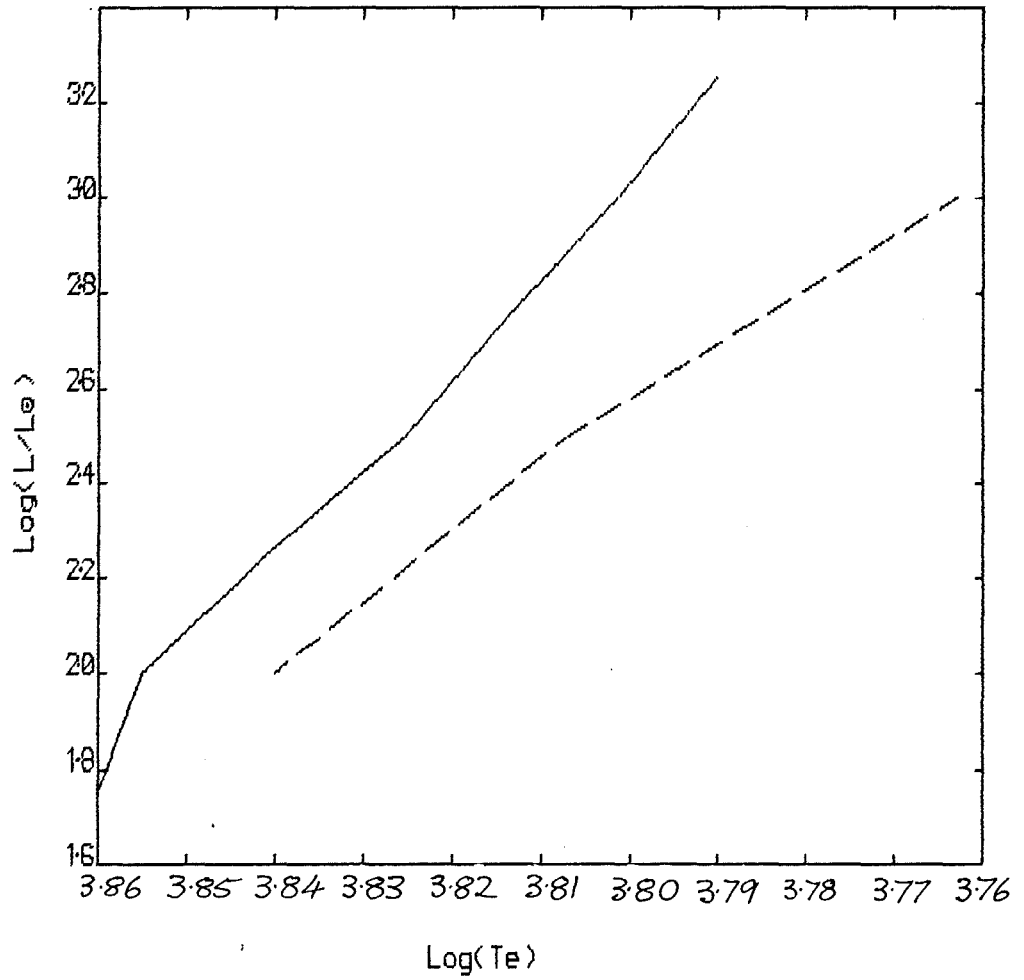


Fig. 7.5

Blue edges for $Z = 0.005$ from;

this work

Carson et al. (1981)

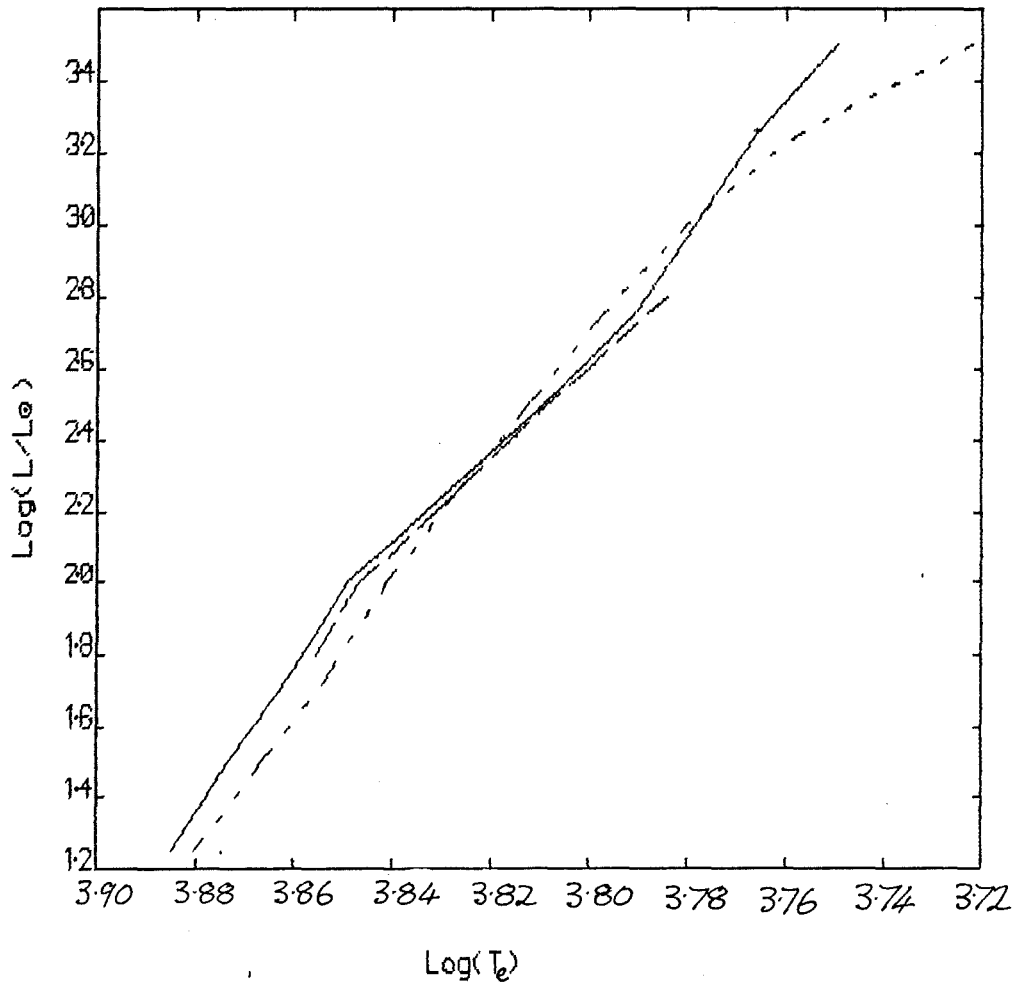


Fig. 7.6

Blue edges for $Z = 0.000$

- = Carson opacity
- = Stellingwerf opacity formula
- · - · - = from King et al. (1981)

edges gives excellent agreement right down to the bend at $\log(L/L_{\odot}) = 2.0$. This implies that the Carson and Los Alamos opacities are indistinguishable so far as blue edges are concerned when metals are absent from the models. Although the Carson and Stellingwerf derived blue edges differ by a greater margin this is still no greater than the uncertainty due to different methods of interpolation for the Carson opacity. Since the Stellingwerf fit can only be expected to hold for a limited range of conditions similar to those found in RR Lyrae stars the high luminosity results might be somewhat uncertain.

When metals are introduced into the models a large difference between the blue edges computed using the two opacities appears. This can be seen clearly from fig. 7.7 which displays results for the linearly interpolated Carson opacity, the Stellingwerf formula, and the cubic spline fit to the Carson opacity. The last set of results is included in order to demonstrate that even when the most pessimistic view is taken of the uncertainties involved in interpolation the difference between the two sets of opacities is still larger. This fundamental difference between the metallicity dependence of blue edges computed using the different opacities was first found by Carson and Stothers (1976). This difference can be seen by comparing figs. 7.8 and 7.9. With the exception of the dubious high luminosity points the Los Alamos (Stellingwerf) blue edges show the same movement to the red with increasing metallicity

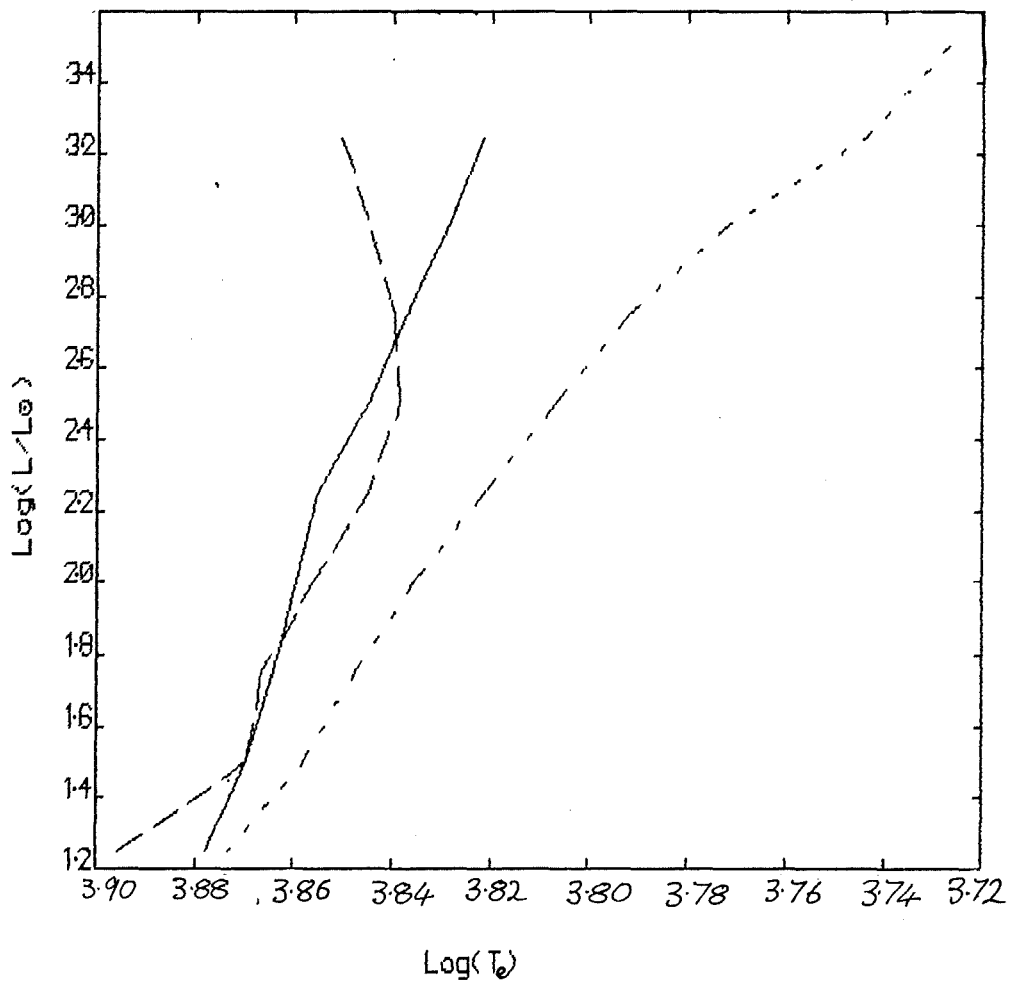


Fig. 7.7

Blue edges for $Z = 0.020$

- = Carson opacity with linear interpolation
- = Carson opacity with fitted spline surface
- · - · - = Stellingwerf opacity formula

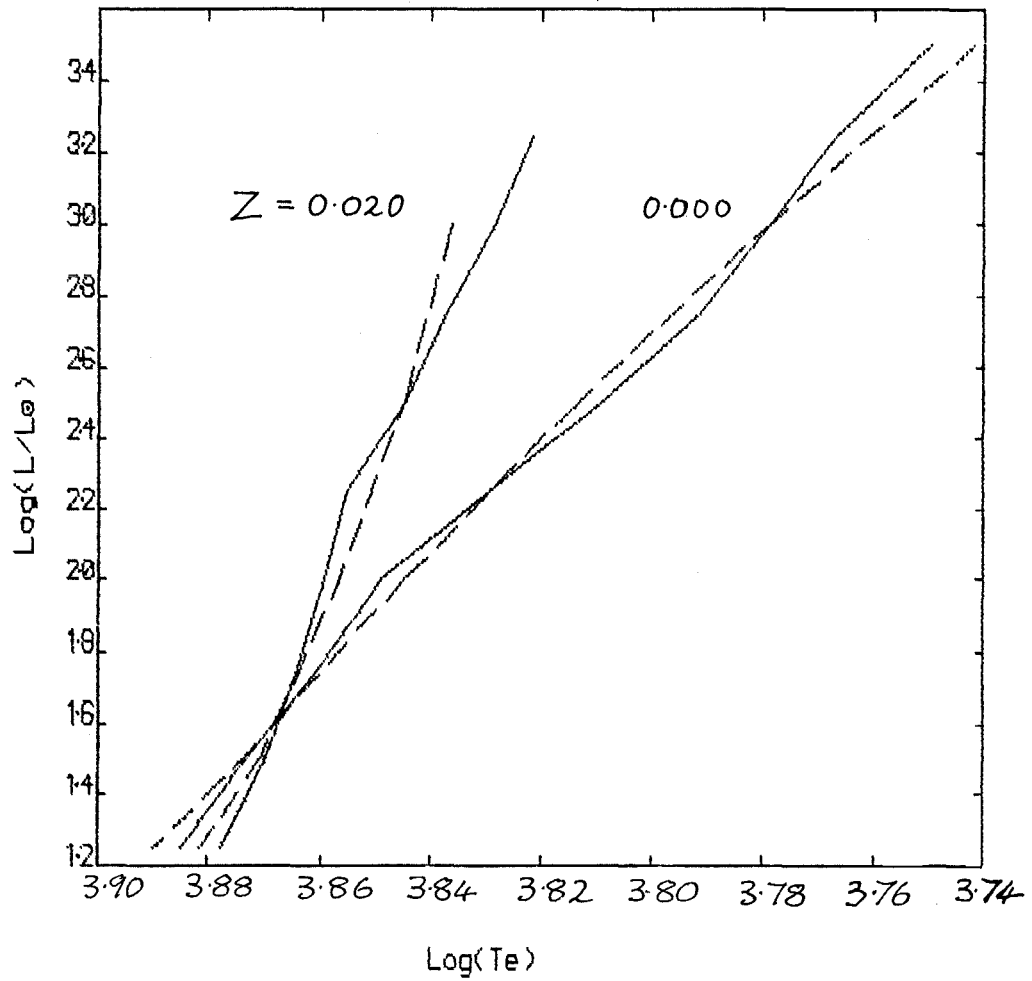


Fig. 7.8

Blue edges for $M = 0.6 M_\odot$ with the Carson opacities for $Z = 0.000$ and 0.020

— = linear interpolation
 - - - = cubic spline interpolation

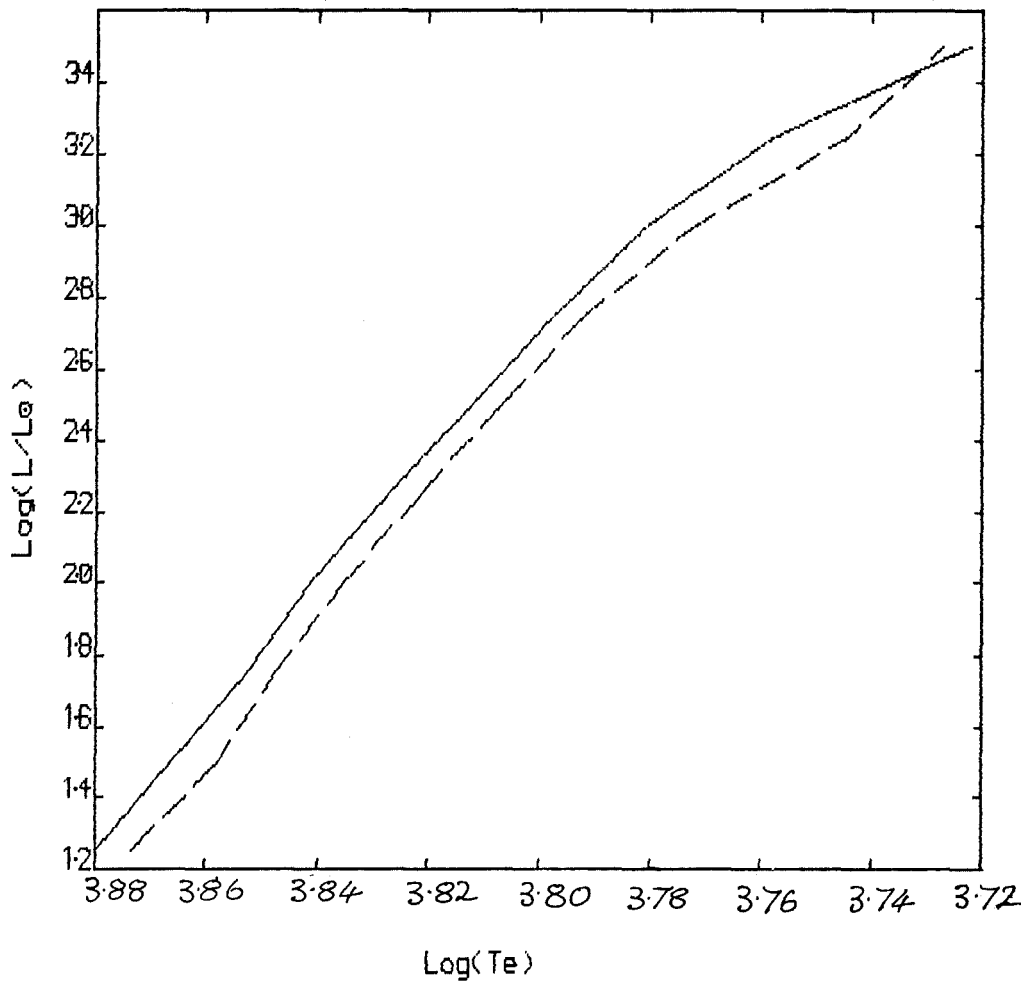


Fig. 7.9

Blue edges for $M = 0.6 M_{\odot}$ with the Stellingwerf opacity formula

— = $Z = 0.000$
 - - - = 0.020

for all luminosities. The blue edges computed using the Carson opacities show the same trend for the low luminosities. However this dependence decreases in strength as the luminosity rises until the blue edges cross at $\log(L/L_{\odot}) \simeq 1.6$. For further increases in luminosity the blue edges show a very strong metallicity dependence with the opposite sense. This is independent of whether or not a spline or linear interpolation is used. The crossover point is well defined and is independent of the method of interpolation. However the swing towards the blue found by Carson et al. (1981) for the $Z = 0.020$ blue edge has not been found in the present calculations for $M = 0.6 M_{\odot}$. It did appear in calculations for higher masses, for example see fig. 7.10 for $M = 2.0 M_{\odot}$. This is probably a result of the differing boundary conditions.

In order to illuminate the mechanism giving rise to the differing metallicity dependences the details of a set of four models are displayed in figs. 7.11 - 7.14. The models are all computed with $M = 0.6 M_{\odot}$ at $\log(L/L_{\odot}) = 3.0$ with $\log(T_{eff}) = 3.76$ and so lie close to the $Z = 0.000$ blue edge. For the Carson opacities cubic spline interpolation is used whilst the Stellingwerf fit represents the Los Alamos opacities. The metallicities used are $Z = 0.000$ and 0.020 . The quantity dW/dm is the work done per unit mass normalised to the total kinetic energy. Its step like appearance results from an averaging over roughly constant masses for the otherwise unmanageable H/HeI ionisation zone.

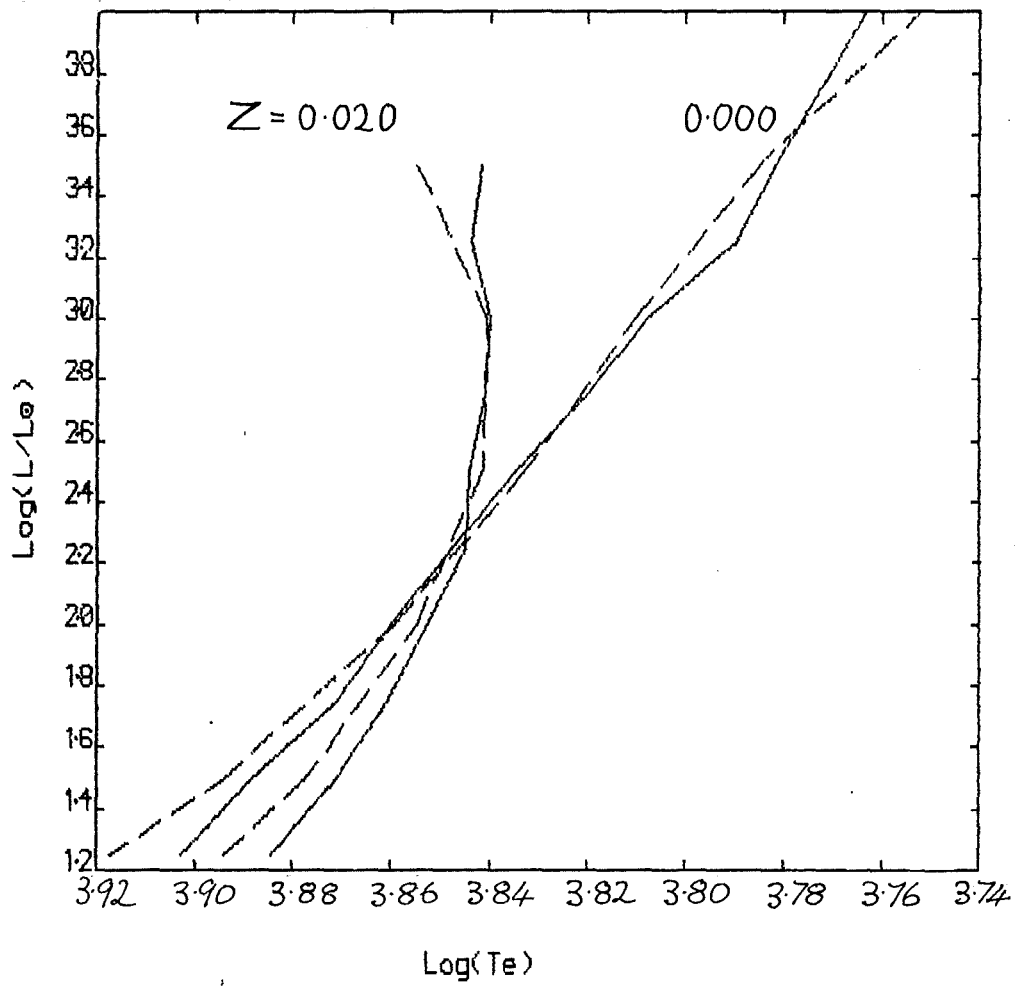


Fig. 7.10

Blue edges for $M = 2.0 M_{\odot}$ with
the Carson opacities for
 $Z = 0.000$ and 0.020

———— = linear interpolation
----- = cubic spline interpolation

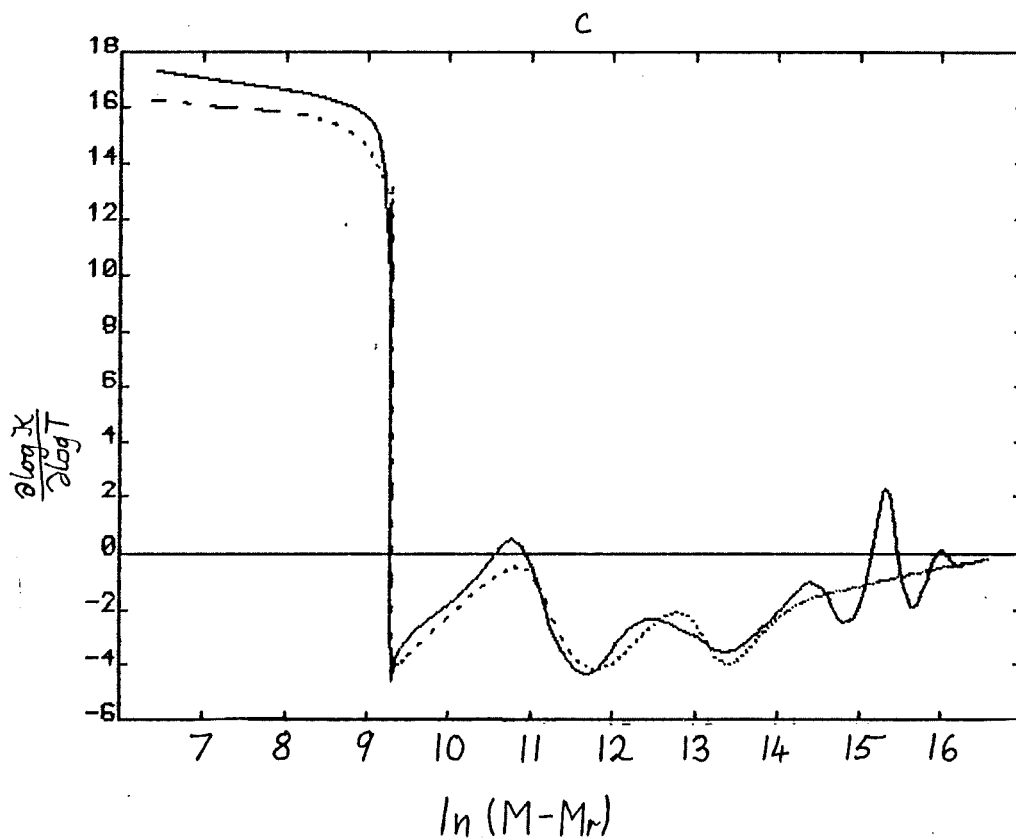
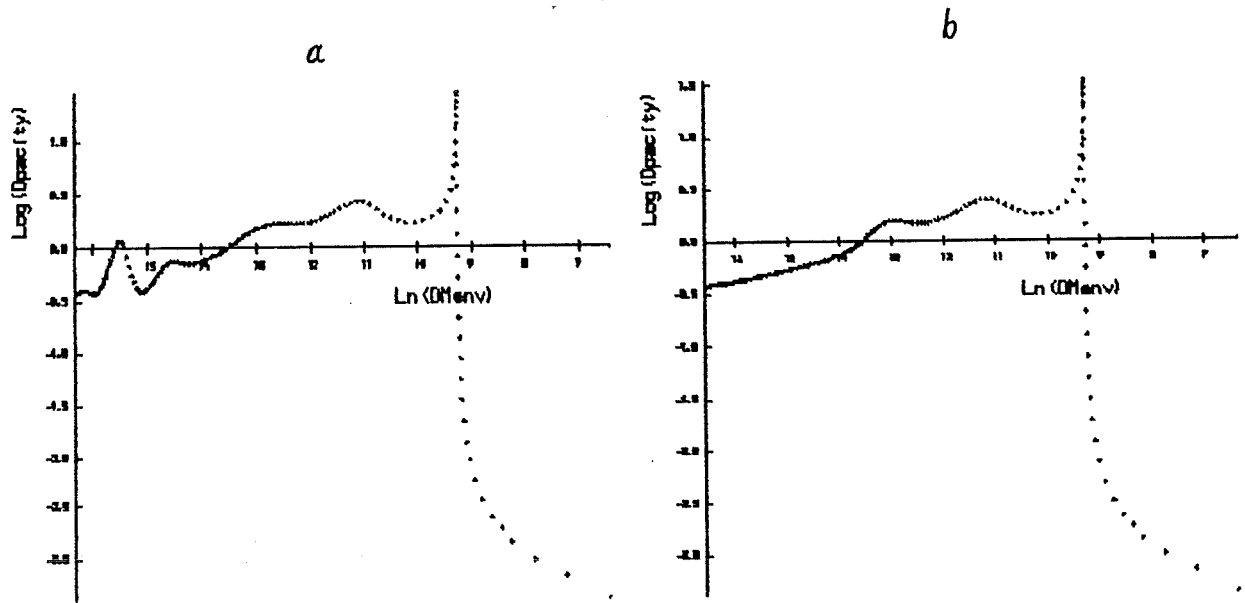


Fig. 7.11 Opacities for $Z = 0.000$

- a) Opacity with mass for Carson opacity
- b) " " " " Stellingwerf formula
- c) Derivative of opacity w.r.t. temperature
- = Carson opacity

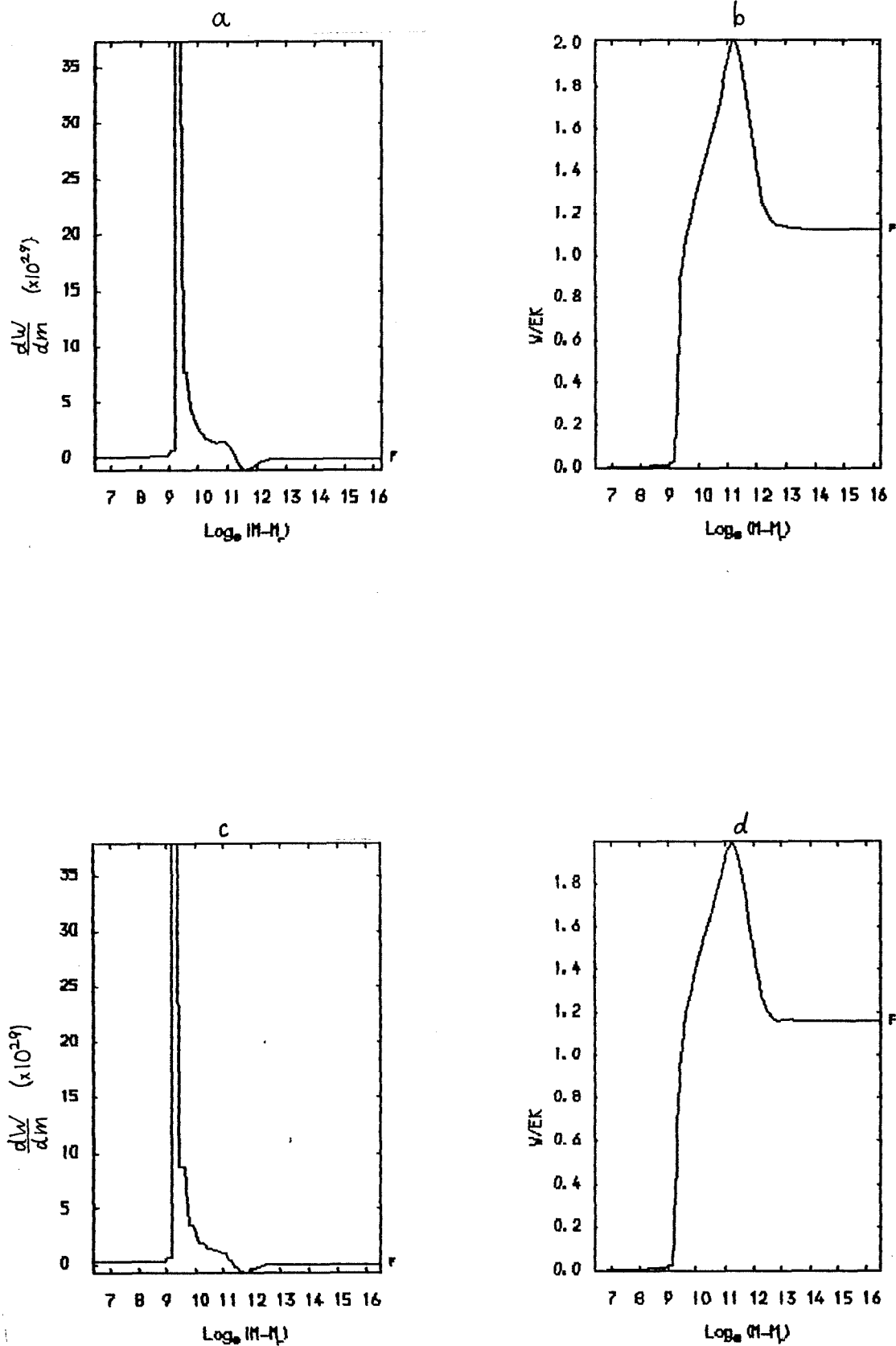


Fig. 7.12 Work functions and integrals for $Z = 0.000$

- a) Work function (normalised to total kinetic energy) for Carson opacity
- b) Work integral for Carson opacity
- c) Work function for Stellingwerf formula
- d) Work integral for Stellingwerf formula

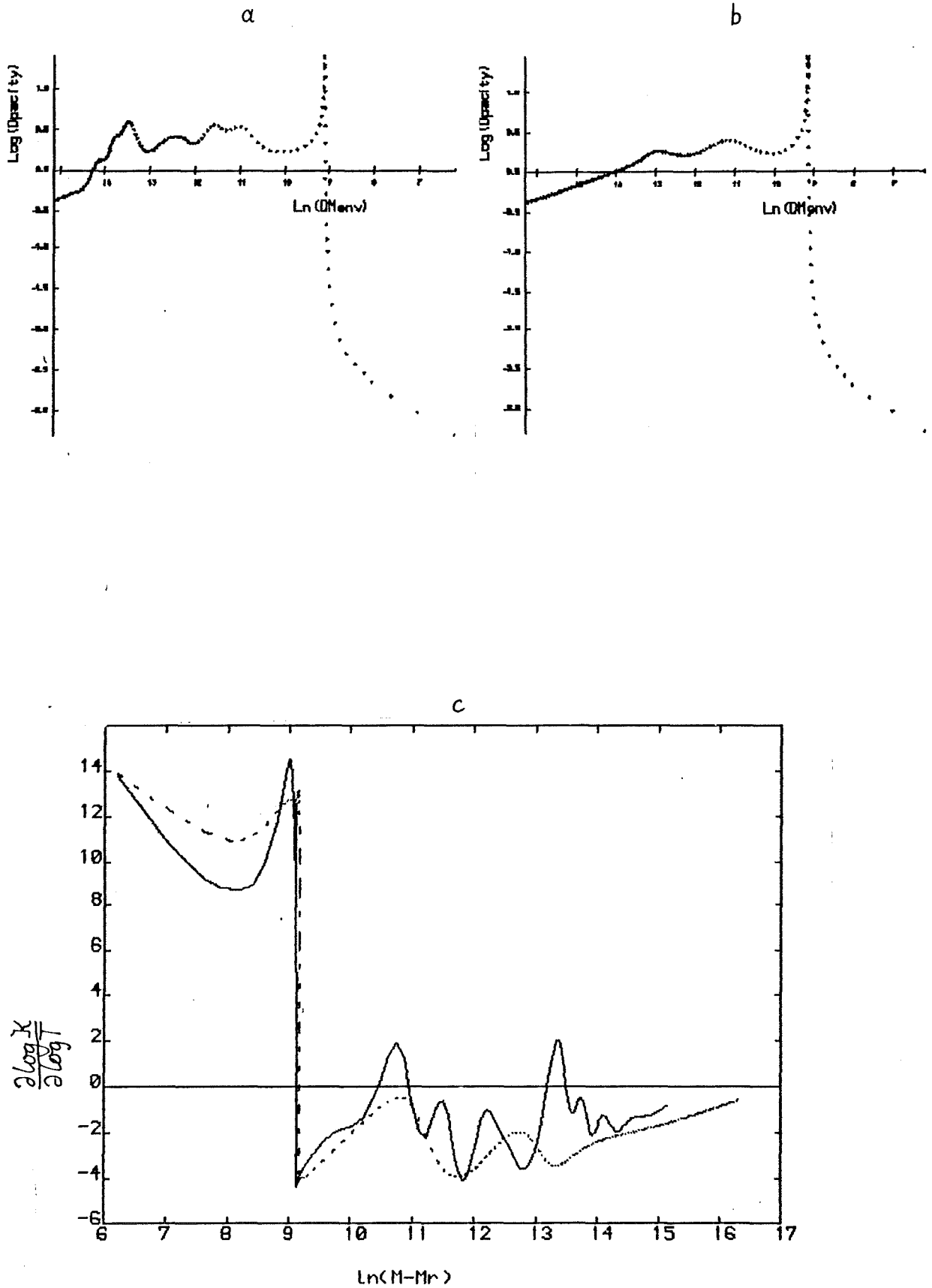


Fig. 7.13

Opacities for $Z = 0.020$

- a) Opacity with mass for Carson opacity
- b) " " " " Stellingwerf formula
- c) Derivative of opacity w.r.t. temperature
- = Carson opacity
- = Stellingwerf formula

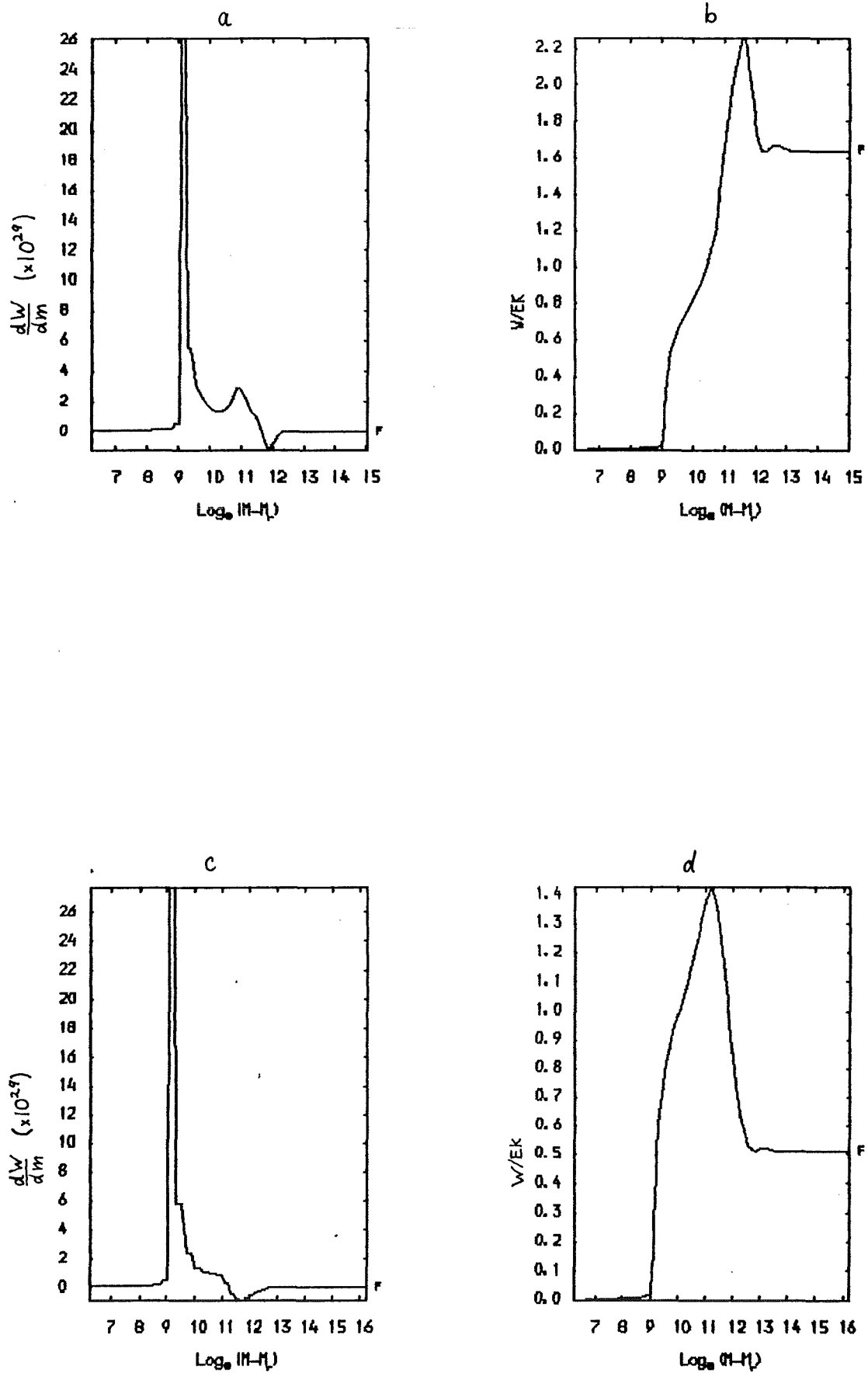


Fig. 7.14 Work functions and integrals for $Z = 0.020$

- a) Work function (normalised to total kinetic energy) for Carson opacity
- b) Work integral for Carson opacity
- c) Work function for Stellingwerf formula
- d) Work integral for Stellingwerf formula

There is little difference between the $Z = 0.000$ opacities (fig. 7.11) except for a curious bump in the Carson model at $\log_e(M-m_r) \approx 15.5$. Little difference in the work functions can be detected, fig. 7.12. The opacity feature deep in the envelope has a negligible effect upon stability because the pulsation amplitude is so small there. There is little to distinguish the $\frac{\omega}{\lambda}$ Los Alamos opacity models of figs. 7.11 and 7.13. However the Carson model, fig. 7.13, for $Z = 0.020$ has a very much larger opacity bump at $\log_e(M-m_r) = 10.5 - 11.0$ for which the temperature derivative is appreciably positive. This region gives rise to a hump in the work function (dW/dm) which peaks at $\log_e(M-m_r) = 11.0$. In addition the sharp drop followed by a new bump ($\log_e(M-m) = 11.5 - 12.0 - 13.0$) greatly reduces the efficacy of the radiative damping. There is little difference in the driving produced by the H/HeI regions ($\sim 0.6 - 0.7$ for both opacities) but the new driving zone ($\Delta(W/E_k) \approx 1.2$ and 0.6 for the Carson and Los Alamos opacities respectively) and the diminished damping ($\Delta(W/E_k) \approx -0.6$ and -0.9 respectively) produce a profound difference.

7.1.2.3 Blue Edges For Different Metallicities -

Sets of blue edges have been computed using the Carson opacity tables for all the metallicities available, that is for $Z = 0.000$, 0.005 , 0.010 , and 0.020 . A number of masses have been used, namely; $M/M_\odot = 0.6$, 0.8 , 1.2 , 2.0 , and 5.0 . These span those likely for

population II variables (0.6 - 0.8) and the masses which have been quoted for RV Tauri variables (Dawson 1979). The limits on the luminosities are arbitrary at the lower end. The problems encountered at the higher luminosities have already been described. In particular the Carson bumps can lead to large regions in which pressure radiation dominates to the extent that in some more extreme cases $P_g/P \sim 10^{-3}$ leading to a failure of the equation of state subroutine.

The results of these calculations are displayed in figs. 7.15 - 19. All of these sequences display the same general behaviour. In all cases there is a more or less well defined crossover point of the blue edges for different metallicities. This effect is most clearly seen in the results for $M = 0.8$ (fig. 7.16). There is a tendency for the crossover point to move to higher luminosities as the mass is increased. In fact, to a high accuracy (the correlation coefficient, $r = 0.998$),

$$\log(L_{x-over}/L_{\odot}) = 0.768 \log(M/M_{\odot}) - 1.453$$

For the more luminous models with high metallicity there is a tendency for blue edge to curl around so the that $dT_{blue-edge}/dL > 0$. This was found by Carson et al. (1981) for the $M = 0.6 M_{\odot}$ models. The effect might be related to the effects found by Saio and Wheeler (1983), and Cox and Stellingwerf (1979). The authors of the latter paper derive a simple expression for the locus of the blue edge in terms of p_r/p and show that the strong effect of radiation pressure on the heat capacity ($p_r/p = 0.1$ gives $C_v/C_{vg} \sim 2$) causes the blue edge to become almost

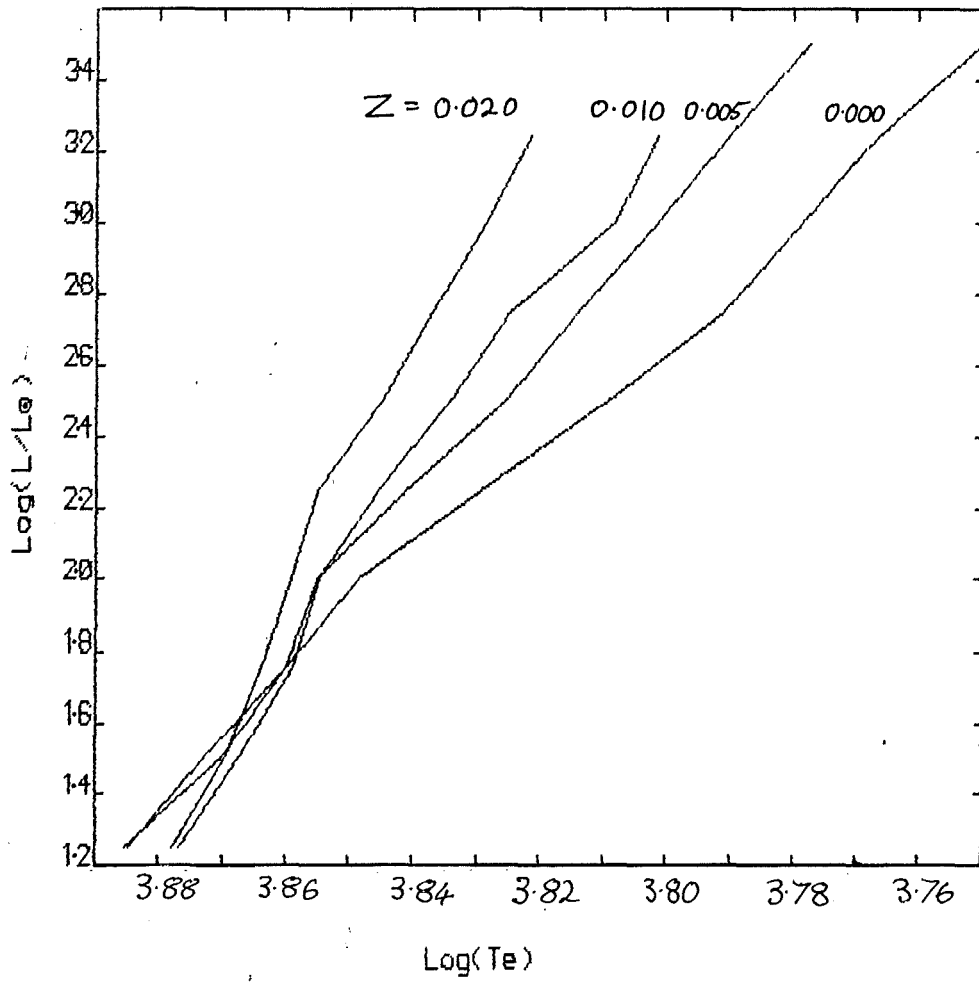


Fig. 7.15 Blue edges for $M = 0.6 M_{\odot}$

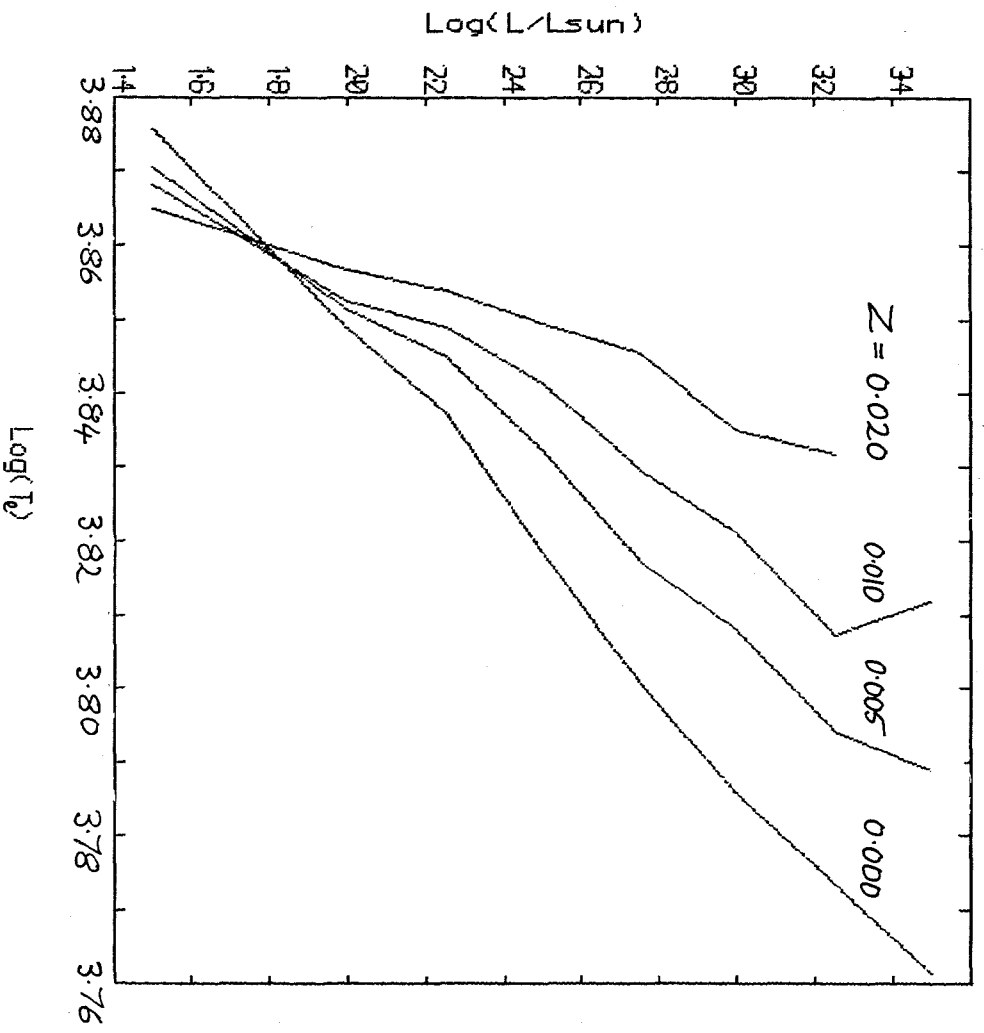


FIG. 7.16 Blue edges for $M = 0.8 M_{\odot}$

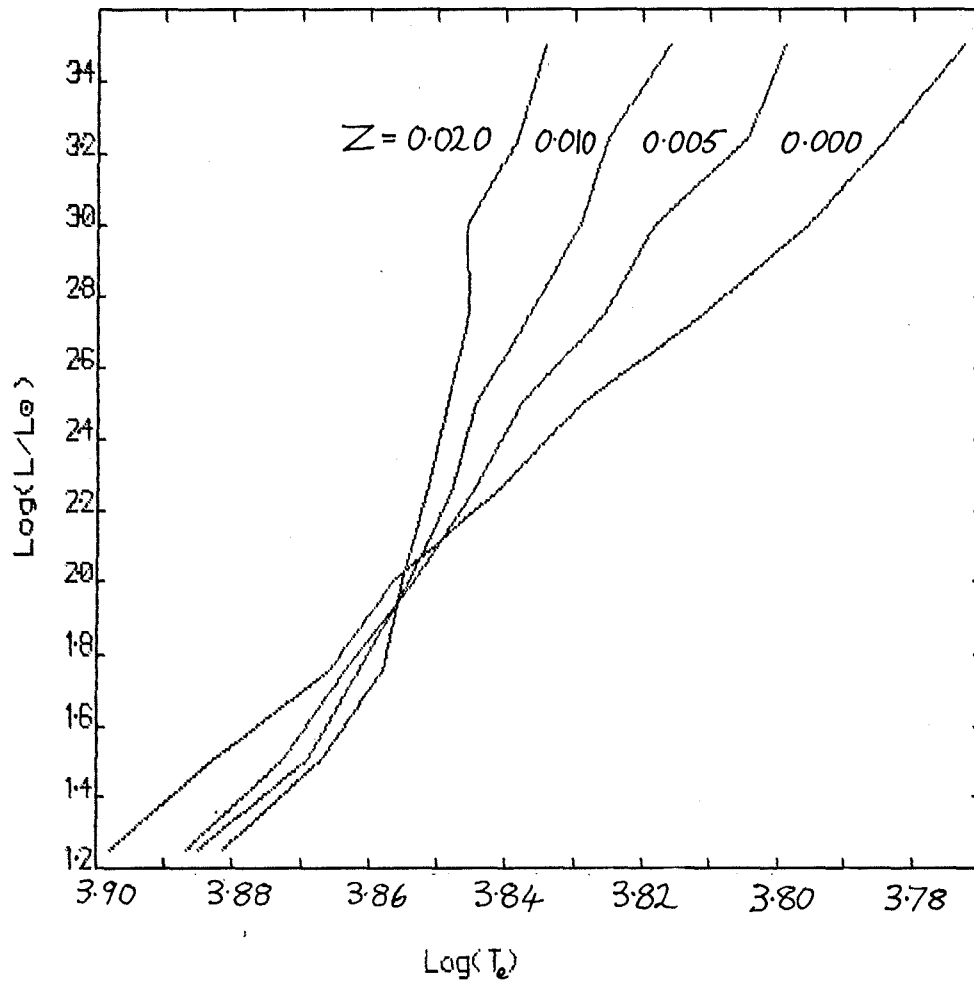


Fig. 7.17 Blue edges for $M = 1.2 M_{\odot}$

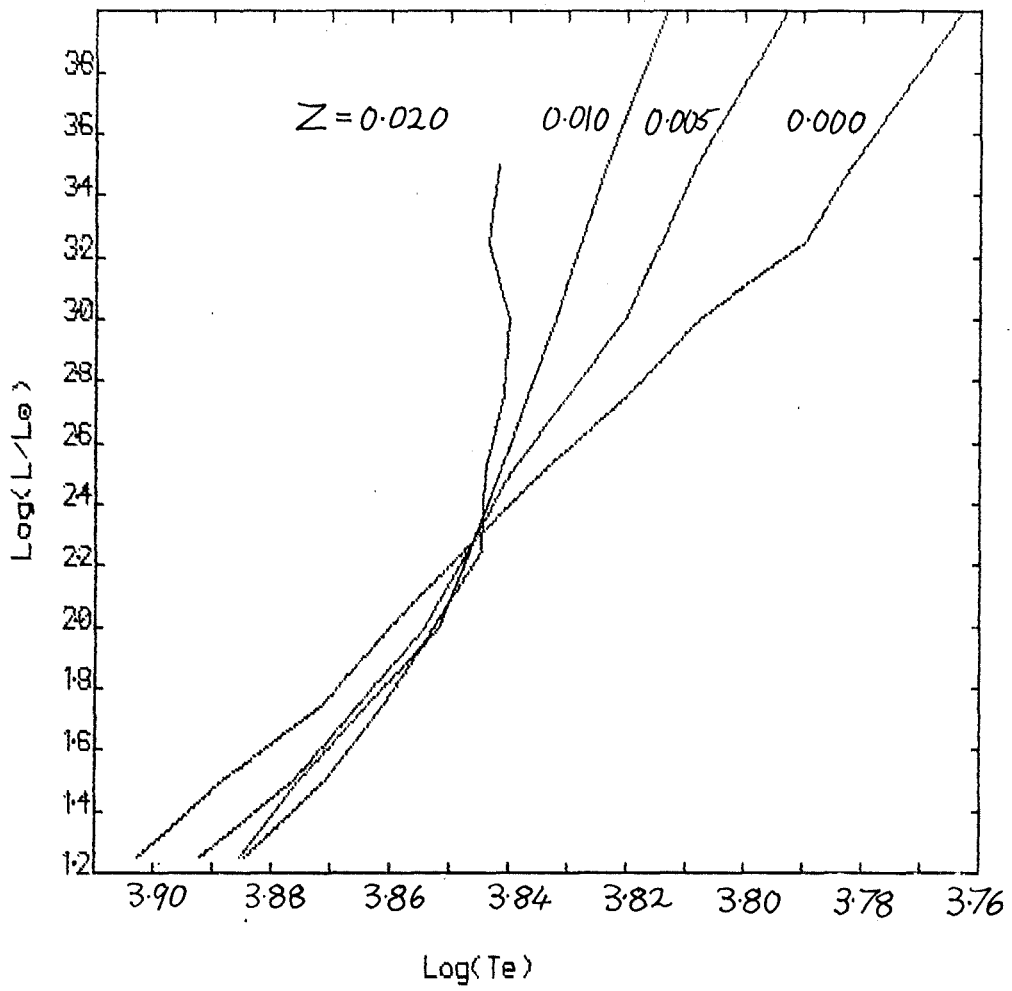


Fig. 7.18 Blue edges for $M = 2.0 M_{\odot}$

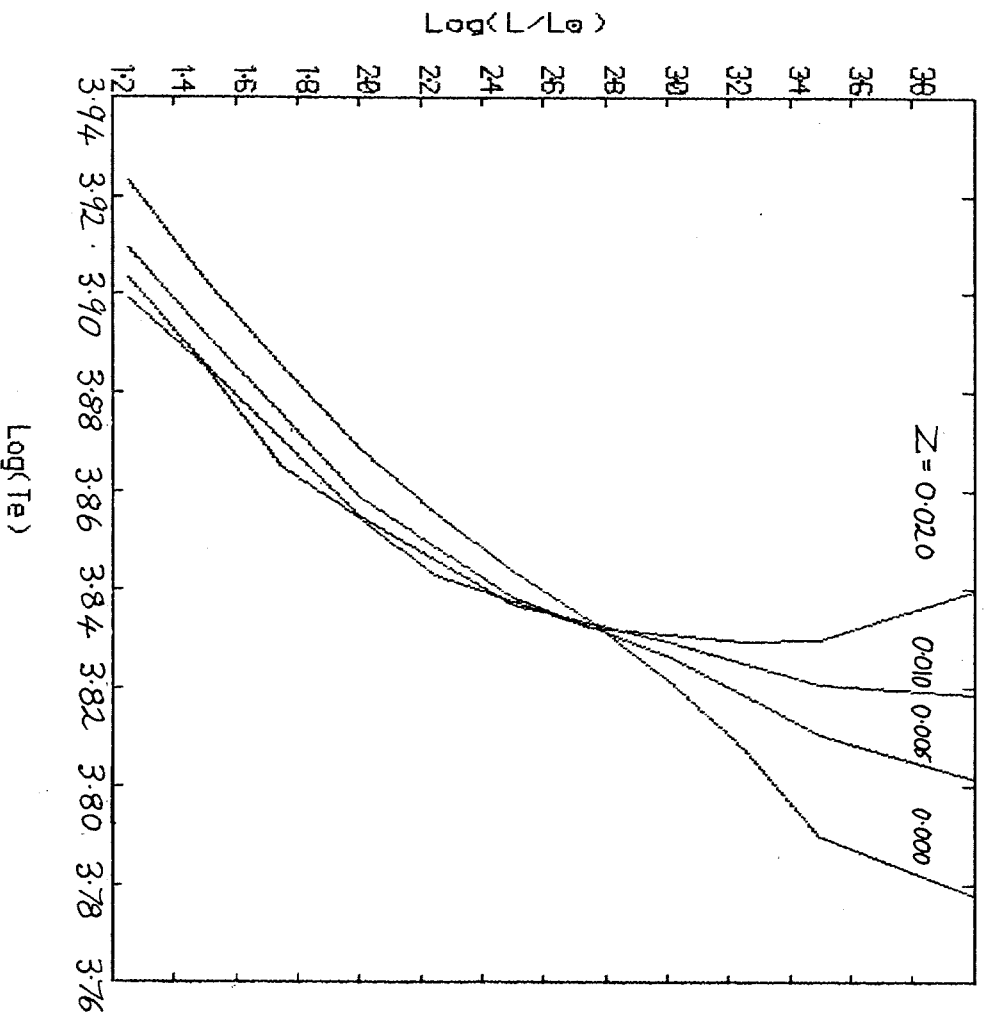


Fig. 7.19 Blue edges for $M = 5.0 M_{\odot}$

horizontal in the $\log(T_{\text{eff}}) - \log(L/L_{\odot})$ plane. However these results imply that an increase in mass raises the luminosity at which this change in behaviour appears and the results of Saio and Wheeler (1983) show the turn around to be much sharper. The appearance of the effect in the relatively low luminosity stars computed with the Carson opacity with high metallicity is probably due to the regions of high radiation pressure induced by the metals bumps. It is probably the details of the model trajectories in the $\log(T) - \log(\rho)$ plane of the opacity table which gives rise to the differing mass dependence.

When the behaviour of the blue edges is viewed in terms of stellar mass it is easy to see for $Z = 0.000$ a trend of increasing temperature for the blue edge with rising mass (fig. 7.20). For $Z = 0.020$ (fig. 7.21) the situation appears to be rather confused. At the lowest and highest luminosities the same trend is probably present. However at a particular luminosity, which increases with mass, the blue edges steepen and the slope of some even reverse. After a further increase in luminosity the slopes return towards their original value. The result is a confused set of crossings for intermediate luminosities.

A single blue edge has been computed for $M = 0.6 M_{\odot}$ with $X = Y = 0.495$, $Z = 0.010$ to examine the dependence upon helium content. Fig. 7.22 shows the blue edges for this and the $Y = 0.25$, $Z = 0.010$ mixtures. The two blue edges are nearly parallel differing

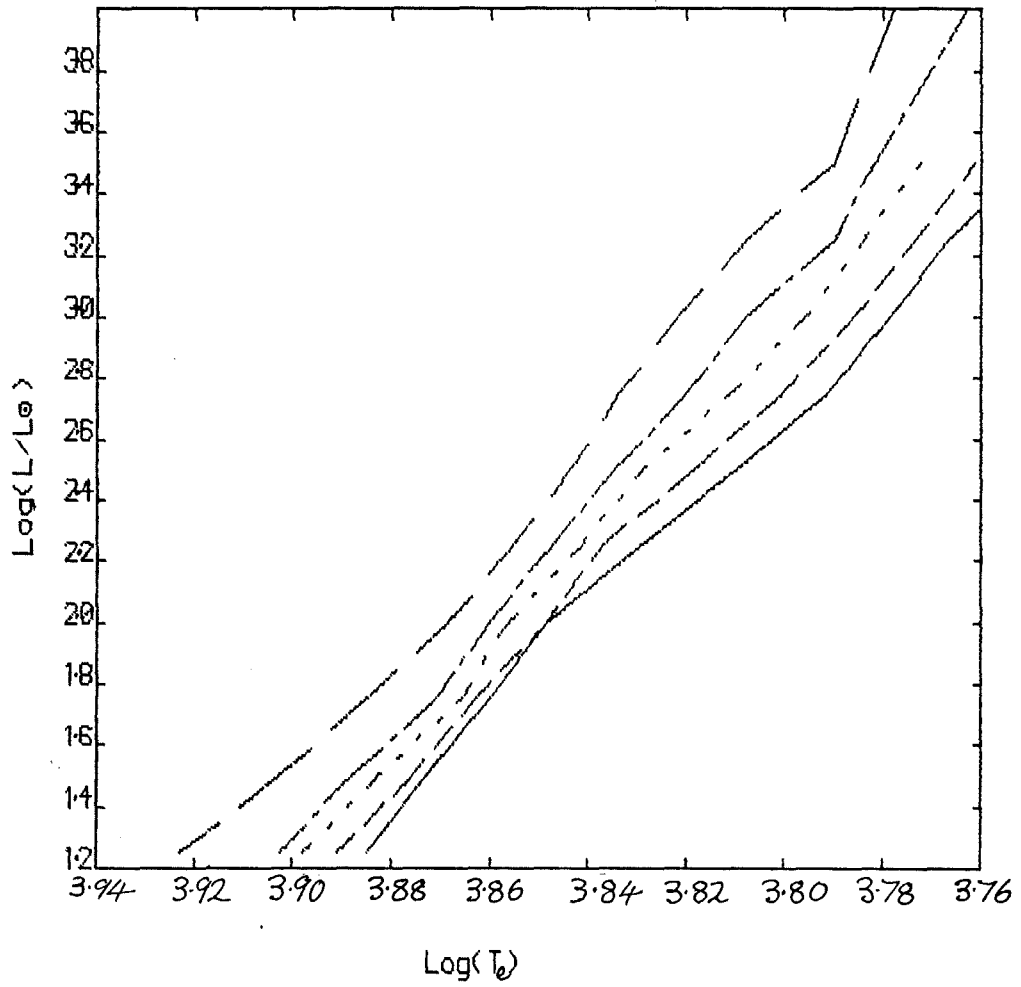


Fig. 7.20

Blue edges for $Z = 0.000$

- = $M/M_{\odot} = 0.6$
- = " = 0.8
- - - - - = " = 1.2
- · - · - = " = 2.0
- - - · - = " = 5.0

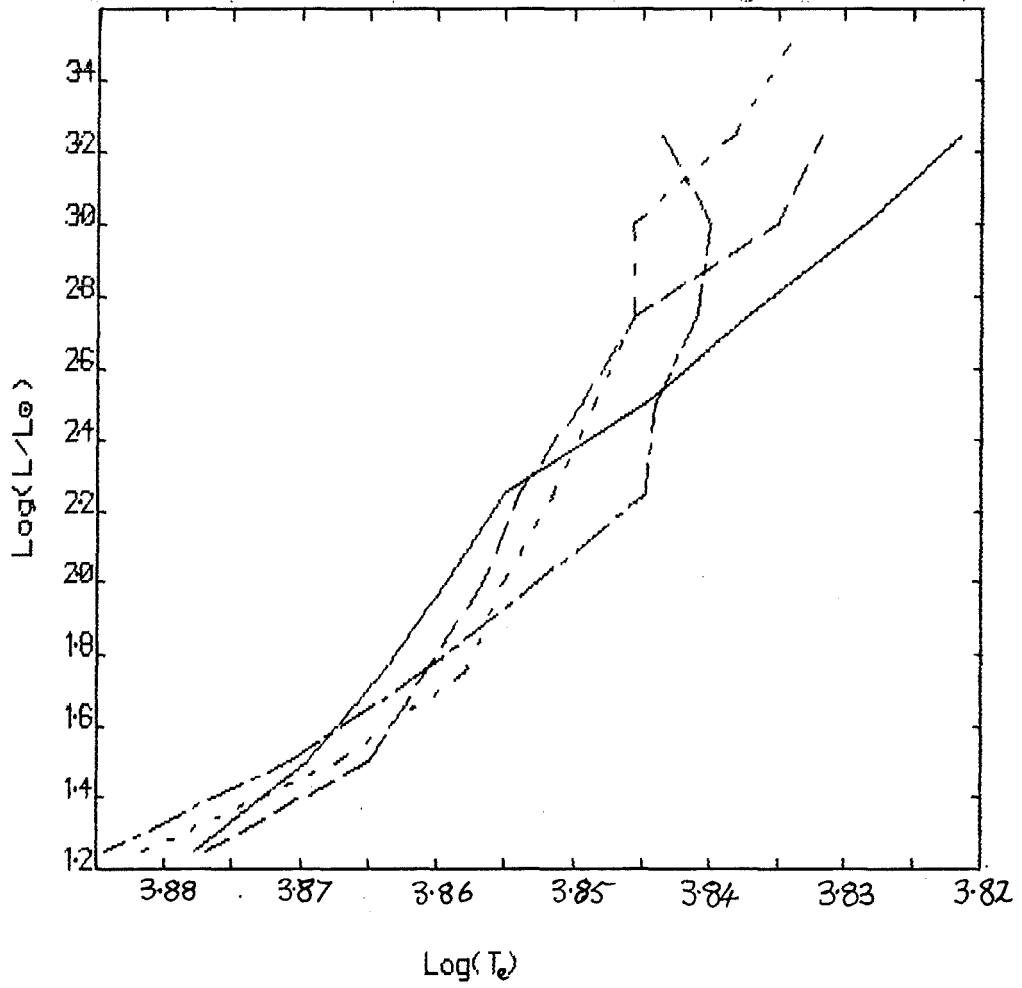


Fig. 7.21

Blue edges for $Z = 0.020$

- = $M/M_{\odot} = 0.6$
- = " = 0.8
- = " = 1.2
- . - . = " = 2.0
- . - . = " = 5.0

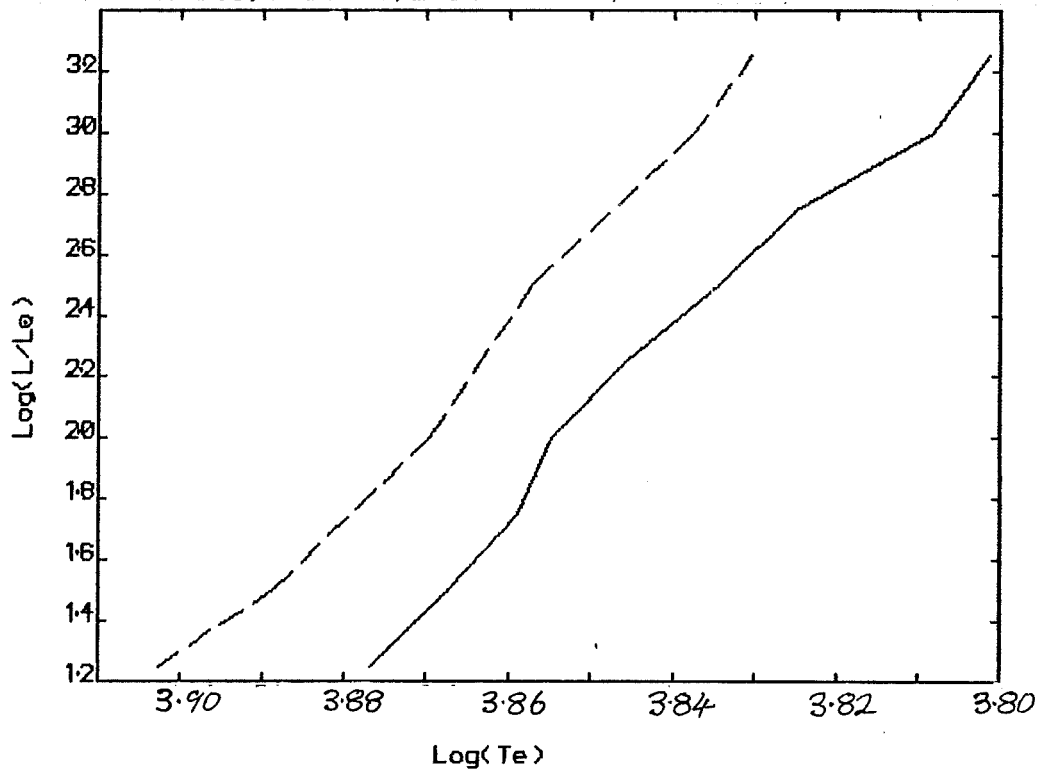


Fig. 7.22

Blue edges for different He abundances
 $Z = 0.010$, $M = 0.6 M_{\odot}$

— = $Y = 0.25$
 - - - = 0.495

by,

$$6 \log(T_{\text{blue edge}}) = (0.53 + 0.011 \log(L/L_{\odot})) \log(Y/0.25)$$

The helium and metallicity dependences both move the blue edges in the same direction for the higher luminosities and so the two effects will be difficult to disentangle unless observations exist which extend down to the metallicity crossover point. The mass dependence is a further complication.

7.1.2.4 The Effect Of The Eddington Approximation -

Blue edges for $M = 0.6 M_{\odot}$ with $Z = 0.00$ and 0.02 were computed using the Eddington approximation due to Unno and Spiegel (1965). The results are displayed in fig. 7.23. As can easily be seen there is no detectable difference whatever. In fact an examination of all the numbers involved shows that at the blue edge differences only appear in the fourth and third figures.

The reason for this is not difficult to see. For there to be any difference between the Eddington and diffusion approximations the radiative relaxation time and the pulsation period must be comparable, i.e.

$$\omega \tau_{\text{rad}} \sim 1$$

where

$$\tau_{\text{rad}} \equiv \frac{c_p T}{2\sigma T^4 K}$$

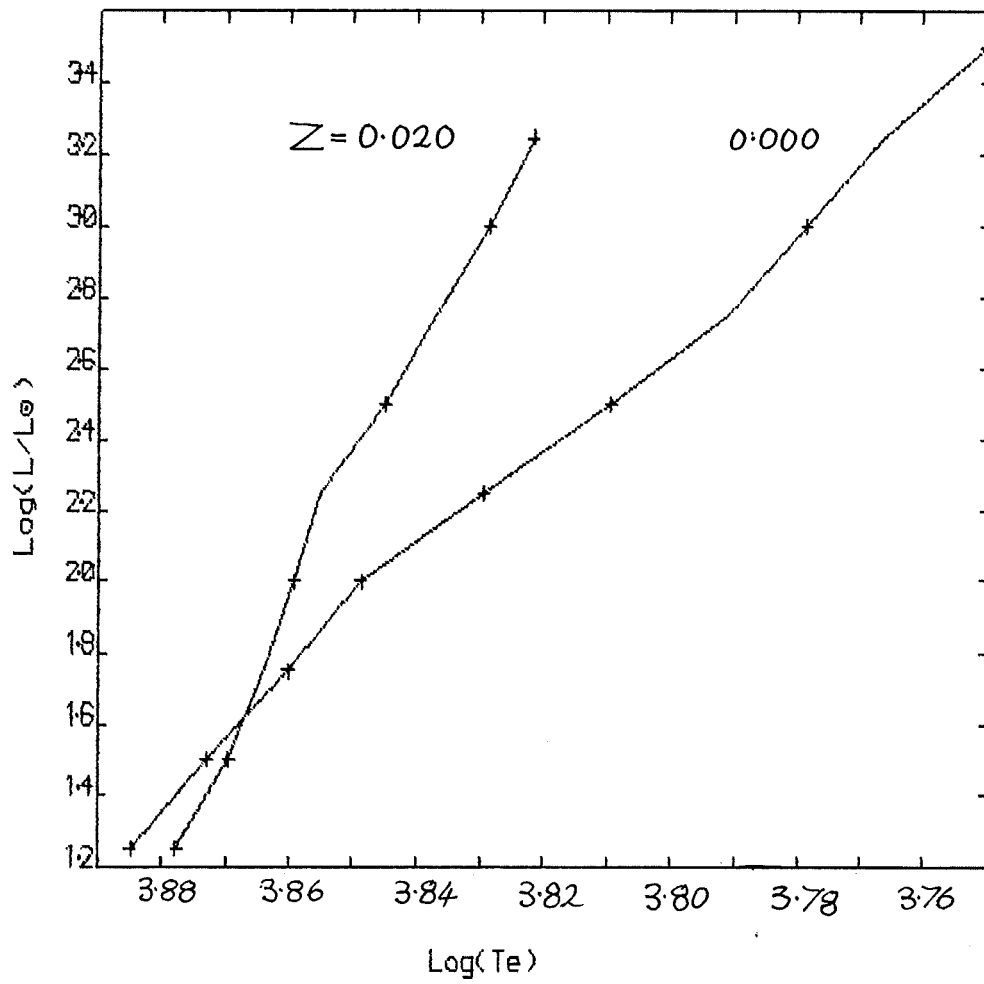


Fig. 7.23

Blue edges using the Eddington approximation

— = diffusion approximation
 + + = Eddington approximation

Since $\kappa \sim \rho^\alpha$ where $\alpha > 0$ this will be most likely to occur near the stars surface. In fact the effects only occur in the outer atmosphere and the mass involved in this region is so small that the work done is negligible. By assuming an isothermal atmosphere, a constant heat capacity, the usual simple approximation for the pulsation frequency, and $\kappa \sim \rho^\alpha T^\beta$ we get

$$\omega \tau_{\text{rad}} \sim \frac{1}{\rho^{(\alpha-1)/2} T^{(\beta+1)/2} L^{1/2}}$$

where $\alpha, \beta > 0$, $\alpha \sim 1$, $\beta \gg 1$. So to get the greatest effect we should look at models at low temperatures.

A sequence of models with;

$$M = 0.6 M_{\odot}$$

$$\text{Log}(L/L_{\odot}) = 3.0$$

$$X = 0.75$$

$$Z = 0.00$$

$$\text{and } \text{Log}(T_{\text{eff}}) = 3.68, 3.70, 3.72, \text{ and } 3.76,$$

using the Stellingwerf opacity formula. The value of $\text{Re}(\omega \tau_{\text{rad}})$ and the amplitude of the temperature perturbation ($\delta T/T$) at the surface for both diffusion and Eddington approximation models are given for the first four modes (see table 7.2). It can be seen that with the exception of the fundamental mode the perturbation is always greater when the Eddington approximation is used. The magnitude of the effect

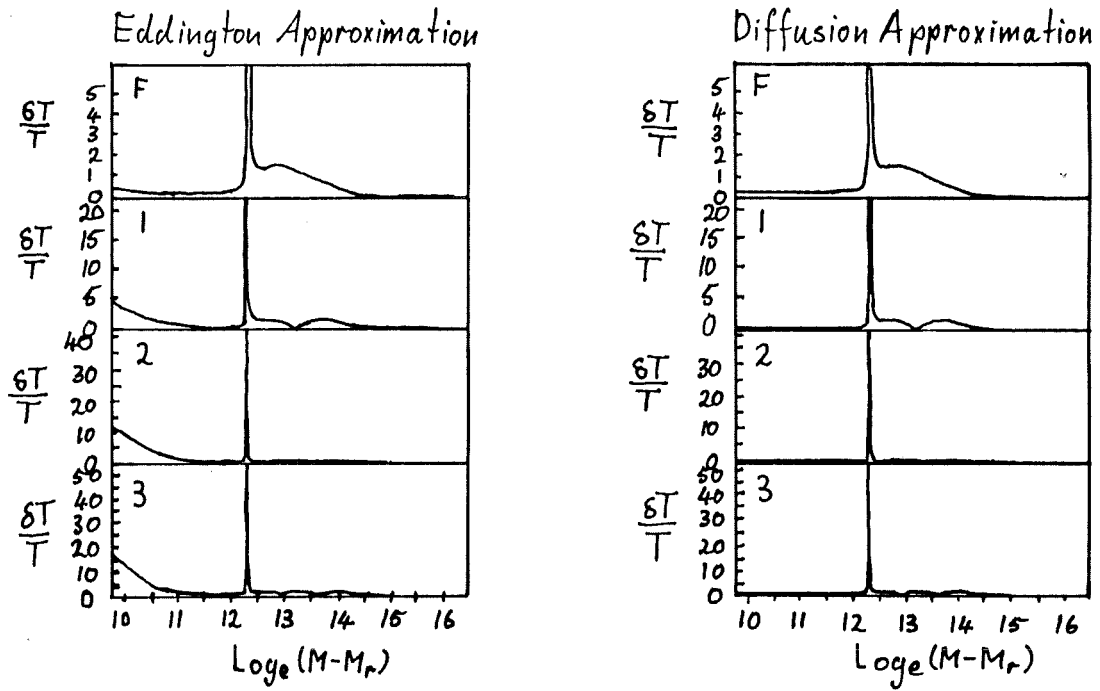


Fig. 7.24 Temperature perturbations for the Eddington and diffusion approximations: $\log(T_{\text{eff}}) = 3.68$.

Table 7.2 Temperature perturbations for the Eddington and diffusion approximations

$\log(T_{\text{eff}}) = 3.68$

Mode	F	1-0	2-0	3-0
$w \chi_{\text{rad}}$	0.09	0.28	0.45	0.52
$(\delta T/T)_{\text{dif}}$	0.22	0.16	0.05	0.32
$(\delta T/T)_{\text{Edd}}$	0.32	4.2	12.	16.

$\log(T_{\text{eff}}) = 3.70$

Mode	F	1-0	2-0	3-0
$w \chi_{\text{rad}}$	0.04	0.11	0.17	0.20
$(\delta T/T)_{\text{dif}}$	0.50	0.24	0.08	0.41
$(\delta T/T)_{\text{Edd}}$	0.22	1.7	4.3	6.4

$\log(T_{\text{eff}}) = 3.72$

Mode	F	1-0	2-0	3-0
$w \chi_{\text{rad}}$	0.03	0.07	0.12	0.14
$(\delta T/T)_{\text{dif}}$	0.44	0.16	0.10	0.28
$(\delta T/T)_{\text{Edd}}$	0.23	1.1	2.8	4.0

$\log(T_{\text{eff}}) = 3.76$

Mode	F	1-0	2-0	3-0
$w \chi_{\text{rad}}$	0.01	0.03	0.04	0.06
$(\delta T/T)_{\text{dif}}$	0.65	0.37	0.09	0.25
$(\delta T/T)_{\text{Edd}}$	0.56	0.68	0.80	1.2

increases considerably as the effective temperature of the model falls. Fig. 7.24 shows the temperature perturbations of the first four modes for the coolest of the models in both approximations.

Studies of pulsation driven mass loss using simplified atmosphere models (for example, Willson and Hill 1979) show that the amount of mass lost depends strongly upon how close to isothermality the atmosphere is. Any tendency of the atmosphere to retain heat leads to a great increase in the mass loss rate (see figs. 12+13 of Willson and Hill) The thermal energy perturbation is proportional to the temperature perturbation and so the use of the Eddington approximation leads to a startling increase in the energy retained and hence, I would expect, the mass loss rate.

7.1.2.5 The Running Wave Boundary Condition -

I have computed a pair of blue edges with $Z = 0.00$ and 0.02 using the running wave boundary condition. The results are displayed in fig. 7.25. At first sight the results look like those expected intuitively. That is, stabilisation for the higher luminosities with $Z = 0.00$. The behaviour for $Z = 0.02$ is a little strange but probably could be explained. However at this point I should recall that a different form of the static model boundary condition, that is one which ^{has} mass lying outside the outer most zone boundary, must be used. When this same boundary condition is used with the standing wave

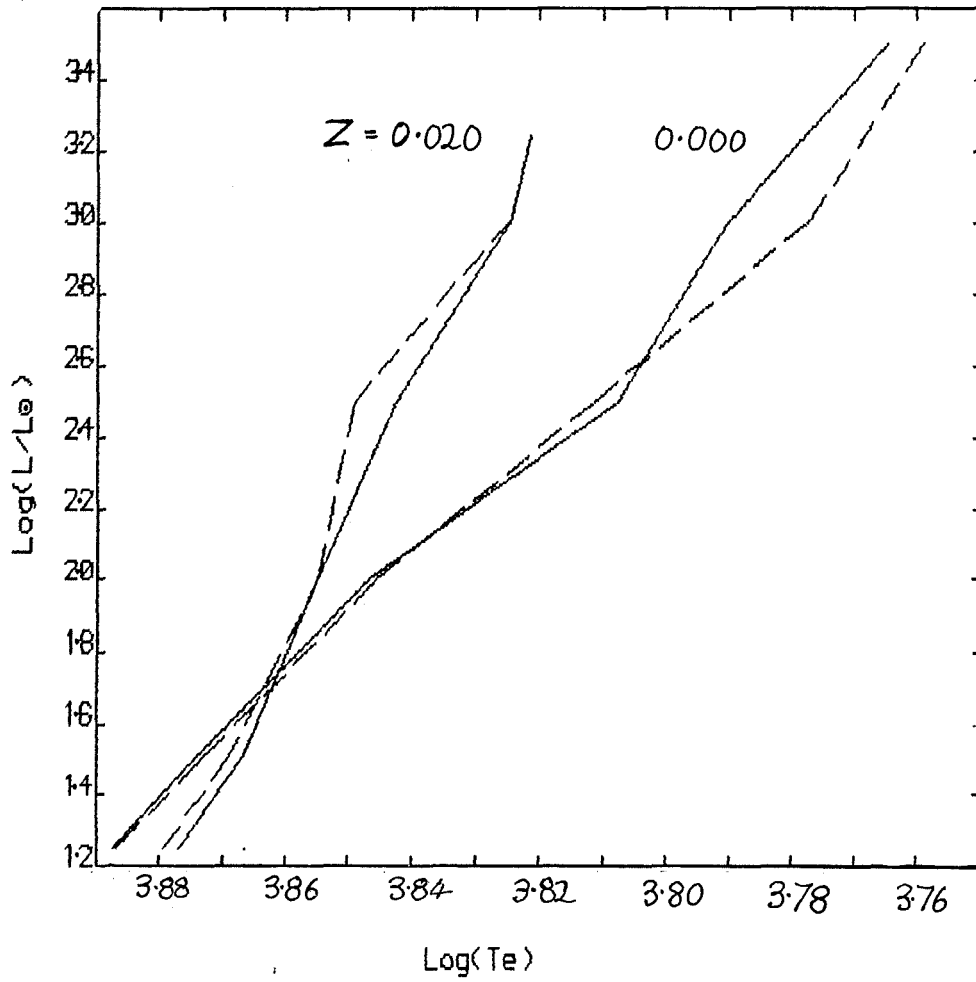


Fig. 7.25

Blue edges using standing and running wave momentum boundary conditions

———— = standing wave with $M_{ext} = 0$
 - - - - = running wave with $M_{ext} > 0$

boundary condition for the pulsation then the results are practically indistinguishable. So it appears that running waves can be dismissed as a source of uncertainty in the blue edge location. On the other hand the presence or absence of matter outside the outermost zone does make a difference. The uncertainty introduced in this way is, at worst, about twice that due to the opacity interpolation.

The introduction of metals into the model greatly increases the opacity near the surface and so since the position of the outer boundary is specified by optical depth reduces the external mass. This probably explains why the uncertainty is much smaller for the $Z = 0.02$ models.

Recently Saio, Wheeler and Cox (1984) have also looked into the momentum boundary condition. They find that so long as the boundary condition gives a finite kinetic energy at infinite radius the eigenfrequencies are insensitive to arbitrary changes of the phase difference between the radial and pressure perturbations at the surface.

Unno (1965) found a similar result for lower L/M values. He could only get significant damping from running waves by postulating hot, dense chromospheres.

7.1.2.6 The Effect Of Convection On The Blue Edges -

Whilst convection is obviously more important towards the red edge of the instability strip there is still convection at the blue edge. The convection is restricted to the H/HeI ionisation zone and carries between about 45 and 96% of the total energy flow. The effect of this is to reduce the height of the H/HeI driving peak in the work function but simultaneously to make it broader. This can quite easily result in an increase of the area under the peak and so increased driving. However this neglects the effects of turbulent viscosity and pressure and, far worse, the nonlocal nature of convection.

The calculations given in this section were made using the approximation

$$8L_c/L_c = 0$$

because of the considerable uncertainties involved in using any more sophisticated approach. An attempt to justify this is given in section 7.1.1. The turbulent viscosity can easily be included in the calculations but near the blue edge the velocity gradient in the H/HeI ionisation zone can be very large with a velocity scale height much less than the mixing length (Gonczi 1981). This is inconsistent with the mixing length theory. A velocity gradient as steep as this would, in a physically correct model, disrupt the convective eddies and so reduce, perhaps even eliminate, the convective heat flow. Conversely one would expect the mixing to smooth out the velocity gradient.

These effects, by definition, cannot be treated in a linear model. Gonczi (1981) has shown that the anomalously large velocity gradient produces a very large viscosity with the dubious consequence of viscosity driving. For this reason the turbulent viscosity is omitted from the calculations of this section.

The results are displayed in fig. 7.26. For the $Z = 0.00$ models the convective blue edge is displaced towards higher temperatures and lies approximately parallel to the radiative blue edge. There is an increase of the displacement with increasing luminosity. At its greatest the displacement is $\delta \log(T_{\text{eff}}) = 0.015$ or about twice the opacity uncertainty. For the $Z = 0.02$ blue edge there is very little difference between the radiative and convective results. Any displacement is always less than the uncertainty introduced by the opacity interpolation and is not consistent in direction. The small magnitude of the effect for this metallicity is simply a result of the increased temperature at the blue edge reducing the convective flux.

7.2 RED EDGES FOR THE $M = 0.6 M_{\odot}$ INSTABILITY STRIP

As is now well known the inclusion of convection in pulsation models with only thermal coupling does not cause the sought after return to stability at low temperatures (see for example Gonczi and Osaki 1980, Baker and Gough 1979) but only an approach to neutral stability, i.e. $\eta \rightarrow 0$. This can be seen for the low luminosity models

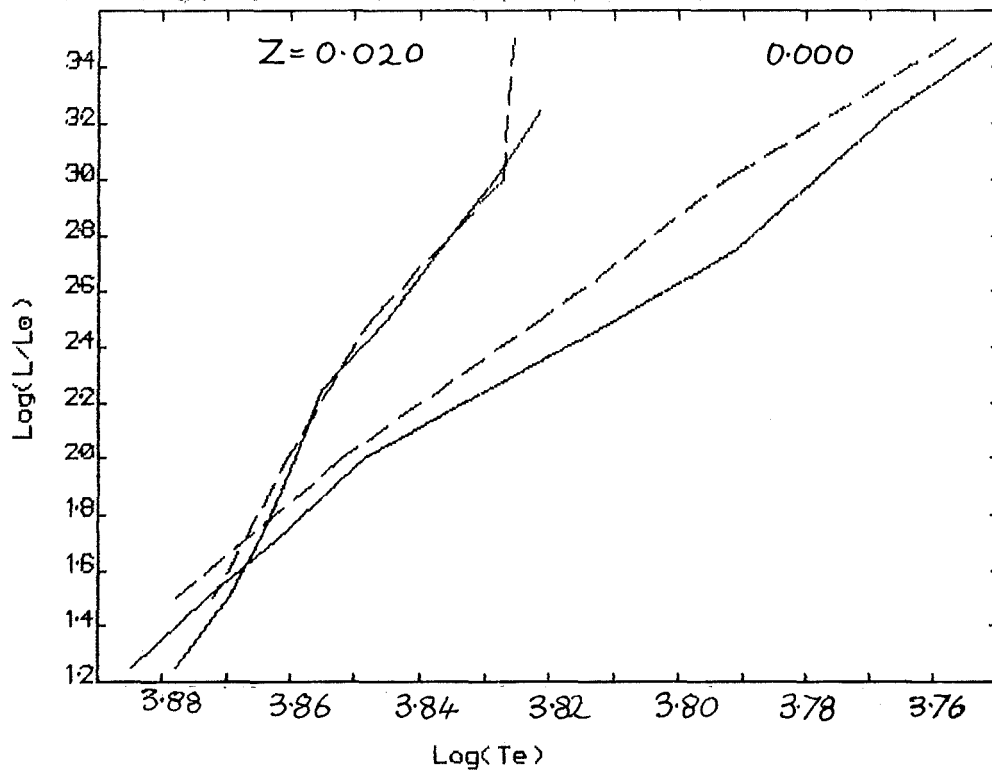


Fig. 7.26 Blue edges for $M = 0.6 M_{\odot}$ with convection

— = radiative models
 - - - = convective models

from fig. 7.27 in which the instability coefficient is plotted for a sequence of models with $M = 0.6 M_{\odot}$, $2.0 < \log(L/L_{\odot}) < 4.0$ and $Z = 0.005$. The Stellingwerf fit to the Los Alamos opacity has been used. As before the perturbation to the convective flux is assumed to be zero. When the convective viscosity terms are included the stability coefficient does pass through zero as the temperature falls for the $\log(L/L_{\odot}) = 2.0$ sequence. This encouraging behaviour is not repeated by any other of the sequences all of which display an obstinate desire to pulsate. The results of the calculations without viscosity are shown in fig. 7.27 and those with viscosity in fig. 7.28. If any of these results can be believed the prediction is that the instability strip should broaden with increasing luminosity and, judging by the high luminosity behaviour, the red edge might well disappear altogether. A look at the H-R diagram for pulsating stars shows a similar effect in the observations with the long period variables and red semiregular variables lying well to the red. However even at its narrowest the calculated instability strip is almost twice as wide as the observed instability strip (see for example Demers and Harris 1974).

In the section on convection theories I stressed that the various theories for the coupling with pulsation do not even agree on the mechanism behind the low temperature return to stability. For this reason I would be surprised by any agreement between theory and observation using the methods available to me.

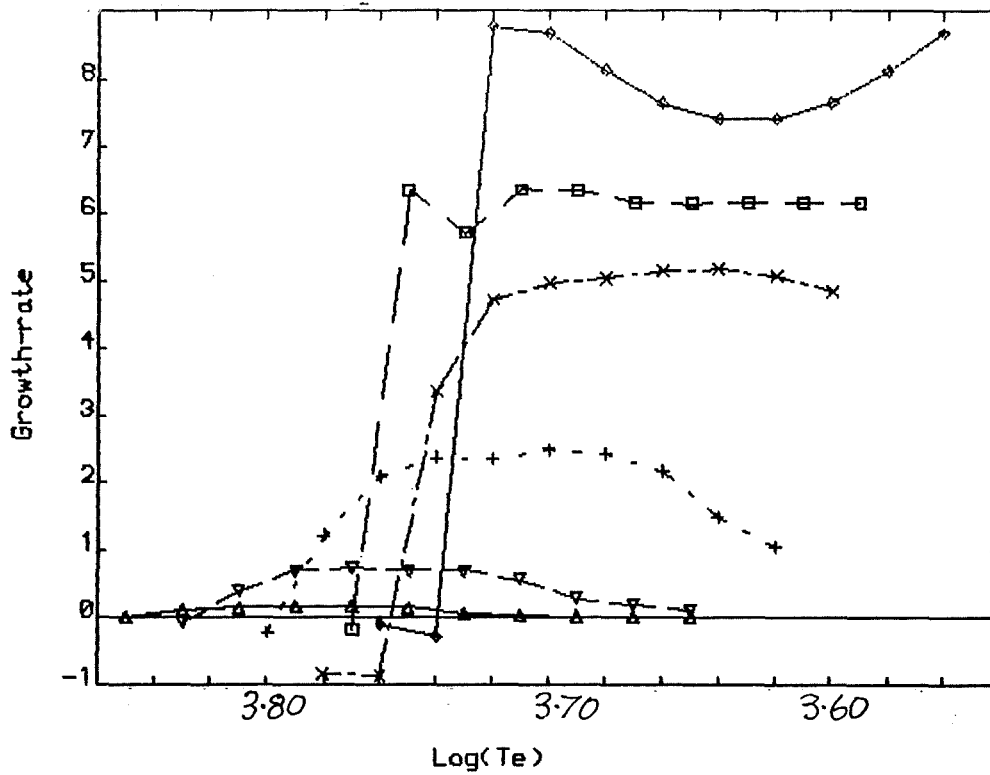


Fig. 7.27 Growth rates for convective models without viscosity using the Stellingwerf opacity formula

$M = 0.6 M_{\odot}$
 $Y = 0.25$
 $Z = 0.005$

$\Delta = \log(L/L_{\odot}) = 2.00$
 $\nabla = \quad \quad \quad 2.50$
 $+ = \quad \quad \quad 3.00$
 $\times = \quad \quad \quad 3.50$
 $\square = \quad \quad \quad 3.75$
 $\diamond = \quad \quad \quad 4.00$

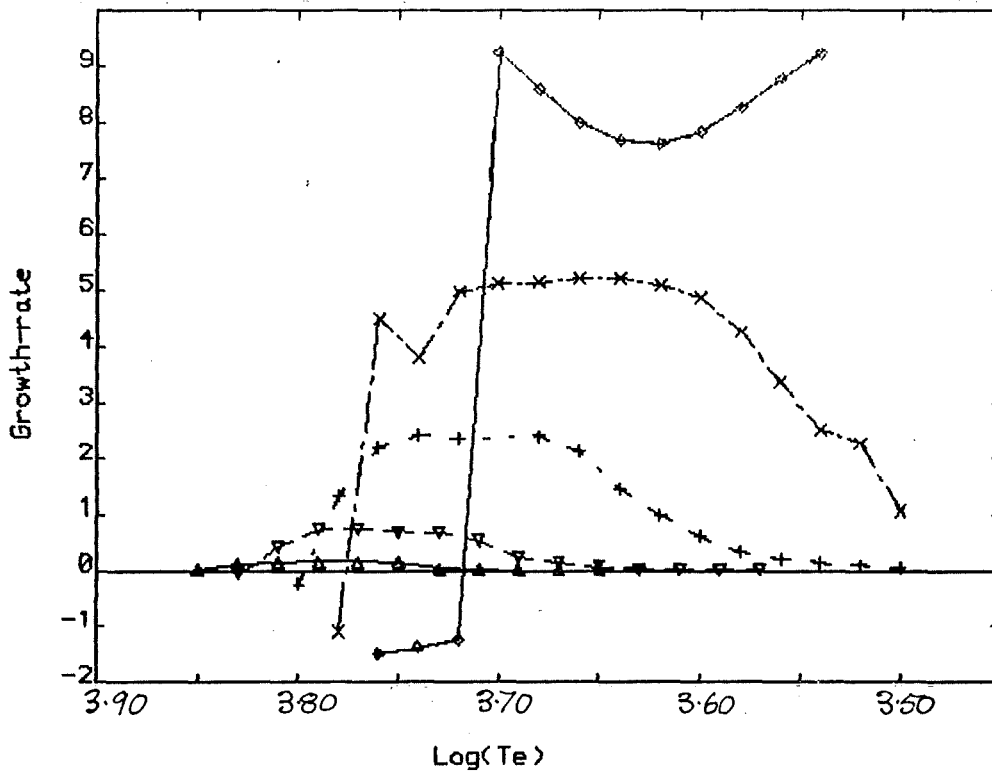


Fig. 7.28 Growth rates for convective models with viscosity but otherwise as above

7.3 NONADIABATIC EFFECTS

It is usually assumed that so far as the period of pulsation is concerned nonadiabatic effects can be neglected. This is not true for high values of L/M . The thermal time scale

$$\tau_{th} = \frac{4\pi r^3 \rho C_p T}{L}$$

as in the discussion of the boundary condition, and the dynamical time scale

$$\tau_{dyn} = \sqrt{\frac{R^3}{GM}}$$

For the system to be nearly adiabatic we must have at each point

$$\frac{\tau_{dyn}}{\tau_{th}} \equiv \frac{\sqrt{R^3}}{\sqrt{GM}} \frac{L}{4\pi r^3 \rho C_p T} \ll 1.$$

Clearly as L/M increases this becomes less likely. Also when $\rho C_p T$ is small enough we get nonadiabaticity whatever the star. In fact we require

$$Re(\omega_i \tau_{th}) \gg 1$$

where ω_i is the frequency for the i^{th} eigenmode. So when nonadiabatic effects do appear they will affect the lowest order modes first and in particular the fundamental mode. This means that the period ratios, for example P_1/P_0 , will be affected. The effect of nonadiabaticity upon the fundamental periods for radiative and convective models lying along a line roughly parallel to the blue edge can be seen in fig. 7.29 for stellar models with $M = 0.6 M_\odot$. At the highest luminosity the nonadiabatic periods are about a factor of three

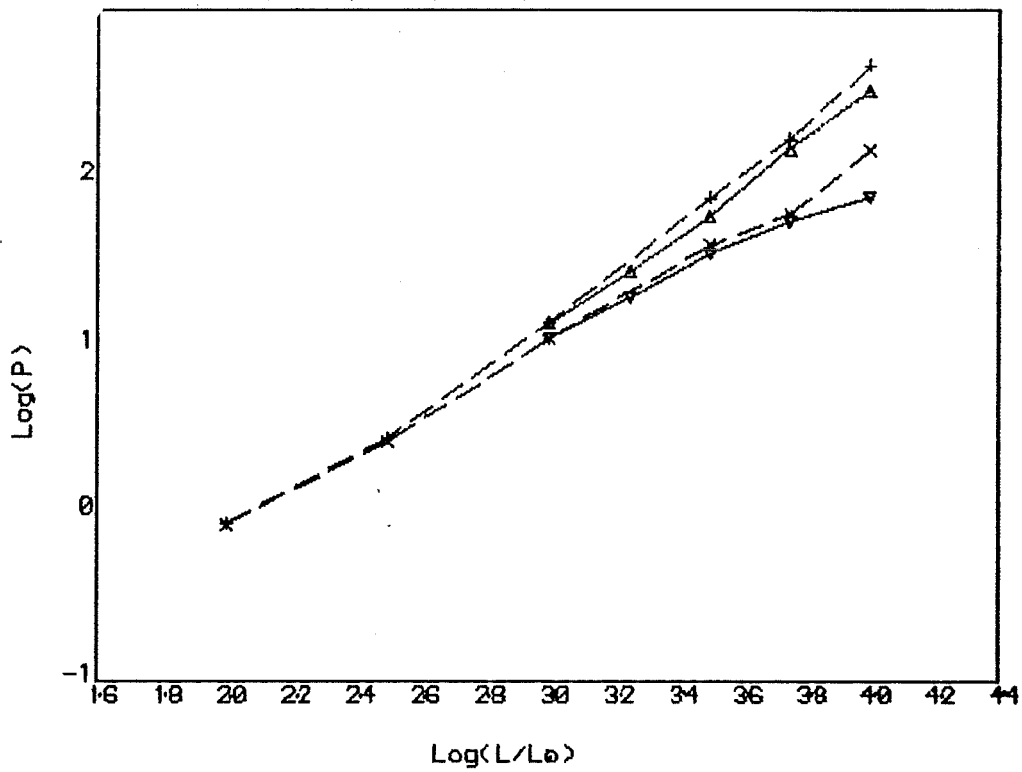


Fig. 7.29 . Adiabatic and nonadiabatic fundamental periods with and without convection using the Stellingwerf opacity formula

$$M = 0.6 M_{\odot}$$

$$Y = 0.25$$

$$Z = 0.005$$

- Δ = Adiabatic, radiative
- + = " convective
- ∇ = Nonadiabatic, radiative
- x = " convective

smaller than their adiabatic counterparts. The immediate consequence of the resulting fall in the gradient of the period increase with luminosity is a turnup in the period luminosity law for a family of stars with constant mass. Van den Bergh (1974) reports having observed this.

Since the overtone periods are very nearly unaffected the nonadiabatic effects on the fundamental period have a radical effect upon the period ratios. P_1/P_0 is plotted in fig. 7.30 for the same sequence of convective models. The important point is that at high values of L/M the adiabatic approximation does not even give the correct qualitative behaviour. Instead of the monotonic decrease of the period ratio found in the adiabatic approximation the function P_1/P_0 has a clearly defined minimum. If we consider a fixed point on the H-R diagram and vary M then a similar behaviour is found. At first as M gets smaller the fundamental period increases but after a while the nonadiabatic effects make themselves felt and as L/M rises still further the period approaches a maximum value (fig. 7.31). Again the period ratio as a function of mass has a clear minimum before rising very rapidly as the mass becomes very small as is shown in fig. 7.32.

The presence of a minimum in the period ratio is of great importance. It means that the period ratio for a pulsating star cannot give an unambiguous estimate of the stars mass. There must be

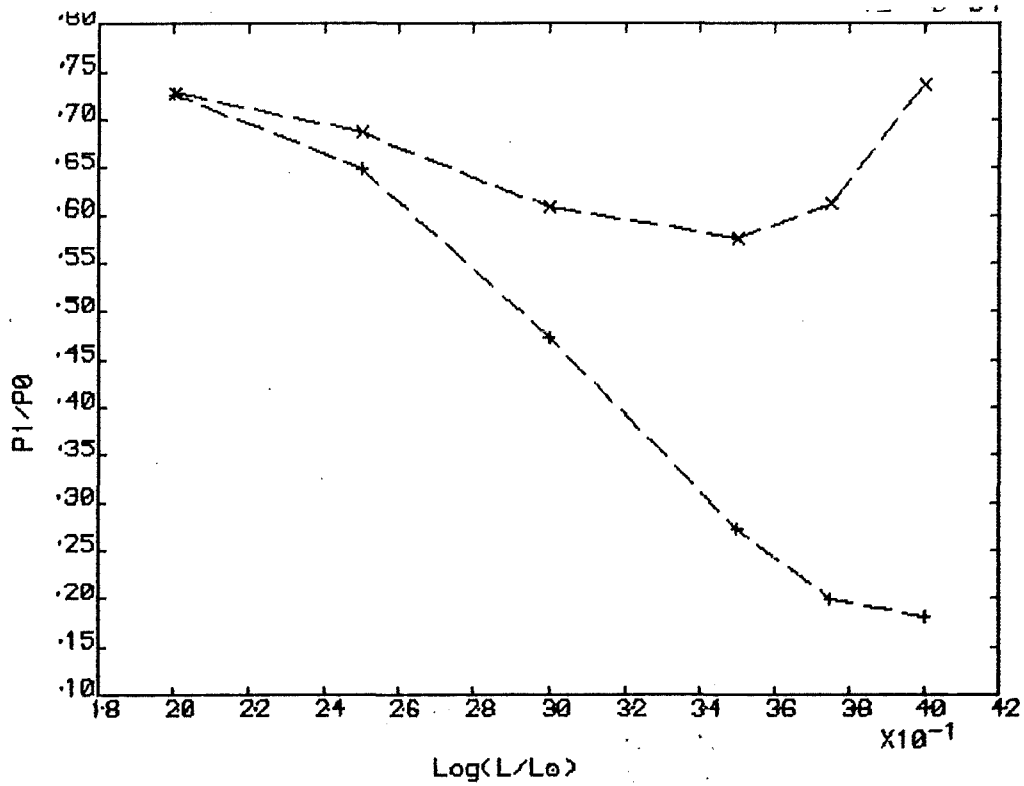


Fig. 7.30

Variation of the adiabatic and nonadiabatic period ratios P_1/P_0 with luminosity parallel to the blue edge using the Stellingwerf opacity formula

$$M = 0.6 M$$

$$Y = 0.25$$

$$Z = 0.005$$

+ = Adiabatic

x = Nonadiabatic

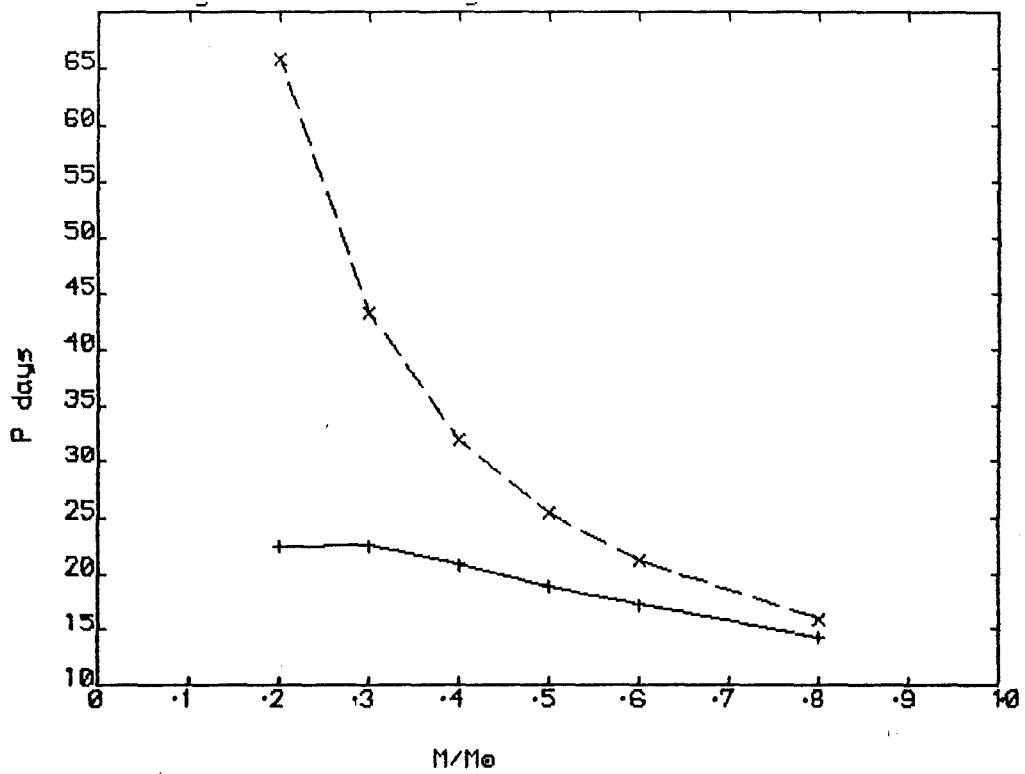


Fig. 7.31 Adiabatic and nonadiabatic fundamental mode periods at different masses for

$$\log(L/L_{\odot}) = 2.94$$

$$\log(T_{\text{eff}}) = 3.725$$

x = Adiabatic
+ = Nonadiabatic

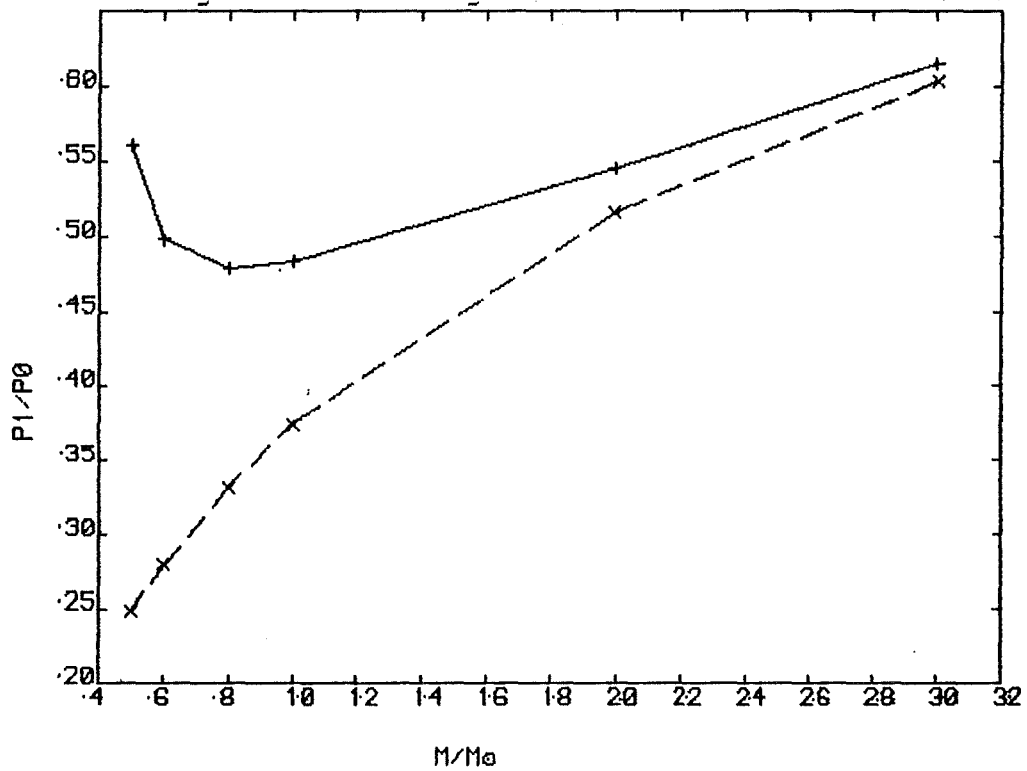


Fig. 7.32 Adiabatic and nonadiabatic period ratios (P_1/P_0) at different masses for;

$$\log(L/L_{\odot}) = 3.44$$

$$\log(T_{\text{eff}}) = 3.725$$

x = Adiabatic
+ = Nonadiabatic

an additional independent source of information to distinguish between high mass (population I) stars and low mass (population II) stars. As an example; this has been completely ignored in Fernie's (1983) analysis of HD161796. His entire argument for this stars apparently anomalous status is based on what I think to be a false derivation of the stars mass using Petersen's (1973) adiabatic period ratios. This is strange since Petersen himself draws attention to the possibility that his data might be inadequate in this type of situation. HD161796 and its relatives will be considered later.

When convection becomes important the picture changes somewhat. The general effect of convection is to reduce the nonadiabatic effects so that the periods tend to lie closer to their adiabatic approximations and so are larger. This can be seen from fig. 7.29. An example of the difference at

$$M = 0.6 M_{\odot}$$

$$\log(L/L_{\odot}) = 3.0$$

$$\log(T_{eff}) = 3.68$$

	P_{ad}	P_{nonad}
Radiative	37.44	30.08
Convective	39.29	36.10

The introduction of turbulent viscosity into the convective model raises the period to 36.21.

When we go to higher luminosities the convection affects the adiabatic period rather more with the result that the ratio $P_{\text{ad}}/P_{\text{non-ad}}$ is nearly the same for radiative and convective models.

$$M = 0.6 M_{\odot}$$

$$\log(L/L_{\odot}) = 4.0$$

$$\log(T_{\text{eff}}) = 3.65 \text{ (radiative)}$$

$$= 3.64 \text{ (convective)}$$

	Radiative		Convective	
	Adiabatic	Nonadiabatic	Adiabatic	Nonadiabatic
F	606.1	172.2	861.0	254.8
1-o	134.7	166.9	152.0	201.1

where F and 1-o indicate the fundamental and 1st overtone.

It is also worth remarking that at this very high luminosity the nonadiabatic effects have begun to creep into the overtone modes.

There is also a noticeable difference between the high luminosity periods computed using the Carson opacities and those incorporating the Stellingwerf opacity formula. Table 7.15 gives a sample of the results. For models constructed using the Carson opacities the adiabatic fundamental period is shorter but the overtone periods are longer. The effects of nonadiabaticity upon the periods are rather greater for the Carson models than for the Stellingwerf models, for example, the ratio $P_{\text{nonad}}/P_{\text{ad}} = 0.49$ for the Carson model but 0.57 for the Stellingwerf model. It can also be seen that the period

Table 7.15

$M = 0.6 M_{\odot}$ $\log(L/L_{\odot}) = 3.5$

$\log(T_{\text{eff}})$	Mode	Carson		Stellingwerf	
		Adiabatic	Nonadiabatic	Adiabatic	Nonadiabatic
3.68	F	143.4	69.2	151.5	87.0
	1-o	30.6	33.7	28.1	33.5
	2-o	24.8	22.1	24.1	23.1
3.66	F	173.5	86.4	186.2	106.0
	1-o	34.5	40.1	32.3	39.9
	2-o	29.4	25.4	28.2	28.0

ratios P_1/P_0 and P_2/P_0 are considerably greater for the Carson opacity models. This differs from the behaviour found for the lower luminosities, for example $\log(L/L_\odot) = 2.00$, where the period ratios for the Carson opacity models are smaller than for the Stellingwerf opacity formula.

7.3.1 The Effects Of Extreme Nonadiabaticity

The nonadiabatic effects described up to this point have all preserved the organisation of the modes found in the adiabatic approximation. There is no radical difference in behaviour even though the periods might be modified considerably. However whilst this investigation was carried out it appeared that every now and again an eigenfrequency would be found which did not fit into the normal scheme (or at least did not conform with my probably naive preconceptions). The most common occurrence is a "mode" with an immensely long period $\sim 10^4$ days. (I say "mode" rather than mode because I doubt its right^{to} claim a "physical" existence.) Since this indicates a value of $|\text{Re}(\omega)/\text{Im}(\omega)| \sim 10^{-20}$ this is almost certainly a "mode" lying on the imaginary axis. To date all of these "modes" have $\text{Im}(\omega) > 0$ indicating stability. Variations in the number of zones in the model under study changes $\text{Im}(\omega)$ considerably. If this is the same "mode" for each different zoning this implies that either it is an artifact of the numerical method or else too sensitive to the numerical details of the model to be worth considering. The latter

point is credible since $|\omega|$ is very small ($\sim 10^{-8} \text{sec}^{-1}$) with an e-folding time $\tau_e \sim 10^4$ days which for a dispersion relation similar to those derived by Saio et al. (1984) would imply a very small wave number. This implies that we could expect the entire star to be involved and so a calculation based on the envelope alone would be expected to fail. The long time scale makes it possible that these "modes" are secular modes, that is, thermal oscillations. However the evidence for this is more than a little flimsy.

Occasionally modes appear with periods which whilst of the same order of magnitude as the more normal periods do not fit into the usual organisation. They are frequently rather longer of period than the fundamental but can also appear amongst the more usual modes. The behaviour of these modes is reminiscent of the strange modes found by Wood (1976), King et al. (1980), Saio and Wheeler (1983), and discussed in detail by Saio, Wheeler and Cox (1984). The authors of the latter paper find that the strange and ordinary modes can be distinguished by the behaviour of the phase of the radius perturbation ($\delta r/r$); for ordinary modes the phase decreases towards the centre of the star whilst for the strange modes it increases. This test has been applied to a number of modes and a selection of the results are given in figs. 7.33-7.39. The details of the models are given in table 7.16.

Table 7.16

Model 1

$M = 0.6 M_{\odot}$
 $\text{Log}(L/L_{\odot}) = 3.5$
 $\text{Log}(T_{\text{eff}}) = 3.68$
 Carson opacity; $X = 0.745$, $Z = 0.005$

Mode	P (days)	Growth Rate
1 (F)	69.16	4.987
2 (Strange)	139.3	-15.44
3 (1-o)	33.65	1.65
4 (?)	$5.7 \cdot 10^{20}$	$-1.9 \cdot 10^{17}$
5 (2-o)	22.11	0.1744

Model 2

$M = 0.6 M_{\odot}$
 $\text{Log}(L/L_{\odot}) = 3.5$
 $\text{Log}(T_{\text{eff}}) = 3.66$
 Carson opacity; $X = 0.745$, $Z = 0.005$

Mode	P (days)	Growth Rate
1 (F)	86.35	5.369
2 (1-o)	40.14	1.04
3 (?)	$1.3 \cdot 10^{19}$	$-4.0 \cdot 10^{15}$
4 (3-o)	15.40	-0.5474
5 (2-o)	25.42	0.0758

Model 3

$M = 0.6 M_{\odot}$
 $\text{Log}(L/L_{\odot}) = 3.5$
 $\text{Log}(T_{\text{eff}}) = 3.68$
 Stellingwerf opacity; $X = 0.745$, $Z = 0.005$

Mode	P (days)
1 (F)	86.97
2 (2-o)	23.05
3 (Strange)	22.03
4 (1-o)	33.52

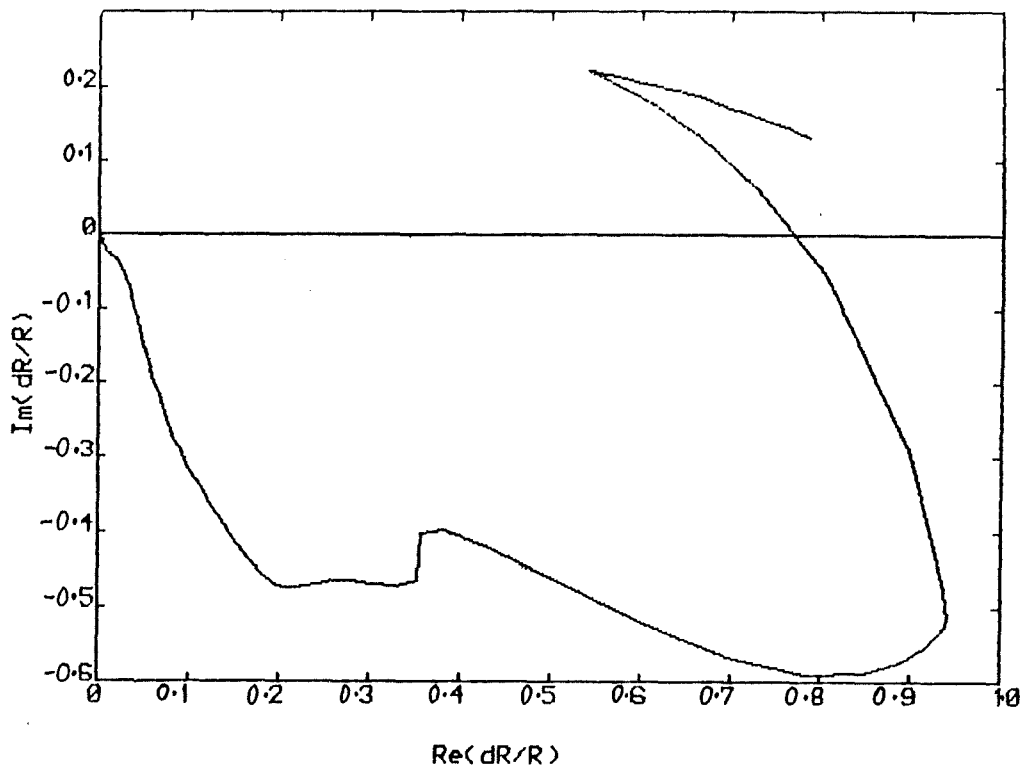


Fig. 7.33 Phase plot for the radial perturbation of mode 1 of model 1 (see table 7.16)
An ordinary mode

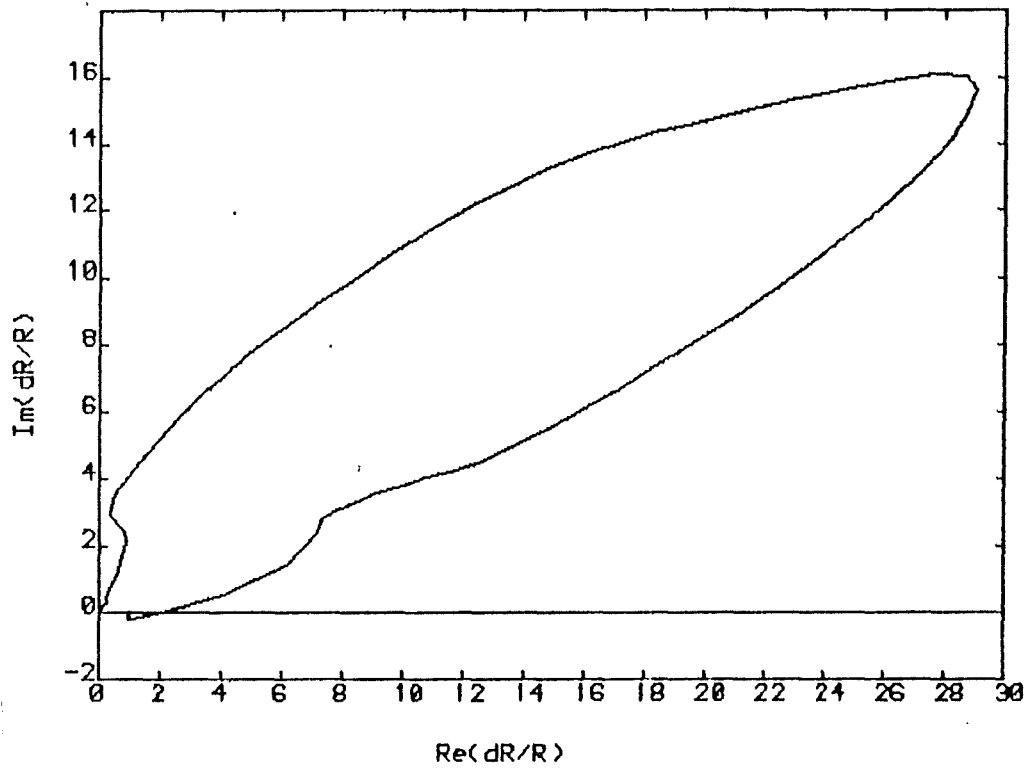


Fig. 7.34 Phase plot for the radial perturbation of mode 2 of model 1 (see table 7.16)
A strange mode

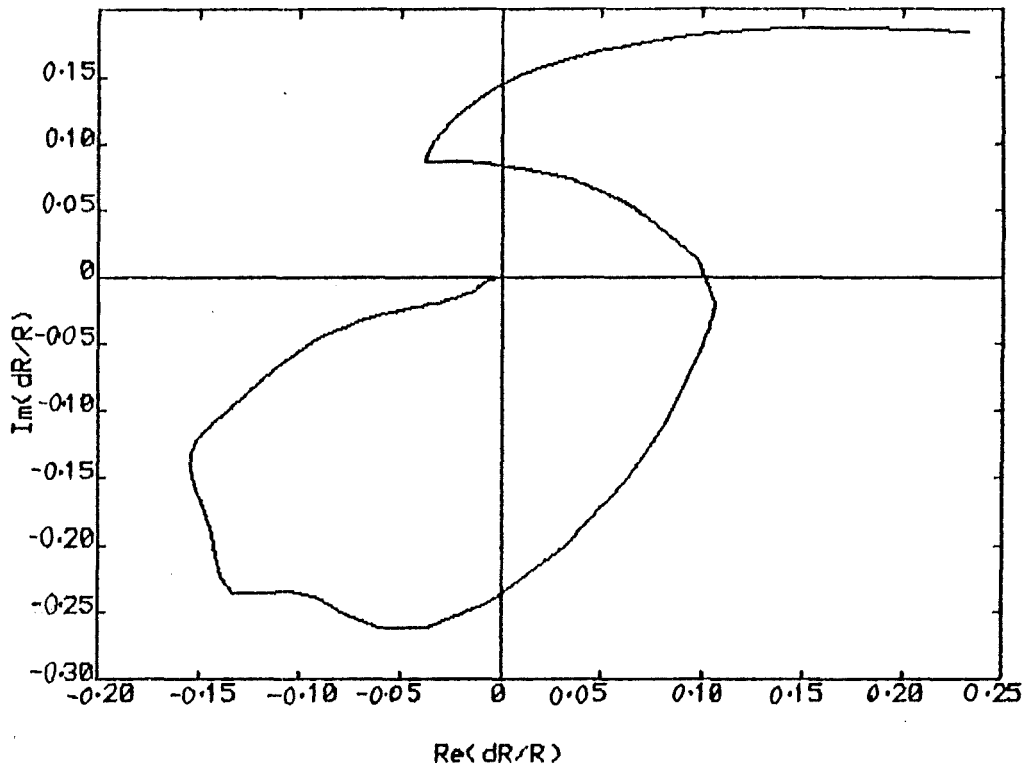


Fig. 7.35 Phase plot for the radial perturbation of mode 3 of model 1 (see table 7.16)
An ordinary mode

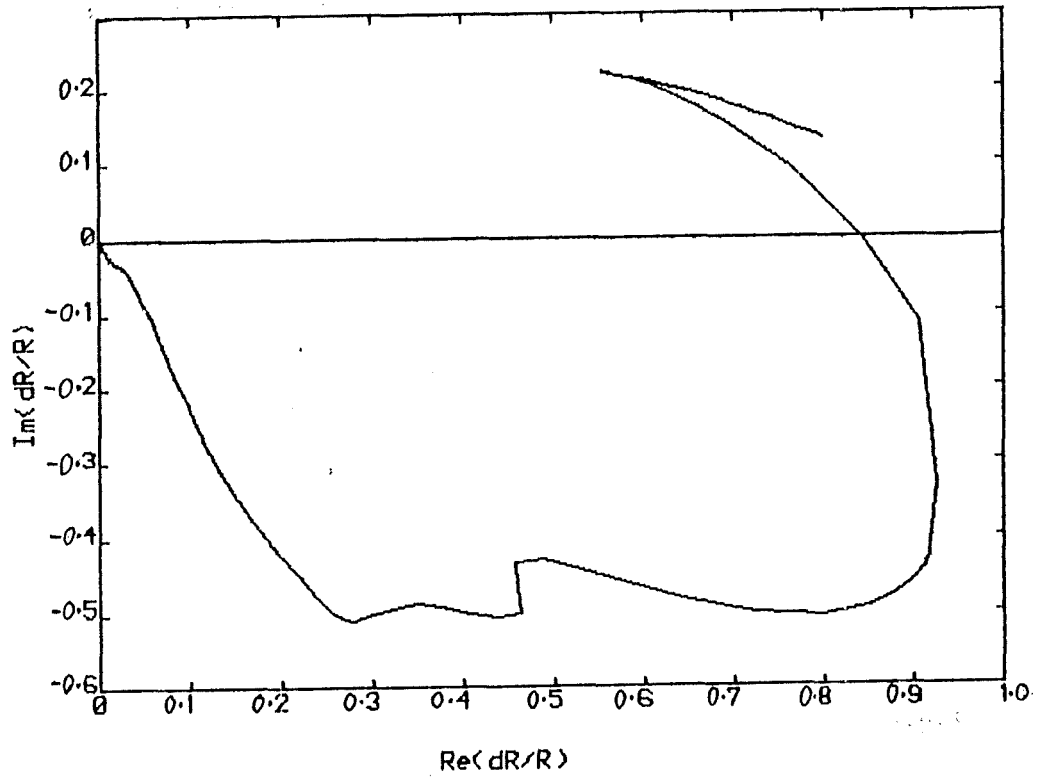


Fig. 7.36 Phase plot for the radial perturbation of mode 1 of model 2 (see table 7.16)
An ordinary mode

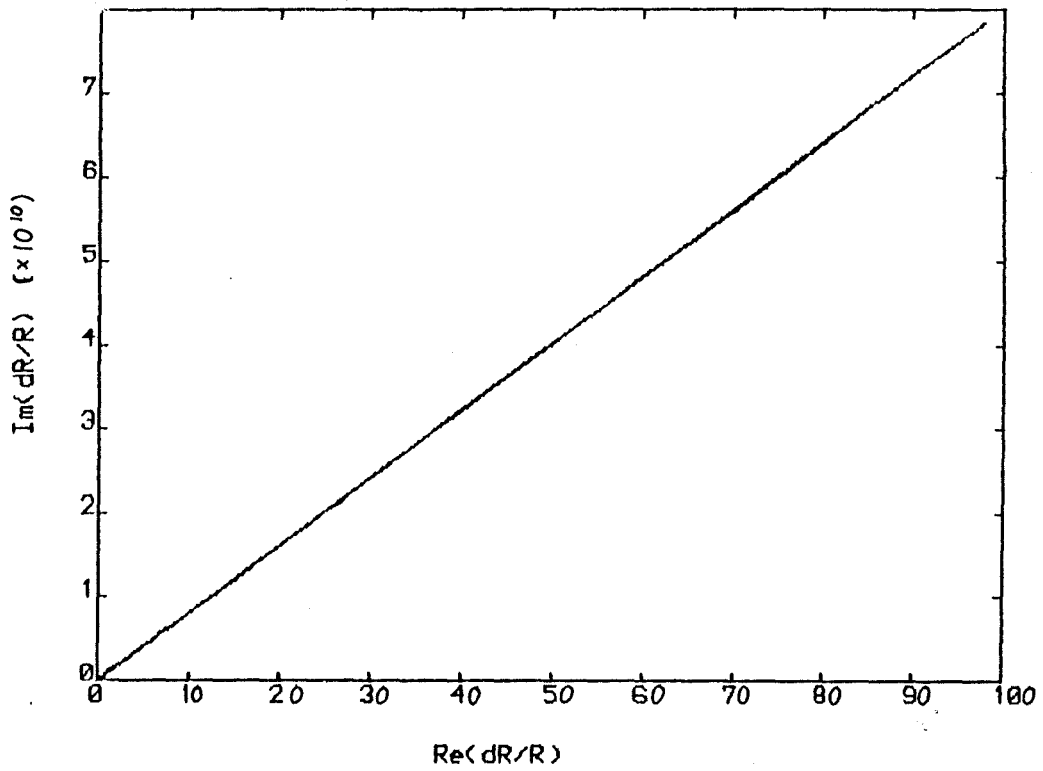


Fig. 7.37 Phase plot for the radial perturbation of mode 3 of model 2 (see table 7.16)
A secular mode ?

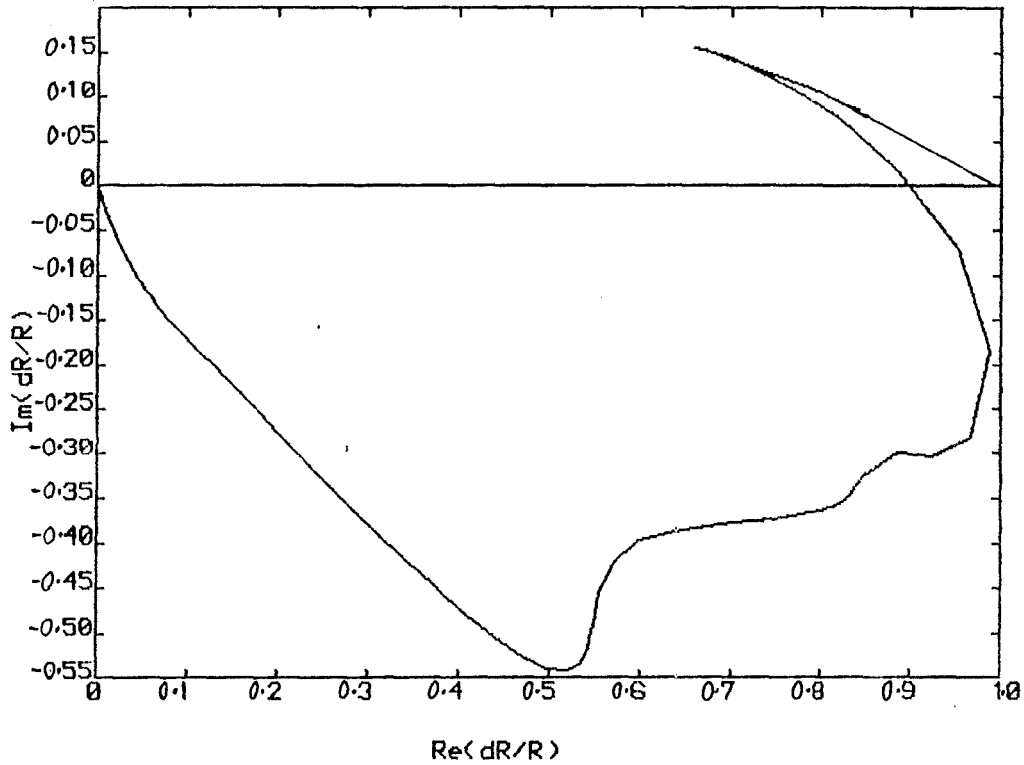


Fig. 7.38 Phase plot for the radial perturbation of mode 1 of model 3 (see table 7.16)
An ordinary mode

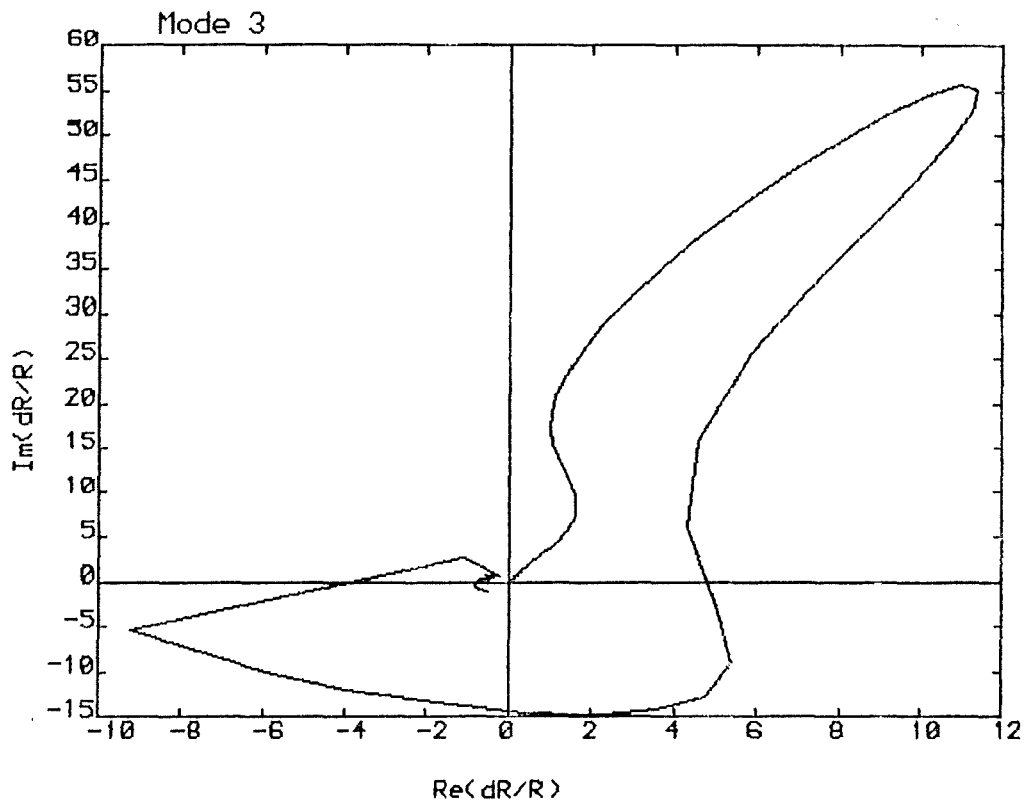


Fig. 7.39 Phase plot for the radial perturbation of mode 3 of model 3 (see table 7.16)
A strange mode

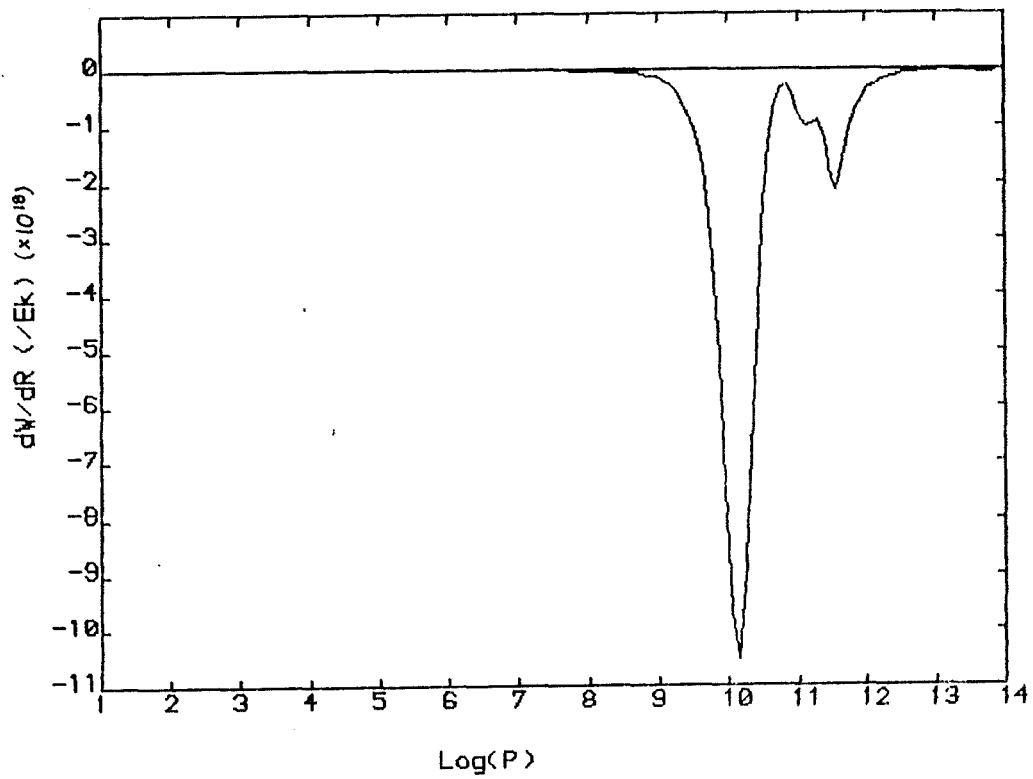


Fig. 7.40 Work function (dW/dR) for mode 3 of model 3
A strange mode

The difference in the behaviour of mode 2 of model 1 from all the others is quite clear, that is a clockwise trajectory from the centre rather than the usual anticlockwise. Mode 3 of model 2 is an example of the phase behaviour of one of the dubious "secular modes". A further example of a strange mode is mode 3 of model 3. A feature which is common to all the strange modes I have identified is that they are all strongly stabilised. Fig. 7.40 shows a work function (dW/dR) for the strange mode from model 3. There is a complete absence of driving. Again this fits with the results of Saio et al. (1984). The examples show this clearly. All the published work on strange modes to date has been concerned with high luminosity helium stars aimed at explaining the R Cor Bor stars. I think that this is the first time that strange modes have been found in stars of a more usual composition. Certainly Fox and Wood (1982) in their study of long period variable models did not find strange modes. The limitations on the time available have not allowed me to make a systematic study of the strange modes, in fact my main interest in them (like that of Messier in nebulae) was to eradicate them from my data.

Saio et al. (1984) have constructed a simple analytic model for the nonadiabatic oscillations in a plane parallel approximation to a star. They show that the oscillations can be understood in terms of coupled thermal and dynamical modes. In the adiabatic limit the coupling of the modes is absent but when the system is highly

nonadiabatic the coupling is strong. The thermal modes are identical to the secular modes. This would tend to suggest that the eigenfrequencies I have found on the imaginary axis are secular modes moving towards shorter periods prior to leaving the axis to become strange modes.

The presence of the strange modes raises a question; have I identified all the modes correctly? A simple check on the phase change of the radial perturbation is sufficient to spot strange modes in the Stellingwerf opacity models. However glitches appear in phase for the Carson opacity models making this test unreliable. It has not been possible to plot the phase diagram for every mode of every model and indeed I probably do not have the resources to do this. However, experience shows that by looking at the continuity of the periods, growth-rates, and phase lags for the modes along a sequence gives a satisfactory method of identification. When the situation is unclear the eigenfunctions etc. can be plotted up. Saio et al. (1984), Fox and Wood (1982) etc. search for their eigenvalues by calculating the discriminant for a model (see section 2.3) along a closed path in the frequency plane. The number of modes located in the loop is given by the total phase change in the discriminant divided by 2π assuming that poles are absent from the loop. The presence of poles reduces the number predicted by one for each pole. This method is very costly in CPU time. Also I have found that the absence of poles cannot be guaranteed which leads to the possibility that modes might be missed.

I suspect that this might have occurred in Fox and Wood (1982). The method I use has been described earlier on. The only modification made to cope with strange modes is that the starting point of the iteration for all the modes is given by

$$\omega_i^{(0)} = \frac{1}{2} (\omega_{\text{nonad}} + \omega_{\text{ad}})$$

where ω_{ad} and ω_{nonad} are the approximate adiabatic and nonadiabatic fundamental eigenfrequencies. Experience shows that for the convective models the first three ordinary modes are almost always found amongst the first five eigenvalues. The situation is a little less satisfactory for the radiative models which accounts for the blank spaces in some of the tables.

7.4 A SURVEY OF THE LUMINOSITY-TEMPERATURE PLANE FOR $M = 0.6 M_{\odot}$

Sequences of radiative and convective models have been constructed using the Carson and Los Alamos (Stellingwerf) opacities for $Z = 0.005$. The aim of this exercise was to provide data for an analysis of the RV Tau, type II cepheid, and SRd star observations. It was also expected that the behaviour of the pulsation models at the high luminosities indicated by the periods would be of considerable interest in themselves. Since models were required which extended further redwards than the red edge of the instability strip defined at lower luminosities convection was included in the main sequences. The convective sequences with both opacities were constructed for

$\log(L/L_{\odot}) = 2.00, 2.50, 3.00, 3.50, 3.75,$ and 4.00 with about eleven models at each luminosity spaced at intervals of 0.02 in $\log(T_{\text{eff}})$. Neither of these sequences include the effects of turbulent viscosity. An additional sequence incorporating turbulent viscosity was constructed using the Stellingwerf opacity formula in order to try to find a red edge to the instability strip and to observe the effects of viscosity in general.

A set of radiative models was constructed to cover a range of $\log(L/L_{\odot}) = 3.00, 3.25, 3.50, 3.75,$ and 4.00 lying on both sides of the blue edge using the Stellingwerf opacity. As noted earlier the Carson opacities do not allow the construction of purely radiative models for the highest of the L/M values. Subsidiary radiative sequences were constructed employing the Carson opacity for $M/M_{\odot} = 0.6$ and 0.8 for comparison with Bridgers (1983) nonlinear models of the CW stars. Again $Z = 0.005$.

Tables (7.17-7.48) of the periods, growth rates, and phase lags for the first three modes (fundamental, first and second overtones), of the period ratios $P_1/P_0, P_2/P_0,$ and $1+P_0/P_1 - P_0/P_2,$ and of the adiabatic periods are given at the end of the chapter.

A comparison of the adiabatic and nonadiabatic overtone periods shows that the i^{th} nonadiabatic overtone period is often closer to the $(i+1)^{\text{th}}$ than the i^{th} adiabatic overtone period. This has already been observed by, for example, Wood (1976), and Saio, Wheeler and Cox

(1984). The very considerable difference between the adiabatic and nonadiabatic fundamental periods for the higher luminosities can be seen clearly.

At the high luminosities the behaviour of the growth rates is not simple. Modes frequently stabilise only to become unstable again before returning to stability as the temperature rises. There is generally one mode, most usually the fundamental, which has a very large positive growth rate. However possession of this large growth rate is sometimes passed on to another mode (see tables 7.20+7.31 for $\log(L/L_{\odot}) = 3.5$). In the Stellingwerf table as the temperature falls the high degree of instability starts at the second overtone, passes to the first overtone and then to the fundamental where it remains. The growth rate crossover for the Carson sequence is shown in fig. 7.41. The strange modes are also displayed in this graph- the strength of their stability is clear to see. The periods for these modes are shown in fig. 7.42. it can be seen that the periods and growth rates do not always show a smooth progression.

Trying to trace blue edges whilst the growth rates behave in this way is not easy. However I have attempted to do this and the results can be seen in figs. 7.43-7.46. There is a considerable difference between the blue edges for the Stellingwerf radiative and convective models. The fundamental blue edges are reasonably similar. In particular, with the exception of a peculiar glitch in the convective

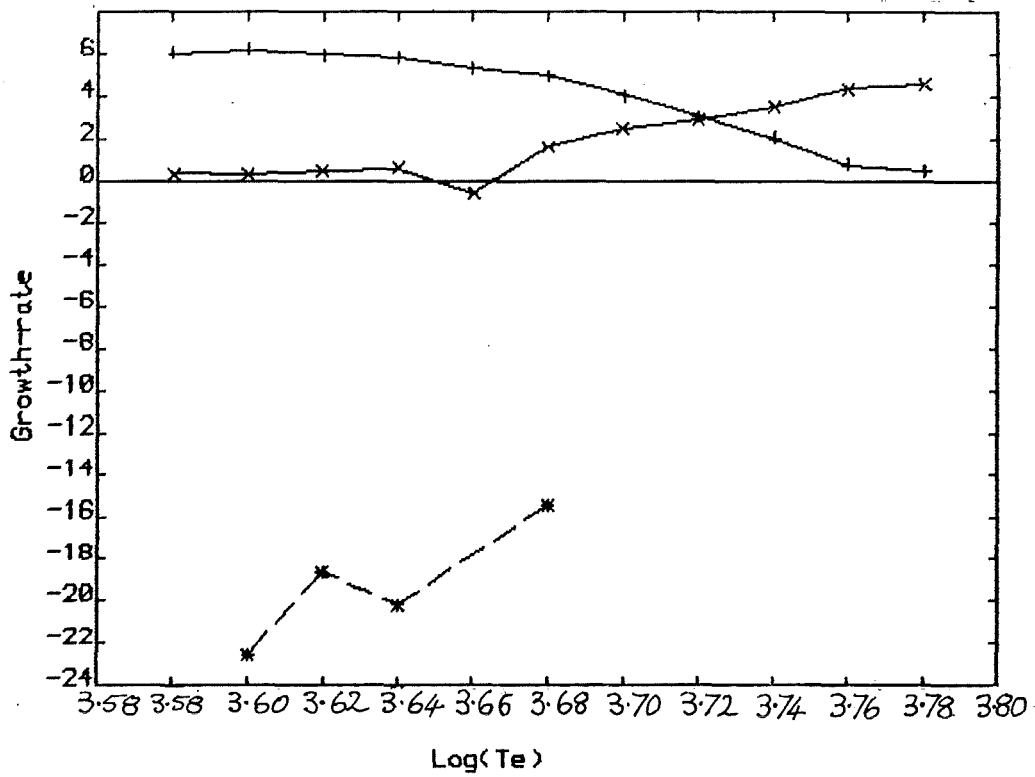


Fig. 7.41

Growth rates for a sequence of convective models incorporating the Carson opacity

$M = 0.6 M_{\odot}$
 $\log(L/L_{\odot}) = 3.5$
 (see table 5.31)

- + = F
- x = 1-o
- * = strange mode

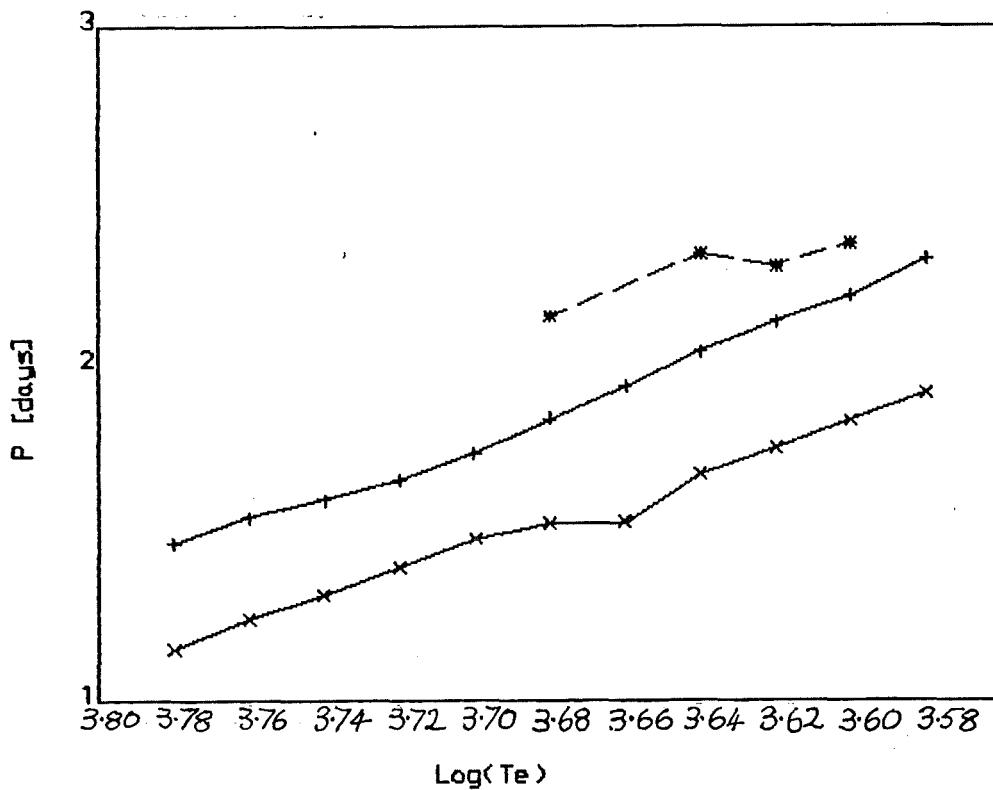


Fig. 7.42

Periods for the models above

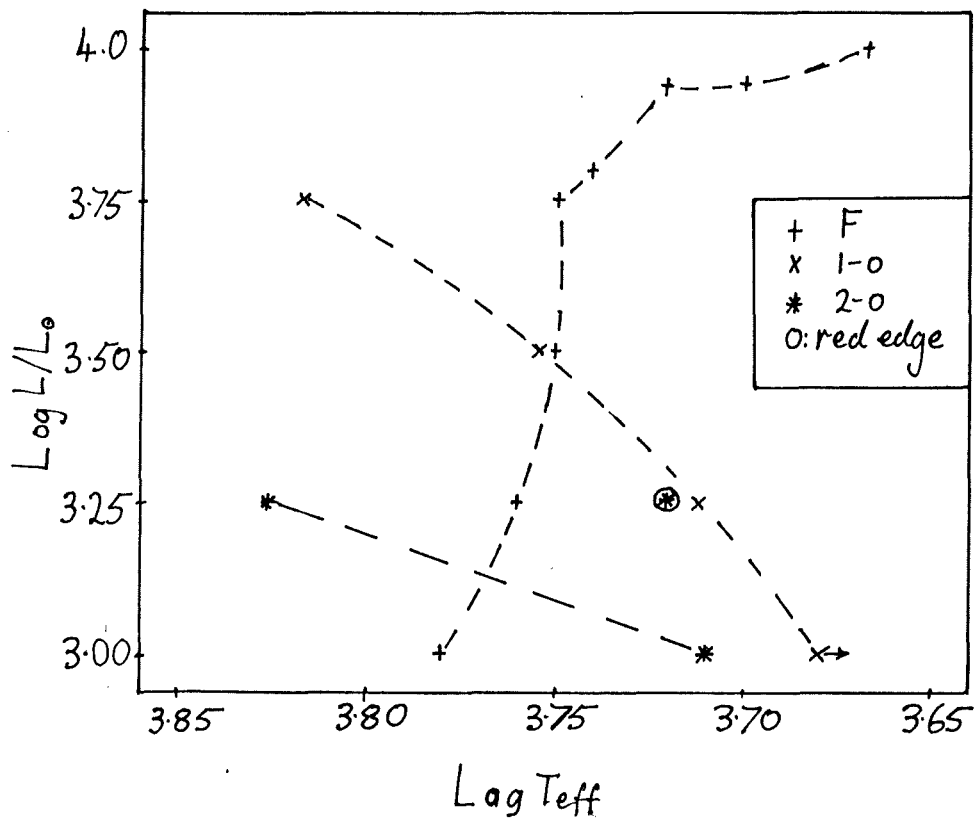


Fig. 7.43

Blue edges for radiative models using the Stellingwerf opacity formula (see tables 5.39 - 5.43)

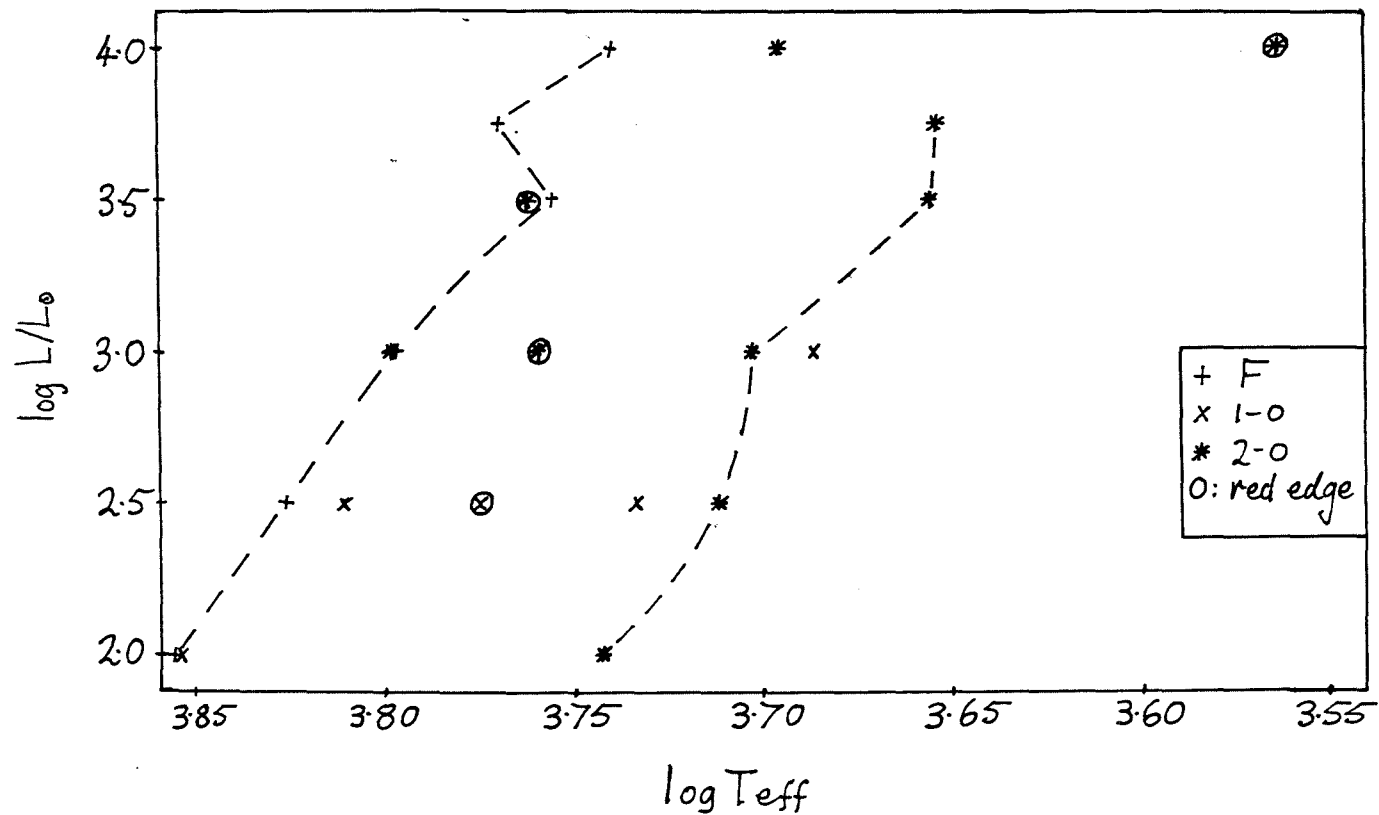


Fig. 7.44

Blue edges for convective models without viscosity using the Stellingwerf opacity for a (see tables 5.17 - 5.22)

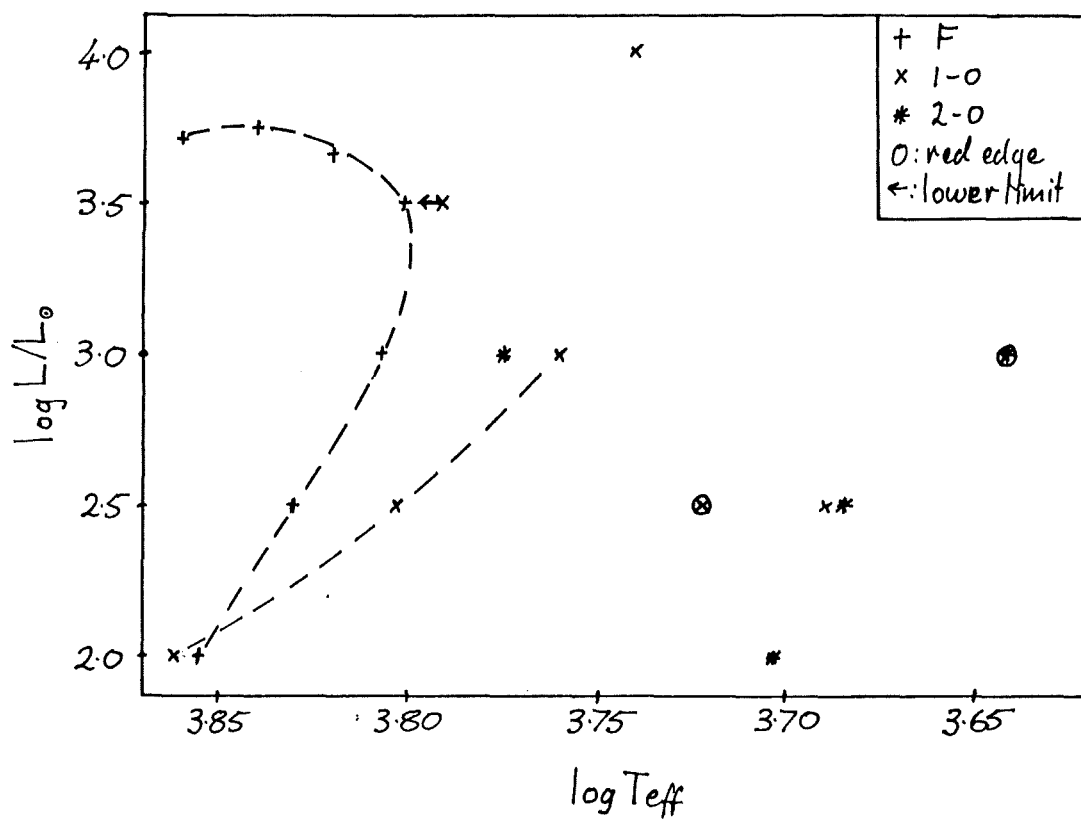


Fig. 7.45

Blue edges for convective models with viscosity using the Stellingwerf opacity formula (see tables 5.23 - 5.27)

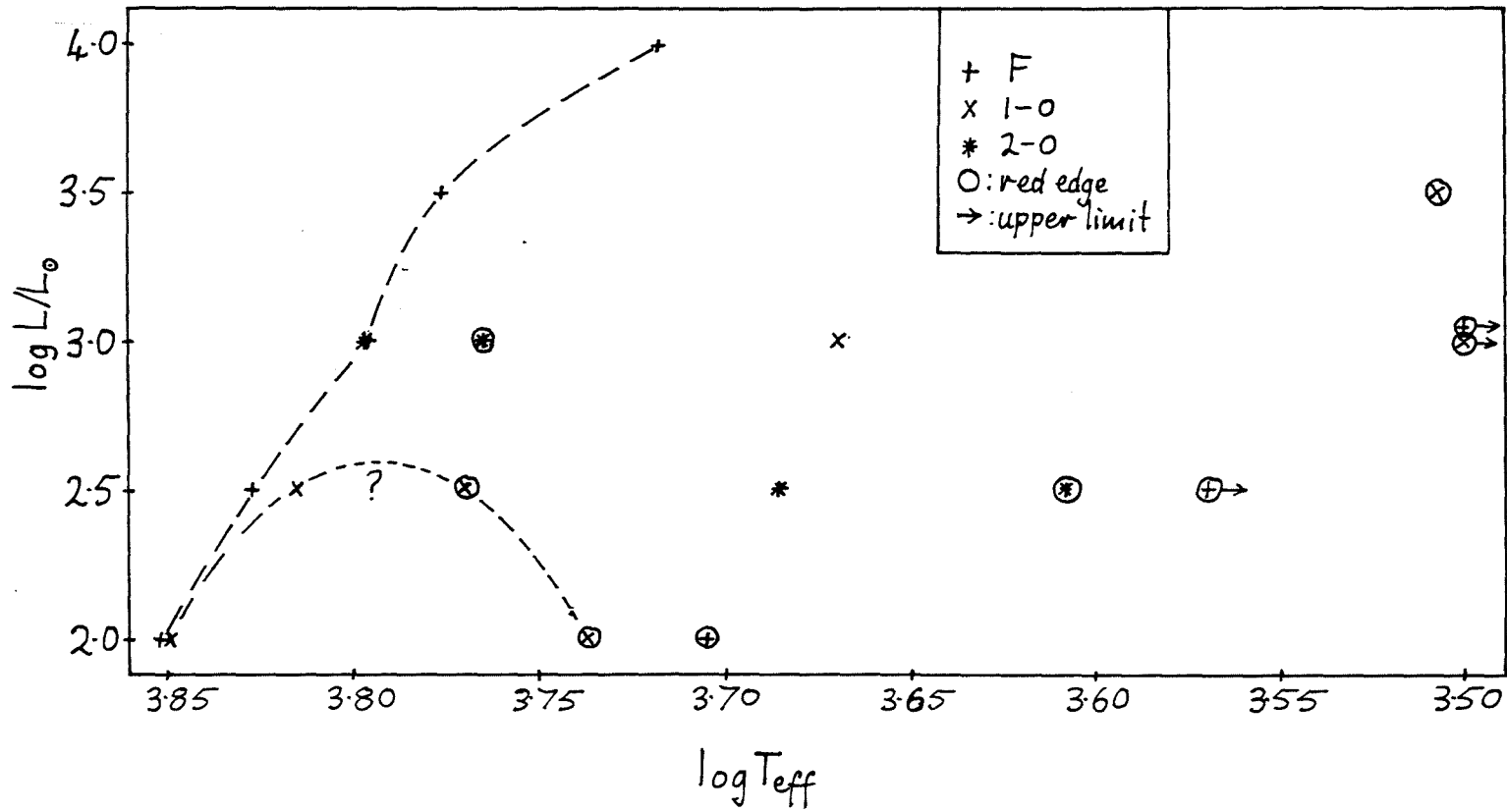


Fig. 7.46

Blue edges for convective models without viscosity using the Carson opacity (see table 5.28 - 5.33)

blue edge without viscosity at $\log(L/L_{\odot}) = 3.5$, they both move towards lower temperature with increasing luminosity. The behaviour of the overtone blue edges for the convective sequences is confusing. It is not possible to construct satisfactory overtone blue edges from this data.

For the Carson opacities the fundamental blue edge is like that for the Stellingwerf formula for $\log(L/L_{\odot}) \approx 3.5$. When $\log(L/L_{\odot}) = 3.75$ and 4.00 there does not appear to be a blue edge. The model sequences have been extended bluewards and the periods and growth rates found for these models may be found in table 7.49. The modes are listed in the order in which they were found and any identification is tentative. For the second of these sequences it can be seen that as far out as $\log(T_{eff}) = 3.88$ there is a highly unstable mode, probably the second overtone, and that the first mode, which is almost certainly the fundamental, is only moderately unstable. The second mode in the table for that luminosity is probably the first overtone and is stable. A complicating factor is the possibility that one of the other of the modes might be a strange mode. There are certainly strange modes on the loose in the $\log(L/L_{\odot}) = 3.5$ sequence (see columns 3 and 4 of the table).

For the $\log(L/L_{\odot}) = 4.00$ extension sequence what appears to be the fundamental mode starts off very unstable at $\log(T_{eff}) = 3.78$. However there is also a stable mode with a nearly identical period.

Passing down the sequence it can be seen that the highly unstable mode no longer has the longest period. For example a 44.10 day mode which is marginally unstable appears. This marginally unstable mode is found in column one of the rest for the rest of this sequence. It is conceivable that this might be an unstable strange mode although no such thing has been found before and the work of Saio et al. (1984) indicates that if it does exist it should be limited to the transition of a mode from strangeness to an ordinary state. The appearance of a mode with a period almost identical to that of the highly unstable mode with a growth rate nearly equal in magnitude but with the opposite sign is an interesting but perplexing feature. Whilst it is well known that the pulsation eigenfrequency exists as part of a conjugate pair ($i\omega$ and $-i\omega^*$) the conjugate of ω is not in general a solution of the equations. This same conjugal relationship has also been found (of course) by Saio, Wheeler and Cox (1984). They have investigated the nonadiabatic behaviour of the modes in their highly nonadiabatic models by artificially modifying the ratio τ_{th}/τ_{dyn} . By varying this parameter from the extreme nonadiabatic limit (0) to the adiabatic limit ($\tau_{th}/\tau_{dyn} \rightarrow \infty$) they obtain a sequence of eigenfrequencies for which the absolute value is plotted in their fig. 15. This graph shows, amongst other things, a pair of modes which in the nonadiabatic limit tend to the same value of $|\omega|$ and which prove to be a complex conjugate pair. So this is not an isolated or unique occurrence but is fairly common amongst very highly nonadiabatic models. In the

appendix to their paper they derive dispersion relationships for simplified models for which they show that in both the adiabatic and nonadiabatic limits the models form complex conjugate pairs.

The information in which I am most interested is the location of the resonances $[0,0;1]$, $[0,0;2]$, and $[0,1;2]$. (Here the notation $[i,j;k]$ denotes the condition $1/P_i + 1/P_j = 1/P_k$.) The loci for these conditions in the luminosity-temperature and period-temperature planes are given in figs. 7.47-7.54. Some of the corresponding data for the adiabatic approximation are also given. The convective sequences for the Stellingwerf opacity formula will be described first. At low luminosities it can be seen that there is little difference between the adiabatic and nonadiabatic data. However as the luminosity increases the two curves part company the adiabatic curve continuing towards lower temperatures whilst nonadiabatic locus swings around back towards higher temperatures. The $[0,0;1]$ locus heads off redwards with almost constant luminosity. A similar thing happens for the $[0,0;2]$ locus. This too swings around and follows a curve lying outside the $[0,0;1]$ line before embarking upon what appears to be a further small loop back on itself. At low luminosity the $[0,0;1]$ curve reaches a minimum luminosity before rising slowly as the temperature falls.

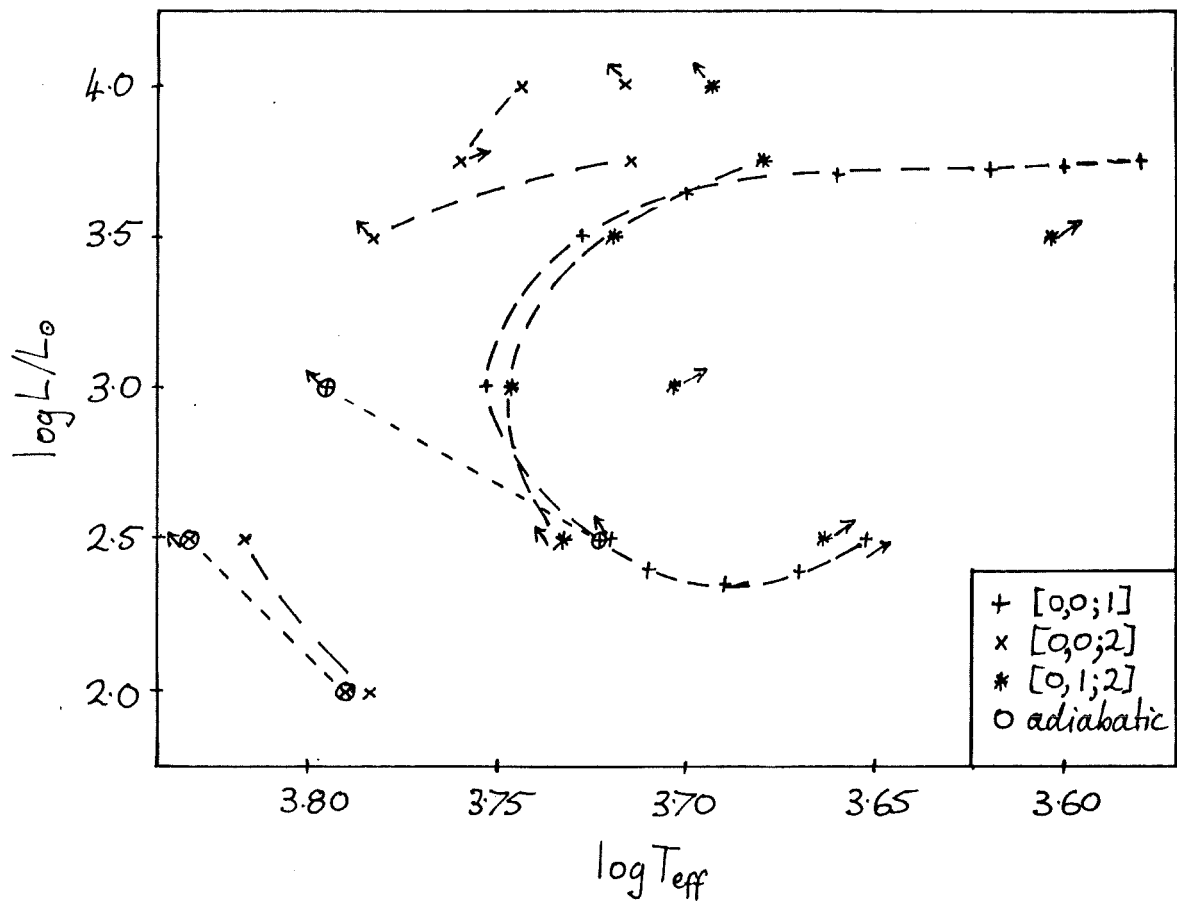


Fig. 7.47

Resonance locations for the convective models using the Stellingwerf opacity. (The arrows indicate the direction in which the resonance parameter increases)

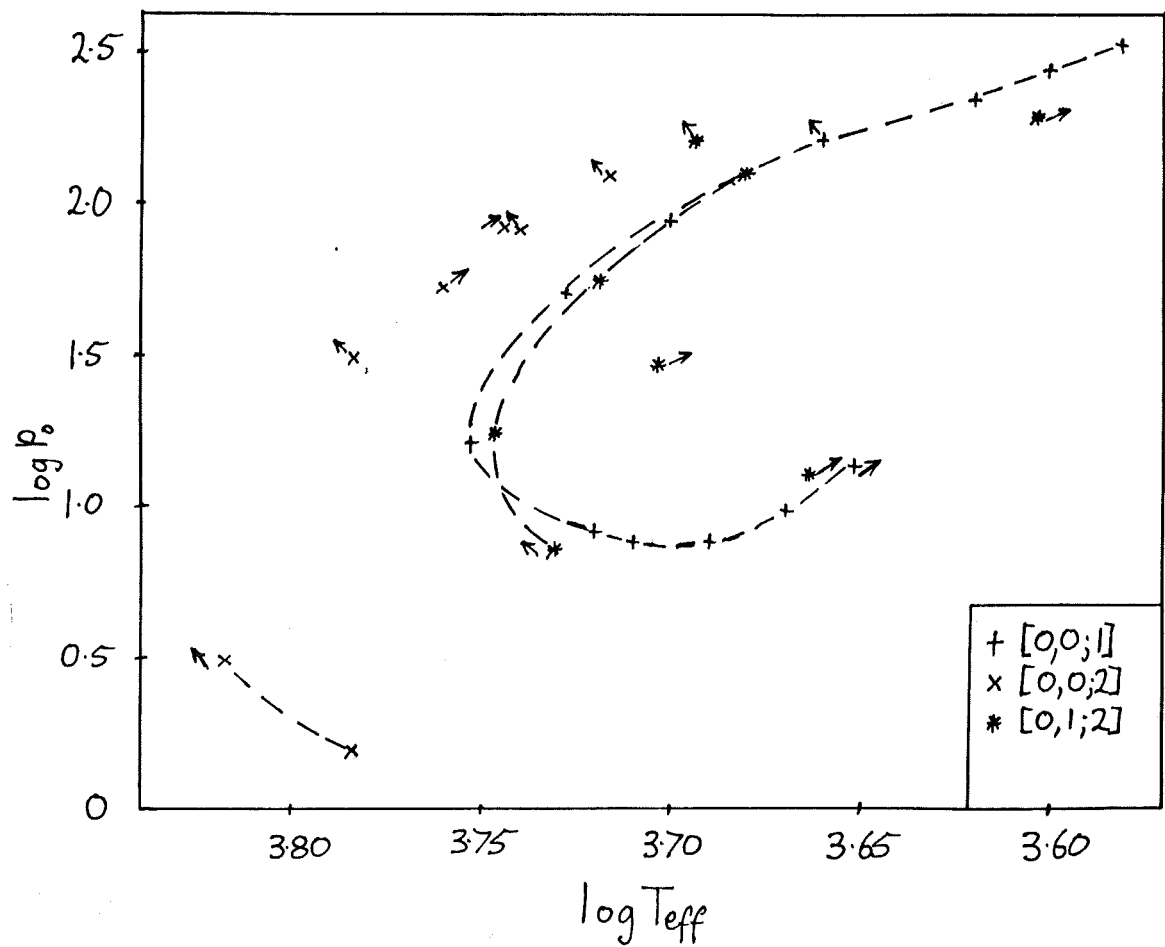


Fig. 7.48

Resonance locations (as above)

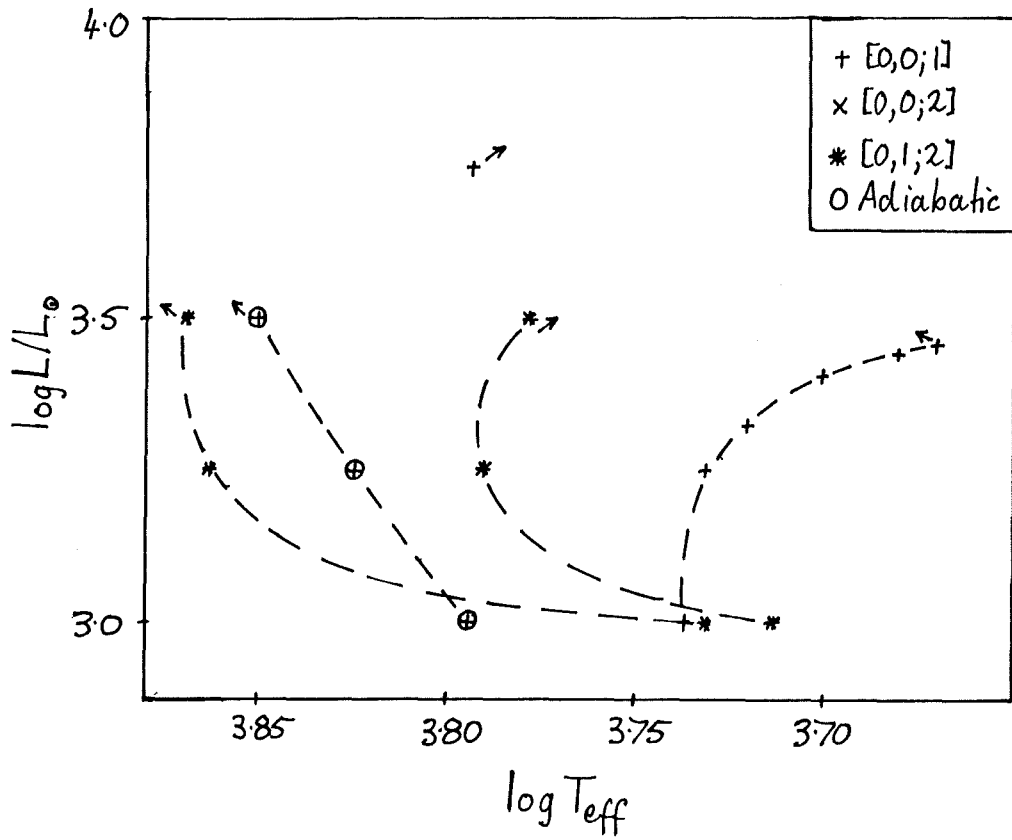


Fig. 7.49 Resonance locations for the radiative models using the Stellingwerf opacity

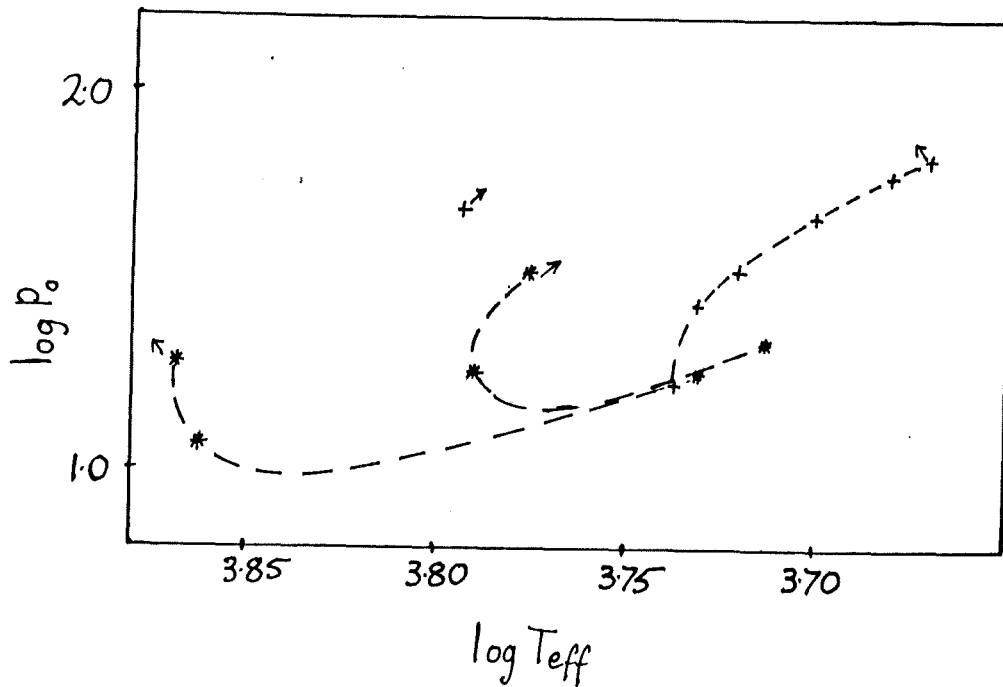


Fig. 7.50 Resonance locations (as above)

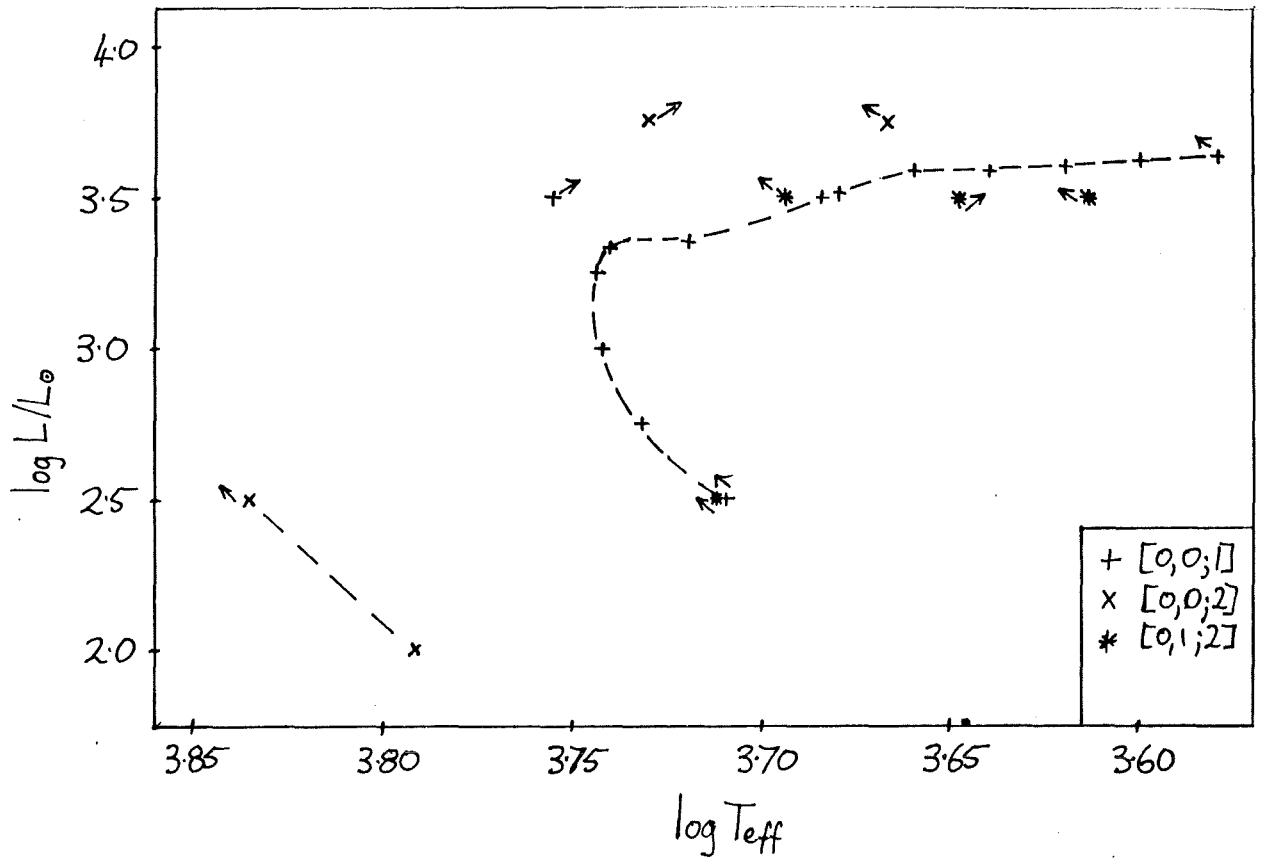


Fig. 7.51

Resonance locations for convective models using the Carson opacity

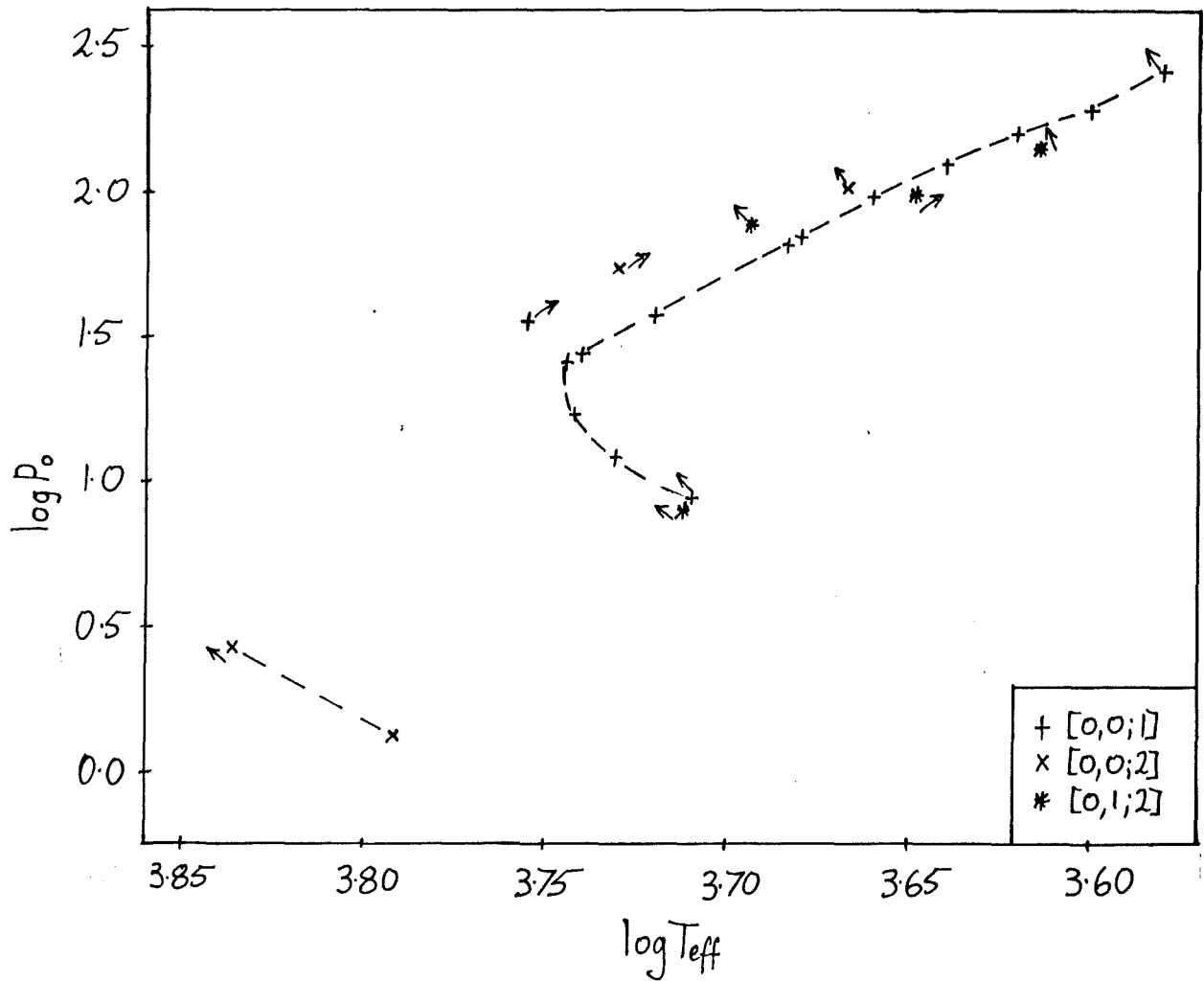


Fig. 7.52

Resonance locations (as above)

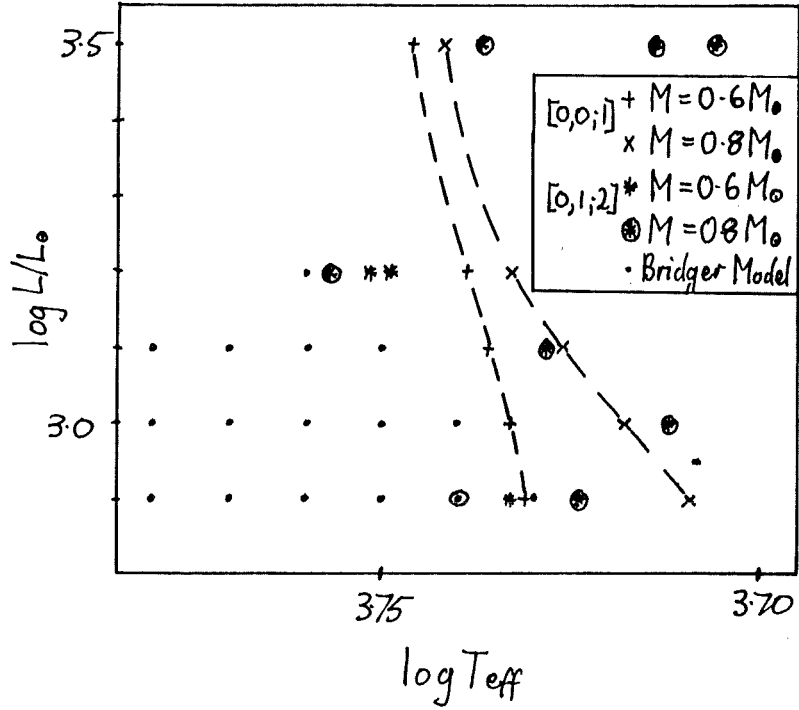


Fig. 7.53 Resonance locations for radiative models using the Carson opacity with $M/M_{\odot} = 0.6 + 0.8$

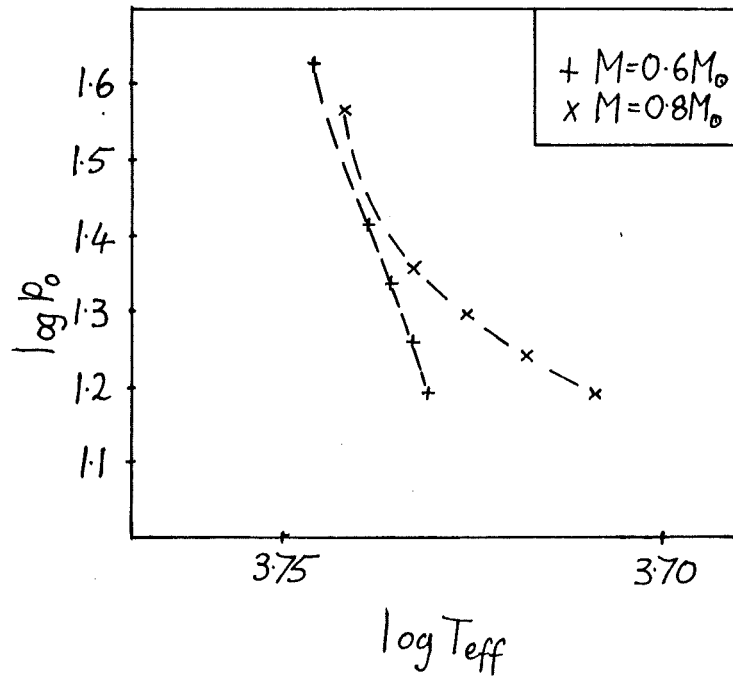


Fig. 7.54 Resonance locations (as above)

The same figures contain the data for the [0,1;2] triple resonance. As can be seen these loci lie very close to the [0,0;1] curve and run almost parallel to it. This is probably of great importance. These loci are so close together that it seems likely that near resonances should occur simultaneously in some models. However this is only conjecture. For anything definite to be said the mode coupling coefficients derived by Buchler and Goupil (1984) must be calculated. Even then it must be borne in mind that they treat the two resonances independently and also that they work under the assumption that $|\text{Im}(\omega)/\text{Re}(\omega)| \ll 1$. This last condition is not satisfied by many of my models, for which $|\text{Im}(\omega)/\text{Re}(\omega)| \sim 0.5$ is not a rarity.

The Stellingwerf radiative models show a different behaviour for the [0,1;2] locus. In this case a pair of resonances for each luminosity exists which rapidly move off bluewards before hinting at a return towards the [0,0;1] locus.

For the Carson convective models life becomes more difficult. A [0,1;2] resonance is found for $\log(L/L_{\odot}) = 2.50$ but disappears for $\log(L/L_{\odot}) = 3.00$ although there are a couple of points at which $1 + P_0/P_1 - P_0/P_2$ is small enough that resonant interaction might take place. At $\log(L/L_{\odot}) = 3.50$ the resonance reappears with a vengeance. There are at least three resonances at this luminosity. For $\log(L/L_{\odot}) = 3.75$ the only triple resonances are of questionable

validity and so I have disregarded them.

Looking at the radiative Carson ^{models} a picture can be seen which is a little like that for the Stellingwerf models. Again the triple resonance crosses the [0,0;1] locus but does not lie close to it over an extended region.

So it looks as if convection is very important to the qualitative behaviour of the resonance locations. When convection is present then the [0,0;1] and [0,1;2] resonance loci are nearly coincident over extended regions of the H-R diagram. The opacity is less important to the qualitative behaviour but does decide the part of the H-R diagram the loci occupy.

In order to be able to say something about the mass dependence of the periods I have computed two auxiliary sequences of models for $M/M_{\odot} = 0.5$ and 0.8 using the Stellingwerf opacity formula with $Z = 0.005$. The fundamental periods from these sequences are given in table 7.50. There is nothing particularly exciting to be said about these models.

Tradition dictates that values of $Q = P\sqrt{\rho}$ be calculated for each of the models in the survey. These values are found in tables 7.51 - 7.68. So far as I can see Qs are only of great value when the stars are either limited to a small region of the H-R diagram and so they vary only slightly and when the pulsations are nearly adiabatic

so that the physical assumption behind the definition is nearly correct. In most cases I prefer to work directly with the periods.

Table 7.3 Blue edges

M=0.6M_⊙ Carson opacity with linear interpolation

Log(L/L _⊙)	Z =			
	0.00	0.005	0.010	0.020
	Log(T _{eff})	Log(T _{eff})	Log(T _{eff})	Log(T _{eff})
1.2500	3.8849	3.8853	3.8768	3.8777
1.5000	3.8730	3.8703	3.8674	3.8695
1.7500	3.8602	3.8600	3.8590	3.8639
2.0000	3.8487	3.8551	3.8547	3.8593
2.2500	3.8294	3.8410	3.8455	3.8551
2.5000	3.8093	3.8254	3.8342	3.8449
2.7500	3.7911	3.8139	3.8247	3.8371
3.0000	3.7786	3.8014	3.8084	3.8285
3.2500	3.7666	3.7902	3.8013	3.8215
3.5000	3.7498	3.7776	----	----

Table 7.4 Blue edges

M=0.8M_⊙ Carson opacity with linear interpolation

Log(L/L _⊙)	Z =			
	0.00	0.005	0.010	0.020
	Log(T _{eff})	Log(T _{eff})	Log(T _{eff})	Log(T _{eff})
1.2500	3.8910	3.8852	3.8803	3.8770
1.5000	3.8757	3.8706	3.8683	3.8650
1.7500	3.8630	3.8611	3.8602	----
2.0000	3.8486	3.8513	3.8524	3.8566
2.2500	3.8372	3.8451	3.8489	3.8540
2.5000	3.8184	3.8322	3.8414	3.8495
2.7500	3.8004	3.8171	3.8297	3.8455
3.0000	3.7856	3.8080	3.8212	3.8351
3.2500	3.7734	3.7943	3.8072	3.8317
3.5000	3.7613	3.7887	3.8116	----

Table 7.5 Blue edges

M=1.2M_⊙ Carson opacity with linear interpolation

Log(L/L _⊙)	Z = 0.00	0.005	0.010	0.020
	Log(T _{eff})	Log(T _{eff})	Log(T _{eff})	Log(T _{eff})
1.2500	3.8980	3.8869	3.8851	3.8815
1.5000	3.8828	3.8729	3.8690	3.8672
1.7500	3.8658	3.8634	3.8614	3.8579
2.0000	3.8564	3.8532	3.8540	3.8551
2.2500	3.8416	3.8450	3.8479	3.8515
2.5000	3.8290	3.8377	3.8444	3.8485
2.7500	3.8109	3.8257	3.8365	3.8456
3.0000	3.7957	3.8184	3.8291	3.8457
3.2500	3.7838	3.8043	3.8251	3.8383
3.5000	3.7726	3.7989	3.8158	3.8342

Table 7.6 Blue edges

M=2.0M_⊙ Carson opacity with linear interpolation

Log(L/L _⊙)	Z = 0.00	0.005	0.010	0.020
	Log(T _{eff})	Log(T _{eff})	Log(T _{eff})	Log(T _{eff})
1.2500	3.9026	3.8922	3.8853	3.8844
1.5000	3.8881	3.8761	3.8751	3.8709
1.7500	3.8710	----	----	3.8609
2.0000	3.8601	3.8542	3.8517	3.8526
2.2500	3.8477	----	----	3.8448
2.5000	3.8345	3.8397	3.8417	3.8441
2.7500	3.8200	----	----	3.8409
3.0000	3.8077	3.8204	3.8322	3.8400
3.2500	3.7899	----	----	3.8436
3.5000	3.7817	3.8084	3.8235	3.8417
4.0000	3.7629	3.7927	3.8131	----

Table 7.7 Blue edges

M=5.0M_⊙ Carson opacity with linear interpolation

Log(L/L _⊙)	Z =			
	0.00	0.005	0.010	0.020
	Log(T _{eff})	Log(T _{eff})	Log(T _{eff})	Log(T _{eff})
1.2500	3.9228	3.9092	3.9033	3.8988
1.5000	3.9028	3.8919	3.8856	3.8854
1.7500	3.8853	----	----	3.8649
2.0000	3.8686	3.8589	3.8548	3.8545
2.2500	3.8556	----	----	3.8431
2.5000	3.8435	3.8384	3.8370	3.8377
2.7500	3.8338	----	----	3.8322
3.0000	3.8218	3.8269	3.8294	3.8310
3.2500	3.8076	----	----	3.8295
3.5000	3.7899	3.8104	3.8205	3.8299
3.7500	----	----	----	3.8348
4.0000	3.7776	3.8015	3.8188	3.8396

Table 7.8 Blue edges

M=0.6M_⊙ Carson opacity with spline interpolation

Log(L/L _⊙)	Z =			
	0.00	0.005	0.010	0.020
	Log(T _{eff})	Log(T _{eff})	Log(T _{eff})	Log(T _{eff})
1.2500	3.8899	3.8855	3.8821	3.8814
1.5000	3.8735	3.8731	3.8707	3.8706
2.0000	3.8449	3.8508	3.8504	3.8565
2.5000	3.8135	3.8287	3.8345	3.8449
3.0000	3.7787	3.8023	3.8170	3.8363
3.5000	3.7418	3.8113	----	----

Table 7.9 Blue edges

M=0.6M_⊙ Carson opacity with;

Log(L/L _⊙)	Stellingwerf		Fitted 2D-spline	
	Z = 0.00 Log(T _{eff})	0.020 Log(T _{eff})	0.000 Log(T _{eff})	0.020 Log(T _{eff})
1.2500	3.8801	3.8733	3.8949	3.8952
1.5000	3.8661	3.8579	3.8756	3.8695
1.7500	3.8524	3.8474	3.8571	3.8663
2.0000	3.8410	3.8352	3.8423	3.8559
2.2500	3.8271	3.8214	3.8264	3.8449
2.5000	3.8123	3.8068	3.8116	3.8384
2.7500	3.7974	3.7919	3.7977	3.8396
3.0000	3.7805	3.7719	3.7842	----
3.2500	3.7580	3.7440	3.7698	3.8505
3.5000	3.7222	3.7271	3.7444	----

Table 7.10 Blue edges

M=0.6M_⊙ Carson opacity linear
Eddington Approximation

Log(L/L _⊙)	Z =	
	0.00 Log(T _{eff})	0.020 Log(T _{eff})
1.2500	3.8849	3.8777
1.5000	3.8730	3.8695
1.7500	3.8602	----
2.0000	3.8487	3.8593
2.2500	3.8294	----
2.5000	3.8093	3.8449
3.0000	3.7787	3.8285
3.2500	----	3.8215
3.5000	3.7498	----

Table 7.11 Blue edges

M=0.6M_⊙ Carson opacity with linear interpolation

Log(L/L _⊙)	Standing wave		Running wave	
	Z = 0.00 Log(T _{eff})	0.020 Log(T _{eff})	0.000 Log(T _{eff})	0.020 Log(T _{eff})
1.2500	3.8864	3.8786	3.8867	3.8793
1.5000	3.8731	3.8689	3.8732	3.8691
2.0000	3.8456	3.8548	3.8456	3.8549
2.5000	3.8111	3.8492	3.8112	3.8492
3.0000	3.7775	3.8249	3.7775	3.8249
3.5000	3.7592	----	3.7592	----

Table 7.12 Blue edges

M=0.6M_⊙ Carson opacity with linear interpolation

Convective models

Log(L/L _⊙)	Z =			
	0.00 Log(T _{eff})	0.005 Log(T _{eff})	0.010 Log(T _{eff})	0.020 Log(T _{eff})
1.5000	3.8780	3.8761	3.8728	3.8722
2.0000	3.8521	3.8548	3.8548	3.8604
2.5000	3.8212	3.8306	3.8371	3.8476
3.0000	3.7922	3.8068	3.8189	3.8272
3.5000	3.7571	----	----	3.8257

Table 7.13 Blue edges

$M=2.0M_{\odot}$, Carson opacity with spline interpolation

Log(L/L _⊙)	Z = 0.00 0.020	
	Log(T _{eff})	Log(T _{eff})
1.2500	3.9175	3.8944
1.5000	3.8938	3.8772
2.0000	3.8593	3.8548
2.5000	3.8327	3.8414
3.0000	3.8103	3.8404
3.5000	3.7849	3.8545
4.0000	3.7520	-----

Table 7.14 Blue edges

$M=0.6M_{\odot}$, Carson opacity with linear interpolation for $X=Y=0.495$ and $Z=0.01$

Log(L/L _⊙)	Log(T _{eff})
1.2500	3.9027
1.5000	3.8886
2.0000	3.8695
2.5000	3.8572
3.0000	3.8374
3.2500	3.8304

Survey Tables

Tables 7.17 - 7.22

Convective models without viscosity
Stellingwerf opacity
 $M = 0.6 M_{\odot}$ $Z = 0.005$

Tables 7.23 - 7.27

Convective models with viscosity
Stellingwerf opacity
 $M = 0.6 M_{\odot}$ $Z = 0.005$

Tables 7.28 - 7.33

Convective models without viscosity
Carson opacity
 $M = 0.6 M_{\odot}$ $Z = 0.005$

Tables 7.34 - 7.38

Radiative models
Stellingwerf opacity
 $M = 0.6 M_{\odot}$ $Z = 0.005$

Tables 7.39 - 7.43

Radiative models
Carson opacity
 $M = 0.6 M_{\odot}$ $Z = 0.005$

Tables 7.44 - 7.48

Radiative models
Carson opacity
 $M = 0.8 M_{\odot}$ $Z = 0.005$

The tables show;

- a) nonadiabatic periods, growth rates (GR), and phase-lags (Ph),
- b) Nonadiabatic and adiabatic resonance parameters, i.e. P_1/P_0 , P_2/P_0 , and $1+P_0/P_1 - P_0/P_2$ (denoted by [0,1;2])
- and c) (often) adiabatic periods.

Table 7.17 $\log(L/L_{\odot}) = 2.00$

Log(T_{eff})	P0	P1	P2	GR0	GR1	GR2	Ph0	Ph1	Ph2
3.85	0.863	0.628	0.483	0.510E-02	0.657E-01-0.164		107.	96.5	21.5
3.83	1.02	0.740	0.558	0.972E-01	0.189	-0.433E-01	150.	151.	152.
3.81	1.21	0.870	0.643	0.139	0.173	-0.504E-01	172.	173.	174.
3.79	1.45	1.02	0.736	0.148	0.114	-0.995E-01	178.	178.	178.
3.77	1.74	1.18	0.835	0.155	0.901E-01-0.749E-01		179.	179.	180.
3.75	2.11	1.36	0.945	0.139	0.886E-01-0.922E-02		179.	180.	-179.
3.73	2.58	1.54	1.06	0.510E-01	0.345E-01	0.184E-01	179.	-180.	-178.
3.71	3.08	1.75	1.22	0.194E-01	0.265E-01	0.442E-01	179.	-179.	-176.
3.69	3.47	2.06	1.45	0.795E-02	0.232E-01	0.530E-01	179.	-178.	-175.
3.67	3.89	2.39	1.75	0.440E-02	0.204E-01	0.453E-01	179.	-177.	-173.
3.65	4.37	2.77	2.07	0.272E-02	0.179E-01	0.342E-01	-179.	-175.	-171.

Nonadiabatic

Adiabatic

Log(T_{eff})	Nonadiabatic			Adiabatic			Log(T_{eff})	P0	P1	P2
	P1/P0	P2/P0	[0,1;2]	P1/P0	P2/P0	[0,1;2]				
3.85	0.728	0.560	0.588	0.727	0.550	0.557	3.85	0.872	0.633	0.479
3.83	0.725	0.547	0.550	0.719	0.535	0.524	3.83	1.03	0.739	0.551
3.81	0.716	0.530	0.508	0.708	0.519	0.487	3.81	1.22	0.863	0.633
3.79	0.701	0.508	0.458	0.694	0.500	0.443	3.79	1.45	1.01	0.726
3.77	0.678	0.480	0.392	0.674	0.477	0.389	3.77	1.74	1.17	0.831
3.75	0.647	0.449	0.317	0.646	0.448	0.317	3.75	2.11	1.36	0.943
3.73	0.597	0.412	0.247	0.596	0.411	0.243	3.73	2.58	1.53	1.06
3.71	0.570	0.396	0.230	0.570	0.395	0.226	3.71	3.08	1.75	1.22
3.69	0.594	0.419	0.300	0.593	0.418	0.296	3.69	3.47	2.06	1.45
3.67	0.614	0.451	0.408	0.614	0.450	0.404	3.67	3.89	2.39	1.75
3.65	0.633	0.474	0.469	0.633	0.473	0.466	3.65	4.37	2.77	2.07

Table 7.18 $\log(L/L_{\odot}) = 2.50$

$\log(T_{eff})$	P0	P1	P2	GRO	GR1	GR2	Ph0	Ph1	Ph2
3.83	2.71	1.87	1.43	-0.729E-01	-0.340	-0.680	111.	7.14	-161.
3.81	3.26	2.16	1.59	0.394	0.168E-01	-0.636	154.	150.	-169.
3.79	4.00	2.54	1.79	0.688	0.792E-01	-0.439	173.	174.	179.
3.77	4.93	2.95	2.03	0.730	-0.276E-01	-0.441	179.	178.	179.
3.75	6.03	3.36	2.25	0.685	-0.821E-01	-0.420	179.	179.	-179.
3.73	7.41	3.83	2.51	0.686	0.231E-01	-0.154	179.	180.	-179.
3.71	9.01	4.34	2.83	0.557	0.679E-01	0.181E-01	179.	-180.	-179.
3.69	10.7	4.92	3.29	0.267	0.962E-01	0.193	178.	-180.	-178.
3.67	12.4	5.78	3.89	0.172	0.138	0.229	178.	-179.	-178.
3.65	13.6	6.86	4.69	0.967E-01	0.139	0.190	179.	-178.	-176.

Nonadiabatic

Adiabatic

$\log(T_{eff})$	Nonadiabatic			Adiabatic			$\log(T_{eff})$	P0	P1	P2
	P1/P0	P2/P0	[0,1;2]	P1/P0	P2/P0	[0,1;2]				
3.83	0.687	0.525	0.552	0.649	0.469	0.409	3.83	2.87	1.86	1.34
3.81	0.664	0.487	0.454	0.628	0.447	0.354	3.81	3.44	2.16	1.53
3.79	0.635	0.448	0.343	0.604	0.422	0.286	3.79	4.14	2.50	1.75
3.77	0.598	0.412	0.246	0.576	0.395	0.202	3.77	5.02	2.89	1.98
3.75	0.557	0.373	0.116	0.546	0.366	0.969E-01	3.75	6.11	3.34	2.23
3.73	0.517	0.339	-0.137E-01	0.513	0.336	-0.228E-01	3.73	7.46	3.83	2.51
3.71	0.482	0.314	-0.108	0.481	0.312	-0.122	3.71	9.02	4.33	2.82
3.69	0.460	0.307	-0.790E-01	0.458	0.303	-0.113	3.69	10.7	4.92	3.26
3.67	0.467	0.314	-0.469E-01	0.465	0.309	-0.863E-01	3.67	12.4	5.78	3.84
3.65	0.503	0.344	0.842E-01	0.502	0.340	0.545E-01	3.65	13.6	6.84	4.64

Table 7.19 $\log(L/L_{\odot}) = 3.00$

$\text{Log}(T_{\text{eff}})$	P0	P1	P2	GRO	GR1	GR2	Ph0	Ph1	Ph2
3.80	9.28	6.28	3.98	-0.226	-1.28	-0.167	142.	-172.	168.
3.78	11.2	6.83	4.82	1.21	-1.29	1.20	168.	-175.	168.
3.76	14.5	7.61	5.50	2.09	-0.868	0.343E-02	177.	179.	179.
3.74	18.8	8.62	5.71	2.36	-0.821	-1.10	179.	-180.	-166.
3.72	23.7	9.47	6.02	2.34	-0.600	-1.55	179.	-179.	-130.
3.70	29.4	10.6	7.97	2.49	-0.169	0.220	179.	-180.	174.
3.68	36.1	12.0	9.41	2.42	0.845E-01	0.173	179.	180.	175.
3.66	43.6	13.8	11.1	2.17	0.354	0.846E-01	179.	178.	177.
3.64	51.6	16.5	13.1	1.49	0.543	0.393E-01	178.	177.	179.
3.62	57.7	20.2	15.6	1.04	0.563	0.558E-01	178.	178.	178.

$\text{Log}(T_{\text{eff}})$	Nonadiabatic			Adiabatic			$\text{Log}(T_{\text{eff}})$	P0	P1	P2
	P1/P0	P2/P0	[0,1;2]	P1/P0	P2/P0	[0,1;2]				
3.80	0.677	0.429	0.146	0.508	0.345	0.748E-01	3.80	11.4	5.78	3.93
3.78	0.609	0.430	0.317	0.474	0.316	-0.505E-01	3.78	13.9	6.61	4.41
3.76	0.525	0.379	0.266	0.437	0.287	-0.200	3.76	17.2	7.52	4.93
3.74	0.457	0.303	-0.112	0.399	0.257	-0.379	3.74	21.3	8.52	5.49
3.72	0.399	0.254	-0.434	0.363	0.231	-0.570	3.72	26.5	9.61	6.12
3.70	0.361	0.271	0.810E-01	0.332	0.212	-0.714	3.70	32.5	10.8	6.88
3.68	0.333	0.261	0.165	0.309	0.201	-0.738	3.68	39.3	12.1	7.90
3.66	0.316	0.255	0.242	0.297	0.199	-0.650	3.66	46.4	13.8	9.25
3.64	0.319	0.255	0.209	0.306	0.204	-0.626	3.64	53.3	16.3	10.9
3.62	0.350	0.271	0.170	0.334	0.217	-0.614	3.62	59.5	19.9	12.9

Table 7.20 $\log(L/L_{\odot}) = 3.50$

$\text{Log}(T_{\text{eff}})$	P0	P1	P2	GR0	GR1	GR2	Ph0	Ph1	Ph2
3.78	31.3	17.9	15.3	-0.821	-0.835	5.20	131.	171.	131.
3.76	33.0	20.5	13.6	-0.873	3.78	-0.781	-180.	157.	-162.
3.74	39.7	22.9	15.5	3.36	1.08	-0.783	174.	172.	-148.
3.72	55.1	25.0	17.2	4.71	0.618	-0.934	176.	173.	-62.7
3.70	71.2	28.6	19.2	4.95	0.633	-1.05	176.	169.	-21.1
3.68	87.0	33.5	23.1	5.03	0.572	-0.810	176.	165.	3.91
3.66	106.	39.9	28.0	5.14	0.484	-0.126	175.	162.	0.511
3.64	130.	47.8	33.8	5.16	0.430	0.459	175.	162.	11.3
3.62	160.	57.3	41.3	5.06	0.440	0.597	175.	162.	15.9
3.60	196.	68.8	51.1	4.84	0.535	0.427	175.	163.	21.1

Nonadiabatic

Adiabatic

$\text{Log}(T_{\text{eff}})$	Nonadiabatic			Adiabatic			$\text{Log}(T_{\text{eff}})$	P0	P1	P2
	P1/P0	P2/P0	[0,1;2]	P1/P0	P2/P0	[0,1;2]				
3.78	0.572	0.489	0.703	0.353	0.242	-0.299	3.78	47.6	16.8	11.5
3.76	0.621	0.412	0.183	0.312	0.221	-0.322	3.76	59.9	18.7	13.2
3.74	0.576	0.390	0.175	0.272	0.201	-0.288	3.74	75.9	20.6	15.3
3.72	0.454	0.313	0.008	0.235	0.184	-0.184	3.72	96.5	22.7	17.7
3.70	0.402	0.270	-0.221	0.206	0.170	-0.313E-01	3.70	122.	25.1	20.7
3.68	0.385	0.265	-0.175	0.186	0.160	0.126	3.68	152.	28.1	24.2
3.66	0.375	0.263	-0.138	0.174	0.152	0.172	3.66	186.	32.3	28.2
3.64	0.367	0.259	-0.128	0.169	0.145	0.454E-01	3.64	225.	37.9	32.7
3.62	0.358	0.258	-0.891E-01	0.171	0.145	-0.579E-01	3.62	264.	45.2	38.3
3.60	0.351	0.261	0.160E-01	0.183	0.155	0.326E-01	3.60	297.	54.3	46.2

Table 7.21 $\log(L/L_{\odot}) = 3.75$

Log(T_{eff})	P0	P1	P2	GR0	GR1	GR2	Ph0	Ph1	Ph2
3.77	50.7	27.6	20.8	-0.189	-1.91	-1.23	133.	-178.	-175.
3.75	53.5	41.9	31.9	0.637	6.35	-1.99	168.	146.	-162.
3.73	60.8	51.9	36.4	5.70	1.32	-2.04	163.	172.	-150.
3.71	87.2	53.3	40.8	6.36	0.690	-2.02	168.	172.	-121.
3.69	112.	60.5	43.8	6.34	0.426	-2.10	168.	171.	-53.8
3.67	135.	71.9	44.6	6.17	0.252	-2.36	167.	171.	-19.3
3.65	164.	86.9	51.1	6.15	0.165	0.520	165.	172.	3.58
3.63	200.	105.	62.0	6.17	0.130	0.646	164.	173.	2.85
3.61	246.	128.	75.8	6.17	0.126	0.548	164.	173.	4.09
3.59	307.	155.	93.1	6.16	0.159	0.356	166.	174.	9.98

Nonadiabatic

Adiabatic

Log(T_{eff})	Nonadiabatic			Adiabatic			Log(T_{eff})	P0	P1	P2
	P1/P0	P2/P0	[0,1;2]	P1/P0	P2/P0	[0,1;2]				
3.77	0.545	0.410	0.396	0.257	0.222	0.381	3.77	107.	27.6	23.8
3.75	0.784	0.596	0.598	0.225	0.199	0.404	3.75	136.	30.6	27.0
3.73	0.854	0.598	0.499	0.199	0.175	0.323	3.73	173.	34.3	30.2
3.71	0.611	0.468	0.500	0.179	0.152	0.131E-01	3.71	219.	39.3	33.4
3.69	0.542	0.393	0.297	0.166	0.133	-0.477	3.69	276.	45.9	36.8
3.67	0.532	0.330	-0.149	0.159	0.120	-1.05	3.67	343.	54.7	41.2
3.65	0.531	0.312	-0.320	0.156	0.111	-1.63	3.65	423.	66.0	46.8
3.63	0.527	0.310	-0.324	0.155	0.105	-2.06	3.63	516.	79.7	54.1
3.61	0.518	0.307	-0.321	0.155	0.103	-2.27	3.61	621.	96.3	63.9
3.59	0.505	0.303	-0.315	0.161	0.107	-2.15	3.59	724.	116.	77.2

Table 7.22 $\log(L/L_{\odot}) = 4.00$

$\log(T_{\text{eff}})$	P0	P1	P2	GRO	GR1	GR2	Ph0	Ph1	Ph2
3.76	76.6	48.0	27.1	-0.108	-2.58	0.921	142.	-173.	-178.
3.74	81.6	54.1	41.3	-0.297	-1.47	-0.180	173.	-162.	169.
3.72	115.	92.1	59.2	8.78	-0.693	-0.627	144.	-176.	-117.
3.70	148.	109.	64.5	8.67	-0.734	-0.723E-01	147.	-170.	2.59
3.68	179.	132.	72.1	8.14	-0.562	0.342	143.	-167.	1.04
3.66	213.	163.	84.9	7.64	-0.520	0.454	137.	-162.	-1.86
3.64	254.	201.	103.	7.41	-0.496	0.360	131.	-157.	-2.62
3.62	309.	248.	127.	7.41	-0.526	0.248	127.	-155.	-0.921
3.60	384.	305.	156.	7.65	-0.670	0.148	128.	-155.	3.80
3.58	493.	379.	191.	8.13	-0.938	0.636E-01	134.	-158.	17.0
3.56	648.	476.	232.	8.66	-1.25	-0.120E-01	142.	-162.	62.4

$\log(T_{\text{eff}})$	Nonadiabatic			Adiabatic			$\log(T_{\text{eff}})$	P0	P1	P2
	P1/P0	P2/P0	[0,1;2]	P1/P0	P2/P0	[0,1;2]				
3.76	0.627	0.353	0.789	0.214	0.151	-0.931	3.76	256.	54.8	38.8
3.74	0.663	0.540	0.491	0.202	0.135	-1.47	3.74	313.	63.1	42.1
3.72	0.802	0.515	0.306	0.191	0.120	-2.11	3.72	384.	73.1	45.9
3.70	0.737	0.437	0.701E-01	0.180	0.107	-2.82	3.70	474.	85.5	50.6
3.68	0.738	0.403	-0.126	0.175	0.985E-01	-3.43	3.68	581.	102.	57.3
3.66	0.765	0.399	-0.198	0.175	0.946E-01	-3.84	3.66	709.	124.	67.1
3.64	0.789	0.406	-0.197	0.177	0.935E-01	-4.03	3.64	861.	152.	80.5
3.62	0.801	0.410	-0.191	0.178	0.926E-01	-4.17	3.62	0.105E+04	187.	97.6
3.60	0.794	0.405	-0.212	0.177	0.908E-01	-4.36	3.60	0.130E+04	230.	118.
3.58	0.769	0.387	-0.285	0.174	0.877E-01	-4.64	3.58	0.164E+04	285.	144.
3.56	0.735	0.358	-0.432	0.169	0.837E-01	-5.02	3.56	0.209E+04	352.	175.

Table 7.23 $\log(L/L_{\odot}) = 2.00$

$\log(T_{\text{eff}})$	P0	P1	P2	GRO	GR1	GR2	Ph0	Ph1	Ph2
3.85	0.863	0.628	0.483	0.673E-02	0.754E-01	-0.141	108.	98.3	31.6
3.83	1.02	0.741	0.558	0.101	0.201	-0.144E-01	150.	152.	153.
3.81	1.22	0.871	0.644	0.140	0.178	-0.334E-01	172.	173.	174.
3.79	1.45	1.02	0.737	0.147	0.113	-0.949E-01	178.	178.	178.
3.77	1.74	1.18	0.836	0.152	0.823E-01	-0.850E-01	179.	179.	180.
3.75	2.11	1.36	0.946	0.130	0.595E-01	-0.594E-01	179.	180.	-179.
3.73	2.58	1.54	1.06	0.304E-01	-0.373E-01	-0.864E-01	179.	-180.	-178.
3.71	3.08	1.75	1.22	0.124E-02	-0.491E-01	-0.618E-01	179.	-179.	-177.
3.69	3.47	2.06	1.46	-0.386E-02	-0.324E-01	-0.490E-01	179.	-178.	-175.
3.67	3.89	2.39	1.75	-0.310E-02	-0.233E-01	-0.337E-01	179.	-177.	-173.
3.65	4.37	2.77	2.07	-0.225E-02	-0.187E-01	-0.250E-01	-179.	-175.	-171.

$\log(T_{\text{eff}})$	Nonadiabatic			Adiabatic		
	P1/P0	P2/P0	[0,1;2]	P1/P0	P2/P0	[0,1;2]
3.85	0.728	0.560	0.587	0.727	0.550	0.557
3.83	0.726	0.547	0.550	0.719	0.535	0.524
3.81	0.717	0.530	0.509	0.708	0.519	0.487
3.79	0.701	0.508	0.458	0.694	0.500	0.443
3.77	0.678	0.480	0.393	0.674	0.477	0.389
3.75	0.647	0.449	0.317	0.646	0.448	0.317
3.73	0.597	0.412	0.246	0.596	0.411	0.243
3.71	0.570	0.396	0.231	0.570	0.395	0.226
3.69	0.594	0.419	0.301	0.593	0.418	0.296
3.67	0.614	0.451	0.408	0.614	0.450	0.404
3.65	0.633	0.474	0.469	0.633	0.473	0.466

Table 7.24 $\log(L/L_{\odot}) = 2.50$

Log(T_{eff})	P0	P1	P2	GRO	GR1	GR2	Ph0	Ph1	Ph2
3.83	2.71	1.86	1.42	-0.672E-01	-0.315	-0.691	112.	20.0	-159.
3.81	3.26	2.16	1.58	0.422	0.905E-01	-0.570	154.	152.	-168.
3.79	4.01	2.55	1.79	0.717	0.128	-0.344	173.	174.	178.
3.77	4.94	2.96	2.03	0.741	-0.913E-02	-0.390	179.	178.	179.
3.75	6.05	3.37	2.25	0.683	-0.834E-01	-0.401	179.	179.	-179.
3.73	7.42	3.83	2.52	0.672	-0.118E-01	-0.225	179.	180.	-179.
3.71	9.02	4.34	2.83	0.525	-0.367E-01	-0.151	179.	180.	-178.
3.69	10.7	4.93	3.30	0.225	-0.702E-01	-0.859E-02	178.	-180.	-177.
3.67	12.4	5.79	3.89	0.129	-0.363E-01	0.285E-01	178.	-179.	-176.
3.65	13.6	6.86	4.70	0.554E-01	-0.139E-01	0.251E-01	179.	-178.	-175.
3.63	14.8	8.09	5.58	0.258E-01	-0.827E-02	0.160E-01	180.	-177.	-173.
3.61	16.1	9.62	6.57	0.123E-01	-0.936E-02	0.196E-02	-179.	-175.	-170.
3.59	18.0	11.5	7.96	0.511E-02	-0.126E-01	-0.180E-01	-178.	-173.	-168.
3.57	22.6	14.6	10.1	0.272E-02	-0.123E-01	-0.286E-01	-177.	-172.	-165.

Nonadiabatic

Adiabatic

Log(T)	P1/P0	P2/P0	[0,1;2]	P1/P0	P2/P0	[0,1;2]
3.83	0.686	0.524	0.550	0.649	0.469	0.409
3.81	0.665	0.484	0.438	0.628	0.447	0.354
3.79	0.636	0.447	0.335	0.604	0.422	0.286
3.77	0.599	0.411	0.240	0.576	0.395	0.202
3.75	0.557	0.373	0.113	0.546	0.366	0.969E-01
3.73	0.517	0.339	-0.108E-01	0.513	0.336	-0.228E-01
3.71	0.481	0.314	-0.106	0.481	0.312	-0.122
3.69	0.460	0.308	-0.760E-01	0.458	0.303	-0.113
3.67	0.467	0.314	-0.449E-01	0.465	0.309	-0.863E-01
3.65	0.503	0.345	0.857E-01	0.502	0.340	0.545E-01
3.63	0.548	0.378	0.178	0.546	0.374	0.154
3.61	0.598	0.409	0.226	0.596	0.404	0.203
3.59	0.642	0.443	0.302	0.641	0.439	0.283
3.57	0.647	0.446	0.304	0.646	0.443	0.292

Table 7.25 $\log(L/L_{\odot}) = 3.00$

Log(T_{eff})	P0	P1	P2	GRO	GR1	GR2	Ph0	Ph1	Ph2
3.80	9.21	6.26	3.93	-0.255	-1.31	-0.215	144.	-170.	169.
3.78	11.1	6.71	5.19	1.32	-1.22	1.11	169.	-175.	169.
3.76	14.6	7.59	5.64	2.21	-0.628	-0.318	177.	178.	-179.
3.74	18.9	8.64	5.96	2.43	-0.684	-0.163	179.	180.	-179.
3.72	23.8	9.52	6.86	2.37	-0.528	0.122	179.	-179.	177.
3.68	36.2	12.1	9.46	2.41	-0.875E-01	0.147	179.	-180.	176.
3.66	43.8	13.9	11.2	2.14	0.714E-01	0.541E-01	179.	-180.	179.
3.64	51.7	16.5	13.2	1.46	0.219	-0.402E-02	178.	179.	-179.
3.62	57.8	20.2	15.7	0.997	0.259	0.205E-01	178.	180.	180.
3.60	62.7	24.7	18.7	0.598	0.222	0.608E-01	179.	-179.	178.
3.58	66.0	29.9	18.1	0.332	0.161	-0.224	180.	-178.	72.3
3.56	71.6	36.1	22.4	0.206	0.112	-0.261	-179.	-176.	151.
3.54	89.3	47.0	32.3	0.135	0.787E-01	0.215	-179.	-175.	178.
3.52	107.	52.7	31.4	0.883E-01	0.626E-01	-0.198	-178.	-173.	142.

Nonadiabatic

Adiabatic

Log(T_{eff})	P1/P0	P2/P0	[0,1;2]	P1/P0	P2/P0	[0,1;2]
3.80	0.680	0.427	0.128	0.508	0.345	0.748E-01
3.78	0.602	0.465	0.512	0.474	0.316	-0.505E-01
3.76	0.521	0.388	0.340	0.437	0.287	-0.200
3.74	0.456	0.315	0.129E-01	0.399	0.257	-0.379
3.72	0.400	0.288	0.026	0.363	0.231	-0.570
3.68	0.335	0.261	0.160	0.309	0.201	-0.738
3.66	0.317	0.256	0.243	0.297	0.199	-0.650
3.64	0.320	0.255	0.212	0.306	0.204	-0.626
3.62	0.350	0.271	0.175	0.334	0.217	-0.614
3.60	0.394	0.298	0.180	0.382	0.243	-0.505
3.58	0.453	0.275	-0.430	0.444	0.280	-0.323
3.56	0.504	0.313	-0.212	0.497	0.320	-0.110
3.54	0.527	0.362	0.136	0.523	0.334	-0.798E-01
3.52	0.491	0.292	-0.381	0.486	0.303	-0.244

Table 7.26 $\log(L/L_{\odot}) = 3.50$

$\log(T_{eff})$	P0	P1	P2	GRO	GR1	GR2	Ph0	Ph1	Ph2
3.78	31.3	17.6	16.7	-1.23	-1.10	5.88	125.	172.	136.
3.76	32.1	22.5	13.7	-0.211	4.50	-0.736	171.	160.	-164.
3.74	38.8	24.6	23.7	3.81	0.459	-1.60	174.	177.	-172.
3.72	55.1	25.6	17.7	4.97	-1.10	0.443	176.	175.	-84.0
3.70	71.4	29.1	20.1	5.12	0.581	-1.39	176.	171.	-37.8
3.68	87.2	34.0	24.3	5.14	0.578	-1.14	176.	166.	-26.9
3.66	107.	40.5	28.7	5.22	0.517	-0.404	175.	163.	-5.84
3.64	131.	48.4	34.3	5.22	0.471	0.556E-01	175.	162.	4.66
3.62	160.	58.0	41.5	5.09	0.479	0.158	175.	163.	8.57
3.60	196.	69.7	51.1	4.87	0.564	-0.124E-01	175.	164.	10.4
3.58	239.	84.0	63.5	4.26	0.692	-0.313	176.	166.	15.2
3.56	276.	102.	78.9	3.36	0.800	-0.524	177.	169.	172.
3.54	318.	123.	96.8	2.52	0.823	-0.615	178.	172.	173.
3.52	421.	151.	121.	2.29	0.918	-0.660	179.	173.	173.

Nonadiabatic

Adiabatic

$\log(T_{eff})$	P1/P0	P2/P0	[0,1;2]	P1/P0	P2/P0	[0,1;2]
3.78	0.565	0.533	-0.229	0.353	0.242	-0.299
3.76	0.703	0.429	-0.577	0.312	0.221	-0.322
3.74	0.635	0.610	0.936	0.272	0.201	-0.288
3.72	0.465	0.321	0.039	0.235	0.184	-0.184
3.70	0.408	0.282	-0.099	0.206	0.170	-0.313E-01
3.68	0.391	0.279	-0.211E-01	0.186	0.160	0.126
3.66	0.379	0.268	-0.862E-01	0.174	0.152	0.172
3.64	0.371	0.263	-0.110	0.169	0.145	0.454E-01
3.62	0.362	0.259	-0.971E-01	0.171	0.145	-0.579E-01
3.60	0.355	0.261	-0.206E-01	0.183	0.155	0.326E-01
3.58	0.351	0.266	0.806E-01	0.204	0.176	0.221
3.56	0.369	0.286	0.214	0.238	0.206	0.341
3.54	0.388	0.305	0.297	0.277	0.237	0.379
3.52	0.358	0.289	0.329	0.266	0.218	0.155

Table 7.27 $\log(L/L_{\odot}) = 4.00$

$\log(T_{\text{eff}})$	P0	P1	P2	GR0	GR1	GR2	Ph0	Ph1	Ph2
3.76	76.1	48.3	30.8	-1.50	-2.34	1.43	147.	180.	-162.
3.74	83.3	53.3	40.7	-1.38	-1.26	-0.059	-180.	-168.	173.
3.72	94.4	58.6	47.0	-1.24	-0.702	-0.138	-172.	-91.5	163.
3.70	150.	110.	64.7	9.25	-0.961	-0.354	147.	-168.	1.01
3.68	181.	133.	73.1	8.60	-0.655	0.268E-01	143.	-166.	1.81
3.66	214.	163.	86.7	8.01	-0.565	0.242	137.	-161.	0.642
3.64	255.	201.	105.	7.70	-0.524	0.255	131.	-157.	-0.190
3.62	309.	248.	128.	7.64	-0.546	0.197	127.	-155.	0.695
3.60	385.	306.	157.	7.84	-0.688	0.114	128.	-155.	4.83
3.58	494.	380.	191.	8.28	-0.955	0.292E-01	134.	-158.	18.1
3.56	649.	478.	232.	8.80	-1.27	-0.550E-01	142.	-162.	63.9
3.54	860.	613.	281.	9.24	-1.61	-0.147	150.	-166.	106.

$\log(T_{\text{eff}})$	Nonadiabatic			Adiabatic		
	P1/P0	P2/P0	[0,1;2]	P1/P0	P2/P0	[0,1;2]
3.76	0.635	0.401	0.767	0.214	0.151	-0.931
3.74	0.640	0.489	0.436	0.202	0.135	-1.47
3.72	0.621	0.498	0.389	0.191	0.120	-2.11
3.70	0.734	0.431	0.428E-01	0.180	0.107	-2.82
3.68	0.736	0.405	-0.112	0.175	0.985E-01	-3.43
3.66	0.764	0.405	-0.158	0.175	0.946E-01	-3.84
3.64	0.789	0.412	-0.158	0.177	0.935E-01	-4.03
3.62	0.802	0.415	-0.162	0.178	0.926E-01	-4.17
3.60	0.795	0.407	-0.196	0.177	0.908E-01	-4.36
3.58	0.770	0.387	-0.282	0.174	0.877E-01	-4.64
3.56	0.736	0.357	-0.440	0.169	0.837E-01	-5.02
3.54	0.713	0.326	-0.663	0.146	0.712E-01	-6.18

Table 7.28 $\log(L/L_{\odot}) = 2.00$

$\log(T_{eff})$	P0	P1	P2	GR0	GR1	GR2	Ph0	Ph1	Ph2
3.85	0.886	0.637	0.489	0.630E-02	0.398E-01	-0.186	85.0	68.9	-29.4
3.83	1.04	0.745	0.561	0.779E-01	0.123	-0.108	122.	119.	104.
3.81	1.24	0.874	0.645	0.168	0.174	-0.347E-01	163.	164.	165.
3.79	1.48	1.02	0.742	0.174	0.138	-0.595E-01	174.	175.	174.
3.77	1.76	1.19	0.848	0.184	0.962E-01	-0.914E-01	177.	177.	177.
3.75	2.10	1.37	0.963	0.177	0.493E-01	-0.104	177.	178.	178.
3.73	2.50	1.58	1.09	0.172	0.555E-01	-0.497E-01	177.	178.	179.
3.71	2.99	1.82	1.24	0.141	0.489E-01	-0.140E-01	176.	178.	179.
3.69	3.57	2.07	1.40	0.912E-01	0.387E-01	0.231E-01	176.	179.	-180.
3.67	4.25	2.35	1.61	0.562E-01	0.442E-01	0.684E-01	177.	180.	-178.
3.65	4.93	2.74	1.88	0.259E-01	0.406E-01	0.758E-01	177.	-180.	-176.

$\log(T_{eff})$	Nonadiabatic			Adiabatic			$\log(T_{eff})$	P0	P1	P2
	P1/P0	P2/P0	[0,1;2]	P1/P0	P2/P0	[0,1;2]				
3.85	0.719	0.551	0.578	0.715	0.538	0.541	3.85	0.895	0.640	0.482
3.83	0.713	0.537	0.541	0.706	0.525	0.512	3.83	1.05	0.744	0.554
3.81	0.704	0.520	0.496	0.695	0.510	0.477	3.81	1.25	0.867	0.636
3.79	0.691	0.502	0.457	0.682	0.493	0.437	3.79	1.48	1.01	0.729
3.77	0.674	0.481	0.406	0.667	0.475	0.394	3.77	1.76	1.17	0.835
3.75	0.654	0.459	0.350	0.650	0.456	0.347	3.75	2.09	1.36	0.954
3.73	0.632	0.437	0.295	0.631	0.437	0.296	3.73	2.49	1.57	1.09
3.71	0.608	0.415	0.236	0.608	0.415	0.237	3.71	2.98	1.81	1.24
3.69	0.580	0.393	0.180	0.580	0.393	0.179	3.69	3.56	2.07	1.40
3.67	0.552	0.379	0.172	0.552	0.378	0.166	3.67	4.26	2.35	1.61
3.65	0.556	0.382	0.182	0.555	0.380	0.173	3.65	4.93	2.74	1.88

Table 7.29 $\log(L/L_{\odot}) = 2.50$

Log(T_{eff})	P0	P1	P2	GRO	GR1	GR2	Ph0	Ph1	Ph2
3.83	2.86	1.89	1.41	0.315E-01	-0.287	-0.425	80.7	-17.1	-161.
3.81	3.40	2.17	1.59	0.261	-0.995E-01	-0.393	126.	117.	-174.
3.79	4.09	2.52	1.41	0.654	0.160	-0.193	161.	164.	179.
3.77	4.99	2.94	2.05	0.833	0.164	-0.180	172.	174.	177.
3.75	6.07	3.40	2.33	0.900	0.963E-01	-0.181	176.	176.	177.
3.73	7.34	3.91	2.63	0.903	0.193E-01	-0.201	178.	177.	179.
3.71	8.87	4.45	2.95	0.836	-0.289E-01	-0.171	177.	177.	180.
3.69	10.7	5.05	3.32	0.783	-0.450E-02	-0.448E-01	177.	178.	180.
3.67	12.9	5.74	3.76	0.718	0.689E-01	0.112	178.	179.	180.
3.65	15.4	6.51	4.30	0.617	0.937E-01	0.215	178.	180.	179.
3.63	18.2	7.46	5.04	0.414	0.142	0.302	-179.	-178.	-179.

Log(T_{eff})	Nonadiabatic			Adiabatic			Log(T_{eff})	P0	P1	P2
	P1/P0	P2/P0	[0,1;2]	P1/P0	P2/P0	[0,1;2]				
3.83	0.663	0.493	0.481	0.628	0.454	0.390	3.83	2.98	1.87	1.35
3.81	0.638	0.468	0.429	0.609	0.434	0.338	3.81	3.56	2.17	1.54
3.79	0.615	0.346	-0.267	0.587	0.412	0.275	3.79	4.27	2.51	1.76
3.77	0.591	0.412	0.266	0.564	0.390	0.206	3.77	5.13	2.90	2.00
3.75	0.561	0.385	0.182	0.542	0.369	0.134	3.75	6.16	3.34	2.27
3.73	0.533	0.359	0.919E-01	0.519	0.349	0.591E-01	3.73	7.39	3.84	2.58
3.71	0.501	0.333	-0.116E-01	0.495	0.329	-0.216E-01	3.71	8.88	4.40	2.92
3.69	0.473	0.311	-0.105	0.472	0.310	-0.108	3.69	10.7	5.03	3.30
3.67	0.447	0.293	-0.177	0.447	0.291	-0.196	3.67	12.8	5.73	3.73
3.65	0.422	0.279	-0.216	0.422	0.275	-0.260	3.65	15.4	6.50	4.24
3.63	0.409	0.276	-0.173	0.409	0.271	-0.246	3.63	18.2	7.43	4.92

Table 7.30 $\log(L/L_{\odot}) = 3.00$

$\log(T_{\text{eff}})$	P0	P1	P2	GRO	GR1	GR2	Ph0	Ph1	Ph2
3.80	10.1	6.03	3.99	0.327	-0.769	-0.438	112.	-175.	163.
3.78	12.0	6.77	4.42	1.05	-0.483	-0.358	149.	169.	175.
3.76	14.4	7.55	5.50	1.66	-0.597E-02	1.14	166.	171.	163.
3.74	17.5	8.69	6.35	2.33	0.287	0.702	173.	174.	168.
3.72	21.5	10.1	7.19	2.70	0.239	0.376	177.	177.	172.
3.70	26.8	11.6	8.21	3.05	0.130	0.277	179.	178.	172.
3.68	33.1	13.1	9.51	3.22	0.195E-01	0.189	178.	178.	172.
3.66	40.3	14.6	11.2	3.51	0.136	0.104	-179.	-180.	177.
3.64	49.7	16.4	13.2	3.52	0.319	-0.828E-02	-178.	180.	-177.
3.62	63.0	18.6	15.5	3.11	0.470	-0.728E-01	178.	174.	-178.
3.60	77.4	21.6	18.2	2.73	0.668	-0.131	178.	172.	-176.

Nonadiabatic				Adiabatic						
$\log(T_{\text{eff}})$	P1/P0	P2/P0	[0,1;2]	P1/P0	P2/P0	[0,1;2]	$\log(T_{\text{eff}})$	P0	P1	P2
3.80	0.597	0.396	0.145	0.487	0.327	-0.813E-02	3.80	12.1	5.87	3.94
3.78	0.564	0.369	0.585E-01	0.457	0.301	-0.135	3.78	14.7	6.72	4.42
3.76	0.525	0.382	0.289	0.430	0.278	-0.265	3.76	17.9	7.68	4.97
3.74	0.498	0.363	0.258	0.405	0.259	-0.396	3.74	21.7	8.77	5.60
3.72	0.470	0.334	0.128	0.380	0.241	-0.530	3.72	26.2	9.99	6.31
3.70	0.434	0.307	0.457E-01	0.357	0.224	-0.664	3.70	31.8	11.3	7.11
3.68	0.395	0.287	0.510E-01	0.335	0.210	-0.784	3.68	38.4	12.9	8.05
3.66	0.363	0.278	0.155	0.312	0.197	-0.875	3.66	46.6	14.6	9.18
3.64	0.329	0.266	0.269	0.289	0.186	-0.901	3.64	56.8	16.4	10.6
3.62	0.295	0.246	0.323	0.266	0.179	-0.842	3.62	69.3	18.5	12.4
3.60	0.278	0.235	0.345	0.253	0.175	-0.750	3.60	83.3	21.1	14.6

Table 7.31 $\log(L/L_{\odot}) = 3.50$

$\log(T_{\text{eff}})$	P0	P1	P2	GRO	GR1	GR2	Ph0	Ph1	Ph2
3.78	29.5	14.2	11.8	0.515	4.62	-1.19	119.	107.	-166.
3.76	35.2	17.4	13.7	0.804	4.39	-0.520	141.	118.	-125.
3.74	39.7	20.6	15.6	2.06	3.50	0.171	158.	125.	-3.84
3.72	45.6	25.0	17.6	3.08	2.94	0.427	166.	135.	7.86
3.70	54.7	30.4	19.7	4.07	2.53	0.226	170.	146.	4.19
3.68	69.2	33.7	22.1	4.99	1.65	0.174	170.	138.	2.32
3.66	86.3	34.0	20.9	5.37	-0.562	-0.640	171.	-46.8	34.5
3.64	109.	47.1	37.4	5.88	0.625	0.184	171.	153.	7.50
3.62	134.	56.7	42.3	5.99	0.501	0.565	172.	161.	14.9
3.60	160.	68.4	48.8	6.24	0.368	0.608	171.	166.	13.0
3.58	206.	81.9	57.1	6.06	0.392	0.520	173.	168.	14.3

Nonadiabatic				Adiabatic						
$\log(T_{\text{eff}})$	P1/P0	P2/P0	[0,1;2]	P1/P0	P2/P0	[0,1;2]	$\log(T_{\text{eff}})$	P0	P1	P2
3.78	0.482	0.399	0.567	0.327	0.221	-0.465	3.78	52.7	17.3	11.7
3.76	0.493	0.389	0.456	0.296	0.207	-0.457	3.76	65.3	19.3	13.5
3.74	0.520	0.393	0.376	0.271	0.195	-0.428	3.74	80.0	21.7	15.6
3.72	0.548	0.385	0.227	0.249	0.186	-0.367	3.72	97.6	24.3	18.1
3.70	0.555	0.361	0.303E-01	0.229	0.177	-0.273	3.70	119.	27.2	21.1
3.68	0.487	0.320	-0.725E-01	0.213	0.173	-0.100	3.68	143.	30.6	24.8
3.66	0.394	0.242	-0.585	0.199	0.169	0.117	3.66	174.	34.5	29.4
3.64	0.432	0.343	0.400	0.187	0.165	0.260	3.66	174.	34.5	29.4
3.62	0.423	0.316	0.196	0.179	0.157	0.222	3.64	210.	39.3	34.5
3.60	0.428	0.264	-0.443	0.171	0.146	-0.416E-01	3.62	255.	45.6	40.0
3.58	0.398	0.277	-0.092	0.161	0.132	-0.394	3.60	315.	54.0	45.8
							3.58	396.	63.8	52.1

Table 7.32 $\log(L/L_{\odot}) = 3.75$

$\text{Log}(T_{\text{eff}})$	P0	P1	P2	GRO	GR1	GR2	Ph0	Ph1	Ph2
3.77	46.7	28.4	22.3	0.494	5.71	-1.67	126.	90.6	-175.
3.75	52.4	33.3	23.6	1.33	5.17	-0.148	143.	94.9	-20.7
3.73	55.3	40.9	26.8	1.77	5.45	0.377	155.	107.	-4.97
3.71	59.2	51.4	41.5	3.99	2.71	0.339	121.	148.	41.0
3.69	76.4	59.6	46.4	5.31	0.994	0.902	144.	149.	31.0
3.67	99.5	71.9	51.1	6.22	0.320	0.889	147.	166.	15.7
3.65	129.	86.2	56.5	6.96	0.194E-01	0.941	149.	177.	7.31
3.63	182.	107.	86.1	3.72	2.36	0.706	168.	129.	36.9
3.61	206.	128.	76.0	7.39	-0.112	0.547	152.	-178.	-2.73
3.59	285.	163.	110.	4.37	0.821	0.191	166.	160.	6.01
3.57	326.	186.	107.	7.28	-0.170	0.250	159.	-178.	6.18

Nonadiabatic				Adiabatic						
$\text{Log}(T_{\text{eff}})$	P1/P0	P2/P0	[0,1;2]	P1/P0	P2/P0	[0,1;2]	$\text{Log}(T_{\text{eff}})$	P0	P1	P2
3.77	0.608	0.478	0.550	0.226	0.197	0.338	3.77	123.	27.7	24.1
3.75	0.635	0.450	0.353	0.204	0.181	0.391	3.75	152.	31.0	27.6
3.73	0.740	0.485	0.288	0.190	0.169	0.330	3.73	185.	35.2	31.2
3.71	0.868	0.701	0.725	0.181	0.157	0.154	3.71	223.	40.3	35.0
3.69	0.780	0.607	0.635	0.176	0.147	-0.100	3.69	266.	46.7	39.1
3.67	0.723	0.513	0.437	0.175	0.138	-0.528	3.67	318.	55.7	43.9
3.65	0.668	0.438	0.213	0.177	0.131	-0.993	3.65	378.	66.9	49.4
3.63	0.588	0.473	0.587	0.180	0.125	-1.45	3.63	449.	80.7	56.0
3.61	0.621	0.369	-0.968E-01	0.179	0.117	-1.97	3.61	546.	97.9	63.8
3.59	0.572	0.386	0.158	0.178	0.111	-2.39	3.59	666.	119.	74.4
3.57	0.571	0.328	-0.294	0.167	0.103	-2.76	3.57	839.	140.	86.0

Table 7.33 $\log(L/L_{\odot}) = 4.00$

$\log(T_{eff})$	P0	P1	P2	GR0	GR1	GR2	Ph0	Ph1	Ph2
3.76	58.3	48.1	26.7	5.82	-1.26	2.32	70.8	158.	-168.
3.72	81.2	57.3	35.3	6.59	1.81	1.40	82.8	-4.47	-154.
3.70	98.2	65.3	39.3	7.06	1.95	1.17	90.3	-0.08	-156.
3.68	123.	73.5	44.2	7.31	1.37	0.998	92.9	-12.6	-165.
3.66	132.	-----	54.0	6.76	-----	1.25	71.7	-----	-162.
3.64	197.	-----	76.4	8.55	-----	0.924	98.9	-----	-155.
3.62	209.	-----	-----	7.88	-----	-----	76.2	-----	-----
3.60	311.	301.	98.6	8.66	-----	1.00	96.6	-----	-171.
3.58	417.	369.	114.	8.78	-----	0.767	109.	-----	-176.
3.56	531.	445.	131.	9.21	-----	0.693	121.	-----	-174.

Nonadiabatic

Adiabatic

$\log(T_{eff})$	Nonadiabatic			Adiabatic			$\log(T_{eff})$	P0	P1	P2
	P1/P0	P2/P0	[0,1;2]	P1/P0	P2/P0	[0,1;2]				
3.76	0.825	0.458	0.029	0.193	0.132	-1.39	3.76	287.	55.3	37.9
3.72	0.706	0.435	0.117	0.190	0.115	-2.42	3.72	397.	75.4	45.7
3.70	0.665	0.400	0.006	0.189	0.110	-2.82	3.70	462.	87.4	50.7
3.68	0.596	0.358	-0.113	0.194	0.107	-3.20	3.68	539.	105.	57.7
3.66	-----	0.409	-----	0.204	0.108	-3.37	3.66	628.	128.	67.7
3.64	-----	0.388	-----	0.214	0.110	-3.41	3.64	735.	157.	80.9
3.62	-----	-----	-----	0.224	0.113	-3.40	3.62	868.	194.	97.9
3.60	0.968	0.317	-1.121	0.234	0.115	-3.40	3.60	0.104E+04	242.	120.
3.58	0.885	0.273	-1.533	0.231	0.111	-3.65	3.58	0.127E+04	294.	142.
3.56	0.838	0.247	-1.855	0.214	0.101	-4.25	3.56	0.163E+04	350.	165.

Table 7.34 $\log(L/L_{\odot}) = 3.00$

Log(T_{eff})	P0	P1	P2	GRO	GR1	GR2	Ph0	Ph1	Ph2
3.90	4.74	3.15	2.27	-1.36	-0.463	-0.465	-33.6	150.	73.8
3.88	5.55	3.66	2.57	-1.41	-0.538	-0.493	-28.7	155.	84.4
3.86	6.47	4.23	2.89	-1.43	-0.624	-0.505	-21.1	162.	99.8
3.84	7.48	4.88	3.23	-1.40	-0.746	-0.484	-8.65	171.	118.
3.82	8.56	5.62	3.62	-1.22	-0.946	-0.428	13.8	-178.	135.
3.80	9.73	6.40	4.04	-0.770	-1.28	-0.350	54.0	-165.	150.
3.78	11.2	7.09	4.49	0.218E-01	-1.65	-0.287	97.9	-150.	161.
3.76	13.4	7.62	5.00	0.963	-1.63	-0.560	126.	-135.	174.
3.74	16.5	8.31	5.67	1.77	-1.00	-1.07	142.	172.	-170.
3.72	20.5	9.47	6.30	2.27	-0.462	-1.36	151.	162.	-156.
3.70	24.9	10.9	7.98	2.56	-0.190	0.117	154.	164.	169.
3.68	30.1	12.4	9.31	2.82	-0.160E-01	0.237E-01	157.	167.	172.

Nonadiabatic

Adiabatic

Log(T_{eff})	Nonadiabatic			Adiabatic			Log(T_{eff})	P0	P1	P2
	P1/P0	P2/P0	[0,1;2]	P1/P0	P2/P0	[0,1;2]				
3.90	0.666	0.479	0.413	0.637	0.480	0.487	3.90	4.39	2.79	2.1
3.88	0.660	0.462	0.352	0.618	0.456	0.427	3.88	5.27	3.26	2.4
3.86	0.655	0.446	0.286	0.595	0.430	0.356	3.86	6.35	3.78	2.7
3.84	0.653	0.433	0.219	0.569	0.403	0.275	3.84	7.68	4.37	3.1
3.82	0.657	0.423	0.160	0.540	0.375	0.184	3.82	9.32	5.04	3.4
3.80	0.658	0.416	0.114	0.510	0.347	0.804E-01	3.80	11.30	5.78	3.9
3.78	0.633	0.401	0.862E-01	0.479	0.320	-0.371E-01	3.78	13.80	6.62	4.4
3.76	0.569	0.373	0.758E-01	0.446	0.293	-0.172	3.76	16.90	7.55	4.9
3.74	0.503	0.343	0.767E-01	0.413	0.267	-0.325	3.74	20.80	8.59	5.5
3.72	0.463	0.308	-0.886E-01	0.382	0.244	-0.487	3.72	25.50	9.74	6.2
3.70	0.436	0.320	0.173	0.357	0.225	-0.640	3.70	31.00	11.10	6.9
3.68	0.414	0.310	0.189	0.335	0.210	-0.772	3.68	37.40	12.50	7.8

Table 7.35 $\log(L/L_{\odot}) = 3.25$

$\log(T_{eff})$	P0	P1	P2	GR0	GR1	GR2	Ph0	Ph1	Ph2
3.89	9.32	5.81	3.72	-1.27	-0.774	-0.489	-42.0	127.	5.25
3.87	11.0	6.66	4.20	-1.40	-0.845	-0.561	-38.7	132.	18.2
3.85	12.8	7.59	4.68	-1.55	-0.910	-0.688	-33.0	139.	41.5
3.83	14.8	8.65	5.22	-1.70	-0.971	-0.835	-24.1	148.	74.6
3.81	16.7	9.88	5.87	-1.79	-1.07	-1.02	-9.04	158.	119.
3.79	18.3	11.4	7.00	-1.67	-1.33	2.83	21.7	171.	106.
3.77	19.5	12.9	8.53	-0.778	-2.09	2.64	90.8	-171.	123.
3.75	22.4	13.6	10.3	0.879	-2.89	2.03	129.	-149.	139.
3.73	27.6	13.7	12.2	2.18	-2.57	1.23	144.	-138.	151.
3.71	34.2	14.5	14.2	2.91	0.664	-1.66	150.	158.	152.
3.69	41.4	17.2	15.7	3.31	0.552	-1.14	153.	159.	177.
3.67	49.8	20.3	18.0	3.69	0.615	-0.942	156.	158.	-163.

Nonadiabatic				Adiabatic						
$\log(T_{eff})$	P1/P0	P2/P0	[0,1;2]	P1/P0	P2/P0	[0,1;2]	$\log(T_{eff})$	P0	P1	P2
3.89	0.624	0.400	0.102	0.605	0.416	0.252	3.89	8.25	4.99	3.4
3.87	0.607	0.383	0.347E-01	0.577	0.389	0.159	3.87	10.00	5.79	3.9
3.85	0.592	0.365	-0.518E-01	0.545	0.360	0.538E-01	3.85	12.20	6.67	4.4
3.83	0.585	0.353	-0.122	0.511	0.332	-0.601E-01	3.83	15.00	7.66	4.9
3.81	0.590	0.351	-0.185	0.476	0.304	-0.187	3.81	18.40	8.74	5.5
3.79	0.619	0.382	-0.315E-02	0.440	0.278	-0.326	3.79	22.60	9.93	6.2
3.77	0.663	0.437	0.218	0.403	0.252	-0.478	3.77	27.90	11.20	7.0
3.75	0.608	0.461	0.473	0.366	0.229	-0.629	3.75	34.60	12.60	7.9
3.73	0.495	0.443	0.761	0.331	0.210	-0.751	3.73	42.80	14.20	8.9
3.71	0.424	0.417	0.960	0.302	0.195	-0.803	3.71	52.80	15.90	10.3
3.69	0.415	0.380	0.779	0.278	0.186	-0.771	3.69	64.40	17.90	12.0
3.67	0.407	0.362	0.696	0.260	0.182	-0.639	3.67	77.90	20.20	14.2

Table 7.36 $\log(L/L_{\odot}) = 3.50$

Log(T_{eff})	P0	P1	P2	GRO	GR1	GR2	Ph0	Ph1	Ph2
3.88	17.9	10.4	6.73	-0.837	-0.887	-3.43	-33.6	122.	63.6
3.86	20.9	11.7	7.36	-0.936	-0.934	-3.41	-27.4	125.	73.8
3.84	24.1	13.0	7.43	-1.04	-0.988	-0.433	-18.0	130.	-19.6
3.82	27.4	14.6	9.24	-1.12	-1.02	-3.23	-4.53	136.	103.
3.80	30.5	16.2	10.2	-1.14	-1.03	-2.64	14.4	145.	118.
3.78	33.2	18.0	11.4	-1.03	-1.08	-1.75	40.9	156.	144.
3.76	35.2	20.2	17.7	-0.608	-1.25	3.26	82.5	168.	128.
3.74	36.9	22.2	15.2	0.605	2.41	-0.766	129.	145.	-153.
3.72	43.3	25.9	17.2	2.60	1.29	-0.689	145.	156.	-109.
3.70	53.6	29.3	27.6	3.58	0.877	-3.54	148.	157.	-122.
3.68	64.7	33.9	28.2	4.10	0.651	-3.20	150.	155.	-77.5
3.66	77.7	39.9	29.5	4.59	0.431	-1.71	151.	156.	-57.8

Log(T_{eff})	Nonadiabatic			Adiabatic			Log(T_{eff})	P0	P1	P2
	P1/P0	P2/P0	[0,1;2]	P1/P0	P2/P0	[0,1;2]				
3.88	0.578	0.376	0.070	0.558	0.343	-0.120	3.88	16.10	8.98	5.5
3.86	0.559	0.352	-0.051	0.520	0.317	-0.235	3.86	19.90	10.30	6.2
3.84	0.541	0.308	-0.117	0.478	0.296	-0.285	3.84	24.60	11.80	7.2
3.82	0.532	0.337	-0.110	0.437	0.282	-0.262	3.82	30.50	13.40	8.6
3.80	0.531	0.334	-0.029	0.396	0.262	-0.287	3.80	38.00	15.10	9.9
3.78	0.543	0.344	-0.065	0.357	0.242	-0.336	3.78	47.30	16.90	11.4
3.76	0.574	0.501	0.746	0.318	0.222	-0.368	3.76	59.10	18.80	13.1
3.74	0.602	0.412	0.233	0.282	0.204	-0.359	3.74	74.00	20.90	15.1
3.72	0.599	0.397	0.151	0.250	0.189	-0.286	3.72	92.40	23.10	17.5
3.70	0.547	0.516	0.887	0.226	0.179	-0.160	3.70	114.00	25.80	20.4
3.68	0.524	0.436	0.617	0.209	0.174	0.246E-01	3.68	138.00	28.90	24.0
3.66	0.513	0.380	0.319	0.198	0.171	0.222	3.66	166.00	32.80	28.4

Table 7.37 $\log(L/L_{\odot}) = 3.75$

$\log(T_{eff})$	P0	P1	P2	GRO	GR1	GR2	Ph0	Ph1	Ph2
3.86	36.1	17.5	15.0	-0.765	-1.17	-4.64	-15.5	134.	105.
3.84	40.3	19.2	16.2	-0.811	-1.24	-4.43	-4.29	135.	111.
3.82	44.0	20.8	18.5	-0.818	-1.40	-4.26	11.7	138.	123.
3.80	47.5	22.8	22.5	-0.751	4.83	-1.75	32.0	89.5	144.
3.78	50.5	27.0	21.0	-0.587	4.97	-2.06	56.0	95.6	155.
3.76	52.9	33.2	22.2	-0.279	5.23	-1.18	85.5	107.	176.
3.74	54.7	42.4	24.3	0.210	5.28	-0.704	120.	122.	-165.
3.72	55.9	55.4	38.4	5.06	0.669	-2.49	133.	143.	-154.
3.70	72.9	57.8	42.8	5.23	0.368	-2.00	136.	152.	-97.9
3.68	89.1	65.4	46.2	5.42	-0.538E-01	-1.31	134.	159.	-30.0
3.66	108.	77.6	50.1	5.77	-0.296	-0.547	132.	170.	-8.83
3.64	130.	93.2	57.4	6.20	-0.389	-0.258E-01	131.	-181.	-2.82

Nonadiabatic

Adiabatic

$\log(T_{eff})$	Nonadiabatic			Adiabatic			$\log(T)$	P0	P1	P2
	P1/P0	P2/P0	[0,1;2]	P1/P0	P2/P0	[0,1;2]				
3.86	0.483	0.416	0.664	0.439	0.290	-0.171	3.86	37.90	16.60	11.0
3.84	0.477	0.403	0.616	0.395	0.283	-0.461E-02	3.84	47.70	18.80	13.5
3.82	0.471	0.420	0.742	0.351	0.271	0.158	3.82	60.20	21.10	16.3
3.80	0.480	0.473	0.967	0.312	0.254	0.272	3.80	75.70	23.60	19.2
3.78	0.534	0.416	0.469	0.276	0.233	0.322	3.78	95.00	26.30	22.1
3.76	0.627	0.420	0.210	0.244	0.211	0.357	3.76	119.00	29.10	25.2
3.74	0.775	0.445	0.432E-01	0.218	0.191	0.371	3.74	149.00	32.40	28.5
3.72	0.991	0.688	0.555	0.197	0.173	0.284	3.72	185.00	36.50	32.0
3.70	0.793	0.586	0.555	0.186	0.157	0.355E-01	3.70	226.00	42.00	35.6
3.68	0.734	0.518	0.433	0.182	0.147	-0.312	3.68	271.00	49.20	39.7
3.66	0.721	0.465	0.238	0.184	0.140	-0.745	3.66	320.00	58.90	44.6
3.64	0.715	0.441	0.129	0.191	0.134	-1.19	3.64	372.00	71.00	50.0

Table 7.38 $\log(L/L_{\odot}) = 4.00$

Log(T_{eff})	P0	P1	P2	GRO	GR1	GR2	Ph0	Ph1	Ph2
3.83	65.0	37.7	----	-0.481	6.34	----	12.7	74.0	----
3.81	67.6	39.4	----	-0.405	-5.55	----	39.1	132.	----
3.79	69.2	44.8	----	-0.341	-5.19	----	62.6	139.	----
3.77	71.0	48.8	----	-0.296	-4.28	----	83.0	153.	----
3.75	72.5	54.1	----	-0.451	-3.18	----	107.	166.	----
3.73	76.9	59.9	43.7	-1.22	-1.68	-0.043	139.	164.	155.
3.71	91.1	63.2	50.2	-1.76	-0.421	-0.086	167.	0.348	154.
3.69	110.	69.1	57.4	-1.55	0.311	-0.366	-174.	-13.8	97.5
3.67	135.	79.0	65.2	-1.14	0.447	-0.352	-157.	-18.0	131.
3.65	172.	167.	93.6	6.98	-0.810	0.137	83.9	-143.	-14.4
3.63	206.	206.	113.	7.20	-0.646	-0.811E-01	79.2	-135.	-1.91

Log(T_{eff})	Nonadiabatic			Adiabatic			Log(T_{eff})	P0	P1	P2
	P1/P0	P2/P0	[0,1;2]	P1/P0	P2/P0	[0,1;2]				
3.83	0.579	----	----	0.250	0.234	0.743	3.85	94.10	25.60	24.1
3.81	0.578	----	----	0.239	0.206	0.331	3.83	120.00	30.00	28.2
3.79	0.647	----	----	0.231	0.182	-0.174	3.81	151.00	36.10	31.1
3.77	0.687	----	----	0.220	0.162	-0.626	3.79	188.00	43.50	34.2
3.75	0.746	----	----	0.209	0.146	-1.08	3.77	230.00	50.50	37.2
3.73	0.779	0.443	0.253E-01	0.201	0.133	-1.57	3.75	278.00	58.10	40.5
3.71	0.694	0.551	0.627	0.198	0.122	-2.11	3.73	332.00	66.90	44.1
3.69	0.628	0.522	0.676	0.198	0.116	-2.58	3.71	394.00	77.80	48.2
3.67	0.587	0.483	0.663	0.207	0.114	-2.92	3.69	461.00	91.30	53.4
3.65	0.969	0.544	0.193	0.222	0.117	-3.01	3.67	531.00	110.00	60.7
3.63	1.00	0.550	0.182	0.241	0.124	-2.88	3.65	606.00	135.00	71.2
							3.63	686.00	165.00	85.4

Table 7.39 $\log(L/L_{\odot}) = 2.9$

$\log(T_{eff})$	P0	P1	P2	GRO	GR1	GR2	Ph0	Ph1	Ph2
3.76	12.0	6.42	4.33	0.816	-0.560	-0.278	110.	-178.	164.
3.75	13.1	6.85	4.63	0.664	-0.581	-0.304	104.	178.	166.
3.74	14.4	7.32	4.87	0.897	-0.499	-0.225	111.	163.	164.
3.73	15.6	7.76	5.07	1.27	-0.323	0.234	126.	152.	154.
3.72	17.2	8.38	5.49	1.29	-0.332	0.206	124.	151.	153.
3.71	18.9	8.91	5.55	1.50	-0.215	-0.489	131.	147.	170.
3.70	20.4	9.48	5.95	1.42	-0.161	-0.647	131.	146.	179.

$\log(T_{eff})$	Nonadiabatic			Adiabatic		
	P1/P0	P2/P0	[0,1;2]	P1/P0	P2/P0	[0,1;2]
3.76	0.537	0.362	0.989E-01	0.461	0.304	-0.117
3.75	0.522	0.353	0.823E-01	0.450	0.295	-0.168
3.74	0.510	0.339	0.146E-01	0.439	0.286	-0.221
3.73	0.499	0.326	-0.637E-01	0.429	0.277	-0.275
3.72	0.486	0.318	-0.843E-01	0.419	0.269	-0.330
3.71	0.471	0.294	-0.283	0.409	0.261	-0.384
3.70	0.465	0.291	-0.280	0.400	0.254	-0.439

Table 7.40 $\log(L/L_{\odot}) = 3.0$

Log(T_{eff})	P0	P1	P2	GRO	GR1	GR2	Ph0	Ph1	Ph2
3.76	14.8	7.87	5.09	0.390	-0.853	-0.484	92.5	-160.	164.
3.75	16.1	8.28	5.29	1.09	-0.601	-0.663	113.	180.	170.
3.74	17.2	8.74	5.62	1.15	-0.540	-0.820	117.	169.	-179.
3.73	18.6	9.24	5.97	1.35	-0.418	-0.924	124.	159.	-170.
3.72	20.5	9.87	6.37	1.52	-0.335	-0.941	127.	155.	-162.
3.71	22.3	10.5	6.81	1.52	-0.310	-0.985	127.	154.	-152.
3.70	24.3	11.2	7.25	1.88	-0.926E-01	-0.966	136.	152.	-144.

Log(T_{eff})	Nonadiabatic			Adiabatic		
	P1/P0	P2/P0	[0,1;2]	P1/P0	P2/P0	[0,1;2]
3.76	0.533	0.345	-0.259E-01	0.436	0.283	-0.245
3.75	0.515	0.329	-0.988E-01	0.425	0.273	-0.305
3.74	0.509	0.327	-0.931E-01	0.414	0.264	-0.365
3.73	0.496	0.320	-0.105	0.403	0.256	-0.425
3.72	0.482	0.312	-0.138	0.393	0.248	-0.487
3.71	0.473	0.306	-0.159	0.384	0.241	-0.548
3.70	0.461	0.299	-0.180	0.374	0.233	-0.611

Table 7.41 $\log(L/L_{\odot}) = 3.1$

$\text{Log}(T_{\text{eff}})$	P0	P1	P2	GR0	GR1	GR2	Ph0	Ph1	Ph2
3.77	16.5	9.02	5.71	0.153	-0.988	-1.02	82.5	-166.	171.
3.76	17.7	9.48	6.05	0.805	-0.892	-1.14	104.	-168.	-179.
3.75	19.4	10.1	6.48	0.737	-0.873	-1.16	102.	-171.	-171.
3.74	21.1	10.6	6.91	0.766	-0.840	-1.17	104.	-176.	-162.
3.73	22.7	11.2	7.32	1.44	-0.576	-1.16	121.	167.	-153.
3.72	25.0	11.9	7.80	1.63	-0.499	-1.08	123.	161.	-142.
3.71	27.0	12.6	8.31	1.83	-0.329	-1.02	128.	155.	-126.
3.70	28.6	13.1	8.86	1.85	-0.132	-1.03	133.	153.	-107.

$\text{Log}(T_{\text{eff}})$	Nonadiabatic			Adiabatic		
	P1/P0	P2/P0	[0,1;2]	P1/P0	P2/P0	[0,1;2]
3.77	0.546	0.346	-0.608E-01	0.424	0.271	-0.337
3.76	0.536	0.342	-0.553E-01	0.412	0.261	-0.404
3.75	0.522	0.333	-0.832E-01	0.400	0.252	-0.470
3.74	0.504	0.327	-0.727E-01	0.389	0.243	-0.537
3.73	0.494	0.323	-0.738E-01	0.378	0.235	-0.604
3.72	0.476	0.312	-0.103	0.368	0.228	-0.670
3.71	0.466	0.308	-0.989E-01	0.358	0.221	-0.735
3.70	0.457	0.309	-0.434E-01	0.348	0.214	-0.799

Table 7.42 $\log(L/L_{\odot}) = 3.2$

$\log(T_{\text{eff}})$	P0	P1	P2	GR0	GR1	GR2	Ph0	Ph1	Ph2
3.77	20.0	11.0	6.93	0.263	-1.03	-1.38	85.5	-175.	-180.
3.76	21.4	11.4	7.36	0.707	-1.05	-1.38	98.9	-170.	-169.
3.75	22.8	11.9	7.83	1.15	-0.893	-1.32	111.	-178.	-157.
3.74	25.8	12.9	8.41	0.705	-0.948	-1.21	101.	-177.	-146.
3.73	27.7	13.4	8.89	1.48	-0.731	-1.06	116.	172.	-130.
3.72	29.1	14.1	9.45	1.75	-0.617	-0.979	125.	165.	-108.
3.71	31.5	14.8	10.0	2.02	-0.475	-0.836	130.	159.	-86.1
3.70	34.0	15.6	10.7	2.22	-0.317	-0.724	134.	157.	-65.3

$\log(T_{\text{eff}})$	Nonadiabatic			Adiabatic		
	P1/P0	P2/P0	[0,1;2]	P1/P0	P2/P0	[0,1;2]
3.77	0.547	0.345	-0.683E-01	0.400	0.249	-0.522
3.76	0.534	0.343	-0.380E-01	0.387	0.239	-0.594
3.75	0.520	0.343	0.669E-02	0.375	0.231	-0.664
3.74	0.501	0.326	-0.768E-01	0.363	0.223	-0.732
3.73	0.486	0.321	-0.532E-01	0.352	0.216	-0.797
3.72	0.482	0.324	-0.116E-01	0.342	0.209	-0.857
3.71	0.468	0.318	-0.652E-02	0.332	0.203	-0.910
3.70	0.459	0.313	-0.150E-01	0.323	0.198	-0.953

Table 7.43 $\log(L/L_{\odot}) = 3.5$

$\log(T_{\text{eff}})$	P0	P1	P2	GR0	GR1	GR2	Ph0	Ph1	Ph2
3.77	34.0	17.5	12.7	-0.626E-01	-0.976	-1.46	80.2	155.	-179.
3.76	34.7	18.0	13.5	0.463	-1.13	-0.943	96.0	160.	-152.
3.75	37.8	19.2	14.3	0.797	-1.04	-0.586	103.	158.	-130.
3.74	51.9	19.9	15.1	-1.43	-1.39	-0.160	39.3	164.	-90.8
3.73	43.3	21.3	15.8	1.42	-1.35	0.636E-01	113.	166.	-57.9
3.72	47.4	23.1	16.7	1.40	-1.36	0.452	114.	171.	-39.8
3.71	52.4	24.5	17.9	1.14	-1.40	0.438	112.	175.	-34.8
3.70	54.2	26.0	18.9	1.77	-1.38	0.553	120.	-180.	-31.8

$\log(T_{\text{eff}})$	Nonadiabatic			Adiabatic		
	P1/P0	P2/P0	[0,1;2]	P1/P0	P2/P0	[0,1;2]
3.77	0.515	0.375	0.274	0.314	0.210	-0.583
3.76	0.521	0.389	0.348	0.301	0.204	-0.583
3.75	0.509	0.379	0.327	0.289	0.198	-0.583
3.74	0.384	0.292	0.181	0.278	0.193	-0.574
3.73	0.492	0.364	0.285	0.267	0.189	-0.553
3.72	0.487	0.353	0.221	0.258	0.185	-0.530
3.71	0.468	0.341	0.207	0.248	0.181	-0.496
3.70	0.481	0.349	0.214	0.240	0.178	-0.456

Table 7.44 $\log(L/L_{\odot}) = 2.9$

$\log(T_{\text{eff}})$	P0	P1	P2	GR0	GR1	GR2	Ph0	Ph1	Ph2
3.76	9.81	5.48	3.85	0.643	-0.343	-0.418	112.	149.	-177.
3.75	10.7	5.87	4.09	0.688	-0.310	-0.420	114.	141.	-177.
3.74	11.7	6.28	4.34	0.770	-0.270	-0.400	118.	137.	-179.
3.73	12.9	6.74	4.62	0.850	-0.229	-0.366	123.	136.	178.
3.72	14.0	7.17	4.88	1.01	-0.116	-0.300	131.	140.	174.
3.71	15.4	7.72	5.21	1.02	-0.158	-0.283	130.	137.	173.
3.70	16.6	8.21	5.52	1.19	0.140E-02	-0.188	138.	146.	171.

$\log(T_{\text{eff}})$	Nonadiabatic			Adiabatic		
	P1/P0	P2/P0	[0,1;2]	P1/P0	P2/P0	[0,1;2]
3.76	0.558	0.392	0.240	0.515	0.350	0.881E-01
3.75	0.548	0.382	0.204	0.504	0.341	0.494E-01
3.74	0.536	0.370	0.165	0.494	0.332	0.103E-01
3.73	0.525	0.359	0.123	0.484	0.323	-0.289E-01
3.72	0.514	0.350	0.883E-01	0.474	0.315	-0.698E-01
3.71	0.501	0.338	0.384E-01	0.465	0.306	-0.111
3.70	0.494	0.332	0.137E-01	0.455	0.299	-0.151

Table 7.45 $\log(L/L_{\odot}) = 3.0$

Log(T_{eff})	P0	P1	P2	GRO	GR1	GR2	Ph0	Ph1	Ph2
3.76	12.0	6.58	4.57	0.692	-0.454	-0.390	109.	177.	173.
3.75	13.1	7.02	4.88	0.583	-0.469	-0.442	103.	161.	176.
3.74	14.4	7.51	5.18	0.679	-0.422	-0.436	107.	146.	177.
3.73	15.6	8.00	5.44	1.07	-0.264	-0.303	126.	146.	172.
3.72	17.1	8.60	5.82	1.02	-0.271	-0.354	122.	145.	174.
3.71	18.8	9.22	6.17	1.18	-0.223	-0.264	128.	144.	171.
3.70	20.5	9.82	6.54	1.38	-0.912E-01	-0.109	136.	146.	168.

Log(T_{eff})	Nonadiabatic			Adiabatic		
	P1/P0	P2/P0	[0,1;2]	P1/P0	P2/P0	[0,1;2]
3.76	0.549	0.381	0.198	0.489	0.329	0.286E-02
3.75	0.534	0.371	0.179	0.478	0.319	-0.412E-01
3.74	0.522	0.360	0.137	0.468	0.310	-0.866E-01
3.73	0.511	0.348	0.830E-01	0.458	0.301	-0.133
3.72	0.503	0.340	0.483E-01	0.448	0.293	-0.179
3.71	0.490	0.328	-0.969E-02	0.438	0.285	-0.227
3.70	0.479	0.319	-0.492E-01	0.429	0.277	-0.275

Table 7.46 $\log(L/L_{\odot}) = 3.1$

Log(T_{eff})	P0	P1	P2	GRO	GR1	GR2	Ph0	Ph1	Ph2
3.77	13.4	7.49	5.13	0.534	-0.640	-0.407	98.9	-161.	164.
3.76	14.6	7.97	5.44	0.654	-0.597	-0.410	104.	-171.	166.
3.75	16.2	8.51	5.72	0.904	-0.516	-0.350	112.	180.	165.
3.74	17.4	8.99	6.04	0.998	-0.439	-0.313	117.	164.	167.
3.73	18.9	9.56	6.37	1.16	-0.351	-0.236	123.	156.	166.
3.72	21.0	10.4	6.82	1.16	-0.368	-0.260	121.	155.	166.
3.71	22.6	10.9	7.14	1.42	-0.225	0.679E-01	130.	150.	160.
3.70	24.7	11.6	7.71	1.60	-0.121	0.362	135.	150.	155.

Log(T_{eff})	Nonadiabatic			Adiabatic		
	P1/P0	P2/P0	[0,1;2]	P1/P0	P2/P0	[0,1;2]
3.77	0.559	0.383	0.177	0.475	0.317	-0.499E-01
3.76	0.545	0.373	0.149	0.463	0.307	-0.102
3.75	0.526	0.354	0.757E-01	0.452	0.297	-0.154
3.74	0.516	0.347	0.521E-01	0.442	0.288	-0.207
3.73	0.505	0.336	0.929E-02	0.431	0.280	-0.259
3.72	0.493	0.325	-0.472E-01	0.421	0.271	-0.313
3.71	0.482	0.316	-0.923E-01	0.412	0.263	-0.368
3.70	0.471	0.312	-0.831E-01	0.402	0.256	-0.424

Table 7.47 $\log(L/L_{\odot}) = 3.2$

$\log(T_{eff})$	P0	P1	P2	GR0	GR1	GR2	Ph0	Ph1	Ph2
3.77	16.5	9.18	6.01	0.524	-0.827	-0.553	94.4	-157.	159.
3.76	18.0	9.66	6.31	0.850	-0.717	-0.496	105.	-165.	161.
3.75	19.4	10.2	6.60	1.05	-0.638	-0.491	114.	-178.	165.
3.74	21.5	10.9	7.07	0.676	-0.694	-0.479	103.	-176.	167.
3.73	23.2	11.5	7.32	1.35	-0.464	-0.643	122.	164.	173.
3.72	25.5	12.4	7.86	1.02	-0.561	-0.740	113.	166.	-180.
3.71	27.6	13.1	8.28	1.61	-0.320	-0.828	128.	154.	-173.
3.70	29.6	13.7	8.82	1.54	-0.199	-0.964	131.	151.	-158.

$\log(T_{eff})$	Nonadiabatic			Adiabatic		
	P1/P0	P2/P0	[0,1;2]	P1/P0	P2/P0	[0,1;2]
3.77	0.555	0.364	0.518E-01	0.450	0.294	-0.173
3.76	0.538	0.351	0.129E-01	0.438	0.284	-0.233
3.75	0.525	0.340	-0.348E-01	0.426	0.275	-0.293
3.74	0.509	0.329	-0.740E-01	0.415	0.266	-0.352
3.73	0.497	0.315	-0.161	0.405	0.257	-0.413
3.72	0.484	0.308	-0.181	0.395	0.250	-0.475
3.71	0.474	0.300	-0.227	0.385	0.242	-0.538
3.70	0.463	0.298	-0.190	0.375	0.234	-0.601

Table 7.48 $\log(L/L_{\odot}) = 3.5$

$\log(T_{\text{eff}})$	P0	P1	P2	GRO	GR1	GR2	Ph0	Ph1	Ph2
3.77	31.8	16.3	10.3	0.127E-01	-0.961	-1.43	73.6	173.	171.
3.76	32.0	16.9	10.9	0.722	-1.06	-1.43	97.4	-180.	-173.
3.75	35.1	18.0	11.7	0.694	-0.963	-1.33	98.8	175.	-163.
3.74	37.2	18.5	12.4	1.37	-1.01	-1.16	112.	-180.	-148.
3.73	41.5	19.8	13.3	0.991	-0.923	-0.983	104.	176.	-131.
3.72	45.1	21.2	14.2	1.08	-0.907	-0.847	107.	172.	-113.
3.71	46.0	21.6	14.9	2.06	-0.682	-0.569	126.	160.	-81.9
3.70	52.6	23.6	16.0	1.52	-0.775	-0.463	116.	163.	-65.8

$\log(T_{\text{eff}})$	Nonadiabatic			Adiabatic		
	P1/P0	P2/P0	[0,1;2]	P1/P0	P2/P0	[0,1;2]
3.77	0.513	0.323	-0.149	0.372	0.225	-0.757
3.76	0.528	0.342	-0.290E-01	0.359	0.216	-0.833
3.75	0.514	0.333	-0.552E-01	0.346	0.208	-0.906
3.74	0.497	0.334	0.165E-01	0.334	0.201	-0.968
3.73	0.478	0.320	-0.350E-01	0.323	0.195	-1.02
3.72	0.471	0.314	-0.591E-01	0.313	0.190	-1.07
3.71	0.471	0.325	0.424E-01	0.303	0.185	-1.10
3.70	0.448	0.304	-0.556E-01	0.294	0.181	-1.12

Table 7.49

Periods and growth rates (GR) for high temperatures with $M = 0.6 M_{\odot}$
 (convective models using the Carson opacity for $Z = 0.005$)

$\text{Log}(L/L_{\odot}) = 3.50$

$\text{Log}(T_{\text{eff}})$	P1	GR1	P2	GR2	P3	GR3	P4	GR4	P5	GR5
3.80	26.51	0.020	91.42	-13.0	10.03	-2.09	14.46	-0.988	----	----
3.82	24.65	-0.315	80.38	-12.11	8.036	-0.970	13.32	-1.04	523.8	-71.5
3.84	21.79	-0.511	67.86	-11.27	7.301	-0.881	4.911	-0.367	8.511	3.31
3.86	19.07	-0.477	67.75	-12.46	6.653	-0.792	7.234	-2.98	10.78	-1.00

$\text{Log}(L/L_{\odot}) = 3.75$

$\text{Log}(T_{\text{eff}})$	P1	GR1	P2	GR2	P3	GR3	P4	GR4	P5	GR5
3.79	41.27	0.575	22.30	-0.759	24.39	5.94	12.63	-0.200	11.12	-0.519
3.80	41.26	0.507	21.28	-0.514	22.51	4.94	20.00	-3.63	12.20	-0.100
3.82	39.29	0.175	21.79	-0.812	19.26	4.08	14.19	-0.453	9.741	-0.350
3.84	34.85	0.007	20.94	-0.842	16.20	4.60	13.16	-0.398	8.640	-0.352
3.86	32.21	0.087	18.88	-0.486	11.64	-0.415	14.31	3.77	6.462	-0.297
3.88	27.02	0.188	15.90	-0.23	10.32	-0.29	12.82	3.54	12.74	-3.54

$\text{Log}(L/L_{\odot}) = 4.00$

$\text{Log}(T_{\text{eff}})$	P1	GR1	P2	GR2	P3	GR3	P4	GR4	P5	GR5
3.78	----	----	50.18	-0.066	50.23	6.07	44.19	-3.72	21.39	0.503
3.82	----	----	33.64	-0.018	39.48	5.09	37.88	-4.63	4.03	-0.071
3.84	44.10	0.14	----	----	32.23	5.22	31.61	-5.07	16.73	0.08
3.86	----	----	29.72	0.06	28.85	5.23	28.44	-5.14	3.358	-0.014
3.88	36.52	0.08	----	----	25.73	4.84	25.63	-4.82	13.61	0.05
3.89	37.05	0.07	24.83	-4.33	24.88	4.35	----	----	13.45	0.047
3.90	33.09	0.05	23.33	4.11	23.32	-4.10	----	----	11.89	0.062

Table 7.50

Stellingwerf opacity models with convection
for $Z = 0.005$

Log(L/L_{\odot})	Log(T_{eff})	$M/M_{\odot} =$	
		0.5	0.8
		P0	P0
2.00	3.85	0.976	0.712
	3.75	2.439	1.693
	3.65	4.956	3.710
3.00	3.80	10.59	7.711
	3.70	33.36	23.25
	3.60	77.14	44.84
4.00	3.76	76.82	70.49
	3.66	234.0	190.8
	3.56	748.2	562.4

Table 7.53

Second overtone mode Q values for $M = 0.6 M_{\odot}$ Stellingwerf opacity for $Z = 0.005$
Convective models without viscosity

$\text{Log}(L/L_{\odot}) = 2.00$	2.50	3.00	3.50	3.75	4.00
$\text{Log}(T_{\text{eff}})$					
3.8500	0.0215	----	----	----	----
3.8300	0.0216	0.0234	----	----	----
3.8100	0.0217	0.0227	----	----	----
3.8000	----	----	0.0223	----	----
3.7900	0.0217	0.0222	----	----	----
3.7800	----	----	0.0235	0.0315	----
3.7700	0.0214	0.0219	----	----	0.0260
3.7600	----	----	0.0234	0.0244	----
3.7500	0.0211	0.0212	----	----	0.0347
3.7400	----	----	0.0212	0.0242	----
3.7300	0.0206	0.0206	----	----	0.0345
3.7200	----	----	0.0194	0.0234	----
3.7100	0.0207	0.0202	----	----	0.0336
3.7000	----	----	0.0224	0.0228	----
3.6900	0.0214	0.0205	----	----	0.0315
3.6800	----	----	0.0230	0.0238	----
3.6700	0.0225	0.0211	----	----	0.0279
3.6600	----	----	0.0237	0.0252	----
3.6500	0.0232	0.0221	----	----	0.0278
3.6400	----	----	0.0243	0.0265	----
3.6300	----	----	----	----	0.0294
3.6200	----	----	0.0252	0.0282	----
3.6100	----	----	----	----	0.0313
3.6000	----	----	----	0.0304	----
3.5900	----	----	----	----	0.0335
3.5800	----	----	----	----	----
3.5600	----	----	----	----	0.0441

Table 7.54

Fundamental mode Q values for $M = 0.6 M_{\odot}$ Stellingwerf opacity for $Z = 0.005$

Convective models with viscosity

$\text{Log}(L/L_{\odot}) = 2.00$ $\text{Log}(T_{\text{eff}})$	2.50	3.00	3.50	4.00
3.8500	0.0384	-----	-----	-----
3.8300	0.0396	0.0443	-----	-----
3.8100	0.0412	0.0465	-----	-----
3.8000	-----	-----	0.0516	-----
3.7900	0.0427	0.0498	-----	-----
3.7800	-----	-----	0.0542	0.0645
3.7700	0.0446	0.0534	-----	-----
3.7600	-----	-----	0.0621	0.0576
3.7500	0.0471	0.0570	-----	-----
3.7400	-----	-----	0.0700	0.0606
3.7300	0.0502	0.0608	-----	-----
3.7200	-----	-----	0.0768	0.0750
3.7100	0.0522	0.0644	-----	-----
3.7000	-----	-----	-----	0.0846
3.6900	0.0512	0.0666	-----	-----
3.6800	-----	-----	0.0886	0.0900
3.6700	0.0500	0.0672	-----	-----
3.6600	-----	-----	0.0934	0.0962
3.6500	0.0489	0.0642	-----	-----
3.6400	-----	-----	0.0960	0.1026
3.6300	-----	0.0608	-----	-----
3.6200	-----	-----	0.0935	0.1091
3.6100	-----	0.0576	-----	-----
3.6000	-----	-----	0.0883	0.1164
3.5900	-----	0.0561	-----	-----
3.5800	-----	-----	0.0810	0.1236
3.5700	-----	0.0614	-----	-----
3.5600	-----	-----	0.0765	0.1244
3.5400	-----	-----	0.0831	0.1248
3.5200	-----	-----	0.0867	0.1439

Table 7.55

First overtone mode Q values for $M = 0.6 M_{\odot}$ Stellingwerf opacity for $Z = 0.005$
Convective models with viscosity

$\text{Log}(L/L_{\odot}) = 2.00$	2.50	3.00	3.50	4.00
$\text{Log}(T_{\text{eff}})$				
3.8500	0.0280	----	----	----
3.8300	0.0287	0.0304	----	----
3.8100	0.0294	0.0308	----	----
3.8000	----	----	0.0351	----
3.7900	0.0300	0.0316	----	----
3.7800	----	----	0.0328	0.0362
3.7700	0.0302	0.0320	----	----
3.7600	----	----	0.0323	0.0404
3.7500	0.0304	0.0317	----	----
3.7400	----	----	0.0320	0.0384
3.7300	0.0299	0.0314	----	----
3.7200	----	----	0.0307	0.0348
3.7100	0.0296	0.0310	----	----
3.7000	----	----	----	0.0345
3.6900	0.0304	0.0307	----	----
3.6800	----	----	0.0296	0.0351
3.6700	0.0307	0.0314	----	----
3.6600	----	----	0.0296	0.0364
3.6500	0.0310	0.0324	----	----
3.6400	----	----	0.0306	0.0379
3.6300	----	0.0332	----	----
3.6200	----	----	0.0327	0.0396
3.6100	----	0.0344	----	----
3.6000	----	----	0.0348	0.0414
3.5900	----	0.0359	----	----
3.5800	----	----	0.0367	0.0435
3.5700	----	0.0396	----	----
3.5600	----	----	0.0386	0.0460
3.5400	----	----	0.0437	0.0483
3.5200	----	----	0.0427	0.0516

Table 7.56

Second overtone mode Q values for $M = 0.6 M_{\odot}$ Stellingwerf opacity for $Z = 0.005$

Convective models with viscosity

$\text{Log}(L/L_{\odot}) = 2.00$ $\text{Log}(T_{\text{eff}})$	2.50	3.00	3.50	4.00
3.8500	0.0215	-----	-----	-----
3.8300	0.0216	0.0232	-----	-----
3.8100	0.0218	0.0225	-----	-----
3.8000	-----	-----	0.0220	-----
3.7900	0.0217	0.0222	-----	-----
3.7800	-----	-----	0.0253	0.0344
3.7700	0.0214	0.0219	-----	-----
3.7600	-----	-----	0.0240	0.0246
3.7500	0.0211	0.0212	-----	-----
3.7400	-----	-----	0.0221	0.0370
3.7300	0.0206	0.0207	-----	-----
3.7200	-----	-----	0.0221	0.0241
3.7100	0.0207	0.0202	-----	-----
3.7000	-----	-----	-----	0.0238
3.6900	0.0215	0.0205	-----	-----
3.6800	-----	-----	0.0232	0.0251
3.6700	0.0225	0.0211	-----	-----
3.6600	-----	-----	0.0239	0.0258
3.6500	0.0232	0.0222	-----	-----
3.6400	-----	-----	0.0245	0.0269
3.6300	-----	0.0229	-----	-----
3.6200	-----	-----	0.0254	0.0283
3.6100	-----	0.0235	-----	-----
3.6000	-----	-----	0.0263	0.0304
3.5900	-----	0.0248	-----	-----
3.5800	-----	-----	0.0222	0.0329
3.5700	-----	0.0274	-----	-----
3.5600	-----	-----	0.0239	0.0356
3.5400	-----	-----	0.0301	0.0380
3.5200	-----	-----	0.0255	0.0414

Table 7.57

Fundamental mode Q values for $M = 0.6 M_{\odot}$ Stellingwerf opacity for $Z = 0.005$

Radiative models

$\text{Log}(L/L_{\odot}) = 3.00$	3.25	3.50	3.75	4.00
$\text{Log}(T_{\text{eff}})$				
3.9000	0.0530	----	----	----
3.8900	----	0.0632	----	----
3.8800	0.0541	----	0.0736	----
3.8700	----	0.0650	----	----
3.8600	0.0549	----	0.0748	0.0839
3.8500	----	0.0658	----	----
3.8400	0.0553	----	0.0751	0.0816
3.8300	----	0.0663	----	0.0797
3.8200	0.0551	----	0.0744	0.0776
3.8100	----	0.0652	----	0.0722
3.8000	0.0546	----	0.0721	0.0729
3.7900	----	0.0622	----	0.0644
3.7800	0.0547	----	0.0684	0.0675
3.7700	----	0.0577	----	0.0576
3.7600	0.0570	----	0.0631	0.0616
3.7500	----	0.0577	----	0.0512
3.7400	0.0611	----	0.0577	0.0555
3.7300	----	0.0620	----	0.0473
3.7200	0.0662	----	0.0589	0.0494
3.7100	----	0.0669	----	0.0488
3.7000	0.0700	----	0.0635	0.0561
3.6900	----	0.0705	----	0.0513
3.6800	0.0737	----	0.0668	0.0597
3.6700	----	0.0739	----	0.0548
3.6600	----	----	0.0699	0.0631
3.6500	----	----	----	0.0609
3.6400	----	----	----	0.0661
3.6300	----	----	----	0.0635

Table 7.58

First overtone mode Q values for $M = 0.6 M_{\odot}$ Stellingwerf opacity for $Z = 0.005$
Radiative models

$\text{Log}(L/L_{\odot}) = 3.00$ $\text{Log}(T_{\text{eff}})$	3.25	3.50	3.75	4.00
3.9000	0.0352	-----	-----	-----
3.8900	-----	0.0394	-----	-----
3.8800	0.0357	-----	0.0427	-----
3.8700	-----	0.0393	-----	-----
3.8600	0.0359	-----	0.0419	0.0407
3.8500	-----	0.0390	-----	-----
3.8400	0.0361	-----	0.0405	0.0389
3.8300	-----	0.0388	-----	0.0463
3.8200	0.0362	-----	0.0396	0.0367
3.8100	-----	0.0386	-----	0.0421
3.8000	0.0359	-----	0.0383	0.0350
3.7900	-----	0.0387	-----	0.0417
3.7800	0.0346	-----	0.0371	0.0361
3.7700	-----	0.0382	-----	0.0396
3.7600	0.0324	-----	0.0362	0.0387
3.7500	-----	0.0351	-----	0.0382
3.7400	0.0308	-----	0.0347	0.0430
3.7300	-----	0.0308	-----	0.0368
3.7200	0.0306	-----	0.0352	0.0490
3.7100	-----	0.0284	-----	0.0338
3.7000	0.0306	-----	0.0347	0.0445
3.6900	-----	0.0293	-----	0.0322
3.6800	0.0304	-----	0.0350	0.0438
3.6700	-----	0.0301	-----	0.0321
3.6600	-----	-----	0.0359	0.0453
3.6500	-----	-----	-----	0.0591
3.6400	-----	-----	-----	0.0474
3.6300	-----	-----	-----	0.0635

Table 7.59

Second overtone mode Q values for $M = 0.6 M_{\odot}$ Stellingwerf opacity for $Z = 0.005$
Radiative models

$\text{Log}(L/L_{\odot}) = 3.00$	3.25	3.50	3.75	4.00
$\text{Log}(T_{\text{eff}})$				
3.9000	0.0254	-----	-----	-----
3.8900	-----	0.0252	-----	-----
3.8800	0.0250	-----	0.0277	-----
3.8700	-----	0.0248	-----	-----
3.8600	0.0245	-----	0.0263	0.0349
3.8500	-----	0.0241	-----	-----
3.8400	0.0239	-----	0.0232	0.0328
3.8300	-----	0.0234	-----	-----
3.8200	0.0233	-----	0.0251	0.0326
3.8100	-----	0.0229	-----	-----
3.8000	0.0227	-----	0.0241	0.0346
3.7900	-----	0.0238	-----	-----
3.7800	0.0219	-----	0.0235	0.0281
3.7700	-----	0.0252	-----	-----
3.7600	0.0213	-----	0.0318	0.0259
3.7500	-----	0.0266	-----	-----
3.7400	0.0210	-----	0.0237	0.0247
3.7300	-----	0.0274	-----	0.0269
3.7200	0.0203	-----	0.0234	0.0339
3.7100	-----	0.0278	-----	0.0269
3.7000	0.0224	-----	0.0327	0.0329
3.6900	-----	0.0267	-----	0.0268
3.6800	0.0228	-----	0.0291	0.0310
3.6700	-----	0.0267	-----	0.0265
3.6600	-----	-----	0.0265	0.0293
3.6500	-----	-----	-----	0.0331
3.6400	-----	-----	-----	0.0292
3.6300	-----	-----	-----	0.0348

Table 7.62

Second overtone mode Q values for $M = 0.6 M_{\odot}$ Carson opacity for $Z = 0.005$
Convective models without viscosity

$\text{Log}(L/L_{\odot}) = 2.00$	2.50	3.00	3.50	3.75	4.00
$\text{Log}(T_{\text{eff}})$					
3.8500	0.0218	----	----	----	----
3.8300	0.0218	0.0231	----	----	----
3.8100	0.0218	0.0227	----	----	----
3.8000	----	----	0.0224	----	----
3.7900	0.0218	0.0175	----	----	----
3.7800	----	----	0.0216	0.0243	----
3.7700	0.0217	0.0222	----	----	0.0278
3.7600	----	----	0.0234	0.0246	----
3.7500	0.0215	0.0219	----	----	0.0257
3.7400	----	----	0.0235	0.0244	----
3.7300	0.0212	0.0216	----	----	0.0254
3.7200	----	----	0.0232	0.0239	----
3.7100	0.0210	0.0211	----	----	0.0342
3.7000	----	----	0.0231	0.0233	----
3.6900	0.0206	0.0207	----	----	0.0333
3.6800	----	----	0.0233	0.0228	----
3.6700	0.0207	0.0204	----	----	0.0320
3.6600	----	----	0.0239	0.0188	----
3.6500	0.0210	0.0203	----	----	0.0308
3.6400	----	----	0.0245	0.0293	----
3.6300	----	0.0207	----	----	0.0409
3.6200	----	----	0.0251	0.0288	----
3.6100	----	----	----	----	0.0314
3.6000	----	----	0.0256	0.0290	----
3.5900	----	----	----	----	0.0396
3.5800	----	----	----	0.0295	----
3.5700	----	----	----	----	0.0335
3.5600	----	----	----	----	0.0249

Table 7.63

Fundamental mode Q values for $M = 0.6 M_{\odot}$ Carson opacity for $Z = 0.005$
Radiative models

$\text{Log}(L/L_{\odot}) = 2.90$ $\text{Log}(T_{\text{eff}})$	3.00	3.10	3.20	3.50
3.7700	----	----	0.0633	0.0645
3.7600	0.0607	0.0630	0.0634	0.0644
3.7500	0.0618	0.0639	0.0648	0.0641
3.7400	0.0634	0.0637	0.0658	0.0677
3.7300	0.0641	0.0643	0.0660	0.0678
3.7200	0.0660	0.0662	0.0679	0.0665
3.7100	0.0676	0.0672	0.0684	0.0672
3.7000	0.0681	0.0683	0.0676	0.0677

Table 7.64

First overtone mode Q values for $M = 0.6 M_{\odot}$ Carson opacity for $Z = 0.005$
Radiative models

$\text{Log}(L/L_{\odot}) = 2.90$ $\text{Log}(T_{\text{eff}})$	3.00	3.10	3.20	3.50
3.7700	----	----	0.0346	0.0355
3.7600	0.0325	0.0335	0.0339	0.0343
3.7500	0.0323	0.0329	0.0337	0.0334
3.7400	0.0322	0.0324	0.0330	0.0338
3.7300	0.0319	0.0319	0.0326	0.0328
3.7200	0.0321	0.0318	0.0323	0.0322
3.7100	0.0319	0.0316	0.0319	0.0316
3.7000	0.0317	0.0315	0.0310	0.0310

Table 7.65

Second overtone mode Q values for $M = 0.6 M_{\odot}$ Carson opacity for $Z = 0.005$
Radiative models

$\text{Log}(L/L_{\odot}) = 2.90$ $\text{Log}(T_{\text{eff}})$	3.00	3.10	3.20	3.50	
3.7700	-----	-----	0.0219	0.0224	0.0244
3.7600	0.0219	0.0217	0.0217	0.0222	0.0242
3.7500	0.0218	0.0210	0.0216	0.0220	0.0239
3.7400	0.0214	0.0208	0.0215	0.0221	0.0236
3.7300	0.0208	0.0206	0.0213	0.0218	0.0230
3.7200	0.0211	0.0206	0.0212	0.0216	0.0227
3.7100	0.0199	0.0205	0.0211	0.0213	0.0227
3.7000	0.0199	0.0204	0.0210	0.0213	0.0224

Table 7.66

Fundamental mode Q values for $M = 0.8 M_{\odot}$ Carson opacity for $Z = 0.005$
Radiative models

$\text{Log}(L/L_{\odot}) = 2.90$ $\text{Log}(T_{\text{eff}})$	3.00	3.10	3.20	3.50	
3.7700	-----	-----	0.0593	0.0615	0.0706
3.7600	0.0573	0.0589	0.0603	0.0626	0.0663
3.7500	0.0583	0.0601	0.0625	0.0630	0.0679
3.7400	0.0595	0.0616	0.0626	0.0651	0.0671
3.7300	0.0612	0.0623	0.0635	0.0656	0.0699
3.7200	0.0620	0.0637	0.0658	0.0673	0.0709
3.7100	0.0636	0.0654	0.0661	0.0679	0.0675
3.7000	0.0640	0.0665	0.0674	0.0680	0.0720

Table 7.67

First overtone mode Q values for $M = 0.8 M_{\odot}$ Carson opacity for $Z = 0.005$
Radiative models

$\text{Log}(L/L_{\odot}) = 2.90$ $\text{Log}(T_{\text{eff}})$	3.00	3.10	3.20	3.50	
3.7700	----	----	0.0332	0.0342	0.0362
3.7600	0.0320	0.0323	0.0329	0.0336	0.0350
3.7500	0.0320	0.0322	0.0328	0.0331	0.0348
3.7400	0.0319	0.0321	0.0324	0.0330	0.0334
3.7300	0.0320	0.0319	0.0321	0.0325	0.0333
3.7200	0.0318	0.0320	0.0326	0.0327	0.0333
3.7100	0.0319	0.0321	0.0319	0.0323	0.0317
3.7000	0.0317	0.0319	0.0317	0.0315	0.0323

Table 7.68

Second overtone mode Q values for $M = 0.8 M_{\odot}$ Carson opacity for $Z = 0.005$
Radiative models

$\text{Log}(L/L_{\odot}) = 2.90$ $\text{Log}(T_{\text{eff}})$	3.00	3.10	3.20	3.50	
3.7700	----	----	0.0227	0.0224	0.0229
3.7600	0.0225	0.0224	0.0225	0.0219	0.0226
3.7500	0.0223	0.0224	0.0221	0.0214	0.0226
3.7400	0.0221	0.0222	0.0217	0.0214	0.0224
3.7300	0.0219	0.0217	0.0214	0.0207	0.0224
3.7200	0.0216	0.0217	0.0214	0.0207	0.0223
3.7100	0.0215	0.0215	0.0209	0.0204	0.0218
3.7000	0.0213	0.0212	0.0211	0.0203	0.0219

CHAPTER 8

APPLICATIONS OF THE LINEAR PULSATION RESULTS: THE RV TAURI STARS

8.1 THE RV AND SRD STARS

In chapter 6 I attempted to show that not only do the RV and SRD stars form fairly well defined groupings in temperature, period, abundance etc. but that these groups appear to form a part of a large system to which the type II cepheid stars, the CW stars in particular, also belong. Evolutionary considerations (Gingold 1974) and pulsation work (e.g. Carson et al. 1981) give fairly well constrained masses for the type II cepheids in the Galaxy and in globular clusters. The latter is a little less than the former but both lie slightly below $0.6 M_{\odot}$ - $M/M_{\odot} = 0.55 - 0.6$ is probably a reasonable range. One property of the RV stars appears not to fit in with the others. This is the luminosity. Takeuti and Petersen (1983), and Du Puy (1973) have shown that the observed data (P , T_{eff} , L) do not combine to give reasonable masses. Their work is based on linear models calculated in the adiabatic approximation. When the nonadiabatic theory is applied to their long period RV example ($\log(L/L_{\odot}) = 2.94$, $\log(T_{eff}) = 3.725$) I

find that it is not possible to get a value for the mass which gives a period anything like the observed period. Fig. 7.31 shows this. The nonadiabatic effects stop the period from rising above ~ 23 days which is well below the observed period of 67.5 (or 135) days. There is in any case little point in going below $0.5 M_{\odot}$ in the search for a mass since a star less massive than this could not hope to attain the luminosity required.

However the fundamental period is not always the longest radial pulsation period. The periods of strange modes, when they are present, are frequently much greater. This prompted Takeuti and Petersen (1983) to suggest that the anomalously long periods of some of the RV stars might be due to pulsation in strange modes. Unfortunately for this idea all the pulsation modes in the linear pulsation models computed in the present work that can ^{be} identified as strange modes are stable. The relevant strange modes are listed in table 8.1. An idea of whether or not these modes might be driven can be gained by comparing the the linear growth - rates, η , with those of the the unstable modes suspected of providing the driving. However when the periods of the two modes under comparison are very different it is not sensible to compare the usual growth rates. A modified growth rate for the strange modes, defined $\eta_s = \eta (P_0/P_S)$, is given in the final column of the table. This makes the stability of the strange modes a little less intimidating. However the damping times are still so very short that I doubt whether they could even be driven

Table 8.1

Strange modes with long periods.

M/M_{\odot}	$\log(L/L_{\odot})$	$\log(T_{\text{eff}})$	Opacity	P_0	η_0	P_s	η_s	$\hat{\eta}_s$
0.50	3.00	3.80	STEL	10.59	-0.942	107.3	-70.2	-6.93
0.50	4.00	3.76	STEL	76.39	-0.932	3850.	-892.	-17.7
0.60	3.50	3.80	W315	26.51	+0.020	91.42	-13.0	-3.77
0.60	3.50	3.82	W315	24.65	-0.315	80.38	-12.1	-3.71
						523.8	-71.5	-3.36
0.60	3.50	3.84	W315	21.79	-0.511	67.86	-11.2	-3.60
0.60	3.50	3.86	W315	19.07	-0.470	67.75	-12.4	-3.49
0.60	4.00	3.56	STEL	531.2	+9.21	3021.	-94.5	-16.6

Opacity: STEL = Stellingwerf formula

W315 = Carson with $Y = 0.25$, $Z = 0.005$

by resonant interaction with another mode. The stability argument against the presence of the strange modes is greatly strengthened by the study by Saio et al. (1984) of modes in highly luminous helium stars. They find that the two most abundant classes of strange modes are unconditionally stable although further small transitional strange modes might become unstable in some circumstances. They however have not found any unstable strange modes. A further problem with the hypothesis that the RV pulsations are the result of strange modes is that the observed luminosities that we are trying to explain are frequently lower than those at which the strange modes appear. I have not found any strange modes for $\log(L/L_{\odot}) < 3.00$ and only one for $\log(L/L_{\odot}) < 3.50$. I conclude that the strange modes cannot be the answer to the problem. However there is another possible entry for the strange modes. Some of the strange modes have periods of around 3000 days or more. It could be that if these modes can be driven they are responsible for the long period oscillations characteristic of the RVb stars and found in at least one of the RVa stars (Mantegazza 1978). If the period of oscillation is sufficiently long then if the usual type of dispersion law is followed the wave length of the mode should be large and perhaps large enough for the mode to penetrate to the energy producing regions of the star. The ξ - mechanism might then be invoked to provide driving for the mode. A probable flaw in the argument is the fact that if the wave - length for the mode is great enough for it to involve the stellar core then the period will

probably be in error.

I can see no way of reconciling the data (P , T_{eff} , L) when P is assumed to be a normal pulsation mode and so at least one of these data must be seriously in error.

Once a decision has been made regarding which observed period (formal or half-formal) will be identified with the fundamental pulsation mode the period can be assumed to be exact. The observed temperatures form what appears to be a consistent and well defined body of data. If there is an error in the photometric temperatures then it is the photometry which underestimates the temperature (for example, compare Dawson's (1979) photometric temperature with Baird's (1984) spectroscopic value for AC Her). An increase in the RV temperatures would only exacerbate the problem. This leaves the luminosity as the prime candidate for correction.

I choose to continue by dropping the luminosity from my set of known quantities.

The precursors of the stars in question are thought to be the horizontal branch (HB) stars. Iben and Rood (1970) have constructed HB star models using an initial helium core mass of $M = 0.475 M_{\odot}$. This can be justified by looking at Eggleton's (1968) calculations for models evolving onto the HB. When neutrino losses are treated and with $Y = 0.3$ he finds a core mass $M/M_{\odot} = 0.48 - 0.50$. By comparing

their models of HB stars with observations of M3 Iben and Rood deduce a variation in total mass of $0.1 - 0.2 M_{\odot}$ and settle for masses of $0.56 M_{\odot}$ at the blue end and $0.76 M_{\odot}$ at the red end of the HB. The work of Demarque and Mengel (1971) yields lower masses of $0.50 - 0.60 M_{\odot}$. From Gingold's (1976) work it can be seen that if the value $M = 0.4664 M_{\odot}$ is accepted for the core mass then the minimum total mass for a star reaching the AGB is about $0.52 M_{\odot}$. If an envelope is less massive than is given by these figures the star runs out of fuel before achieving a crossing of the instability strip at luminosities sufficiently high for our purpose. If the core mass is lower then this minimum total mass is likewise lower and vice versa. This implies that $M = 0.5 M_{\odot}$ is probably the lowest pre-AGB stellar mass that we need consider and that the range in mass is, thankfully, small. I have thus adopted $M = 0.6 M_{\odot}$ as my canonical type II cepheid, RV and SRd star mass. The sequences of pulsation models calculated for $M = 0.6 M_{\odot}$ can now be used to study these stars. Any mass dependence can be tied down using the $M/M_{\odot} = 0.5$ and 0.8 data which should bracket all the values permitted by the evolution calculations for pre-He shell flash models. I impose the latter qualification because the observations offer strong evidence for extensive mass loss at the high luminosities encountered (e.g. Gehrz 1972). This implies that the post-He shell flash masses will be lower, perhaps significantly lower.

If the mass range is sufficiently small, if it can be assumed that the variations in mass are not correlated with the other parameters, and if all the stars pulsate in the same mode then the pulsation period can be substituted for the luminosity to make up the set of variables specifying a star. However a caveat is in order. The assumption regarding the pulsation mode might be in error since UU Her shows two pulsation modes. The RV-like mode has a shorter period and so is probably the first overtone. One would hope that overtone pulsation is a rare occurrence. UU Her will be looked at in detail in a later section. For now it is sufficient to observe that for the great majority of stellar models with $\log(L/L_{\odot}) > 3.5$ the fundamental mode growth rate is positive and very much larger than all of the others implying that the fundamental mode should predominate.

Using periods rather than luminosity we can immediately compare the theoretical blue edges with the observations. Figs. 8.1 + 8.2 show the blue edges derived using convective models, $M=0.6M_{\odot}$ with the Carson opacities for $Z = 0.005$ and 0.000 , and the Stellingwerf formula for $Z = 0.005$ together with the observations for the Galactic stars and the globular cluster stars. For both sets of observations there is virtually no evidence to support the shape of the Carson opacity blue edge for $Z = 0.005$ and, although it is very shaky, it would seem that the slope is too great. It would seem that the $Z = 0.000$ Carson or the Stellingwerf blue edge fit the results a little better. In the case of the globular clusters this is reasonable because we expect a

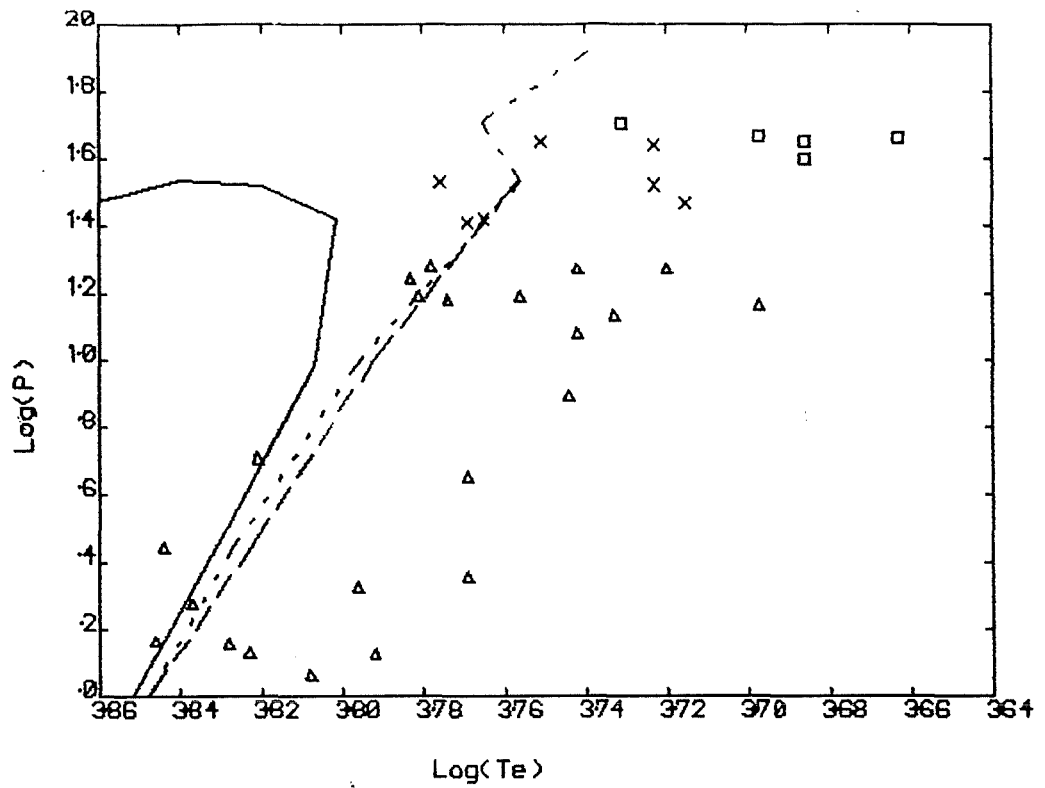


Fig. 8.1 Theoretical blue edges superimposed on the observations for the globular cluster stars.

----- = Stellingwerf opacity formula $Z = 0.005$
 ————— = Carson opacity $Z = 0.005$
 - · - · - = " " $Z = 0.000$

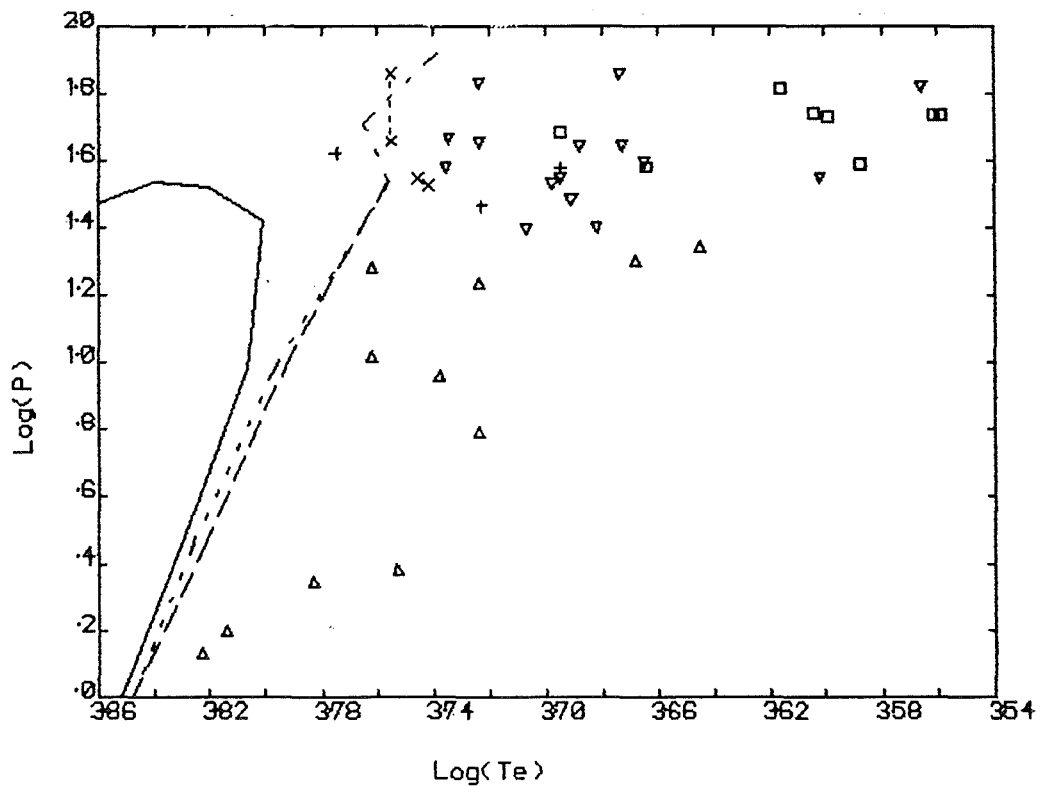


Fig. 8.2 As above but for the field stars.

low metallicity (see chapter 6). However for the bulk of the field RV and type II cepheid stars $Z = 0.005$ (or $[A/H] = -0.6$) is a reasonable value. It is just conceivable that the shape of the Carson $Z = 0.005$ blue edge can be seen in the Galactic observations but since it is determined by only a couple of data points I am inclined to dismiss it. Again it is not inconceivable that the glitch in the Stellingwerf opacity blue edge is present in both sets of observations, and again I think it best forgotten. The blue edges both need to be shifted in temperature whatever opacity is used. This can be accomplished by increasing either or both of the mass and helium abundance to fit the cluster data or the reverse in the case of the Galactic data. Carson et al. (1981) derive a mass smaller for the cluster stars than for the Galactic stars using theoretical light curves. This implies that the helium abundance for the cluster stars should be rather greater than for the Galactic stars. A value of $Y = 0.32$ for the globular cluster stars and around 0.22 for the galactic stars would be reasonable. As noted earlier the temperatures of the RV stars tend to err on the lower side and so reduce the slope of the blue edge or increase the inferred helium abundance. A corrected blue edge would then move towards the Carson opacity blue edge. The errors on the theoretical blue edges ($6 \log(T_{eff}) \approx 0.02$ at the very worst, more likely half this value) make a considerable contribution to the uncertainty which is of the order of magnitude of the He dependence effect. The errors are however large enough that these conclusions

are very uncertain. Little can be said other than that the observations form fairly well defined instability strips for which the locations of the blue edges are in broad agreement with the theoretical results.

Given the data (P , T_{eff}) for the stars together with an assumed mass and the linear pulsation calculations for this mass it is possible to calculate luminosities for the stars. This has been done and the results compared with the observed luminosities. The method used for the calculations was to fit a formula of the form

$$\begin{aligned} \log(L/L_{\odot}) = & a_0 + a_T \cdot \log(T) + a_P \cdot \log(P) \\ & + a_{TP} \cdot (\log(T)) \cdot (\log(P)) \\ & + a_{TT} \cdot (\log(T))^2 + a_{PP} \cdot (\log(P))^2 \end{aligned}$$

to the data. All of these terms are found to be significant. The reduced multiple correlation coefficient calculated with either or both of the square terms missing are noticeably smaller than with them. The errors on the coefficients are all below 5%. The data for the calculations are drawn from table 6.2. Kwee's (1967) data are included in order to help estimate uncertainties and also because the Galactic data of Demers and Harris (1974) has luminosities which are derived using the $P - M_V$ law for the cluster data and so are not independent of the periods.

Table 8.2a

Predicted luminosities and residuals using
the Stellingwerf opacity for the cluster

type II cepheids. (*Data from Kwee*).

		$\log(P)$	$\log(L_p/L_\odot)$	$\log(T_{\text{eff}})$	$\log(L_o/L_\odot)$	$\log(L_p/L_o)$
M2	1	1.192	3.081	3.769	2.822	0.259
	5	1.244	3.125	3.765	2.881	0.244
	6	1.286	3.150	3.760	2.952	0.198
M3	154	1.184	3.102	3.774	3.078	0.024
M5	42	1.410	3.369	3.767	3.237	0.132
	84	1.423	3.353	3.762	3.204	0.149
M10	2	1.273	3.120	3.758	2.912	0.208
	3	0.896	2.634	3.756	2.543	0.091
M13	1	0.164	1.992	3.787	2.108	-0.116
	2	0.708	2.508	3.774	2.474	0.034
	6	0.325	2.062	3.765	2.045	0.017
M15	1	0.158	2.197	3.835	2.058	0.139
M80	1	1.194	3.071	3.767	2.629	0.442
ω Cen	29	1.168	2.667	3.699	2.879	-0.212
	43	0.063	1.985	3.810	2.199	-0.214
	48	0.651	2.428	3.771	2.490	-0.062
	60	0.130	2.124	3.826	2.139	-0.015
	61	0.357	2.117	3.771	2.206	-0.089
	92	0.129	1.951	3.785	1.997	-0.046

Table 8.2a (continued)

Predicted luminosities and residuals using
the Stellingwerf opacity for the cluster

type II cepheids. (*Data from Demers + Harris.*)

	log(P)	log(Lp/L _⊙)	log(T _{eff})	log(L _o /L _⊙)	log(Lp/L _o)
W Cen 29	1.168	2.658	3.697	2.844	-0.186
43	0.063	1.977	3.808	2.122	-0.145
48	0.651	2.418	3.769	2.410	0.008
60	0.130	2.110	3.823	2.062	0.048
61	0.357	2.109	3.769	2.126	-0.017
92	0.129	1.977	3.792	1.910	0.067
M3 154	1.184	3.102	3.774	3.010	0.092
M80 1	1.194	3.003	3.756	2.555	0.448
M13 1	0.164	2.259	3.846	2.030	0.229
2	0.709	2.773	3.821	2.462	0.311
6	0.325	2.191	3.796	2.082	0.109
M10 2	1.273	3.022	3.742	2.839	0.183
3	0.896	2.573	3.744	2.471	0.102
M14 1	1.272	2.896	3.720	2.843	0.053
2	0.445	2.580	3.844	2.133	0.447
7	1.134	2.797	3.733	2.537	0.260
17	1.082	2.782	3.742	2.531	0.251
76	0.276	2.339	3.837	2.460	-0.121
M15 1	0.158	2.163	3.828	1.879	0.284
M2 1	1.192	3.158	3.781	2.722	0.437
5	1.244	3.244	3.783	2.769	0.475
6	1.284	3.266	3.778	2.834	0.432

Table 8.2a (continued)

Predicted luminosities and residuals using
the Stellingwerf opacity for the cluster

RV stars.

		$\log(P)$	$\log(L_p/L_\odot)$	$\log(T_{\text{eff}})$	$\log(L_o/L_\odot)$	$\log(L_p/L_o)$
M5	42	1.410	3.382	3.769	3.206	0.176
	84	1.423	3.373	3.765	3.173	0.200
ω Cen	1	1.470	3.119	3.715	3.105	0.014
M2	11	1.530	3.608	3.776	3.238	0.370
M56	6	1.650	3.604	3.751	2.799	0.805
M22	8	1.525	3.240	3.723	2.692	0.548
	9	1.642	3.401	3.723	2.452	0.949

Table 8.2a (continued)

Predicted luminosities and residuals using
the Stellingwerf opacity for the cluster

SRd stars.

		$\log(P)$	$\log(L_p/L_\odot)$	$\log(T_{\text{eff}})$	$\log(L_o/L_\odot)$	$\log(L_p/L_o)$
M3	138	1.600	3.121	3.686	2.566	0.555
	225	1.650	3.185	3.686	2.634	0.551
M13	11	1.665	3.078	3.663	2.832	0.246
M22	5	1.666	3.271	3.697	2.636	0.635
M56	3	1.706	3.545	3.731	2.506	1.039
M3	95	1.713	3.021	3.640	2.839	0.182

Table 8.2a (continued)

Predicted luminosities and residuals using
the Stellingwerf opacity for the field

type II cepheids. (*Data from Kwee*).

	$\log(P)$	$\log(L_p/L_\odot)$	$\log(T_{\text{eff}})$	$\log(L_o/L_\odot)$	$\log(L_p/L_o)$
527 Sgr	0.100	2.052	3.817	2.117	-0.065
2 Aql	0.223	2.078	3.794	2.144	-0.066
839 Sgr	0.265	2.082	3.785	2.149	-0.067
UY Eri	0.344	2.211	3.796	1.918	0.293
AU Peg	0.380	2.030	3.742	1.923	0.107
465 Oph	0.453	2.125	3.749	2.147	-0.022
AP Her	1.017	2.830	3.765	2.725	0.105
1072 Sgr	1.127	3.038	3.776	2.954	0.084
802 Sgr	1.130	2.956	3.762	2.776	0.180
410 Sgr	1.140	3.056	3.776	2.970	0.086
CS Cas	1.167	3.092	3.776	2.994	0.098
FI Sct	1.173	3.100	3.776	3.002	0.098
1187 Sgr	1.179	3.020	3.762	2.824	0.196
741 Sgr	1.182	3.024	3.762	2.828	0.196
CZ Sct	1.188	3.032	3.762	2.836	0.196
AL Sct	1.193	3.039	3.762	2.840	0.199
377 Sgr	1.210	3.061	3.762	2.856	0.205
481 Oph	1.215	3.068	3.762	2.864	0.204
CO Sct	1.233	3.182	3.776	3.062	0.120
W Vir	1.238	3.098	3.762	2.884	0.214
1303 Sgr	1.267	3.229	3.776	3.098	0.131
CC Lyr	1.380	3.353	3.771	3.214	0.139

Table 8.2a (continued)

Predicted luminosities and residuals using
the Stellingwerf opacity for the field

type II cepheids. (*Data from Demers + Harris*).

	$\log(P)$	$\log(L_p/L_\odot)$	$\log(T_{\text{eff}})$	$\log(L_o/L_\odot)$	$\log(L_p/L_o)$
RU Cam	1.346	2.630	3.645	3.004	-0.374
RS Peg	1.299	2.674	3.668	2.903	-0.229
κ Pav	0.957	2.613	3.738	2.564	0.049
AU Peg	0.380	2.070	3.753	2.195	-0.125
ST Pup	1.281	3.156	3.762	2.808	0.348
SW Tau	0.199	2.141	3.814	2.057	0.084
XX Vir	0.130	2.110	3.823	1.994	0.116
AL Vir	1.012	2.807	3.762	2.604	0.203
TX Del	0.790	2.366	3.724	2.463	-0.097
UY Eri	0.346	2.156	3.783	2.177	-0.021
W Vir	1.236	2.873	3.724	2.747	0.126

Table 8.2a (continued)

Predicted luminosities and residuals using
the Stellingwerf opacity for the field

RV(A) stars.

	$\log(P)$	$\log(L_p/L_\odot)$	$\log(T_{eff})$	$\log(L_o/L_\odot)$	$\log(L_p/L_o)$
RV Tau	1.595	3.003	3.665	3.972	-0.969
U Mon	1.664	3.512	3.735	3.124	0.388
R Sct	1.857	3.389	3.674	3.516	-0.127
V Vul	1.578	3.397	3.736	3.440	-0.043
UZ Oph	1.641	3.185	3.688	4.008	-0.823
DY Aql	1.818	2.831	3.566	2.768	0.063
564 Oph	1.548	2.679	3.602	4.172	-1.493
TT Oph	1.485	3.003	3.691	2.800	0.203
TX Oph	1.830	3.678	3.724	4.264	-0.586
SS Gem	1.650	3.418	3.724	2.380	1.038
R Sge	1.548	3.105	3.695	2.732	0.373
TW Cam	1.640	3.100	3.673	3.972	-0.872
DF Cyg	1.396	2.979	3.707	3.340	-0.361
SU Gem	1.399	2.853	3.682	3.212	-0.359
RX Cap	1.531	3.100	3.698	0.900	2.200

Table 8.2a (continued)

Predicted luminosities and residuals using
the Stellingwerf opacity for the field

RV(β) stars.

	$\log(P)$	$\log(L_p/L_\odot)$	$\log(T_{eff})$	$\log(L_o/L_\odot)$	$\log(L_p/L_o)$
AC Her	1.577	3.142	3.695	2.036	1.106
EQ Cas	1.465	3.160	3.723	1.502	1.658
EP Lyr	1.620	3.737	3.775	0.140	3.597

Table 8.2a (continued)

Predicted luminosities and residuals using
the Stellingwerf opacity for the *field*
RV(C) stars

	$\log(P)$	$\log(L_p/L_\odot)$	$\log(T_{\text{eff}})$	$\log(L_\odot/L_\odot)$	$\log(L_p/L_\odot)$
UU Her	1.653	3.637	3.755	3.288	0.349
453 Oph	1.547	3.420	3.746	3.453	-0.033
360 Cyg	1.526	3.363	3.742	4.158	-0.795

Table 8.2a (continued)

Predicted luminosities and residuals using
the Stellingwerf opacity for the field

RV(C) star UU Her assuming that the

RV behaviour takes place in the 1st

overtone mode.

	$\log(P)$	$\log(L_p/L_\odot)$	$\log(T_{\text{eff}})$	$\log(L_\odot/L_\odot)$	$\log(L_p/L_\odot)$
UU Her	1.845	3.931	3.755	3.288	0.643

Table 8.2a (continued)

Predicted luminosities and residuals using
the Stellingwerf opacity for the field

SRd stars.

	$\log(P)$	$\log(L_p/L_\odot)$	$\log(T_{\text{eff}})$	$\log(L_o/L_\odot)$	$\log(L_p/L_o)$
SX Her	1.728	2.858	3.599	4.265	-1.407
TX Per	1.589	2.673	3.588	4.178	-1.505
WY And	1.736	2.732	3.561	4.480	-1.748
RU Cep	1.736	2.726	3.559	5.414	-2.688
Z Aur	1.744	2.896	3.604	4.504	-1.608
TW Aql	1.681	3.279	3.695	3.897	-0.618
SV UMa	1.580	2.979	3.664	3.958	-0.979
AB Leo	1.814	3.027	3.616	4.662	-1.635

Table 8.2a (continued)

Predicted luminosities and residuals using
the Stellingwerf opacity for the field

SRd stars but with the Flower (1976)

bolometric corrections.

	$\log(P)$	$\log(L_p/L_\odot)$	$\log(T_{\text{eff}})$	$\log(L_o/L_\odot)$	$\log(L_p/L_o)$
SX Her	1.728	2.858	3.599	4.111	-1.253
TX Per	1.589	2.673	3.588	3.937	-1.264
WY And	1.736	2.732	3.561	3.734	-1.002
RU Cep	1.736	2.726	3.559	4.588	-1.862
Z Aur	1.744	2.896	3.604	4.371	-1.475
TW Aql	1.681	3.279	3.695	3.881	-0.602
SV UMa	1.580	2.979	3.664	3.921	-0.942
AB Leo	1.814	3.027	3.616	4.566	-1.539

Table 8.2b

Predicted luminosities and residuals using
the Carson opacity for the cluster

type II cepheids. (*Data from Kwee*).

		$\log(P)$	$\log(L_p/L_\odot)$	$\log(T_{\text{eff}})$	$\log(L_o/L_\odot)$	$\log(L_p/L_o)$
M2	1	1.192	3.101	3.769	2.822	0.279
	5	1.244	3.154	3.765	2.881	0.273
	6	1.286	3.188	3.760	2.952	0.236
M3	154	1.184	3.115	3.774	3.078	0.037
M5	42	1.410	3.412	3.767	3.237	0.175
	84	1.423	3.404	3.762	3.204	0.200
M10	2	1.273	3.159	3.758	2.912	0.247
	3	0.896	2.652	3.756	2.543	0.109
M13	1	0.164	2.017	3.787	2.108	-0.091
	2	0.708	2.508	3.774	2.474	0.034
	6	0.325	2.092	3.765	2.045	0.047
M15	1	0.158	2.127	3.835	2.058	0.069
M80	1	1.194	3.093	3.767	2.629	0.464
ω Cen	29	1.168	2.699	3.699	2.879	-0.180
	43	0.063	1.988	3.810	2.199	-0.211
	48	0.651	2.433	3.771	2.490	-0.057
	60	0.130	2.081	3.826	2.139	-0.058
	61	0.357	2.139	3.771	2.206	-0.067
	92	0.129	1.983	3.785	1.997	-0.014

Table 8.2b (continued)

Predicted luminosities and residuals using
the Carson opacity for the cluster

type II cepheids. (*Data from Demers+Harris*).

		$\log(P)$	$\log(L_p/L_\odot)$	$\log(T_{\text{eff}})$	$\log(L_o/L_\odot)$	$\log(L_p/L_o)$
ω Cen	29	1.168	2.688	3.697	2.844	-0.156
	43	0.063	1.984	3.808	2.122	-0.138
	48	0.651	2.425	3.769	2.410	0.015
	60	0.130	2.075	3.823	2.062	0.013
	61	0.357	2.133	3.769	2.126	0.007
	92	0.129	2.001	3.792	1.910	0.091
M3	154	1.184	3.115	3.774	3.010	0.105
M80	1	1.194	3.037	3.756	2.555	0.482
M13	1	0.164	2.157	3.846	2.030	0.127
	2	0.709	2.686	3.821	2.462	0.224
	6	0.325	2.185	3.796	2.082	0.103
M10	2	1.273	3.072	3.742	2.839	0.233
	3	0.896	2.597	3.744	2.471	0.126
M14	1	1.272	2.950	3.720	2.843	0.107
	2	0.445	2.447	3.844	2.133	0.314
	7	1.134	2.837	3.733	2.537	0.300
	17	1.082	2.816	3.742	2.531	0.285
	76	0.276	2.247	3.837	2.460	-0.213
M15	1	0.158	2.111	3.828	1.879	0.232
M2	1	1.192	3.161	3.781	2.722	0.439
	5	1.244	3.247	3.783	2.769	0.478
	6	1.284	3.280	3.778	2.834	0.446

Table 8.2b (continued)

Predicted luminosities and residuals using
the Carson opacity for the cluster RV stars.

		$\log(P)$	$\log(L_p/L_\odot)$	$\log(T_{eff})$	$\log(L_o/L_\odot)$	$\log(L_p/L_o)$
M5	42	1.410	3.423	3.769	3.206	0.217
	84	1.423	3.420	3.765	3.173	0.247
ω Cen	1	1.470	3.198	3.715	3.105	0.093
M2	11	1.530	3.653	3.776	3.238	0.415
M56	6	1.650	3.699	3.751	2.799	0.900
M22	8	1.525	3.328	3.723	2.692	0.636
	9	1.642	3.509	3.723	2.452	1.057

Table 8.2b (continued)

Predicted luminosities and residuals using
the Carson opacity for the cluster SRd stars.

		$\log(P)$	$\log(L_p/L_\odot)$	$\log(T_{eff})$	$\log(L_o/L_\odot)$	$\log(L_p/L_o)$
M3	138	1.600	3.204	3.686	2.566	0.638
	225	1.650	3.278	3.686	2.634	0.644
M13	11	1.665	3.144	3.663	2.832	0.312
M22	5	1.666	3.376	3.697	2.636	0.740
M56	3	1.706	3.664	3.731	2.506	1.158
M3	95	1.713	3.052	3.640	2.839	0.213

Table 8.2b (continued)

Predicted luminosities and residuals using
the Carson opacity for the field

type II cepheids. (*Data from Kwee*).

	$\log(P)$	$\log(L_p/L_\odot)$	$\log(T_{\text{eff}})$	$\log(L_\odot/L_\odot)$	$\log(L_p/L_\odot)$
527 Sgr	0.100	2.035	3.817	2.117	-0.082
2 Aql	0.223	2.086	3.794	2.144	-0.058
839 Sgr	0.265	2.098	3.785	2.149	-0.051
UY Eri	0.344	2.203	3.796	1.918	0.285
AU Peg	0.380	2.065	3.742	1.923	0.142
465 Oph	0.453	2.154	3.749	2.147	0.007
AP Her	1.017	2.844	3.765	2.725	0.119
1072 Sgr	1.127	3.044	3.776	2.954	0.090
802 Sgr	1.130	2.980	3.762	2.776	0.204
410 Sgr	1.140	3.063	3.776	2.970	0.093
CS Cas	1.167	3.100	3.776	2.994	0.106
FI Sct	1.173	3.109	3.776	3.002	0.107
1187 Sgr	1.179	3.047	3.762	2.824	0.223
741 Sgr	1.182	3.051	3.762	2.828	0.223
CZ Sct	1.188	3.059	3.762	2.836	0.223
AL Sct	1.193	3.066	3.762	2.840	0.226
377 Sgr	1.210	3.090	3.762	2.856	0.234
481 Oph	1.215	3.097	3.762	2.864	0.233
CO Sct	1.233	3.195	3.776	3.062	0.133
W Vir	1.238	3.130	3.762	2.884	0.246
1303 Sgr	1.267	3.245	3.776	3.098	0.147
CC Lyr	1.380	3.388	3.771	3.214	0.174

Table 8.2b (continued)

Predicted luminosities and residuals using
the Carson opacity for the field

type II cepheids. (*Data from Demers & Harris.*)

	$\log(P)$	$\log(L_p/L_\odot)$	$\log(T_{\text{eff}})$	$\log(L_o/L_\odot)$	$\log(L_p/L_o)$
RU Cam	1.346	2.599	3.645	3.004	-0.405
RS Peg	1.299	2.683	3.668	2.903	-0.220
κ Pav	0.957	2.642	3.738	2.564	0.078
AU Peg	0.380	2.102	3.753	2.195	-0.093
ST Pup	1.281	3.192	3.762	2.808	0.384
SW Tau	0.199	2.116	3.814	2.057	0.059
XX Vir	0.130	2.075	3.823	1.994	0.081
AL Vir	1.012	2.823	3.762	2.604	0.219
TX Del	0.790	2.389	3.724	2.463	-0.074
UY Eri	0.346	2.166	3.783	2.177	-0.011
W Vir	1.236	2.923	3.724	2.747	0.176

Table 8.2b (continued)

Predicted luminosities and residuals using
the Carson opacity for the field RV(A) stars.

	$\log(P)$	$\log(L_p/L_\odot)$	$\log(T_{eff})$	$\log(L_o/L_\odot)$	$\log(L_p/L_o)$
RV Tau	1.595	3.057	3.665	3.972	-0.915
U Mon	1.664	3.621	3.735	3.124	0.497
R Sct	1.857	3.515	3.674	3.516	-0.001
V Vul	1.578	3.490	3.736	3.440	0.050
UZ Oph	1.641	3.278	3.688	4.008	-0.730
DY Aql	1.818	2.639	3.566	2.768	-0.129
564 Oph	1.548	2.562	3.602	4.172	-1.610
TT Oph	1.485	3.071	3.691	2.800	0.271
TX Oph	1.830	3.823	3.724	4.264	-0.441
SS Gem	1.650	3.528	3.724	2.380	1.148
R Sge	1.548	3.187	3.695	2.732	0.455
TW Cam	1.640	3.176	3.673	3.972	-0.796
DF Cyg	1.396	3.044	3.707	3.340	-0.296
SU Gem	1.399	2.897	3.682	3.212	-0.315
RX Cap	1.531	3.181	3.698	0.900	2.281

Table 8.2b (continued)

Predicted luminosities and residuals using
the Carson opacity for the field RV(B) stars.

	$\log(P)$	$\log(L_p/L_\odot)$	$\log(T_{eff})$	$\log(L_o/L_\odot)$	$\log(L_p/L_o)$
AC Her	1.577	3.229	3.695	2.036	1.193
EQ Cas	1.465	3.239	3.723	1.502	1.737
EP Lyr	1.620	3.797	3.775	0.140	3.657

Table 8.2b (continued)

Predicted luminosities and residuals using
the Carson opacity for the field RV(C) stars.

	$\log(P)$	$\log(L_p/L_\odot)$	$\log(T_{eff})$	$\log(L_o/L_\odot)$	$\log(L_p/L_o)$
UU Her	1.653	3.729	3.755	3.288	0.441
453 Oph	1.547	3.503	3.746	3.453	0.050
360 Cyg	1.526	3.446	3.742	4.158	-0.712

Table 8.2b (continued)

Predicted luminosities and residuals using
the Carson opacity for the field SRd stars.

	$\log(P)$	$\log(L_p/L_\odot)$	$\log(T_{\text{eff}})$	$\log(L_o/L_\odot)$	$\log(L_p/L_o)$
SX Her	1.728	2.773	3.599	4.265	-1.492
TX Per	1.589	2.513	3.588	4.178	-1.665
WY And	1.736	2.494	3.561	4.480	-1.986
RU Cep	1.736	2.478	3.559	5.414	-2.936
Z Aur	1.744	2.832	3.604	4.504	-1.672
TW Aql	1.681	3.386	3.695	3.897	-0.511
SV UMa	1.580	3.029	3.664	3.958	-0.929
AB Leo	1.814	3.020	3.616	4.662	-1.642

Table 8.2b (continued)

Predicted luminosities and residuals using
the Carson opacity for the field SRd stars

but with the Flower (1976) bolometric corrections.

	$\log(P)$	$\log(L_p/L_\odot)$	$\log(T_{\text{eff}})$	$\log(L_o/L_\odot)$	$\log(L_p/L_o)$
SX Her	1.728	2.773	3.599	4.111	-1.338
TX Per	1.589	2.513	3.588	3.937	-1.424
WY And	1.736	2.494	3.561	3.734	-1.240
RU Cep	1.736	2.478	3.559	4.588	-2.110
Z Aur	1.744	2.832	3.604	4.371	-1.539
TW Aql	1.681	3.386	3.695	3.881	-0.495
SV UMa	1.580	3.029	3.664	3.921	-0.892
AB Leo	1.814	3.020	3.616	4.566	-1.546

Table 8.2c

Coefficients in the fitting formula
for $\log(L/L_{\odot})$ as a function of P_0, T_{eff} .

	Stellingwerf	Carson
a_0	151.71	-55.135
a_T	-82.565	27.920
a_P	-9.6349	-8.0325
a_{PT}	2.7799	2.3140
a_{PP}	0.20757	0.30331
a_{TT}	11.352	-3.3964

Tables 8.2(a + b) give the data derived in this manner together with the observed luminosities and a residual defined as $\log(L_p/L_o)$ where L_p and L_o are the predicted and observed luminosities respectively. The coefficients in the fitted formula are given in tables 8.2c. Period - luminosity plots are to found in figs. 8.3 and 8.4 and the corresponding residuals are given in figs. 8.5 and 8.6.

The residuals for the globular cluster stars show the simplest distribution. All of the type II cepheids (from Demers and Harris 1974), all but two of the RV Tau stars, and all but one of the SRd stars have residuals which lie in a band of width $\log(L_p/L_o) \approx 0.6$. This band slopes so that the residuals increase slowly with period and is displaced to lie above zero. Looking at fig. 8.7 which displays the residuals for the type II cepheids from Kwee's (1967) work as well as the later Demers and Harris (1974) data we see that the breadth of the residual band for the former is about one half of that of the latter. The mean displacement of the band is almost $\log(L_p/L_o) = 0.055$. In fact it is only a few of the Demers and Harris (1974) stars which cause the large spread in the residuals. If these are ignored then there is little difference between the two samples.

A better idea of the source of the residuals can be gained by looking at the mean residuals for each cluster with more than one member. I find:

	Demers + Harris	Kwee
ω Cen	-0.04 +/- 0.10	-0.106 +/- 0.086
M13	0.22 +/- 0.10	-0.022 +/- 0.083
M2	0.448 +/- 0.024	0.234 +/- 0.032
M10	0.143 +/- 0.057	0.150 +/- 0.083
M5	0.188 +/- 0.017	0.141 +/- 0.012
Mean	0.19 +/- 0.18	0.08 +/- 0.14

So a large part of the scatter comes from differences between the clusters. This might conceivably be due to real differences between the clusters but since the pattern is not the same for both sets of data I think it more likely to be due to observational error. The correlation of the residuals with period for the whole set of data does not appear for individual clusters although this is probably explained by the small numbers of stars involved. For ω Cen there might be a correlation (i.e. $r = -0.53$ giving a probability of correlation of 72%) but it has the opposite slope.

The width of the residual band could come from a number of sources. Assuming in turn that each of the potential sources of error is the only source the range of variations can be estimated. These are;

Source	Range
Mass	46%
$\log(T_{eff})$	0.05 - 0.12
M_{bol}	0. ^m 9

If the width is entirely attributable to a range in mass then this gives us masses as low as $M = 0.37 M_{\odot}$ for type II cepheids, a value which is precluded by the evolutionary calculations.

The observed luminosity is dependent upon the bolometric correction which in its turn is strongly dependent upon the observed effective temperature. This dependence is greatest at low temperatures where $d(\text{B.C.})/dT_{\text{eff}} \approx +7$ from whence it falls to zero, that is, too great a temperature will underestimate the observed luminosity. Since a rise in the temperature produces a rise in the predicted luminosity L_p/L_o will be increased or vice versa. This in turn reduces the spread in temperature implied by the width of the band of L_p/L_o values giving an upper value at the lower temperatures of around 0.05 rather than 0.12 although it will still be large at high temperatures. If the temperature is the sole contributor to the spread in the residuals the implication is that a considerable part of the width of the type II cepheid instability strip is attributable to error. The same conclusion has also been suggested by Harris (1981) on the basis of new, though sparse, observations. This seems to imply that it would be reasonable to assume that a large part of the spread in the residuals can be ascribed to uncertainties in the effective temperatures.

The final option is to assume that all of the spread is attributable to the luminosity or bolometric magnitude and so the error must lie in either the bolometric corrections assumed or in the distance moduli used. The most modern bolometric constants for metal poor stars are those calculated by Bohm-Vitense (1973) from stellar atmosphere models. These were used whenever a bolometric correction was not supplied by Dawson (1979). The bolometric corrections used by Dawson are derived from data used by Schlesinger (1969) in a study of globular cluster stars and are a part of the calibration of the D.D.O. system (by Osborn 1973). A more recent set of bolometric corrections are those derived from observations of population I stars by Flower (1977). A comparison of the bolometric corrections from all three sources shows that the uncertainty is no greater than ± 0.5 . An additional uncertainty appears in the case of the RV, and to a lesser extent the SRd, stars because these stars possess circumstellar shells which make the flux distribution diverge from a black-body curve.

Accounting for the rise in the mean residuals with period is difficult. It is unlikely that this is the result of a decrease in mass with increasing period since this would imply a very low mass at long periods ($M = 0.29 M_{\odot}$) and, of course, a fairly high mass ($M = 0.88 M_{\odot}$) at short periods. A possibility is that a consistent overestimate of the temperature at all periods leads through the bolometric constant to the observed effect. However this contradicts the tendency of the photometry to underestimate the effective

temperatures of the RV stars.

The consistency of the residuals for all of the three types of star, with three exceptions, implies that the assumption that they all have similar mass is vindicated. (The three high residual stars are ringed in fig. 8.3 + 8.8.) It also suggests that the assumption that the pulsation period of the SRd stars should be half the formal period is sensible. The RV and SRd stars are now clearly separated on the period-luminosity diagram for the predicted periods. As with the observations, when the predicted luminosities are used the RV stars form an extension of the type II cepheids whilst the SRd stars lie a little below them. A turnup in the period-luminosity curve at $\log(P) \approx 1.2$ seen in the observed data is almost imperceptible when the predicted luminosities are used.

Moving to the field stars a rather different picture presents itself. Looking at fig. 8.7 which shows the residuals for the type II cepheids drawn from Demers and Harris (1974), and from Kwee (1967), we can see that the scatter is probably a little less for these stars than for their cluster counterparts. The scatter for the Kwee data is, with the exception of one point, considerably less than that for the Demers and Harris data ($\Delta_{DH} / \Delta_{Kwee} = 0.20/0.079$). There is a negligible correlation of the residuals from the latter data but a barely significant correlation from the Kwee data which has a positive slope ($\log(Lp/Lo) = 0.15\log(P) + C$) like the cluster data. Because

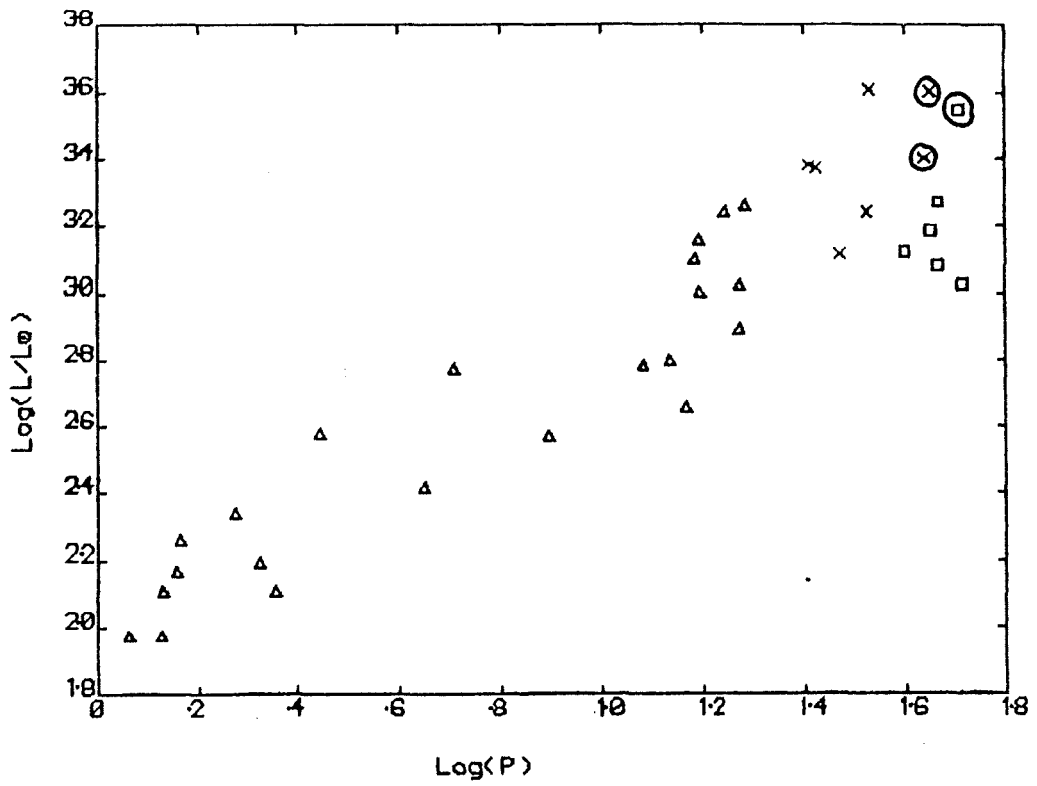


Fig. 8.3 Period - luminosity plot using the predicted luminosities for the globular cluster stars.

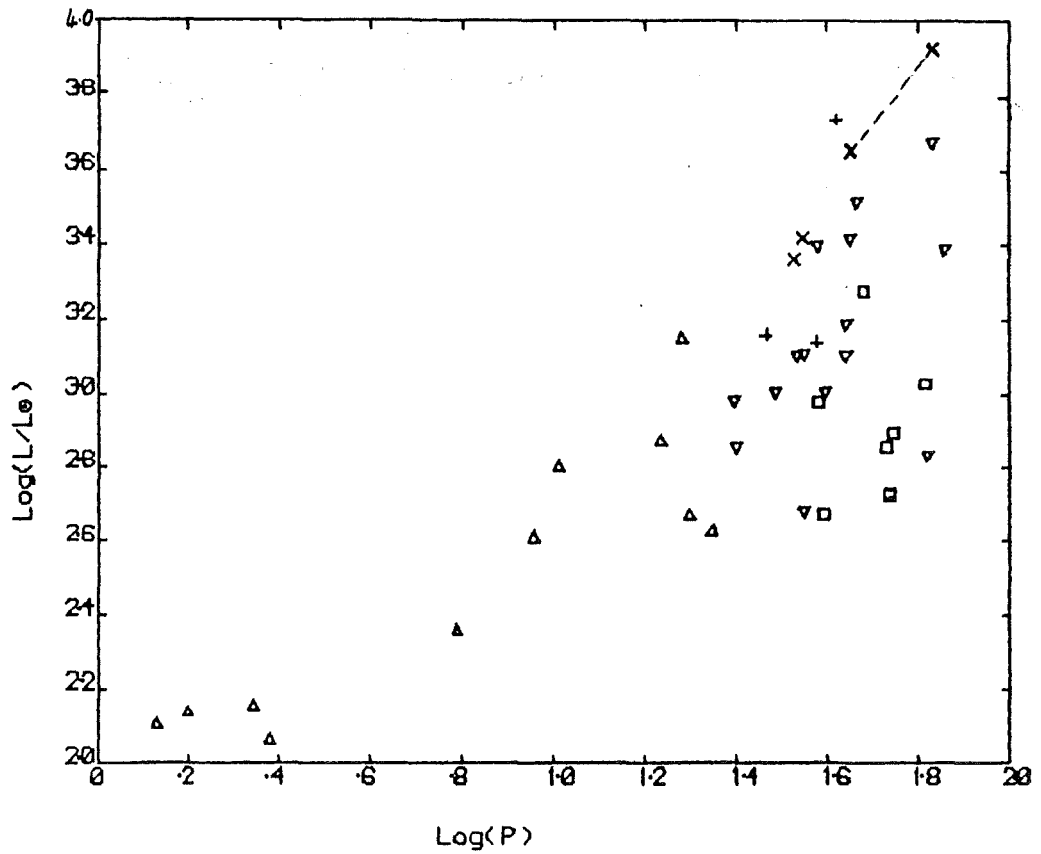


Fig. 8.4 As above but for the field stars.

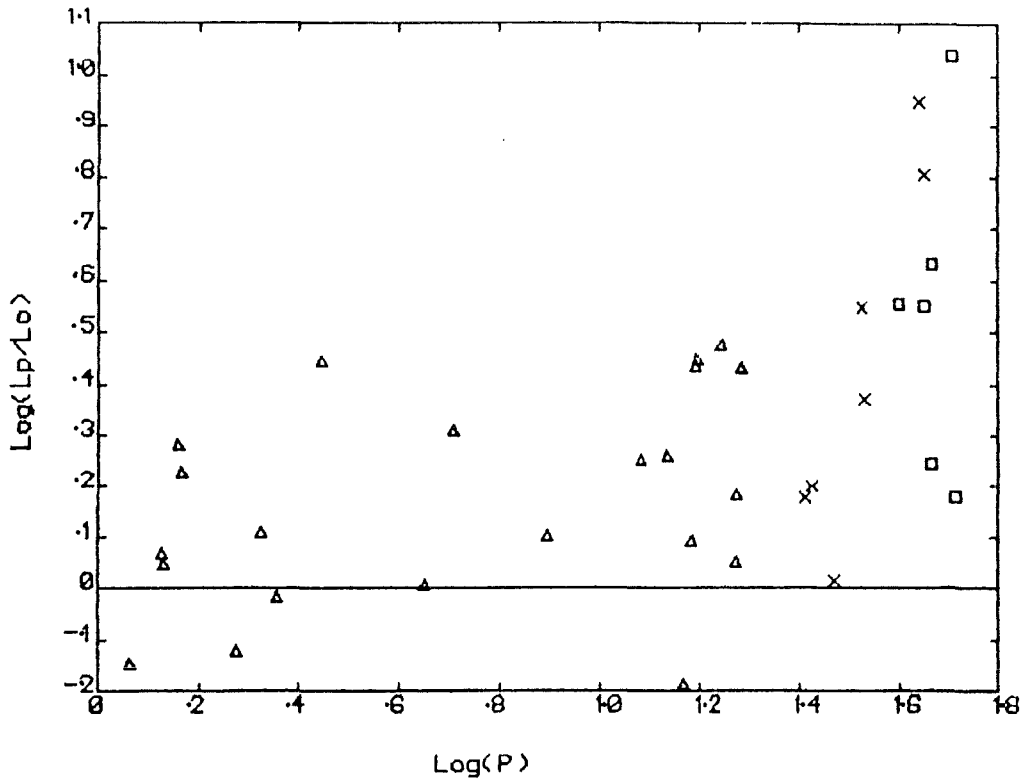


Fig. 8.5 Luminosity residuals $\log(L_p/L_o)$ for the globular cluster stars.

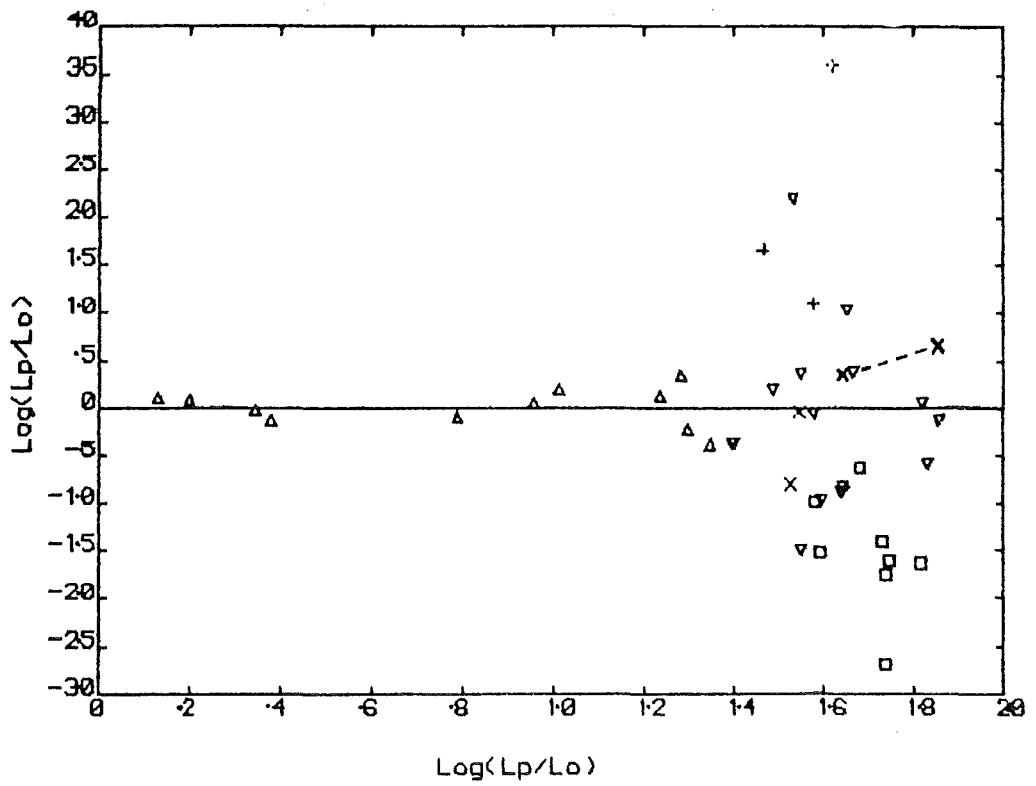


Fig. 8.6 As above but for the field stars.

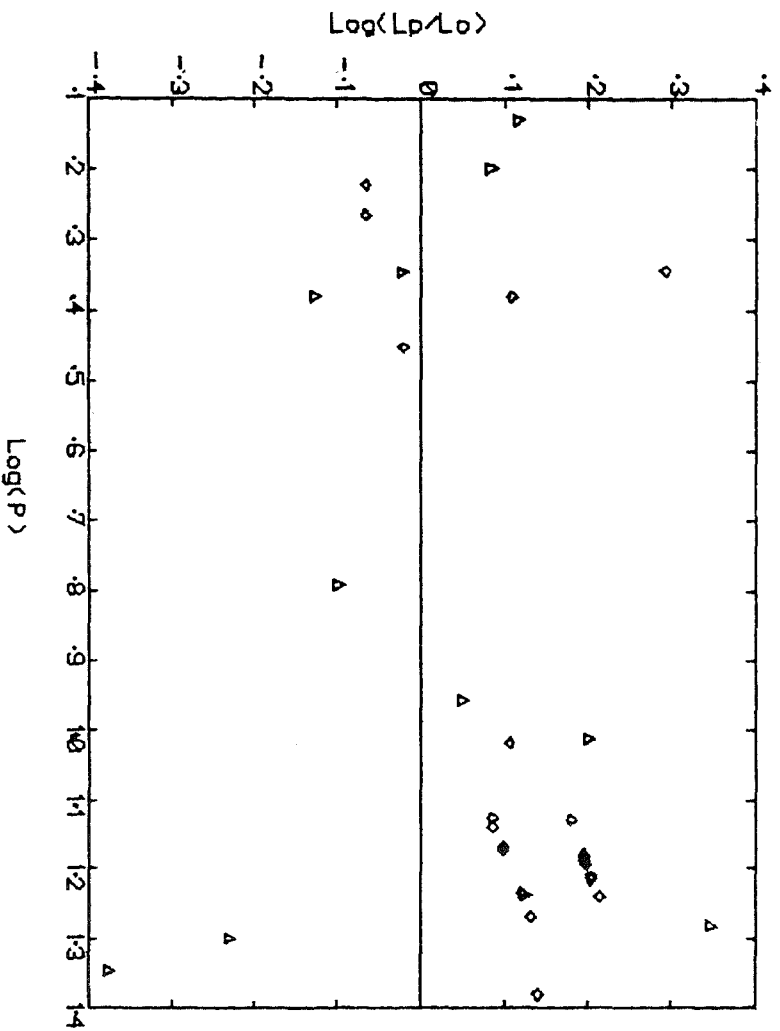


Fig. 8.7 Luminosity residuals for the field stars from the observations of:
 Dewers and Harris Δ
 and Kwee \diamond

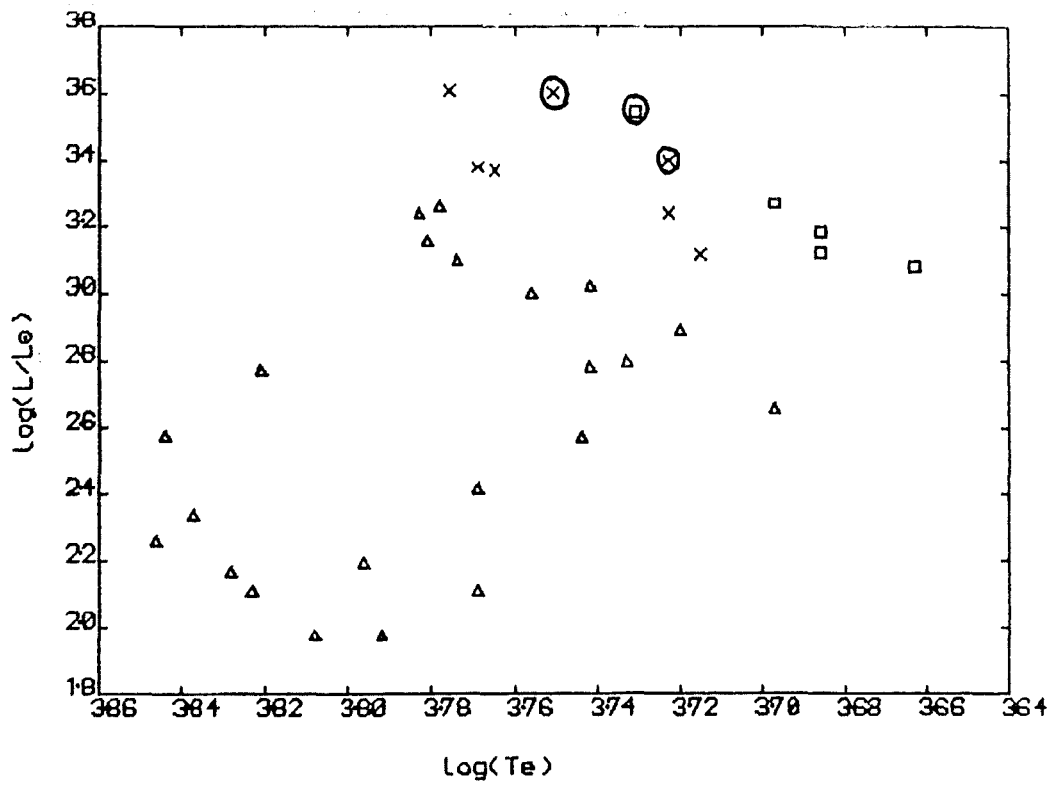


Fig. 8.8 The H-R diagram using the predicted luminosities for the globular cluster stars.

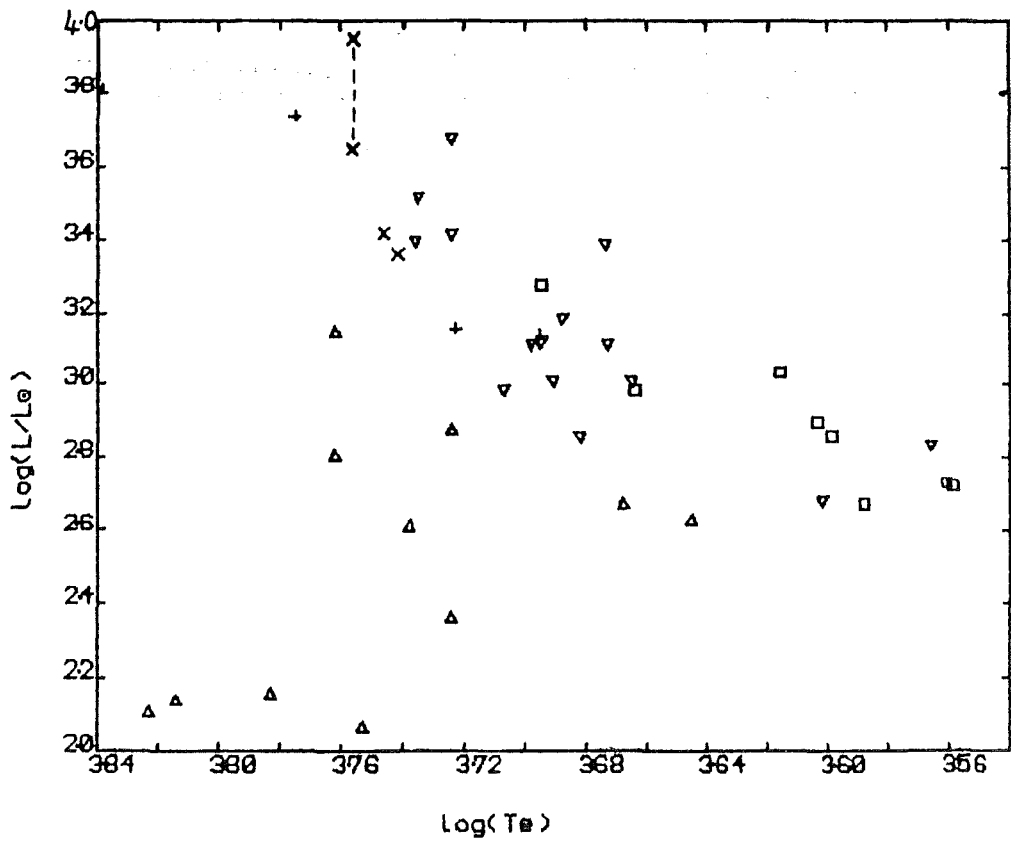


Fig. 8.9 As above but for the field stars.

the Demers and Harris (1974) luminosities are derived from the period-luminosity law for the cluster stars they will not be used after this point. The zero point for the residuals from Kwee's field data is 0.01 as opposed to -0.09, with a slope of 0.20, for the cluster data. Within the bounds set by the uncertainties there is little difference between the cluster and the field stars so far as the predicted luminosities are concerned.

For the field RV and SRd stars we find a rather dismal situation. All of the SRd residuals are negative and they can be as large as $\log(L_p/L_o) = -2.7$. However almost all of the observed luminosities were calculated using the bolometric corrections extrapolated from Bohm-Vitense's (1973) figures. Using Flower's (1977) numbers greatly reduces the SRd residuals of which the largest is now $\log(L_p/L_o) = -1.9$ with most less negative than -1.54. The adjustments to the model required to reduce these residuals to zero are very large. For example, an increase of the mass by a factor of about 150 (clearly nonsense), an increase of the temperature by a factor of 2.3, or some serious error in the observed luminosities is needed. The modified mass would be around 90 M_{\odot} which is well outside the upper limit on the mass imposed by Dawson's (1979) own photometry. This would imply a considerable inconsistency in his results. It is also inconsistent with the independently verified metals abundances of the stars (e.g. Preston 1963). Further alternatives include the possibility that the pulsation is in a very high order pulsation mode

or that the effects of nonadiabaticity are so immense that they shrink the periods to the values observed for the observed luminosities. However I think it important that the theory and observations are in as good agreement for the cluster SRd stars (and RV stars) as for the type II cepheids. This makes me inclined to accept the predicted luminosities and reject the observed luminosities.

Moving on to the RV Tauri variables we again find residuals (tables 8.2 (a + b)) of the same order of magnitude as for the SRd stars. In this case they are not consistently of one sign. There are seven RV(A) stars with positive residuals against eight with negative residuals. The mean residual is -0.09 ± 0.9 and there is a very high probability that they are completely uncorrelated with period. There is however a strong dependence on the observed luminosity and also weaker correlations with temperature and the predicted luminosity. It would seem that there is little connection between the luminosities and the rest of the observed data. For the stars showing the large negative residuals the same arguments hold as for the SRd stars and the result is that there is no consistent interpretation of the data. In the case of the large positive residuals it is even more difficult to invoke a change in the stars' masses since there are strict lower limits imposed not only by the evolution calculations but also by the pulsation calculations.

A closer look at the residuals for the RV(A) stars is in order. If I drop all the stars which have fewer than four measurements of the M_V then although the very largest of the residuals go away some very large values remain. These include RV Tau for which $\log(L_p/L_o) = -0.97$ with nine measurements and SS Gem for which $\log(L_p/L_o) = +1.04$ with four measurements. It can also be seen (Table 8 of Dawson 1979) that for all of the remaining stars there is reasonable phase coverage. For either the RV(A₁) or RV(A₂) stars or for the entire set of RV(A) stars in this reduced sample the mean residuals are still close to zero (-0.11 ± 0.52 , $+0.18 \pm 0.97$, -0.00 ± 0.67). Dawson (1979) has observed that his masses vary with phase (less so for the RV(A₂)s than for the RV(A₁)s). However it seems at least as likely that the larger part of the errors are random rather than systematic.

The cluster RV stars are all classified as RV(C) and so a comparison of these stars in the field and in clusters is sensible. None of the cluster RV stars exhibits a negative residual but one of the field RV(C) stars has a large negative residual ($\log(L_p/L_o) = -1.0$). However with the exception of this rogue point (a mere 33% of the sample!) the rest of the field stars can be made to conform to the pattern displayed by the cluster stars. Needless to say I do not find this convincing.

In the case of the RV(B) stars it is already known that the luminosities determined using the D.D.O. photometry are unreliable and so the large residuals should not come as a surprise.

Dawson (1979) has looked into possible errors in the D.D.O. photometric $\langle M_V \rangle$ values by comparing them with Du Puy's (1973) figures. He shows that the residual ($\langle M_V \text{D.D.O.} \rangle - \langle M_V \text{Du Puy} \rangle$) is correlated with the mass determined using either the D.D.O. or the Du Puy magnitudes although the slopes carry opposite signs. Going further he is able to tie the problem down to a flaw in the luminosities or surface gravities given by the D.D.O. system indicating contamination of the colour C(45-48) (where $45 \equiv 4500 \text{ \AA}$, $48 \equiv 4800 \text{ \AA}$ filters). The only features which could be responsible for the contamination are $H\beta$ (4861 \AA) and the TiO band (4761 \AA). In the latter case the luminosity is lower than it should be but higher in the former. There is little difference between the residuals for the RV(A₂) stars (which show both Balmer emission and TiO absorption) and the RV(A₁) stars (which have neither) but the SRd stars which generally show very strong Balmer emission have the large negative residuals predicted by this explanation.

Very recently Mantegazza (1984) has made an analysis of the D.D.O. photometric data on the RV and SRd stars. He derives four factors (orthonormal variables) which are linear combinations of the four D.D.O. colours and shows that in the planes defined by pairs of

factors the stars separate into fairly well defined groups. However in all the factors there is a large contribution from the suspect C(45-48) colour. This makes me wonder just what it is that the factors are measuring although the results do seem to imply that there is useful information in all the colours.

It seems worth while to give the H-R diagrams which result from using the predicted luminosities along with the observed temperatures from which they are derived. These H-R diagrams form figs 8.8 and 8.9. They hold no surprises. The only odd point is that the field SRd stars occupy a patch of the diagram at rather low luminosities.

The main alternative source of observed RV Tauri luminosities is the work of Du Puy (1973) described in chapter 6. He derives the well known P-M relation with a positive slope. A look at figs. 8.3 and 8.4 shows that the $\langle M_V \rangle$ values calculated using the luminosities derived from the linear pulsation results in conjunction with Dawson's temperatures very probably are not in agreement with this observed relationship. The calculation of the M_V values confirms this. For the globular clusters the predicted P- M_V relations are:

Type II cepheids:

$$\begin{aligned} \text{Kwee} \quad M_V &= -2.40 \log(P) + 0.02 \\ &\quad \pm 0.16 \quad \pm 0.15 \end{aligned}$$

$$\begin{aligned} \text{D + H} \quad M_V &= -1.99 \log(P) - 0.33 \\ &\quad \pm 0.21 \quad \pm 0.18 \end{aligned}$$

RV Tau:

$$\begin{aligned} M_V &= -1.9 \log(P) - 0.8 \\ &\quad \pm 2.1 \quad \pm 3.2 \end{aligned}$$

In the latter case there is a 10% probability that the sample is uncorrelated. The SRd stars show a negligible correlation: it is 80% probable that they are not correlated in M_V and $\log(P)$. In the case of the field stars I find the following relations for M_V predicted using the linear pulsation results:

Type II cepheids:

$$\begin{aligned} \text{Kwee} \quad M_V &= -2.68 \log(P) + 0.23 \\ &\quad \pm 0.11 \quad \pm 0.12 \end{aligned}$$

$$\begin{aligned} \text{D + H} \quad M_V &= -1.48 \log(P) - 0.26 \\ &\quad \pm 0.37 \quad \pm 0.34 \end{aligned}$$

RV(A):

$$\begin{aligned} M_V &= -2.0 \log(P) + 0.4 \\ &\quad \pm 1.7 \quad \pm 2.7 \end{aligned}$$

For neither the field nor the cluster RV stars is the slope of the $P - M_V$ relation positive. In the case of the globular cluster RV stars the various observed $P - M_V$ relations underestimate the

luminosity. For the field RV stars the M_v values, determined from parallax measurements, are on average overestimated. In any case the wide range of temperatures makes a simple $P - M_v$ relation inappropriate for the field stars. In the following table the observed $\langle M_v \rangle$ values from the combined cluster data of table 6.4.7 (C), from Du Puy's cluster data (DPC) and from his observed $P - M_v$ relation for the field (DPF) are compared with the values predicted using Dawson's temperatures with the linear pulsation results:

	C	DPC	DPF	Predicted
Cluster	-2.52	-2.97	-	-3.70
Field	-	-	-2.86	-3.15

So whilst the predictions of individual magnitudes show the wrong trends, the mean magnitudes are "reasonably" close to the value predicted by the $M = 0.6 M_{\odot}$ model. In the case of the field stars the implied luminosities differ by only 30%.

8.1.1 Resonances

There are two main alternatives for the resonance hypothesis as applied to the RV Tau stars. Christy (1966) found that in his RV-like model the formal period was twice the fundamental pulsation period and proposed that this was a result of the resonance $P_1/P_0 = 2/3$. A double resonance of this kind does not exist in the lowest order nonlinear terms (e.g. Buchler and Goupil 1984) but might well be found in higher order terms. For example, terms with time dependences

involving 3ω are already found in the second order perturbation equations. However this resonance condition could occur in the lower order terms as part of a triple resonance $[0,1;j]$ for which $P_j/P_0 = 2/5$. The tendency for some RV light curves to show frequent variations of light amplitude could reflect an imperfect satisfaction of the resonance conditions.

Figs. 8.10 and 8.11 show the resonance loci for the Stellingwerf opacity models computed with and without convection in the $\text{Log}(T_{\text{eff}}) - \text{Log}(P_0)$ plane for $M = 0.6 M_{\odot}$ with the usual composition. The $P_2/P_0 = 0.5$ resonance can be seen clearly cutting across the instability strip for $P_0 \simeq 1.6 - 4.0$ days. This is widely believed to give rise to the secondary bumps on many of the BL Her light and velocity curves (e.g. Simon and Schmidt 1976, Carson et al. 1981). Carson et al. (1981) find that the bumps are displayed over a fairly wide range of the period ratio, that is,

$$0.46 < P_2/P_0 < 0.56$$

which translates into a temperature range of,

$$3.85 < \log(T_{\text{eff}}) < 3.75$$

for a $\log(L/L_{\odot}) = 2.00$ sequence. At longer periods the $[0,0;1]$ and $[0,1;2]$ resonance loci cross the instability strip. They then turn upwards to run up through the RV Tau portion of the instability strip. Another branch of the $[0,0;2]$ locus lies on the upper edge of the RV segment of the instability strip. A branch of the $[0,1;2]$ locus skirts the lower edge of the W Vir/RV Tau instability strip before

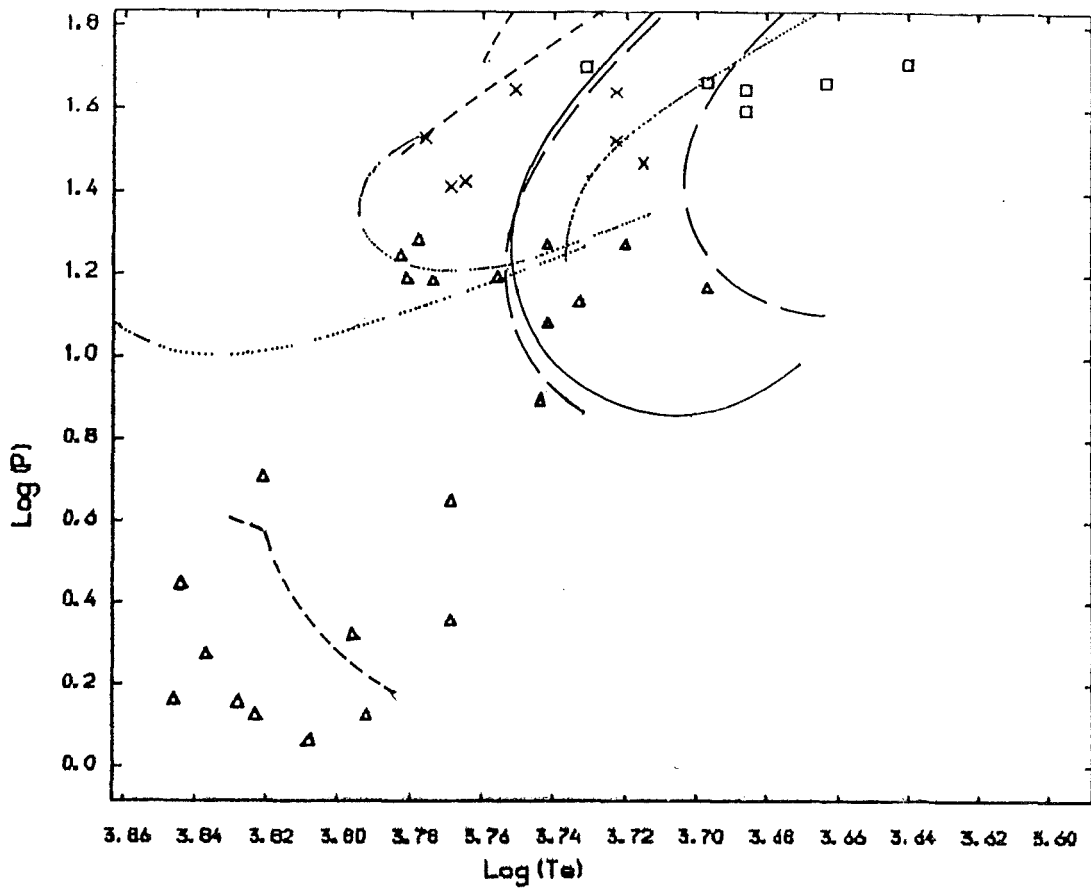


Fig. 8.10 The theoretical resonance loci superimposed on the observations for the globular cluster stars.

- = [0,0;1] (with convection)
- = [0,0;2] (with convection)
- · - · - = [0,1;2] (with convection)
- = [0,0;1] (radiative)
- = [0,1;2] (radiative)

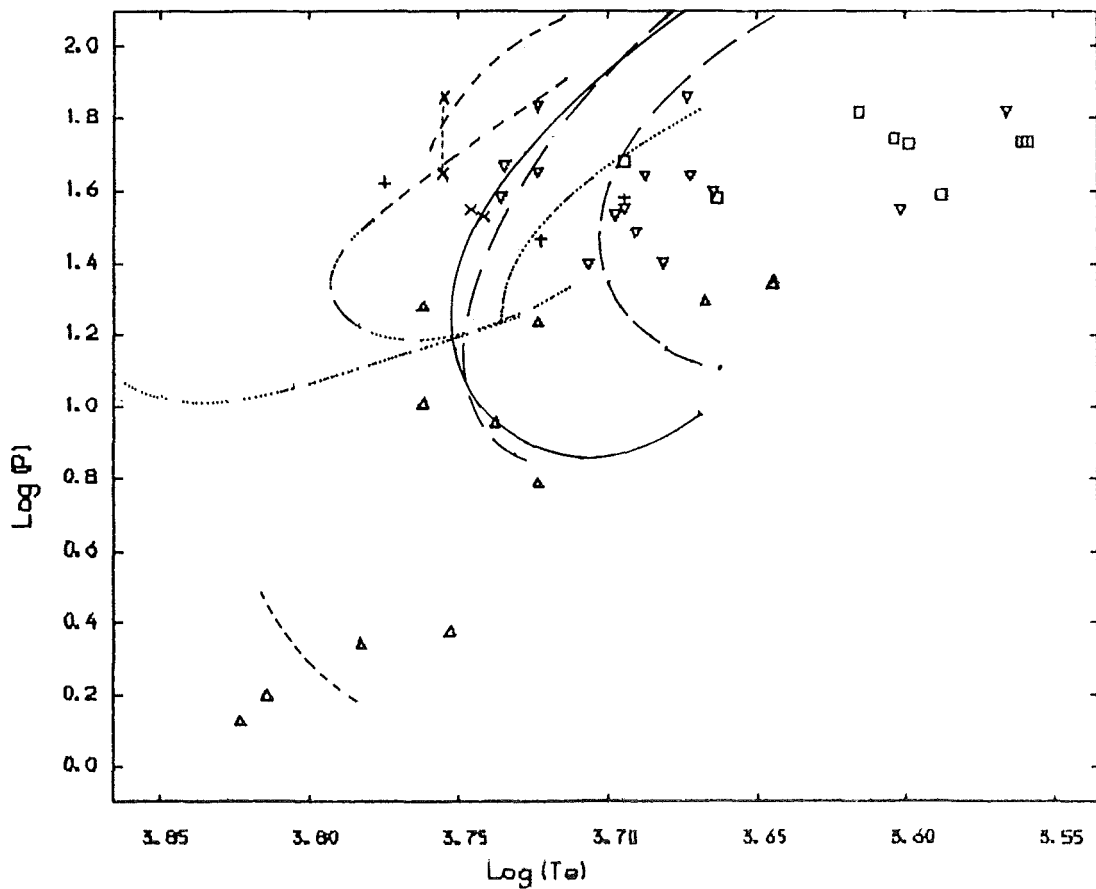


Fig. 8.11 As above but for the field stars.

passing through the SRd stars.

We need to know whether or not resonant interactions will be able to excite the secondary modes which in a harmonic oscillator would be stable. For the lower branches of the $[0,0;i]$ resonance locus when the nonlinear terms are ignored the fundamental mode is unstable whilst the resonant overtone modes are stable. Using the resonance theory directly involves the calculation of the coupling coefficients—a very lengthy process. The alternative method is to look for phenomena in other well known stars and try and use this knowledge to predict whether or not resonances will be important in the RV and SRd stars.

Although there is the same pattern in the linear instability coefficients for the $[0,0;2]$ and lower branch $[0,0;1]$ resonances, only the first shows evidence of an interaction. That is, there is a clear bump on the BL Her light and velocity curves which is not found in the relevant W Vir star light and velocity curves. The amplitude equations for a double resonance $[0,0;j]$ given by Buchler and Goupil (1984) are;

$$\frac{da_0}{dt} = \kappa_0 a_0 + i \frac{\Delta\Omega}{2} a_0 + P_0 a_0^* a_j$$

$$\frac{da_j}{dt} = \kappa_j a_j - i \Delta \Omega a_j + \mathcal{P}_j a_0^2$$

where a_i is the complex amplitude of the i^{th} mode, $\Re_i \equiv \text{Re}(\omega_i)$, $\Im_i \equiv -\text{Im}(\omega_i)$, $\Omega \equiv 0.25(2\Re_i + \Re_j)$, $\Delta_{ij} \equiv 0.5(2\Re_i - \Re_j)/\Omega$, $|\Delta_{ij}| \ll 1$, and \mathcal{P}_j are the coupling coefficients. To find out whether or not the amplitude of the overtone mode will grow to a finite amplitude under the influence of the fundamental mode Dziembowski (1982) assumes a_0 is constant and integrates the second equation to obtain the time development of a_j . Assuming $\kappa_0 > 0$, $\kappa_j < 0$ he finds,

$$|a_j| \propto |a_0|^2 \frac{(1 - \cos \Delta \Omega t)}{\sqrt{\kappa_j^2 + (\Delta \Omega)^2}}.$$

I cannot duplicate this result but find that for $t \rightarrow \infty$, with $\kappa_j < 0$,

$$a_j \longrightarrow \frac{\mathcal{P}_j a_0^2}{i \Omega \Delta - \kappa_j}.$$

Of course this is only reasonable if the overtone amplitude is sufficiently small that

$$\frac{da_0}{dt} \approx 0.$$

However both results predict that the overtone mode should always appear. This appears to contradict the observations which suggest (Carson et al. 1981) that the appearance of the BL Her bumps is a threshold phenomenon with a minimum total amplitude below which the

interaction does not take place. (However for a system where the signs on both the linear instability coefficients are reversed, a parametric resonance, there is a threshold amplitude, i.e. a minimum overtone amplitude.) The only escape from this contradiction would be for there to be radical differences between the coupling coefficients for the two different resonances. However it would have to be a very substantial difference to bring about such a large effect. I think that it is more likely that the resonance theory as described in the literature is not an adequate description of the real state of affairs.

The alternative hypothesis for the BL Her bump formation is the echoed pulse model suggested by Christy (1968). From a study of velocity histories Christy (1968) found that in each period a double pulse is generated which travels to the surface and core of the star where both portions are reflected to meet up again at or very near to their birthplace. Simon (1977) and more recently Whitney (1983) have suggested that these two mechanisms are one and the same thing described in two different languages. Whitney (1983) attempts to show that the conditions imposed on the sound travel times for the pulses for them to meet at their place of generation are equivalent to the simultaneous satisfaction of temporal and spatial resonance conditions. It is the fortuitous location of the antinodes of the second overtone eigenfunction which enables this mode to satisfy the spatial resonance condition. However Whitney (1983) does not go

further and examine whether or the coupling coefficients of the quasi-linear resonance theories impose a similar restriction. This is a pity. However he does provide the suggestion of a reason for the $[0,0;2]$ resonance to be favoured over other $[0,0;1]$ resonances. The question I would like answered is whether or not the $[0,1;2]$ resonance will be similarly favoured. However the conclusion which must be drawn is that not enough is known to be able to extrapolate the observations of the lower luminosity stars to the RV and SRd stars and so predict the modal content of their pulsations.

The discussion above provides us with no means for predicting reliably how resonances will affect the stability of modes. However for the longer periods once the resonance loci have turned back blue - wards both the fundamental and first overtone are unstable. The fundamental is generally the most strongly unstable with growth rates frequently as large as 6 or more. The implication is that whatever mechanism it is that suppresses the first overtone mode on the shorter period, W Vir, branch of the $[0,0;1]$ locus will probably not operate on the longer period branch.

We can get some idea of whether or not the resonant interactions will be of importance to the properties of the stars in the following way. Buchler and Goupil (1984) point out that the condition for a resonance to be important is that

$$|\Delta| \lesssim \frac{\kappa}{\Omega}.$$

(This of course says nothing about the effect that the resonance will have.) If we calculate the smallest of $4\pi|\Delta_{0j}|/\max(|\mu_0|, |\mu_j|)$ and $4\pi|\Delta_{0r}|/\max(|\mu_0|, |\mu_r|, |\mu_z|)$, which we call R , for all the points of a model sequence we should get a reasonable idea of which models can exhibit resonances. This has been done for the convective models, without viscosity, computed using the Stellingwerf opacity formula. The results form fig. 8.12. For $\log(L/L_\odot) < 2.5$ we find $\log(R) \gg 0$ for most of the models (i.e. the logarithms are largely greater than zero) making only brief excursions into the region where resonances will take hold. For $\log(L/L_\odot) \approx 2.5$ the picture is much the same except that most of the models $\log(R) \approx 0$. At higher luminosities points for which $\log(R) \gtrsim 0$ are the exception and the bulk of the points now lie around $\log(R) \approx -1$. So we can see that when the luminosity becomes great enough resonances should play an important part in the behaviour of stars across a large part of the HR diagram. Very similar results are found for the Carson opacity convective models and for the Stellingwerf opacity radiative models. If it is the case that RV Tauri behaviour is the result of resonances or near resonances these results suggest why the behaviour is so widespread. However it might be that taking the largest of the growth - rates of whatever sign for the comparison is not a good idea. Basing a

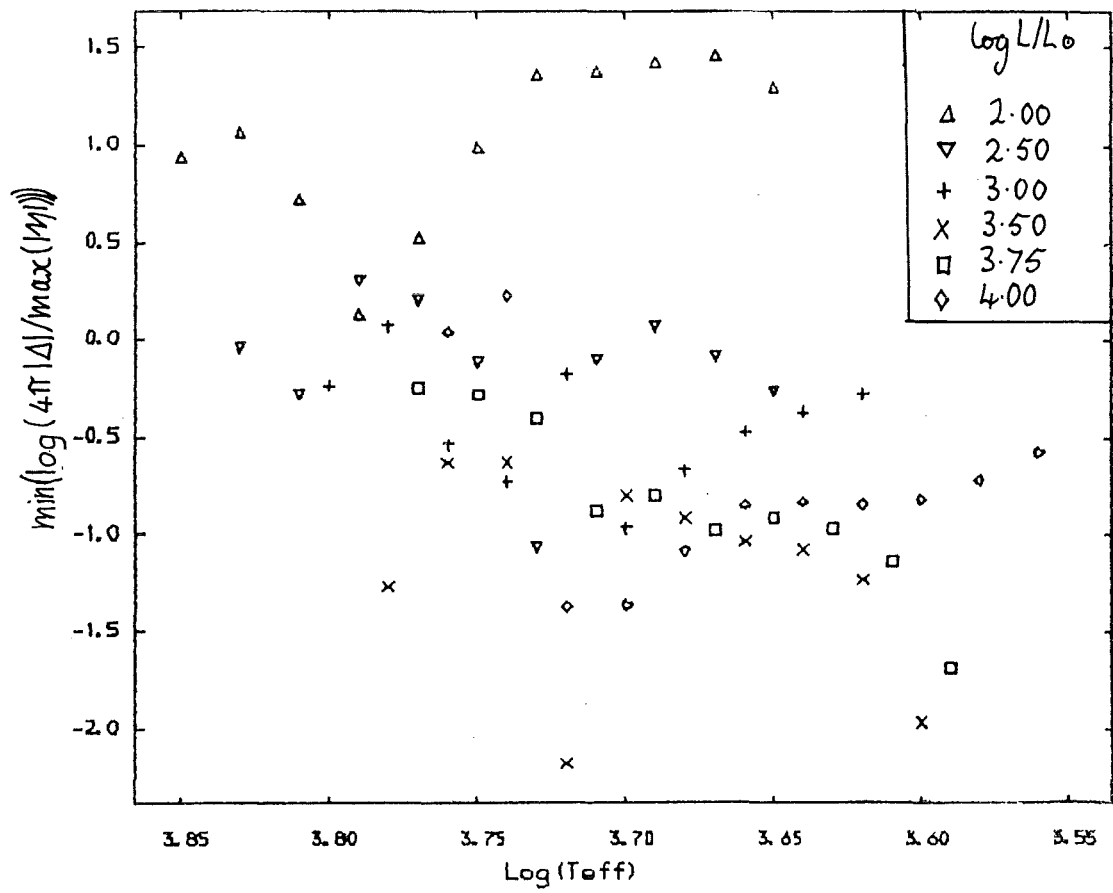


Fig. 8.12 $4\pi|\Delta|/\max(|M_i|)$ using the data derived using the Stellingwerf opacities and convection.

criterion for the presence of resonances on a very large negative growth - rate is a little dubious. So the experiment has been tried again but this time with $|\max(\mu_i, \mu_j)|$ etc. for the denominator. The results are a little less impressive. However for $\log(L/L_\odot) > 2.5$ and $\log(T_{\text{eff}}) > 3.75$ the same basic message comes through as before.

Table 8.3 contains the values of the period ratios P_1/P_0 and P_2/P_0 along the $[0,1;2]$ resonance locus for convective and radiative models constructed using the Stellingwerf opacity. Almost all of the values for P_1/P_0 for the convective models are close to or below $1/2$. For $\log(L/L_\odot) = 4.0$ in the convective models $P_1/P_0 = 0.74$ and for $\log(L/L_\odot) > 3.25$ in the radiative models there are ratios as high as 0.62 . Christy's (1966) hypothesis demands a very accurate satisfaction of the resonance condition because in his model there was not any evidence for beat periods or other effects of non-commensurability. It must also be fairly frequently satisfied in real life for such highly repeatable light curves as that for AC Her to exist.

To see whether or not the version of the resonance hypothesis advocated by Takeuti and Petersen (1983) will work the observed RV and SRd data must be shifted upward (in $\log(P_0)$) by 0.3 . If this is done (it is easily visualised) then using the convective models with the Stellingwerf opacity for the globular clusters the RV stars now lie above the $[0,0;1]$ resonance locus but coincide with a branch of the

Table 8.3

Values of period-ratios along the [0,1;2] locus

	$\log(L/L_{\odot})$	$\log(T_{\text{eff}})$	P_1/P_0	P_2/P_0
C STEL	2.50	3.732	0.521	0.343
		3.663	0.480	0.324
	3.00	3.746	0.477	0.323
		3.703	0.367	0.268
	3.50	3.719	0.456	0.313
		3.603	0.352	0.260
	3.75	3.680	0.565	0.349
	4.00	3.693	0.737	0.424
R STEL	3.00	3.731	0.484	0.326
		3.713	0.454	0.312
	3.25	3.862	0.601	0.375
		3.790	0.620	0.383
	3.50	3.868	0.567	0.362
		3.778	0.545	0.353
C W315	2.50	3.712	0.505	0.335

C = Convective; R = Radiative

Opacity: STEL = Stellingwerf opacity

W315 = Carson opacity; $Y=0.25$ $Z=0.005$

[0,0;2] locus. The SRd stars will now lie below the [0,0;1] locus. If the radiative models are used instead then all the stars lie above the [0,0;1] locus. The same trick moves almost all the Galactic RV stars onto or closer to one or other resonance loci. The two coolest RV(A) stars along with the bulk of the cool SRd stars still lie below all the resonance loci.

So there is no problem involved with making the RV stars lie on or near to a resonance locus and it is likely that all of the RV and SRd stars are to some extent affected by resonances. This is true for either of the alternate resonance hypotheses. What I cannot say on the basis of the linear results is how strong the effects of the modal interactions are. This really needs fully nonlinear hydrodynamical models. However the failure of nonlinear models (Simon, Cox and Hodson 1980; Buchler and Regev 1981) to explain the double - mode cepheids is worrying and bodes ill for such an enterprise.

Something which can easily be done is to guess the ratio of the amplitudes for the modes thought to be involved in the interaction and simply add the two, or more, waves together. This has been tried using period ratios from a great many of the more luminous linear models. The wave form adopted is:

$$|\sin(\pi t/P_j)|$$

since this gives the rounded maximum and sharp minimum characteristic of the RV light curves. Unfortunately the results are not inspiring.

Only for a very small range in the period ratio does the result look much like an RV light curve (i.e. $P_2/P_1 = 2/3$). Other values of the period ratio produce a light curve which is too irregular for even the most wayward of the RV stars. It could well be that this experiment is too naive to be a reasonable test, but taken at face value it makes the resonance hypothesis look inadequate for the task of producing RV light curves.

There is more evidence to support the view that the interaction of two or more modes cannot give a complete explanation of the RV light curves. Klyus (1981) has carried out Fourier analysis and autocorrelation analysis on the light curve of R Sct. He finds three significant periods of 71, 143, and 348 days in the power spectrum. It is worth remarking that if the overtone modes were present in sufficient strength to cause the characteristic shape of the RV light curves then they should surely appear in the power spectrum as significant peaks. The autocorrelation function decays rapidly with the shift applied so that for a shift of 2000 days it has fallen below the error limits. This indicates that there is a stochastic element in the light curve. Klyus proceeds by isolating the oscillation associated with each period using narrow band filters and shows, by means of autocorrelation functions, that all three of the modes have a stochastic element. Klyus (1981) makes a number of suggestions to account for the stochastic element, none of which I find very plausible. However the atmospheres of pulsating star models losing

mass (e.g. Willson and Hill 1979, Wood 1979, Tuchman, Sack and Barkat 1979) show highly irregular motions. The RV stars are known to have lost mass and at least one has been shown to be losing mass and models of RV stars show similar effects (Christy 1966, Bridger 1983). I think that this makes it very likely that pulsation driven mass loss is the source of the stochastic element in the RV light curves and that the mass loss is responsible for the alternation.

8.2 A DETERMINATION OF THE MASS AND LUMINOSITY OF UU HER

It is worth looking at the double mode RV(C) star UU Her in some detail because the knowledge of the additional period makes it possible, in principle, to determine the mass and luminosity independently. However UU Her is peculiar in a number of ways. Its most striking peculiarity is the presence, at different times but perhaps sometimes simultaneously, of two distinct oscillations in the light curve (Payne - Gaposhkin, Brenton and Gaposhkin 1943). There are segments of the light curve for which the period is 71.06 days and which look like cepheid light curves. Other portions are RV - like in shape and have a formal period of 90.40 days. However in addition to these modes identified by Payne - Gaposhkin et al. (1943) I find that there are three pieces of the light curve for which a period of about 45 days is most appropriate. Payne - Gaposhkin et al. (1943) suggest that a fundamental and a first - overtone pulsation period can be identified

$$P = 71.06 \text{ days}$$

$$P = 45.20 \text{ days.}$$

UU Her is also rather more metal poor ($[Fe/H] = -1.27$, Dawson 1979) than the other RV(C) stars ($[Fe/H] \approx -0.8$) but is similar in this respect to the globular cluster RV star M2 v11 ($[Fe/H] = -1.28$) and to the low metallicity SRd stars. It is also marginally the hottest of the RV(C) stars with

$$\log(T_{eff}) = 3.755$$

according to Dawson's (1979) D.D.O. photometry. Dawson also derives a mass for UU Her of $M = 0.36 M_{\odot}$ which is approximately independent of phase. This is not only considerably lower than his masses for all of the other RV stars but also much lower than the core masses expected for stars in this region of the H-R diagram (Eggleton 1968, Iben and Rood 1970, Gingold 1976).

Taking Dawson's (1979) UBV photometry obtained concurrently with the D.D.O. photometry and using the Bohm - Vitense (1973) $(B-V)_0 - \log(T_{eff})$ calibrations for metal poor super - giants gives after de - reddening

$$\log(T_{eff}) = 3.815 + 0.088$$

$$-0.051$$

However using the UBV data from Preston et al. (1963) gives

$$\log(T_{eff}) = 3.769 + 0.035$$

$$-0.038$$

or if Flower's (1977) temperature calibrations for normal super - giants are substituted,

$$\log(T_{eff}) = 3.808 + 0.028 \\ - 0.042$$

So the temperature derived for UU Her is highly uncertain even when identical methods are used.

Given two periods, which I assume are correctly identified, and an effective temperature it is possible to determine independently a mass and a luminosity for a star. The only remaining assumption to be made is that the star has a uniform chemical composition. This is assumed to be $(X,Y) = (0.745,0.25)$ since the metallicity is unimportant and for consistency with the other models in this study. After some preliminary probing, model sequences were constructed for $\log(T_{eff}) = 3.770, 3.755$ and 3.740 using the Stellingwerf opacity formula and the same convection as described earlier. The results of the calculations are displayed as tables 8.4 - 8.6 as lines of constant mass and luminosity in the $P_0 - (P_1/P_0)$ plane in fig. 8.13(a - c). UU Her is marked on each of the figures as a cross. From this data the mass and luminosity for each temperature are determined using a two dimensional nonlinear fit. The masses and luminosities are:

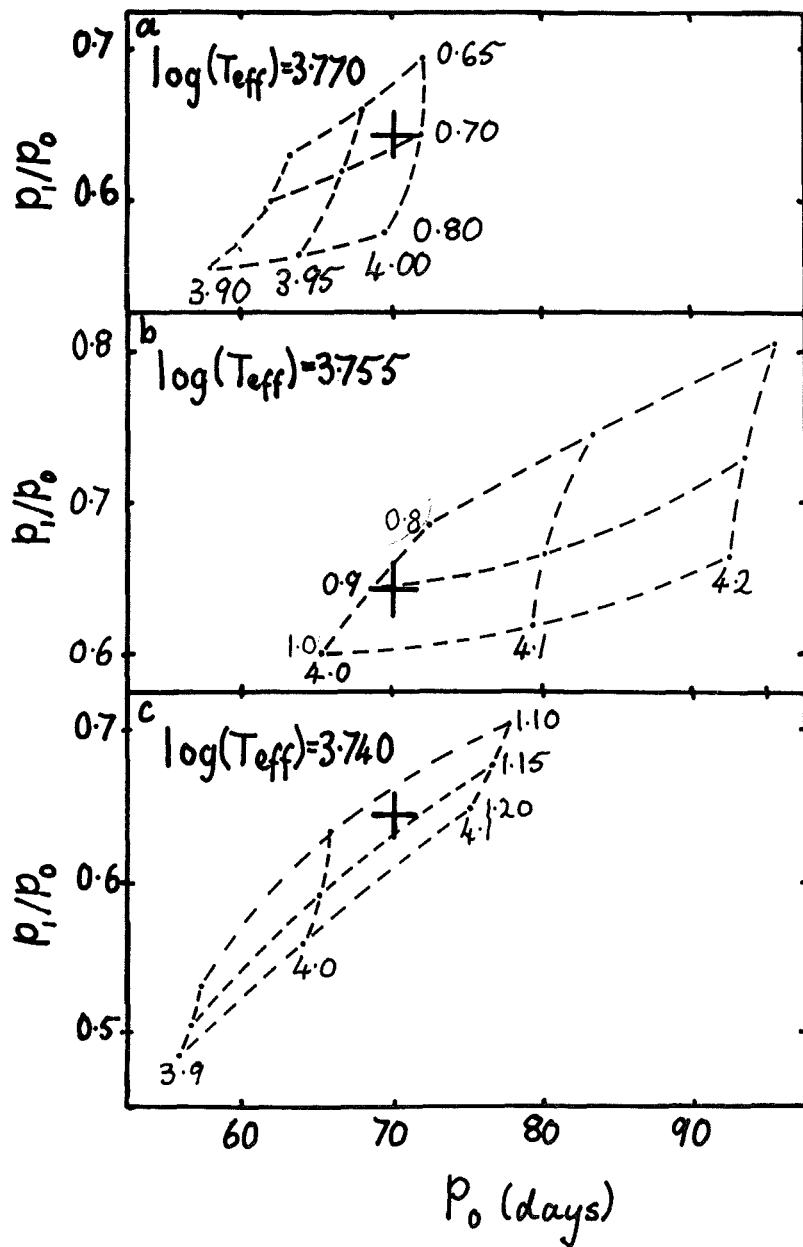


Fig. 8.13 Lines of constant mass and luminosity in $P_0 - P_1/P_0$ plane for $\log(T_{\text{eff}}) = 3.770, 3.755, 3.740$ together with UU Her.

$\log(T_{\text{eff}})$	M/M_{\odot}	$\log(L/L_{\odot})$	M_{bol}
3.740	1.1566	4.0425	-5.35
3.755	0.9287	4.0253	-5.30
3.770	0.7064	3.9924	-5.22

The mass derived using Dawson's (1979) D.D.O. effective temperature is rather higher than the mass ($0.6 M_{\odot}$) assumed previously for the RV stars. It is far higher than Dawson's mass calculated directly from the observations. However when the UBV effective temperature from Preston et al. (1963) is used the mass, whilst still larger than expected, is coming closer to the original assumption of $0.6 M_{\odot}$. Use of Dawson's (1979) UBV effective temperature or the alternative Preston et al. figure would close the gap.

It is unfortunate that the estimates of effective temperatures cover such a large range as to prevent a definitive determination of the mass and luminosity for this star. The reason for the difference is not at all obvious. It is clear that there is a considerable difference between the values of U, B, and V observed by Preston et al. and by Dawson. One possibility is that Dawson, with only six observations, failed to get sufficiently good phase coverage whereas Preston et al. made extensive observations covering three periods. However three of Dawson's six (B-V) values lie outside the limits of the observations of Preston et al. ($0.4 < (B-V) < 0.6$) as does his mean value ($\langle B-V \rangle = 0.36$). So either there are systematic errors

present in one or both of the sets of observations or the colour of UU Her has itself changed in the interval between the two observations. The phenomenon which springs to mind is sporadic mass emission which would presumably add a circumstellar component to the reddening law. However the possibility of systematic errors must be borne in mind.

An explanation is needed for the unique (amongst RV stars) modal behaviour displayed by UU Her. A look at tables 7.17 - 7.22 shows us that for temperatures lower than a certain value, at $\log(L/L_{\odot}) > 3.5$ the growth rate for the fundamental period is far greater than that for the overtones. We can thus expect the fundamental mode to be dominant, perhaps to the exclusion of other modes, for the bulk of the RV stars. However running down a model sequence towards higher temperatures it can be seen that the first overtone growth rate rises abruptly and the fundamental growth rate falls until after a short transition region the situation is reversed. This can be seen in more detail by comparing the growth rates given in tables 8.4 - 8.6 for the different temperatures. UU Her is, as observed earlier, unusually hot and indeed falls in this overtone dominated region.

An attempt can also be made to explain the presence of RV behaviour in the shorter period pulsation mode but not the longer period mode if it is assumed that the RV behaviour is the result of mass loss or incipient mass loss as in a number of nonlinear models

Table 8.4

Models for UU Her with $\log(T_{\text{eff}}) = 3.770$

M/M_{\odot}	$\log(L/L_{\odot})$	P_0	P_1	P_1/P_0	η_0	η_1
0.65	3.90	62.99	39.97	0.635	-0.127	7.00
	3.95	67.88	44.80	0.660	-0.114	7.11
	4.00	72.17	50.21	0.696	-0.133	7.33
0.70	3.90	61.84	36.92	0.597	-0.132	6.73
	3.95	66.50	41.37	0.621	-0.114	6.97
	4.00	71.92	46.40	0.645	-0.092	7.06
0.80	3.90	57.94	32.17	0.555	-0.240	6.51
	3.95	63.67	35.89	0.564	-0.165	6.60
	4.00	69.41	40.17	0.579	-0.112	6.73

Table 8.5

Models for UU Her with $\log(T_{\text{eff}}) = 3.755$

M/M_{\odot}	$\log(L/L_{\odot})$	P_0	P_1	P_1/P_0	η_0	η_1
0.80	4.00	72.64	49.71	0.684	0.393	6.87
	4.10	83.33	62.02	0.744	0.231	7.73
	4.20	95.61	77.07	0.806	0.037	8.10
0.90	4.00	68.45	44.14	0.645	0.375	6.41
	4.10	82.14	54.80	0.667	0.396	6.99
	4.20	93.59	68.45	0.731	0.234	7.85
1.00	4.00	65.29	39.38	0.603	0.351	5.71
	4.10	79.20	49.06	0.619	0.431	6.45
	4.20	92.38	61.39	0.665	0.370	7.27

Table 8.6

Models for UU Her with $\log(T_{\text{eff}}) = 3.740$

M/M_{\odot}	$\log(L/L_{\odot})$	P_0	P_1	P_1/P_0	η_0	η_1
1.10	3.90	57.41	30.34	0.528	2.48	2.13
	4.00	65.97	41.70	0.632	1.95	3.12
	4.10	77.76	54.83	0.705	1.46	4.90
1.15	3.90	56.77	28.60	0.504	2.54	2.06
	4.00	65.14	38.61	0.593	2.07	2.73
	4.10	76.47	51.84	0.678	1.56	4.43
1.20	3.90	56.08	27.16	0.484	2.59	1.99
	4.00	64.19	36.02	0.561	2.17	2.52
	4.10	75.25	48.91	0.650	1.65	3.96

(Christy 1966, Stobie 1969, Bridger 1983). If an impulse approximation is adopted for the atmospheric "particles" (Willson and Hill 1979) then a time scale, t_A , for the relaxation of the atmosphere from a shock can be derived. When $t_A/P \sim 1$, where P is the requisite pulsation period, the atmosphere is unable to relax between successive shocks and so is forced to expand. There is observational evidence to support the relation of t_A/P to mass loss in long period variable stars (Bowers and Kerr 1977). So if there is more than one period alternately present with similar amplitudes (since t_A is a function of the velocity amplitude) we should expect any phenomena connected with mass loss to be strongest in the shorter period mode. This appears to be the case for UU Her.

The alternative hypothesis for the RV behaviour (modal interaction) must also be considered. Numerical experiments in which two waves with the required period ratio of the form $|\sin(\pi t/P)|$ were combined produced very unconvincing RV behaviour. Although nonlinear interaction terms must have some effect upon the light curve I do not think that they can be responsible for the alternation characteristic of RV light curves. In UU Her it is presumably the nonlinear interaction of the modes which governs the switching back and forth between the 70 and 45 day modes.

8.3 A DETERMINATION OF THE MASS AND LUMINOSITY FOR THE HIGH LUMINOSITY F STAR HD161796

HD161796 is one of a number of high luminosity A and F stars found in the field. It is frequently compared with 89 Her and spectroscopic studies suggest that both stars have population I compositions (Searle, Sargent and Jugaku 1963; Abt 1960). However high luminosity A and F stars are also found in globular clusters. For example, HD116745 is, with $M_V = -3.3$, visually the brightest star in ω Cen (Sargent 1965; Cannon and Stobie 1973; Dickens and Powell 1973). Recently high resolution spectroscopy has shown HR4912 (Luck, Lambert and Bond 1983) and HD46703 (Luck and Bond 1984) to be metal poor with compositions suggesting that they are old, low mass stars. A preliminary reexamination of HD161796 by Luck, Lambert and Bond (Luck et al. 1983) gives indications that it too is metal poor.

A number of the 89 Her stars show light variations with time scales of the order of a few weeks. In the case of 89 Her itself (Ferne 1981) these are largely irregular, HD46703 (Luck and Bond 1984; Bond 1970) appears semiregular, and HR4912 (Luck et al. 1983) has a period or periods between 44 and 68 days. HD161796 (Ferne 1983) is unique because it is known to have periods of 43 and 62 days. During the time it was observed the star switched from pulsation with a period of 62 days to quiescence to pulsation with a period of 43 days. For both modes the light amplitude is small (0.07^m and 0.09^m).

respectively). Curiously the star is able "switch on" its pulsation instantaneously at full amplitude with no growth being visible.

The motivation for studying HD161796 lies in its association with HR4912. HR4912 has been studied in depth by Luck et al. (1983) who, on the basis of high resolution spectroscopic evidence, conclude that it is very similar in composition to the SRd stars. This leads them to describe the star as the brightest of the SRd stars. So it seems reasonable to assume that HD161796 is also a close relative of the SRd stars and on that basis to look at the mass and luminosity given by pulsation theory in the hope that this will shed light on the SRd stars.

Assuming that the periods given earlier are the fundamental (P_0) and first overtone (P_1) mode pulsation periods Fernie is able to derive a mass using Petersen's (Petersen 1973) theoretical pulsation data. He finds $M \approx 20 M_\odot$. Other methods based upon the assumption that this star is a relative of the classical cepheid variables yield similar masses. Using a radius derived from the cepheid period - radius relation and a temperature ($T_{\text{eff}} = 6300 \pm 170\text{K.}$) from his photometry he finds $\log(L/L_\odot) = 4.93$ or $M_{\text{bol}} = -7.5$. By using the Barnes - Evans surface brightness method (Barnes, Evans and Moffett 1978) and his own calibration for diametric amplitude with light amplitude (Fernie 1977) derived for classical cepheids Fernie obtains a similar luminosity.

Takeuti (1983) has constructed a number of linear, adiabatic pulsation models with similar masses ($M/M_{\odot} = 13.2 - 30$) and finds that this mass determination is justified. He also suggests that a triple resonance for which $1/P_0 + 1/P_1 = 1/P_2$ (as in double mode cepheids), with P_1 and P_2 being identified with the observed periods, is an alternative. However nonlinear studies by the same author appear to predict stability of the models.

My reason for detailing the previous mass determination is to make it clear that the entire analysis hangs upon the identification of the star as a population I star of high mass. The mass determined appears at first sight to be unique (within the error limits). However this is not the case. The results from linear, nonadiabatic pulsation calculations of stars with high mass - luminosity ratios (Takeuti 1983; Fox and Wood 1981) show that the period ratios P_j/P_0 are not monotonic functions of P_0 but show a distinct minimum. It follows that for given effective temperature (T_{eff}), P_0 and P_1 there will be two possible masses (and luminosities).

To determine the alternative, lower mass solution for HD161796 a set of linear, nonadiabatic pulsation models were computed. Stellingwerf's (1975) formula for the opacity was used for all the calculations with a "population II" composition of $(Y,Z) = (0.25,0.005)$ for the majority of the models and $(0.25,0.000)$ for a further short sequence. The mixing - length was chosen to be

equal to the pressure scale height. The effective temperatures used were; $\log(T_{\text{eff}}) = 3.78, 3.80, \text{ and } 3.82$. Periods and growth rates for the three pulsation modes with the longest periods form tables 8.7, 8.8 and 8.9. The first two modes are the fundamental and first overtone modes. It will be noticed that in one or two cases the fundamental period is shorter than the overtone period. An inspection of the eigenfunctions for modes shows that the fundamental mode eigenfunction acquires an extra node as the luminosity increases along a sequence but that there is a continuum of properties along this sequence. This seems like the best basis for making the identification. The third mode, for which the eigenfrequency is almost equal to the complex conjugate of the overtone, is probably a strange mode as defined by Saio et al. (1984). This mode is labelled with the subscript 's' (P_s). The same authors also show that the complex conjugal relationship of the latter two modes is a natural consequence of extreme nonadiabaticity, that is, where $|\eta/4\pi| \rightarrow 0$ does not hold.

A comparison of the models for the two different compositions shows that the effect of varying the metallicity is small. It seems reasonable to suppose that the observed modes will be the marginally stable fundamental and the highly unstable first overtone. Fig. 8.14 shows P_1/P_0 plotted as a function of P_0 for $\log(T_{\text{eff}}) = 3.82$. There is no problem in finding a mass for HD161796. The results of the mass and luminosity determination are;

Table 8.7

Models for HD161796 with $\log(T_{\text{eff}}) = 3.78$

Z	M/M _⊙	log(L/L _⊙)	P ₀	P ₁	P _s	P ₁ /P ₀	P _s /P ₀	η ₀	η ₁	η _s
0.005	0.60	4.0	71.41	50.69	43.93	0.710	0.615	-0.241	6.74	-4.18
		3.9	62.57	38.97	33.44	0.629	0.534	-0.292	6.75	-3.34
		3.8	53.72	30.62	27.66	0.570	0.515	-0.379	6.43	-2.16
	0.55	4.0	71.24	57.12	50.19	0.802	0.705	-0.287	6.71	-3.86
		3.9	63.50	43.49	37.26	0.685	0.587	-0.282	6.71	-3.86
		3.8	55.15	33.84	29.07	0.614	0.527	-0.340	6.60	-2.90
	0.50	4.0	69.94	66.17	59.58	0.946	0.852	-0.386	6.80	-4.73
		3.9	63.82	49.26	42.64	0.772	0.668	-0.320	6.74	-4.19
		3.8	56.35	37.87	32.18	0.672	0.571	-0.323	6.71	-3.57
0.45	4.0	68.39	79.33	74.28	1.160	1.086	-0.322	6.97	-5.26	
	3.9	62.99	57.53	50.92	0.913	0.808	-0.445	6.74	-4.41	
	3.8	57.00	43.24	36.95	0.759	0.648	-0.359	6.74	-3.96	

Table 8.8

Models for HD161796 with $\log(T_{\text{eff}}) = 3.80$

Z	M/M _⊙	log(L/L _⊙)	P ₀	P ₁	P _s	P ₁ /P ₀	P _s /P ₀	η_0	η_1	η_s
0.005	0.60	4.0	68.07	45.82	42.77	0.673	0.628	-0.372	6.41	-5.55
		3.9	59.56	34.29	31.51	0.576	0.529	-0.518	5.96	-4.79
		3.8	51.01	25.92	22.68	0.508	0.445	-0.660	5.49	-3.62
	0.55	4.0	67.87	52.34		0.771		-0.325	6.62	
		3.9	60.44	38.75	35.88	0.641	0.594	-0.456	6.20	-5.24
		3.8	52.44	29.15	26.54	0.556	0.506	-0.594	5.76	-4.34
	0.50	4.0	67.30	57.36		0.852		-0.275	6.49	
		3.9	60.65	44.64	41.65	0.736	0.687	-0.403	6.42	-5.56
		3.8	53.58	33.25	30.60	0.621	0.571	-0.528	6.03	-4.95
0.45	4.0	65.32	69.29	66.71	1.061	1.021	-0.217	6.82	-6.11	
	3.9	59.79	53.05	50.11	0.887	0.838	-0.361	6.66	-5.85	
0.000	0.50	4.0	67.08	57.76		0.861		-0.325	6.57	
		3.9	60.41	44.97		0.744		-0.485	6.49	
		3.8	53.26	33.49		0.629		-0.617	6.11	

Table 8.9

Models for HD161796 with $\log(T_{\text{eff}}) = 3.82$

Z	M/M _⊙	log(L/L _⊙)	P ₀	P ₁	P _s	P ₁ /P ₀	P _s /P ₀	η_0	η_1	η_s
0.005	0.6	4.0	66.23	39.66	38.30	0.599	0.578	-0.448	6.23	-5.86
		3.9	57.08	29.50	28.31	0.517	0.496	-0.617	5.57	-5.06
		3.8	48.17	22.11	22.02	0.459	0.441	-0.756	4.93	-1.47
	0.55	4.0	66.59	45.34	43.90	0.681	0.659	-0.371	6.53	-6.19
		3.9	58.42	33.46	32.25	0.573	0.552	-0.543	5.92	-5.52
		3.8	49.94	24.99	23.83	0.500	0.477	-0.695	5.28	-4.65
	0.50	4.0	65.95	53.13	51.69	0.806	0.784	-0.289	6.85	-6.50
		3.9	59.20	38.60	37.28	0.652	0.630	-0.462	6.26	-5.90
		3.8	51.49	28.63	27.56	0.556	0.535	-0.622	5.65	-5.22
0.45	4.0	64.36	64.46	63.21	1.002	0.982	-0.196	7.24	-6.93	
	3.9	58.93	45.78	44.39	0.777	0.753	-0.376	6.59	-6.23	
	3.8	52.52	33.44	32.24	0.637	0.614	-0.539	6.02	-5.67	

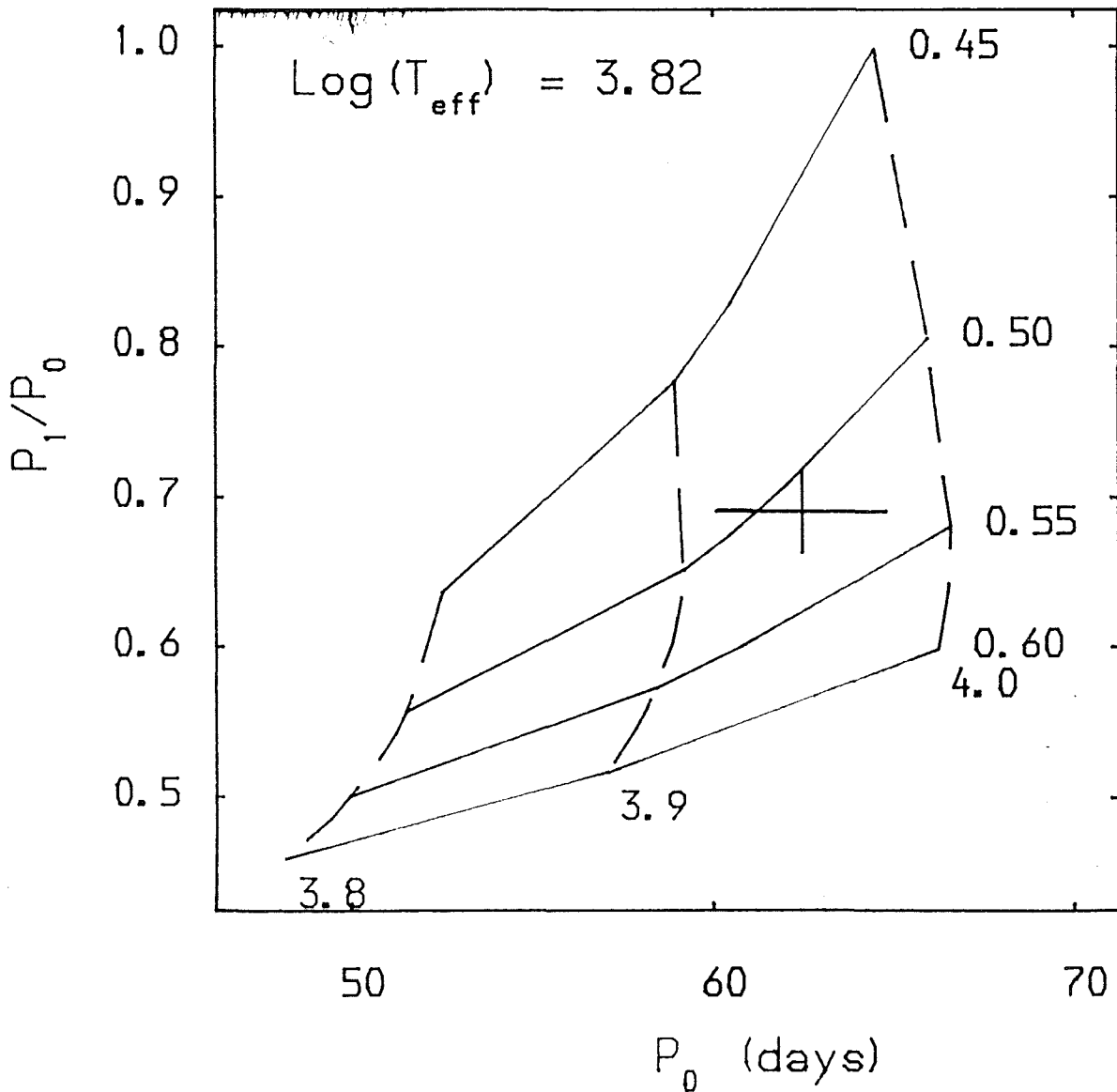


Fig. 8.14 Lines of constant mass and luminosity in the $P_0 - P_1/P_0$ plane for $\log(T_{\text{eff}}) = 3.82$ together with HD161796.

$\log(T_{eff})$	M/M_{\odot}	$\log(L/L_{\odot})$	M_{bol}
3.78	0.540	3.886	-4.956
3.80	0.539	3.925	-5.052
3.82	0.511	3.946	-5.105
	± 0.031	± 0.034	± 0.085

The errors given in the table are derived from the errors on the observed periods alone. When the error on the temperature quoted by Fernie is taken into account then additional uncertainties of about $0.017 M_{\odot}$ and 0.023 on the mass and $\log(L/L_{\odot})$ respectively. The main uncertainty in the model is probably the value of the mixing length. A set of models with $\log(T_{eff}) = 3.80$, $M = 0.54 M_{\odot}$, and $\log(L/L_{\odot}) = 3.925$ using ratios of the mixing length and pressure scale height of 0.5, 1.0, and 2.0 were computed. The variations in the fundamental period and in the period ratio (P_1/P_0) are less than 1% and 5% respectively. This implies a negligible effect on the results. So the total uncertainties on the mass, $\log(L/L_{\odot})$, and M_{bol} can be estimated to be $0.023 M_{\odot}$, 0.041 , and 0.10 respectively.

The modal interaction must be considered. Resonant interactions become important when the condition $|\Delta| \lesssim |\eta/4\uparrow|$ is satisfied. Here $\Delta_{ij} = 2(P_j/P_i - 1/2)/(P_j/P_i + 1/2)$ for a double mode resonance, $P_j/P_i \approx 1/2$, or $\Delta_{ijk} = P_i/P_k/(1 + P_i/P_j) - 1$ for the triple mode resonance. As an example consider the model with $M = 0.55 M_{\odot}$ and $\log(L/L_{\odot}) = 4.0$ for $\log(T_{eff}) = 3.82$. There are three values of $|\eta/4\uparrow|$ which are 0.030, 0.52, and 0.49 for the respective modes.

The three relevant Δ 's are; $\Delta_{01} = 0.31$, $\Delta_{05} = 0.27$, and $\Delta_{15} = -0.39$ so it is clear that all these three modes should be considered in the interaction. However because the resonance theory requires that $|\eta/4\pi| \ll 1$ to be able to make quantitative predictions of stability and limit cycles we can go no further. However it seems at least possible that the large growth rates involved (the of amplitude of the overtone could increase by a factor of $\exp(6.5/2)$ in a single period) can explain the rapidity with which HD161796 begins its pulsations. The influence of the highly stable strange mode might also result in the low amplitude of the pulsation.

Pulsation theory gives us a choice of two masses for HD161796. The low mass interpretation can provide the correct periods for a reasonable population II mass, can explain the existence of pulsations, and perhaps go some way toward explaining the details of the pulsation. The mass and luminosity fit well with the interpretation of these stars as post - asymptotic giant branch (AGB) stars (Luck et al. 1983, Luck and Bond 1984) based upon the results of high resolution spectroscopy. On the other hand a representative high mass model, computed using the same composition, opacity, and mixing - length as before, with $M = 20 M_{\odot}$, $\log(L/L_{\odot}) = 5.15$ and $\log(T_{\text{eff}}) = 3.80$ for which $P_0 = 63.7$, $P_1 = 43.7$, $\eta_0 = -0.41$, and $\eta_1 = -0.71$ cannot explain the instability. It also demands an explanation of the anomalously large distance of the star from the Galactic plane which is implied by the derived luminosity. The

results from the surface - brightness method are derived using the assumption that the mass is high and so cannot be regarded as independent evidence for that hypothesis. Even if the high mass is correct it still requires a large upward extrapolation in period and a large downward extrapolation in light amplitude to use the method. So, on the whole, I think that the low mass interpretation is the simpler and more natural of the two alternatives.

Further theoretical study of this star should be interesting. The combination of a near perfect sinusoidal light curve and a very small amplitude make it a "text - book" example of a weakly nonlinear pulsator. This should serve to make it useful for comparisons of resonance theories which, hopefully, will be developed without the restrictions on the nonadiabaticity. More observations of HD161796 are required to increase our knowledge of the interaction and in particular to determine whether or not the same ephemeris is maintained from one appearance of a mode to another. If the latter effect is observed then it would confirm that the light curve is the result of a sustained multi - mode pulsation rather than being sporadically excited.

CHAPTER 9

NONLINEAR MODELS

9.1 THE NONLINEAR PROGRAMME

The nonlinear, hydrodynamic pulsation programme used for the work described in this chapter was written by Dr. T.R. Carson and I am indebted to him for allowing me to use it. This programme is based on Christy's (1967) methods, that is to say it employs a semi - implicit differencing scheme with correct centring in time and space to second order. An explicit integration of the dynamical equations is carried out at the start of each time - step and then the equation for energy conservation, the radiative transfer equation (in the diffusion approximation), and the equation of state are solved simultaneously by iteration on the temperatures using a Newton - Raphson method. As in Christy's work all of the energy is assumed to be transferred by radiation (and conduction). Convection is completely ignored. The difference equation used for the radiative transfer equation is Christy's final form. The finite difference method is unable to cope with shock waves by itself and the presence of a shock wave prompts

the dynamical variables on either side of the shock to oscillate wildly with a short wavelength about the true solution. This aberrant oscillation of the zones, which can be likened to the oscillations of atoms in a crystal, is suppressed in this application by the introduction of an artificial viscosity which smears all velocity variations over a number of zones rather than the single zone which they would otherwise occupy. The form used for the artificial viscosity is that given by Stellingwerf (1975).

The boundary conditions used at the surface of the star are not the same as those used by Christy (1967). Rather than set the pressure at the outer boundary to $P_N = 0$ the expression $P_N = P_{Nrad}$ is used. The boundary condition for the radiation equation has also been improved so that the Stefan - Boltzmann equation, $L = 4\pi R_{ph}^2 T_{eff}^4$, is satisfied properly. Christy used the approximation $R = r_{N+1}$ which whilst fine for such stars as the RR Lyrae variables which have very shallow atmospheres is a poor approximation for the type II cepheids. In the programme used here the radius R may be found by interpolation in temperature to T_{eff} or by taking the radius of the zone with a temperature closest to T_{eff} . Initially some problems were experienced using the "exact" form of this boundary condition and so a number of models were constructed using the latter approximation. This seems to make little difference.

The base of the envelopes, at which the lower boundary conditions are applied, is set so that $R_{\text{inner}}/R_{\text{L}} = 0.05 - 0.10$

The division of the model into zones is performed using one of two algorithms. One is a simple zoning by mass as described by Christy (1967) in which the mass of each successively deeper zone is greater than the last by a constant factor which is generally between 1.3 and 1.1 but which in some of the models to described here could be as small as 1.00003. The alternative is more sophisticated and attempts to increase the resolution of the model in the outer envelope. In this case the star is divided up into zones across which the sound travel time is roughly equal and so the time - step prescribed by the Courant condition is optimised. The result is fine zoning near the surface but fairly coarse zoning near the base of the envelope.

For all of the models the equation of state is computed in situ and includes the first five positive ionisation states for H, He, O, and Mg together with the relevant negative ions. A number of models were computed with the inclusion of hydrogen molecules.

Two opacities were used for the calculations both of which are based on the Carson (1976) table for $Y = 0.25$ and $Z = 0.005$. One of these is essentially identical to that used in the linear pulsation work described earlier and by Bridger (1983) in his study of the W Vir stars. That is for temperatures above $\log(T_{\text{eff}}) = 3.8$ the Carson

table is used whilst for the lower temperatures values computed using the Christy formula are substituted for the original data. A number of models were also computed using a molecular and grain opacity interpolated from Alexander's (1975) data (his more recent, rather more accurate data, Alexander 1983, cannot be used because it is too sparse). This is used for temperatures below $\log(T_{eff}) = 3.9$ in the same way as the Christy data.

The models are started with an initial velocity perturbation given by

$$U(r) = -10 (r/R_{ph})^5 \text{ km/s.}$$

Plots of the difference between the time varying bolometric magnitude and its equilibrium value at the surface are made as a matter of course. The radius and velocity for the zone interface which corresponded to the photosphere in the equilibrium model are also plotted. The work function and integrated work function can also be plotted up.

The period of the oscillation used in the calculation of the work function and listed as a representative period for the star is determined deep in the envelope.

9.2 MODELS WITH "STANDARD" PHYSICS

These models were constructed using the usual Eddington Approximation boundary condition for the luminosity and so do not take into account the effects of spherical geometry. It follows that the temperatures in the models will never fall much below 80% of the effective temperature and so the formation of molecules and molecular opacities can safely be ignored. The models were constructed for the following parameters:

Log(L/L _⊙)	Log(T _{eff})				
3.2	3.76	3.74	3.72	3.70	3.65
3.5	3.74	3.72	3.70		

The limit for successful radiative models is thought to be about $\log(T_{eff}) = 3.70$. However, this is fairly arbitrary and a model was constructed at the cooler temperature to see just what would happen. All of the models were constructed with approximately 50 zones distributed using the equal sound travel time algorithm. As an experiment a number of models were constructed using the $P_N = 0$ boundary condition sometimes in combination with the Christy luminosity boundary condition.

9.2.1 The Sequence For $\text{Log}(L/L_0) = 3.2$

$\text{Log}(T_{\text{eff}})$	P (days)	Growth - rate
3.76	21.2	0.43
3.74	24.5	0.89
3.72	30.2	1.35
3.70	29.34 - 0.131N	1.8
3.65	51.86 - 1.07N	1.6

(Here N is the cycle number for the pulsation.)

The peak kinetic energies and periods for these models are plotted in figs. 9.1 and 9.2 respectively. For each model the peak kinetic energy executes a rapid almost perfectly exponential rise which halts abruptly. For the hottest of the models this is followed by a phase of roughly constant peak kinetic energy. However as we move along the sequence to lower temperatures it can be seen that the constancy of peak kinetic energy disappears until for the coolest model massive period to period variations are apparent. On the whole, though, the peak kinetic energy can be seen to increase as the equilibrium temperature decreases as does the initial growth - rate. An immediate consequence of this erratic behaviour is the loss of the most useful criterion for determining whether or not the pulsation is fully grown. However because the growth - rates are so large it is safe to assume that in the cooler models all transients have died out within a few periods.

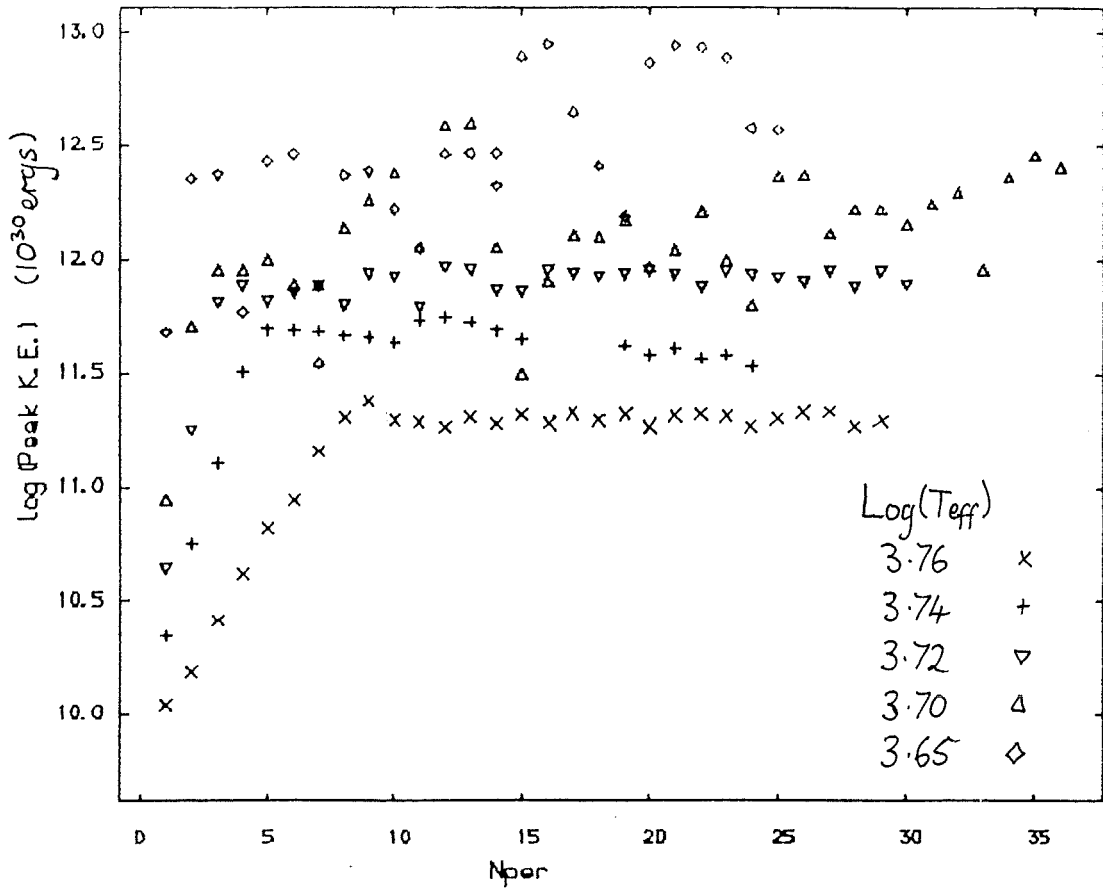


Fig. 9.1 Peak kinetic energies for the model sequence with $\log(L/L_{\odot}) = 3.2$

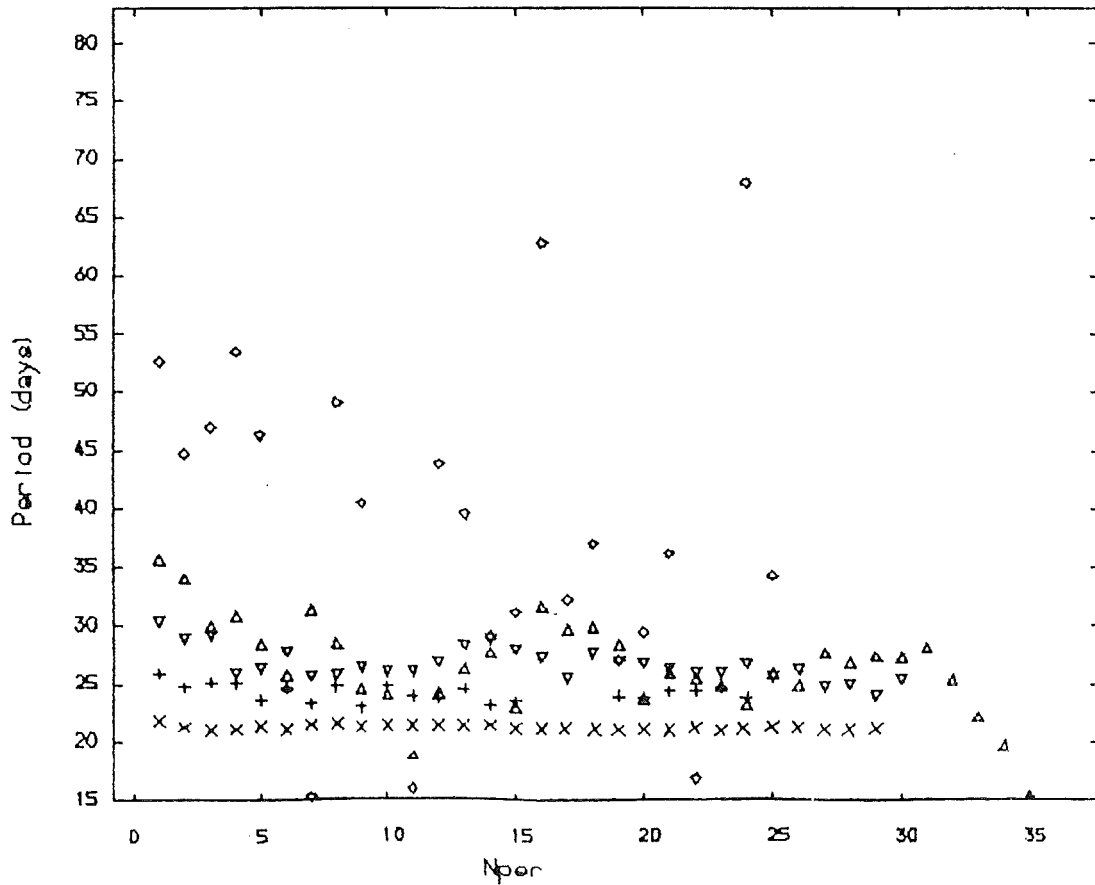


Fig. 9.2 Periods for the same models as above

Fig. 9.2 shows us that the same erratic behaviour also appears in the periods determined deep in the envelope from the radii. The periods determined well after the initial growth fall off as time progresses and so are given above as a linear formula for the cooler models. A feature of the $\log(T_{eff}) = 3.65$ model is the doubling up of periods and also the occurrence of a number of very short periods. The period formula is determined with these outlying periods omitted. All of these features are the result of the violent behaviour of the outermost layers of the stars. Because of the period variations it makes no sense to phase the data and plot up a single period, rather, whole slices of the data are plotted instead.

We can move now to an examination of the individual models.

9.2.1.1 $\log(T_{eff}) = 3.76$ -

Fig. 9.3 shows the radius, radial velocity, and light curves for a number of periods for this model. In the notation of Kwee (1967) the light curve is "crested". The light and velocity curve for this model are very like many of those found in Bridger's (1983) survey of hotter and less luminous models. An examination of the radii throughout the model shows that from the sixth and seventh period on the outermost zone boundary oscillates with a formal period twice that of the rest of the star. Every second period the descending outer zone meets the zone below as it ascends and is driven out again to a

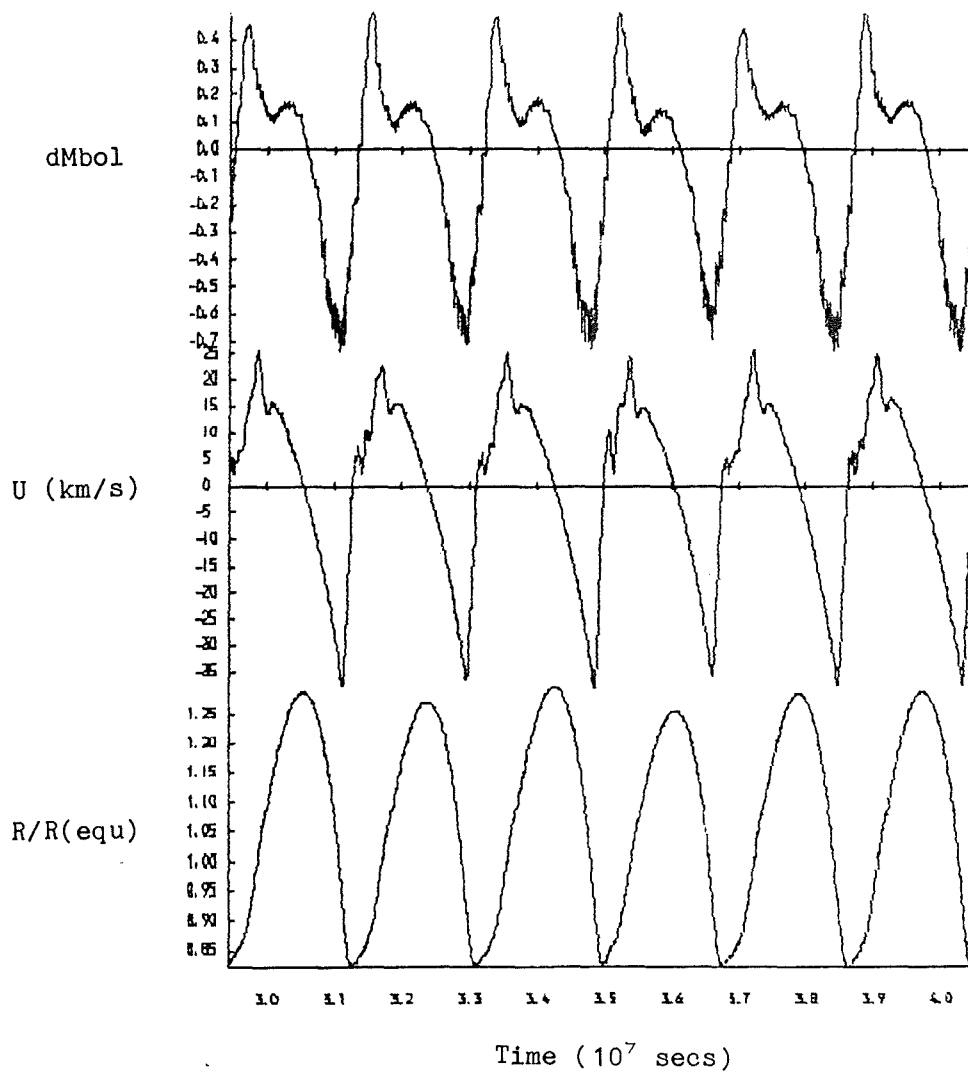


Fig. 9.3 $\text{Log}(L/L_{\odot}) = 3.2$, $\text{log}(T_{\text{eff}}) = 3.76$

great distance (from $55 R_{\odot}$ to $70 R_{\odot}$). After a while the period of the outer layer doubles again. The shock which results from the encounters of the outer zone with the rest of the star dissipates energy and produces a dip in the work function near the surface and the effect of this is reflected in the variations of the peak kinetic energy as can be seen in fig. 9.2. The accompanying cyclic variation in the light amplitude is about 0.06 and the variation in the light minimum about 0.035.

9.2.1.2 $\text{Log}(T_{\text{eff}}) = 3.74 -$

In most ways the early history of this model is identical to that of the previous model. However here the alternation is rather stronger and an examination of the radii for all of the zone boundaries shows that now a large proportion of the matter outside of the photosphere is involved. From period 14 onwards the light amplitude of the even numbered periods is $1^{\text{m}}.6 - 1^{\text{m}}.7$ whilst that for the other periods is $1^{\text{m}}.1 - 1^{\text{m}}.4$. The depth of minima alternate with variations of $0^{\text{m}}.2 - 0^{\text{m}}.3$ although at period 23 the order of the alternation reverses. Light, radius, radial velocity curves are shown in fig. 9.4. From period 26 on the peak kinetic energy oscillates around $3 \cdot 10^{11}$ ergs on a time scale of about 12 periods. As can be seen in fig. 9.5 the crest on the light curve decays slowly until period 18 at which point the star enters a new stage in its life. At this point the light amplitude falls for a couple of periods and the

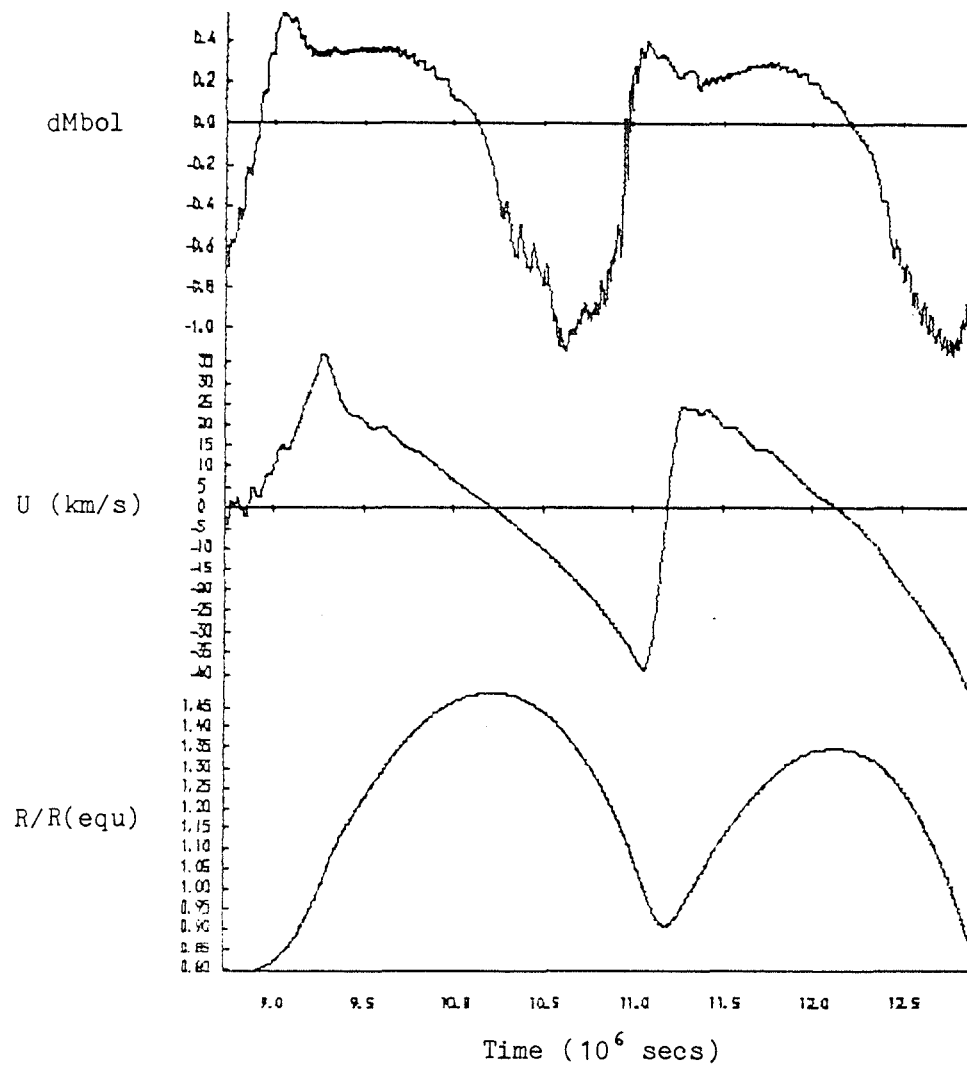


Fig. 9.4 $\text{Log}(L/L_{\odot}) = 3.2$, $\text{log}(T_{eff}) = 3.74$

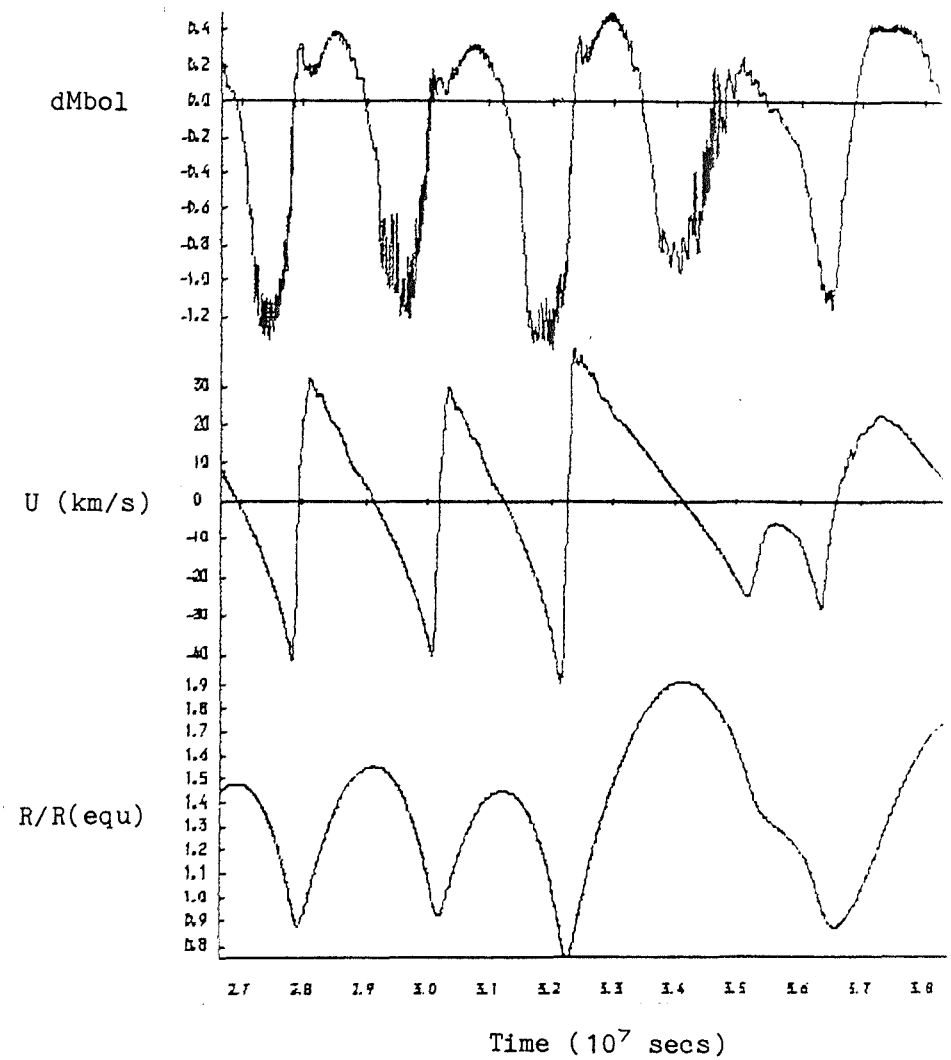


Fig. 9.5 $\text{Log}(L/L_{\odot}) = 3.2$, $\text{log}(T_{eff}) = 3.74$
(continued)

light curve loses the crest altogether. This change in the light curve is a result of the expulsion of the outer mass zone and the subsequent relaxation of the disturbed underlying zones as can be seen from fig. 9.6. From this point on the model degenerates steadily with the luminosity undergoing a steady decline in mean value and amplitude until eventually the model crashes through there being too small a density in the outer zone. As the mean light output diminishes there is an accompanying loss of detail from the light curve until it almost perfectly smooth, fig. 9.7. The curious behaviour of the luminosity at the outer zone boundary is not shared by that at the next boundary down. In fact there is a slowly growing luminosity gradient in the outer zone which implies, through the conservation of energy, that the heat content of this zone is steadily increasing. The mean effective temperature remains constant and so because of the nature of the luminosity boundary condition, the mean temperature of the outer zone must also remain roughly constant. With the rapid increase of the volume of the outer zone the gas pressure here soon falls well below the radiation pressure and reaches a lower limit. An application of the first law of thermodynamics using the well known expressions for the internal energy and pressure of radiation tells us that the outer zone is indeed expanding! We find that

$$\frac{\partial L}{\partial m} = -u \left(\frac{d \log u}{dt} + \frac{1}{3} \frac{d \log V}{dt} \right)$$

and since $V \rightarrow 1/\Delta M \cdot 4\pi/3 R^3$ as $R_{ph}/R \rightarrow 0$, and also $dR/dt \rightarrow v_{\infty}$

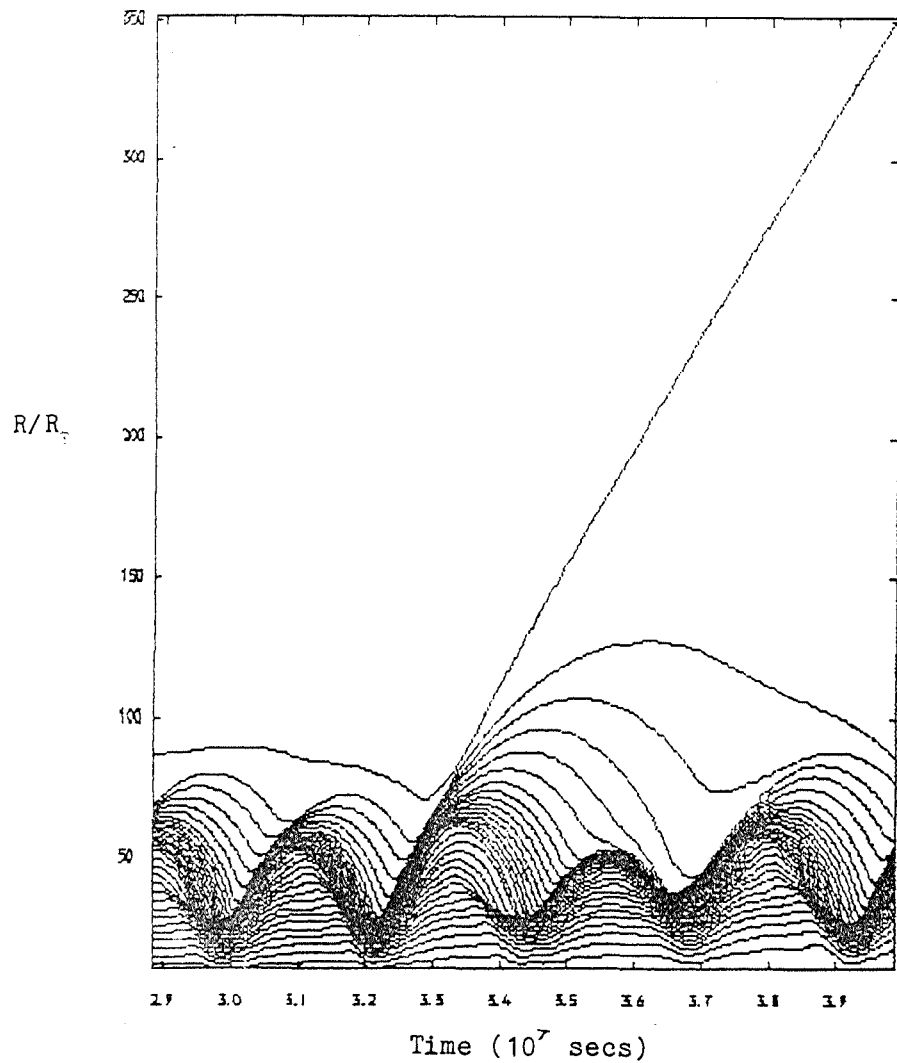


Fig. 9.6 $\text{Log}(L/L_{\odot}) = 3.2$, $\text{log}(T_{\text{eff}}) = 3.74$
Radii of zone boundaries

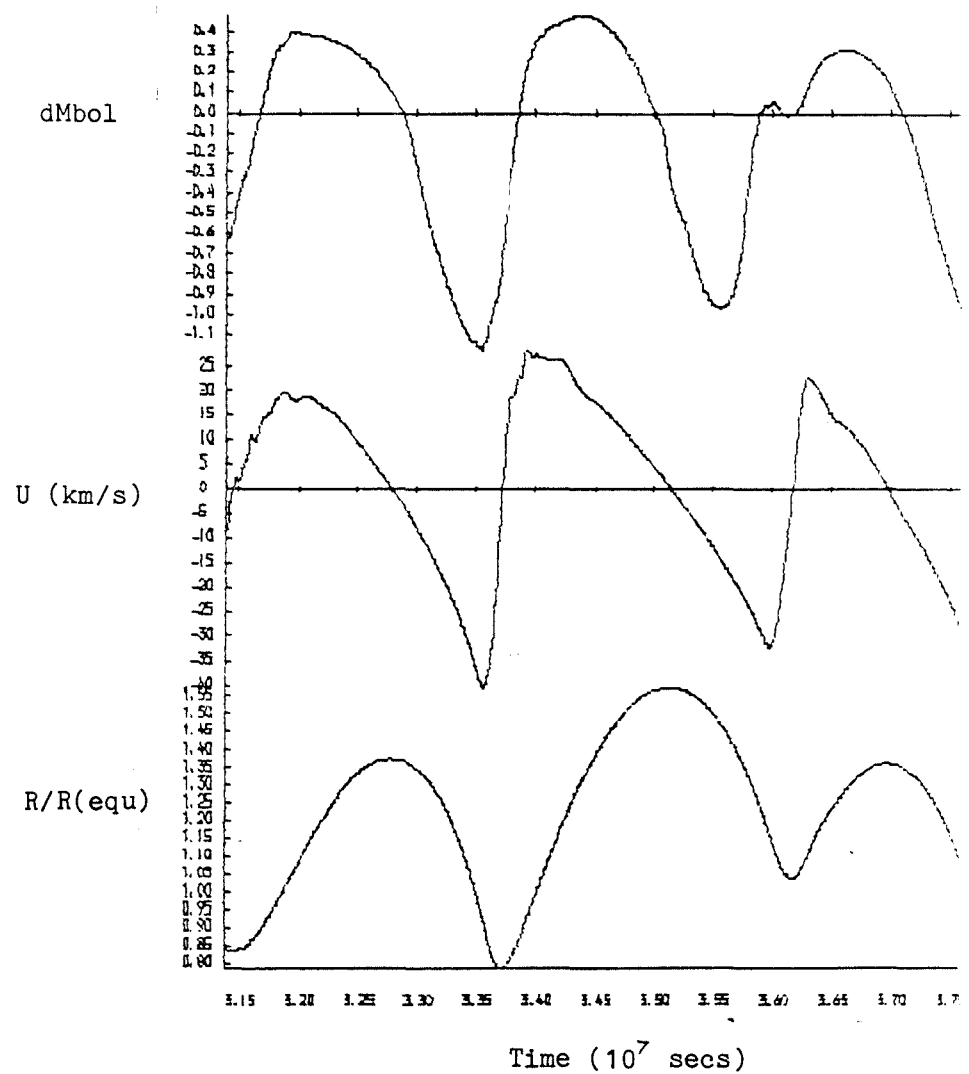


Fig. 9.7 $\text{Log}(L/L_{\odot}) = 3.2$, $\text{log}(T_{\text{eff}}) = 3.74$
(continued)

$$\frac{\partial L}{\partial M} \longrightarrow - \frac{4V_{\infty}}{3C} \frac{R^2}{R_{ph}^2} \frac{L}{\Delta M}$$

and so the luminosity gradient is negative and rapidly increases in magnitude as the outer radius moves off to infinity. Many workers in the field appear to study the luminosity at the base of the outer zone rather than at the top because it is more "reliable". This might be the case but I feel that it is conceptually wrong and so I persist in using the outer boundary as my reference point. Either the drop in luminosity is real and so should be found in nature or the model of the outer boundary is incorrect and should be investigated and not hidden.

However during the more tranquil moments of the model it does show behaviour very like that of some of the W Vir / incipient RV Tauri stars discussed by Erleksova (1970) (e.g. SZ Mon, and MZ Cyg). The magnitude of the amplitude variations in the model is as great as or greater than those found in these stars. The loss of the outer mass zone is accompanied by a disturbance in the light curve with a temporary reduction in amplitude which is reminiscent of disturbances found in some RV light curves from time to time.

9.2.1.3 $\text{Log}(T_{\text{eff}}) = 3.72 -$

The tendency to greater irregularity is continued in this model. The outer zone is expelled more quickly than before and the light rapidly develops marked differences in the depth of alternate minima. This can be seen in figs. 9.8 - 9.10. The last figure shows the light curve after the "decay" has well and truly set in. Whilst it is tempting to see these light curves as reasonably good representations of RV Tauri, or in the last moments as SRd, light curves it is easily seen that the cycle length is more likely three times the pulsation period. However there are some portions of some RV Tauri light curves, and R Sct is probably the best example, which do show behaviour a little like this. Fig. 9.11 shows the work integral for a period from this model. Two features are of interest. The first is that the work integral is not zero as is the case in models of perfectly periodic stars. Also noticeable is the presence of damping in the very outer layers of the model. This can be traced back to the presence of strong shock waves in the zones undergoing the long period oscillations.

As an experiment a further model was constructed for these parameters but with the luminosity boundary condition replaced by the Christy approximation. Fig. 9.12 shows the peak kinetic energies for both models and the periods are displayed as fig. 9.13. It is easy to see that although the first model, using the accurate boundary

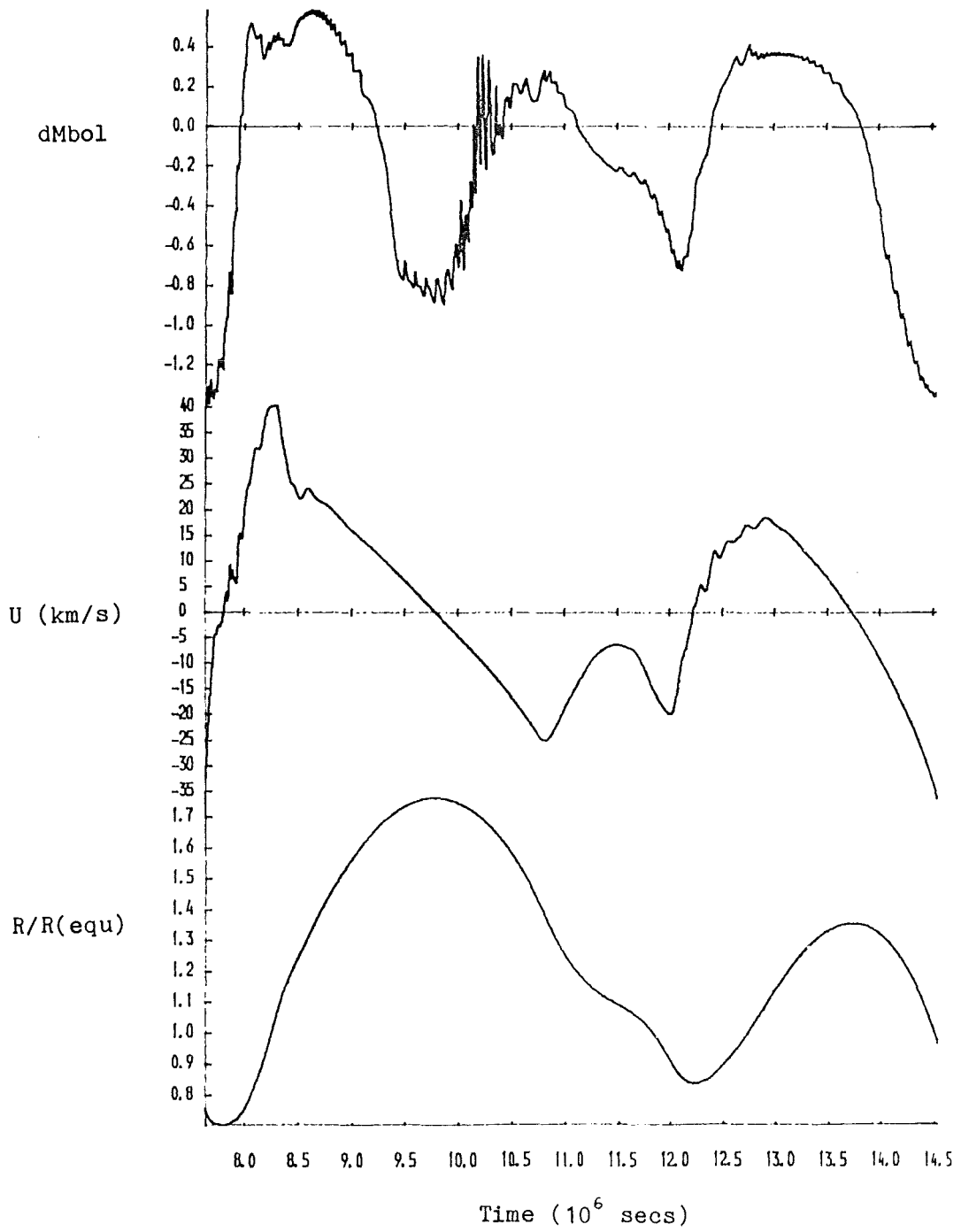


Fig. 9.8 $\text{Log}(L/L_{\odot}) = 3.2$, $\text{log}(T_{\text{eff}}) = 3.72$

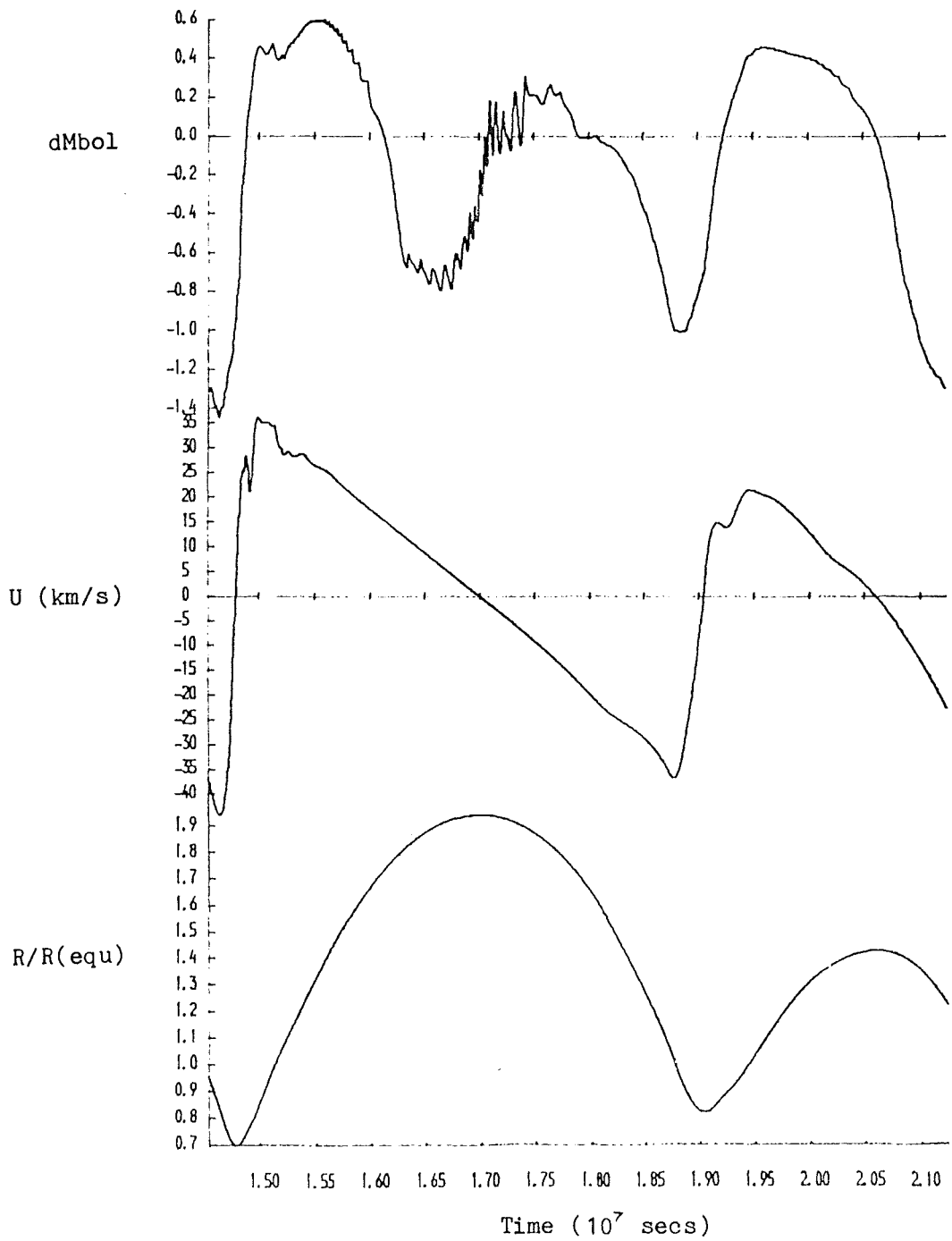


Fig. 9.9 $\text{Log}(L/L_{\odot}) = 3.2$, $\text{log}(T_{eff}) = 3.72$
(continued)

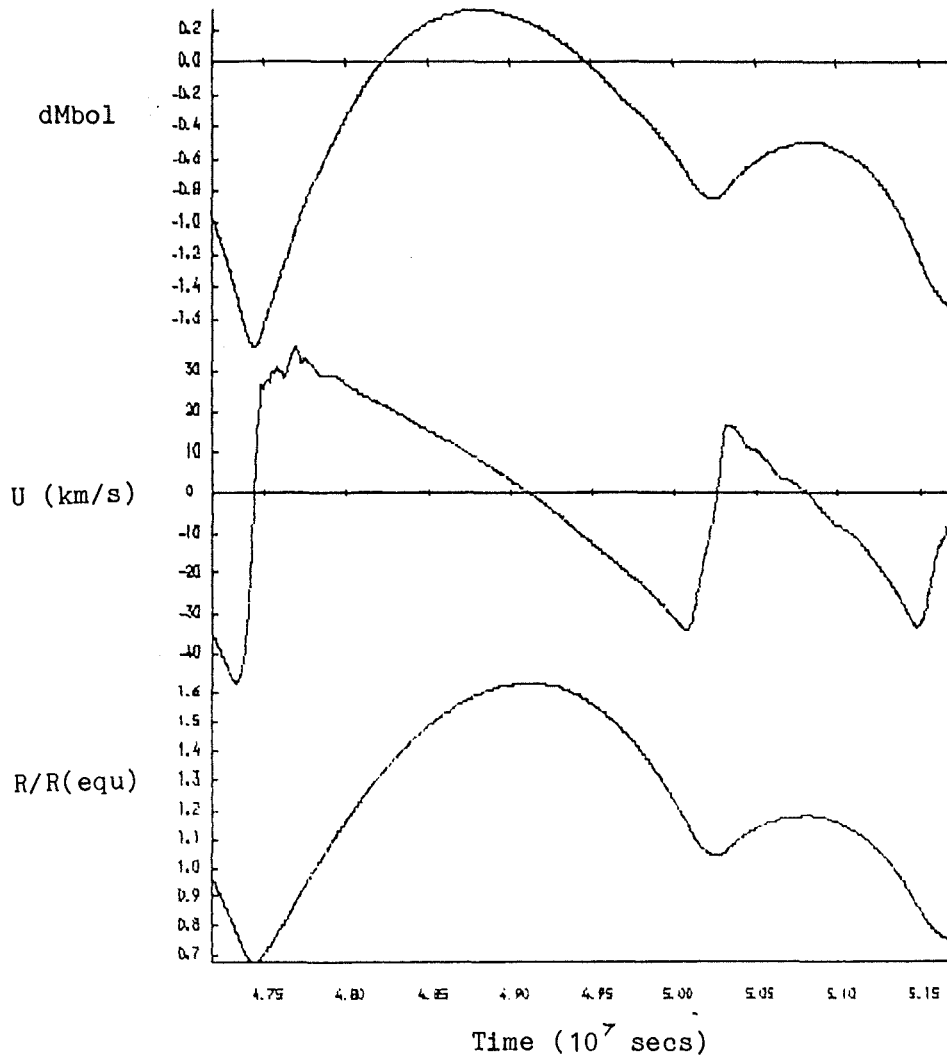


Fig. 9.10 $\text{Log}(L/L_{\odot}) = 3.2$, $\log(T_{\text{eff}}) = 3.72$
(continued)

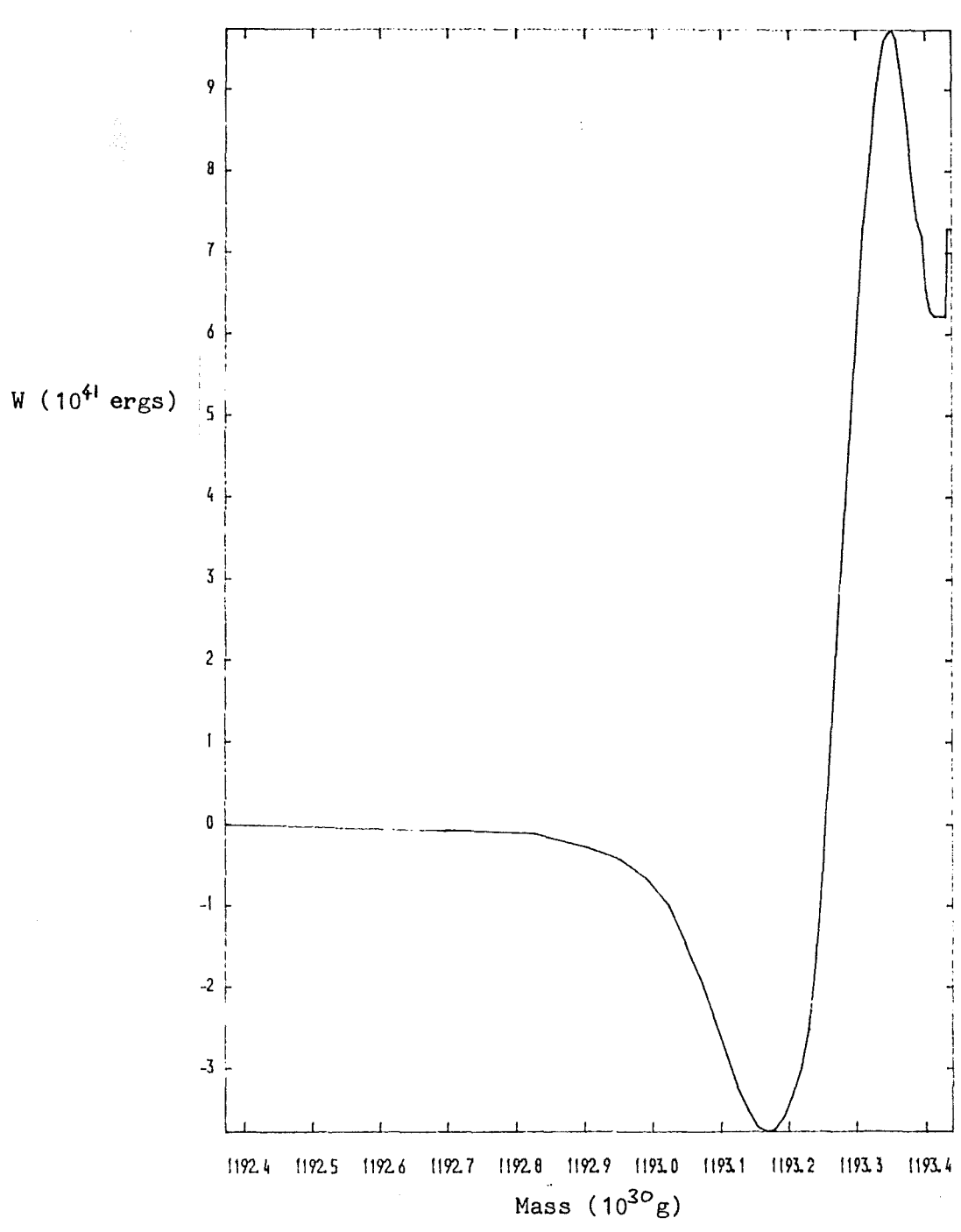


Fig. 9.11 Work integral for $\log(T_{\text{eff}}) = 3.72$

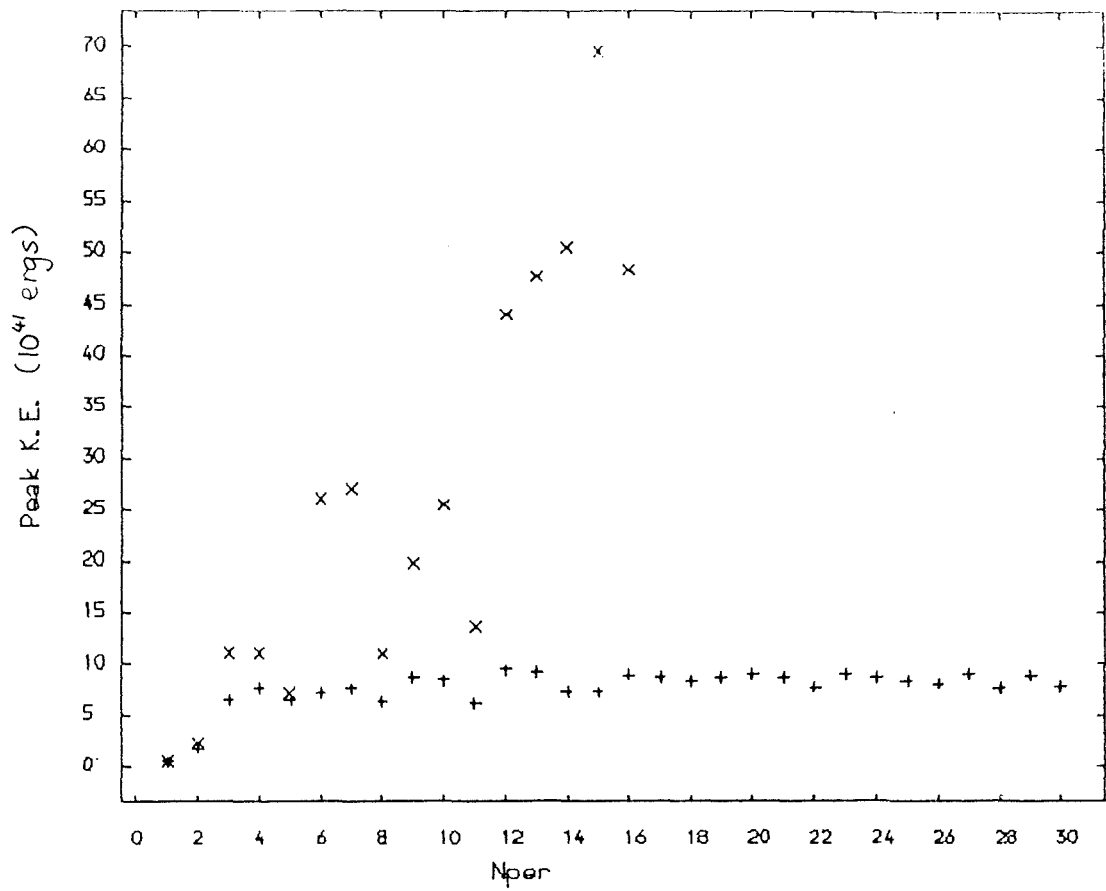


Fig. 9.12 Peak kinetic energies for $\log(L/L_{\odot}) = 3.2$, $\log(T_{\text{eff}}) = 3.72$ with luminosity determined at R_{ph} , +, and at r_{NH} (Christy), x

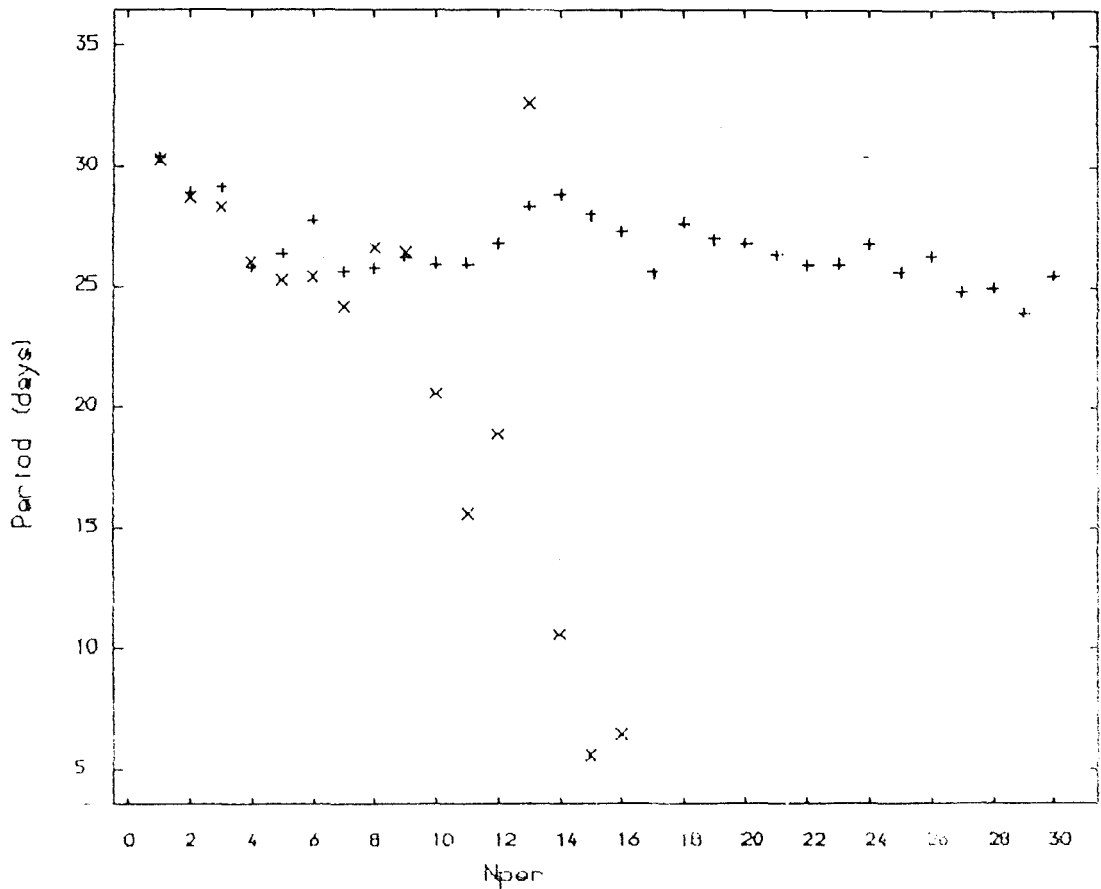


Fig. 9.13 Periods for the same models as above

condition, is far from regular the second model is far more violent and disintegrates rapidly. The light curve is originally similar to that of the first model but soon degenerates with the appearance of large luminosity spikes at rising light which come to dominate the original light maxima. A reason for trying the Christy boundary condition was the observation that since the base of the outer zone is used to relate the outer zone luminosity and temperature this would allow the temperature to fall off as the expansion proceeded. However the flaw in this is that the effective temperature is tied to the temperature in the outer zone and so this too is dragged down. The result is a large scale expansion of the outer envelope and wild oscillation of the lower zones which rapidly make the calculation unreliable because they no longer resolve the structure of the model properly.

9.2.1.4 $\text{Log}(T_{\text{eff}}) = 3.70 -$

Again there is the increase in irregularity which is to be expected. The alternation of the light curve sets in gently at the third period and grows from there on as can be seen from figs. 9.14 and 9.15. The outer zone is ejected during periods 5 to 6 and from this point on the light curve begins to smooth out although it is still reasonably reliable for a further four or five periods. From here on the light curve degenerates until it turns into something very bizarre indeed (fig. 9.16). Perhaps surprisingly this not unlike some

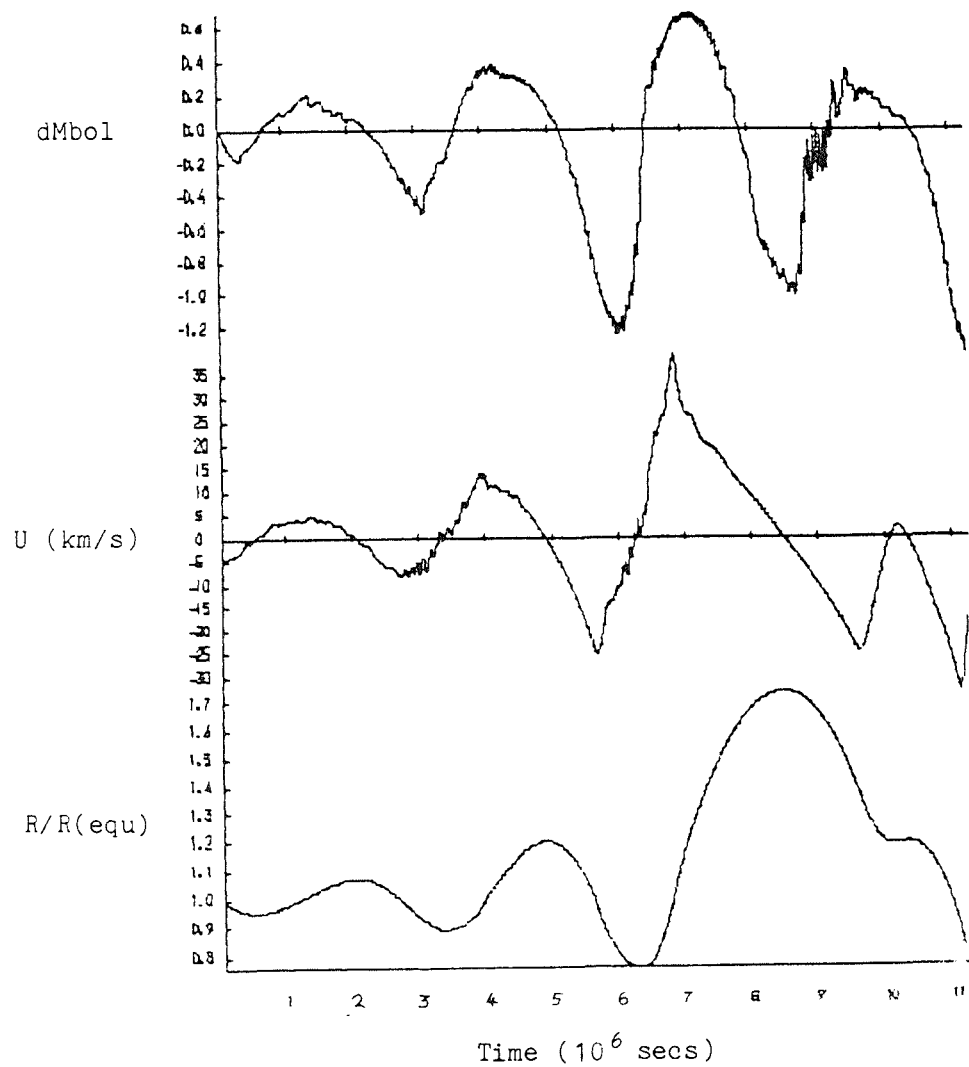


Fig. 9.14 $\text{Log}(L/L_{\odot}) = 3.2$, $\text{log}(T_{\text{eff}}) = 3.70$

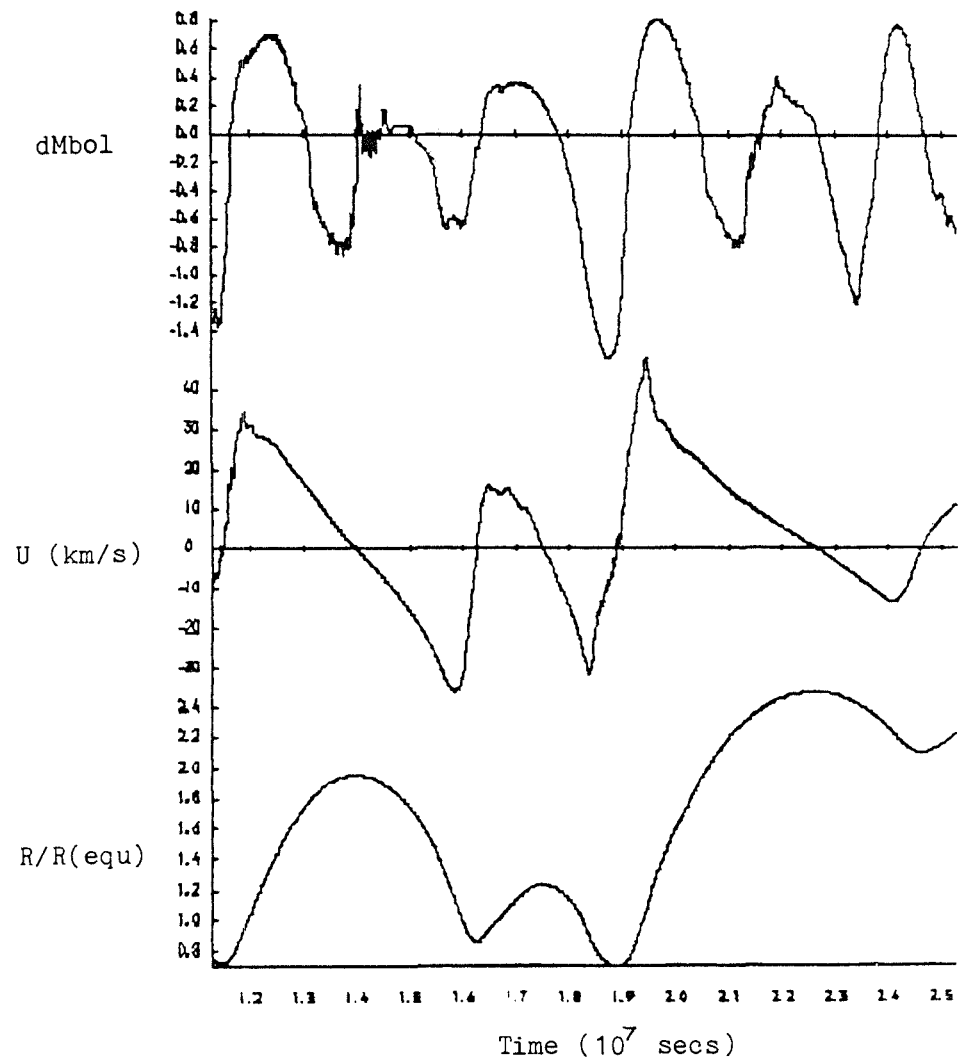


Fig. 9.15 $\text{Log}(L/L_{\odot}) = 3.2$, $\text{log}(T_{\text{eff}}) = 3.70$
(continued)

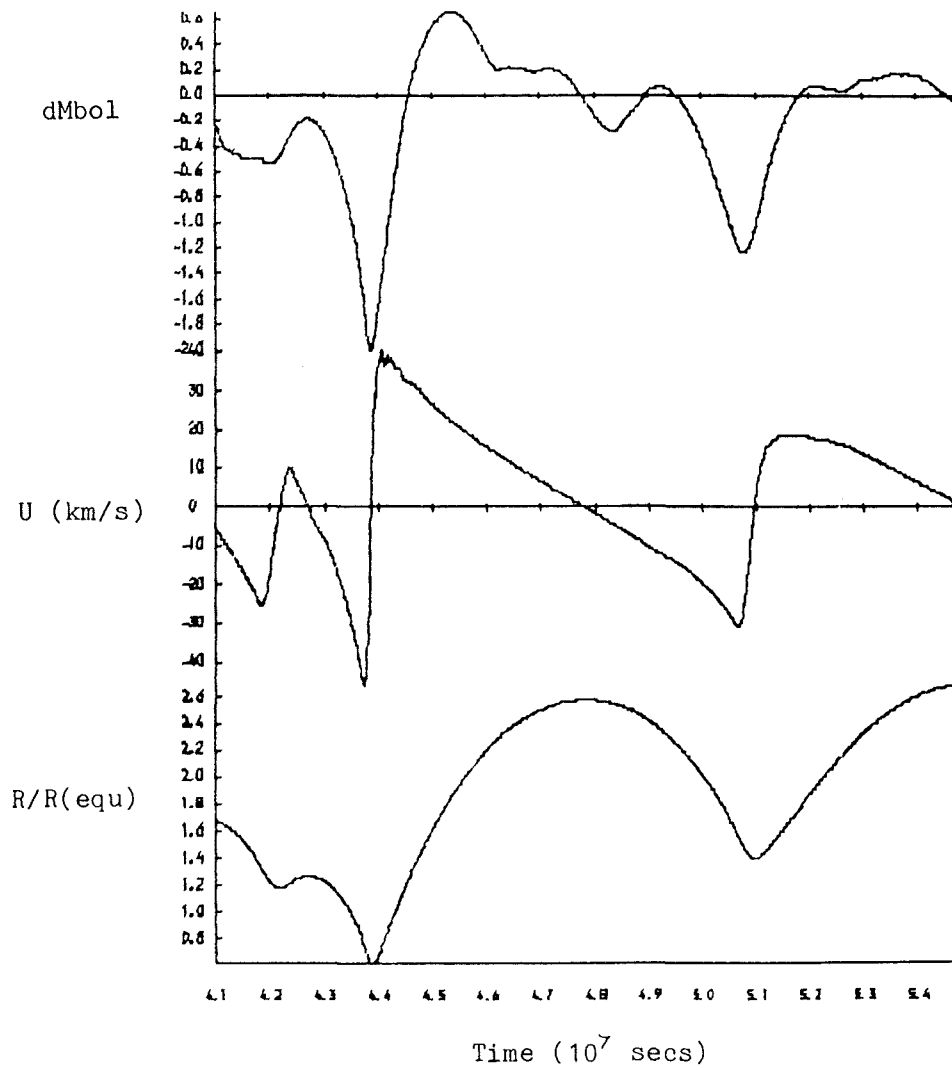


Fig. 9.16 $\text{Log}(L/L_{\odot}) = 3.2$, $\text{log}(T_{\text{eff}}) = 3.70$
(continued)

of the weirder pieces of the light curve for R Sct. However it must be remembered that by this point the model is not at all reliable. An examination of the histories of the radii throughout the star shows that matter is regularly thrown out from around $55 R_{\odot}$ to up to $\sim 185 R_{\odot}$ over a stretches of 5 to 6 periods.

9.2.1.5 $\text{Log}(T_{\text{eff}}) = 3.65 -$

A portion of the early radius, velocity, and luminosity curves for this model are presented as fig. 9.17. A feature of the model is for a large emission of radiation, during which a large part of the model is thrown out to a large distance, to be followed by a luminosity spike which barely clears the equilibrium luminosity. This is followed by a small hump which does not reach the equilibrium luminosity followed by a cycle of "normal" variation after which the sequence is repeated.

A point which all of the models which eject mass have in common is that in every case no matter how violent the ejection, only one zone is ejected. This fixes a fairly crude upper limit on the mass loss rate of around $10^{-5} M_{\odot}/\text{yr}$ for the models. However the coarse zoning of these models makes this a very loose upper limit. At least twice as many zones would be required to make any serious comment on the mass loss rates. Doubling the number of mass zones produces an immediate doubling of the CPU time required (from 7 - 10 hrs to

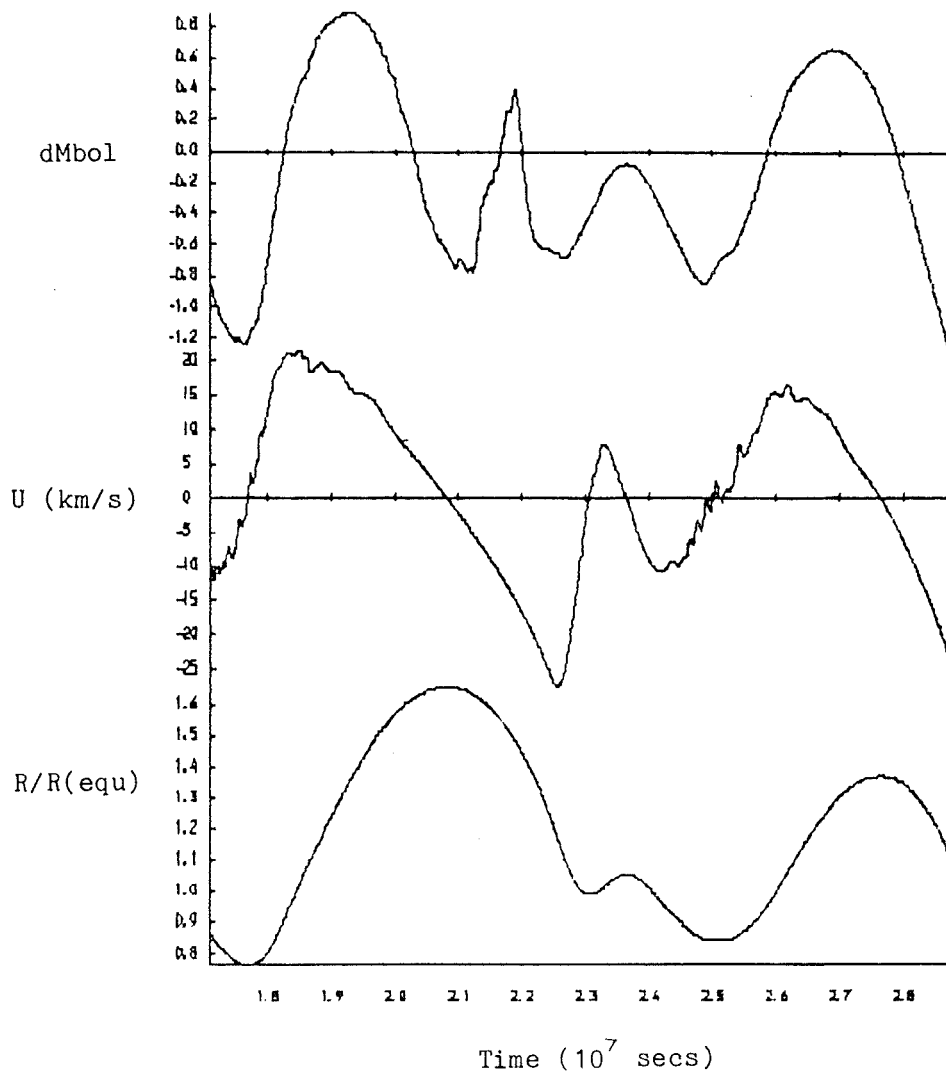


Fig. 9.17 $\text{Log}(L/L_{\odot}) = 3.2$, $\text{log}(T_{\text{eff}}) = 3.65$

14 - 20 hrs) which is further increased by a factor of 2 through the influence of the Courant condition. With the computing system available this was felt to be prohibitive.

9.2.2 The Sequence For $\text{Log}(L/L_{\odot}) = 3.5$

$\log(T_{\text{eff}})$	P (days)	Growth - rate	Peak K.E.
3.74	41.486	??	$9.539 \cdot 10^{39}$
3.72	38.2 - 45.0	+0.7	4.6 10^{41} 47 zones
	35 - 45	+0.7	6 10^{41} 35 zones
3.70	46.8 - 0.24N	+1.2	6 - 15 10^{41}

With the exception of the hottest model in the sequence, which is very nearly stable, the models of this sequence show much the same characteristics as the previous, lower luminosity models. The erratic behaviour is stronger than before and the "decay" of the models more rapid.

9.2.2.1 $\text{Log}(T_{\text{eff}}) = 3.72 -$

Figs. 9.18 and 9.19 show the peak kinetic energies and periods for the two models. There is a general qualitative agreement between the two models and, in particular, the periods follow very similar trends towards the end of the models lives. The 47 zone model is, however, much less erratic in its behaviour and also the peak kinetic energies tend to be smaller than for the more coarsely zoned counterpart. It appears that the 35 zone model is overdriven.

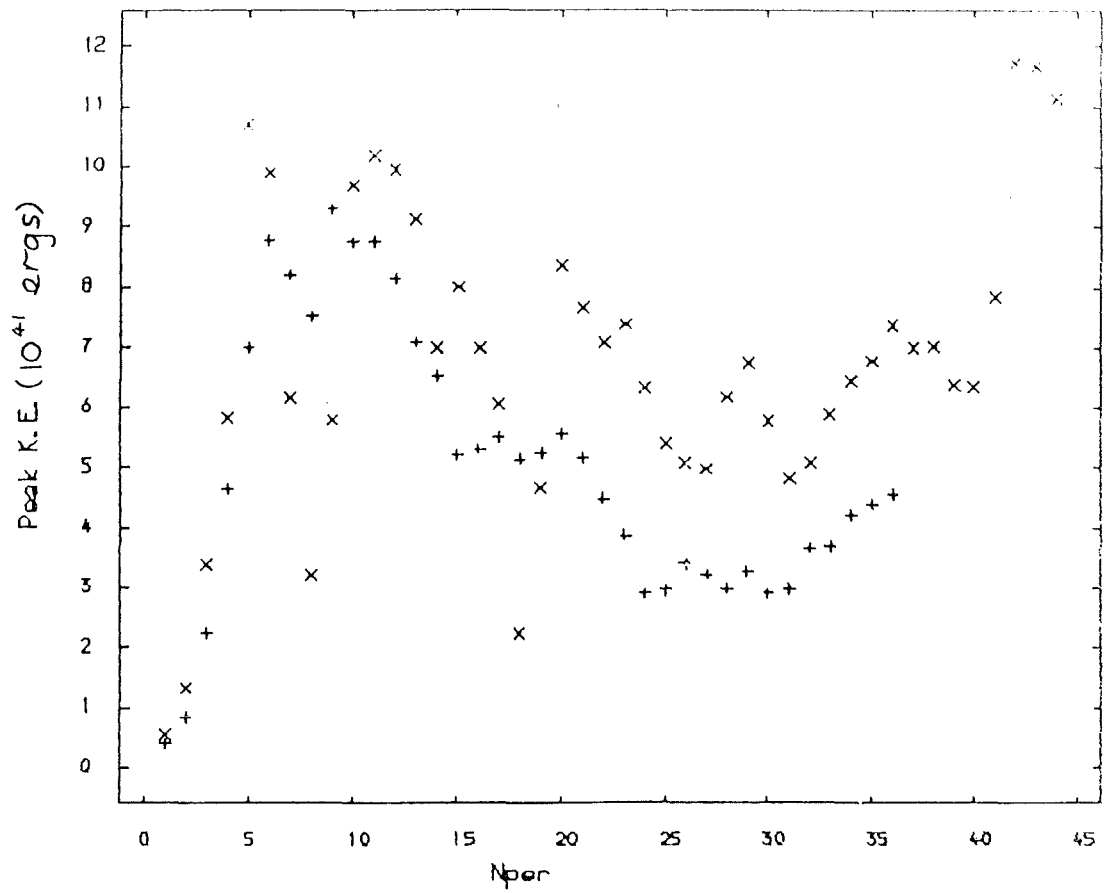


Fig. 9.18 Peak kinetic energies for
 $\log(L/L_{\odot}) = 3.5$, $\log(T_{\text{eff}}) = 3.72$ with:
 + 47 zones
 x 35 zones

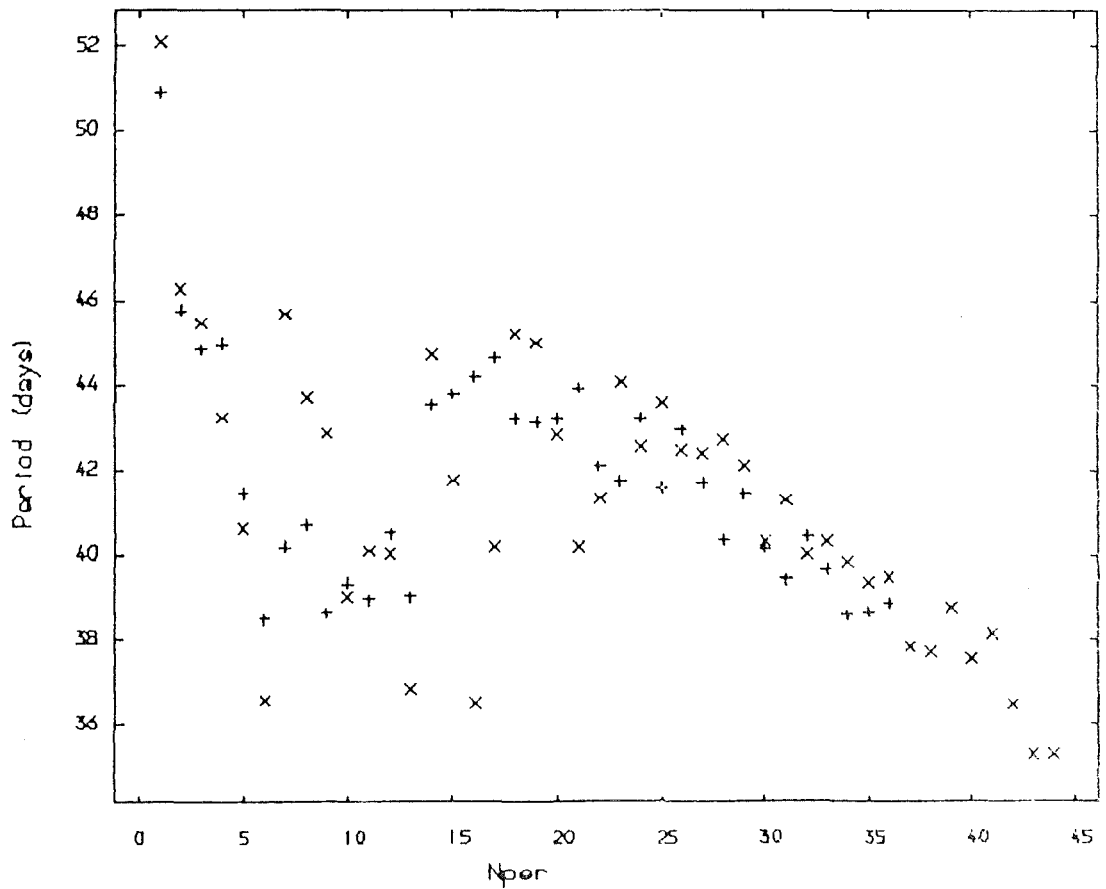


Fig. 9.19 Periods for the same models as above

Whether the root of the problem lies in the radiative damping region deep in the model or in the surface layers where damping through shocks occurs cannot be said for certain. However a comparison of work integrals for the two models shows a small difference in the radiative damping regions but probably a larger difference in the outer layers. It must be stressed that the aperiodicity makes the comparison of these work integrals precarious because they are averaged over frequently quite different periods.

The first 12 periods are plotted for the 47 zone model and form fig. 9.20. Periods 12 to 23 are plotted for the 35 zone model as fig. 9.21. Whilst the general features of this last plot are to be found in the more finely zoned model they are much more subdued. A point worth noting is that the decline of the period is apparently not amplitude dependent. However this figure and the histories of the radii for all zones, except for the surface and the deepest zones, (fig. 9.22) forms a good example of the RV - like behaviour. Two pulsations with a large amplitude during which matter is thrown out are followed by a period with a low light output and small amplitude as the matter returns to its original place. A weak ejection with a low light output is then followed by a period with a strong ejection and high light output. Following this ejection the light output drops greatly and the pulsation amplitude is very greatly reduced by the transfer of kinetic energy to the outer zones. This kind of sequence appears repeatedly. during the time covered by the figures matter

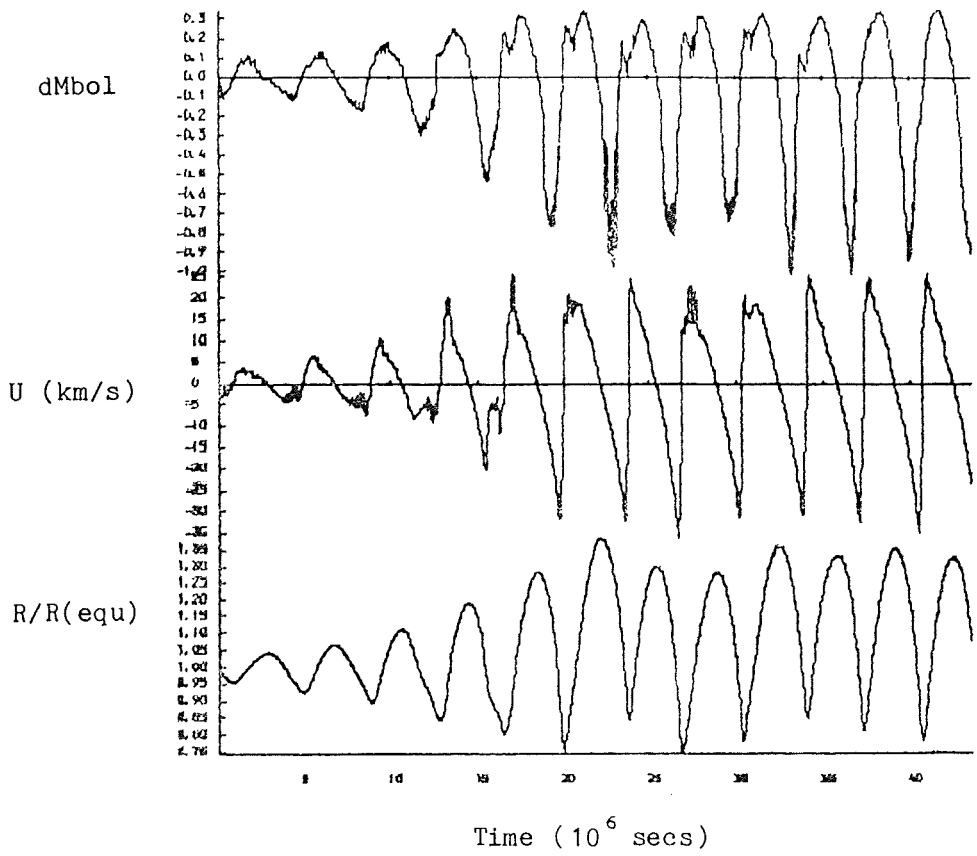


Fig. 9.20 $\text{Log}(L/L_{\odot}) = 3.5$, $\text{log}(T_{eff}) = 3.72$
 first 12 periods with 47 zones

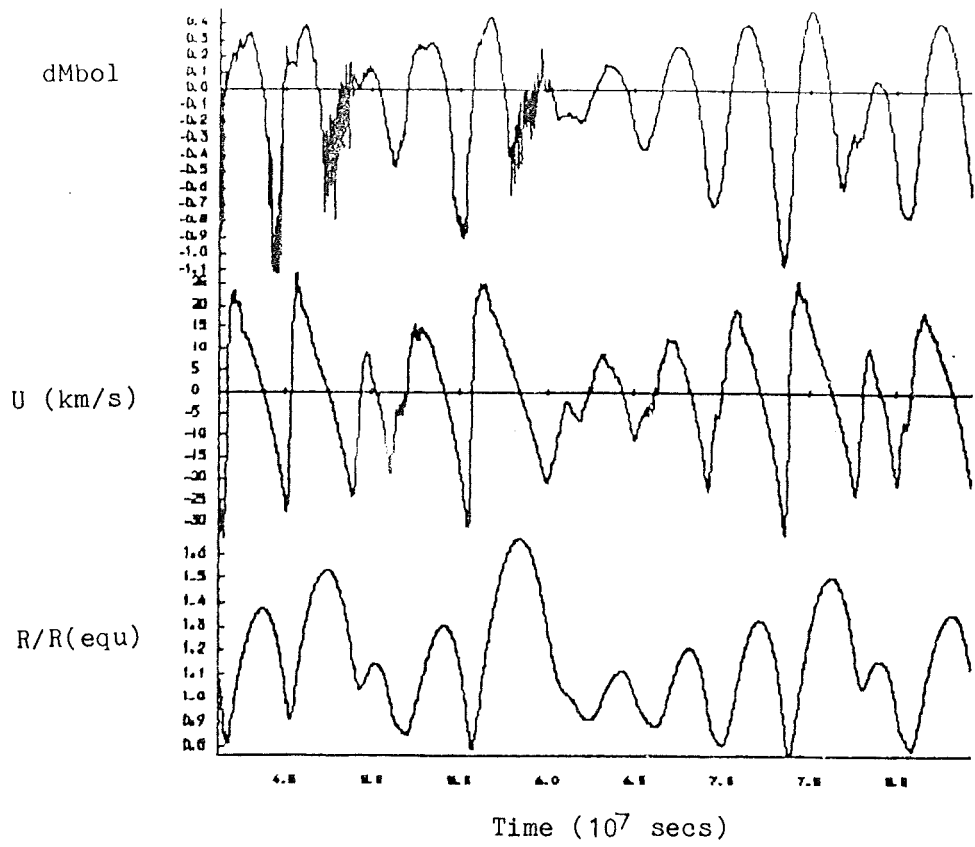


Fig. 9.21 $\text{Log}(L/L_{\odot}) = 3.5$, $\text{log}(T_{\text{eff}}) = 3.72$
with 35 zones

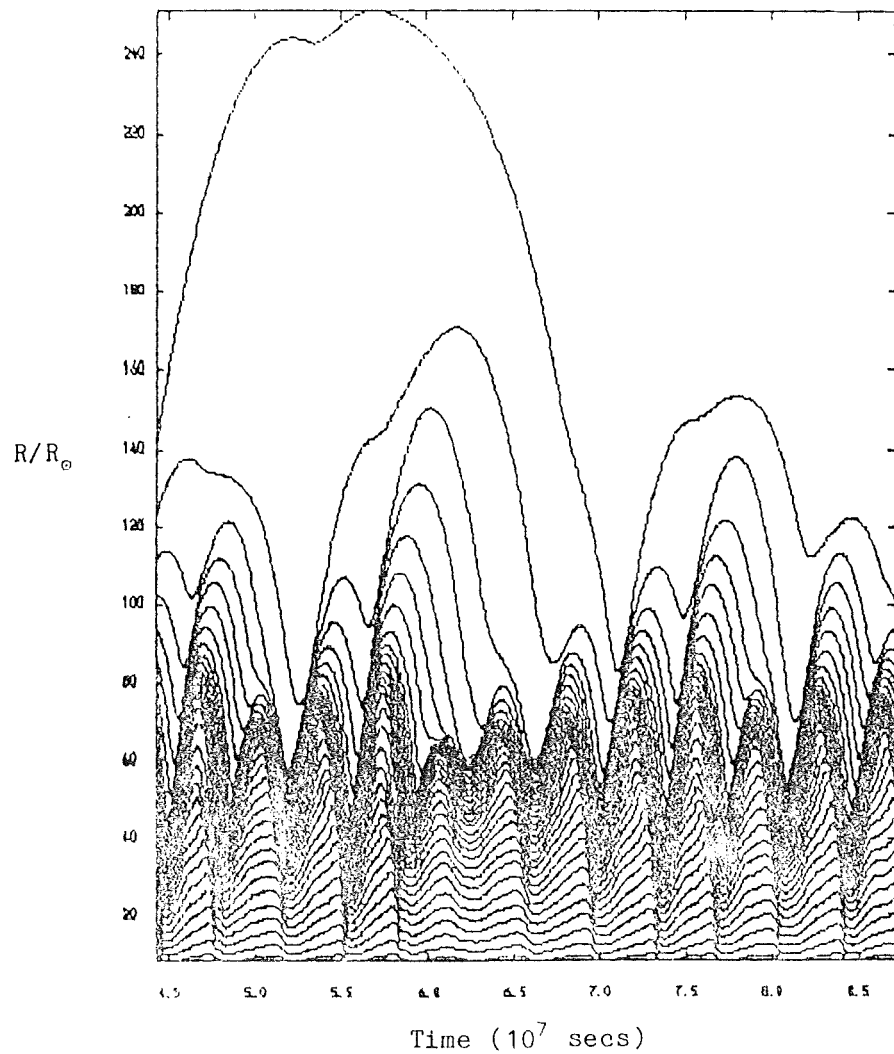


Fig. 9.22 $\text{Log}(L/L_{\odot}) = 3.5$, $\text{log}(T_{\text{eff}}) = 3.72$
Radii of zone boundaries

travels through great distances, $\sim 60 - 70 R_{\odot}$ being typical. The mass involved in these motions is considerable, $\sim 3 \cdot 10^5 M_{\odot}$.

$$9.2.2.2 \quad \text{Log}(T_{\text{eff}}) = 3.70 -$$

Numerical problems prevented the construction of a model with the usual 50 zones and the best that could be managed was 38 zones. Figs. 9.23 and 9.24 are plots of the peak kinetic energy and period for this model. Most of the life of this model is shown in figs. 9.25 to 9.27. Beyond period 50 the model can be regarded as fatally flawed by the expansion. The peak kinetic energy undergoes wild oscillations in the latter stages of the model as the result of cyclic expulsions of large quantities of matter to large distances. Most of this matter remains bound. However this is the only model in which more than one zone reaches escape velocity. By the time 50 periods (5.55 years) have passed 6 zones amounting to $\sim 4 \cdot 10^5 M_{\odot}$ have been expelled. So this gives us a mass loss rate of $7 \cdot 10^6 M_{\odot}/\text{yr}$. However the probable inadequacy of the zoning and, of course, of the luminosity boundary condition means that these figures should be treated with scepticism. The deep dip in the peak kinetic energy at periods 7 to 9 is the result of the expulsion of the outer layers. This event is followed by the contraction of the inner layers of the stellar envelope and a concomitant fall in the pulsation period. The lost kinetic energy is presumably emitted as radiation and converted to potential energy of the outer layers. Very similar effects have been reported by authors

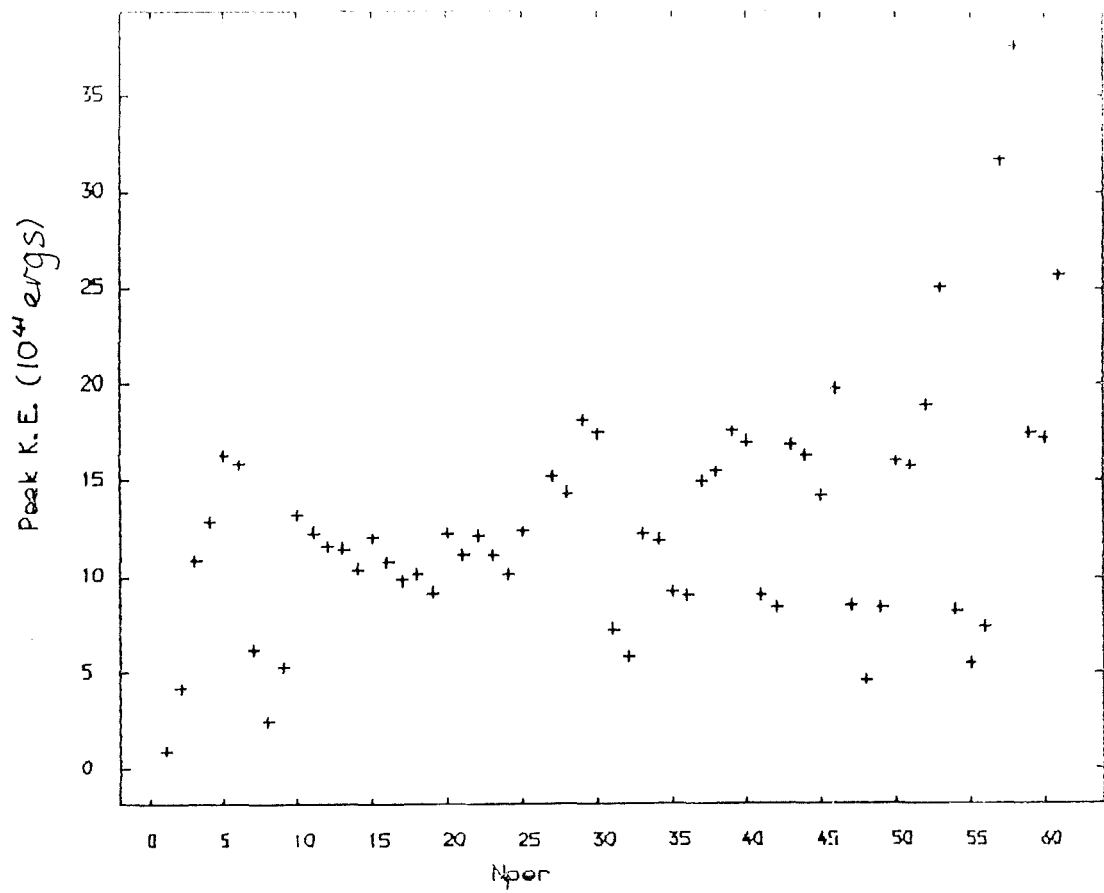


Fig. 9.23 Peak kinetic energies for
 $\log(L/L_{\odot}) = 3.5$, $\log(T_{eff}) = 3.70$

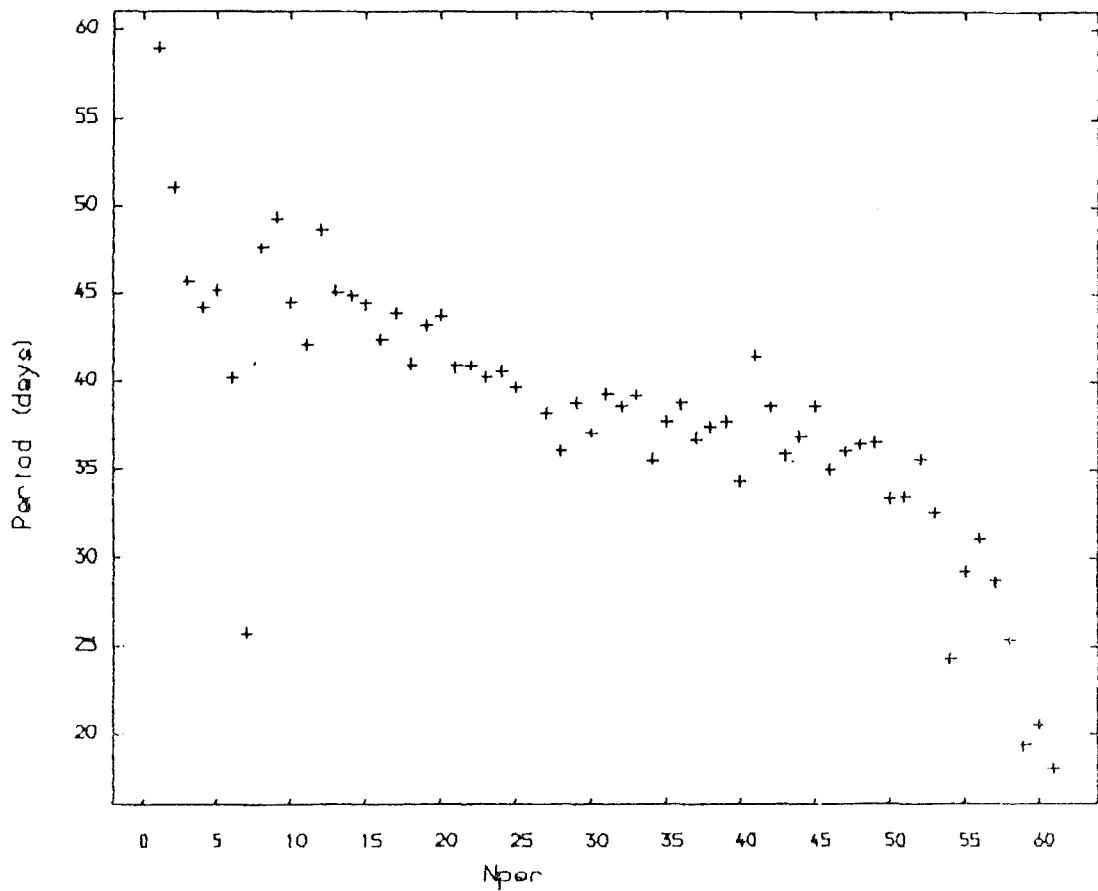


Fig. 9.24 Periods for same models as above

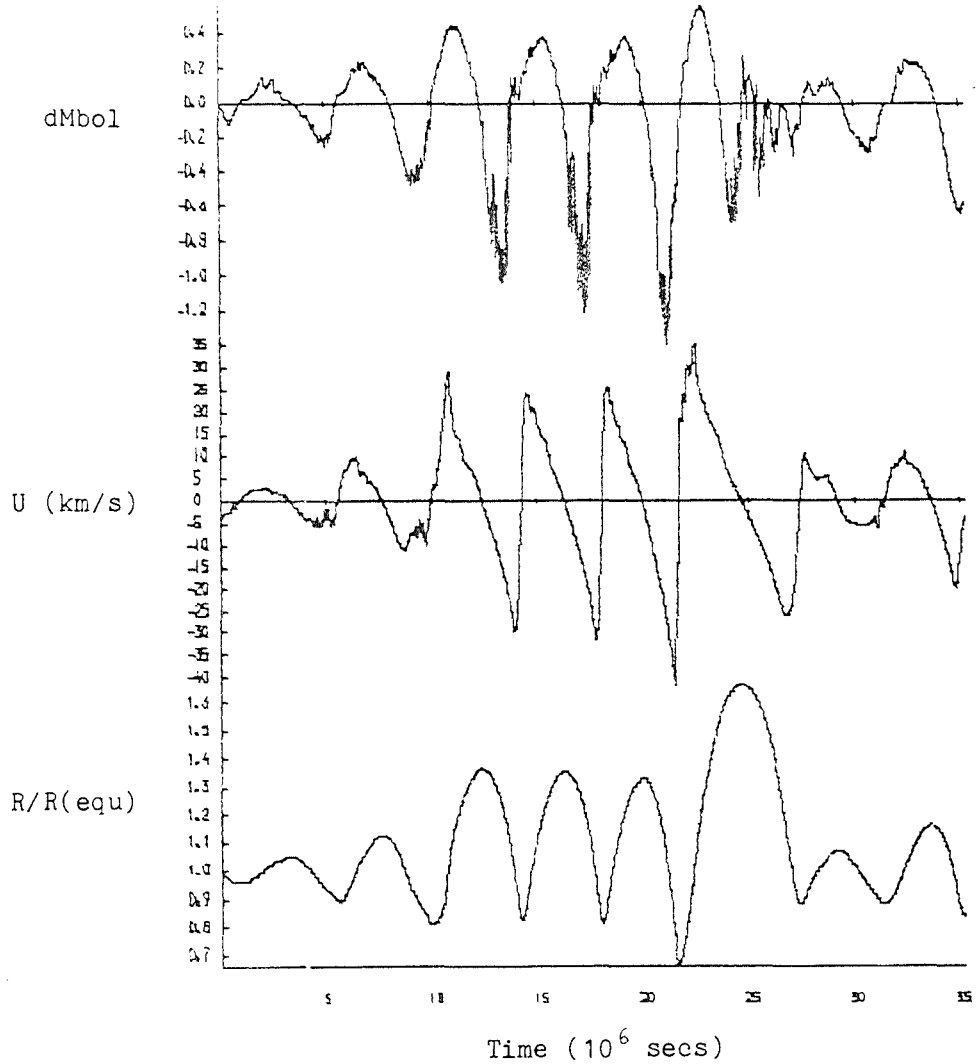


Fig. 9.25 $\text{Log}(L/L_{\odot}) = 3.5$, $\text{log}(T_{eff}) = 3.70$

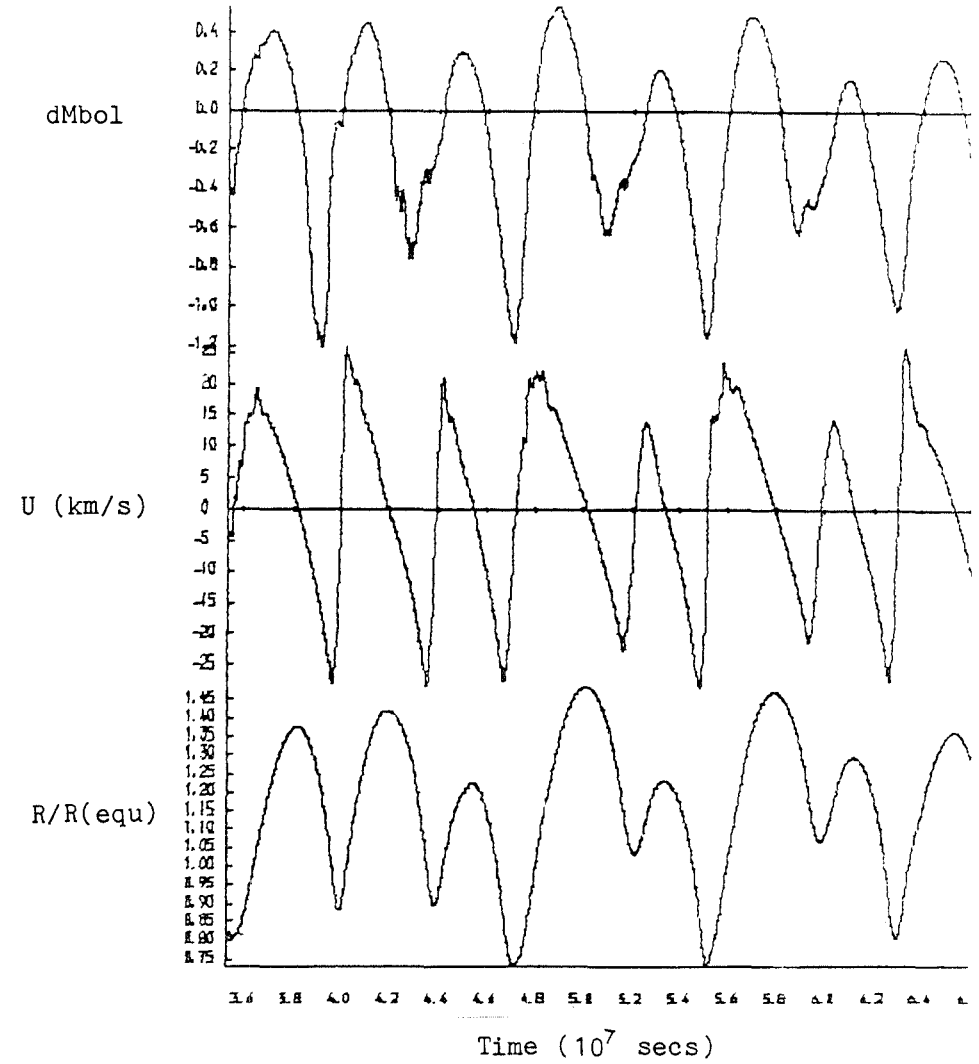


Fig. 9.26 $\text{Log}(L/L_{\odot}) = 3.5$, $\text{log}(T_{eff}) = 3.70$
(continued)

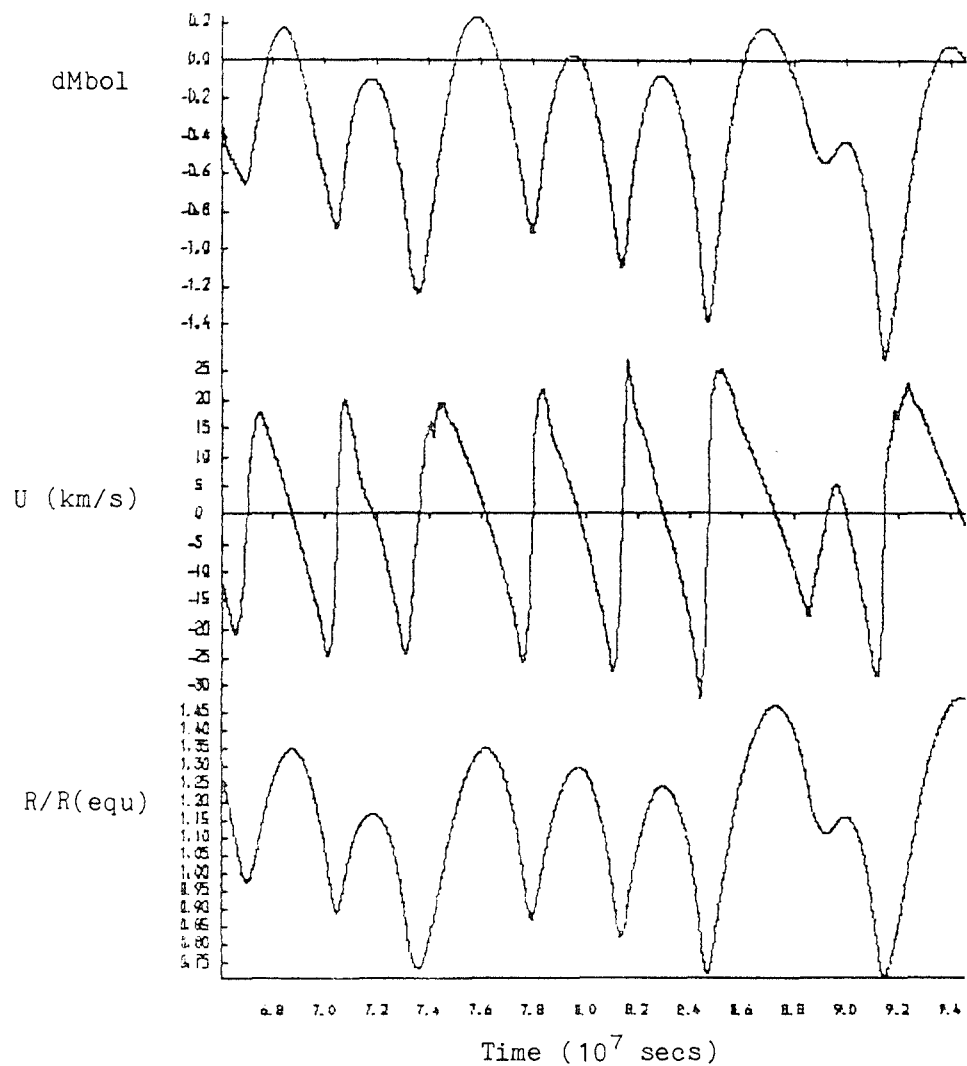


Fig. 9.27 $\log(L/L_{\odot}) = 3.5$, $\log(T_{eff}) = 3.70$
(continued)

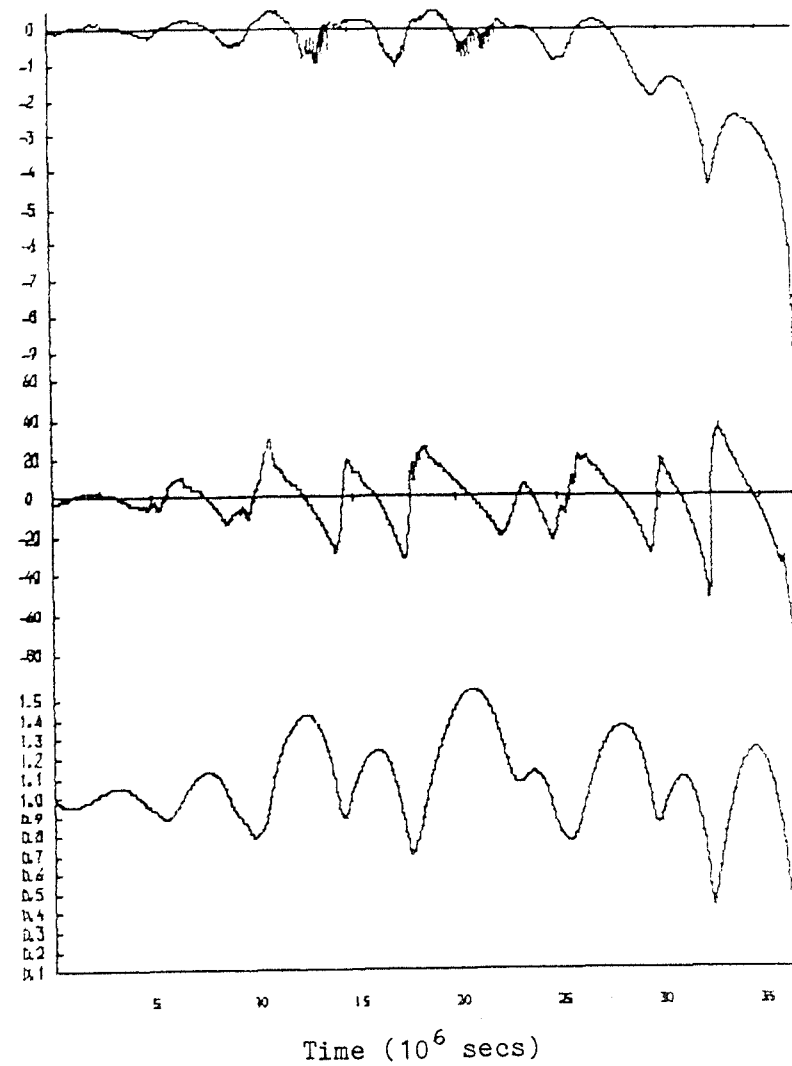


Fig. 9.28 $\log(L/L_{\odot}) = 3.5$, $\log(T_{eff}) = 3.70$,
but with $P = 0$ at outer boundary

working on nonlinear models of long period variable stars (Keeley 1970; Wood 1974). Here too a decrease in the mean radius and pulsation period is observed.

A further model was constructed for these parameters identical in every way except that the pressure at the surface was assumed to be zero. This model quite literally exploded and so affords an excellent example of the inadequacy of both the $P = 0$ and the Eddington Approximation boundary condition. Fig. 9.28 shows the entire life of this model including its eventual extinction.

9.2.3 Driving Of The Pulsations

For the $\log(L/L_{\odot}) = 3.2$, $\log(T_{eff}) = 3.76$ model it can be seen from the work function, displayed as fig. 9.29, that most of the driving is found in the region of the HeII ionisation zone ($\log \rho \approx -8.5$, $\log(T) \approx 4.6 - 4.7$) which, on consulting the opacity tables, is seen to coincide with the HeII hump on the opacity. The H/HeI ionisation appears to contribute little. Just outside the H/HeI ionisation zone there is a considerable damping region. This damping is the result of dissipation of kinetic energy by shock waves running up into the atmosphere.

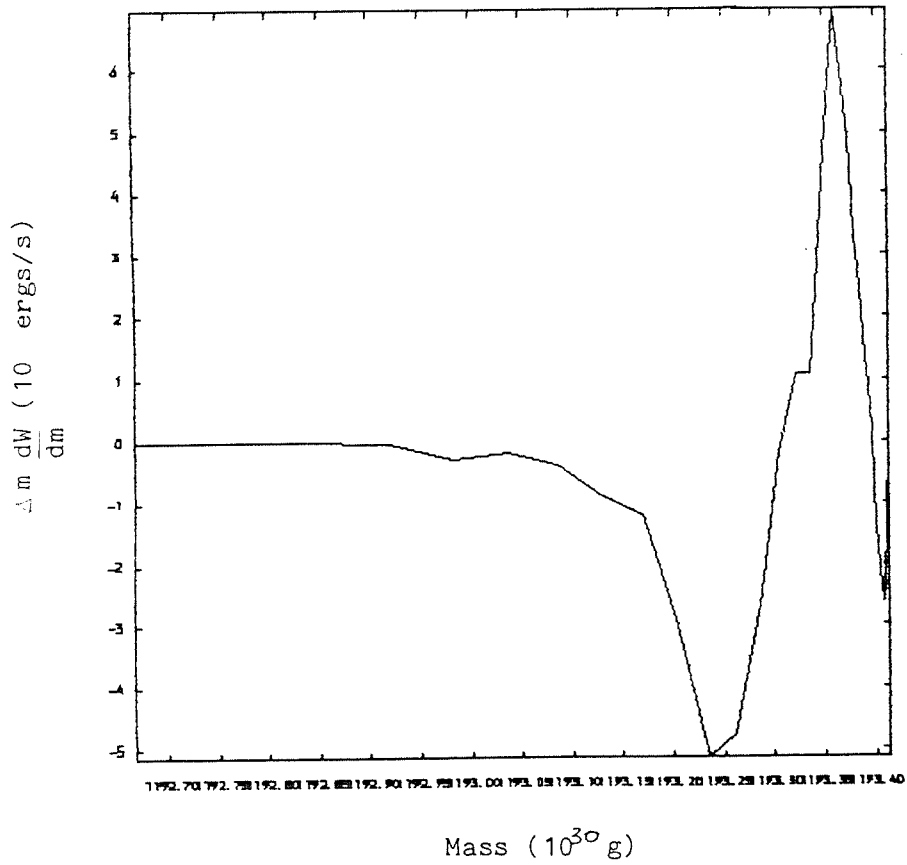


Fig. 9.29 Work/zone for $\log(L/L_{\odot}) = 3.2$,
 $\log(T_{\text{eff}}) = 3.76$

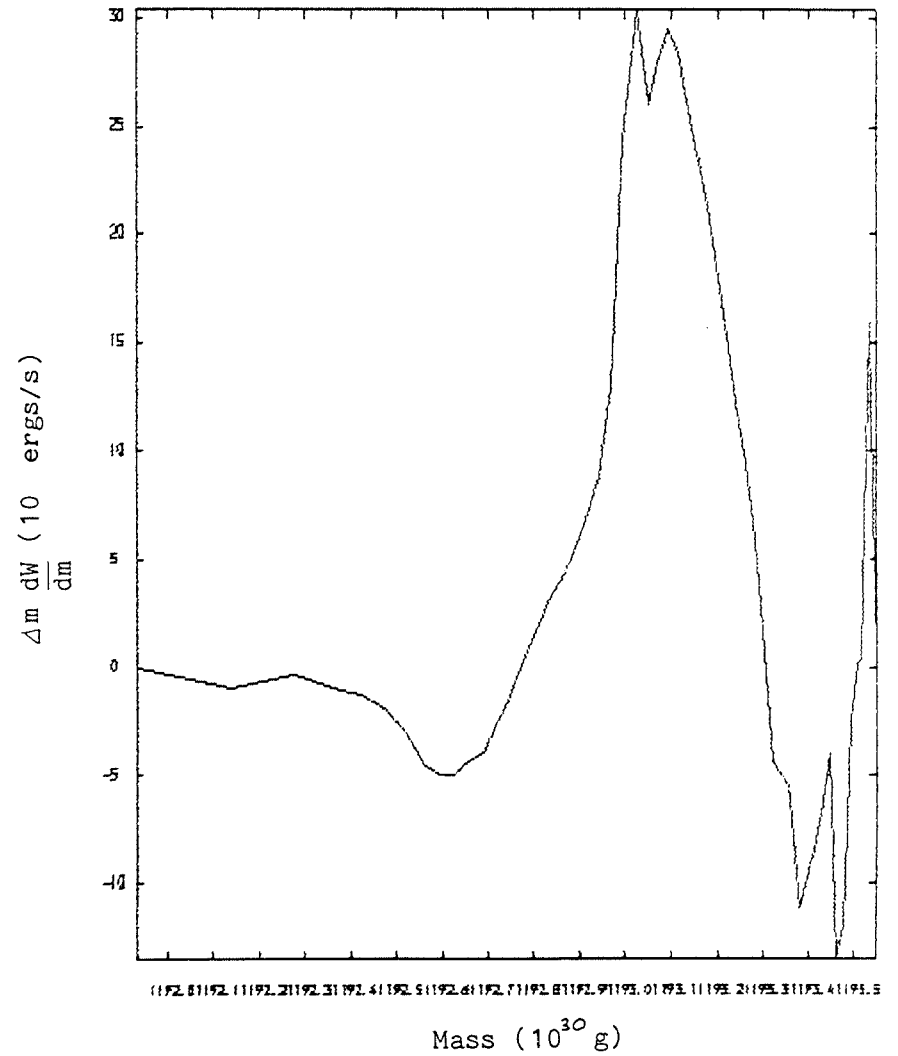


Fig. 9.30 Work/zone for $\log(L/L_{\odot}) = 3.2$,
 $\log(T_{\text{eff}}) = 3.65$

When the $\log(T_{eff}) = 3.65$ model for the same luminosity is examined it is found that the shape and location of the driving peaks vary greatly from one period to the next. In fact it is clear that the motion is nowhere near periodic. For most of the later periods there appears to be a single large driving peak which is frequently located at low temperatures. Thus we can tentatively say that a great deal of the driving appears to be the work of H/HeI ionisation zone. However the uncertainty of the temperatures at the peak and the presence of very strong shock dissipation which distorts its shape makes this uncertain. During some of the periods the radiative damping deep in the envelope is almost nonexistent and almost all of the dissipation is provided by massive shocks in the atmosphere. Even if convection were to change the dissipation by 100% the damping from this mechanism would still be nearly negligible in comparison with the shock damping. For this reason the amplitude of the pulsation might not be so badly affected by the absence of convection as might be feared. Fig. 9.30 shows the work function for this model. Returning to a hotter model this time with $\log(T_{eff}) = 3.72$ we find the main peak of the driving at $\log(T_{eff}) = 4.55$ followed by a shoulder at $\log(\rho) = 4.6 - 4.65$ (fig. 9.11). The latter can again be identified with the HeII ionisation feature in the opacity with confidence. The main feature seems again to occur at too high a temperature to be the result of H/HeI ionisation. In this model too the damping due to shock waves in the atmosphere is again frequently greater than the

contribution of the deep radiative damping region.

9.3 SPHERICAL GEOMETRY IN THE ATMOSPHERE

The luminosity boundary condition described earlier is derived from the Eddington Approximation for a plane parallel atmosphere and likewise the diffusion equation also assumes plane parallel geometry. The boundary condition most often used incorporates the equation

$$T_o^4 = 1/2 T_{eff}^4,$$

where T_o is the temperature at the stars surface (or more correctly, in the outer most zone). This is likely to be a poor approximation in stars such as the longer period W Vir stars and the RV Tauri stars. Fadeev and Tutukov (1981) have attempted to improve this boundary condition by using the radiative dilution coefficient for spherical geometry, W . They have

$$F = T_{eff}^4 / W$$

or

$$T_o^4 = W T_{eff}^4,$$

where $W = 1/2(1 - \sqrt{1 - (R_{ph}/R)^2})$, R is the photospheric radius and F is the radiation flux. Clearly when R_{ph}/R is close to 1 this reduces to the usual expression. (However consider Bridger's (1983) model for which $\log(L/L_\odot) = 2.9$ and $\log(T_{eff}) = 3.74$; $R_{ph}/R = 0.932$, which is fairly close to 1, but $W = (1/2) 0.64!$) Now if the outer boundary is at a distance much greater than the photospheric radius then the surface temperature

$$T_o^4 \rightarrow 1/4 (R_{ph}/R)^2 T_{eff}^4$$

→ 0

This is particularly important when mass loss occurs since then the outer radius tends to infinity. This behaviour of the temperature at the outer zone offers a solution to the problems encountered with the luminosity at the outer boundary. We have, as before

$$V \rightarrow 4\pi/3 \ 1/\Delta m \ R^3, \ U \rightarrow aT^4 V, \ P \rightarrow 1/3 \ U/V, \ \text{and } dR/dt \rightarrow v_{\infty},$$

but now $T^4 \sim 1/R^2$.

So we find that

$$\frac{\partial L}{\partial m} \approx - \frac{4V_{\infty}}{3c} \frac{L}{\Delta m}.$$

This analysis, as does that for the original boundary condition, includes the reasonable assumption that $d \log(\langle L \rangle) / dt$ is much smaller than $d \log(\langle R \rangle) / dt$ (where $\langle x \rangle$ is the value of x averaged over a pulsation period.) A more detailed treatment of the luminosity at the outer boundary follows this section. This confirms the basic result.

Although the use of the radiation dilution coefficient at the outer boundary greatly improves the behaviour of that zone it introduces an inconsistency into the radiative transfer equation. Logically the differential equation for the mean intensity J or, in the equilibrium diffusion approximation, T should include the effects of spherical geometry. This has been attempted by some authors (Paczynski 1969; Fox and Wood 1982) in static models or linear pulsation calculations. However the ad hoc representations of the geometry do not inspire confidence and in the work of Fox and Wood can allow an optical depth which decreases with depth in the stellar

model. To the best of my knowledge spherical geometry has never been treated properly in any nonlinear pulsation calculations. The sole attempt to date has been the work of Fadeev and Tutukov.

Fadeev and Tutukov (1981) used the radiation dilution boundary condition to construct a model with the following parameters;

$$M = M_{\odot}$$

$$\log(T_{eff}) = 3.74$$

$$\log(L/L_{\odot}) = 3.5$$

and with a population II composition. The equation of state included molecular hydrogen but the opacity was that calculated by Cox and Stewart (1969) and this does not take into account the contribution of molecules to the opacity. Fadeev and Tutukov found that an extended envelope was produced and that mass was lost ($\sim 10^{-6} M_{\odot}$) as the result of the action of strong shocks in the atmosphere. They investigated the propagation of the shocks in the atmosphere and conclude that radiative losses from the shocks are negligible unless the shock is exceedingly strong. The light curve for their model has unequal minima and is somewhat like an RV light curve.

9.4 THE LUMINOSITY AT THE OUTER BOUNDARY

The behaviour of the luminosity at the outer boundary can be studied in a little more detail than in the cursory treatment outlined above. In the case where radiation dilution is ignored we write,

$$L = 4\pi R^2 \sigma T^4,$$

where L is the luminosity at the outer boundary and T the temperature of the outer zone. We assume that variations of the photospheric radius R_{ph} , and also the radius at the base of the outer zone, are negligible when compared with the rapid growth of the outer radius, R . The mass of the outer zone is denoted Δm and the luminosity at the base of the outer zone is $L_1(t)$ and is assumed to be periodic. Since

$$\frac{\partial L}{\partial m} = -T \frac{dS}{dt} = -\frac{dU}{dt} - \frac{1}{3} U \frac{d \log V}{dt},$$

we have

$$\frac{L - L_1}{\Delta m} = -\frac{dU}{dt} - \frac{1}{3} \frac{dR}{dt}.$$

As before we assume that the gas pressure has fallen to zero, and that the only contribution to dV/dt is from the expansion of the outer boundary. So now we have,

$$\frac{L - L_1}{\Delta m} = -U \left(4 \frac{dR}{dt} + \frac{d \log L}{dt} \right).$$

We assume that $dR/dt \rightarrow v_0$, an assumption which is backed up by the nonlinear models. We can now substitute for U in terms of L , R , R_{ph} , Δm , etc.,

$$\frac{L - L_1}{\Delta m} = -\frac{\alpha}{\sigma} \frac{L}{4\pi R_{ph}^2} \frac{4\pi R^2}{3 \Delta m} \left(4 \frac{v_0}{R} + \frac{1}{L} \frac{dL}{dt} \right),$$

so,

$$L - L_1 = -\frac{4}{3c} \left(\frac{R_0 + v_0 t}{R_{ph}} \right)^2 \left(4 v_0 L + (R_0 + v_0 t) \frac{dL}{dt} \right),$$

where we have assumed $R = R_0 + v_0 t$ and where c is the speed of light.

We now define $\alpha = 4v/3c$ and rearrange to get,

$$\frac{dL}{dt} + \frac{R_{ph}^2 + 4\alpha(R_0 + v_\infty t)^2}{\alpha(R_0 + v_\infty t)^2} L = \frac{v_\infty R_{ph}^2}{\alpha(R_0 + v_\infty t)^3} L_1(t).$$

A formal solution is easily obtained,

$$L = \left(\frac{R_0}{R_0 + v_\infty t}\right)^4 e^{\frac{K}{2}\left(\left(\frac{R_0}{R_0 + v_\infty t}\right)^2 - 1\right)} L_0 + K L_1 \left(\frac{R_0}{R_0 + v_\infty t}\right)^4 e^{\frac{K}{2}\left(\frac{R_0}{R_0 + v_\infty t}\right)^2} \int_0^t \left(\frac{R_0}{R_0 + v_\infty t'}\right)^{-1} e^{-\frac{K}{2}\left(\frac{R_0}{R_0 + v_\infty t'}\right)^2} \frac{v_\infty dt'}{R_0},$$

where L_0 is the value of L at $t = 0$, and we define $K = R_{ph}^2/\alpha R^2$. To simplify the problem we assume that L_1 is constant i.e. that we are interested only in the mean luminosity. Consider the case where $v_\infty t/R_0 \ll 1$. We can expand in terms of this parameter so that,

$$L \approx \left(1 - 4\frac{v_\infty t}{R_0}\right) \left(e^{-k\frac{v_\infty t}{R_0}} L_0 + \left(1 + \frac{v_\infty t}{R_0} - e^{-k\frac{v_\infty t}{R_0}}\right) L_1\right)$$

where terms in $1/K \sim \alpha$ are assumed to be small. Or, in terms of the luminosity gradient, we have,

$$\frac{L - L_1}{\Delta m} \approx \left(1 - 4\frac{v_\infty t}{R_0}\right) e^{-\frac{K v_\infty t}{R_0}} \frac{L_0 - L_1}{\Delta m} - 3\frac{v_\infty t}{R_0} \frac{L_1}{\Delta m}.$$

When the expansion is at an advanced stage, i.e. $v_\infty t/R_0 \gg 1$, we can define $x = R_0/v_\infty t$ and then for the second term on the RHS we have

$$\begin{aligned} & K L_1 x^4 e^{\frac{K}{2}x^2} \int_x^1 \frac{e^{-\frac{K}{2}x'^2}}{x'^3} dx' \\ & < K L_1 x^4 e^{\frac{K}{2}x^2} \int_x^1 \frac{dx'}{x'^3} \\ & = K L_1 \frac{x^2}{2} (1 - x^2) e^{\frac{K}{2}x^2} \end{aligned}$$

Assuming now $Kx^2 \rightarrow 0$ we get,

$$L < \left(\frac{R_0}{v_{\infty} t}\right)^4 \left(1 + \frac{k}{2} \left(\frac{R_0}{v_{\infty} t}\right)^2\right) e^{-\frac{k}{2}} L_0 \\ + \frac{k}{2} \left(\frac{R_0}{v_{\infty} t}\right)^2 \left(1 + \frac{k}{2} \left(\frac{R_0}{v_{\infty} t}\right)^2\right) L_1,$$

and so

$$L \sim \frac{k}{2} \left(\frac{R_0}{v_{\infty} t}\right)^2 L_1$$

when the expansion is well advanced.

When radiation dilution is included life is much simpler. For R sufficiently large that $R_{ph}/R \ll 1$ we have

$$W \rightarrow \frac{1}{4} \left(\frac{R_{ph}}{R}\right)^2$$

and so,

$$L = 4\pi R_{ph}^2 \sigma T^4 \cdot 2 \frac{R^2}{R_{ph}^2}.$$

So now,

$$\frac{L - L_1(t)}{\Delta M} = -\frac{1}{2} \frac{4}{3c} \frac{1}{\Delta M} \left(2 v_{\infty} L + (R_0 + v_{\infty} t) \frac{dL}{dt}\right)$$

and so,

$$\frac{dL}{dt} + 2 \left(\frac{1+\alpha}{\alpha}\right) \left(\frac{v_{\infty}}{R_0 + v_{\infty} t}\right) L = \frac{2}{\alpha} \left(\frac{v_{\infty}}{R_0 + v_{\infty} t}\right) L_1(t).$$

The solution for constant L_1 is simple,

$$L = \left(\frac{R_0}{R_0 + v_{\infty} t}\right)^{2\left(\frac{\alpha+1}{\alpha}\right)} L_0 + \frac{1}{\alpha+1} \left(1 - \left(\frac{R_0}{R_0 + v_{\infty} t}\right)^{2\left(\frac{\alpha+1}{\alpha}\right)}\right) L_1$$

or,

$$\frac{L - L_1}{\Delta M} = \left(\frac{R_0}{R_0 + v_{\infty} t}\right)^{2\left(\frac{\alpha+1}{\alpha}\right)} \frac{L_0 - L_1}{\Delta M} - \alpha \frac{L_1}{\Delta M},$$

where $\alpha = 4v_{\infty}/3c$ is again assumed to be small.

In both cases the initial conditions are quickly wiped out by the expansion, but in the case where radiation dilution is included the luminosity gradient remains very small and the luminosity does not deviate greatly from that of the underlying star. This is in stark contrast with the case where the usual Eddington Approximation boundary condition is in force and for which the exterior luminosity falls rapidly with time as the expansion proceeds. This simple model explains the curious behaviour found in the models reasonably well.

9.5 MODELS CONSTRUCTED USING RADIATION DILUTION

The intention here was to repeat the survey described above but with radiation dilution included in the luminosity boundary condition. However numerical problems appeared which although eventually eradicated from luminosities up to and including $\log(L/L_{\odot}) = 3.4$ could not be squeezed out of the $\log(L/L_{\odot}) = 3.5$ models. The greatly reduced time available suggested that attention be limited to a very few models. These models were constructed for

$$\log(T_{eff}) = 3.70$$

$$\log(L/L_{\odot}) = 3.2, 3.4$$

Because the new boundary condition allows the temperature at the outer zone to fall very considerably it is now essential that the molecular opacity be included. Molecular hydrogen was also included in the main models. A pair of models was constructed with molecules

omitted from the equation of state in order to get a crude estimate of the effects of molecular dissociation as opposed to the dominant, opacity effects. A model was constructed at the lower luminosity with all contributions from molecules omitted. Also the effects of halving or quadrupling the artificial viscosity constant and removing the viscosity cutoff were examined.

9.5.1 Features Common To All Of The Models

As with most of the cooler models described above the outer zone is ejected from these models. The cyclic boosting of large quantities of matter to large distances (~ 10 equilibrium radius) is again present. However a less welcome feature of the models is the appearance of luminosity spikes at rising light. Whatever I do these will not go away. Another feature seen in all of these models, as well as in the previous sequences, is a contraction of the inner envelope. This gives rise to the initial decrease of period seen in the earlier models and in the present set. The contraction of the model naturally gives rise to an increase of the effective temperature and it is perhaps worth remarking that the RV stars are known for being bluer than would be expected from their spectra.

The most pleasing thing about these models is that the decrease in mean luminosity and the smoothing out of the light curve at the outer boundary associated with the escape of the outer zone has

entirely disappeared, as was to be expected.

9.5.2 The Model For $\text{Log}(L/L_{\odot}) = 3.2$

The light, radial velocity, and radius curves for all 38 periods of this model are given in figs. 9.31 and 9.32. The peak kinetic energy and periods for this model and for a model from which the formation of molecular hydrogen was omitted are shown as figs. 9.33 and 9.34 respectively. Whilst there is considerable variation of the period from cycle to cycle the tendency for the period to fall off has almost disappeared. There is still, however, an initial fall in period associated with the initial contraction of the mean photospheric radius. This event can be seen in the plot of the photospheric radius and radii centred on the mass element associated with the equilibrium photosphere which forms fig. 9.35. It is clear that the mean photospheric radius has contracted from about $50 R_{\odot}$ to close to $40 R_{\odot}$ which should lead to a 10% rise in the mean effective temperature for the model. This rise in effective temperature is sufficient to carry the model from $\log(T_{\text{eff}}) = 3.70$ to 3.74, i.e. about half way across the instability strip.

Whilst the periods determined for radii deep in the envelope are useful as a guide they are not observable. For this reason periods have been calculated for the models from the times of light minimum. As can be seen from fig. 9.36 these periods are rather more variable

than the others. They lie within a range of 23 -39 days. The mean period calculated for the light curve is:

$$P = 29.0 \pm 1.9 \text{ days}$$

It is instructive to look at the phases of the light minima. A plot of the phases forms fig. 9.37. The phase varies in what appears to be a periodic manner. The amplitude of this variation is large, ~ 0.8 , although the scatter around the mean oscillation of the phase is probably less than 0.2. Is this sort of behaviour found in the RV stars? Fig. 9.38 is a reproduction of fig. 13 from Payne - Gaposhkin et al. (1943) and is a collection of plots of phase of light minimum for a number of RV stars. (N.B. the period used by Payne - Gaposhkin et al. is twice the pulsation period and so for comparison purposes the phase and cycle they give should be doubled.) It can be seen that all of the RV stars show a scatter in the phase of up to 0.8 and only for V Vul is the scatter much less than 0.4. Whether or not any of the stars shows a periodic phase variation with a comparable period, is open to debate. However it is clear that the variations in phase of minima are comparable for the stars and for this model.

Whether the variation of the phase really is periodic or is the result of random variations of the period is open to question. Consider fig. 9.39 which shows phases calculated for 100 periods scattered randomly around a specified mean. There is a disconcerting tendency for these phases to take on the appearance, at least for short stretches, of periodicity. Before anything conclusive can be

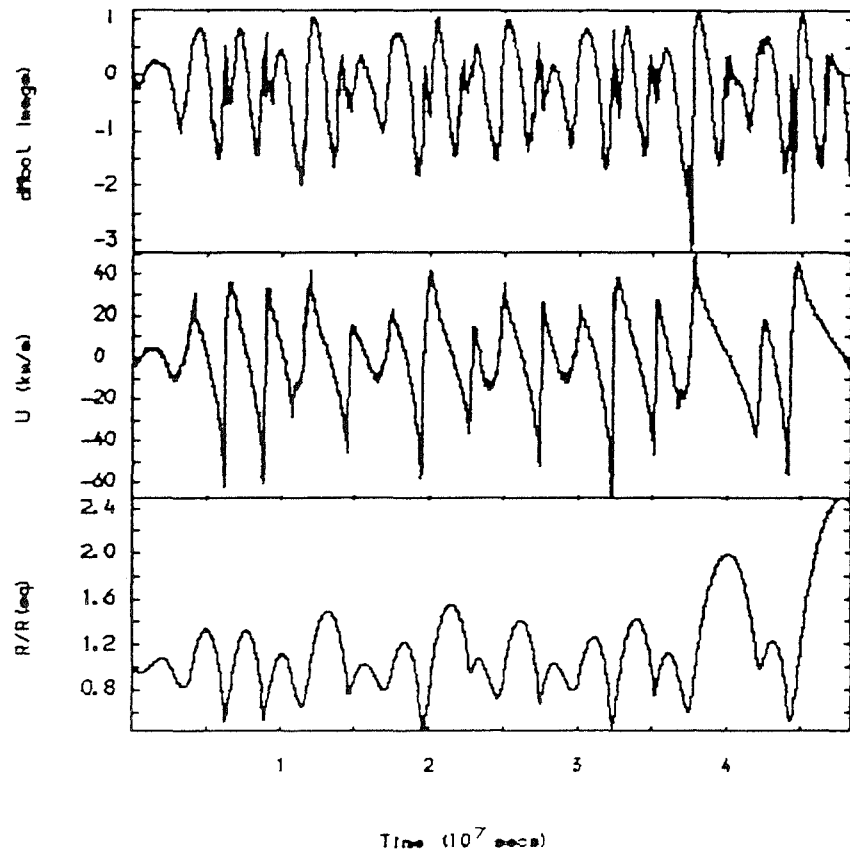


Fig. 9.31 $\log(L/L_{\odot}) = 3.2$, $\log(T_{\text{eff}}) = 3.70$

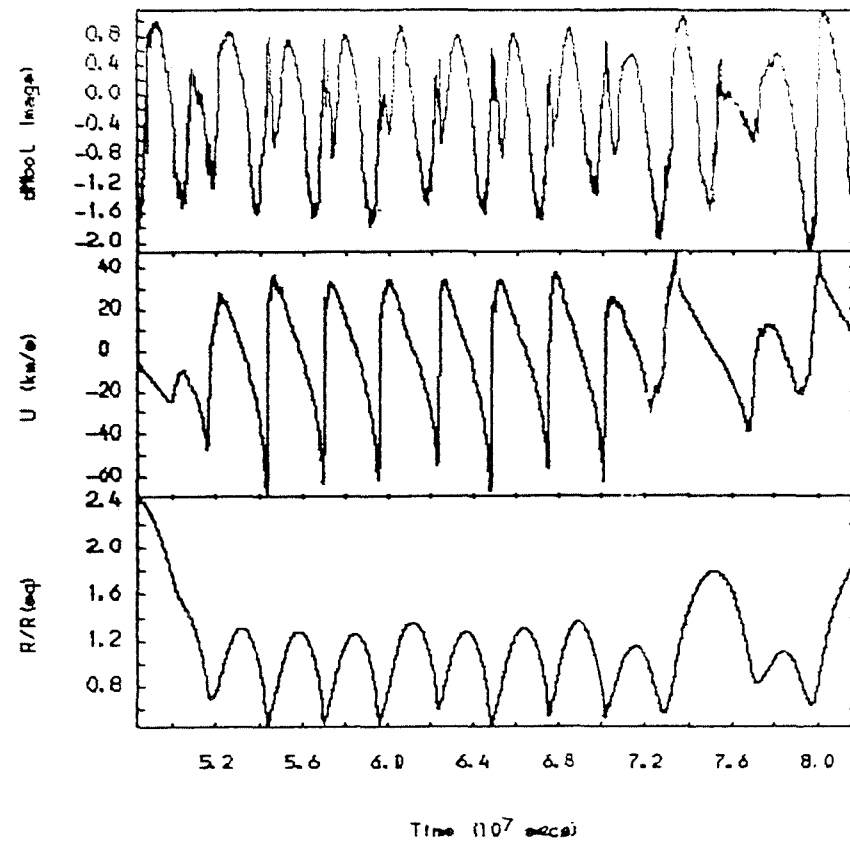


Fig. 9.32 $\log(L/L_{\odot}) = 3.2$, $\log(T_{\text{eff}}) = 3.70$
(continued)

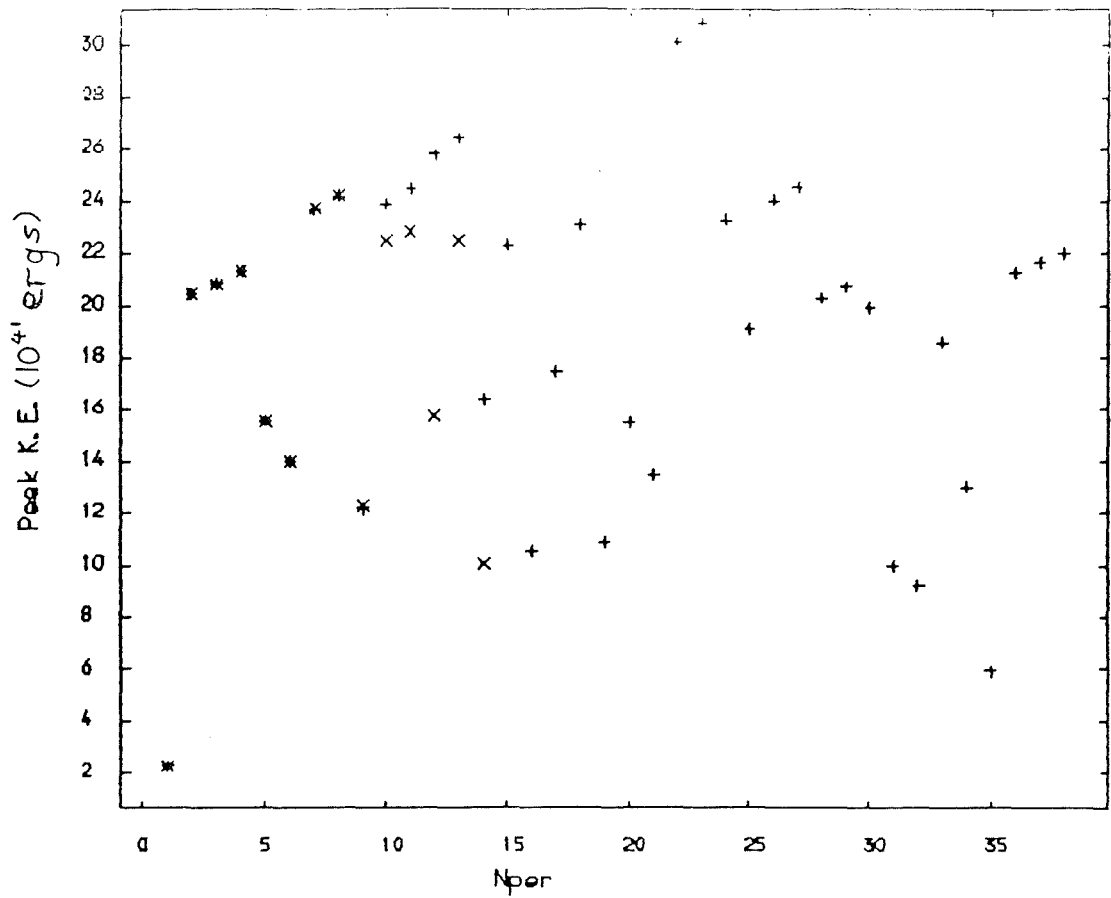


Fig. 9.33 Peak kinetic energies for
 $\log(L/L_{\odot}) = 3.2$, $\log(T_{\text{eff}}) = 3.70$
 + all molecular contributions
 x molecular hydrogen omitted

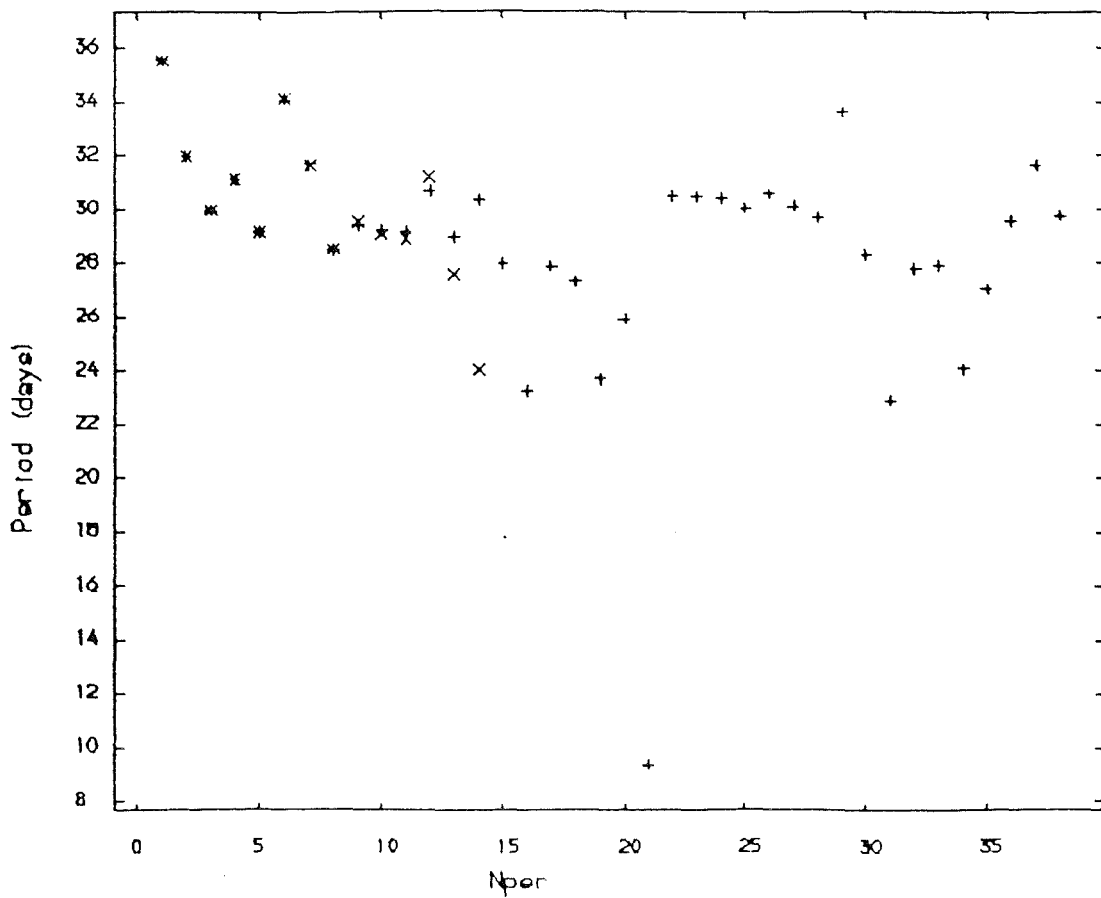


Fig. 9.34 Periods (deep in the envelope) for
 $\log(L/L_{\odot}) = 3.2$, $\log(T_{\text{eff}}) = 3.70$
 + all molecular contributions
 x molecular hydrogen omitted

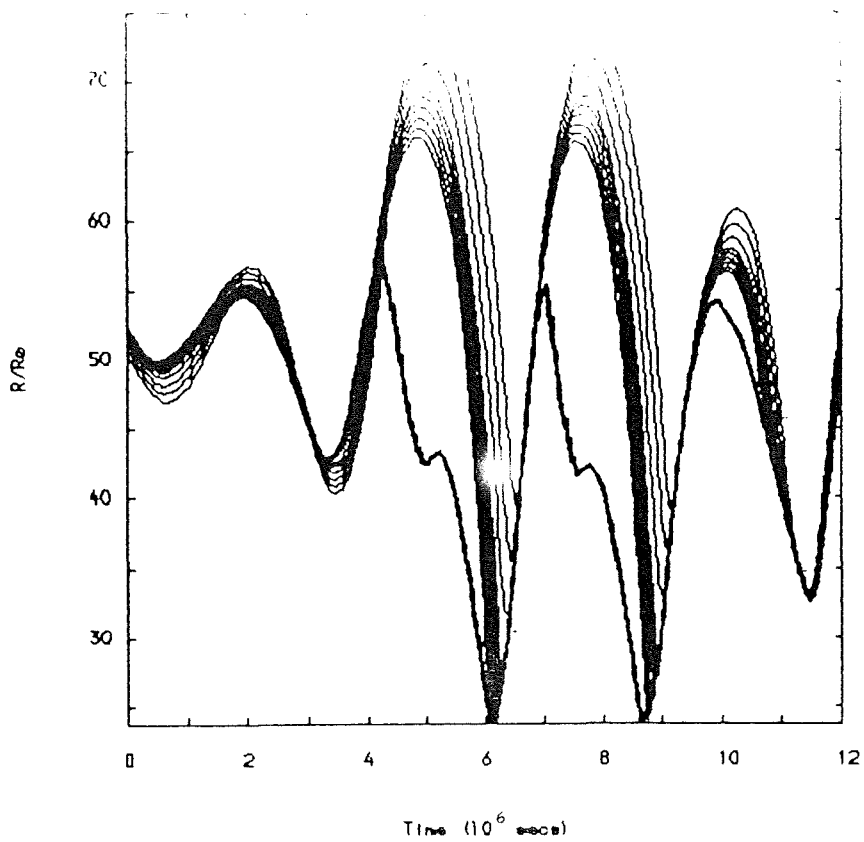


Fig. 9.35 $\text{Log}(L/L_{\odot}) = 3.2$, $\text{log}(T_{\text{eff}}) = 3.70$
 Thick line: photospheric radius
 Thin lines: zone boundary radii
 centred on the equilibrium
 photospheric mass zone

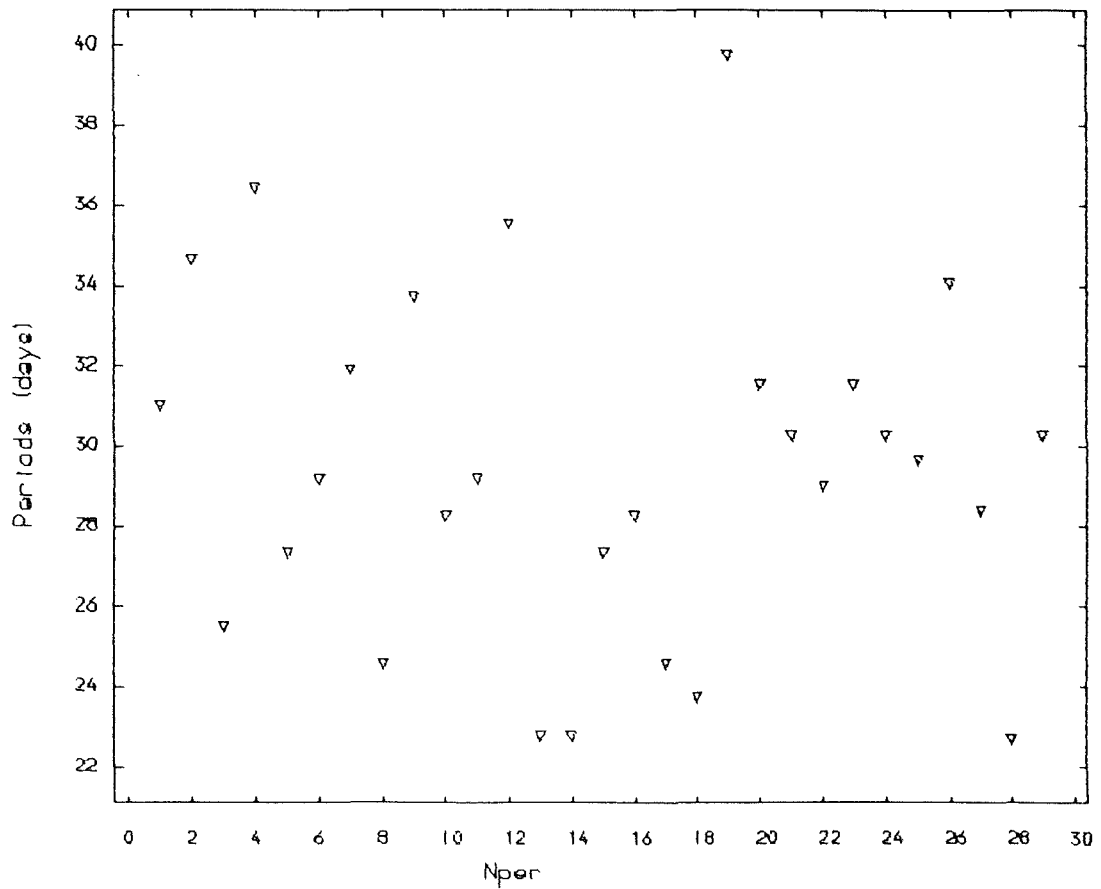


Fig. 9.36 Periods determined from the light
 curve for $\text{Log}(L/L_{\odot}) = 3.2$,
 $\text{log}(T_{\text{eff}}) = 3.70$

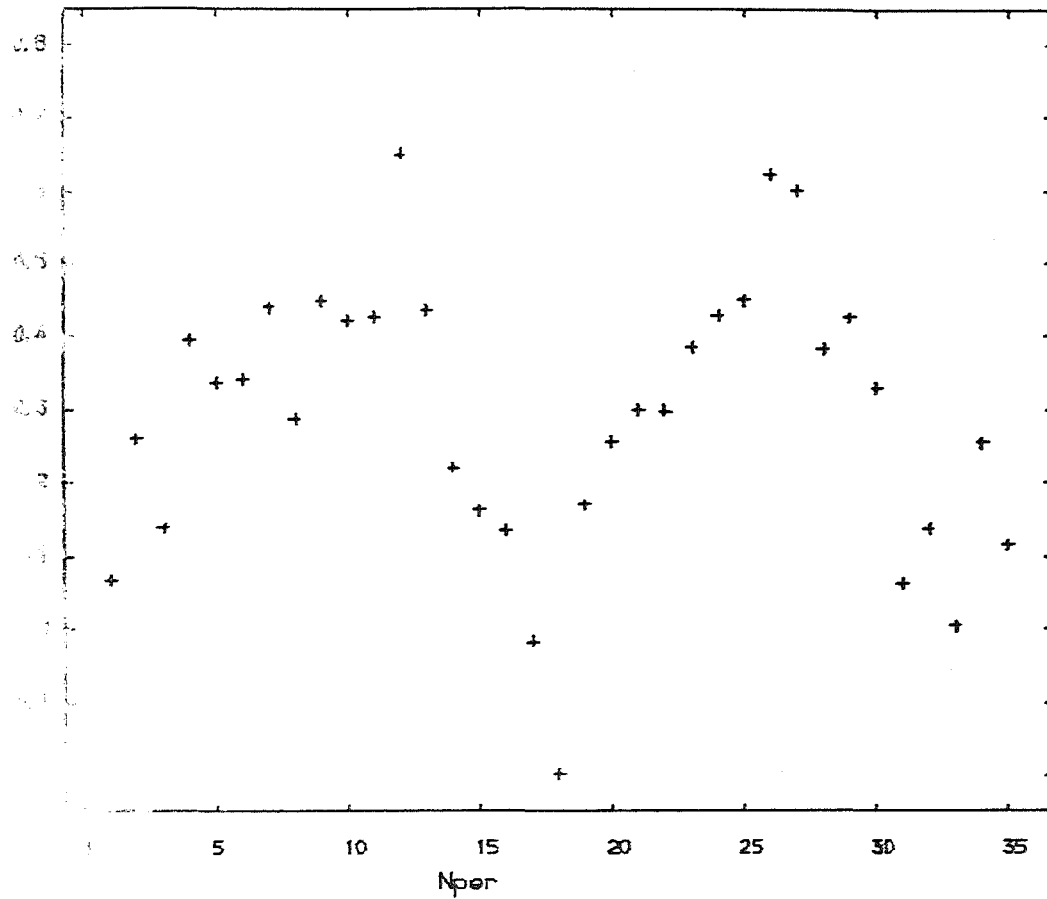


Fig. 9.37 Phase of light minima for
 $\log(L/L_{\odot}) = 3.2$, $\log(T_{eff}) = 3.70$

[02

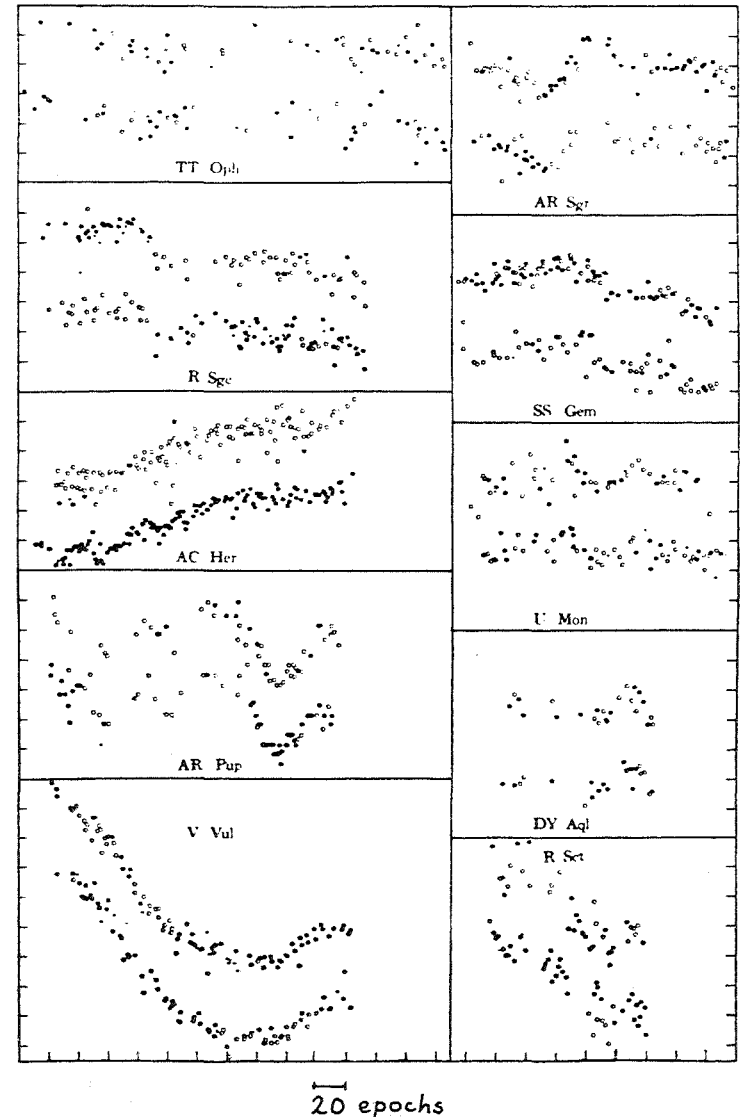


Fig. 9.38 Phases of minima for selected RV Tau stars
 (from Payne-Gaposhkin et al. 1943)
 N.B. phased using double period
 ● Primary minima

OSerially...

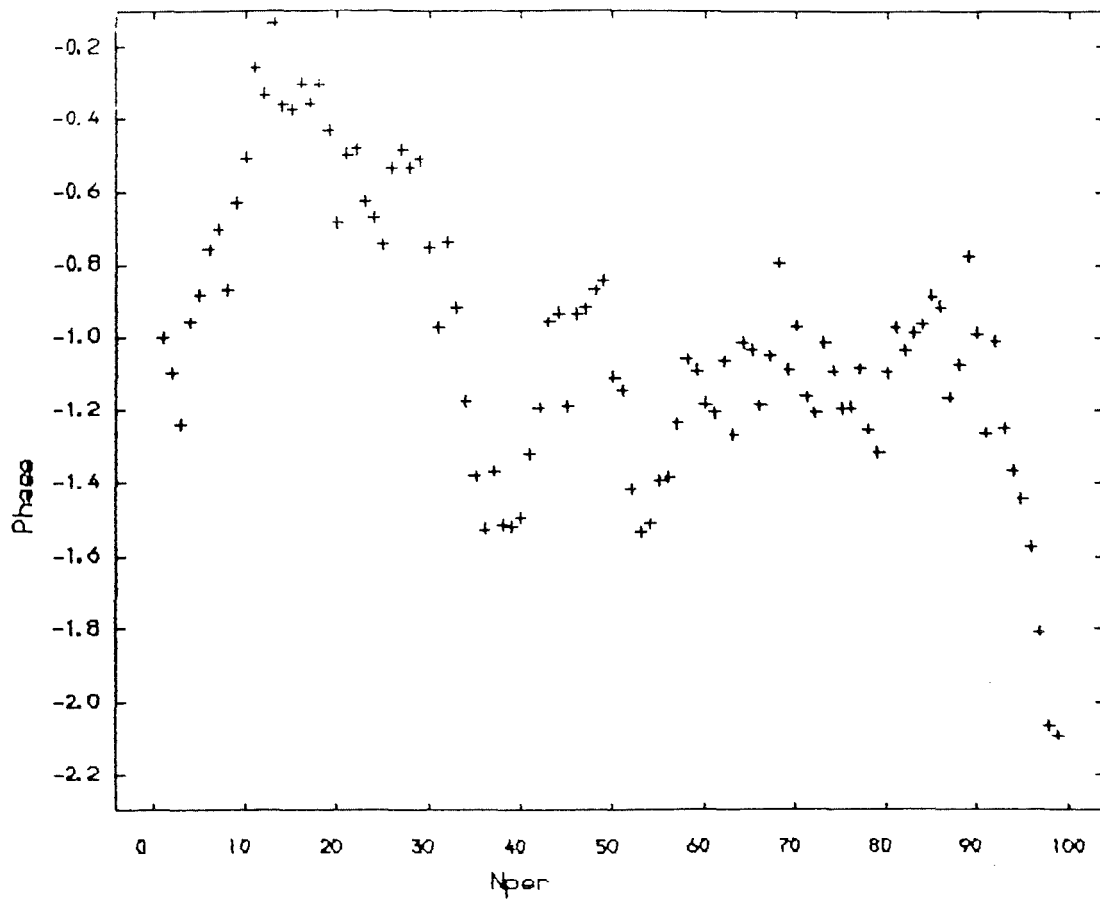


Fig. 9.3? Phases of minima for randomly generated periods

said regarding the question of periodicity in the phase of light minima proper statistical tests (Lacy 1973) would have to be carried out on far larger sets of data. For now I think it suffices to say that similar behaviour is found in both the model and in the observations.

Whilst the light curve is certainly not regular it is difficult to see it as a typical RV Tauri light curve. However it does look somewhat like the light curve of the rather atypical RV Tau star, TT Oph. A feature of possible interest is the deep minimum at $T = 3.75 \cdot 10^8$ secs. at the end of period 14. This minimum coincides with the infall of a zone and then the immediate expansion of a great many zones, fig. 9.40, involving a mass of $8.5 \cdot 10^{-6} M_{\odot}$. The matter involved remains bound. As usual with a large expansion phase the peak kinetic energy for this period is much reduced. That of the following period is much greater but is followed by another fall. From here over the next 3 periods the cycle is repeated with another large expansion taking place. The result of these expansions is the creation of an extended atmosphere for about 7 - 8 periods with large amounts of matter lying up to $200 R_{\odot}$ or more from the stars centre. Some of this gas moves through very large distances, $100 R_{\odot}$, over 2 - 3 periods frequently with speeds as great as 60 km/sec. There is thus plenty of scope for explaining the existence of high redshift lines and the large distances travelled by material as observed by Baird (1984) in AC Her. However it must be pointed out the in AC Her the

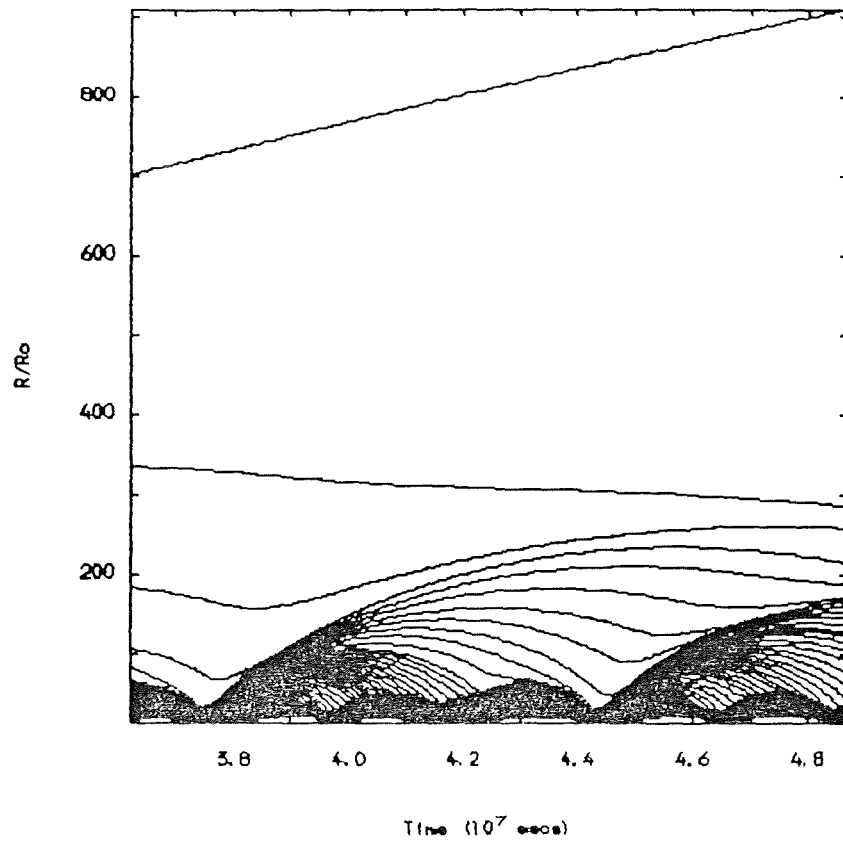


Fig. 9.40 $\text{Log}(L/L_{\odot}) = 3.2$, $\text{log}(T_{\text{eff}}) = 3.70$
 radii of zone boundaries at the very
 deep minimum ($T = 3.75 \cdot 10^7$ secs) and
 afterwards

high redshift lines occur at rising light whereas in this model they are found a little earlier in phase on the preceding falling light.

It is also difficult to compare the star with the model because the temperatures could well be very different. I say could because Baird (1984) finds an effective temperature $\log(T_{eff}) = 3.78$ from the line spectrum whereas Dawson (1979) derives $\log(T_{eff}) = 3.69$ from his D.D.O. photometry. The effective temperature for the equilibrium model was $\log(T_{eff}) = 3.70$ but that for the nonlinear model is closer to $\log(T_{eff}) = 3.74$. This makes any conclusions drawn from a comparison of theory and observation precarious. However for what it is worth fig. 9.41 shows the movements of the zones 34 - 42 centred on the equilibrium photospheric mass element and the photosphere itself. The next figure, fig. 9.42, shows the velocity curves for the zones and for the photosphere. A point of interest here is the fact that the photospheric velocity and so presumably those at other fixed optical depths is very like the light curve. This has been found to be the case in some RV stars. An example of this is AC Her (Bopp 1984). It is conceivable that at least part of the uncertainty in the observed temperature for AC Her might be explained by the presence of an extended atmosphere such as that found in the model. Mihalas (1978) makes the important point that a colour temperature for an extended atmosphere will be lower, frequently by a large factor, than the actual temperature. This fits with the fact that the photometric temperature is lower than the line temperature. Also he points out

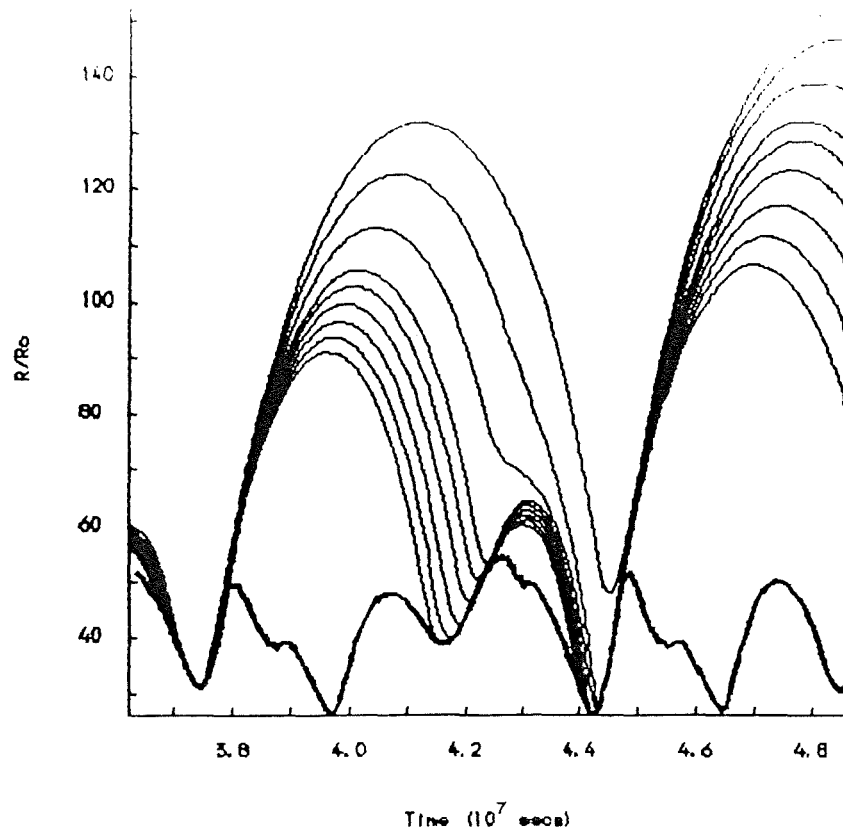


Fig. 9.41 $\log(L/L_{\odot}) = 3.2$, $\log(T_{\text{eff}}) = 3.70$
 Thick line: photospheric radius
 Thin lines: zone boundary radii
 centred on the equilibrium
 photospheric mass zone

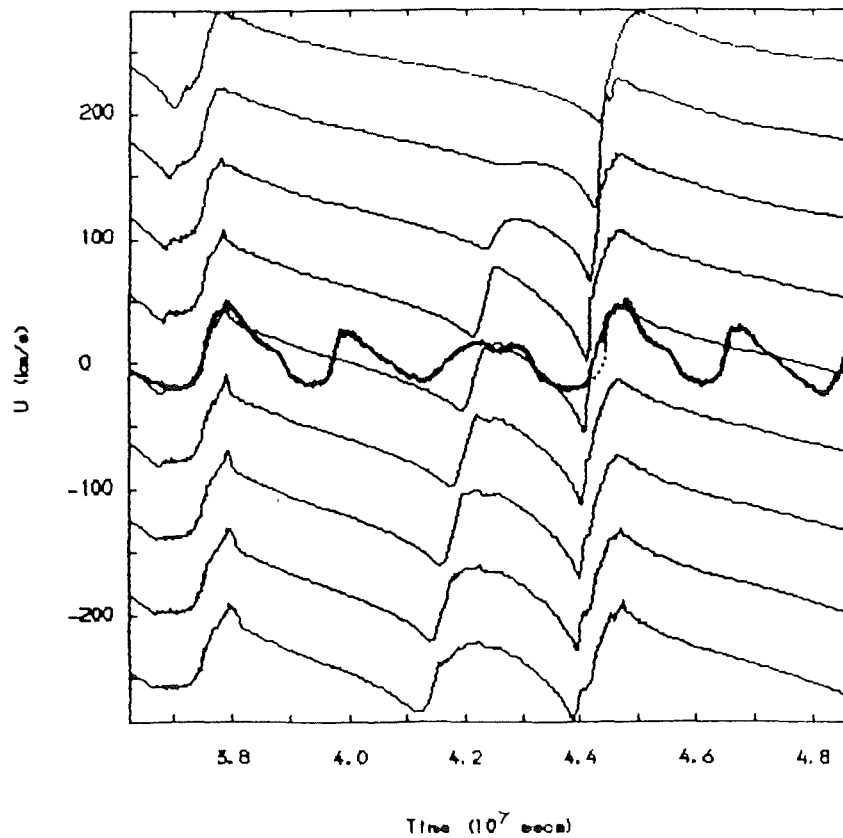


Fig. 9.42 $\log(L/L_{\odot}) = 3.2$, $\log(T_{\text{eff}}) = 3.70$
 Thick line: velocity at photospheric radius
 Thin lines: velocities at zone boundary radii
 centred on the equilibrium photospheric
 mass zone

that when the flux distribution for the star is compared with a Planck function for the colour temperature then the star will appear to show both ultraviolet and infrared flux excesses. The RV stars show these excesses and although a large part of these excesses is undoubtedly due to metal paucity and the presence of circumstellar matter a contribution due to the above effect cannot be ruled out.

9.5.3 The Model For $\text{Log}(L/L_{\odot}) = 3.4$

The move to a higher luminosity again accentuates the irregularities in the model. Figs. 9.43 and 9.44 are plots of the peak kinetic energy and period (determined deep in the envelope) for the main model and for a model computed without molecular hydrogen in the equation of state but with molecular opacity. A great deal of irregularity is obvious with the peak kinetic energies varying over a factor of ten. In fig. 9.45 the periods for the light curve are plotted. The mean period for the light curves is;

$$P = 36.23 \pm 0.14 \text{ days.}$$

Again the irregularity is plain to see and, as for the lower luminosity model, the irregularity is greater than for the periods of the radii. However when the phases of the light minima are plotted, fig. 9.46, then some semblance of order appears. As in the previous model the phases appear to vary periodically this time with a cycle length of twenty - six mean pulsation periods. Again it is probably not possible to make a definite statement on whether or not the

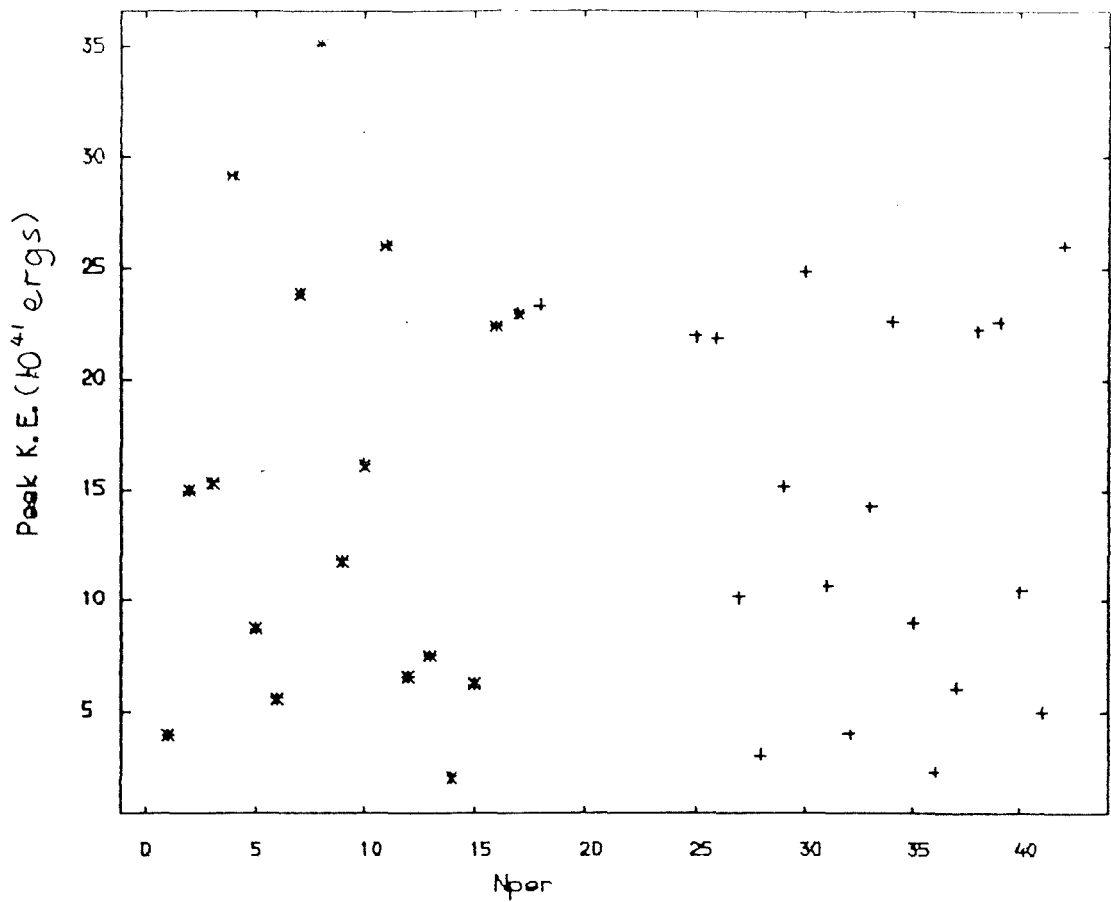


Fig. 9.43 Peak kinetic energies for
 $\text{Log}(L/L_{\odot}) = 3.4$, $\text{log}(T_{\text{eff}}) = 3.70$
 + all molecular contributions
 x molecular hydrogen omitted

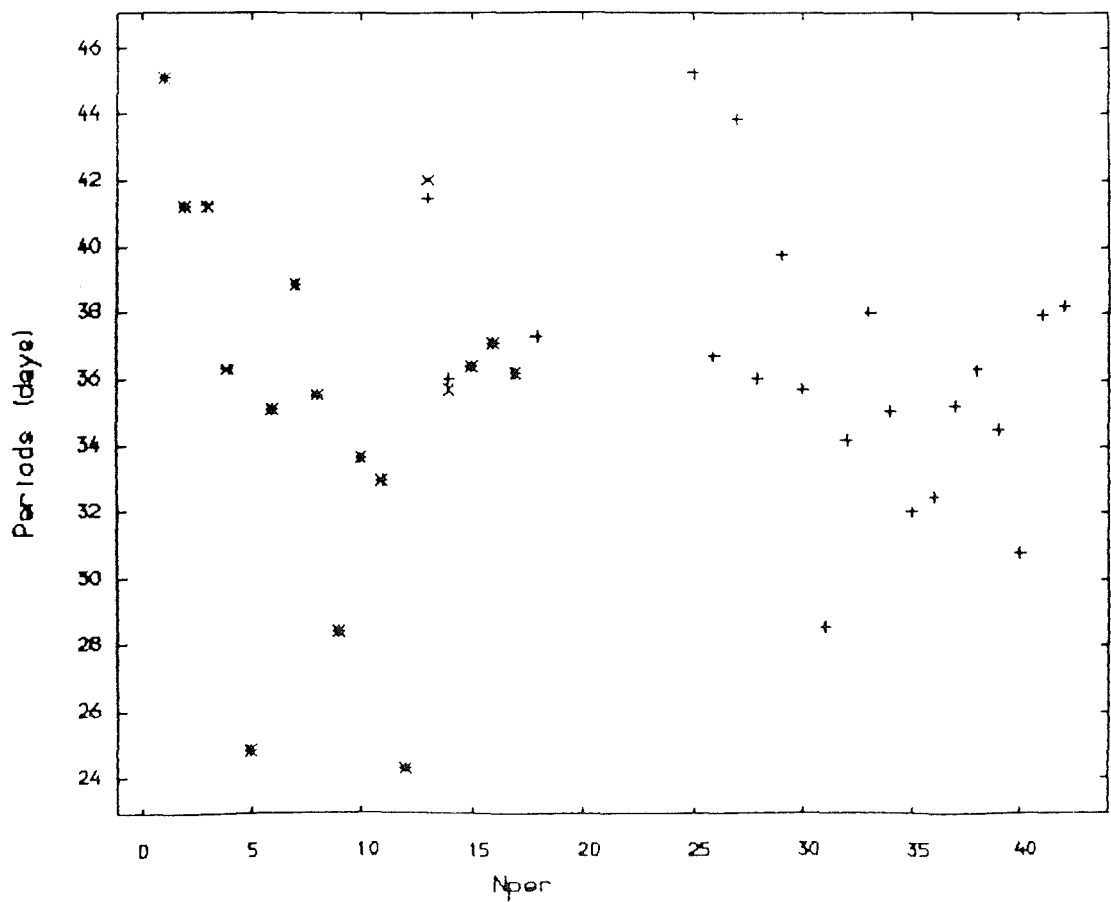


Fig. 9.44 Periods (deep in envelope) for
 $\text{Log}(L/L_{\odot}) = 3.4$, $\text{log}(T_{\text{eff}}) = 3.70$
 + all molecular contributions
 x molecular hydrogen omitted

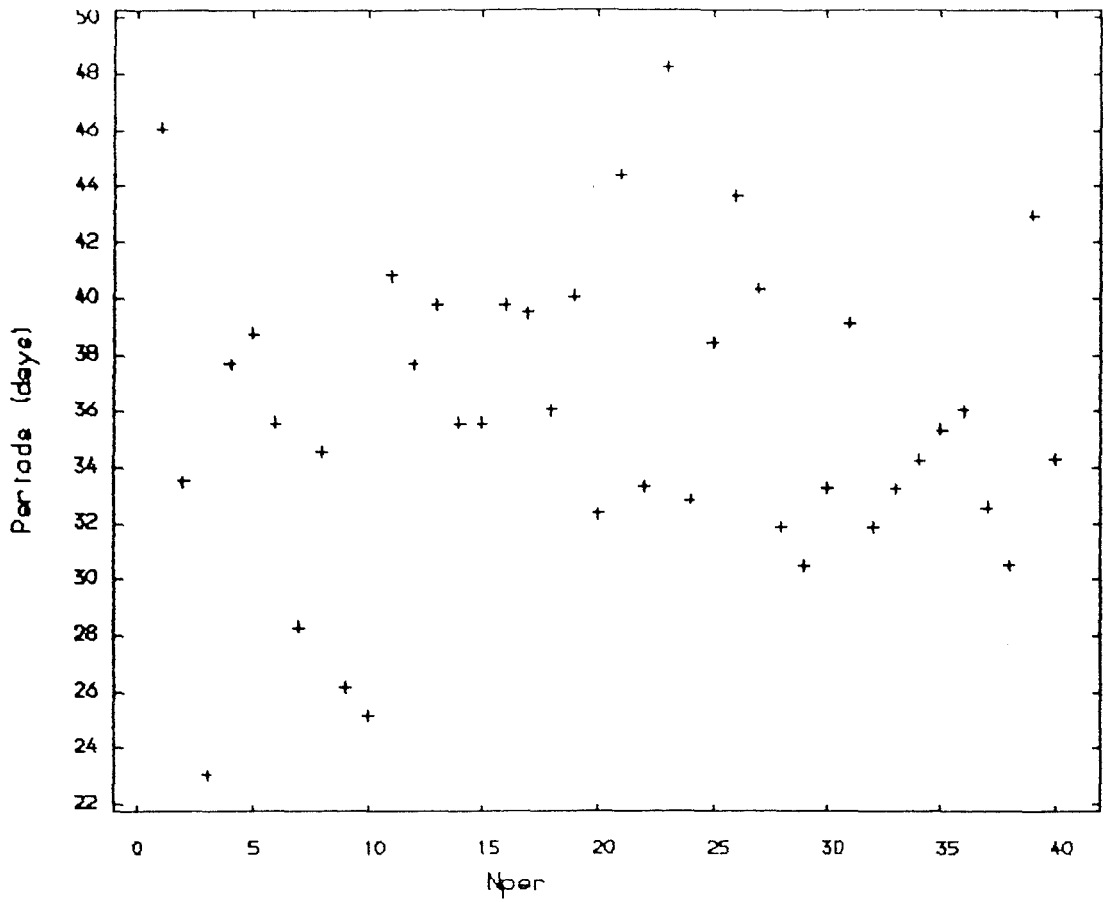


Fig. 9.45 Periods determined from the light curve for $\text{Log}(L/L_{\odot}) = 3.4$, $\text{log}(T_{\text{eff}}) = 3.70$

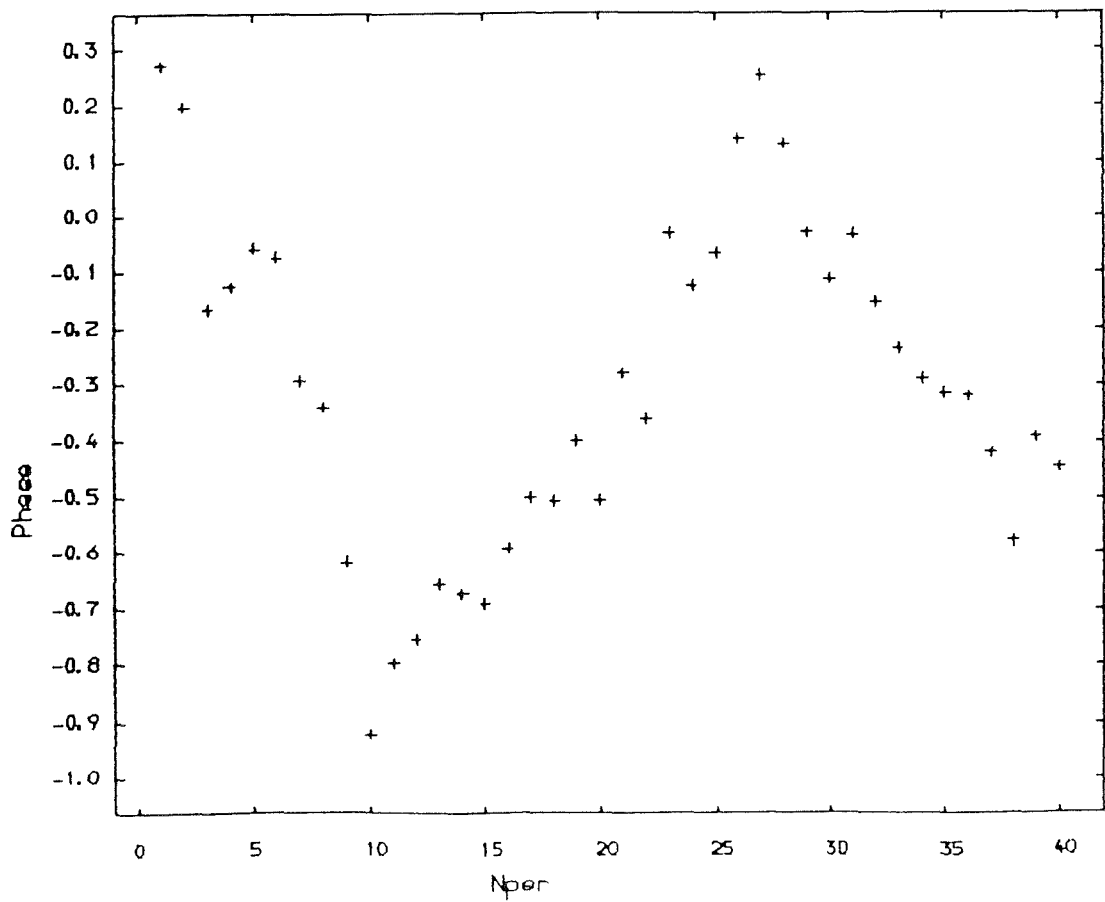


Fig. 9.46 Phases of light minima for $\text{log}(L/L_{\odot}) = 3.4$, $\text{log}(T_{\text{eff}}) = 3.70$

variation is truly periodic.

Unfortunately it was not possible to make plots of long stretches of the light - curve, etc. However figs. 9.47 - 9.49 contain a number of slices of the data. The luminosity spikes are still present but are much reduced in amplitude and much less frequent than in the lower luminosity model. A recurring feature of this model is a sudden drop in amplitude of the pulsation. The pulsation then grows from this reduced amplitude back to the original strength in much the same way as the pulsation grows from the initial perturbation. After a few periods of large amplitude pulsation the amplitude falls off again and so the cycle is repeated. It is just possible that this quasi periodic variation of the amplitude might be the result of a beat between two modes but the asymmetric profile of the variation argues against this. Perhaps more importantly a beat would be expected to give a more systematic variation. There seems to be little to distinguish the low amplitude phases of the pulsation except that they tend to be associated with the infall of the previously accelerated matter and to follow a period during which a moderate expansion of the lower atmosphere took place. In many ways the light curve for this model is like that of R Sct and perhaps AR Pup and U Mon.

A striking feature of this model is the very great extent of the atmosphere. Although it is still bound the atmosphere now extends out to $2000 R_{\odot}$ for periods 38 - 42 ($T = 11.6 - 13.2 \cdot 10^8$ secs) as can be

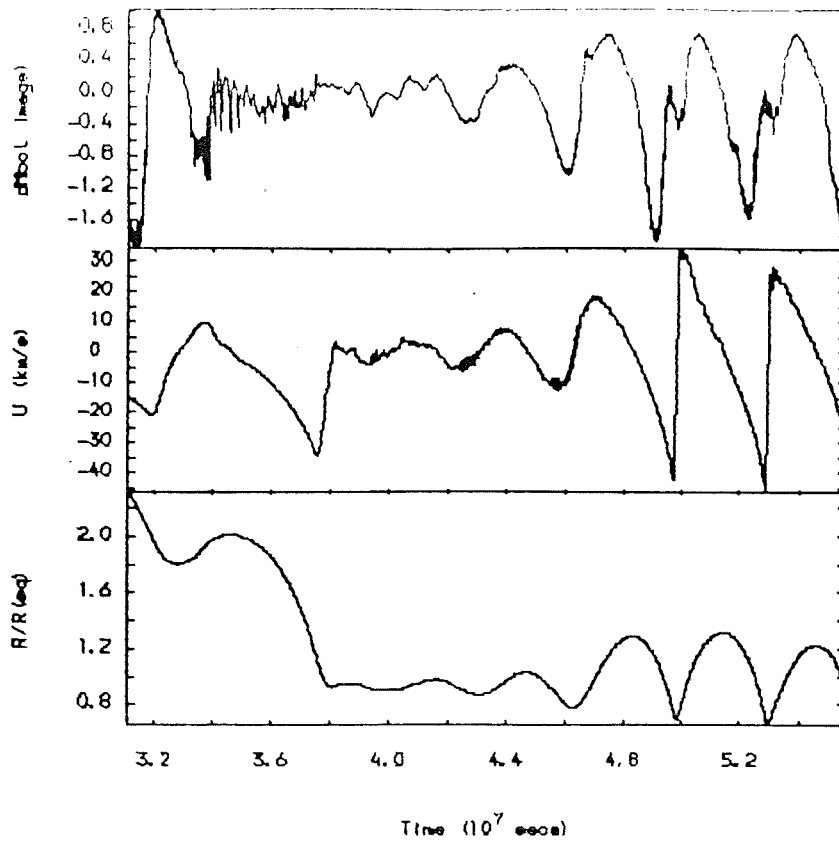


Fig. 9.47 $\text{Log}(L/L_{\odot}) = 3.4$, $\log(T_{\text{eff}}) = 3.70$

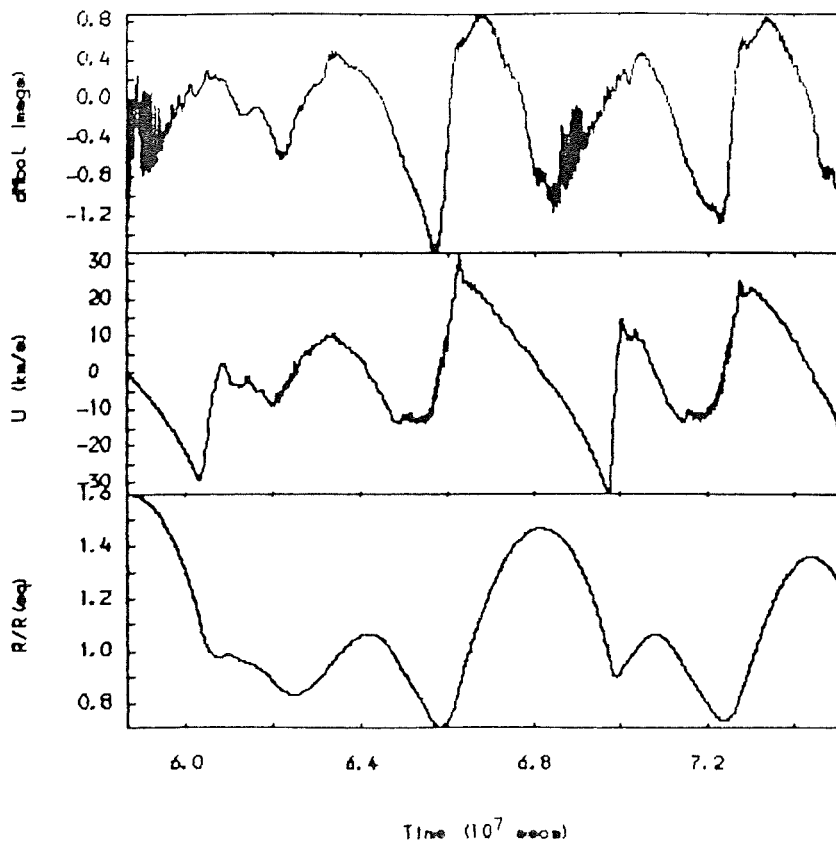


Fig. 9.48 $\log(L/L_{\odot}) = 3.4$, $\log(T_{\text{eff}}) = 3.70$
(continued)

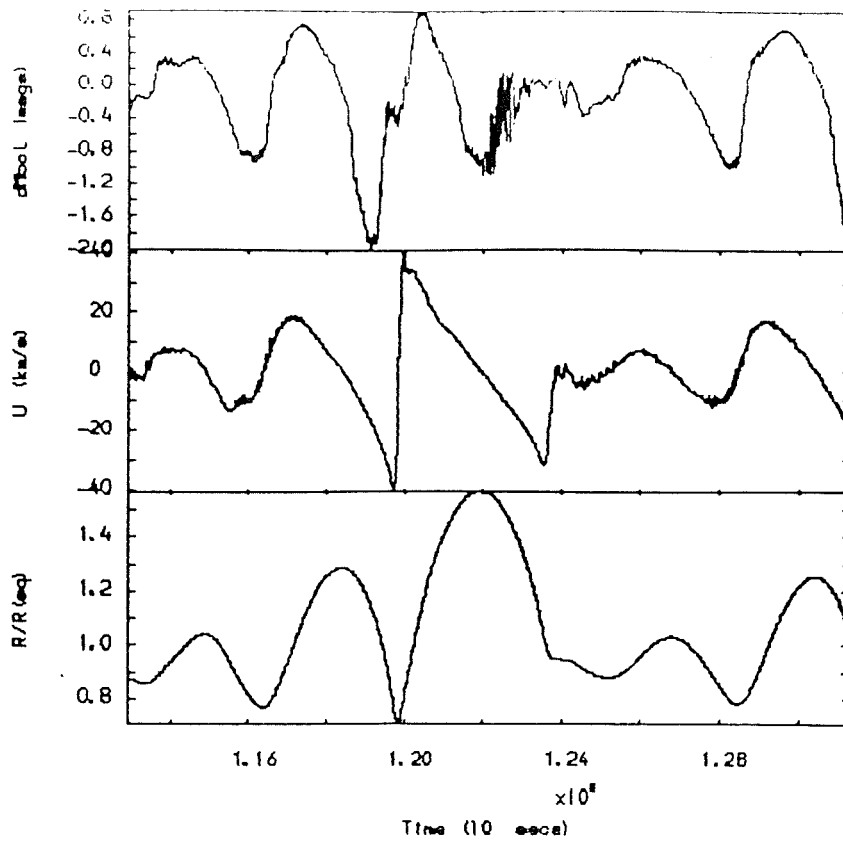


Fig. 9.49 $\text{Log}(L/L_{\odot}) = 3.4$, $\text{log}(T_{\text{eff}}) = 3.70$
(continued)

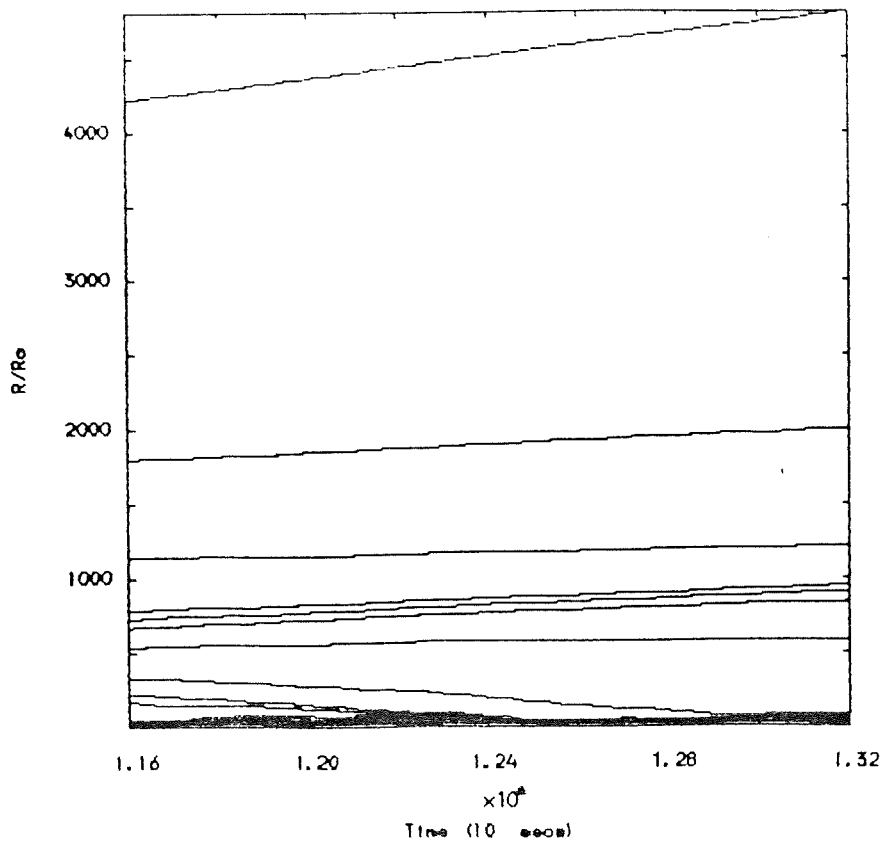


Fig. 9.50 $\text{Log}(L/L_{\odot}) = 3.4$, $\text{log}(T_{\text{eff}}) = 3.70$
Formation of the highly extended atmosphere

seen from fig. 9.50. However even after 4.2 yrs only the outer layer has reached escape velocity and so the mass loss rate is,

$$M < 2.4 \cdot 10^{-6} M_{\odot}/\text{yr}.$$

The mass in the extended atmosphere between 500 and 2000 R_{\odot} is $\sim 2.6 \cdot 10^{-5} M_{\odot}$. Temperatures are low enough, ~ 600 K, to permit the formation of dust. Thus the infrared observations (Gehrz 1972) seem to fit in with theory.

9.5.4 The Deep Minimum For The $\text{Log}(L/L_{\odot}) = 3.2$ Model

A very deep minimum was observed recently in R Sct by Howell et al. (1983). A curious feature of this minimum ($\sim 3^m$ dimmer than mean light) was the presence of almost all spectral lines as emission lines rather than in absorption. The only absorption features present were the TiO bands. For this reason a close look at the very deep minimum at $T = 3.75 \cdot 10^7$ secs in the $\text{log}(L/L_{\odot}) = 3.2$ model is suggested.

Looking at the model at the deep minimum we find that at $T = 3.75358 \cdot 10^7$ secs the star is very greatly compressed with densities of $> 5 \cdot 10^{-8}$ g/cm³ above the photosphere and below the atmospheric shock. This shock is formed at the point at which the tenuous infalling atmosphere meets the rising material below. This shock is shown up clearly in the velocity profiles in fig. 9.51. The velocity across the shock is 46 km/sec and the ratio of the densities on either side is $1.9 \cdot 10^{-8} / 4.4 \cdot 10^{-10} \sim 44$ indicating a strong shock. Fig. 9.52 shows

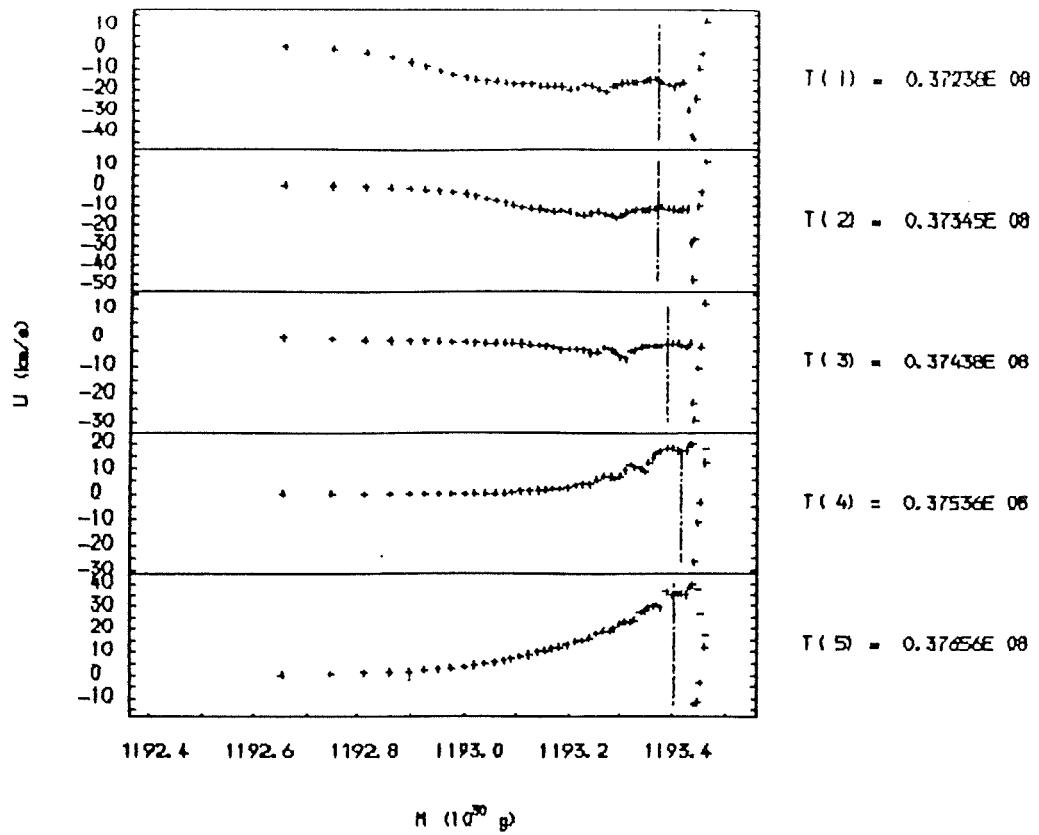


Fig. 9.51 Velocity profiles for
 $\text{Log}(L/L) = 3.2$, $\text{log}(T) = 3.70$
 at the very deep minimum
 (Vertical line indicates photosphere
 and -s indicate escape velocity)

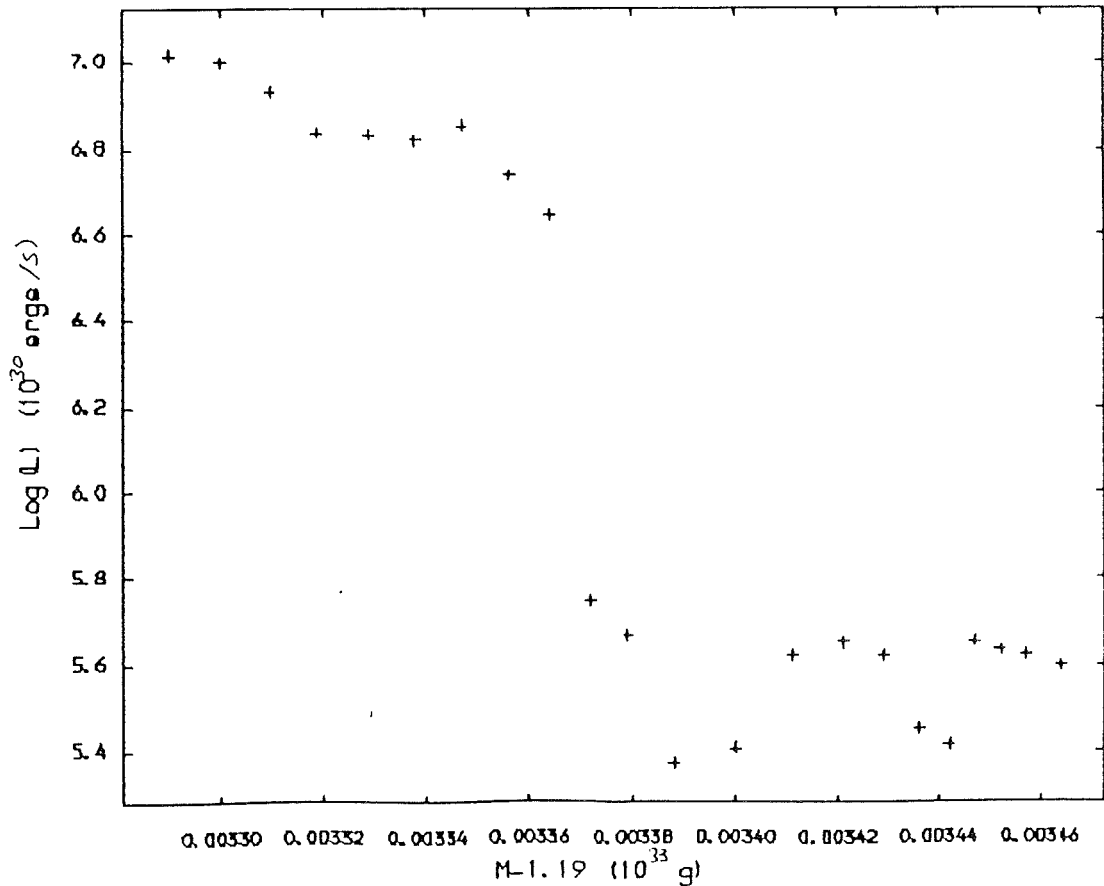


Fig. 9.52 Luminosity profile for
 $\text{Log}(L/L) = 3.2$, $\text{log}(T) = 3.70$
 at the very deep minimum
 ($T = 3.7536 \cdot 10$ secs)

the variation of the luminosity with mass in the outer part of the model. Below the photosphere the luminosity falls off very steeply towards the surface as the result of the compression effect on absorption. There is thus a region in which the heat of the gas is rising rapidly. Further out beyond the photosphere we encounter the shock where there is a considerable rise in the luminosity. Presumably this luminosity is generated by the shock although it is very difficult to get a reasonable estimate of the shock power because the density is poorly resolved outside the shock and changes greatly from zone to zone. The increase in luminosity at the shock accounts for about 49% of the total luminosity at the surface. Presumably a sizeable proportion of this will be in the form of emission lines and will thus be able to account for the strength of emission at the deep minimum though whether this can help explain the lack of line absorption I do not know. A problem with this explanation of the emission strength at the deep minimum is that the shock is moving outwards with a velocity of 20 km/s whereas the emission lines from R Sct are very nearly stationary with respect to the stellar centre of gravity. However, moving back to the situation shown in the velocity profile before this one we find that although the luminosity is not as low as before, only $1^{*}7$ below the mean luminosity, 66% of the luminosity is generated in the shock zone, and the shock is moving inwards only at 1.5 km/s. This fits the observations much better although there is a difference in time of about 2.5 days ($\Delta\phi = 0.07$)

between the deep minimum and this stage of the shock.

9.5.5 Damping Through Running Waves

The creation of an extended atmosphere raises the possibility that damping of the pulsations by running waves might occur. Consider the values of $(\partial \log(p)/\partial r)^{-1}/R$ in the outermost parts of the star. For period 7 of the model for $\log(L/L_{\odot}) = 3.4$ the values are;

1.13, 0.29, 0.12,.....

The large value in the outer zone certainly suggests that running waves might be important here. However bearing the negative results for the linear models constructed with the running wave boundary condition in mind detailed calculations must be made before any conclusion can be drawn.

9.5.6 Omission Of Molecules From The Equation Of State

The differences between the peak kinetic energies developed by models with and without hydrogen molecules in the equation of state can be seen in figs. 9.33 and 9.43. At the outset there is no difference to be seen for models at either luminosity. The outer layers of the model are still too hot to allow the formation of molecular hydrogen at sufficiently high densities. However by period 8 for the $\log(L/L_{\odot}) = 3.2$ model differences have begun to creep in and by the 10^4 period the peak kinetic energy for the model incorporating

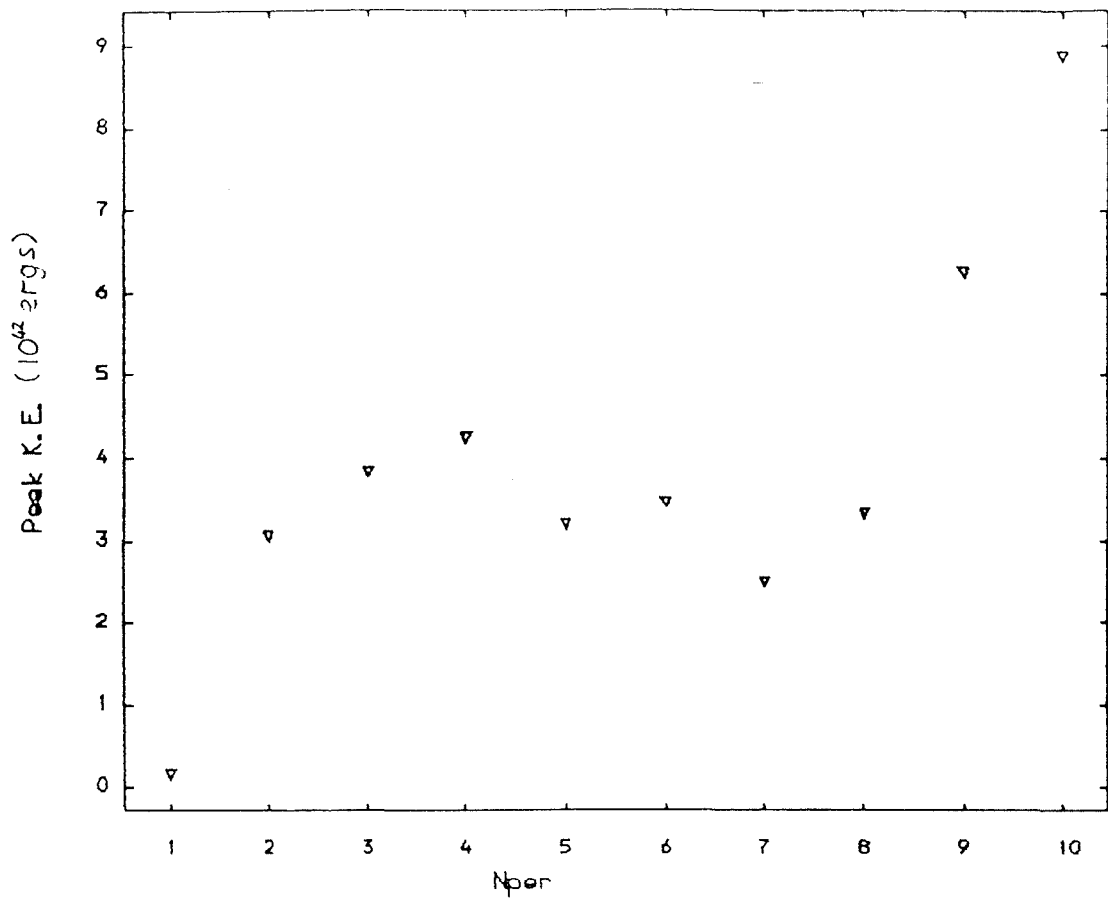


Fig. 9.53 Peak kinetic energies for
 $\text{Log}(L/L_{\odot}) = 3.2$, $\text{log}(T_{eff}) = 3.70$
 with all molecular contributions omitted

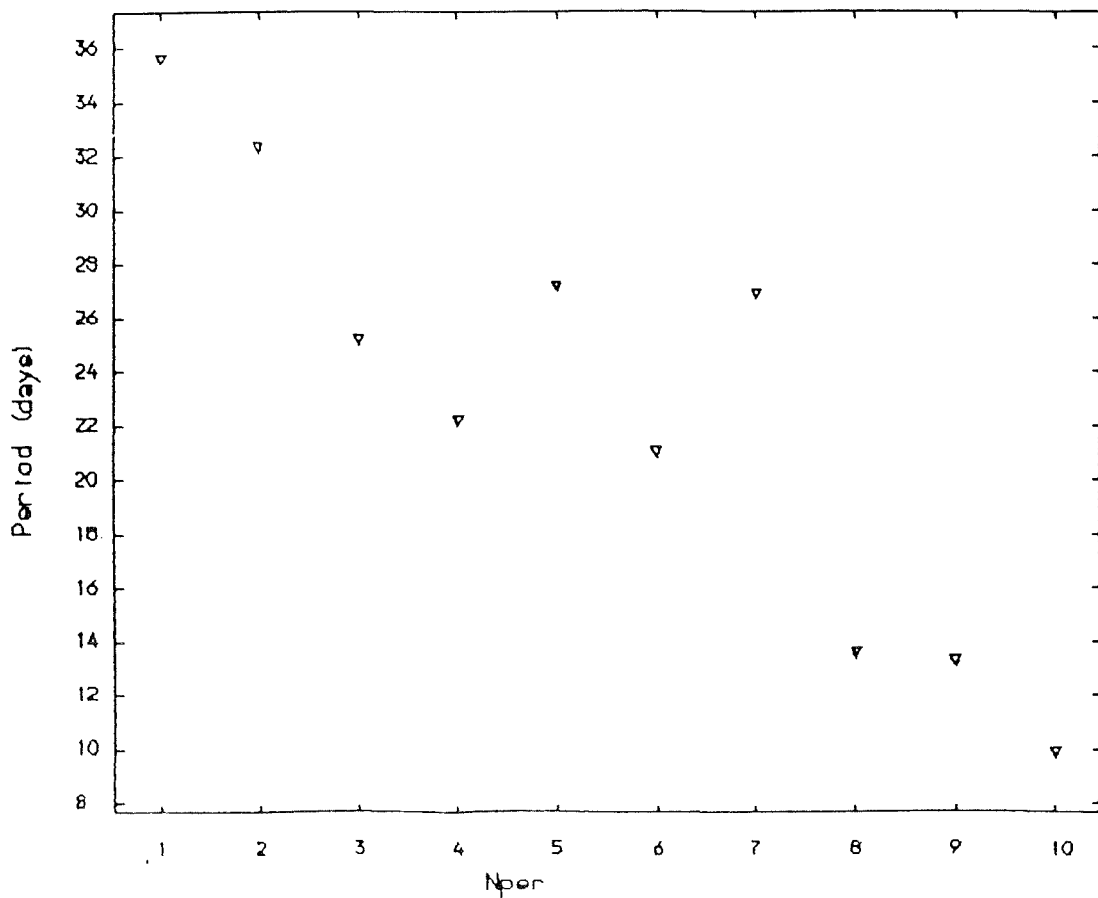


Fig. 9.54 Periods (deep in envelope) for
 $\text{Log}(L/L_{\odot}) = 3.2$, $\text{log}(T_{eff}) = 3.70$
 with all molecular contributions omitted

molecular hydrogen is noticeably larger than in the other model of the same luminosity. It is impossible to use the work integrals to confirm the appearance of H_2 driving because the differences introduced by the aperiodicity in the two models mask any that might be caused by a new source of driving. The peak kinetic energies for the two higher luminosity models are very nearly identical all 17 periods over which they were both run. This is presumably a result of the lower densities in the atmosphere although, again, this cannot be conclusively confirmed.

When the light curves for the models with and the models without molecular hydrogen in the equation of state are compared it is found that for the models with $\log(L/L_\odot) = 3.2$ the RV - like property of the light curve is stronger in the model from which molecular hydrogen is excluded. For the higher luminosity models there are no significant differences between the two light curves even though these model was run for longer than the previous pair. The peak kinetic energies are the same down to 3 significant figures and this is true of all of the variables except for the period which is different in the third figure for two adjacent periods by ~ 0.5 days. However the sum of these two periods for the two models differs only by 0.3 days.

9.5.7 Omission Of All Molecular Effects

When molecules are entirely neglected the growth of the pulsations is spectacular. It was not possible to construct a high luminosity model and so this discussion must be limited to the $\log(L/L_{\odot}) = 3.2$ model. The peak kinetic energy and the periods for the low luminosity model without molecules form figs. 9.53 and 9.54. As can be seen the peak kinetic energies, after a brief lull, undergo a precipitous rise and the periods show an equally startling decrease. After 10 periods the model died and refused all attempts at resuscitation. Clearly the inclusion of a molecular opacity is essential to the nonlinear modelling of these stars.

9.5.8 The Effects Of Varying The Artificial Viscosity

A number of experiments were carried out for $\log(L/L_{\odot}) = 3.2$. Halving the artificial viscosity constant results in a 20% lowering of the peak kinetic energy during the reliable, early phase of the models but unpredictable results later. This is coupled with a very ragged light curve indicative of spurious oscillations in the zone variables and so an artificial viscosity this low should not be used. On the other hand a quadrupling of the artificial viscosity constant increases the peak kinetic energies by 5 - 10%. This is linked with an increase of the height of the luminosity spikes and so as little advantage could be seen in using this value of the constant all

further models were computed using the usual value of 1.

Removal of the artificial viscosity cutoff for weak shock waves makes a small decrease ($< 5\%$) in the peak kinetic energy.

Changes of 5 - 10% in the peak kinetic energy are, I think, negligible when the uncertainties in other approximations and due to zoning are recalled. One important point is that the luminosity spikes are apparently not sensitive to the details of the artificial viscosity even though they do arise from shocks.

9.5.9 The Luminosity Spikes

These features appear at rising light during most periods of the $\log(L/L_{\odot}) = 3.2$ model and a few periods of the higher luminosity model. The spike is associated with the emergence of a shock wave from the photosphere of the model. A spike in the luminosity can be traced through a model, see fig. 9.55 and 56, and can be seen to move with the shock in the optically thick envelope. However when the shock reaches the photosphere the excess luminosity is very quickly radiated away. How does this compare with a more "normal" model? Looking at a simple crested W Vir model, e.g. Bridger's (1983) model for $\log(L/L_{\odot}) = 3.1$, $\log(T_{\text{eff}}) = 3.75$, we see that the same basic pattern is present. In this case the shock induced spike nearly merges with the hump which arrives slightly later and becomes the crest at light maximum. So there is nothing strange about the

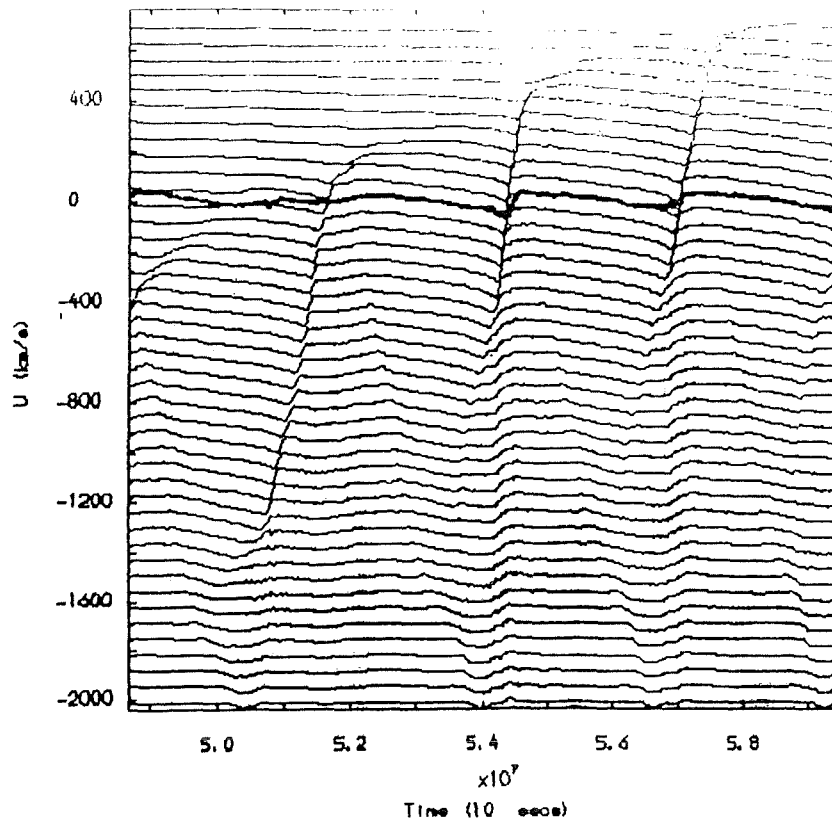


Fig. 9.55 $\text{Log}(L/L_{\odot}) = 3.4$, $\text{log}(T_{\text{eff}}) = 3.70$
 Velocities at zone boundaries and
 photospheric velocity (thick line)
 Note periodic shocks

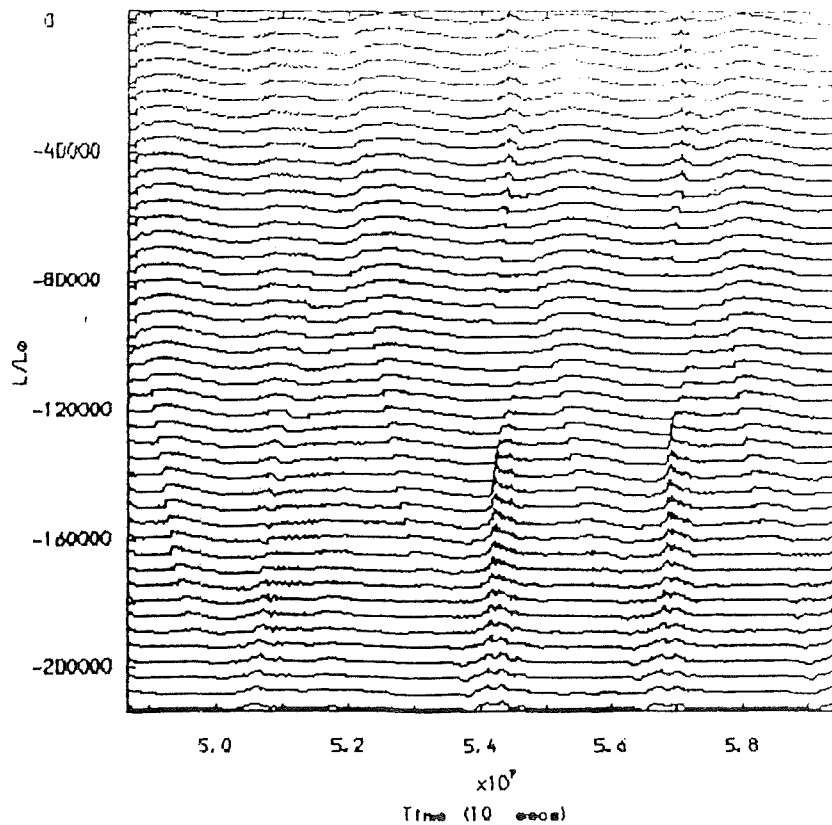


Fig. 9.56 $\text{Log}(L/L_{\odot}) = 3.4$, $\text{log}(T_{\text{eff}}) = 3.70$
 Luminosity at zone boundaries,
 for comparison with fig. 9.55

mechanism responsible for the formation of the luminosity spikes.

9.5.10 The Validity Of The Equilibrium Diffusion Approximation

In section 7.1.2.4 it was shown that by using a model for radiative transport in which departures from equilibrium are taken into account considerable differences could occur in the linear temperature perturbations near the surface of a stellar model. For perturbations with a time scale roughly equal to the fundamental period these differences are marginal but on shorter time scales very large increases in the amplitude of the temperature perturbations can occur. When radiation is the only mechanism for heat transport we have, as before,

$$J = B + \frac{1}{4\pi} \frac{dQ}{dt}$$

so a reasonable way to measure the departures from equilibrium is to define $\tau_Q = (d(\log(Q))/dt)$ and compare this with the radiative relaxation time scale τ_{rad} defined previously.

When this is done it is found that for most of the atmospheric zones $\tau_{rad}/\tau_Q < 10^{-2}$ most of the time. However for short periods of time $\tau_Q/\tau_{rad} < 2$ occurs in the outer zone. This implies a figure for $\omega\tau_{rad}$ which on the basis of the increases in the temperature perturbations near the surface of cool linear models implies a very considerable increase of the temperature perturbations in these nonlinear models. In particular it indicates that shocks will not be

isothermal in the outer layers of the stars. As remarked earlier Christy (1966) has also drawn attention to the shortcomings of the equilibrium diffusion approximation when strong shocks are present. In a model constructed at the lower luminosity without molecular opacity the ratio became small, i.e. $\tau_Q \kappa_{\text{rad}} \ll 1$ throughout a good deal of the atmosphere. This is a direct result of the very large differences (by factors of up to $\sim 10^5$) between the opacity with molecules and that without. It was originally thought that the assumption of radiative equilibrium was responsible for the occurrence of the luminosity spikes and that the inclusion of the nonequilibrium term would lengthen the rise time for the luminosity emitted at the shocks and so smooth the spike away. However the spikes are fully formed at the base of the atmosphere where the equilibrium approximation appears to ^{be} _A satisfied and so the attribution of the luminosity spikes to nonequilibrium effects seems unlikely.

The large departures from isothermality implied by all of these results should, according to, for example, Willson and Hill 1979, imply an increase, probably a large increase, in the mass loss rate. (However Fadeev and Tutukov 1981 invoke the inadequacies of the equilibrium diffusion approximation as an explanation for what they see as an overestimate of the mass loss rate for their model for FG Sge.) Thus the inclusion of some approximate treatment of nonequilibrium effects in radiative transfer is indicated for future models of stars where mass loss is suspected and perhaps even for

those where it is not. An interesting point is the possibility that nonequilibrium effects might be composition dependent and that this might partially explain the differences between RV and SRd light curves. For example a comparison of opacities with molecules included for $Z = 0.001$ and 0.005 (roughly $[Fe/H] = -0.6$ and -1.3), which are reasonable values for field SRd and RV stars respectively, shows that in the latter case the opacities at low temperatures frequently differ by factors of up to 5. This would presumably produce differences by a similar factor in the radiative relaxation time scale and increase the amount of heat retained in the SRd atmospheres.

9.5.11 Shock Waves

All of the nonlinear models constructed using the radiation dilution show strong shock waves. The strongest of these shocks are formed at the point where the tenuous infalling atmosphere meets the relatively dense material below. A specific example of this is the shock associated with the very deep minimum of the $\log(L/L_{\odot}) = 3.2$ model discussed in section 9.5.4. In this case the velocity across the shock was relatively small, 25 km/s. However, large velocities of infall occur frequently and 40 km/s is common in models at both luminosities. In the lower luminosity model infall velocities of ~ 60 km/s are common and occur roughly every second period. The high velocity of the infalling material meeting the rising denser gas produces a very strong shock.

Figs. 9.57 to 9.60 show "snapshots" of the velocity profiles through the low luminosity model with mass as the abscissa. Working through the sequence, the infall velocity rises to 60 km/s whilst the photosphere moves out through the mass as the next expansion phase approaches. The photosphere catches the shock at $T = 1.96 \cdot 10^7$ sec. and following this the velocity across the shock doubles as the envelope moves into expansion. From here on the photosphere recedes into the star and the shock moves towards the surface. Eventually the shock reaches the surface having accelerated the atmosphere into fairly rapid expansion. Soon after this the envelope moves into contraction and by $T = 2.18 \cdot 10^7$ sec. a new shock is forming just above the photosphere. However this shock remains well above the photosphere and does not grow to quite the same strength as the previous shock. Fig. 9.61 repeats the final frame but with radius as the abscissa. From this can be seen the sharp change in velocity and density at the shock and also the expansion of the atmosphere. Another example of the very strong shock forming on the photosphere is shown in figs. 9.62 and 9.63 and also fig. 9.64. The traces of an earlier shock can be seen in the very outermost layers of these figures. All three of these shocks appear at rising light as can be seen by an examination of fig. 9.31 and this is true for all other occurrences of the phenomenon.

Figs. 9.57 - 9.64 Velocity profiles for
 $\log(L/L_{\odot}) = 3.2, \log(T_{eff}) = 3.70$

+ velocity at zone boundary
- escape velocity at same point
vertical line indicates photosphere

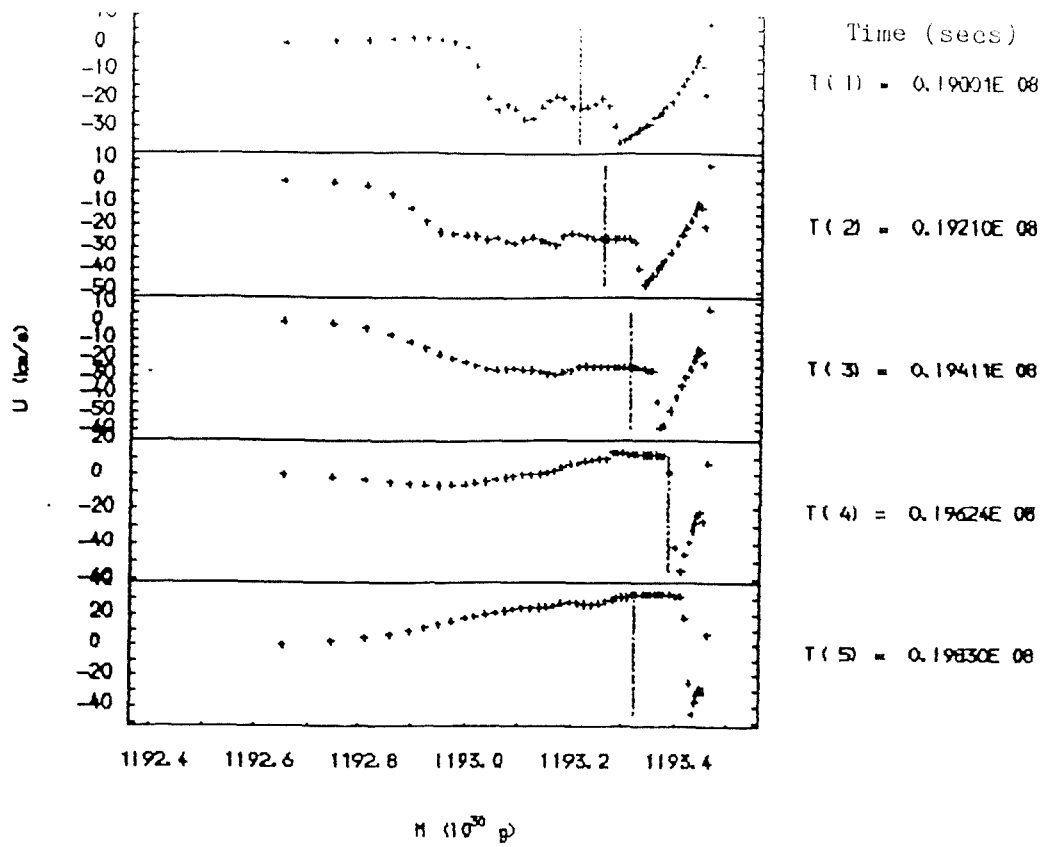


Fig. 9.57 Velocity profiles with mass

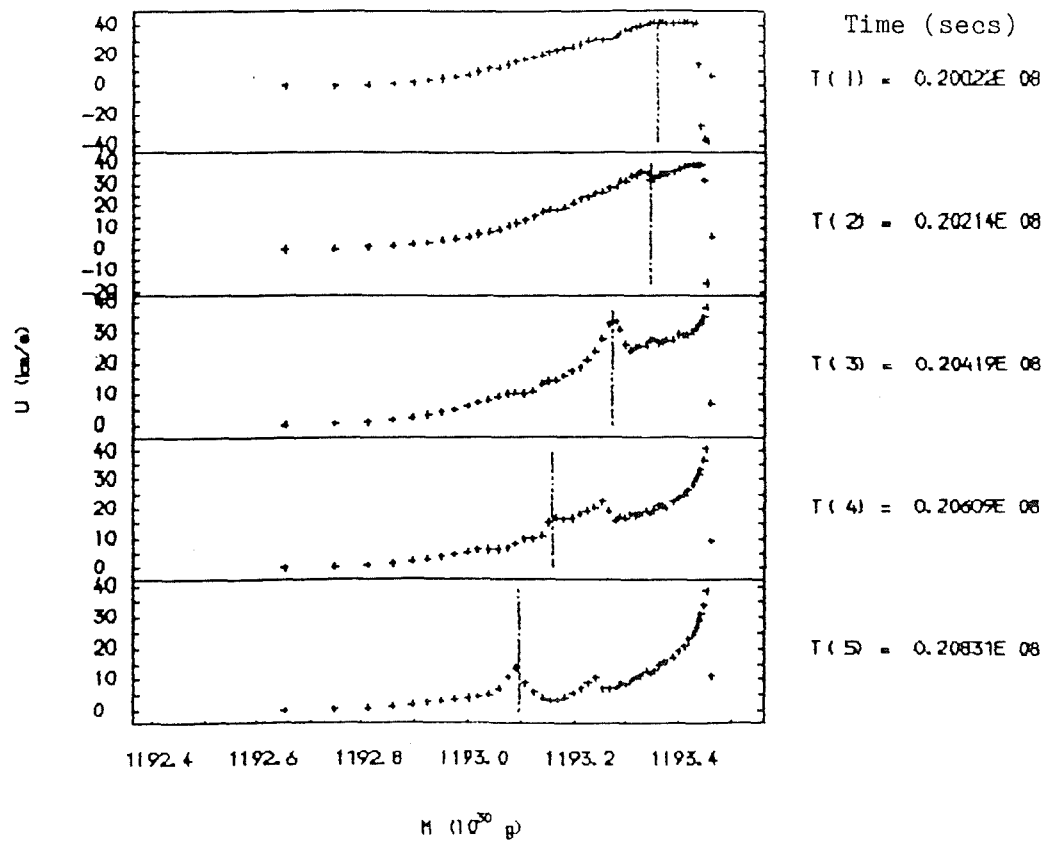


Fig. 9.58 Velocity profiles with mass

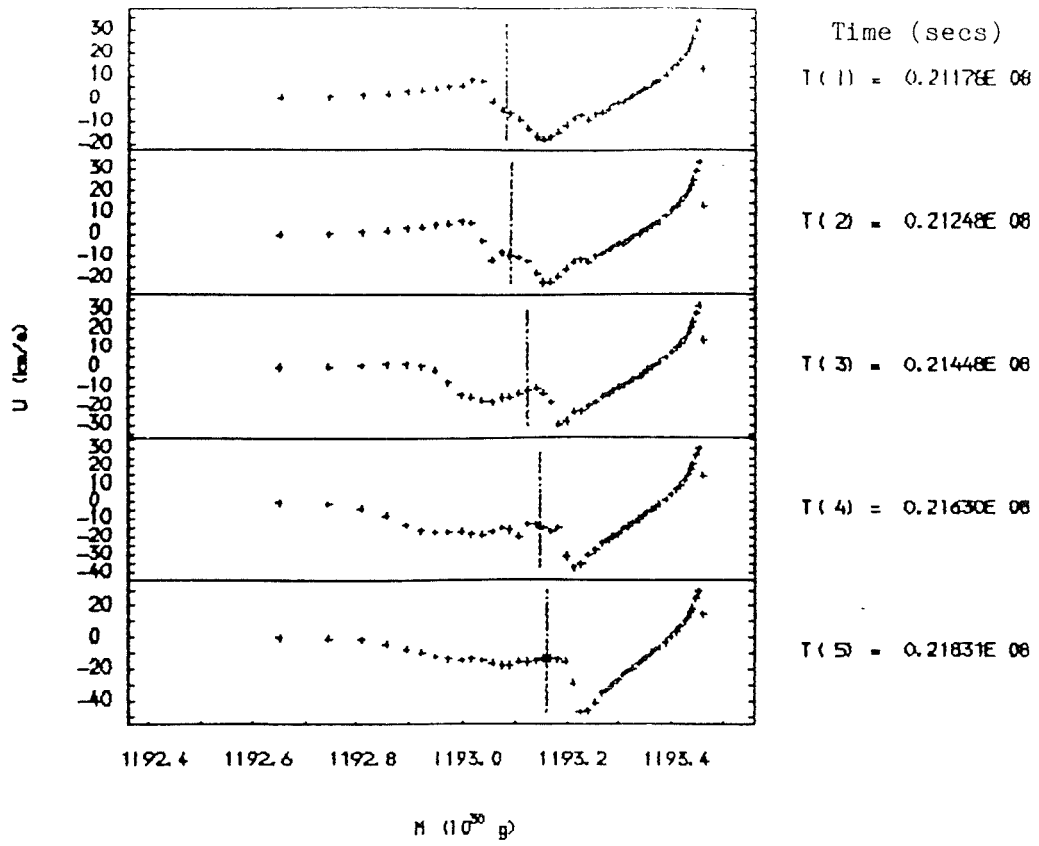


Fig. 9.59 Velocity profiles with mass

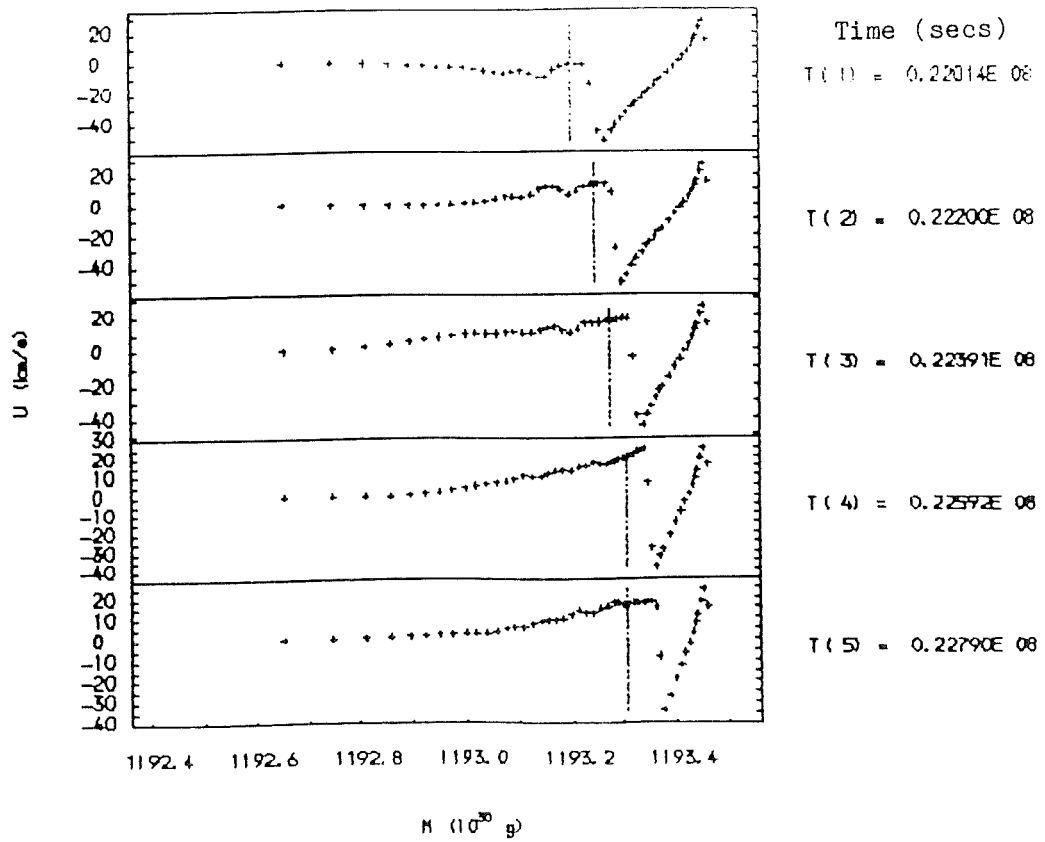


Fig. 9.60 Velocity profiles with mass

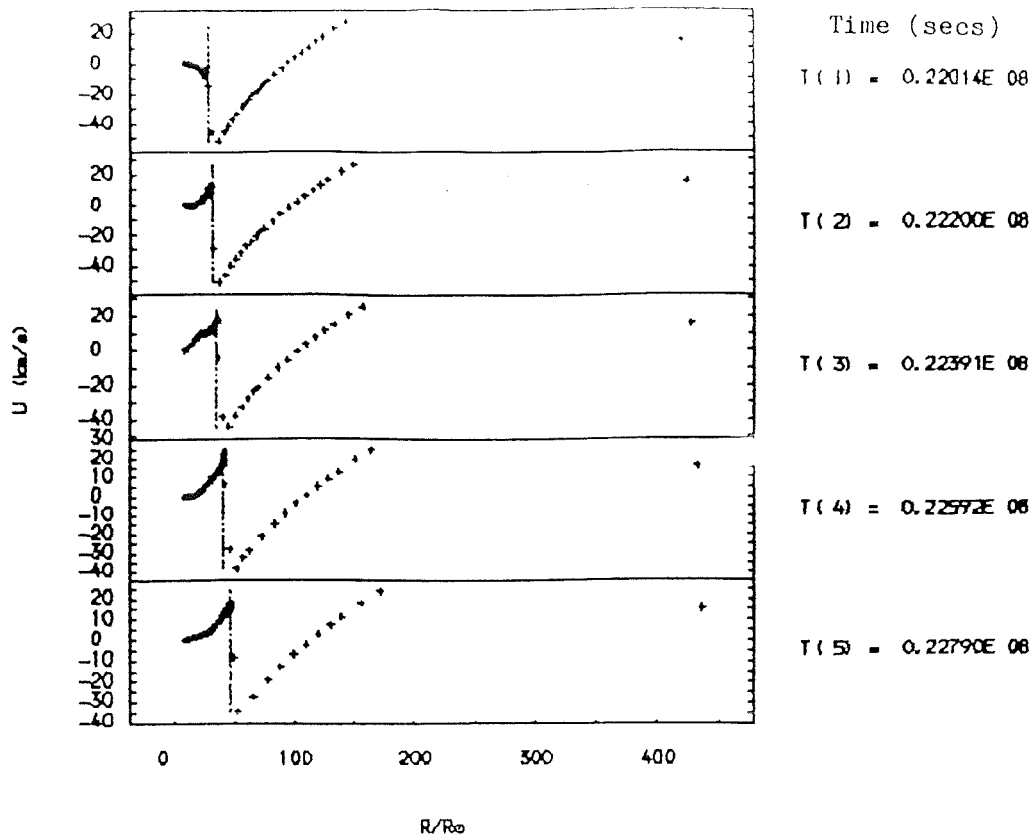


Fig. 9.61 Velocity profiles with radius

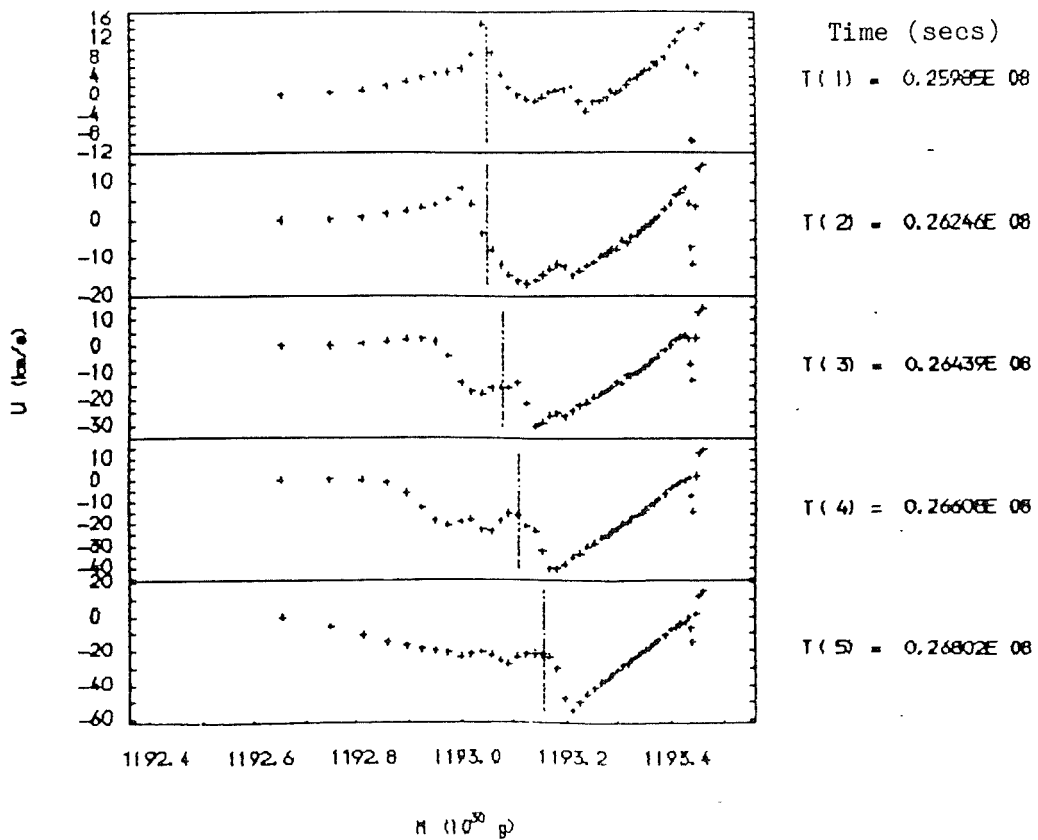


Fig. 9.62 Velocity profiles with mass

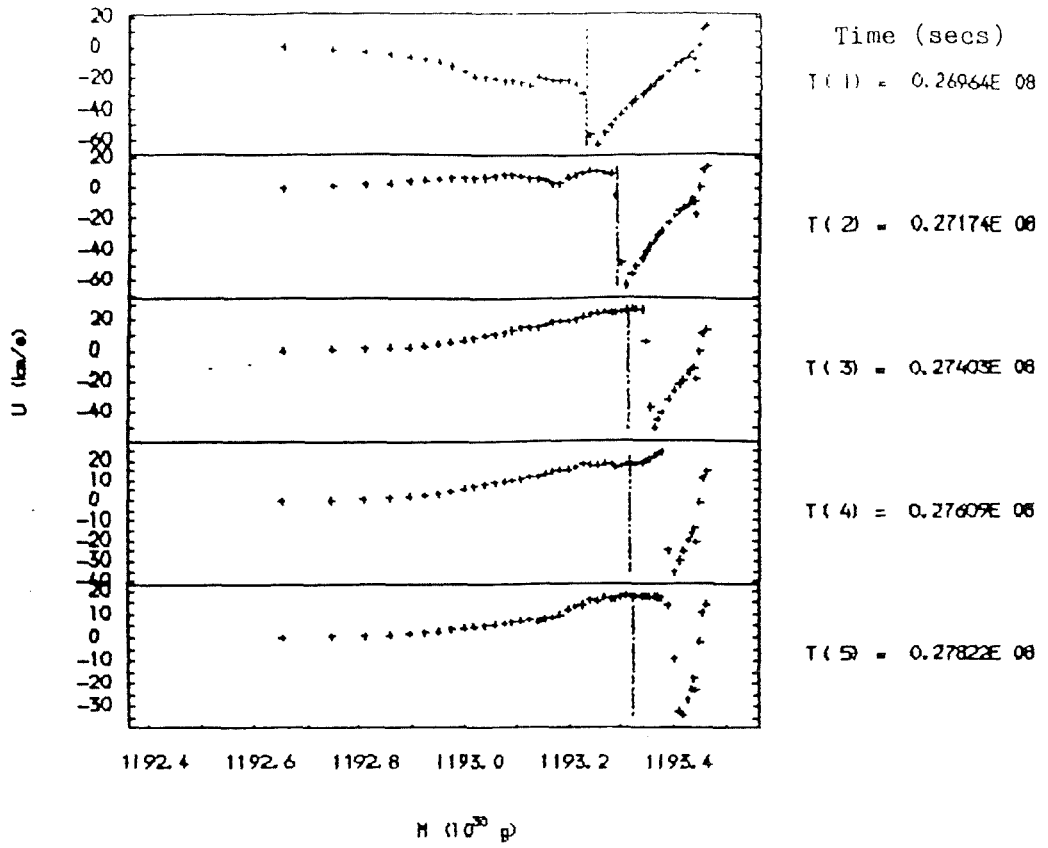


Fig. 9.63 Velocity profiles with mass

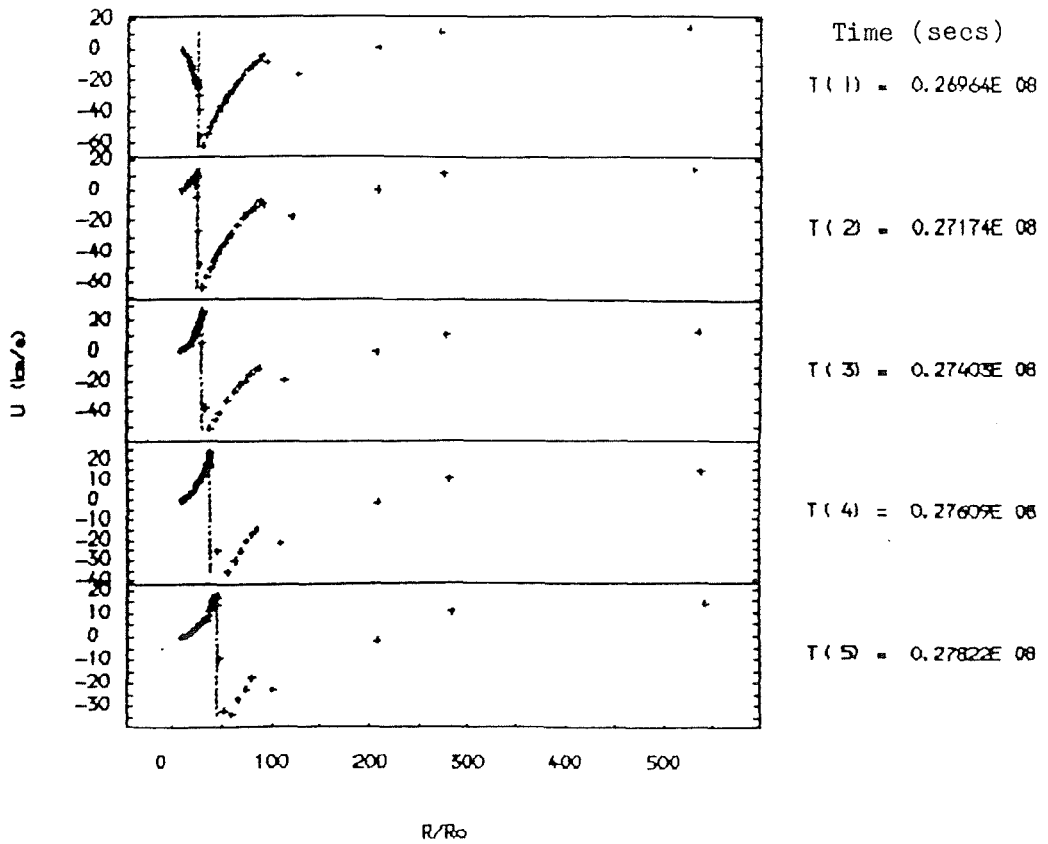


Fig. 9.64 Velocity profiles with radius

How would these shocks appear to the observer? To answer this question properly requires details of the line forming regions, that is, of the line optical depths and radiative recombination for the shock emission. However a rough idea of the lines present can probably be gained by looking at the mass above and below the shock and the shock strength. For the first shock there will initially be two redshifted absorption systems with some emission in between. The blue absorption system should move to the blue slowly with the emission and weaken until as the photosphere reaches the shock this absorption system disappears. Simultaneously the highly red - shifted system moves redwards and the emission grows in strength as the shock power increases (by a factor of ~ 8 since the shock power is proportional here to velocity cubed). Very soon after this the photosphere recedes and the now blue - shifted absorption component reappears as the shock moves towards the surface. The emission and the redshifted lines will fade as the matter the shock meets grows increasingly tenuous. As the envelope moves to contraction, after a false start, a new shock begins to form above the photosphere. In this case the shock remains above the photosphere and so a blue component probably ^{will} always be present. As before the shock moves outwards towards the surface but weakens before it reaches the surface because the next contraction phase has set in. The final shock looks similar to the first shock with the initial blue absorption component fading out as the emission rises followed by a reappearance of a much

bluer blue component as the shock leaves the photosphere for the surface.

Whilst it must be remembered that the zoning is too coarse and the physics too poor for these models to treat shocks accurately the results do seem to match up tolerably well with the observations of Baird (1982, 1984). In every case the strong shock appears at light minimum and grows through rising light. In the case of the deep minima the blue absorption component does not appear immediately but only after the blue shifted emission has been in evidence for some while and the highly red - shifted line system fades well before light maximum is reached. The velocities for the various components seem to be about right. Also the prediction is that the blue component should be more heavily veiled than the red which matches the observations whereas Baird's (1984) two shock model predicts the reverse. Baird's model is based upon the two shock model for long period variable star shocks due to Willson and Hill (1979) which has been severely criticised by Wood (1981). Wood's simpler alternative is much the same as the one suggested by the behaviour of the shocks in my less luminous model.

CHAPTER 10

CONCLUSION

The main aim of the present study was to make a theoretical interpretation of the RV Tauri variables. However as a preliminary to this investigation a number of sources of uncertainty in pulsation calculations in the linear approximation were investigated, but many of which will also affect nonlinear calculations. An attempt has been made to try and quantify the errors incurred in calculating the linear pulsation models. It was found that the uncertainties on the physical variables increase rapidly as the model is integrated inwards from the surface towards the centre of the star. The fractional errors remain reasonable (i.e. $\ll 1$) throughout most lower luminosity stars, e.g. RR Lyrae stars, but become rather large at the envelope base in some more luminous stellar models typical of the longer period W Vir stars. An important cause of the limiting accuracy was found to be the accuracy with which the equation of state was solved. However these errors are very probably overestimated to a large degree and so should not be unduly worrying. It was not possible to carry the analysis

through to obtain simple expressions for the errors on the pulsation variables for the full nonadiabatic problem. However the errors for the adiabatic problem are well known and easily calculated. These are found to be small. An idea of the way errors affect the pulsation results was gained by use of a "Monte Carlo" type simulation of errors imposed at various stages between the calculation of the static models and the linear pulsation calculation. This showed that in the most reasonable case the errors were very small indeed for the periods and larger, though still small enough to give at least three figures of accuracy, on the growth - rates. As a spin - off from the errors analysis a method for studying the effects of variations of input physics, in particular the opacity, on the static stellar models and on the linear pulsation results was developed. This, whilst tractable, has yet to be applied. It should offer considerable advantages over methods previously used to study such effects in pulsation models (although other authors have applied an equivalent method to static models.)

The effects of using varying partition functions in the equation of state rather than the more usual constant values were investigated through the extension of an approximation found in the literature. The results are disappointing for the giant stars showing only negligible effects. This is not the case, however, in main sequence stellar models for which observable effects should be present. This has not been pursued.

Some time was spent on calculating and comparing fundamental mode blue - edges calculated using the Carson opacities, as an example of an opacity with a metals bump, and the Los Alamos opacities. The intention was to look for metallicity dependences in observations which might set limits on the accuracy of the respective opacities. However the comparison of these blue - edges with observations of type II cepheids and RV Tauri stars gave inconclusive results.

Other physical approximations investigated included the use of a nonequilibrium Eddington approximation, previously used only in nonradial calculations, in place of the usual diffusion approximation. Whilst this did not affect the complex eigen - frequencies of the models it does produce a greatly increased temperature perturbation near to the stellar surface. On the strength of work on pulsation driven mass - loss found in the literature it is suggested that this should increase the mass - loss rates appreciably. Another point investigated was the effect of a running wave boundary condition at the stellar surface. This was thought to be a possible source of uncertainty because of the considerable extent of the atmospheres of many of the stars under investigation. On the other hand the running waves were found to have no appreciable effect upon the periods or stability of any of these models. However the presence or absence of matter outside the surface boundary was found to affect stability slightly. The introduction of convection into the stellar models was also found to have an effect upon the stability near the blue - edge

of the instability strip pushing the edge slightly to the blue for the lowest metallicity models.

A large number of linear pulsation calculations using both of the two alternative sources of opacities and with or without some form of convection for use in the ^{analysis} of the RV Tauri stars were presented. On the basis of the trends found in the intercomparisons of the W Vir, RV Tauri, and SRd stars which were discussed in the review (chapter 6) a single mass was assumed for all three classes of star. Using this assumption luminosities based upon the observed periods and effective temperatures were calculated using the linear pulsation theory data. These luminosities were then compared with the observed luminosities by calculating residuals ($\log(L_p/L_o)$). A considerable spread was found in the residuals which can be translated into a spread in the effective temperatures almost as large as the width of the instability strip. This suggests that the instability strip is considerably narrower for the type II cepheids than is generally thought. This is in accord with some recent observations (Harris 1981). However the mean residuals at each period are larger than zero and increase with period. This remains to be properly explained but there does seem to be scope for such an explanation in terms of errors on the distance scale for clusters, bolometric corrections, and the effective temperatures. Even so trends common to the W Vir, RV Tauri, and SRd stars in the globular clusters suggest that the assumption of a single mass and of a close relationship is reasonable. When the data for the

field RV Tauri and SRd stars drawn from Dawson (1979) are placed under scrutiny it quickly becomes obvious that unless the assumptions are wildly wrong there is no real relation between the stars within the classes. For example for mass differences to be the sole source of the large residuals the masses would have to vary from one star to another by factors of as much as 100. Another source of observed luminosities (Du Puy 1976) was considered for these stars and the residuals in this case ^{were} found to be very much smaller.

One suggestion to account for the peculiar, characteristically semi - regular RV Tauri light curves is that a resonance between pulsation modes might exist. This has been examined using the linear pulsation results and it is found that over a considerable portion, if not all, of the RV Tauri region of the HR diagram modal interaction should be possible. However it is not possible to make any predictions regarding the actual state of affairs on the basis of the linear results because the necessary theory does not yet exist.

There is one RV Tauri star, UU Her, which possesses two pulsation periods and for this reason it is possible to deduce a mass and luminosity founded purely on the knowledge of these two periods and the observed effective temperature. This has been done and yields values for the mass between 0.7 and 1.2 M_{\odot} for log. effective temperatures in the range 3.77 and 3.74 whilst the luminosity is very nearly $10^4 L_{\odot}$ for all reasonable temperatures. It is unfortunate that

the effective temperature is so poorly known. However it is possible to explain the unique biperiodic behaviour of this star as being the result of its high temperature which places it in a region of the HR diagram where the linear growth rates for the fundamental and first overtone modes are comparable. For all the other, cooler RV Tauri and SRd stars the fundamental mode is far more unstable and the overtone much less unstable or, frequently, stable.

A peculiar, high luminosity F - star, HD161796, which is thought on the basis of spectroscopy to be a post - asymptotic giant branch star and probably closely related to the SRd stars has been analysed in a similar manner. In this case a far more tightly constrained mass of $0.50 - 0.54 M_{\odot}$ was derived in agreement with the evolutionary arguments. It was argued on the basis of the linear growth rates that this low mass interpretation is far more plausible than the original suggestion of a high mass. A mechanism was suggested tentatively to explain the amplitude and biperiodicity of the light curve.

A limited number of nonlinear pulsation models have also been constructed with a view to explaining the nature of the RV Tauri pulsations. No great success can be claimed but a number of the features found in the observed light curves and spectroscopy are found in the models. These features include the variation in depths of minima and the tendency for the stars to undergo periods of relative quiescence. Occasional deep minima have also been observed and a

variability in the period is usually present. This last feature is, though, more a feature of SRd stars than the RV Tauri stars. The behaviour of the material above the photosphere is erratic but cyclic and involves the movements of large masses out to many times the equilibrium photospheric radius. Strong shocks and very high infall velocities observed in a number of RV Tauri atmospheres are also present in models. It is possible that other atmospheric phenomena are also present in the models. Some slight mass loss is observed initially but the recurrent mass loss suggested by some of the observations is not found.

However there are a number of considerable flaws in the models. It is suggested that the use of the equilibrium diffusion equation for radiative transport is not valid. An alternative to this approximation is the Eddington Approximation used for some of the trial linear calculations and the results of those calculations do indeed suggest an increased mass loss rate. A further problem is seen to lie in the dubious approximation to spherical geometry in the atmosphere used in the more reliable models.

Obviously much more work remains to be done not only in terms of computation but also on the underlying theory needed to cope with the RV Tauri stars. A realistic but tractable treatment of sphericity in a pulsating atmosphere is required and the best starting point for this might well be the Unno and Kondo (1976) extension of the well

known equilibrium Eddington approximation to spherical geometry. This should be used to provide the geometric input to a solution of Castor's (1972) equations for radiative transfer in a spherically symmetric moving atmosphere. The omnipresent convection problem must also be resolved. At present the most promising path forwards seems to be that laid out by Stellingwerf (1982 etc.) and this, at least, will be incorporated into models for the future.

The RV Tauri stars are similar to the Long Period Variables (LPVs) in that they also are losing mass through pulsational driving. However the LPV stars cannot hope to be studied without using convection and so the effects of convection and mass loss cannot be easily disentangled. The RV Tauri stars probably can be studied without the incorporation of convection and so this provides a way of studying mass loss separated from convection. In particular the switch from W Vir to RV Tauri behaviour at a reasonably well defined period or luminosity provides a test for the validation of a theory for pulsationally driven mass loss. However quite apart from this the RV Tauri and SRd stars are of considerable interest in their own right. If, as seems, possible the high luminosity F - stars are the next stage in the evolution of, at least, the SRd stars then these stars are at the penultimate point of evolution of the low mass stars. However I cannot claim to have offered any real proof for this speculation.

APPENDIX A

REFERENCES

- Aalberg, J.H., Nilson, E.N., and Walsh, J.L., (1967)
"The Theory of Splines and Their Applications"
- Abt, H.A., (1960)
Astrophys. J., 131, 99
- Alexander, D.R., (1975)
Astrophys. J. Suppl., 29, 363
- Alexander, D.R., Johnson, H.R., and Rypma, R.L., (1983)
Astrophys. J., 272, 773
- Allen, C.W., (1973)
"Astrophysical Quantities", 3rd. edn.,
Athlone Press, University of London
- Baade, T.G., and Swope, H., (1963)
Astr. J., 68, 435
- Baird, S.R., (1981)
Astrophys. J., 245, 408
- Baird, S.R., (1982)
Publs astr. Soc. Pacif., 94, 850
- Baird, S.R., (1984)
Publs astr. Soc. Pacif., 96, 72
- Baker, N.H., (1966)
"Stellar Evolution", eds. Stein, R.F., Cameron, A.G.F.,
Plenum Press: N.Y.
- Baker, N.H., and Kippenhahn, R., (1962)
Z. Astroph., 54, 114
- Baker, N.H., and Kippenhahn, R., (1965)
Astrophys. J., 142, 868
- Baker, N.H., and Gough, D.O., (1979)
Astrophys. J., 234, 232
- Barnes, T.G., and Du Puy, D.L., (1975)
Astrophys. J., 200, 364
- Barnes, T.G., Evans, D.S., and Moffet, T.J., (1978)
Mon. Not. R. astr. Soc., 183, 285
- Bednarek, T.A., (1975)
"Cepheid Modeling", eds. Fischel, D., Sparks, W.M.,
Washington, D.C.:NASA

- Bohm-Vitense, E., (1958)
Z. Astroph., 46, 108
- Bohm-Vitense, E., (1973)
Astr. Astrophys., 24, 447
- Bond, H.E., (1970)
Astrophys. J. Suppl., 22, 117
- Bowers, P.F., and Kerr, F.J., (1977)
Astron. Astrophys., 57, 115
- Bridger, A., (1983)
Ph.D. Thesis, University of St. Andrews, U.K.
- Buchler, J.R., and Goupil, M.J., (1984)
Astrophys. J., 193, 177
- Buchler, J.R., and Regev, O., (1981)
Astrophys. J., 250, 776
- Cannon, R.D., and Stobie, R.S., (1973)
Mon. Not. R. astr. Soc., 162, 207
- Carson, T.R., (1971)
Prog. in High Temp. Phys. and Chem., 3, 99
- Carson, T.R., (1976)
Ann. Rev. Astr. Astrophys., 14, 95
- Carson, T.R., Huebner, W.F., Magee, N.H., and Merts, A.L., (1984)
Astrophys. J., 283, 468
- Carson, T.R., Mayers, D.F., Stibbs, D.W.N., (1967)
Mon. Not. R. astr. Soc., 140, 483
- Carson, T.R., and Stothers, R., (1976)
Astrophys. J., 204, 461
- Carson, T.R., and Stothers, R., (1982)
Astrophys. J., 259, 440
- Carson, T.R., Stothers, R., and Vemury, S.K., (1981)
Astrophys. J., 244, 230
- Castor, J.I., (1971)
Astrophys. J., 166, 109
- Christy, R.F., (1966)
Astrophys. J., 144, 108
- Christy, R.F., (1966a)
Astrophys. J., 145, 337
- Christy, R.F., (1967),
Methods in Computational Science, 7, 191
- Christy, R.F., (1968)
Q. Jl R. astr. Soc., 9, 13
- Cloutman, L.D., (1973)
Astrophys. J., 184, 675
- Conte, S.D., and de Boor, C., (1972)
"Elementary Numerical Analysis",
- Cox, A.N., (1965)
"Stars and Stellar Systems", 8, 195,
eds., Aller, L.H., McLaughlin, D.B.
- Cox, A.N., Stewart, J.N., Eilers, D.D., (1965)
Astrophys. J. Suppl. Ser. 11, 1

- Cox, A.N., and Stewart, J.N., (1970)
Astrophys. J. Suppl., 19, 243
- Cox, J.P., (1980)
"Theory of Stellar Pulsation",
Princeton University Press, Princeton, N.J.
- Cox, J.P., and Giuli, R.T., (1968)
"Principles of Stellar Structure", (Gordon and Breach: N.Y.)
- Cox, J.P., and Stellingwerf, R.F., (1979)
Publs astr. Soc. Pacif., 91, 319
- Cox, M.G., (1972),
J. Inst. Maths. Applics., 10, 134
- Dawson, D.W., (1979)
Astrophys. J. Suppl. 41, 97
- De Boor, C. (1972),
J. Approx. Theory, 6, 50
- Demers, S., and Harris, W.E., (1974)
Astr. J., 79, 627
- Demarque, P., and Mengel, J.G., (1971)
Astrophys. J., 171, 583
- Deupree, R.G., (1975)
Astrophys. J., 198, 419
- Deupree, R.G., (1977a)
Astrophys. J., 211, 509
- Deupree, R.G., (1977b)
Astrophys. J., 214, 502
- Deupree, R.G., (1977c)
Astrophys. J., 215, 232
- Deupree, R.G., (1977d)
Astrophys. J., 215, 620
- Deupree, R.G., Hodson, S.W., (1976)
Astrophys. J., 208, 426
- Dickens, R.J., and Powell, A.L.T., (1973)
Mon. Not. R. astr. Soc., 161, 249
- Du Puy, D.L., (1973)
Astrophys. J., 185, 597
- Dziembowski, W., (1982)
Acta. Astron., 32, 147
- Eggleton, P.P., (1968)
Mon. Not. R. astr. Soc., 140, 387
- Eggleton, P.P., (1983)
Mon. Not. R. astr. Soc., 204, 449
- Epstein, R.E., Gudmundsson, E.H., and Pethick, C.J., (1983)
Mon. Not. R. astr. Soc., 204, 471
- Erleksova, G.E., (1970)
Inf. Bull. Variable Stars, 1663
- Fadeev, Yu., and Tutukov, A.V., (1981)
Mon. Not. R. astr. Soc., 195, 811
- Fernie, J.D., (1977)
Mon. Not. R. astr. Soc., 180, 339
- Fernie, J.D., (1981)

- Astrophys. J., 243, 576
Ferne, J.D., (1983)
Astrophys. J., 265, 999
Fischel, D., and Sparks, W.M., (1971)
Astrophys. J., 164, 359
Flower, P.J., (1977)
Astr. Astrophys., 54, 31
Fox, M.W., and Wood, P.R., (1982)
Astrophys. J., 259, 198
Fricke, K., Stobie, R.S., and Strittmatter, P.A., (1971)
Mon. Not. R. astr. Soc., 154, 23
Gehrz, R.D., (1972)
Astrophys. J., 178, 715
Gehrz, R.D., and Hackwell, J.A., (1974)
Astrophys. J., 193, 385
Gehrz, R.D., and Woolf, N.J., (1970)
Astrophys. J., 161, 213
Gingold, R.A., (1974)
Astrophys. J., 193, 177
Gingold, R.A., (1976)
Astrophys. J., 204, 116
Gonczi, G., (1981)
As.Ap., 96, 138
Gonczi, G. (1982)
Astr. Astrophys., 110, 1
Gonczi, G., and Osaki, Y., (1980),
Astr. Astrophys., 84, 304
Gough, D.O., (1977)
Astrophys. J., 214, 196
Griem, H.R., (1967)
Astrophys. J., 147, 1092
Harris, H.C., (1981)
Astr. J., 86, 719
Harris, H.C., (1984)
I.A.U. Colloq., 82
Harris, H.C., and Wallerstein, G., (1984)
Astr. J., 89, 379
Henyey, L.G., Forbes, J.E., and Gould, N.L. (196?)
Astrophys. J., 139, 306
Howell, S.B., Bopp, B.W., and Noah, P.V., (1983)
Publs astr. Soc. Pacif., 95, 762
Hubbard, W.B., and Lampe, M., (1968)
Astrophys. J., Suppl. Ser. 18, 297
Iben, I. (1971)
Astrophys. J., 166, 131
Iben, I., and Rood, R.T., (1970)
Astrophys. J., 161, 587
Jeffery, C.S., (1982)
Ph.D. Thesis, University of St. Andrews, U.K.
Joy, A.H., (1952)

- Astrophys. J., 115, 25
Karp, A.H., (1975)
Astrophys. J., 201, 641
Keeley, D.A., (1970)
Astrophys. J., 161, 657
Keeley, D.A., (1977)
Astrophys. J., 211, 926
King, D.S., Cox, A.N., and Hodson, S.W., (1981)
Astrophys. J., 244, 242
King, D.S., Wheeler, J.C., Cox, J.P., Cox, A.N.,
and Hodson, S.W., (1980)
"Nonradial and Nonlinear Stellar Pulsation",
eds. Hill, H.A., Dziembowski, W.A., Springer-Verlag
Klyus, I.A., (1981)
Soviet Astron., 25, 207
Kraft, R.P., (1979)
Ann. Rev. Astr. Astrophys., 17, 309
Kukarkin, B.V., Kholopov, P.N., Efremov, Yu.N.,
Kukarkina, N.P., Kurochkin, N.E., Medvedeva, G.I.,
Perova, N.B., Fedorovich, V.P., and Frolov, M.S., (1969)
"General Catalogue of Variable Stars", 3 edn.
Kukarkin, B.V., Kholopov, P.N., Efremov, Yu.N.,
Kukarkina, N.P., Kurochkin, N.E., Medvedeva, G.I.,
Perova, N.B., Pskovsky, Yu.P., Fedorovich, V.P.,
and Frolov, M.S., (1971)
"First Supplement to Third Edition of the
General Catalogue of Variable Stars"
Kukarkin, B.V., Kholopov, P.N., Efremov, Yu.N.,
Kukarkina, N.P., Kurochkin, N.E., Medvedeva, G.I.,
Perova, N.B., Pskovsky, Yu.P., Fedorovich, V.P.,
and Frolov, M.S., (1974)
"Second Supplement to Third Edition of the
General Catalogue of Variable Stars"
Kukarkin, B.V., Kholopov, P.N., Efremov, Yu.N.,
Kukarkina, N.P., Kurochkin, N.E., Medvedeva, G.I.,
Perova, N.B., Pskovsky, Yu.P., Fedorovich, V.P.,
and Frolov, M.S., (1976)
"Third Supplement to Third Edition of the
General Catalogue of Variable Stars"
Kwee, K.K., (1967)
B.A.N., 19, 260
Kwee, K.K., (1968)
B.A.N., 19, 374
Lacy, C.H., (1973)
Astr. J., 78, 90
Lang, K.R., (1974)
"Astrophysical Formulae", Springer-Verlag
Ledoux, P., and Walraven, Th., (1958)
Handbuch der Physik, 51, 605
Lloyd-Evans, T., (1970)

- The Observatory, 90, 254
- Luck, R.E., (1981)
Publs astr. Soc. Pacif., 93, 211
- Luck, R.E., and Bond, H.E., (1984)
Astrophys. J., 279, 729
- Luck, R.E., Lambert, D.L., and Bond, H.E., (1983)
Publs astr. Soc. Pacif., 93, 413
- Mantegazza, L. (1978)
Inf. Bull. Variable Stars, 1500
- Mantegazza, L., (1984)
Astr. Astrophys., 135, 300
- Mihalas, D., (1978)
"Stellar Atmospheres", 2 edn.,
W.H. Freeman and Co., San Fransisco
- Osborn, W., (1973),
Astrophys. J., 186, 725
- Paczynski, B. (1969)
Acta Astron., 19, 1
- Payne-Gaposhkin, C., Brenton, V.K., and Gaposhkin, S., (1943)
Ann. Astr. Obs. Harv. Coll., 113, 65
- Petersen, J.O., (1973)
Astr. Astrophys., 27, 89
- Pilachowski, C.A., (1984)
Astrophys. J., 281, 614
- Preston, G.W., (1962)
Astrophys. J., 138, 320
- Preston, G.W., (1964)
Astrophys. J., 140, 173
- Preston, G.W., Kreminski, W., Smak, J., and Williams, J.A. (1962),
Astrophys. J., 137, 401
- Preston, G.W., and Wallerstein, G., (1963)
Astrophys. J., 138, 820
- Ralston, A., (1965)
"A First Course in Numerical Analysis",
McGraw-Hill, New York
- Refsdal, S., and Stabell, R., (1972)
Astr. Astrophys., 20, 19
- Rosino, L., (1951)
Astrophys. J., 113, 60
- Rosino, L., (1978)
Vistas in Astron., 22, 39
- Rosseland, S. (1949),
"The Pulsation Theory of Variable Stars",
Dover, New York
- Saio, H., (1980)
Astrophys. J., 240, 685
- Saio, H., and Wheeler, J.C., (1983)
Astrophys. J., 272, L25
- Saio, H., Wheeler, J., and Cox, J.P., (1984)
Astrophys. J., 281, 318

- Sanford, R.F., (1955)
Astrophys. J., 121, 318
- Sargent, W.L.W., (1963)
Astrophys. J., 137, 268
- Schwarzschild, M., (1958)
"Structure and Evolution of Stars",
Dover, New York
- Schlesinger, B.M., (1969)
Astrophys. J., 157, 533
- Simon, N.R., (1977)
Astrophys. J., 217, 160
- Simon, N.R., (1981)
Bull. A.A.S., 13, 871
- Simon, N.R., (1982)
Astrophys. J., 260, L87
- Simon, N.R., Cox, A.N., and Hodson, S.W., (1980)
Astrophys. J., 237, 550
- Simon, N.R., and Schmidt, E.G., (1976)
Astrophys. J., 205, 162
- Spiegel, E.A., (1963)
Astrophys. J., 138, 216
- Stellingwerf, R.F., (1974)
Ap J., 192, 139
- Stellingwerf, R.F., (1975)
Astrophys. J., 195, 441
- Stellingwerf, R.F., (1976)
Astrophys. J., 206, 543
- Stellingwerf, R.F., (1982a)
Astrophys. J., 262, 330
- Stellingwerf, R.F., (1982b)
Astrophys. J., 262, 339
- Stellingwerf, R.F., (1983a)
Preprint
- Stellingwerf, R.F., (1983b)
Preprint
- Stobie, R.S., (1969)
Mon. Not. R. astr. Soc., 144, 485
- Stobie, R.S., (1970)
Mon. Not. R. astr. Soc., 148, 1
- Stothers, R., (1963)
Astr. J., 68, 242
- Stothers, R., (1964)
Publs astr. Soc. Pacif., 76, 98
- Stothers, R.S., (1976)
Astrophys. J., 204, 853
- Takeuti, M., (1983)
The Observatory, 103, 292
- Takeuti, M., and Petersen, J.O., (1983)
Astr. Astrophys., 117,
- Ulrich, R.K., (1976)

- Astrophys. J., 207, 546
- Unno, W., (1964)
Publs astr. Soc. Japan, 17, 205
- Unno, W., (1967)
Publs astr. Soc. Japan, 19, 140
- Unno, W., (1976)
"Problems of Stellar Convection", IAU, Colloq., 38,
Ed. Zahn, J.D., Reidel: Dordrecht.
- Unno, W., Osaki, Y., Ando, H., and Shibahashi, H., (1979)
"Nonradial Oscillations of Stars", Tokyo University Press
- Unno, W., and Spiegel, E.A., (1966),
Publs astr. Soc. Japan, 18, 85
- Van den Bergh, S., (1974)
Astr. J., 72, 72
- Wenzel, W., (1961)
Inf. Bull. Variable Stars, 27
- Whitney, C.A., (1983)
Astrophys. J., 274, 830
- Wilkinson, J.H., (1963)
"Rounding Errors in Algebraic Processes", (H.M.S.O.)
- Willson, L.A., and Hill, S.J. (1979)
Astrophys. J., 225, 854
- Wood, P.R., (1974)
Astrophys. J., 190, 609
- Wood, P.R., (1976)
Mon. Not. R. astr. Soc., 174, 531
- Wood, P.R., (1979)
Astrophys. J., 227, 220
- Wood, P.R., (1981)
"Physical Processes in Red Giant Stars",
eds. Iben, I., Renzini, A., Reidel
- Yoshioka, K., (1979)
Publs astr. Soc. Japan, 31, 23